公开举报西安石油大学职称评审不公正、学术不端（一稿切片三发，三稿六发）不处理，基金管理单位对基金项目申报、执行中的弄虚作假行为（三稿六发，篡改文章题目、会议名称、举办地，滥标基金号，标注基金号文章与项目书研究内容截然不同等）不处理，学术不端、弄虚作假教师在内部举报中一路绿灯提职升级，符合条件教师无缘职称晋升反被降级

尊敬的西安石油大学、陕西省教育厅、陕西省科技厅、国家自然科学基金委：

本人是西安石油大学教师，2023 年 11 月参加西安石油大学职称评审，期间与本人一起参评职称评审的两名教师存在明显的学术不端行为，本人在西安石油大学计算机学院 2023 年 11 月 15 日公示学院推荐排序后，第一时间就李小和、王静怡老师存在的学术不端行为向计算机学院院办和领导提交书面异议（详见附录 1）。计算机学院不接收本人的书面异议，让本人向学校纪委提交。本人向学校纪委提交后（详见附录 2、附录 3），纪委让计算机学院调查。计算机学院对学术不端行为的调查不符合学校文件相关要求（应上学校学术道德委员会集体讨论研究，计算机学院说学校学术道德委员会主任决定不上会由计算机学院自行调查），计算机学院组织 2 位校外专家、2 位学院专家进行评议，但计算机学院枉顾专家意见，所谓“综合”专家意见的调查结论刻意包庇纵容。本人不服，2023 年 11 月 22 日向西安石油大学纪委提起复议（详见附录 4），西安石油大学纪委回复有进一步调查结论会向我回复，但一直杳无音信，截至目前未有复议结论。后本人于 2023 年 12 月 22 日就西安石油大学职称评审过程中对学术不端举报存在的推诿、搪塞行为向陕西省教育厅教师工作部举报（详见附录 5），教师工作部受理后截止目前未回复调查结论。本人于 2023 年 12 月 12 日就王静怡在基金申请、执行过程中存在的弄虚作假、经费使用不当、基金标注、发表论文与基金

合同不一致等一系列科研不端行为向陕西省科技厅（详见附录 6）、国家自然科学基金委举报（详见附录 7），相关机构受理后，截止目前未回复调查结论。

西安石油大学相关机构受理后，调查过程中存在推诿、搪塞等一系列行为，作为主体责任单位一直未认真、积极履行职责。职称评审中虽然有文件、有监督等相关规定，但真正遇到举报学术不端，这些文件、监督逐个失效。存在学术不端的老师在举报过程中一路绿灯，通过学院推荐、学科组评审、学校评审，顺利晋升副教授。2024 年 7 月，西安石油大学计算机学院进行聘岗，计算机学院又以李小和、王静怡具有副教授身份而分别聘岗教师岗 6 级和教师岗 7 级。本人于计算机学院公示当天向计算机学院聘岗工作领导小组提交书面异议和两位老师学术不端的证明材料（详见附录 8），计算机学院答复未见到上级关于两位老师学术不端的最终调查结论，学院认为两位老师不存在学术不端。计算机学院两位老师在职称评审中存在的学术不端和弄虚作假行为违反了教育部《新时代高校教师职业行为十项准则》第七条第八条之规定，详见附录 8 中的教育部《新时代高校教师职业行为十项准则》文件。王静怡老师 2016 年入职，至 2019 年一直聘为教师岗 9 级，因成果薄弱未完成助推，人事处当时要求王静怡老师转岗，王静怡不愿意后被降为教师岗 10 级。2020 年王静怡因获批国基金升为教师岗 9 级。2023 年王静怡以一稿双发且论文成果薄弱仅压线但顺利晋升职称，2024 年 7 月新一轮聘岗由教师岗 9 级升为 7 级。李小和老师 2011 年入职，一直教师岗 9 级。2020 年担任计科系主任，聘为教师岗 8 级。2023 年一稿切片香肠论文三发且论文成果薄弱仅压线但顺利晋升副教授职称，聘为教师岗 7 级。2024 年 7 月新一轮聘岗李小和老师由教师岗 7 级升为 6 级。本人 2012 年入职，2013/2015/2018/2019 年科技分所在系最高。2012-2015 年聘为教师岗 9 级，考核合格。2016-2019 年聘为教师岗 8 级，考核合格。2020-2023 年聘为教师岗 7 级，考核合格。2019、2020、2021、2023 年参评副教授四次，均学院推荐最后一名，均未出学科组。2024 年 7 月聘岗，学院以考核虽然合格但不具有副教授职称，被降聘为教师岗 8 级。本人觉得，成果单薄且学术不端的教师在职称评审、聘岗中一路绿灯、升职升级严重损害了职称和聘岗的公信力，损害了教师的权益和工作的积极性，破坏了学院的风气，请求西安石油大学和相关上级机关能重视学术不端问题，认真、公正开展调查，维护高校教师群体职称评审的公正性，使真正有志于教育、学术

的教师能更多的感受到公正，能在职称评审这样重要的工作中感受到尊重。

西安石油大学在此次调查过程中，多名领导和老师在调查过程中与我沟通，但是更多的是推诿，少有人能真正面对问题。在此，我将沟通中与我交流的问题顺便也整理一下，也算是书面的公开的回复一下各位领导和老师。对于沟通中涉及的各位领导和老师，本人不具名，真实性本人负责。沟通内容很多，本人仅以领导或老师比较多涉及的问题以问答形式汇总为 11 个问题。举报学术不端重在证据材料，举报过程中我提交的材料和相关学术不端的涉事论文我都是在数据库上下载的，任何人只要能够访问 CNKI 和 EI 数据库都能够下载到。我也应相关领导要求对于论文中重复发表内容进行了黄色标注，作为附录一并公开。在此，我对于对我评职称及举报过程中表示关心和理解的各位专家教授、领导、同事、老师表示诚挚的感谢！

问题 1：你举报学术不端的目的是什么？是不是因为你副教授职称没有评审通过？

答 1：我举报王静怡和李小和学术不端确实和我副教授职称评审没有通过有关，这点我不回避。我和王静怡、李小和一起参评副教授，这两位老师都存在明显的学术不端。职称通过的名额是有限的，这两位老师不仅学术不端，且我知道王静怡老师在评职称前向学院评委老师提前打招呼、做工作，这种行为严重损害了其他参评教师的权益。学术不端的老师想方设法打招呼、做工作并顺利通过评审，符合条件的老师多次参评不能通过，所以我举报王静怡和李小和老师学术不端。另外一方面，我本人认为这两位老师学术不端根据西安石油大学职称评审文件理应一票否决，而这两位老师首次参评在被举报学术不端的情况下仍然一路绿灯，提职升级，我认为这个风气存在重大问题，所以我举报这两位老师学术不端也有遏制不良风气的目的。

问题 2：学校职称评审材料公示环节，你发现王静怡和李小和老师公示的文章存在学术不端的问题了没有？

答 2：我就是在公示环节发现这两位老师的文章存在学术不端的。

问题 3：那你为什么没有在公示环节举报这两位老师学术不端？

答 3：因为我和这两位老师是一个学院的，我发现他们两位文章存在学术不端，但同时我也发现他们的文章太薄弱刚刚压线，而我在文章、专利、讲课、获

奖、社会任职这些方面都明显优于这两位老师，我觉得学院推荐排序这两位老师应该不会对我造成影响，所以我没有在材料公示环节举报。但学院推荐排序后，我竟然排在这两位老师之后，我就向学院举报他们两位学术不端了。另外根据西安石油大学职称评审办法以及相关安排，职称评审全过程接受监督举报。另根据人力资源部规定，职称评审通过后，如存在学术不端弄虚作假依然可以随时举报。所以我在学院推荐排序结果公示后向学院递交书面异议以及按照学院要求向西安石油大学纪委提交举报材料，也是符合西安石油大学职称评审办法和相关工作安排的，也是有效的，也是被西安石油大学纪委所受理的。

问题 4：学院推荐排序将这两位老师排在你之前，这是学院评委投票的，跟这两位老师无关啊，你为什么要举报这两位老师呢？

答 4：学院推荐排序会上，对王静怡的评价，在会上在教授间就产生了争议。但有一位教授力挺，所以王静怡就排在前面了。另外，学院推荐排序会之前，王静怡就找参会的评委打招呼，这也是有悖于公平竞争的。我举报之后，计算机学院开展了所谓调查，两名校外专家认为是存在学术不端行为的，一名学院专家认为不好评价，只有一名学院专家明确认为不存在学术不端。王静怡学院推荐排序会前打招呼、搞活动，损害参评教师权益，所以不能认为我举报的这两位老师是躺枪的。

问题 5:你和王静怡是不是有个人恩怨，所以你才举报她？

答 5：我和王静怡在一个办公室，我和她入职前不认识。我和她是同事关系，没有任何个人恩怨。只是因为评职称，她违规做了好多工作，并且学术不端、一贯弄虚作假，损害了我的权益，且败坏了风气，所以我才举报她。

问题 6:2020 年有人举报王静怡国基金项目存在问题，那个人是不是你？

答 6:2020 年我也收到了那封举报信，那封举报信是校内群发的。那封信我也看了，写的还算是有理有据，但是缺少真凭实据。学院这次有教授问过我，我在此说明一下，2020 年的那封举报信不是我写的。不是严重损害我的权益，我没有那个精力去举报她，毕竟王静怡不管怎么样申请到国基金也算是学院的业绩。

问题 7：参评副教授的这几年，你觉得评审公平吗？

答 7：我觉得西安石油大学职称评审大面上还算是公平的，但确实也存在一

些问题，也存在明显不公平的情况。职称评审制度执行层面不落地，师德师风学术不端没有引起重视，一旦有些参评老师做工作，就很容易突破职称评审的一系列环节，监督流于形式，形同虚设。西安石油大学有很多专家教授，很多专家教授在专业上校内校外都有知名度。这些专家不仅业务精湛，人品还很好，但是这些专家可能并不会花很多的精力在人际交往。在目前学校的职称评审的环境中，职称评审就一个“评”字，这个“评”字就很定性，不打分无量化，就很玄，如果突破个别活动能力强的专家教授就会造成职称评审的严重不公正。就像 2023 年 11 月职称评审前李小和老师在我跟前就经常打击我这个屡次评职称不过的人，说评职称重点就一个“评”字，你职称大表不用花那么多精力。个别人的严重不公正、突破职称评审带来的损害是全面的，对学校、对教师工作的损害非常大。以我来说，2019 年参评副教授，当时学院 7 名教师参评副教授 6 名通过，我本人没有通过学科组。2019 年没有通过，我将我的材料打印出来找学校的德高望重的专家看了，当时有专家看了后说第一年没过就没过，材料没问题继续参评第二年肯定就过了。在石油大学还没有听说三年不过的，不要太在意。另一位专家见面的时候说，我之前就在数据库查过你的文章，应该是没有问题的。你也找找你们学院的领导。我当时没有当回事，想着学院领导肯定不会有问题。2020 年参评副教授，当时学院 2 名教师参评副教授 1 名通过，我本人依然没有通过学科组。这时候，有位领导好心提醒我，评职称一定要在会上有人替你说话。而我认为评职称就是评材料。2021 年参评副教授，学院就我 1 人参评，我本人依然没有通过学科组。2022 年心灰意冷未参评。2023 年参评副教授，学院 3 名教师参评副教授 2 名被我在院内推荐排序环节举报学术不端的教师顺利通过，不仅晋升职称，并且 2024 年 7 月还提级聘岗。此次举报之后，我才清楚的发现我被刻意针对了。

问题 8：希望你不要再举报了，举报也没有用，你觉得呢？

答 8：存在学术不端的老师一直提职升级，对符合条件的老师就是一种打击和排挤，难道不能在内部举报的情况下，借此机会开展调查、公正处理，进而扭转风气，给更多有志于教学、科研的教师以机会吗？！内部举报到现在，确实没有用，并且很可笑。我们三个人本来在一个办公室，我内部举报之后学院给李小和老师调换办公位了，给王静怡调换办公楼了。如果内部举报一直推诿、搪塞，我会考虑公开举报的。

问题 9：如果公开举报，你考虑过被举报的这两位老师可能会丧失教职、丢了饭碗吗？

答 9：根据西安石油大学职称评审办法，如果调查查实，这两位老师最多就是撤销以学术不端的成果获得的职称，并不会丢掉饭碗。我本人的意愿仅仅是得到公平公正的对待，能端好自己的饭碗，是评审的不公正使我不能端好自己的饭碗。这两位老师以学术不端才获得的薄弱压线成果，各方面做工作将我排挤掉不能获得职称晋升，我举报他们由内部举报到公开举报，也是不得已而为之。

问题 10：公开举报是你的权力，但你考虑过对西安石油大学可能造成的不良影响吗？你考虑过对你个人的影响吗？

答 10：公开举报，可能会对西安石油大学短时期内造成一定的不良影响。但是，如果学校能以此为契机，刮骨疗伤，我想会重新获得广大教师的认可，广大教师也能在职称评审这样的重要环节中获得更加公平公正的对待，学校的工作肯定能上一个更高的台阶。对我个人的影响，我想如果学校这次采取的不是解决问题，而是解决提出问题的人，我会坦然、理性面对。穿小鞋、打击报复这些不是不可能，但我更愿意相信西安石油大学的领导还是有格局的，学校正处于爬坡阶段，我们现在最需要做的是解决问题，而不是解决提出问题的人。职称评审中存在的问题，事关每一个教师的发展，事关学校的发展进步，如果必须有人指出存在的问题，我愿意做那个人。

问题 11：你的举报材料我看过了，写的很具体，但是你有没有想过如果你公开举报，这些材料其他老师看到了，以后谁还敢和你共事？

答 11：这一点我觉得领导想多了，西安石油大学有很多有才华的老师，不是人人都搞学术不端，也不是人人都搞一稿多发或是弄虚作假的。真正行的端坐的正的人是不会怕的，因为我所提供的材料都是 CNKI 或 EI 数据库下载的，任何人都可以下，任何受过科研培训的人都能下载、整理、标注，这是最基本的技能，石油大学应该所有的老师都具有这个能力的。我只想内部举报使问题得到解决，但没有办法，最终只能公开举报，我想绝大多数如果面临我这个情况的老师，都是能够理解甚至支持我的。

此致

敬礼

2024 年 9 月 10 日

附录：

1. 职称推荐排序异议书（2023 年 11 月 16 日向计算机学院领导提交）.....8-9

2. 对于两位老师学术不端行为的反映（2023 年 11 月 16 日向西安石油大学纪委和科技处提交）.....10-41

3. 补充说明对于计算机学院职称评审推荐排序的异议（2023 年 11 月 16 日向西安石油大学纪委提交）.....42-43

4. 对计算机学院调查不满，请求纪委复议（2023 年 11 月 22 日向西安石油大学纪委提交）..... 44-46

5. 陕西省教育厅申诉申请书（2023 年 12 月 12 日向陕西省教育厅教师工作部提交）.....47-204

6. 向陕西省科技厅举报王静怡基金申请、执行过程中的学术不端、弄虚作假行为（2023 年 12 月 12 日向陕西省科技厅机关纪委提交）.....205-268

7. 向国家自然科学基金委举报王静怡基金申请、执行过程中的学术不端、弄虚作假行为（2023 年 12 月 12 日向基金委科研诚信建设办公室提交）..269-333

8. 向计算机学院聘岗工作小组领导提交聘岗异议书（2024 年 7 月 9 日向计算机学院聘岗领导小组领导提交）.....334-397

附录1

尊敬的王院长：

2023 年 11 月 15 日计算机学院进行了 2023 年副教授职称评审推荐排序，排序结果是李小和（第一）、王静怡（第二）、本人（第三）。本人对排序结果有异议，主要有以下五点理由：

（1）科研论文李小和老师权威三类 1 篇，核心二类 2 篇；发明专利 2 项。王静怡老师权威二类 1 篇，权威三类 1 篇，核心一类 1 篇；发明专利 2 项。两位老师核心以上均为 3 篇，属于刚刚符合副教授职称评审条件。本人权威三类 3 篇，核心一类 1 篇，核心二类 2 篇，核心以上为 6 篇。发明专利 4 项。以上工作业绩均为排名第一和第二的两位老师的两倍，这样的排名显然不公平。

（2）李小和老师符合职称评审论文条件的论文的“sptially constrained Fuzzy c-means clustering algorithm for image segmentation”（权威三类）和“空间加权模糊 C 均值聚类图像分割算法”（核心二类）属于中英文一稿双投，属于学术不端行为，因此，李小和老师不符合论文要求“核心以上三篇，至少有一篇权威”的基本要求。王静怡老师符合职称评审论文条件的第一篇论文的“Research on the changing trend of farmland area in China and its driving factors from 1996 to 2016”（权威三类）和“近 20 年中国耕地数量变化趋势及其驱动因子分析”（核心一类）属于中英文一稿双投，属于学术不端行为，因此，王静怡老师不符合论文要求“核心以上三篇，至少有一篇权威”的基本要求。

（3）本人因在自动化学报发表文章，成为中国自动化学会会员；因在计算机学会会刊发表文章，成为中国计算机学会会员；并担任核心（CSCD）期刊《计算机应用研究》审稿专家。因发表文章引起青岛海尔集团研发部门注意，应邀为青岛海尔集团研发部门提供技术咨询服务。而推荐排名在本人之前的两位老师均没有在学会担任职务，也没有学术方面的社会服务，显然本人在学术方面要优于排名在本人之前的两位老师。

（4）本人主持完成教改项目 2 项，李小和老师和王静怡老师均没有主持完成的教改项目。

（5）教学比赛方面，本人两次在学院获得教学比赛第一名（一等奖），校教学质量优秀奖和校课堂教学创新大赛三等奖。王静怡老师获得校教学比赛三等和二等各一次。教学比赛方面本人成绩优于李小和老师，与王静怡老师相当。

本人在学院兢兢业业工作，重视同事友谊，一直与人为善，但无法回避客观存在的竞争关系。尤其是两位老师压线符合职称评审条件甚至于论文一稿多投而不符合职称评审条件的情况下，两位老师的推荐排序依然在本人之前，这样的结果本人从内心实在无法认同。综合以上五点理由，尤其是第一和第二点理由，本人认为学院此次职称评审推荐排序存在明显的不公正现象。请求学院对以上情况进行核实，公平公正的进行职称评审推荐排序。

此致

敬礼

2023 年 11 月 16 日

附录2

尊敬的学校科技处并纪委领导：

本人 2019 年、2020 年、2021 年参加了三次职称评审，院系推荐排序不公正本人并非第一次遇到。但是，没有像今年这样材料差距相当大且明显的不公正排序。2023 年 11 月 15 日计算机学院进行了 2023 年副教授职称评审推荐排序，排序结果是李小和（第一）、王静怡（第二）、本人（第三）。科研论文李小和老师权威三类 1 篇，核心二类 2 篇；发明专利 2 项。王静怡老师权威二类 1 篇，权威三类 1 篇，核心一类 1 篇；发明专利 2 项。两位老师核心以上均为 3 篇，属于刚刚符合副教授职称评审条件。本人权威三类 3 篇，核心一类 1 篇，核心二类 2 篇，核心以上为 6 篇。发明专利 4 项。以上工作业绩均为排名第一和第二的两位老师的两倍，这样的排名显不公平。本人对排序结果有异议，主要有以下两点理由：

（1）李小和老师符合职称评审论文条件的论文的“sptially constrained Fuzzy c-means clustering algorithm for image segmentation”（权威三类）和“空间加权模糊 C 均值聚类图像分割算法”（核心二类）以及“adaptive spatially weighted fuzzy c-means clustering for image segmentation”（一般期刊）三篇属于结构、内容、结论、实验等高度重复。

“空间加权模糊 C 均值聚类图像分割算法”发表于 2017 年，“sptially constrained Fuzzy c-means clustering algorithm for image segmentation”发表于 2019 年，“adaptive spatially weighted fuzzy c-means clustering for image segmentation”发表于 2022 年，三篇文章都是研究模糊 C 均值算法用于图像分割。2017 年的论文就已经指出将图像的像素空间关系加到模糊 C 均值算法中可以提高图像分割鲁棒性和准确度。2019 年的论文与 2017 的论文相比就额外加入了一个距离加权因子，2022 年的论文与 2019 年的论文相比就额外加了一个中值滤波算子。实际上，对模糊 C 均值聚类算法在图像分割应用中加入像素空间约束关系（如各种距离因子、中值算子等等）在 2010 年前后大家都有共识也有很多论文发表，这三篇文章之间的工作变化很小，加距离因子加权或是加中值算子都是常规操作，李小和老师如果要继续发表这样的工作理应在一篇文章中在同样的实验条件、参数设置下进行对比分析。但李小和老师将这样常规的已经形成共识的小的微调操作拆分成三篇文章发表，且三篇文章引言、FCM 算法描述、结构、实验、结论

存在高度雷同。李小和老师的这三篇文章存在中英文三次重复发表，属于学术不端行为，因此，李小和老师不符合论文要求“核心以上三篇，至少有一篇权威”的基本要求。

（2）王静怡老师符合职称评审论文条件的第一篇论文的“Research on the changing trend of farmland area in China and its driving factors from 1996 to 2016”（权威三类）和“近 20 年中国耕地数量变化趋势及其驱动因子分析”（核心一类）属于中英文一稿双发，属于学术不端行为，因此，王静怡老师不符合论文要求“核心以上三篇，至少有一篇权威”的基本要求。

“Research on the changing trend of farmland area in China and its driving factors from 1996 to 2016”（权威三类）于 2018 年发表在 MTMCE2018 会议上，后该文又以中文形式在引言部分加入了三篇参考文献发表在《中国农业资源与区划》上。除去新加的三篇参考文献在引言部分两篇文章存在一点细微差异外，两篇文章数据、图、表、实验方法、讨论与结论完全一样，属于典型的一稿双发表。

另根据〔2023〕143 号关于印发《西安石油大学职称评审暂行实施办法》第二十一条 申请人提供的各类成果应当与其申报专业相同或相近，非本专业及非相近专业成果原则上不予认定。王静怡老师的符合职称评审论文条件的三篇论文

“comparison on quantitative inversion of characteristicion in salinized soils with heperspectral based on support vector regression and partial least squares regression”“research on the changing trend of farmland area in China and its driving factors from 1996 to 2016”“近 20 年中国耕地数量变化趋势及其驱动因子分析”都属于土地方向，而王静怡老师本、硕、博均为通信方向，这三篇文章的研究方向并不是王静怡老师的研究方向，而是这三篇文章第二作者任职于陕西土地集团的李晓明（王静怡丈夫）的研究方向。王静怡老师不管是在计算机学科还是在通信学科，这三篇文章都不是王静怡老师的研究方向。因此，根据〔2023〕143 号关于印发《西安石油大学职称评审暂行实施办法》第二十一条这三篇文章原则上应不予认定。除去这三篇文章，王静怡老师自己的研究方向上只发表了 2 篇一般期刊论文。

综合以上两点，两位老师均存在学术不端问题，请求科技处及时进行核查处理，妥善解决问题。

随信提交两位老师重复发表的相关论文 5 篇一式两份，并对内容重复部分以黄色进行标注。

此致

敬礼

2023 年 11 月 16 日

DOI: 10.3969/j.issn.1673-064X.2017.05.017 中图分类号: TP391.4
文章编号: 1673-064X(2017)05-0102-05 文献标识码: A

空间加权模糊 C 均值聚类图像分割算法

李小和,屈 展,王魁生,卢胜男

(西安石油大学 计算机学院,陕西 西安 710065)

摘要: 为了提高模糊 C 均值聚类(FCM)算法用于图像分割时对噪声的鲁棒性,在 FCM 算法中引入了图像像素的邻域约束,提出一种空间加权模糊 C 均值聚类图像分割算法。首先根据邻域像素的模糊隶属度函数值,定义像素分类标记的局部先验概率,然后将该局部先验概率融入标准的 FCM 算法的目标函数中,从而提出一种空间加权模糊 C 均值聚类图像分割算法。仿真实验通过合成图像和真实图像验证了该算法的有效性和鲁棒性。

关键词: 图像分割算法; 模糊 C 均值聚类; 空间加权

Spatial Weighted Fuzzy C-means Clustering Algorithm for Image Segmentation

LI Xiaohe,QU Zhan,WANG Kuisheng,LU Shengnan

(College of Computer Science,Xi'an Shiyou University,Xi'an 710065,Shaanxi,China)

Abstract: Fuzzy C-means clustering (FCM) is an unsupervised clustering method,which is widely used in image segmentation. A spatial weighted fuzzy C-means clustering algorithm for image segmentation is proposed in order to overcome the sensitivity of the standard FCM algorithm to noises and other imaging artifacts. Firstly,the local prior probabilities of pixel classification marks are defined are defined according to the fuzzy membership function value of neighborhood pixels,and then those local prior probabilities are incorporated into the objective function of the standard FCM. Simulation experiments show the effectiveness and robustness of the proposed algorithm through both synthetic and real images.

Key words: image segmentation algorithm; fuzzy C-means clustering; spatial weighting

李小和,屈展,王魁生,等. 空间加权模糊 C 均值聚类图像分割算法[J]. 西安石油大学学报(自然科学版),2017,32(5):102-106.

LI Xiaohe,QU Zhan,WANG Kuisheng,et al. Spatial weighted fuzzy C-means clustering algorithm for image segmentation[J]. Journal of Xi'an Shiyou University(Natural Science Edition),2017,32(5):102-106.

收稿日期: 2016-09-01

基金项目: 国家自然科学基金项目(51674200);西安石油大学青年科技创新基金项目(2013BS021)

作者简介: 李小和(1974-),男,博士,讲师,研究方向: 图像处理与模式识别。E-mail: lixh@xsyu.edu.cn

(C)1994-2022 China Academic Journal Electronic Publishing House. All rights reserved. http://www.cnki.net

引 言

图像分割是指根据图像的灰度、颜色或者纹理等特征将图像划分成若干个互不相交的区域,使得这些特征在每个区域内表现出一致性或相似性。图像分割是从图像处理到图像分析的关键步骤,也是图像理解的前提和基础[1]。模糊 C 均值聚类[2](Fuzzy C-means,FCM)算法是一种无监督的聚类方法,近年来被广泛地应用于图像分割领域[3-10]。然而标准的 FCM 算法用于图像分割时没有考虑像素的空间位置关系,因此 FCM 算法对噪声特别敏感。

为了进一步提高 FCM 算法用于图像分割时对噪声的鲁棒性,Ahmed 等[5]通过在 FCM 的目标函数中对像素颜色特征引入邻域约束提出了 FCM_S 算法,但 FCM_S 算法在每一步迭代时都需对邻域像素的颜色特征进行一系列计算,因此时间复杂度较大。Chen 等[6]用邻域像素颜色特征的均值或中值取代邻域像素的颜色特征从而提出了 FSM_S1 和 FSM_S2 算法,由于邻域信息的均值或中值可在迭代之前计算,因此,FSM_S1 和 FSM_S2 算法在保持 FSM_S 算法优越性的同时,降低了 FSM_S 算法的复杂度。Pham[7]通过在 FCM 的目标函数中对模糊隶属度函数值引入邻域约束项提出了 RFCM 图像分割算法。Krindis 和 Chatzis 通过在 FCM 目标函数中引入局部邻域因子,提出了 FLICM 算法[8]。Feng 等[9-10]借助马尔可夫随机场(MRF)在 FCM 算法中引入邻域约束,提出了 GFCM 算法。GFCM 算法在每一步迭代过程中,需要通过对像素的模糊隶属度函数值去模糊化得到一个临时分割场,然后运用 MRF 理论计算出像素属于每一类的局部条件概率,最后将该局部条件概率引入到 FCM 算法的目标函数。

为了进一步提高 FCM 图像分割算法对噪声的鲁棒性,本文首先根据邻域像素的模糊隶属度函数值定义像素分类标记的局部先验概率,然后将该局部先验概率融入到标准 FCM 算法的目标函数,提出一种空间加权模糊 C 均值聚类(SWFCM)图像分割算法。

1 模糊 C 均值聚类

给定样本集 $X=\{\boldsymbol{x}_i \mid 1\leqslant i\leqslant N,\text{且}\ \boldsymbol{x}_i\in \mathbf{R}^d\}$,$d$ 为样本空间维数。为了将这 N 个样本划分为 C 类,FCM 算法通过对目标函数迭代优化实现集合划分。FCM 算法[2]的目标函数定义为

$$J_{\mathrm{FCM}}(\boldsymbol{U},\boldsymbol{V})=\sum_{k=1}^{C}\sum_{i=1}^{N}\mu_{ik}^{m}\|\boldsymbol{x}_i-\boldsymbol{v}_k\|^2。\tag{1}$$

式中:$\boldsymbol{U}=[\mu_{ik}]$为模糊隶属度函数值矩阵,$\mu_{ik}$ 为第 i 个样本属于第 k 类的模糊隶属度函数值;$\boldsymbol{V}=[\boldsymbol{v}_1,\boldsymbol{v}_2,\cdots,\boldsymbol{v}_C]$ 为聚类中心矩阵,$\boldsymbol{v}_k$ 为第 k 个类的中心;m 为模糊加权指数,控制聚类结果模糊程度,$m\in[1,+\infty)$。其中 $\boldsymbol{U}$ 满足约束条件

$$\boldsymbol{U}\in\{\mu_{ik}\in[0,1]\mid\sum_{k=1}^{C}\mu_{ik}=1,\forall i,0<\sum_{i=1}^{N}\mu_{ik}<N\forall k\}。\tag{2}$$

FCM 算法的目标函数 J_{FCM} 是样本到聚类中心的距离平方的加权累积和,它反映了在某种差异性定义下的类内紧致一致度,J_{FCM} 越小,聚类的结果越紧致。采用 Lagrange 乘子法可求得在约束条件下使目标函数 J_{FCM} 取局部最小值的必要条件为:

$$\boldsymbol{v}_k=\frac{\sum_{i=1}^{N}\mu_{ik}^{m}\boldsymbol{x}_i}{\sum_{i=1}^{N}\mu_{ik}^{m}},k=1,2,\cdots,C;\tag{3}$$

$$\mu_{ik}=\frac{\|\boldsymbol{x}_i-\boldsymbol{v}_k\|^{-2/(m-1)}}{\sum_{j=1}^{C}\|\boldsymbol{x}_i-\boldsymbol{v}_j\|^{-2/(m-1)}};$$

$$k=1,2,\cdots,C;\ i=1,2,\cdots,N。\tag{4}$$

FCM 算法的具体步骤为:

① 确定聚类数目 C、参数 m,以及迭代停止阈值 ε;

② 采用随机的方法初始化模糊隶属度函数值;

③ 根据式(3),用当前模糊隶属度函数值更新聚类中心;

④ 根据式(4),用当前聚类中心更新模糊隶属度函数值;

⑤ 重复第③到④步,直到满足终止迭代条件:

$$\|\boldsymbol{v}_{\mathrm{new}}-\boldsymbol{v}_{\mathrm{old}}\|<\varepsilon,\tag{5}$$

式中,$\boldsymbol{v}_{\mathrm{new}}$ 为当前迭代的聚类中心,$\boldsymbol{v}_{\mathrm{old}}$ 为前一步迭代的聚类中心。

通过上述步骤,可得到各类的聚类中心,以及各个样本属于各类的模糊隶属度函数值,从而完成模糊聚类划分。若采用 FCM 算法进行图像分割,则这里的样本指的是图像像素的灰度、颜色或者纹理等特征。

2 空间加权模糊 C 均值聚类

在进行图像分割时,为了得到连通区域,通常希望相邻的像素尽可能分割到相同的区域,因此需要在 FCM 算法中引入邻域约束。根据邻域像素的模糊

(C)1994-2022 China Academic Journal Electronic Publishing House. All rights reserved. http://www.cnki.net

隶属度函数值,定义第 i 个像素属于第 k 类的局部先验概率

$$\pi_{ik}=\frac{\sum_{r\in N_i}u_{rk}^{b}}{\sum_{k=1}^{C}\sum_{r\in N_i}u_{rk}^{b}},\tag{6}$$

式中,N_i 为第 i 个像素的邻域,参数 b 为惩罚因子。由式(6)可知,对于任意的 $r\in N_i$,μ_{ik} 越大,π_{ik} 越大。也就是说,图像的第 i 个像素的邻域像素属于第 k 类的模糊隶属度函数值越大时,π_{ik} 越大。

本文将定义的分类标记的局部先验概率 π_{ik} 融入到标准 FCM 的目标函数中,提出了 SWFCM 图像分割算法。SWFCM 算法的目标函数定义为

$$J_{\mathrm{SWFCM}}=\sum_{k=1}^{C}\sum_{i=1}^{N}(1-\pi_{ik})u_{ik}^{m}\|\boldsymbol{x}_i-\boldsymbol{v}_k\|^2。\tag{7}$$

由式(7)和(6)可知,第 i 个像素到第 k 类中心的距离越小,且第 i 个像素及其邻域像素属于第 k 类的模糊隶属度函数值越大时,J_{SWFCM} 越小。因此,最小化目标函数 J_{SWFCM},可使相邻像素尽可能划分到相同的类。

类似标准 FCM 算法,采用 Lagrange 乘子法可求得在约束条件式(2)下使目标函数 J_{SWFCM} 取局部最小的必要条件为:

$$\boldsymbol{v}_k=\frac{\sum_{i=1}^{N}u_{ik}^{m}(1-\pi_{ik})\boldsymbol{x}_i}{\sum_{i=1}^{N}u_{ik}^{m}(1-\pi_{ik})};\tag{8}$$

$$u_{ik}=\frac{[(1-\pi_{ik})\|\boldsymbol{x}_i-\boldsymbol{v}_k\|^2]^{-1/(m-1)}}{\sum_{k=1}^{C}[(1-\pi_{ik})\|\boldsymbol{x}_i-\boldsymbol{v}_k\|^2]^{-1/(m-1)}}。\tag{9}$$

SWFCM 算法的具体步骤为:

① 确定聚类数目 C、参数 m 以及迭代停止阈值 ε;

② 采用随机的方法初始化模糊隶属度函数值;

③ 根据式(6),计算局部概率 π_{ik};

④ 根据式(8),用当前模糊隶属度函数值更新聚类中心;

⑤ 根据式(9),用当前聚类中心更新模糊隶属度函数值;

⑥ 重复第③—⑤步,直到满足终止迭代条件 $\|\boldsymbol{v}_{\mathrm{new}}-\boldsymbol{v}_{\mathrm{old}}\|<\varepsilon$。

根据上述步骤对图像像素进行聚类后,可按照一定的规则对像素的模糊聚类结果进行去模糊化,从而将其转化为确定性分类,完成图像分割。一种比较直接的去模糊化方法是将各个像素划分至其最大模糊隶属度函数值所对应的类。若

$$l_i=\arg\max_{1\leqslant k\leqslant C}\mu_{ik},\tag{10}$$

则将第 i 像素划分到第 l_i 类。

3　实验结果

为了验证本文提出的 SWFCM 图像分割算法的有效性和鲁棒性,选择人工合成图像和真实图像作为测试图像,并将 SWFCM 算法的分割结果与 FCM、FCM_S1、RFCM、FLICM 和 GFCM 算法的分割结果进行对比。选择参数 $\varepsilon=0.0001$,$b=1.6$。由于 FCM 算法在 $m=2$ 时,能够得到比较理想的聚类结果,因此选择参数 $m=2$。邻域系统为二阶邻域系统。

本文首先通过人工合成图像验证 SWFCM 算法的有效性和鲁棒性。合成图像的大小为 96×96 像素,由灰度值分别为 50、100、150 和 200 的 4 类像素组成,然后给该合成图像分别加上高斯噪声、椒盐噪声,以及高斯噪声和椒盐噪声的混合噪声。图 1(a)

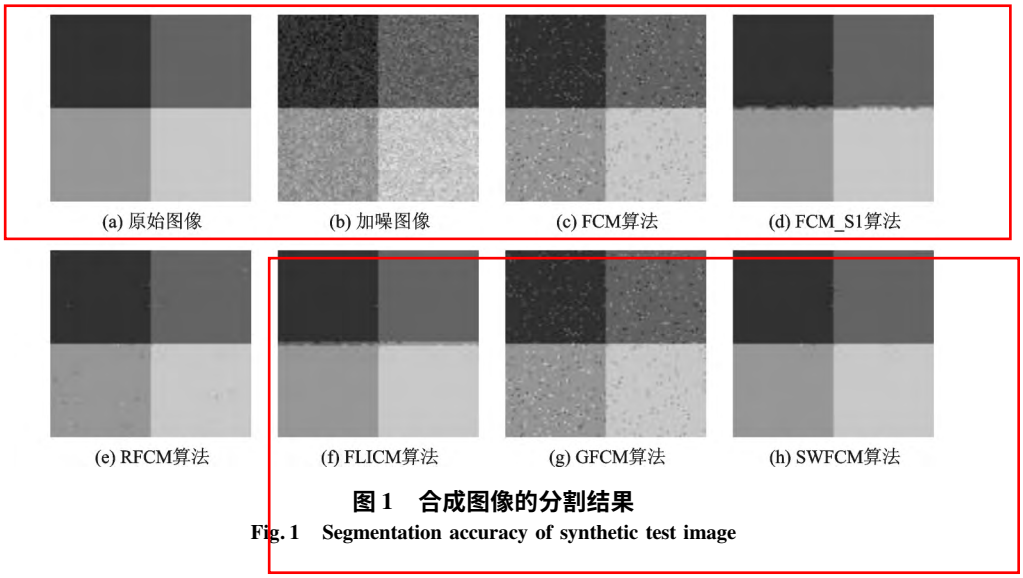


图 1　合成图像的分割结果

Fig. 1　Segmentation accuracy of synthetic test image

(C)1994-2022 China Academic Journal Electronic Publishing House. All rights reserved.　http://www.cnki.net

为原始合成图像，图 1(b) 为加上高斯噪声后的图像。图 1(c) 到(h) 分别为 FCM、FCM_S1、RFCM、FLICM、GFCM 和 SWFCM 算法对图 1(b) 的分割结果。表 1 为 6 种算法在不同噪声下的分割准确率(*SA*) 。这里 *SA* 指的是正确分割的像素数除以图像的总像素数[6] 。参数 $C=4$。由图 1 和表 1 可以发现，FCM、FCM_S1、RFCM、FLICM 和 GFCM 算法在不同程度上受到噪声的影响，分割准确率相对较低，而本文提出的 SWFCM 算法分割准确率最高，能够得到比较理想的分割结果。

表 1 合成图像的分割准确率

Tab. 1 segmentation accuracy on synthetic test image

噪声类型	分割准确率/%					
	FCM	FCM_S1	RFCM	FLICM	GFCM	SWFCM
高斯噪声	94.61	98.69	99.74	98.13	95.29	99.92
椒盐噪声	95.95	93.16	96.39	91.96	96.39	99.80
混合噪声	90.08	92.62	95.29	89.49	90.72	99.35

图 2 为标准测试图像 eight 加上高斯噪声与椒盐噪声的混合噪声后的分割结果。图 2(a) 为 eight 标准测试图像，大小为 308 × 242 像素。图 2(b) 为加上高斯噪声和椒盐噪声后的 eight 图像。图 2(c) 到(h) 分别为 FCM、FCM_S1、RFCM、FLICM、GFCM 和 SWFCM 算法的分割结果。选择参数 $C=2$。通过图 2 可以发现，FCM、FCM_S1、RFCM、FLICM 和 GFCM 算法在一定程度上受到噪声的影响，分割结果相对较差，分割结果包含较多的孤立像素点，本文提出的 SWFCM 算法能够得到比较满意的分割结果。

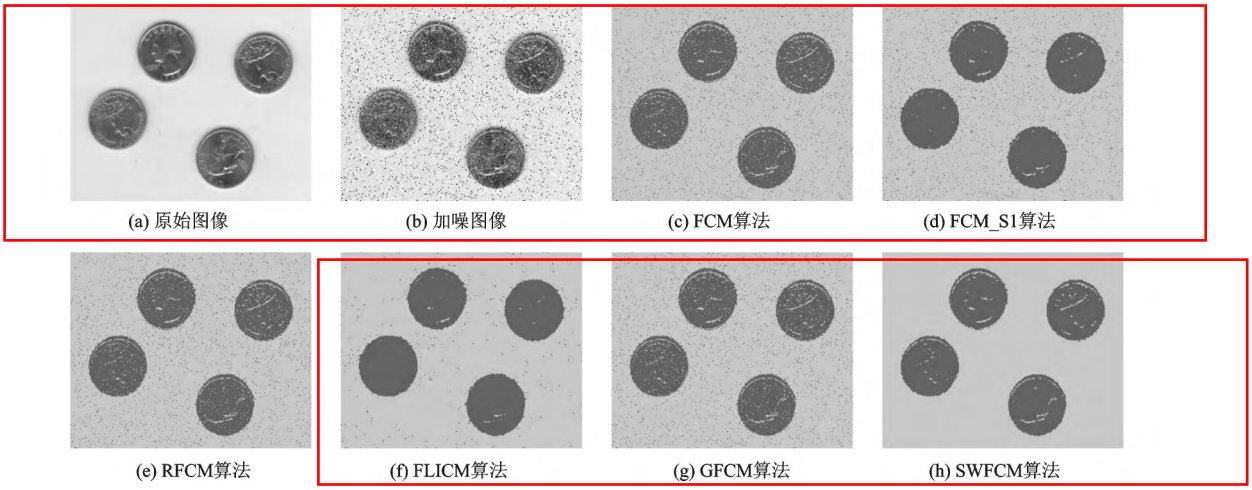


图 2 eight 标准图像加噪声后的分割结果

Fig. 2 Segmentation results of a real image corrupted by noise

4 结 论

标准的 FCM 算法用于图像分割时，由于没考虑相邻像素的关系，对噪声特别敏感，易产生孤立的像素点。为了提高 FCM 图像分割算法对噪声的鲁棒性，本文首先定义了像素分类标记的局部先验概率，然后将该概率融入到 FCM 算法的目标函数中，提出了空间加权模糊聚类图像分割算法。

本文在定义局部先验概率时，没有考虑邻域像素的距离的影响。在式(6) 中引入像素的距离信息，是下一步的研究方向。

参 考 文 献:

[1] ZHANG H，FRITTS J E，GOLDMAN S A. Image segmentation evaluation: a survey of unsupervised methods [J] . Computer Vision and Image Understanding，2008，110(2) : 180-260.

[2] BEZDEK J C. Pattern recognition with fuzzy objective function algorithms [M] . New York: Plenum Press，1981.

[3] LI XH，ZHANG TY，QU Z. Image segmentation using fuzzy clustering with spatial constraints based on Markov random field via Bayesian theory [J] . IEICE Transactions on Fundamentals of Electronics，Communications and Computer Sciences，2008，E91A(3) : 723-729.

[4] LIU G Y，ZHANG Y，WANG A M. Incorporating adaptive

(C)1994-2022 China Academic Journal Electronic Publishing House. All rights reserved. http://www.cnki.net

local information into fuzzy clustering for image segmentation [J]. IEEE Trans. Image Process, 2015, 24(11): 3990-4000.

[5] AHMED M N, YAMANY S M, MOHAMED N, et al. A modified fuzzy C-means algorithm for bias field estimation and segmentation of MRI data [J]. IEEE Transactions on Medical Imaging, 2002, 21(3): 193-199.

[6] CHEN S C, ZHANG D Q. Robust image segmentation using FCM with spatial constraints based on new kernel-induced distance measure [J]. IEEE Transactions on Systems, Man, and Cybernetics: Part B, 2004, 34(4): 1907-1916.

[7] PHAM D L. Spatial models for fuzzy clustering [J]. Computer Vision and Image Understanding, 2001, 84(2): 285-297.

[8] KRINIDIS S, CHATZIS V. A robust fuzzy local information c-means clustering algorithm [J]. IEEE Trans Image Process, 2010, 19(5): 1328-1337.

[9] FENG Y Q, CHEN W F. Brain MR image segmentation using fuzzy clustering with spatial constraints based on Markov random field theory [C]. 2nd International Conference on Information and Computing Science, 2004: 188-195.

[10] 冯衍秋,陈武凡,梁斌,等. 基于 Gibbs 随机场与模糊 C 均值聚类的图像分割新算法 [J]. 电子学报, 2004, 32(4): 645-647.
FENG Yanqiu, CHEN Wufan, LIANG Bin, et al. A new algorithm for image segmentation based on Gibbs random field and fuzzy C-means cluatering [J]. Acta Electronica Sinica, 2004, 32(4): 645-647.

责任编辑: 张新宝

(上接第 101 页)

[8] 高炜欣,胡玉衡,穆向阳,等. 埋弧焊 X 射线焊缝图像缺陷分割检测技术 [J]. 仪器仪表学报, 2011, 32(6): 1215-1224.
GAO Weixin, HU Yuheng, MU Xiangyang, et al. Real-time detection and segmentation of submerged-arc welding defects in X-ray radiography images [J]. Chinese Journal of Scientific Instrument, 2011, 32(6): 1215-1224.

[9] 马婧华,汤宝平,宋涛. 基于自适应本征维数估计流形学习的相空间重构降噪方法 [J]. 振动与冲击, 2015, 34(11): 29-34.
MA Jinghua, TANG Baoping, SONG Tao. Phase space reconstruction method for vibration signal's noise reduction based on adaptive intrinsic dimension estimation manifold learning [J]. Journal of Vibration and Shock, 2015, 34(11): 29-34.

[10] 蒋全胜,贾民平,胡建中,等. 基于拉普拉斯特征映射的故障模式识别方法 [J]. 系统仿真学报, 2008, 20(20): 5710-5713.
JIANG Quansheng, JIA Minping, HU Jianzhong, et al. Method of fault pattern recognition based on laplacian eigenmaps [J]. Journal of System Simulation, 2008, 20(20): 5710-5713.

[11] 王旭辉,舒平,曹立. 基于 ROC 曲线寻优的支持向量机性能研究 [J]. 计算机科学, 2010, 37(8): 240-242.
WANG Xuhui, SHU Ping, CAO Li. Performance evaluation with optimization strategy for support vector machine based on ROC curve [J]. Computer Science, 2010, 37(8): 240-242.

[12] 王欣,高炜欣,武晓朦,等. 基于模糊模式识别的焊缝缺陷图像检测 [J]. 西安石油大学学报(自然科学版), 2016, 31(4): 115-121.
WANG Xin, GAO Weixin, WU Xiaomeng, et al. Image detecting of weld defect based on fuzzy pattern recognition [J]. Journal of Xi'an Shiyou University(Natural Science Edition), 2016, 31(4): 115-121.

[13] 王宏涛,孙剑伟. 基于 BP 神经网络和 SVM 的分类方法研究 [J]. 软件, 2015, 36(11): 96-99.
WANG Hongtao, SUN Jianwei. Research on the classification method based on BP neural network and SVM [J]. Computer Engineering & Software, 2015, 36(11): 96-99.

责任编辑: 董　瑾

(C)1994-2022 China Academic Journal Electronic Publishing House. All rights reserved.　http://www.cnki.net

Journal of Physics: Conference Series

PAPER • **OPEN ACCESS**

Spatially Constrained Fuzzy c-Means Clustering Algorithm for Image Segmentation

To cite this article: Xiaohe Li *et al* 2019 *J. Phys.: Conf. Ser.* **1237** 032024

View the article online for updates and enhancements.

You may also like

- Breast density quantification with cone-beam CT: a post-mortem study
Travis Johnson, Huanjun Ding, Huy Q Le et al.
- Simulation studies of mechanical stresses in REBaCuO superconducting ring bulks with infinite and finite height reinforced by metal ring during field-cooled magnetization
H Fujishiro, M D Ainslie, K Takahashi et al.
- An edge-sensitive simplification method for scanned point clouds
Shifan Liu, Jin Liang, Maodong Ren et al.

This content was downloaded from IP address 219.144.164.16 on 16/11/2023 at 00:13

IOP Conf. Series: Journal of Physics: Conf. Series **1237** (2019) 032024 doi:10.1088/1742-6596/1237/3/032024

Spatially Constrained Fuzzy c-Means Clustering Algorithm for Image Segmentation

Xiaohe Li[1, 2], Zhan Qu[2], and Xiaojing Yang[1]

[1]College of Computer Science, Xi'an Shiyou University, Xi'an 710065, China

[2]The Key Laboratory of Well Stability and Fluid & Rock Mechanics in Oil and Gas Reservoir of Shaanxi Province, Xi'an Shiyou University, Xi'an 710065, China

E-mail: lixh@xsyu.edu.cn; zhqu@xsyu.edu.cn; xjyang@xsyu.edu.cn

Abstract. The fuzzy c-means (FCM) clustering is an unsupervised clustering method, which has been widely used in image segmentation. In this paper, a spatially constrained fuzzy c-means clustering algorithm for image segmentation is proposed to overcome the sensitivity of the FCM clustering algorithm to noises and other imaging artifacts. Firstly, the local prior probabilities of pixel classification are defined according to the fuzzy membership function values of neighbouring pixels, and then those local prior probabilities are incorporated into the objective function of the standard FCM. Thus, the local spatial information embedded in the image is incorporated into the FCM algorithm. Experimental results on the synthetic and real images are given to demonstrate the robustness and validity of the proposed algorithm.

1. Introduction

As an important part of image processing, image segmentation is considered to be one of the key and most difficult techniques in computer vision [1]. The goal of image segmentation is to divide an image into several disjoint regions, which are homogeneous with respect to some characteristics such as gray level, color, texture, etc. Fuzzy c-means (FCM) clustering method [2] has been widely used in image segmentation and its success chiefly attributes to the introduction of fuzziness for the belongingness of each image pixel. This allows the clustering procedure to retain more original image information than the crisp or hard segmentation methods. However, the standard FCM clustering method is sensitive to noise and other imaging artifacts, since it does not consider any spatial information in an image.

To solve this problem, a variety of studies incorporating local spatial information into the original FCM clustering method have been proposed [3-10]. In some methods, the spatial context was embedded in the objective function of FCM clustering. Pham [6] applied a spatial penalty on the membership functions. The penalty term leads to an iterative algorithm that allows the estimation of spatially smooth membership functions. A FCM_S algorithm, proposed by Ahmed [7], modified the FCM objective function to compensate the intensity inhomogeneity and allow the labeling of a pixel to be influenced by the labels in its immediate neighborhood. However, this method is very time-consuming to compute the neighborhood terms in each iteration step. To address this problem, Chen and Zhang [8] applied the mean-filter image and the median-filter image to simplify the neighborhood term of FCM_S, and proposed the FCM_S1 and FCM_S2, respectively. The extra mean-filtered image and median-filtered image introduced by these two algorithms can be computed in advance, so the computational complexity can be considerably reduced. Cai [9] proposed a generalized fuzzy c-means algorithm for fast and robust image segmentation. Krindis and Chatzis [10] proposed a fuzzy local

Content from this work may be used under the terms of the Creative Commons Attribution 3.0 licence. Any further distribution of this work must maintain attribution to the author(s) and the title of the work, journal citation and DOI.
Published under licence by IOP Publishing Ltd

information c-means (FLICM) clustering algorithm. In this algorithm, a fuzzy local factor was introduced for solving the problem of noise sensitive and image detail lost. However, the objective function of FLICM is formulated without setting any parameter that controls the effect of this factor. Feng and Chen [11] used the spatial context constraint on the objective function of FCM, which is referred as GFCM. The spatial constraint based on MRF theory is defined as refusable level. The main drawback of the GFCM algorithm is that the hard maximum membership classification is necessary to compute the prior probabilities during the iteration.

Inspired by the ideas of GFCM algorithm, a novel spatially constrained fuzzy c-means (SCFCM) for image segmentation is proposed in this paper. At first, the local prior probabilities of pixel classification are defined according to the fuzzy membership function values of neighboring pixels, then those local prior probabilities are incorporated into the objective function of the standard FCM. Thus, the local spatial information embedded in the image is incorporated into the segmentation process. Therefore, the proposed method can effectively reduce the impact of noises and other imaging artifacts.

The rest of paper is organized as follows. Section 2 reviews the FCM clustering method briefly. The new image segmentation method is presented in Section 3. The experimental comparisons are presented in Section 4. Finally, conclusions are given in Section 5.

2. Fuzzy c-means clustering

The FCM clustering was first proposed by Dunn [12] and further improved by Bezdek [2]. Mathematically, the standard FCM clustering partitions an image X into c clusters by minimizing the objective function

$$J_{\mathrm{FCM}} = \sum_{k=1}^{c}\sum_{i=1}^{n} u_{ik}^{m} \left\| x_i - v_k \right\|^2 \tag{1}$$

where $X = \{x_1, x_2, \ldots, x_n\}$ denotes an image with n pixels, v_k is the prototype of the center of cluster k and u_{ik} is the fuzzy membership function of the pixel i belonging to the cluster k. The fuzzy partition matrix $U = [u_{ik}]$ satisfies

$$U = \left\{ u_{ik} \in [0,1] \middle| \sum_{k=1}^{c} u_{ik} = 1, \forall i, 0 < \sum_{i=1}^{n} u_{ik} < n, \forall k \right\} \tag{2}$$

The parameter m control the fuzziness of the membership function.

Using the Lagrange multiplier method, the objective function J_{FCM} can be minimized iteratively. the update equations of membership functions u_{ik} and the cluster centers v_k are given as follows:

$$u_{ik} = \frac{\left(\left\| x_i - v_k \right\|\right)^{-2/(m-1)}}{\sum_{j=1}^{c}\left(\left\| x_i - v_j \right\|\right)^{-2/(m-1)}} \tag{3}$$

$$v_k = \frac{\sum_{i=1}^{n} u_{ik}^{m} x_i}{\sum_{i=1}^{n} u_{ik}^{m}} \tag{4}$$

Apparently, the FCM algorithm does not use any spatial information in an image. i.e., the segmentation process is solely based on the histogram of image. Therefore, the FCM clustering method is sensitive to noises and imaging artifacts.

3. Proposed Algorithm

In this work, the local prior probabilities of each pixel are defined. Then those probabilities are incorporated into the FCM objective function, and a new spatially constrained fuzzy c-means (SCFCM) algorithm for image segmentation is presented.

3.1 Definition of the local prior probability

Given the membership function u_{ik} of FCM algorithm, the local prior probability is defined as

$$\pi_{ik} = \frac{\left(\sum_{j\in N_i} w_j u_{jk}\right)^b}{\sum_{k=1}^{c}\left(\sum_{j\in N_i} w_j u_{jk}\right)^b} \tag{5}$$

Where b is the constant strength factor, w_j is a weight coefficient depending on their distance from the central pixel. The influence of the neighbouring pixels is controlled by w_j, and it can be obtained by

$$w_j = \exp\left(-\frac{L_{ij}^2}{2d^2}\right) \tag{6}$$

Where L_{ij} is the spatial Euclidian distance between pixels i and j, and $d = (s-1)/4$, s is the size of the neighborhood window. The strength of w_j decreases as the distance between pixel i and j increases.

Comparing to GFCM algorithm, those prior probabilities can be computed directly from the membership functions of neighborhood pixels, and the hard maximum membership segmentation is unnecessary during the iteration. Furthermore, the spatial Euclidian distance between pixels has be incorporated into those prior probabilities. Therefore, the local prior probability defined in this paper has better characteristics, compared with GFCM algorithm.

3.2 SCFCM algorithm

By incorporating the local prior probability π_{ik} into the standard FCM objective function, the objective function of the proposed algorithm is formulated as

$$J_{\text{SCFCM}} = \sum_{k=1}^{c}\sum_{i=1}^{n}(1-\pi_{ik})u_{ik}^m \|x_i - v_k\|^2 \tag{7}$$

Similar to the standard FCM clustering method, the J_{SCFCM} can be minimized iteratively. The membership functions u_{ik} and the cluster centers v_k are updated as follows:

$$v_k = \frac{\sum_{i=1}^{n} u_{ik}^m (1-\pi_{ik}) x_i}{\sum_{i=1}^{n} u_{ik}^m (1-\pi_{ik})} \tag{8}$$

$$u_{ik} = \frac{\left[(1-\pi_{ik})\|x_i - v_k\|^2\right]^{-1/m}}{\sum_{k=1}^{c}\left[(1-\pi_{ik})\|x_i - v_k\|^2\right]^{-1/m}} \tag{9}$$

Thus, the SCFCM algorithm is given as follows:

Step 1: Set the parameter m, and the number of the clusters c.

Step 2: Initialize the membership functions randomly.

Step 3: Calculate the local prior probabilities using (5)-(6).

Step 4: Update the cluster center v_k using (8).

Step 5: Update the membership functions u_{ik} using (9).

Step 6: In case of convergence, exit; Otherwise, go to Step 3.

4. Experimental Results

To demonstrate the robustness and validity of the SCFCM method, we compare the performance of our proposed SCFCM algorithm with the FCM, FCM_S1, FLICM and GFCM algorithms. The experiment will be done on the synthetic and real images corrupted by noises respectively. We set the fuzzy parameter $m=2$, and $b=1.8$ for the proposed algorithm. The size of neighbourhood window is 3×3.

In the first experiment, a synthetic test image with 128×128 pixels, as shown in Fig. 1(a), is used to compare the performance of the proposed algorithm with others. The image contains four classes with intensity values 0, 70, 140 and 210. We compare the performance of above five algorithms on the synthetic test image, which is divided into 4 classes. The test image is corrupted by "Gaussian", "salt & pepper" and hybrid "Gaussian" and "salt & pepper" noises, respectively, and the segmentation results are shown in Table 1 and Fig. 1. Table 1 gives the average segmentation accuracy (SA) of the five algorithms on three different noisy images, where SA is defined as the sum of the correctly classified pixels divided by the sum of the total number of pixels [8]. Fig. 1 shows the results on synthetic test image corrupted by "Gaussian" noises. we can see that FCM, FCM_S1, FLICM and GFCM are, respectively, influenced by the noises more or less., which indicates that these algorithms lack enough robustness to noises, while the proposed SCFCM algorithm removes almost all the added noises. Compared to the FCM, FCM_S1, FLICM and GFCM algorithm, we can see that the proposed SCFCM algorithm achieves much better segmentation.

Table 1 SA% of five algorithms on synthetic test image.

Noise type	FCM	FCM_S1	FLICM	GFCM	SCFCM
Gaussian	98.21	99.08	98.53	98.79	99.98
Salt & Pepper	95.81	95.38	95.92	96.47	98.33
Hybrid noise	94.53	95.68	95.58	95.71	98.55

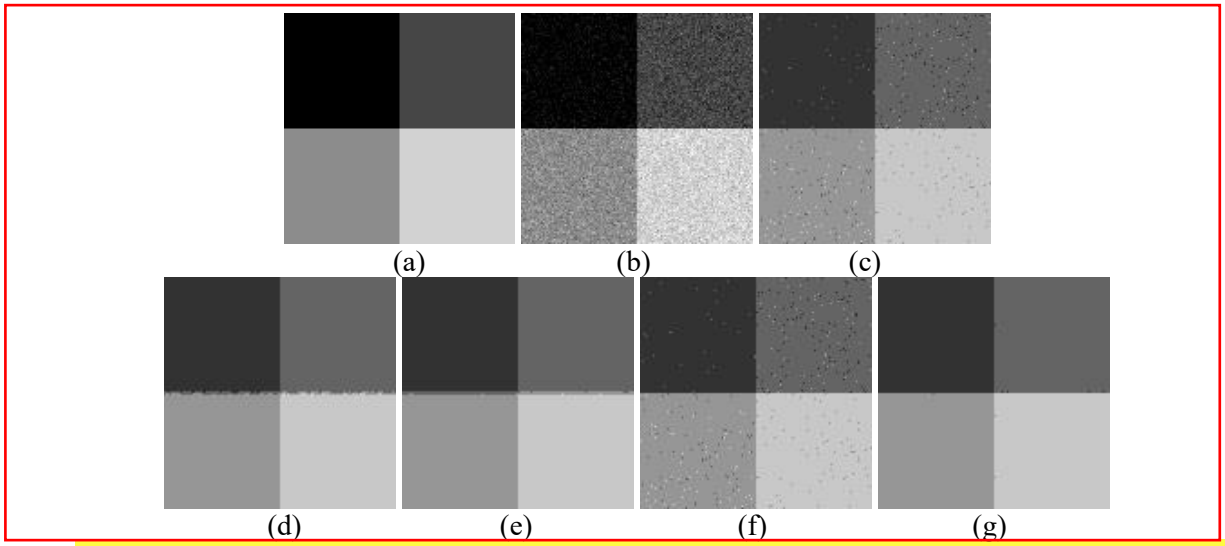


Fig. 1 Segmentation results of five algorithms on synthetic test image. (a) Original image. (b) Noise image. (c) FCM. (d) FCM_S1. (e) FLICM. (f) GFCM. (h) SCFCM.

Fig. 2 presents a comparison of segmentation results on a real image with 308×242 pixels as shown in Fig. 2(a). Fig. 2(b) is the original image corrupted by hybrid "Gaussian" and "salt & pepper" noises. Fig. 2(c)-(g) present the results applying the five algorithms on Fig. 2(b), respectively. We use $c = 2$ in the experiment. Visually, FCM, FCM_S1, FLICM and GFCM are respectively affected by the noises to different extents, while the proposed SCFCM algorithm achieves an outstanding segmentation. From Fig. 2(c)-(g), It can be concluded that the SCFCM algorithm is less sensitive to noises than other algorithms.

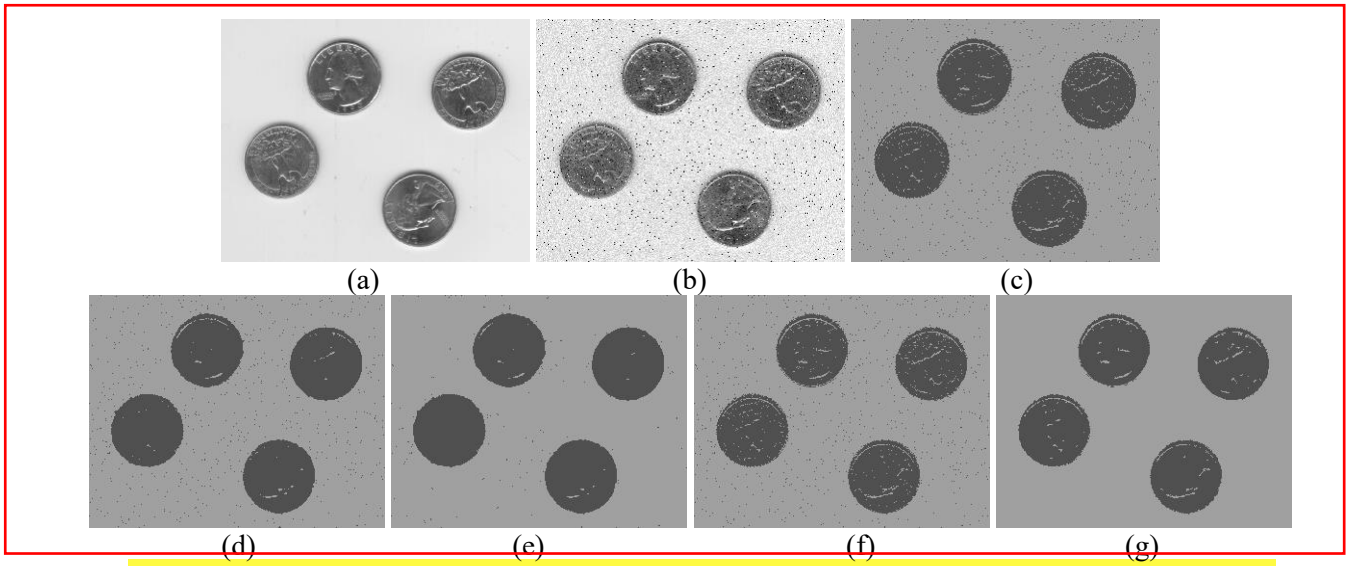


Fig. 2 Segmentation results of five algorithms on a real image corrupted by hybrid "Gaussian" and "salt & pepper" noises. (a) Original image. (b) Noise image. (c) FCM. (d) FCM_S1. (e) FLICM. (f) GFCM. (h) SCFCM.

5. Conclusions

In this paper, we have presented a novel spatially constrained fuzzy c-means clustering algorithm for image segmentation. Firstly, the local prior probabilities of pixels are defined according to the fuzzy membership function values of neighbouring pixels, then those local prior probabilities are incorporated into the objective function of the standard FCM. By this way, the local spatial information embedded in the image is incorporated into the FCM clustering algorithm. Experimental results on the synthetic and real images have demonstrated the robustness and validity of the proposed algorithm.

Acknowledgments

This work was supported by the National Natural Science Foundation of China under grant no. 51674200 and The Youth Foundation of Xi'an Shiyou University under grant no. 2013BS021.

References

[1] H. Zhang, J.E. Fritts, and S. A Goldman. Image segmentation evaluation: A survey of unsupervised methods[J]. Computer Vision and Image Understanding, 2008, 110(2): 260-180.

[2] J.C. Bezdek, Pattern recognition with fuzzy objective function algorithms[M], Plenum, New York, 1981.

[3] X.H. Li, T.Y. Zhang, Z. Qu. Image segmentation using fuzzy clustering with spatial constraints based on Markov random field via Bayesian theory[J]. IEICE Transactions on Fundamentals of Electronics, Communications and Computer Sciences, 2008, E91A(3): 723-729.

[4] F. Li, J. Qin. Robust fuzzy local information and Lp-norm distance-based image segmentation

method[J]. IET Image Processing, 2017, 11(4), 217-226.
[5] J. Zhang, et al. Adaptive image segmentation method based on the fuzzy c-means with spatial information[J]. IET Image Processing, 2018, 12(5): 785-792.
[6] D.L. Pham. Spatial models for fuzzy clustering[J]. Computer vision and image understanding, 2001, 84: 285-297.
[7] M.N. Ahmed, S.M. Yamany, N. Mohamed, A.A. Farag, and T. Moriarty. A modified fuzzy *c*-means algorithm for bias field estimation and segmentation of MRI data[J]. IEEE Trans. Med. Imaging, 2002, 21: 193-199.
[8] S.C. Chen, D.Q. Zhang. Robust image segmentation using FCM with spatial constraints based on new kernel-induced distance measure [J]. IEEE Trans. Syst. Man Cybern. B, 2004, 34(4): 1907–1916.
[9] W.L. Cai, S.C. Chen and D.Q. Zhang. Fast and robust fuzzy c-means clustering algorithms incorporating local information for image segmentation [J]. Pattern Recognition, 2007, 40: 825-838.
[10] S. Krinidis, V. Chatzis. A robust fuzzy local information c-means clustering algorithm[J]. IEEE Trans. Image Process, 2010, 19(5): 1328-1337.
[11] Feng Y. and Chen W. Brain MR image segmentation using fuzzy clustering with spatial constraints based on Markov random field theory[C]. In:Proc of MIAR 2004 (LNCS 3150,Beijing). Berlin: Springer-Verlag, 2014, 188-195.
[12] J.C. Dunn. A fuzzy relative of the ISODATA process and its use in detecting compact well separated clusters[J]. J. Cybern., 1973, 3(3): 32–57.

2022 7th International Conference on Intelligent Computing and Signal Processing (ICSP) | 978-1-6654-7857-1/22/$31.00 ©2022 IEEE | DOI: 10.1109/ICSP54964.2022.9778366

Adaptive spatially weighted fuzzy c-means clustering for image segmentation

Xiaohe Li
School of Computer Science
Xi'an Shiyou University
Xi'an, China
lixh@xsyu.edu.cn

Zhan Qu
School of Petroleum Engineering
Xi'an Shiyou University
Xi'an, China
zhqu@xsyu.edu.cn

***Abstract*—Fuzzy c-means (FCM) clustering algorithm is a popular algorithm in the field of image segmentation. In this paper, an adaptive spatially weighted FCM clustering (ASWFCM) is proposed, to improve the performance of image segmentation. Through defining the weight of each pixel neighborhood and incorporating the spatial weights into the traditional Fuzzy c-means objective function, the image information which related to local spatial is integrated into the segmentation approach. Because of those spatial weights of neighboring pixels are fully adapted to the local image content and can effectively detect the anisotropy of neighborhood, the proposed algorithm improves the robust to noise. Both synthetic and real image experimental results verify the accuracy and the robustness of the ASWFCM method.**

Keywords- clustering, image segmentation, ASWFCM

I. INTRODUCTION

Image segmentation is an important task in image understanding and computer vision [1]. In image segmentation processing, an image is divided into several disjoint regions, each of which has the same characteristics with others, such as gray level, color, texture, and other characteristics. One of the most classical fuzzy clustering methods [3-12] is fuzzy c-means (FCM) algorithm [2]. The advantage of this algorithm is mainly due to the ambiguity introduced by the attributes of each image pixel. However, none of the spatial information in the image context is considered in the standard FCM algorithm, resulting in the performance of the algorithm deteriorates.

In order to improve the effectiveness of the standard FCM, smoothing the image before clustering is an effective method. It should be noted that smoothing filtering operation may result in the loss of image information, especially the loss of important image details at the boundary or edge. Moreover, the trade-off between smoothing and clustering cannot be controlled. Therefore, to improve the performance of image segmentation, researchers put forward a lot of local spatial information should be brought into the standard FCM method. By adding the spatial neighborhood term into objective function of FCM, Ahmed et al. [4] proposed FCM_S algorithm. Through using information obtained in different windows containing the image, each pixel in an image is classified through the accumulated local FCM_S approach [5]. In order to decrease the computational complexity of FCM_S, Chen and Zhang [6] proposed two variant FCM_S1 and FCM_S2, which are replaced with average filtering and median filtering images to simplify FCM_S item neighborhood. FCM_S1, FCM_2, as well as FCM_S have the same key parameter. which is adopted to control the trade-off between a pixel and its neighbors. Because of the fact that the key parameter has a crucial impact on the performance of these approaches, and the selection of the key parameter is carried out through experiments, usually using trial and error experiment, this algorithm has its limitations. Wang et al. [7] adjusted the effect of the neighborhood according to the homogeneousness of the neighboring pixels, but weights for the neighbors of each neighborhood term still have the same value. Krindis and Chatzis [8] presented a fuzzy local information c-means (FLICM) clustering method. By introducing a novel fuzzy local neighborhood factor to the objective function, both image quality and noise robustness are ensured. FLICM, however, the objective function is not set any parameters to control the influence of the factors. Li and Qin [9] improved the robustness of FLICM by using *Lp*-norm distance.

To solve the above problems, an adaptive spatially weighted fuzzy c-means (ASWFCM) method is proposed. Firstly, the weight of each pixel neighborhood is defined, and then combining the weights and the FCM objective function. Due to those spatial weights of neighboring pixels are completely adaptive to the local content of the image, the ASWFCM algorithm proposed in this paper could reduce the impact of noise and other imaging artifacts on image segmentation effectively.

This paper is organized as follows. Sec.1 is the introduction. FCM clustering algorithm is reviewed briefly in Sec.2. In Sec. 3, the detailed proposed algorithm is presented. Both synthetic and real image experimental results are shown in Sec.4, and the conclusion is given in Sec. 5.

II. FUZZY C-MEANS CLUSTERING

The FCM clustering algorithm divides the image X into c clusters by minimizing the objective function

$$J_{\mathrm{FCM}} = \sum_{k=1}^{c}\sum_{i=1}^{n} u_{ik}^{m}\|x_i - v_k\|^2 \qquad (1)$$

where $X = \{x_1, x_2, \ldots, x_n\}$ denotes an image with n pixels, u_{ik} is the membership degree of the pixel i belonging to the cluster k , and satisfies $u_{ik} \in [0,1]$ and $\sum_{k=1}^{c} u_{ik} = 1$ for any pixel i,

Authorized licensed use limited to: Shanghai Jiaotong University. Downloaded on November 17,2023 at 11:42:29 UTC from IEEE Xplore. Restrictions apply.

the prototype of the center of cluster k is denoted as v_k. Parameter m is the weighting exponent on each fuzzy membership which is usually set to 2.

$$u_{ik} = \frac{(\|x_i - v_k\|)^{-2/(m-1)}}{\sum_{j=1}^{c}(\|x_j - v_k\|)^{-2/(m-1)}} \quad (2)$$

$$v_k = \frac{\sum_{i=1}^{n} u_{ik}^m x_i}{\sum_{i=1}^{n} u_{ik}^m} \quad (3)$$

Apparently, the information in image context is not taken into consideration in FCM algorithm. Every pixel is considered as isolated. Therefore, the performance of FCM algorithm is greatly affected by noise.

III. PROPOSED ALGORITHM

In this work, the spatial weights for neighbors of each pixel are defined. Through incorporating the spatial weights into the traditional Fuzzy c-means objective function, an adaptive spatially weighted FCM (ASWFCM) algorithm is proposed to improve the effect.

A. Definition of the local weights

Letting $X = \{x_1, x_2, \ldots, x_n\}$ denotes an image with n pixels, which x_i is the gray value of the ith pixel. For each pixel x_i, the median value of its neighboring pixels value is expressed as follows.

$$m_i = med\{x_r, r \in N_i\} \quad (4)$$

where N_i stands for the set of neighbors falling into a window around x_i. The l_1 distance between x_r and m_i is computed by

$$\sigma_{ir} = |x_r - m_i| \quad (5)$$

The weight for pixel $x_r (x_r \in N_i)$ is defined as

$$\xi_{ir} = \exp\left(-\beta \frac{\sigma_{ir}}{\sigma_i}\right) \quad (6)$$

where β is the strength factor, σ_i represents the maximal value of σ_{ir}.

$$\sigma_i = \max_{r \in N_i} \sigma_{ir} \quad (7)$$

Finally, the obtained weights are normalized so that the sum of them equals to one.

$$w_{ir} = \frac{\xi_{ir}}{\sum_{r \in N_i} \xi_{ir}} \quad (8)$$

The weights for neighborhood N_i is denoted by $W_i = \{w_{ir}, r \in N_i\}$. It can be concluded from (4)-(8) that if a pixel's gray value is far away from the median value of its neighbors, the pixel will have a very small weight. This means that w_{ir} measures the similarity between the pixel x_r and the majority of N_i. That is to say, those weights of neighboring pixels are totally adaptive to the local image content. The calculated weights of two neighborhoods selected from a synthetic image is shown in Figure 1. The Figure 1 (a) gives the pixel's gray values in a neighborhood selected from the boundary area and the estimated weights. The Figure. 1 (b) gives the pixel's gray values in a neighborhood selected from the smooth area and the estimated weights. From Figure. 1, it can be easily seen that weights of noise pixels in the neighborhood are relatively small. The calculated weights in two examples illustrate that this approach could effectively detect the anisotropy of neighborhood.

133	208	197
143	211	194
137	215	**241**

0.0133	0.1600	0.2680
0.0213	0.1390	0.2328
0.0161	0.1153	0.0341

(a)

42	69	66
73	**97**	76
80	**95**	68

0.0115	0.1570	0.1174
0.2312	0.0227	0.1729
0.1147	0.0275	0.1425

(b)

Figure 1. Two neighborhoods selected from a synthetic image and the estimated weights, where edge or noise pixels are highlighted in boldface. (a) neighborhood selected from a boundary area and the estimated weights. (b) neighborhood selected from a smooth area and the estimated weights.

B. ASWFCM algorithm

We incorporate the local spatial weights W_i into the standard FCM objective function and then obtain the novel objective function of ASWFCM below:

$$J_{\text{ASWFCM}} = \sum_{k=1}^{c}\sum_{i=1}^{n} u_{ik}^m \sum_{r \in N_i} w_{ir}\|x_i - v_k\|^2 \quad (9)$$

This novel objective function can be minimized iteratively, which is similar to the traditional FCM algorithm. J_{ASWFCM} in its local minimal extreme could satisfy two conditions

$$u_{ik} = \frac{\left(\sum_{r \in N_i} w_{ir}\|x_r - v_k\|^2\right)^{-1/(m-1)}}{\sum_{j=1}^{c}\left(\sum_{r \in N_i} w_{ir}\|x_r - v_j\|^2\right)^{-1/(m-1)}} \quad (10)$$

$$v_k = \frac{\sum_{i=1}^{n} u_{ik}^m \sum_{r \in N_i} w_{ir} x_r}{\sum_{i=1}^{n} u_{ik}^m} \quad (11)$$

Based on this, the step of ASWFCM algorithm is shown as follows.

Step 1: Setting the number of the clusters c, and the fuzzy parameter m.

Authorized licensed use limited to: Shanghai Jiaotong University. Downloaded on November 17,2023 at 11:42:29 UTC from IEEE Xplore. Restrictions apply.

Step 2: Initializing the membership functions randomly.

Step 3: Calculating weights W_i using (4)-(8).

Step 4: Updating the cluster centers v_k using (11).

Step 5: Updating the membership functions u_{ik} using (10).

Step 6: Exiting if the result is convergence and skipping to Step 4 otherwise.

If the weight $w_{ir} = 0$ for $i \neq r$ and $w_{ir} = 1$ for $i = r$, the ASWFCM algorithm is the same as traditional FCM. In this case, the ASWFCM algorithm can be regarded as an extension of the standard FCM. Compared with those improved FCM-type clustering schemes described in introduction, such as FCM_S, FLICM et al., the main novelty of the ASWFCM algorithm is that the effect of neighborhood is completely adaptive to the local content of the image. And thus the ASWFCM algorithm could reduce the impact of noise and other imaging artifacts on image segmentation effectively.

IV. EXPERIMENTAL RESULTS

In order to verify the accuracy and the robustness of this method, both the synthetic image and real image experimental results are analyzed. In order to further illustrate the effectiveness of the algorithm, the performance between ASWFCM and FCM, FCM_S1, FLICM algorithms is compared. Set the parameters $m = 2$, $\beta = 3$, and $N_R = 9$ (a 3×3 window centered around each pixel) in the experiments.

In condition of "Gaussian" (zero mean), "salt & pepper", hybrid "Gaussian" and "salt & pepper" noise, these four algorithms are applied to a synthetic test image which size is 128×128 pixels, and the test image possesses four classes with intensity values 0, 70, 140 and 210. The results are shown in TABLE I and Figure 2. TABLE I describes the segmentation accuracy (SA) of the four algorithms under different noise, where σ_g denotes the standard deviation of Gaussian noise. Segmentation accuracy is Defined as the ratio of the sum of correctly classified pixels to the total number of pixels [4]. In condition of the synthetic image obtained in "Gaussian" ($\sigma_g = 10$), 5% "salt & pepper" noise and the parameter $c = 4$, the result is shown in Figure 2. From Figure 2, we notice that FCM, FCM_S1 and FLICM are affected by the noise obviously, in other words, all these three algorithms lack enough robustness to noise. Meanwhile, the result obtained by the proposed ASWFCM algorithm removes almost all the additional noise. Combined Table 1 and Figure 2, it could be concluded that the algorithm proposed in this paper is less sensitive to noise than other algorithms and achieves relatively satisfactory results.

TABLE I. SA% OF FOUR METHODS ON SYNTHETIC TEST IMAGE

Noise types and level	FCM	FCM_S1	FLICM	ALWFCM
Gaussian (σ_g=15)	96.54	99.12	99.35	99.62
Gaussian (σ_g=20)	89.74	99.05	99.30	99.49
Gaussian (σ_g=25)	82.50	98.97	99.15	99.29
salt & pepper (10%)	92.66	92.51	90.81	99.07
salt & pepper (15%)	88.84	87.82	85.22	98.20
salt & pepper (20%)	85.31	84.83	79.58	98.10

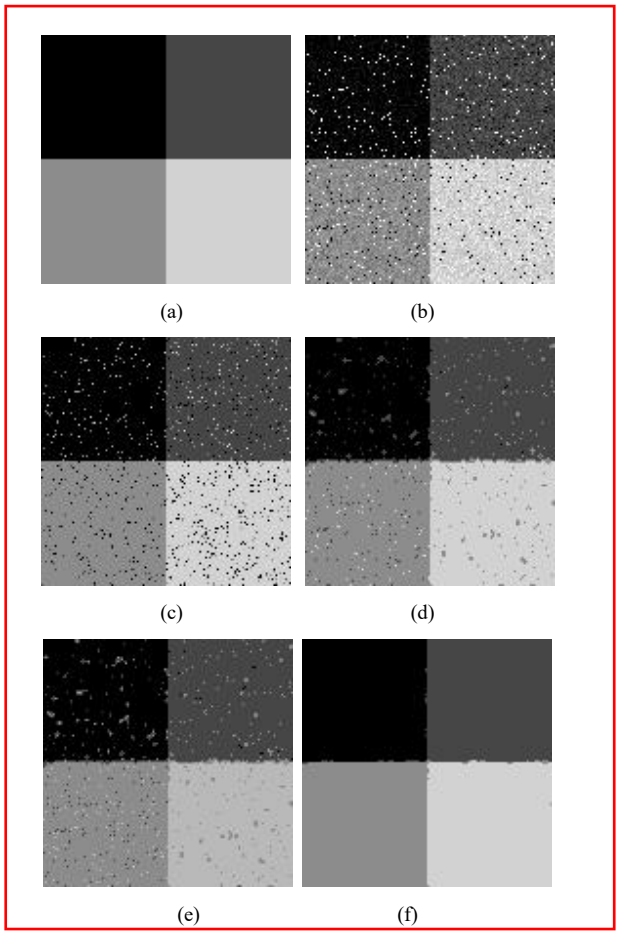


Figure 2. Comparison of segmentation results on synthetic test image. (a) Original image. (b) The same image with hybrid noise. (c) Segemention result obtained by FCM. (d) Ssegemention result obtained by FCM_S1. (e) Segemention result obtained by FLICM result. (f) Segemention result obtained by ASWFCM.

图3的叙述错误，图3(a)是原图，图3(b)是加噪声图

Figure 3 illustrates the clustering results obtained by different algorithms on a real image with 308×242 pixels. Figure 3 (a) shows the real image which in "Gaussian" (σg=10) and 5% "salt & pepper" noise background. Figure 3 (b) is the original image. Figure 3 (c)-(f) present the segmentation results of the four algorithms based on Figure 3 (b), respectively. Due to FCM, FCM_S1 and FLICM are all influenced by hybrid noise, all these three algorithms lack enough robustness to noise, which is shown in Figure 3 (c)-(d). Furthermore, the effect of noise can be basically eliminated through the proposed ASWFCM algorithm, as shown in Figure 3(f). In a word, compared to the above three algorithms, the ASWFCM algorithm proposed in this paper achieves much better segmentation result under hybrid noise condition, and the effectiveness of the algorithm is verified.

Authorized licensed use limited to: Shanghai Jiaotong University. Downloaded on November 17,2023 at 11:42:29 UTC from IEEE Xplore. Restrictions apply.

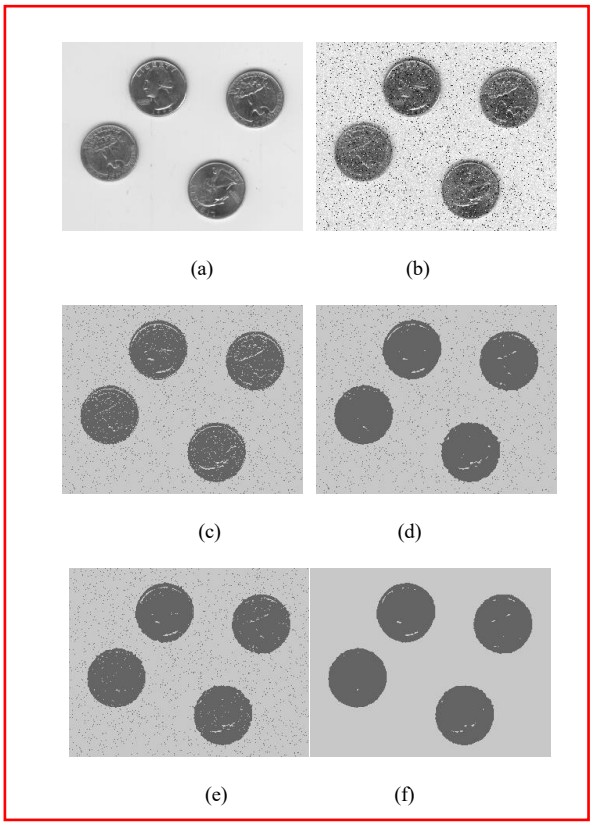


Figure. 3 Comparison of segmentation results on real image. (a) Original image. (b) The same image with hybrid noise. (c) Segemention result obtained by FCM. (d) Segemention result obtained by FCM_S1. (e) Segemention result obtained by FLICM. (f) Segemention result obtained by ASWFCM.

V. CONCLUSIONS

In this paper, the neighboring weights which are completely adaptive to the local content of the image have been defined. This weighting method could not only detect the anisotropy of neighborhoods effectively but also reduce the impact of edges and noise on image. By incorporating those weights into the traditional FCM objective function, a novel adaptive locally weighted fuzzy c-means clustering approach has been presented. Experimental results illustrated that the novel ASWFCM algorithm satisfied both the accuracy and the robustness in image segmentation processsing. Our future work will focus on incorporating the spatial distances of neighboring pixel into the weighting method proposed in this paper.

ACKNOWLEDGMENT

This work is supported by the National Natural Science Foundation of China under grant No. 51974255 as well as The Youth Foundation of Xi'an Shiyou University under grant No. 2013BS021.

REFERENCES

[1] H. Zhang, J.E. Fritts, and S. A Goldman, "Image segmentation evaluation: A survey of unsupervised methods," Computer Vision and Image Understanding, vol. 110(2), pp. 260-180, 2008.

[2] J.C. Bezdek, Pattern recognition with fuzzy objective function algorithms, Plenum, New York, 1981.

[3] X.H. Li, T.Y. Zhang, Z. Qu, "Image segmentation using fuzzy clustering with spatial constraints based on Markov random field via Bayesian theory," IEICE Transactions on Fundamentals of Electronics, Communications and Computer Sciences, vol. E91A(3), pp. 723-729 2008.

[4] M.N. Ahmed et al., "A modified fuzzy c-means algorithm for bias field estimation and segmentation of MRI data," IEEE Trans. Med. Imaging, vol. 21(3), pp. 193–199, 2002.

[5] J. Zhang, et al., "Adaptive image segmentation method based on the fuzzy c-means with spatial information," IET Image Processing, vol. 12(5), pp. 785-792, 2018.

[6] S.C. Chen, D.Q. Zhang, "Robust image segmentation using FCM with spatial constraints based on new kernel-induced distance measure," IEEE Trans. Syst. Man Cybern. B, vol 34(4), pp. 1907–1916, 2004.

[7] Z.M. Wang et al., "An adaptive spatial information-theoretic fuzzy clustering algorithm for image segmentation," Computer Vision and Image Understanding, vol. 117(10), pp. 1412-1420, 2013.

[8] S. Krinidis, V. Chatzis, "A robust fuzzy local information c-means clustering algorithm," IEEE Trans. Image Process, vol. 19(5), pp. 1328-1337, 2010.

[9] F. Li, J. Qin, "Robust fuzzy local information and Lp-norm distance-based image segmentation method," IET Image Processing, vol. 11(4), pp. 217-226, 2017.

[10] J.C. Dunn, "A fuzzy relative of the ISODATA process and its use in detecting compact well separated clusters," J. Cybern., vol. 3(3), pp. 32–57, 1973.

[11] Dhirendra Kumar, R. K. Agrawal, Puneet Kumar, "Bias-Corrected Intuitionistic Fuzzy C-Means With Spatial Neighborhood Information Approach for Human Brain MRI Image Segmentation," IEEE Transactions on Fuzzy Systems, vol. 30(3), pp. 687-700, 2022.

[12] Tao Lei, Peng Liu, Xiaohong Jia et al, "Automatic fuzzy clustering framework for image segmentation," IEEE Transactions on Fuzzy Systems, vol. 28(9), pp. 2078-2091, 2020.

Authorized licensed use limited to: Shanghai Jiaotong University. Downloaded on November 17,2023 at 11:42:29 UTC from IEEE Xplore. Restrictions apply.

PAPER • OPEN ACCESS

Research on the changing trend of farmland area in China and its driving factors from 1996 to 2016

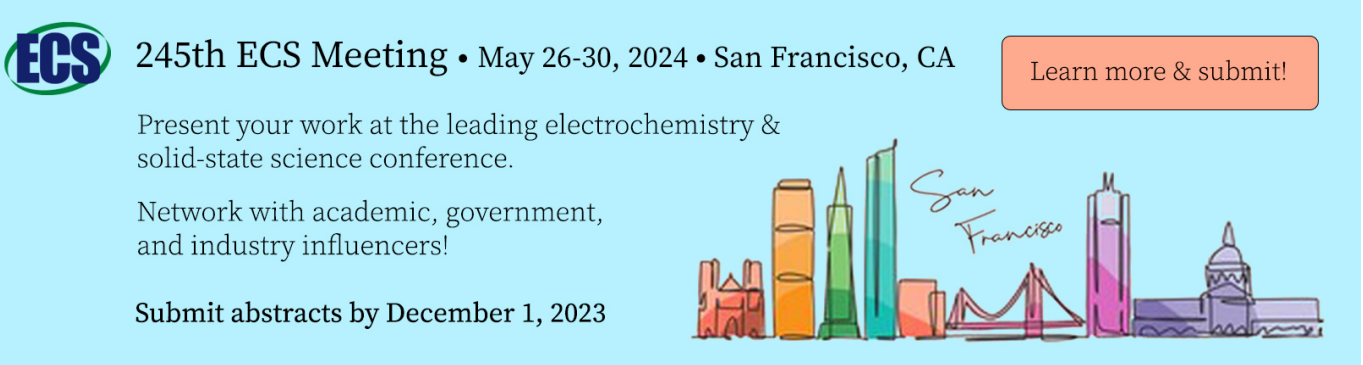
To cite this article: J Y Wang and X M Li 2018 *IOP Conf. Ser.: Mater. Sci. Eng.* **392** 062097

View the article online for updates and enhancements.

中文文章叫近20年，英文文章是1996 to 2016,文章完全一样

You may also like

- The 300 years cropland changes reflecting climate impacts and social resilience at the Yellow River–Huangshui River Valley, China
Qiong Chen, Liang Emlyn Yang, Jing Luo et al.
- Analysis and Research on the Value of Farmland Transfer Based on Environmental Protection Evaluation System
Zhenyu Zhang, Minghua Tian, Jianjun Li et al.
- High Standard Farmland Construction and Soil Conservation Evaluation
Jing Zhang and Lu Sun



This content was downloaded from IP address 219.144.164.16 on 16/11/2023 at 00:29

Research on the changing trend of farmland area in China and its driving factors from 1996 to 2016

J Y Wang [1] and X M Li[2*]

[1]Xi'an Shiyou University, Xi'an China, 710065

[2]Shaanxi Provincial Land Engineering Construction Group，Xi'an China, 710075

*Corresponding author: xmlisdc@126.com

Abstract. The paper was to research the changing trend of farmland area from 1996 to 2016. The original data of farmland area of China in these years were collected, data mining technology was used, and ARIMA model was chosen to predict each other between the two periods of 1996-2008 and 2008-2016, so the original farmland area data could be corrected and normalized. Then correlation analysis was used to study the driving factors. The trend research result showed, the farmland area decreased from 1996 to 2016, the decreasing rate was faster before 2004, and then it decreased slowly. The correlation analysis result showed, the added value proportion of primary industry, the total population, and the urban population were the most important driving factors, their coefficients were 0.959, -0.918 and -0.896 respectively. It could be concluded by the result that the industry configuration and the urbanization could affect the farmland area changing with the development of social economy.

1. Introduction

China is a great agricultural country, and the farmland is one very important resource which is related to food security. However, the vigorous demand for lands brings great challenge for farmland protection with the promotion of socialist modernization construction [1]. The research on farmland area change and its driving factors in China has always been one popular problem. The statement was refuted that China's cultivated land has been descending since 1957 based on the analysis of the actual change of the cultivated land area [2]. The farmland area changing trend, spatial characteristics and the driving factors in China for a period of time before 2007 were studied [3-5]. And in different scales such as the scale of province or in some part of China, the dynamic change trend of farmland was studied [6-8]. Since 1980s, with the development and application of 3S technology, many scholars studied the farmland change using the RS images such as Landsat TM images [9, 10]. And the analysis approaches in the study of the driving forces of land use change in large regions were explored by using digital satellite remote sensing data of China [11]. Not only the changes in China's cultivated land but also those in some provinces were analyzed based on remote sensing data such as Landsat TM/ETM+, NOAA, SPOT dataset [12, 13].

The statistic data sources of cultivated land in China are various, for example, the international organizations such as FAQ, WRI (the world resources institute), and different departments of China such as MLR (the ministry of land and resources), MOA (the ministry of agriculture), the bureau of statistics of PRC. However, the statistical data supplied by MLR are considered the most authoritative [14]. But the data from the MLR are not regularly entire in the demanded periods, and there was a jumping phenomenon with the farmland area from 2008 to 2009, that's because the data of 2008 was

Content from this work may be used under the terms of the Creative Commons Attribution 3.0 licence. Any further distribution of this work must maintain attribution to the author(s) and the title of the work, journal citation and DOI.
Published under licence by IOP Publishing Ltd

based on the first national land use survey, and the data of 2009 was based on the second national land use survey, that's seemly illogical. At present, most scholars analyze the farmland area change by the exiting data directly while ignoring the accuracy of the statistic data, or they just focused on some periods before 2008 or after 2009 evading the jumping years. Only a few scholars researched the farmland area in different historical periods [14, 15]. In this paper, the researched years included the years of before and after the second national land use survey. The method of data mining was introduced to analyze the relation between the two periods of the years before 2008 and the years after 2009, so the changing trend of China's farmland area could be reflected more scientifically. At the same time, the driving factors were studied based on data normalization. And this is not found in the present research, which could be useful for studying China's farmland changing trend.

2. Data and methods

2.1. Data acquisition

2.1.1. Data of farmland area in China

The farmland area of China, especially in the historical periods, has been hard for statistic for a long time. The national department of land management have been announcing the changing situation each year since 1986. In order to obtain the veracious statistical data of farmland in China, the first national land use survey was operated from 1984 to 1996. The survey result showed there was 1.95 billon mu (1 mu = 666.66 m^2) of farmland in China by the day of Oct.31 1996 [15], which was considered the most credible result at that time [16]. Then, the farmland area of each year from 1996 to 2008 can all be obtained from the statistical bulletin of the year.

In order to obtain more veracious statistical data of farmland, the second national land use survey was operated from 2007 to 2009. The survey result showed there was 2.03 billon mu of farmland in China by the year of 2009 [15]. And since then the land use change survey has been operated each year. And the farmland area from 2007 to 2016 can be obtained from the national service platform of land use survey result. Because new methods and technologies were applied with the second national land use survey, some farmlands which were not found in the first survey were found in the second survey, and there was a jumping phenomenon with the farmland area from 2008 to 2009, which would be specially researched after a while for analyzing the changing trend of farmland area.

2.1.2. Data of driving factors

Land is closely related to the human social and economic development. The national farmland change is influenced by the geographical and climate conditions, social and economic development, flood and waterlogging disaster and so on [1]. For researching the driving factors influencing the farmland changing, three kinds of factors were introduced for comparison and selection. One kind were the comprehensive factors reflecting the national economic development, and they were the gross national income (GNI), the gross domestic product (GDP), the primary industry added value and its ratio, the second industry added value and its ratio, the third industry added value and its ratio, the gross agricultural output value, per capita GDP, industrial added value, architectural added value. Another kind were special factors reflecting the level of urbanization, and they were the national population, the urban population, and the rural population. The third kind was the special factors reflecting the natural disaster, and they were the damage area and the grain yield. There were in total of 17 factors which were used for analysis [17]. And data of all factors for the recent 20 years could be obtained from the web site of the national bureau of statistics.

2.2. Study methods

In this paper, the national farmland area dada from 1996 to 2016 years were collected and analysed to study the changing trend, and the correlation analysis was operated to research the driving factors. While studying the changing trend of farmland from 1996 to 2016, according to the found jumping

phenomenon with the data from 2008 to 2009, the data mining technology was introduced. First, the farmland area of the year 2009 can be predicted with the data of 1996 to 2008. And the farmland area of the year 2008 can also be predicted reversely with the data of 2009 to 2016. Then, based on the predicted data and the practically collected data of the farmland of the years 2008 and 2009, the mathematical ratio relation between the farmland area of 2008 and 2009 could be analysed and obtained, so the jumping phenomenon could be solved with the ratio. At last, all the farmland data from 1996 to 2016 should be normalized for researching the changing trend more scientifically.

ARIMA (Autoregressive Integrated Moving Average) model was chosen for prediction with data mining, which was promoted by Box and Jenkins, it's a very famous and useful time-sequence forecast method, and that's just the needed one in this paper.

3. Analysis on the farmland area changing trend from 1996 to 2016

3.1. The analysis based on the original statistic data of farmland area

By collecting and analysing the original statistic data of farmland area for years of 1996-2016, the result showed that the national farmland area decreased year by year, as Figure1, and the decreasing speed was the most quick from 2000 to 2004. While the farmland area jumped from 1.826 billion mu in 2008 to 2.031 billion mu in 2009. And after 2009, the farmland area decreased very slowly.

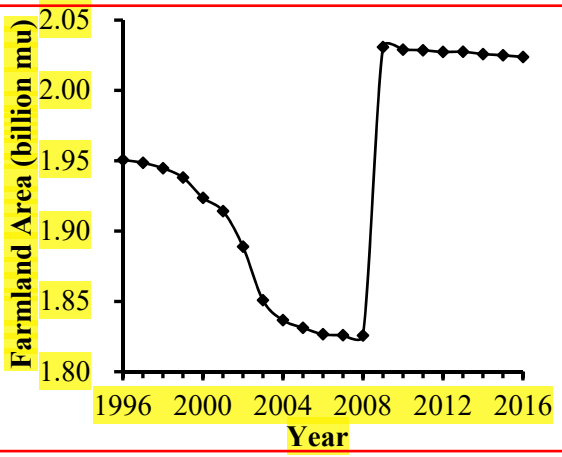


Figure 1. Changing Trend for Farmland Area of 1966-2016 Based on Original Statistic Data

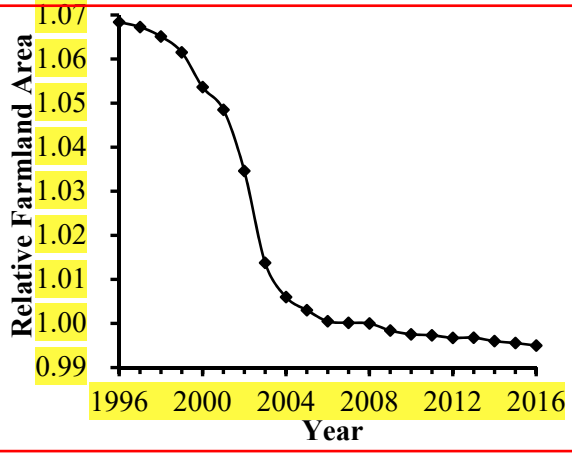


Figure 2. Changing Trend for Farmland Area of 1966-2016 Based on Revised Statistic Data

China finished the first national land use survey in 1996, and the second in 2009, so the jumping phenomenon just happened in the division years of the twice land use survey. Whether the national farmland increased by about 200 million mu in the year of 2009 or not should be studied deeply. And by reviewing literatures [14, 15, 18], it could be concluded that the main reason was that more advanced technologies were introduced while the second land use survey, so some farmlands lost of statistic in the first land use survey were found in the second time, and the accuracy of the statistic result was improved. In this paper, the farmland data for the recent 20 years were based on twice different land use survey and different technology conditions. We can easily studied the changing trend in each period before or after the second land use survey, while all the data of farmland area must be revised and normalized if we want to study the continual time-sequence changing trend from 1996 to 2016, then they might be comparable.

3.2. Revision of farmland area based on data mining technology

Data mining technology is much useful for time-sequence prediction, and by that, in this paper, the farmland area of the year 2009 was predicted with the farmland data of the years from 1996 to 2008, the ratio α between the farmland area of 2009 and that of 2008 could be obtained. And the farmland area of the year 2008 was also predicted reversely with the farmland data of the years from 2009 to

2016, the ratio β between the farmland area of 2009 and that of 2008 could also be obtained. Then, for reflecting the ratio more scientifically, we could get the ratio ρ by the average of α and β.

SPSS software was used for prediction in this paper, by analyzing and comparing, the model of ARIMA was used in both of the prediction and the reverse prediction. The model used while predicting the farmland area of the year 2009 was ARIMA(1,1,2) (r^2=0.975**), and the model used while predicting reversely the farmland area of the 2008 was ARIMA(1,1,4) (r^2=0.966**), both of the two models were significant in the level of 0.01, with that, the predicted farmland area of the year 2009 was 1820.08 million mu, the reversely predicted farmland area of the year 2008 was 2030.98 million mu, so we can get α=0.996899887, β=0.999895617, and then ρ=0.998397752, so we could use the ρ value as the revision ratio of the data of the two different periods.

3.3. Trend analysis based on the revised data of farmland area

All the original farmland area data were revised with the ratio ρ and normalized into relative values for reflecting the changing trend more scientifically. Based on the study of the previous paper, the relative farmland area of the years from 1996 to 2008 were calculated with the denominator of the farmland area of the year 2008, the relative farmland area of the years from 2009 to 2016 were calculated with the denominator of the farmland area of the year 2009 while revised by multiply the ratio ρ. Then the continual changing trend of farmland area from 1996 to 2016 could be obtained, shown as Figure 2, which showed the national farmland area decreased year by year. Before the 2004, the decreasing rate was faster, and after that the decreasing rate trends to be slower, especially after 2009, the farmland area trends to be stable.

4. Analysis on driving factors

A total of 17 factors were collected in this paper, and their descriptive statistical characters were shown in table 1. In order to study the driving factors, correlations between the farmland area and the factors were analysed, and then, by comparing the correlation coefficients shown as table 2. the driving factors could be chosen out.

Table 1. Descriptive Statistical Characters of All Factors from 1996 to 2016

Factors	*Min.*	*Max.*	*Ave.*	*Std.*	Factors	*Min.*	*Max.*	*Ave.*	*Std.*
x_1	7078	74114	30444.70	225956.60	x_{10}	589.8	5398	2287.2	16332.77
x_2	7181.4	74412.7	30571.87	226519.84	x_{11}	2953	24786	11653.28	79508.29
x_3	1387.8	6367.1	3124.07	17742.62	x_{12}	439.3	4952.2	1962.3	15992.73
x_4	8.556	19.325	12.11	3.28	x_{13}	122389	138271	131047.71	4702.17
x_5	3382.8	29623.6	13562.92	94949.58	x_{14}	37304	79298	58413.24	12989.27
x_6	39.810	47.559	45.33	2.00	x_{15}	58973	85085	72634.48	8313.40
x_7	2410.7	38422	13884.89	114605.84	x_{16}	43070	62144	52326.48	5812.06
x_8	33.569	51.634	42.56	4.47	x_{17}	21770	54688	41009.48	10706.30
x_9	1354	5928.8	2884.26	16570.35					

**In the table, x_1 means the gross national income (GNI), billion yuan; x_2 means the gross domestic product (GDP), billion yuan; x_3 means the primary industry added value, billion yuan; x_4 means the proportion of primary industry added value, %; x_5 means the second industry added value, billion yuan; x_6 means the proportion of second industry added value, %; x_7 means the third industry added value, billion yuan; x_8 means the proportion of third industry added value, %; x_9 means gross agricultural output value, billion yuan; x_{10} means per capita GDP, billion yuan; x_{11} means industrial added value, billion yuan; x_{12} means architectural added value, billion yuan; x_{13} means the national population, $*10^4$; x_{14} means the urban population, $*10^4$; x_{15} means the rural population, $*10^4$; x_{16} means the grain yield, $*10^4$ t; x_{17} means damage area, $*10^3$ ha; and the same as follows.*

Table 2. Correlation Coefficients between Original/Relative Farmland Area and Factors

	Original data	Relative data		Original data	Relative data
Relative data	-0.142	1.000	x_9	0.686	-0.709
x_1	0.649	-0.746	x_{10}	0.651	-0.749
x_2	0.652	-0.745	x_{11}	0.638	-0.784
x_3	0.663	-0.736	x_{12}	0.688	-0.716
x_4	-0.274	0.959	x_{13}	0.433	-0.918
x_5	0.647	-0.774	x_{14}	0.488	-0.896
x_6	-0.519	0.259	x_{15}	-0.518	0.880
x_7	0.649	-0.717	x_{16}	0.752	-0.524
x_8	0.433	-0.819	x_{17}	-0.514	0.708

As shown in table 2, the correlation coefficients between the original farmland area and the factors were poor because of the jumping phenomenon. However, by analyzing the correlations between the revised farmland area and the factors, we could find, the proportion of the first industry added value had the best correlation with the farmland area, its coefficient was up to 0.959. The national total population was secondary to it, and its correlation coefficient was -0.918, then the urban population and the rural population were secondary to that sequentially, which means the first industry added value, the national total population, the urban population and the rural population were the most important driving factors. According to the research result, we could conclude that it was mainly the national industry structure and the urbanization construction that influence the farmland changing.

5. Conclusion and discussion

Land has both of its own natural and social characters, and it's just all of the factors including society, economy, and policy factors that influence the statistics of farmland area for a long time. So it's difficult for a long-time changing trend research. The period studied in this paper was across twice national land use survey, and there happened to be a jumping phenomenon, but this couldn't reflect the boost of farmland area from 2008 to 2009. The reasons of the phenomenon were studied, that was mainly because RS, GIS and some other new technologies were applied in the second national land use survey, the survey and statistics were more standardized, so the accuracy was apparently promoted, which made the farmlands lost of statistics before found in the second land use survey. Therefore, in order to study the changing trend for a period across twice land use survey, the quantitative relation of the farmland area between the twice survey must be studied and obtained. In this paper, with data mining technology, revision and normalization of farmland area, the research result could reflect the changing trend more actually.

Research results showed China's farmland area decreased year by year from 1996 to 2016, especially before 2004, the decreasing rate was fast, and after that year the decreasing rate tended to be slow. As to the driving factors, it's the proportion of the primary industry added value in the aspect of the national industry structure and the national population, the urban population in the aspect of urbanization construction which were the main driving factors influencing the farmland changing. Because of the ecological restoration after the year of 1999, the farmland decreased rapidly [14, 19]. In 2004, the land management law was revised, which strengthened the protection and the requisition-compensation balance of farmland, and that's much useful for retaining farmland. In this paper, only the farmland area data from 1996 to 2016 were used to study the changing trend, and in present time, China pay much attention to farmland protection, not only including the quantity, but including the land quality with core of productivity in order to realize the protection of the trinity of quantity, quality and ecology [20]. In the future research, the changing trend of farmland area would be studied deeply.

The years of 1966 to 2016 were introduced in this paper to study the changing trend because the demand of statistical data for longer-time sequence was difficult to be satisfied. In future research, based on the collected statistical data, the data mining, remote sensing interpretation and some other methods would be applied to compensate the lack of some factors, so we wish we could obtain a longer time-sequence changing trend.

References

[1] Zhao Q G, Zhou S L, Wu S H and Ren K. 2006. Cultivated Land Resources and Strategies for Its Sustainable Utilization and Protection in China, *Acta Pedologica Sinica*,43(4): 662-72.
[2] Bi Y Y and Zheng Z Y. 2000. The Actual Changes of Cultivated Area Since The Founding of New China**,** *Resources Science*, 22(2): 8-12.
[3] Li X B. 1999. Change of arable land area in China during the past 20 years and its policy implications, *Journal of Natural Resources*, 14(4): 329-33.
[4] Cao Y G, Yuan C, Zhou W, Tao J and Hua R. 2008. Analysis on D iving Forces and Provincial Differences of Cultivated Land Change in China. *China Land Science*, 22(2): 17-22.
[5] Huang Z H and Wu C F. 2009. Empirical Study of Cultivated Land Change and Socio-economic Factors in China. *Journal of Natural Resources*. 24(2): 192-9.
[6] Yu T, Cao Y G and Xu J X. 2016. Driving Force of Cultivated Land Change in China Based on Different Scales. *Chinese Agricultural Science Bulletin*, 2016, 32(24): 194-8.
[7] Wu X, Wang S R, Shang H Y and Wang Z J. 2017. Analysis of Dynamic Change and Driving Forces of Cultivated Land in NingXia During The Past 18 Years. *Chinese Journal of Agricultural Resources and Regional Planning*. 38(8):98-104.
[8] Guo L Y, Wang D L and Wang J Y. 2012. Analysis of the Arable Land Change and Its Causes in the Eastern Coastal China Over the Last Decades. *Chinese Journal of Agricultural Resources and Regional Planning*. 33(1):6-10.
[9] Zhang G P, Liu J Y and Zhang Z X. 2003. Spatial-temporal Changes of Cropland in China for the Past 10 Years Based on Remote Sensing. *Acta Geographica Sinica*. 58(3): 323-32.
[10] Tian G J, Zhuang D F and Liu M L. 2003. The Spatial-temporal Dynamic Change of Cultivated Land in China in 1990s. *Advance in Earth Sciences*. 18(1): 30-6.
[11] Liu X H,Wang J F,Liu J Y, Liu M L and Meng B. 2005. Quantitative Analysis Approaches to the Driving Forces of Cultivated Land Changes on A National Scale.*Transactions of the Chinese Society of Agricultural Engineering*. 21(4):56-60.
[12] Xu L L, Li B L, Yuan Y C, Gao X Z, Liu H J and Dong G H. 2015. Changes in China's Cultivated Land and the Evaluation of Land Requisition-Compensation Balance Policy from 2000 to 2010. *Resources Science*. 37(8): 1543-51.
[13] Li J G, He C Y, Shi P J, Chen J, Gu Z H and Xu W. 2004. Change Process of Cultivated Land and Its Driving Forces in Northern China during 1983-2001. *Acta Geographica Sinica*. 59(2): 274-82.
[14] Feng Z M, Liu B Q and Yang Z. A Study of the Chaning Trend of Chines Cultivated Land Amount and Data Reconstructing:1949-2003. *Journal of Natural Resources*, 20(1): 35-43.
[15] Tan Y Z, He J, Yue W Z, Zhang L and Wang Q R. 2017. Spatial Pattern Change of the Cultivated Land before and after the Second National Land Survey in China. *Journal of Natural Resources*, 32(2): 186-97.
[16] Lin G C S, Ho S P S. 2003. China's land resources and land-use change: insights from the 1996 land survey. *Land Use Policy*, 20(2): 87-107.
[17] Fu Z Q, Cai Y L, Yang Y X and Dai E F. 2001. Research on the Relationship of Cultivated Land Change and Food Security in China. *Journal of Natural Resources*, 16(4): 313-9.
[18] Zhang Y Q and Yang Z S. 2013. Comparative Analysis of Two Investigations of Land Resource in China. *Scientific and Technological Management of Land and Resources*. 30(2): 100-4.
[19] Xu X L, Cai Y M, Zhang K L and Zheng W Y. 2005. Study on Dynamic Change of Cultivated Land Resources and Causes of the Changes. *China Population Resources and Environment.* 15(3): 75-9.
[20] Tan Y Z, Wu C F, Wang Q R, Zhou L Q and Yan D. 2005. The Change of Cultivated Land and Ecological Environment Effects Driven by the Policy of Dynamic Equilibrium of the Total Cultivated Land. *Journal of Natural Resources*. 20(5): 727-34.

第40卷，第8期
2019年8月
中国农业资源与区划
Chinese Journal of Agricultural Resources and Regional Planning
Vol. 40, No. 8, pp171-176
August, 2019

doi: 10.7621/cjarrp.1005-9121.20190821

中文文章叫近20年，英文文章是1996 to 2016, 文章完全一样

·资源利用·

近20年中国耕地数量变化趋势及其驱动因子分析*

王静怡[1]，李晓明[2※]

（1. 西安石油大学计算机学院，陕西西安 710065；2. 陕西省土地工程建设集团有限责任公司，西安 710075）

摘 要 【目的】研究“二调”前后近20年我国耕地面积的变化趋势及其影响因子，为促进耕地保护和土地资源的高效集约节约利用提供决策支撑。【方法】基于1996—2016年耕地数量的原始统计数据，利用数据挖掘技术选用ARIMA模型，基于两次全国土地调查时间段耕地数量数据进行相互预测和反推，即利用1996—2008年耕地数量数据预测2009年耕地数量，利用2009—2016年数据反推2008年耕地数量，从而实现数据的校正和比值归一化的目的，进一步研究近20年内我国耕地数量的变化趋势，并通过相关性分析研究遴选出其驱动因子。【结果】趋势研究结果表明，近20年内我国耕地数量呈现逐年递减的趋势，其中2004年之前递减速度较快，之后递减速度趋缓。相关性分析结果显示，第一产值增加值占比、年末总人口数，以及城镇人口数是影响耕地数量变化的重要驱动因子，其相关系数分别为0.959，-0.918，-0.896。【结论】从研究结果可以推论，我国在社会经济发展中的产业结构布局，以及城镇化建设进程对耕地数量变化产生了重要的影响。

关键词 数据挖掘 ARIMA模型 耕地数量 变化趋势 驱动因子

中图分类号：P96 **文献标识码**：A **文章编号**：1005-9121【2019】08171-06

0 引言

我国是一个农业大国，耕地资源直接关系到国家粮食安全问题，是确保“中国人的饭碗牢牢端在自己手中”的重要基础。同时，在加快推进我国社会主义现代化建设进程中，经济建设对土地的旺盛需求也对耕地保护带来了极大的挑战[1]。对于我国耕地的变化趋势及其影响驱动力的研究，一直都是一个热点问题，甚至有专家学者通过史册文献资料的查证对过去300年我国部分省区耕地资源数量变化及驱动因素进行了研究[2]。

目前，对于我国耕地变化趋势的研究，多基于对统计数据进行分析，从空间尺度上可以分为国家尺度和区域尺度的研究。其中，对于国家尺度上的研究，由于统计标准、技术手段等多种因素的限制，2008—2009年数据发生明显的跳跃式变化，所以绝大部分的研究均处于2008年之前的部分时间段内，如毕于运等[3]通过对我国建国至1996年实有耕地面积的收集整理研究分析了其变化分析；李秀彬[4]对1999年我国前20年耕地面积变化的总体趋势、空间特征和驱动因子进行了研究；曹银贵[5]研究分析了1996—2005年全国耕地变化的情况及其影响的主要因子；黄忠华、吴次芳等利用1978—2007年我国耕地、经济增长、城镇化、地方财政收入数据分析了社会经济因素对耕地变化的影响[6]。以上研究均将时间局限在2008年之前，而回避了2008—2009年耕地统计数据跳跃的现象，这不利于科学研究我国耕地的变化趋势和指导耕地保护工作。对于区域尺度，如省级，甚至市县级尺度，由于统计基数较小，受统计方法、技术标准等因素的影响不大，几乎各个省份区域都有专家对其耕地变化和驱动因子进行了大量研究，如郭丽英等[7]

收稿日期：2018-03-26

作者简介：王静怡（1984—），女，陕西榆林人，博士、讲师。研究方向：资源利用和数据科学

※通讯作者：李晓明（1983—），男，山东烟台人，博士、高级工程师，硕士生导师。研究方向：土地资源利用和遥感信息。Email: xmlisdc@126.com

* 资助项目：陕西省教育厅科研计划项目“无线MARC系统中联合网络—信道编码的优化设计研究”（18JK0626）

(C)1994-2022 China Academic Journal Electronic Publishing House. All rights reserved. http://www.cnki.net

分析了 1996—2008 年我国沿海地区耕地变化的基本态势、时空特征及其主导成因；吴霞等[8]选取 1997—2014 年宁夏耕地面积数据分析耕地面积变化趋势及其驱动因子；武江民等[9]专门针对甘肃兰州市研究其耕地动态变化与驱动力的定量关系。还有学者则基于基于国家、区域、省域、市县不同尺度研究了中国耕地变化的驱动力[10]；

20 世纪 80 年代以来，随着遥感等 3S 技术的发展应用，诸多学者开始不仅仅局限于统计数据的应用，开始借助遥感信息技术对耕地变化进行研究。如张国平、刘纪元等[11]利用中国资源环境数据库及遥感影像对 20 世纪 80 年代末至 2000 年的中国耕地时空变化进行了分析；田光进、庄大方等[12]通过对遥感图像解译研究 80 年代末与 90 年代末 10 年间耕地时空动态变化特征；刘旭华，王劲峰等使用中国 1987—1989 年和 2000 年两期土地利用遥感调查数据，探索定量化研究国家尺度土地利用变化的驱动力[13,14]；许丽丽等[15]基于中分辨率卫星遥感数据，深入分析了 2000—2010 年中国耕地变化及其空间差异，并对中国耕地占补平衡政策的实施效果进行了评估；李景刚等[16]选取 1983—2001 年 NOAA 等遥感数据分析了北方 13 省的耕地变化与驱动力。遥感信息技术的应用开拓了耕地变化研究的新途径，但是由于遥感解译的精度仍有待于进一步提高，所以一定程度上制约了对于耕地变化的研究。

多来以来，我国对于耕地数量的数据统计有多种来源，其中以国土资源部的统计数据被认为最权威[17]。由于遥感影像解译精度，与实地调查统计相比仍有一定差距，所以大部分学者仍采用统计数据进行研究，而且大多避开了数据有明显变化的过渡年份。目前仅有极少数学者对过渡年份前后时间段的统计数据变化一并进行了相关的分析[17,18]。针对两次全国土地调查的统计数据的跳跃式变化，文章研究提出了基于数据挖掘技术研究分析两个时间段的数量关系，以更科学地反映耕地数量的变化趋势，同时基于校正数值研究影响耕地变化的驱动因子，这在目前的研究中尚未见到，对于科学反映我国耕地变化趋势具有积极的意义。

1 数据与方法

1.1 数据获取

1.1.1 全国耕地数量数据

我国耕地数量，尤其是历史时期的耕地数量，长期以来难以确定。国家土地管理部门从 1986 年开始，每年统计并公布我国耕地的增减情况，虽然还有其他职能部门的统计数据，但仍以国土资源部的数据最为权威[17]。为准确掌握全国耕地数量，1984—1996 年国务院安排开展了全国第一次大规模的土地利用现状调查，数据成果统计到了 1996 年 10 月 31 日，结果表明，1996 年全国耕地面积约为 1.300 亿 hm^2（19.51 亿亩）[18]，这一统计数据被认为具有最高可信度[19]。随后，1996—2008 年耕地面积数据均可直接从统计公报中查得。

为进一步准确掌握耕地土地基础数据，国家于 2007 年 7 月 1 日起，启动了第二次全国土地调查，数据统计时间节点为 2009 年 12 月 31 日，统计结果显示 2009 年我国耕地面积为 1.354 亿 hm^2（20.31 亿亩）[18]。随后的每年都有二调变更调查，2007—2016 年每年的全国耕地面积都可以从国家土地调查成果服务平台直接查得。由于第二次全国土地调查采用的技术方法的改进等原因，2008 年与 2009 年的耕地数量存在“跳跃”现象，为科学分析耕地的变化趋势，这一现象问题在后文中进行了着重的研究处理。

1.1.2 驱动因子数据

土地与人类社会的经济发展密不可分，全国耕地变化是在地理背景制约下、社会经济条件、灾害等自然条件共同驱动下发生的[1]，为探索研究耕地变化的驱动因子，该文主要选取了 3 方面共 17 个因子指标做遴选分析：一方面是反映全国经济发展水平的综合类指标，包括国民总收入、国内生产总值、第一产业增加值及比例、第二产业增加值及比例、第三产业增加值及比例、人均国内生产总值、工业增加值、建筑业增加值、农业总产值；另一方面是反映社会城镇化水平的指标，包括年末总人口、城镇人口、乡村人口；还有第三方面是反映自然灾害的指标，包括受灾面积和粮食产量[20]。上述因子指标近 20 年的数据均

(C)1994-2022 China Academic Journal Electronic Publishing House. All rights reserved. http://www.cnki.net

直接从国家统计局网站查得。

1.2　研究方法

该文研究通过对近 20 年全国耕地数量数据的分析处理，研究其变化趋势，进而通过与选取的因子进行相关性分析，研究其变化的驱动因子。其中，在对 1996—2016 年耕地面积的数据分析中，针对 2008—2009 年数据的跳跃现象，通过数据挖掘，一方面利用 1996—2008 年数据预测 2009 年数据，另一方面利用 2009—2016 年数据反推 2008 年数据，基于上述两种相互预测或反推得出的数值，分析 2008 年和 2009 年耕地数量的数据比例关系，进而对 1996—2016 年耕地面积数据进行比值归一化，以探索研究耕地面积的变化趋势。

该文在数据挖掘预测中，通过遴选对比最终采用的为 ARIMA 模型，即自回归积分滑动平均模型(Autoregressive Integrated Moving Average Model)，是由博克思(Box)和詹金斯(Jenkins)提出的著名时间序列预测方法，主要是指将非平稳时间序列转化为平稳时间序列，然后将因变量仅对它的滞后值以及随机误差项的现值和滞后值进行回归所建立的模型，适用于该文的研究。

2　近 20 年耕地数量变化趋势分析

2.1　基于耕地数量原始统计数据的变化趋势及分析

通过对收集整理的 1996—2016 年耕地数量数据分析，如图 1，可以看出，1996—2008 年全国耕地面积逐年减少，其中以 2000—2004 年递减速度最快；2008—2009 年耕地面积数据出现跳跃，由 1.217 亿 hm^2(18.26 亿亩)增至 1.354 亿 hm^2(20.31 亿亩)；2009—2016 年耕地面积递减速度非常缓慢。

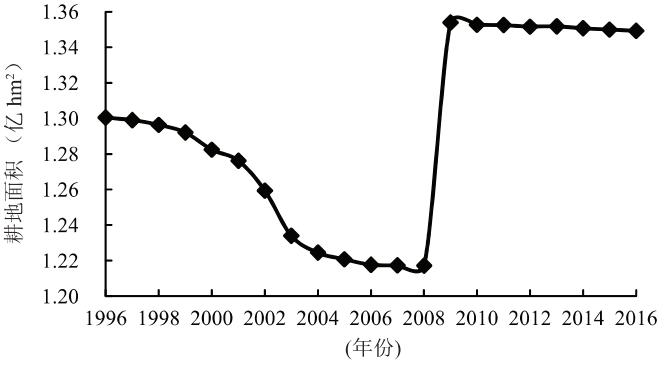


图 1　1996—2016 年基于原始统计数据的耕地数量变化趋势

1996 年国家完成了第一次大规模的土地利用现状调查；2009 年第二次全国土地利用现状调查完成。由此可见，2008—2009 年耕地面积数据的跳跃正是一调与二调数据的分界年份。全国耕地面积是否真的增多了约 0.14 亿 hm^2(2 亿亩)，经文献查阅分析[17,18,21]，主要原因在于二调采用了更为先进的技术手段，将以往少报的耕地面积统计入库，进一步提高了数据的准确度。所以，近 20 年全国耕地数量的统计数据是基于两次不同的技术水平，可直接分别研究各自时段内的变化趋势，但如果要研究连续 20 年时间段内的变化趋势，就须对两个时间段的数据进行校正，使之具有可对比性。

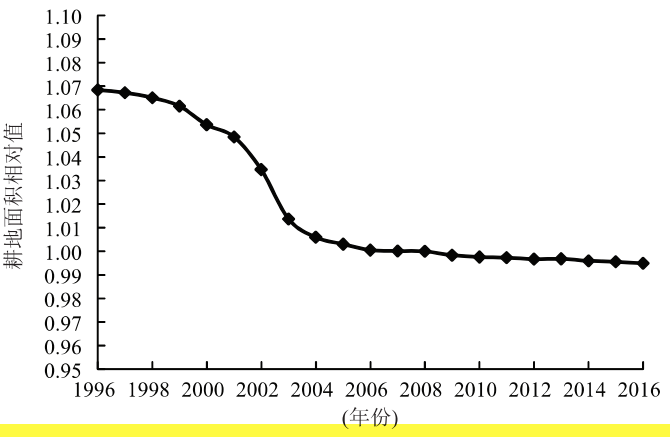


图 2　1996—2016 年基于校正后相对数据的耕地变化趋势

2.2　基于数据挖掘的耕地数量校正

数据挖掘技术在时间序列上具有强有力的预测功能，该文首先利用 1996—2008 年耕地数量数据，预测 2009 年的耕地数量，由此得出 2009 年与 2008 年耕地数量的比值关系 α；然后利用 2009—2016 年耕地数量数据，反推 2008 年的耕地数量，由此得出 2009 年与 2008 年耕地数量的比值关系 β；为更为科学地反映 2009 年与 2008 年耕地数量的比值关系，取利用正向预测与反向反推两种方法得出的 α 与 β 的算数平均值 ρ 作为实际的数量比值关系。

该文研究在预测过程中，利用 SPSS 软件，通过比较分析，在正向预测 2009 年数值和反向反推 2008

(C)1994-2022 China Academic Journal Electronic Publishing House. All rights reserved.　http://www.cnki.net

年数值中均选用 ARIMA 模型，其中正向预测选用的模型为 ARIMA（1，1，2）（$r^2=0.975^{**}$），反向反推选用的模型为 ARIMA（1，1，4）（$r^2=0.966^{**}$），两者均在 0.01 水平呈现显著性。由此，基于 1996—2008 年数据预测得出的 2009 年耕地数量为 1.213 387 亿 hm^2（18.200 8 亿亩），基于 2009—2016 年数据反推得出的 2008 年耕地数量为 1.353 987 亿 hm^2（20.309 8 亿亩），进一步可得出 $\alpha=996\ 899.887\ E-6$，$\beta=999\ 895.617\ E-6$，则 $\rho=998\ 397.752\ E-6$，由此推测 2009 年与 2008 年耕地数量的比值为998 397.752 E－6，即可为两个时间段数据的校正系数。

2.3 基于耕地数量校正相对值的变化趋势分析

为进一步客观的反映近 20 年的耕地数量变化趋势，对全部年份数据进行比值归一化及系数校正，在前文研究基础上，首先对 1996—2008 年全部原始耕地数量数据以 2008 年耕地数量为基数计算得到的比值即为其耕地数量相对值，对 2009—2016 年全部原始耕地数量数据以 2009 年耕地数量为基数计算得到的比值，再乘以校正系数 ρ，即为其相应年份的耕地数量相对值。由此可以得出 1996—2016 年耕地数量的变化趋势，如图 2 所示，可以看出，近 20 年全国耕地数量是呈现递减趋势的，其中 2004 年以前，递减速度较快，2004 年以后耕地数量递减速度较缓，尤其是 2006 年以后耕地数量递减速度趋于稳定。

3 耕地数量变化驱动因子分析

该文研究共收集了 1996—2016 年共 17 个因子指标，首先进行描述性特征统计，如表 1 所示；然后，通过分析耕地数量与各因子指标的相关性（表 2），进行对比分析，以此遴选出耕地数量变化的驱动因子。

表 1 1996—2016 年各因子指标的描述性统计特征

因子	最小值	最大值	平均值	标准差
国民总收入（亿元）	70 780	741 140	304 446.950	225 956.601
国内生产总值（亿元）	71 814	744 127	305 718.670	226 519.843
第一产业增加值（亿元）	13 878	63 671	31 240.710	17 742.619
第一产业增加值占比（%）	8.556	19.325	12.114	3.280
第二产业增加值（亿元）	33 828	296 236	135 629.240	94 949.577
第二产业增加值占比（%）	39.810	47.559	45.327	1.999
第三产业增加值（亿元）	24 107	384 220	138 848.860	114 605.836
第三产业增加值占比（%）	33.569	51.634	42.560	4.472
人均国内生产总值（亿元）	5 898	53 980	22 872	16 332.770
工业增加值（亿元）	29 530	247 860	116 532.760	79 508.293
建筑业增加值（亿元）	4 393	49 522	19 623	15 992.727
年末总人口（万人）	122 389	138 271	131 047.710	4 702.171
城镇人口（万人）	37 304	79 298	58 413.240	12 989.267
乡村人口（万人）	58 973	85 085	72 634.480	8 313.397
农业总产值（亿元）	13 540	59 288	28 842.620	16 570.347
粮食产量（万 t）	43 070	62 144	52 326.480	5 812.061
受灾面积（万 hm^2）	2 177	5 468.8	4 100.948 0	1 070.630

由表 2 可以看出，基于原始统计的耕地面积研究其与各因子指标的相关性，由于数据的跳跃不足以反映耕地变化的实际趋势，与各因子指标的相关性均不高。基于校正后的耕地数量的相对值，研究其与各因子指标的相关性，可以发现，与第一产值增加值占比的相关性最高，相关系数高达 0.959；与年末总人口的相关性次之，为负相关，系数为 －0.918，城镇人口和乡村人口与之的相关性也较高，即第一产业增加值占比，总人口以及城镇人口数量与耕地数量的变化相关性较好，是重要的驱动因子。由此，可以推论出国家产业结构布局调整、我国城镇化建设水平是影响我国耕地数量变化的重要因素条件。耕地作为第一产

(C)1994-2022 China Academic Journal Electronic Publishing House. All rights reserved. http://www.cnki.net

表 2　耕地面积与各因子的相关系数矩阵

	原始统计耕地面积	校正后耕地面积相对值		原始统计耕地面积	校正后耕地面积相对值
原始统计耕地面积	1	-0.142	人均国内生产总值	0.651	-0.749
校正后耕地面积相对值	-0.142	1	工业增加值	0.638	-0.784
国民总收入	0.649	-0.746	建筑业增加值	0.688	-0.716
国内生产总值	0.652	-0.745	年末总人口	0.433	-0.918
第一产业增加值	0.663	-0.736	城镇人口	0.488	-0.896
第一产业增加值占比	-0.274	0.959	乡村人口	-0.518	0.88
第二产业增加值	0.647	-0.774	农业总产值	0.686	-0.709
第二产业增加值占比	-0.519	0.259	粮食产量	0.752	-0.524
第三产业增加值	0.649	-0.717	受灾面积	-0.514	0.708

业的最重要的载体之一，与第一产业增加值密切正相关，我国产业结构中对于第一产业布局要求会直接诱使我国耕地的变化。而城镇化建设过程中，一方面由于城镇建设会直接占用大量的耕地，另一方面，城镇化建设中大量的农民人口直接进入城镇生活，或者进城务工而导致耕地撂荒，所以城镇化建设水平与耕地变化呈现密切的负相关。

4　结论与讨论

土地本身既有自然属性，又有社会属性，对于耕地数量的统计长期以来受社会、经济、政策等诸多因素的影响，导致难以对其进行长时间序列的趋势研究。该文研究的时间序列跨度全国两次土地调查的统计数据，两个时间阶段的数据具有明显的跳跃性，但并不代表 2009 年耕地数量真的比 2008 年大幅度增长。究其原因，主要是由于第二次全国土地调查中应用遥感等新方法、统一了标准，提高了调查的技术水平和准确度，使原来因少报、漏报、瞒报等各种原因未被统计到的耕地重新统计入库，所以要研究跨两个阶段的整体变化趋势，就必须研究建立其数值量化关系。该文通过数据挖掘，并对耕地数量进行校正和比值归一化，研究结果比较准确地反映了我国耕地变化趋势的实际情况。

研究结果表明，近 20 年，我国耕地数量呈现递减趋势，其中 2004 年以前递减速度较快，2004 年以后递减速度趋缓，我国产业结构布局方面，主要是第一产业增加值占比，以及我国人口总数方面，主要是城镇化人口数量是影响变化的主要驱动因子。由于 1999 年后开始生态退耕导致耕地数量迅速减少[17,22]，2004 年国家《土地管理法》修订后强调要加强耕地保护，实行占补平衡，对我国耕地的数量变化产生了积极作用。该文仅对近 20 年我国耕地数量的变化趋势进行了分析；现在国家加强耕地保护，不仅以数量为基础，更关注质量，以产能为核心，实现数量、质量和生态的三位一体保护[23]，下一步将对全国耕地质量的变化趋势进一步分析研究。同时，该文研究通过相关性分析研究提出了主要驱动因子，下一步还将进一步对驱动因子的贡献率进行量化分析研究。

该文研究仅对 1996—2016 年耕地数量的变化趋势进行了分析研究，由于对诸多指标因子数据统计的完整性需求，未对更长时间的耕地变化趋势进行研究。下一步，将在对统计数据分析的基础上，通过对遥感影像的数据挖掘，深入研究更长时间序列的变化趋势。

参考文献

[1] 赵其国，周生路，吴绍华，等. 中国耕地资源变化及其可持续利用与保护对策. 土壤学报，2006，43（4）：662－672.

[2] 葛全胜，戴君虎，何凡能，等. 过去 300 年中国部分省区耕地资源数量变化及驱动因素分析. 自然科学进展，2003，13（8）：825－832.

[3] 毕于运，郑振源. 建国以来中国实有耕地面积增减变化分析. 资源科学，2000，22（2）：8－12.

[4] 李秀彬. 中国近 20 年来耕地面积的变化及其政策启示. 自然资源学报，1999，14（4）：329－333.

(C)1994-2022 China Academic Journal Electronic Publishing House. All rights reserved.　http://www.cnki.net

[5] 曹银贵，袁春，周伟，等. 中国耕地变化的驱动因子及其省域差异分析. 中国土地科学，2008，22（2）：17－22.
[6] 黄忠华，吴次芳，杜雪君. 我国耕地变化与社会经济因素的实证分析. 自然资源学报，2009，24（2）：192－199.
[7] 郭丽英，王道龙，王介勇. 中国沿海地区耕地变化及其成因分析. 中国农业资源与区划，2012，33（1）：6－10.
[8] 吴霞，王世荣，尚红莺，等. 宁夏近 18 年来耕地面积动态变化及驱动力分析. 中国农业资源与区划，2017，38（8）：98－104.
[9] 武江民，赵学茂，党国锋. 甘肃兰州市耕地动态变化与驱动力关系定量研究. 干旱区资源与环境，2010，24（12）：33－38.
[10] 于天，曹银贵，许婧雪. 基于不同尺度的中国耕地变化驱动力研究进展. 中国农学通报，2016，32（24）：194－198.
[11] 张国平，刘纪远，张增祥. 近 10 年来中国耕地资源的时空变化分析. 地理学报，2003，58（3）：323－332.
[12] 田光进，庄大方，刘明亮. 近 10 年中国耕地资源时空变化特征. 地球科学进展，2003，18（1）：30－36.
[13] 刘旭华，王劲峰，刘纪远，等. 国家尺度耕地变化驱动力的定量分析方法. 农业工程学报，2005，21（4）：56－60.
[14] 刘旭华，王劲峰，刘明亮，等. 中国耕地变化驱动力分区研究. 中国科学 D 辑地球科学，2005，35（11）：1087－1095.
[15] 许丽丽，李宝林，袁烨城，等. 2000—2010 年中国耕地变化与耕地占补平衡政策效果分析. 资源科学，2015，37（8）：1543－1551.
[16] 李景刚，何春阳，史培军，等. 近 20 年中国北方 13 省的耕地变化与驱动力. 地理学报，2004，59（2）：274－282.
[17] 封志明，刘宝勤，杨艳昭. 中国耕地资源数量变化的趋势分析与数据重建：1949—2003. 自然资源学报，2005，20（1）：35－43.
[18] 谭永忠，何巨，岳文泽，等. 全国第二次土地调查前后中国耕地面积变化的空间格局. 自然资源学报，2017，32（2）：186－197.
[19] Lin G C S，HO S P S. China´s land resources and land-use change：insights from the 1996 land survey. land Use Policy，2003，20（2）：87－107.
[20] 傅泽强，蔡运龙，杨友孝，等. 中国粮食安全与耕地资源变化的相关分析. 自然资源学报，2001，16（4）：313－319.
[21] 张雅琼，杨子生. 我国两次土地资源调查的对比分析. 国土资源科技管理，2013，30（2）：100－104.
[22] 徐宪立，蔡玉梅，张科利，等. 耕地资源动态变化及其影响因素分析. 中国人口·资源与环境，2005，15（3）：75－79.
[23] 谭永忠，吴次芳，王庆日，等. “耕地总量动态平衡”政策驱动下中国的耕地变化及其生态环境效应. 自然资源学报，2005，20（5）：727－734.

RESEARCH ON THE CHANGE TREND OF FARMLAND QUANTITY IN CHINA FOR RECENT 20 YEARS AND ITS DRIVING FACTORS*

Wang Jingyi[1], Li Xiaoming[2]※

(1. Xi´an Shiyou University, Xi´an, Shaanxi 710065, China;
2. Shaanxi Provincial Land Engineering Construction Group, Xi´an, Shaanxi 710075, China)

Abstract The research aims to research the changing trend of farmland quantity for recent 20 years before and after the second national land use survey. It could provide decision support for farmland protection and efficient use of land resources. The original data of farmland area from 1996 to 2016 were collected, data mining technology was introduced, and ARIMA model was chosen to predict the farmland quantity each other based on the farmland area of the twice land use survey, which meant to predict the farmland quantity of 2009 with the farmland quantity of the years from 1996 to 2008, and to predict the farmland quantity of 2008 inversely with the farmland quantity of the years from 2009 to 2016, so the original farmland area data could be corrected and normalized. Then the changing trend of farmland quantity for recent 20 years was studied furtherly and correlation analysis was used to study the driving factors. The trend research result showed, the farmland area decreased year by year for recent 20 years, the decreasing rate was faster before 2004, and then it decreased slowly. The correlation analysis result showed, the added value proportion of primary industry, the total population, and the urban population were the most important driving factors which influenced the farmland quantity change, their coefficients were 0.959, －0.918 and －0.896 respectively. It could be concluded by the result that the industry configuration and the urbanization could affect the farmland quantity with the development of social economy.

Keywords data mining; ARIMA model; farmland quantity; change trend; driving factors

(C)1994-2022 China Academic Journal Electronic Publishing House. All rights reserved. http://www.cnki.net

附录3

补充说明对于计算机学院职称评审推荐排序的异议

尊敬的学校纪委领导：

（1）2023 年 11 月 15 日计算机学院进行了 2023 年副教授职称评审推荐排序，会上刘某某教授首先发言力推王静怡老师，但是王静怡老师的学术成果存在争议，这种争议源于三年前王静怡老师申请的国基金遭到公开信举报，当时学校很多人都收到了这封公开信。当年学院给出的调查结论是王静怡老师的国基金项目是借鸡生蛋。会上有教授为此与刘某某教授产生了争执。刘某某教授认为应该按照既定事实排序。其他教授及副教授系主任均未发言表态。在这种情况下，学院职称评审组未按照西石大人〔2023〕143 号关于印发《西安石油大学职称评审暂行实施办法》的通知第 41 条相关规定：基层单位评审推荐组**根据申请人的思想政治条件、教育教学水平、学术水平、工作业绩和社会贡献，并参考民主评测结果，进行充分评议**的要求，**在未进行充分评议的情况下单独使用手机匿名投票的结果进行排序**，最终存在学术争议的王静怡老师排在材料明显占优的老师之前，且会场上只公布了排序结果，并未公布手机投票的具体票数。

（2）计算机学院以往的职称推荐都会开全院大会，由拟评职称老师公开述职再进行评议，例如本人参评的 2019 年和 2020 年都是召开全院大会述职，2021 年学院只有本人一人参评副教授不存在排序问题没有召开全院大会述职，但是 2023 年三人参评副教授却只召开职称评审组 12 人的会，从组织形式来看不符合学校要求的基层单位对职称评审推荐应该精心组织的基本要求，也不符合计算机学院职称评审以往的惯例。

（3）〔2023〕143 号关于印发《西安石油大学职称评审暂行实施办法》第十九条特殊情况下的职称评审问题第九款经学校认定有剽窃他人成果及**违反学术道德者，取消其参评资格**，并按国家有关规定处理。2023 年 11 月 15 日职称评审推荐排序结果公示后，本人第一时间向学院排序结果提出异议并指出两位老师存在学术不端问题，学院拖延推诿不予处理。学院做法消极且不负责任，违反了〔2023〕143 号关于印发《西安石油大学职称评审暂行实施办法》第十九条的相关规定。

（4）〔2023〕143 号关于印发《西安石油大学职称评审暂行实施办法》第第四十九条 拟推荐人员**公示无异议后，依次排序向学校专业学科组推荐**。计算

机学院职称评审推荐排序结果2023年11月15日公示后，本人第一时间提出异议。但学院推诿拖延不予处理，不知目前是否仍将存在问题（学术不端）的排序公示结果向学校专业学科组推荐？计算机学院如不采取相应处理，继续依旧向学校专业学科组推荐，则计算机学院的做法就违反了第四十九条的相关规定。

我也知道，有些情况下，制造问题的人不是问题，指出问题的人是问题，此次提出异议必将成为有些人的眼中钉、肉中刺，但我愿意相信学校纪委会从大局学校发展出发，对不公正现象以及学术不端进行查处，扭转不良风气，促进建立更公正的评价环境，使更多的教师能投入更多心力于教学科研，真正推动学校发展。请学校纪委依据〔2023〕143 号关于印发《西安石油大学职称评审暂行实施办法》和西石大科〔2022〕182 号关于印发《西安石油大学学术道德与科研诚信管理办法（试行）》的通知等文件的相关规定，履行监督职责，促使本人提出的问题能够第一时间得到妥善解决。

此致

敬礼

2023年11月16日

附录4

本人对计算机学院关于学术不端的调查程序和结论不满，请求复核

尊敬的纪委职称评审联合检查组领导：

今天上午纪委综合室领导对我举报的学术不端行为的调查结果进行了回复。学术不端行为受理后，纪委将相关举报材料对人事处和科技处进行了转办，学院进行了调查，组织了两名院内教授和两名校外教授进行了对相关论文进行了评议，学院综合专家意见认为不存在学术不端。本人对调查流程及结果均不服，特此提出异议，请纪委领导履行监督职责，推动相关职能部门能真正认真、本着对学校发展和当事人发展的出发点开展调查工作。具体不服的原因有以下几点：

（1）计算机学院进行调查，委托了两位院内教授和两位校外教授对涉嫌重复发表的论文进行了评阅。因为纪委综合室不给我调查反馈书面意见，也坚决不允许我对调查反馈材料复印也不允许我拍照，我只能根据自己现场阅的情况进行说明，无法做到绝对与原件逐字完全一致。现在反馈回来的结果可以清楚的看出，贵州大学田有亮教授认为李小和老师的三篇论文是用改进很少的方法研究同一个问题，差别很少，雷同很多。王静怡老师的两篇论文属于将同一工作先英文投会议发表，后又用中文在中文期刊发表，田教授认为建议作者至少应扩展新内容 70%以上再发表。西安邮电大学陈彦萍教授认为李小和老师的三篇论文结构、内容重复很多。认为王静怡老师的论文雷同很多。学院程国建教授认为李小和老师的三篇论文做了一些改进，有重复。王静怡老师的雷同无法简单合理界定。学院刘某某教授认为李小和的三篇均存在改进，王静怡有权对自己的英文论文翻译后扩展再发表。四位专家中，两位校外专家均认为李小和老师的三篇论文针对统一问题改进很少，重复很多。两位校外专家均认为王静怡老师的两篇论文雷同，田有亮教授认为王静怡老师如要将同一工作的英文文章再次发表应至少扩充新内容 70%以上。学院专家程国建教授认为李小和老师三篇论文存在重复，王静怡老师的雷同无法简单合理界定。综合来看，四位教授中，只有刘某某教授明确指出两位老师均无学术不端。其他三位教授反而均指出两位老师的论文中存在的学术不端表现。

（2）计算机学院委托两位院内教授评议两位老师学术不端的论文，而这两位教授都是 2023 年 11 月 15 日计算机学院职称评审推荐排序会上参会的教授。

本人对计算机学院的评审推荐排序不满，如果要评议两位老师的涉嫌论文学术不端，计算机学院应避开邀请参加过评审推荐会的教授再次评议。

（3）对于四位教授中只有一位院内教授认为不存在学术不端，两位校外教授明确指出论文中存在的学术不端表现，一位院内教授认为无法简单合理界定，这样的情况下，计算机学院以“综合专家意见，认为不存在学术不端”，这种结论显然不负责任，“综合”两字不应被滥用，“综合”不应无视专家的意见，“综合”不应该成为不公正的代名词。

（4）计算机学院以对三位教师投票进行排序，对于我提出的本人教育教学、科研论文、社会服务等方面均优于李小和和王静怡老师，计算机学院再次以排序是综合评定为由掩盖其不公正。根据校发西石大人〔2023〕143 号 关于印发《西安石油大学 职称评审暂行实施办法》第 49 条，基层单位评审推荐根据申请人的思想政治条件、教育教学水平、学术水平，三位老师的思想政治条件均为合格，本人教育教学、科研论文、社会服务等方面均优于李小和和王静怡老师，为什么本人要排在三位老师的最后？综合评定不应成为不公正的代名词。

（5）计算机学院在向职能部门人事处反馈的书面意见中提到，我本人的学会任职、期刊审稿人、解决企业技术问题获得媒体报道、以及担任海尔技术咨询专家为海尔提供技术咨询服务等不属于社会服务，这不符合西石大人〔2023〕143 号 关于印发《西安石油大学 职称评审暂行实施办法》第 49 条第十七条第六款的规定，我的这些业绩属于文件规定的社会服务中的科技服务、重要学术组织或期刊兼职、专家咨询等内容。本人除了校外社会服务外，还积极参与专业认证、专业建设、学科评估等校内公共服务。而李小和老师和王静怡老师没有校外社会服务内容，只有校内社会服务。因此，本人在社会服务这一项中也明显优于李小和老师和王静怡老师。计算机学院的“综合评定”到底是如何综合评定的，这显然属于不公正推荐排序。

（6）计算机学院在向职能部门人事处反馈的书面意见中提到，学院报请学校学术道德委员会主任，认为无需上会讨论。按照西石大科〔2022〕182 号 关于印发《西安石油大学学术道德与科研诚信管理办法（试行）》的通知第十二条 学术不端行为受理后，交由院（系）等依托单位按照相关程序组织开展调查，提供学术判断（包括学术不端行为责任人的确认、调查过程、事实认定及理由、

调查结论等）；然后交由校学术道德专门委员会核实，提出初步认定处理意见；最后交由校学术委员会认定和处理。计算机学院应将学术判断（包括学术不端行为责任人的确认、调查过程、事实认定及理由、调查结论等）等交由校学术道德专门委员会核实，而不是含糊的报请校学术道德专门委员会主任。计算机学院应将调查的专家意见、本人的书面意见、两位老师涉嫌学术不端的论文等完整交由校学术道德专门委员会，由校学术道德专门委员会提出处理意见。目前人事处反馈给纪委的调查材料中并未见到校学术道德专门委员会的处理意见。这属于调查程序不完整。

综合以上六点，本人对计算机学院所谓的调查过程以及调查结论“两位老师不存在学术不端”不满，请求纪委依据职称评审的监督职责，责成职能部门依据《西安石油大学学术道德与科研诚信管理办法（试行）》的通知真正依据专家评议意见给出是否存在学术不端的结论，公正的开展调查，并向校学术道德专门委员会报送完整的调查材料以便校学术道德专门委员会核实处理。

此致

敬礼

2023 年 11 月 22 日

附录5

申诉申请书

陕西省教育厅人事处 教师工作处：

您好，我是西安石油大学计算机学院的一名教师，现向贵处申诉西安石油大学职称评审中对于举报参评教师存在涉嫌重复发表的学术不端行为采用消极应对走流程、调查程序不完整不规范、事实不清、推诿搪塞等问题，致使存在涉嫌学术不端且成果单薄压线的老师一路绿灯通过职称评审进而公示，成果明显丰富且完全符合条件的教师在学院排末尾向学科组推荐进而无缘于职称晋升。在2023年西安石油大学计算机学院的职称评审推荐排序上，存在显著不公，且王静怡老师存在严重的学术不端。2023年11月15日计算机学院职称推荐排序公示后，我向学院提出异议。学院答复我不存在不公，程序没有问题。我提出了书面意见，指出王静怡老师存在学术不端，计算机学院不接收书面材料，让我向相关部门反映。我于2023年11月17日将书面意见以及涉嫌学术不端的论文向纪委提交，后纪委向人事处转办。人事处转办给科技处，科技处转办给计算机学院开展自查。计算机学院开展调查后，又存在调查程序不完整不规范、调查结论不依据专家意见等包庇纵容情况，我对计算机学院的调查存在异议。2023年11月26日，西安石油大学2023年职称拟晋升人员公示，公示期为2023年11月26日-12月1日。2023年11月29日我向西安石油大学人事处提交书面异议。具体有以下六点理由：

（1）计算机学院进行调查，委托了两位本学院教授和两位校外教授对涉嫌重复发表的论文进行了评阅。因为纪委综合室不给我调查反馈书面意见，也坚决不允许我对调查反馈材料复印也不允许我拍照，我只能根据自己现场阅的情况进行说明，无法做到与原件逐字绝对完全一致。现在反馈回来的结果可以清楚的看出，贵州大学田有亮教授认为王静怡老师的两篇论文属于将同一工作先英文投会议发表（文章[5]），后又用中文在中文期刊发表（文章[6]），田教授认为建议作者至少应扩展新内容70%以上再发表。西安邮电大学陈彦萍教授认为王静怡老师的论文（文章[5]和文章[6]）雷同很多。计算机学院程国建教授认为王静怡老师的雷同（文章[5]和文章[6]）无法简单合理界定。计算机学院刘某某教授认为王静怡有权对自己的英文论文翻译后扩展再发表。四位专家中，两位校外专家均认

为王静怡老师的两篇论文（文章[5]和文章[6]）雷同，田有亮教授认为王静怡老师如要将同一工作的英文文章再次发表应至少扩充新内容 70%以上。计算机学院程国建教授认为王静怡老师的雷同无法简单合理界定。综合来看，四位教授中，只有刘某某教授明确指出王静怡无学术不端。其他三位教授都指出王静怡的两篇论文雷同很多。

（2）计算机学院委托两位院内教授评议王静怡老师涉嫌学术不端的论文，而这两位教授都是 2023 年 11 月 15 日计算机学院职称评审推荐排序会上参会的教授。需要指出的是，程国建教授因与王静怡有合作研究关系（程国建教授或指导研究生发表论文标注王静怡国基金基金号），并不适宜担任评阅专家。本人对计算机学院的评审推荐排序不满，如果要评议王静怡老师的论文是否涉嫌学术不端，计算机学院应避开邀请参加过评审推荐会的教授和与王静怡有合作研究的教授评议。应该邀请独立第三方的教授对涉嫌重复发表的论文进行评议，并请专家明确给出是否存在重复发表的结论。

（3）对于四位教授中只有一位院内教授认为不存在学术不端，两位校外教授明确指出论文中存在的学术不端表现（雷同），一位院内教授认为无法简单合理界定，这样的情况下，计算机学院以“综合专家意见，认为不存在学术不端”，这种结论显然不负责任，“综合”两字不应被滥用，“综合”不应无视专家的意见，“综合”不应该成为不公正的代名词。

（4）计算机学院以对教师以投票进行职称评审推荐排序，对于我提出的本人教育教学、科研论文、社会服务等方面均优于王静怡老师，计算机学院再次以排序是基于综合评定为由掩盖其不公正。我 2023 年 11 月 15 日对计算机学院的排序提出异议后，计算机学院答复我排序是基于投票。我质疑排序应该基于思想政治条件、教育教学水平、学术水平和社会服务，计算机学院向人事处的答复又变成了排序是基于综合评价。根据校发西石大人〔2023〕143 号 关于印发《西安石油大学职称评审暂行实施办法》第 49 条，基层单位评审推荐根据申请人的思想政治条件、教育教学水平、学术水平，两位老师的思想政治条件均为合格，本人教育教学、科研论文、社会服务等方面均优于王静怡老师，为什么本人要排在王静怡老师之后？综合评定不应成为不公正的代名词。

（5）计算机学院在向职能部门人事处反馈的书面意见中提到，本人的学会任职、期刊审稿人、解决企业技术问题获得媒体报道、以及担任海尔技术咨询专家为海尔提供技术咨询服务等不属于社会服务，这不符合西石大人〔2023〕143号关于印发《西安石油大学职称评审暂行实施办法》第49条第十七条第六款的规定，本人的这些业绩属于文件规定的社会服务中的科技服务、重要学术组织或期刊兼职、专家咨询等内容。本人除了校外社会服务外，还积极参与专业认证、专业建设、学科评估等校内公共服务。而王静怡老师没有校外社会服务内容，只有校内社会服务。因此，本人在社会服务这一项中也明显优于王静怡老师。计算机学院的“综合评定”到底是如何综合评定的？这显然属于不公正推荐排序。

（6）计算机学院在向职能部门人事处反馈的书面意见中提到，学院报请学校学术道德委员会主任，认为无需上会讨论。按照西石大科〔2022〕182 号关于印发《西安石油大学学术道德与科研诚信管理办法（试行）》的通知第十二条 学术不端行为受理后，交由院（系）等依托单位按照相关程序组织开展调查，提供学术判断（包括学术不端行为责任人的确认、调查过程、事实认定及理由、调查结论等）；然后交由校学术道德专门委员会核实；最后交由校学术委员会认定和处理。计算机学院应将学术判断（包括学术不端行为责任人的确认、调查过程、事实认定及理由、调查结论等）等交由校学术道德专门委员会核实，而不是含糊的报请校学术道德专门委员会主任，校学术道德专门委员会主任认为无需上会讨论。调查组应将调查的专家意见、本人的书面意见、两位老师涉嫌学术不端的论文等完整交由校学术道德专门委员会，由校学术道德专门委员会核实，最后由校学术委员会认定和处理。目前人事处反馈给纪委的调查材料中并未见到校学术道德专门委员会的意见。这属于调查程序不完整。

综合以上六点，本人对计算机学院所谓的调查过程以及调查结论“不存在学术不端”存在异议，希望学校能真正依据西石大人〔2023〕143 号关于印发《西安石油大学职称评审暂行实施办法》、西石大科〔2022〕182 号关于印发《西安石油大学学术道德与科研诚信管理办法（试行）》的通知等文件，真正重视职称评审对于教师及学校发展的重要意义，真正重视学风建设，真正落实对学术不端零容忍、一票否决，真正切实公平公正评价教师，责成计算机学院依据《西安石油大学学术道德与科研诚信管理办法（试行）》的通知公正的开展调查，真正依

据专家评议意见给出是否存在学术不端的负责任的学术判断，并向校学术道德专门委员会报送完整的调查材料以便校学术道德专门委员会核实处理。

2023 年 12 月 11 日，西安石油大学人事处当面答复，调查结果为仅仅告知我结论：不存在学术不端。但对于学术道德委员会是否上会核实、校学术委员会是否认定、事实认定及理由等内容均不予以告知。我又当面陈述意见，希望学校对我提出的六点理由给出具体的答复不要一味的仅仅告知结论。人事处记录后说会向科技处告知我的意见。2023 年 12 月 12 日，人事处电话答复，说领导非常重视，现在再次告知我结论：不存在学术不端。我再次提出希望对六点理由给出具体的答复。人事处告知我他们只是调查结论的应用方，具体过程无法告知。

王静怡老师涉嫌学术不端的情况在此向省教育厅做一说明，具体包括王静怡老师的学习、工作经历以及涉嫌存在学术不端的情况。

1.王静怡老师的教育经历为本、硕、博均为通信工程。具体学习经历为：

2010/03~2016/06，西安电子科技大学，通信与信息系统，博士

2007/09~2010/03，西安电子科技大学，通信与信息系统，硕士

2002/09~2006/07，西安邮电大学，通信工程，学士

具体工作经历为：

2016/07~至今，西安石油大学计算机学院，教师

2. 王静怡老师涉嫌学术不端主要表现为成果发表中存在连续多次重复发表的情况。王静怡老师第 1 次重复发表出现在 2013 年读博士期间，第 2 次重复发表出现在 2016 年读博士期间，第 3 次重复发表出现在入职西安石油大学后 2019 年。6 篇论文涉嫌重复发表，具体如下：

(1)读博士期间第 1 次重复发表

[1] 王静怡, 李颖, 孙岳. 速率兼容网络 LDPC 码的设计[C]//中国通信学会. 第十七届全国青年通信学术年会论文集. 西安电子科技大学综合业务网理论及关键技术国家重点实验室, 2012:5.

[2] 王静怡*, 李颖, 孙岳. 适用于网络 LDPC 码的速率兼容算法. 西安电子科技大学学报,2013, 40(2): 13-17.

文章[1]和[2]属于中文一稿双发。文章[1]于 2012 年 7 月底在会议上发表，文章[2]于 2013 年 4 月于西安电子科技大学学报上发表。文章[2]既没有引用文章[1],文章

[2]也没有在首页对文章已经发表过做任何说明，文章[1]和[2]完全雷同，属于重复发表。文章[1]和[2]的名字经过刻意调整顺序重构。

(2)读博士期间第 2 次重复发表

[3] Jingyi Wang, Shuling Che, Ying Li, Optimal design of the Joint network LDPC Codes over Orthogonal Multiple-Access Relay Channel. 2013 5th International Conference on Intelligent Networking and Collaborative Systems, 2013. XI'AN: IEEE, 622-625.

[4] Jingyi Wang*, Shuling Che, Ying Li and Junlong Wang, Optimal design of Joint network LDPC Codes over Orthogonal Multiple-Access Relay Channel. International Journal of Grid and Utility Computing, UK., 2016, 7(1): 68-74.

文章[3]和文章[4]属于英文一稿双发，文章[3]2013 年发表，文章[4]2016 年发表。文章[4]首页虽有标注了文章[4]为文章[3]的改写和扩展，但两篇文章整体内容、结构、图表以及结论雷同，且整段整段的文字写法均完全一样，雷同率至少超过60%以上，也就是说文章[3]和[4]的大部分（过半）雷同，文章[4]不具备科研成果三性中的新颖性，属于明显不符合成果发表规范。

另文章[3]在申报陕西省科技厅项目基于信息物理融合的智能油田监控系统关键技术研究（2020GY-038）（已立项）时论文名字被篡改为 Jingyi Wang*, Shuling Che, Ying Li and Junlong Wang. Optimal design of the joint network LDPC codes for half-duplex coopreative multi-Access relay channel. 2013 5th International Conference on Intelligent. 2013. USA: IEEE, 622-625.

“Optimal design of the joint network LDPC codes for half-duplex coopreative multi-Access relay channel”在 EI 数据库中经过检索不存在，后通过文章发表时间、页码范围搜索发现文章[3]应为：

Jingyi Wang, Shuling Che, Ying Li, Optimal design of the Joint network LDPC Codes over Orthogonal Multiple-Access Relay Channel. 2013 5th International Conference on Intelligent Networking and Collaborative Systems, 2013. XI'AN: IEEE, 622-625。

另于王静怡 2016 年 4 月博士论文末尾攻读博士期间论文成果（博士论文 99 页）未发现会议论文“Optimal design of the joint network LDPC codes for half-duplex

coopreative multi-Access relay channel”而是会议论文“Optimal design of the Joint network LDPC Codes over Orthogonal Multiple-Access Relay Channel”。

由此可见王静怡老师为避免论文同名易被发现一稿双发，将文章[3]名称由“Optimal design of the Joint network LDPC Codes over Orthogonal Multiple-Access Relay Channel”篡改成了“Optimal design of the joint network LDPC codes for half-duplex coopreative multi-Access relay channel”，但在文章[4]的首页王静怡老师准确写出 2013 年会议论文名称为“Optimal design of the Joint network LDPC Codes over Orthogonal Multiple-Access Relay Channel”。王静怡将会议名称由“2013 5th International Conference on Intelligent Networking and Collaborative Systems”改为了“2013 5th International Conference on Intelligent”，会议举办地由“XI’AN”改为了“USA”，可见此番篡改论文名称、会议名称、会议举办地属于刻意为之。

(3)入职西安石油大学后第 3 次重复发表，并作为评职称成果提交压线职称评审论文最低条件

[5] WangJingyi , Li Xiaoming*.Research on the changing trend of farmland area in China and its driving factors from 1996 to 2016[C]. IOP Conference Series Materials Science and Engineering, IOP Conference Series: Earth and Environmental Science(EES), 6 月 22 日~24 日, 珠海, 中国, 2018.

[6]王静怡,李晓明*.近 20 年中国耕地数量变化趋势及其驱动因子分析*[J].中国农业资源与区划,2019,40(08):171-176.

文章[5]和[6]属于中英文一稿双发，文章[5]英文先于 2018 年在国内举办的国际会议发表，文章[6]为 2019 年在国内中文期刊发表。文章[6]中对文章之前已经发表情况未做任何说明，也没有引用[5]。王静怡第 1 次重复发表始于 2013 年，2016 年第 2 次重复发表时在文章[4]的首页还标注了此论文曾经发表，此次为改写扩展的说明。但在 2019 年第 3 次重复发表时，却在文章[6]中对文章[5]曾经发表过没有做任何说明，这说明王静怡重复发表是明知故犯。为了避免被易于发现一稿双发，文章[5]的名字“Research on the changing trend of farmland area in China and its driving factors **from 1996 to 2016**”在文章[6]再次重复发表时改成了“**近 20 年**中国耕地数量变化趋势及其驱动因子分析 ”。文章[6]在文章[5]的 20 篇参考文

献基础上仅增加了 3 篇参考文献，文章[6]和[5]雷同率超过 90%，文章[6]和[5]整体内容、结构、图表以及结论高度雷同，仅仅在第一部分介绍部分有少量差异，其余均雷同，雷同率超过 90%。文章[6]不具备科研成果三性中的新颖性，属于重复发表。

最后，恳请陕西省教育厅人事处、教师工作处亲自调查或委托独立第三方调查，如果举报属实请求取消王静怡的职称评审资格或撤销其通过学术不端所获副教授职称并公开通报处理结果，借此申诉促使西安石油大学能进一步公正评价教师，优化职称评审办法及细则，真正重视学风建设，使在办公室主打聊天、人际活动且在科研活动中持续涉嫌重复发表且成果单薄的教师能得到惩戒，使兢兢业业从事教学、科研、社会服务的老师能有机会获得公平公正和发展，最终使得我们西安石油大学能发展的更好。

随信附王静怡重复发表论文[1]-[6]、博士学位论文、西石大人〔2023〕143 号关于印发《西安石油大学职称评审暂行实施办法》、西石大科〔2022〕182 号关于印发《西安石油大学学术道德与科研诚信管理办法（试行）》的通知。

此致

敬礼

2023 年 12 月 12 日

The Design of Rate Compatible Network LDPC Codes

Jingyi Wang，Ying Li，Yue Sun，
State Key Lab. of Integrated Service Networks, Xidian Univ., Xi'an , China

Abstract: This paper studies the design of rate compatible network LDPC codes and proposes a rate-compatible puncturing algorithm, which can obtain the minimum error probability. First, based on the structure of network LDPC codes, the recovery error probability is derived. Then an algorithm of finding variable nodes to be deleted based on the tanner graph of network LDPC codes is proposed, which is aimed at minimizing the decoding error probability and optimizing the puncturing pattern. Simulation results show that the proposed methods of rate-compatible network-LDPC codes have 0.4dB of gain at $BER=10^{-4}$ in error performance compare to the existing punctured methods.

Keywords: multi-access relay channel; Network-LDPC code; rate-compatible; puncturing

速率兼容网络 LDPC 码的设计

王静怡，，李颖，孙岳
西安电子科技大学　综合业务网理论及关键技术国家重点实验室，西安，中国，710071

摘　要：本文研究了网络 LDPC 码的速率兼容算法设计，提出了一种可以获得最低译码错误概率的速率兼容删余算法。首先针对网络 LDPC 码的结构特点，推导了译码恢复错误概率，并基于网络 LDPC 码的 Tanner 图搜索需要删余的变量节点，并以达到最小译码错误概率为目标，获得最优的删余图样。仿真结果表明，与采用现有算法获得的网络 LDPC 码相比，采用所提的改进速率兼容算法获得的网络 LDPC 码的性能在 $BER=10^{-4}$ 时有 0.4 个 dB 的性能增益。

关键词：多址接入信道；网络 LDPC 码；速率兼容；删余

1　引言

无线通信系统中采用中继协作传输技术，可以获取额外的分集增益，从而改善系统性能。但是，对于多址接入中继网络，有多个节点同时需要中继节点帮助转发数据，传统的译码转发或者放大转发模式，会使得中继转发效率降低。因此，通过在中继节点设计有效的联合网络-信道编码算法，在改善接收端性能的同时提高转发效率，是目前的研究热点之一。文献[4]利用低密度奇偶校验(LDPC)码，针对多址接入中继信道设计了一种网络 LDPC 码，并指出可以通过调整中继节点转发数据量来实现中继转发效率和接收端译码性能的有效折中。但是，文中并没有给出具体实现算法，本文将在此基础上，研究适用于网络 LDPC 码的速率兼容算法。

速率兼容码的概念由文献[1]首次提出，文中研究了速率兼容卷积码的设计。删余是实现速率兼容的一种常用方法，即通过将低码率母码中的某些编码比特删余来获取高码率码。速率兼容 LDPC 码的设计是近几年研究热点，文献[2，3]通过分组和排序操作，将 LDPC 码的变量节点按照迭代恢复次数进行分类，设计了 LDPC 码速率兼容删余算法。

资助信息：国家自然基金项目(61072064)；国家科技重大专项(2010ZX03003-003-03)；长江学者和创新团队发展计划资助(IRT0852)；中央高校科研业务费专项资金项目(K50510010026).

(C)1994-2023 China Academic Journal Electronic Publishing House. All rights reserved.　http://www.cnki.net

2 适用于多址接入中继信道的网络 LDPC 码

由两个源节点和一个中继节点构成的多址接入中继网络模型如图 1 所示，两个源节点与目的节点之间的信息传输由广播发送和中继转发两个阶段完成。在广播阶段，两个源节点分别向中继节点和目的节点广播发送编码序列 X_1 和 X_2；在中继转发阶段，中继节点首先对接收信号进行译码，得到两个源节点的估计数据，然后对译码得到的估计数据重新进行联合编码，并将编码序列 X_R 转发至目的节点。目的节点则根据收到的信号进行联合译码，得到两个源节点的估计信息。

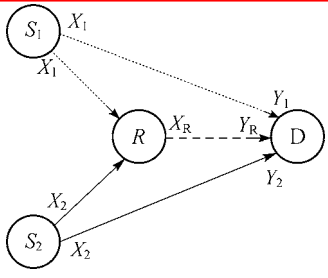


图 1　多址接入中继信道模型

在目的节点端将两个源节点和中继节点采用的 LDPC 码综合考虑，得到如下校验矩阵

$$\boldsymbol{H}=\begin{pmatrix}\boldsymbol{H}_1 & \boldsymbol{0} & \boldsymbol{0}\\ \boldsymbol{0} & \boldsymbol{H}_1 & \boldsymbol{0}\\ \boldsymbol{A} & \boldsymbol{B} & \boldsymbol{C}\end{pmatrix} \qquad (0)$$

式中，$\boldsymbol{H}_1$ 是源节点采用 LDPC 码的校验矩阵，$\boldsymbol{H}_3=(\boldsymbol{A}\quad \boldsymbol{B}\quad \boldsymbol{C})$ 是中继节点采用 LDPC 码的校验矩阵和 $\boldsymbol{0}$ 是零矩阵。由于式(1)中包括了源节点和中继节点所采用 LDPC 码的校验矩阵，并且中继节点是对两个源节点的数据进行联合编码，因此文献[4]称之为网络 LDPC 码，该码的 Tanner 图如图 2 所示。

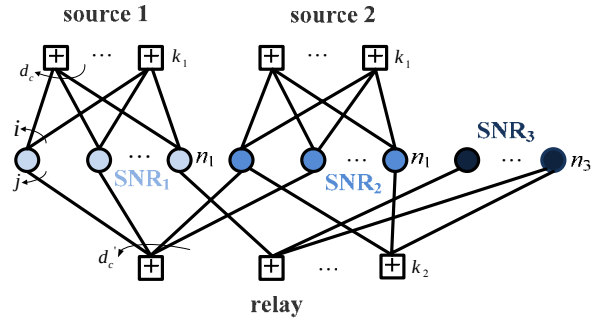


图 2　网络 LDPC 码的 Tanner 图

由图 2，网络 LDPC 码的 Tanner 图中包含上下两层子图，其中上层子图包含 $2k_1$ 个校验节点，它们与变量节点连接关系由式(1)中的 $\boldsymbol{H}_1$ 确定；下层子图包括 k_2 个校验节点，它们与变量节点的连接关系由式(1)中的 $\boldsymbol{H}_3$ 确定。图中每个变量节点的度用 (i,j) 表示，其中 i 为变量节点与上层校验节点相连的边数，j 为变量节点与下层校验节点相连的边数，d_c 和 d_c' 分别表示上层和下层校验节点的度数。

3 速率兼容网络 LDPC 码的设计

3.1 几个定义

定义 1(n 步恢复变量节点)：第 n 次迭代译码时才可以恢复的被删除的变量节点称为 n 步恢复变量节点，用 n-SR 表示。n-SR 的集合用群 G_n 表示。

定义 2(幸存校验节点)：如果一个一步恢复的删余变量节点至少与一个校验节点相连，且与这个校验节点相连的其它变量节点没有都被删余掉，那么这个校验节点就是幸存校验节点。图 3 中的校验节点 S_1 和 S_2 即为幸存校验节点。相反，校验节点 D 即为死校验节点。

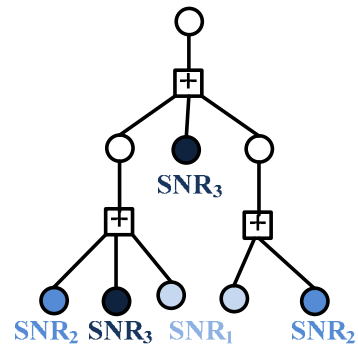


图 3　网络 LDPC 码的恢复树(横线圆表示幸存的变量节点 $S(v)$，竖线圆表示删掉的变量节点)

定义 3(幸存变量节点)：与幸存校验节点相连的其它没有被删除的变量节点称为幸存变量节点。

定义 4(等效幸存邻居变量节点数)：假设网络 LDPC 码所有编码比特在传输过程中受 K 种噪声干扰，对应噪声方差分别为 $\sigma_1^2>\sigma_2^2>\cdots>\sigma_K^2$，令每个受到噪声干扰最大(噪声功率为 σ_1^2)的幸存邻居变量节点的等效幸存邻居变量节点数为 1，则受其他噪声干扰的幸存邻居变量节点的等效幸存邻居变量节点数定义为

$$\alpha_i=\left(\log\left[1-\phi\left[\frac{2}{\sigma_i^2}\right]\right]\Big/\log\left[1-\phi\left[\frac{2}{\sigma_1^2}\right]\right]\right)\leqslant 1 \qquad (0)$$

(C)1994-2023 China Academic Journal Electronic Publishing House. All rights reserved.　http://www.cnki.net

式中，$i=1,2,\cdots,K$。

$$\phi(x)=\begin{cases}\dfrac{1}{\sqrt{4\pi x}}\displaystyle\int_R \tanh\frac{u}{2}e^{-\frac{(u-x)^2}{4x}}su & x>0\\ 0 & x=0\end{cases}。$$

3.2 译码恢复错误概率

将网络 LDPC 码的删余变量节点 v 的所有幸存邻居变量节点按照其所通过信道的噪声功率的大小分为 b 类，假设第 t 类的噪声功率为 $\sigma_t^2(t=1,2,\cdots,b)$，且 $\sigma_1^2>\sigma_2^2>\cdots>\sigma_b^2$,并设第 t 类包括 S_t 个变量节点，记为 $\{v_1^t,\cdots,v_s^t,\cdots v_{S_t}^t\}$。与 LDPC 码类似，首先估计每次迭代过程中网络 LDPC 码的每个变量节点的均值更新，并由此计算该节点的恢复错误概率。

$\rho^{up}(x)=\sum_{k=1}^{d_c}\rho_k^{up}x^{k-1}$ $\rho^{low}(x)=\sum_{k=1}^{d_c'}\rho_k^{low}x^{k-1}$ 假设校验节点的度分布分别为 $\rho^{up}(x)=\sum_{k=1}^{d_c}\rho_k^{up}x^{k-1}$ 和 $\rho^{low}(x)=\sum_{k=1}^{d_c'}\rho_k^{low}x^{k-1}$，其中 η 是上层变量节点与校验节点相连的边数占总边数的比例，$\lambda_{i,j}$ 是与度为 (i,j) 的变量节点连接的边数占总边数的比例。$m_{i,j}^{l-1}$ 和 $n_{i,j}^{l-1}$ 分别表示第 $(l-1)$ 次迭代时，变量节点传给上下层的校验节点的对数似然比的均值。第 l 次迭代时，上下层校验节点的均值更新过程如下：

$$m'^{l}=\sum_k\rho_k^{up}\phi^{-1}\left(\left(\frac{1}{\eta}\sum_{i\geqslant0,j\geqslant0}\frac{i}{i+j}\lambda_{i+j}\phi(m_{i,j}^{l-1})\right)^{\sum_{t=1}^{b}S_t\alpha_t}\right)$$

$$n'^{l}=\sum_k\rho_k^{low}\phi^{-1}\left(\left(\frac{1}{1-\eta}\sum_{i\geqslant0,j\geqslant0}\frac{j}{i+j}\lambda_{i+j}\phi(n_{i,j}^{l-1})\right)^{\sum_{t=1}^{b}S_t\alpha_t}\right)\quad()(1)$$

当上下层的校验节点向被删余的度为 (i,j) 变量节点 $v\in G_{l+1}$ 传递消息时，该消息的对数似然比的均值分别为:

$$m'^{l}=\sum_k\rho_k^{up}\phi^{-1}\left(\left(\frac{1}{\eta}\sum_{i\geqslant0,j\geqslant0}\frac{i}{i+j}\lambda_{i+j}\phi(m_{i,j}^{l-1})\right)^{\sum_{t=1}^{b}S_t\alpha_t}\right)$$

$$n'^{l}=\sum_k\rho_k^{low}\phi^{-1}\left(\left(\frac{1}{1-\eta}\sum_{i\geqslant0,j\geqslant0}\frac{j}{i+j}\lambda_{i+j}\phi(n_{i,j}^{l-1})\right)^{\sum_{t=1}^{b}S_t\alpha_t}\right)$$

其中，α_t 表示每个幸存邻居变量节点的等效幸存邻居变量节点数，S_t 表示与变量节点 v 相连的校验节点没有被删余的变量节点数，变量节点 m_L v 的总等效幸存邻居变量节点数为 $\sum_{t=1}^{b}S_t\alpha_t$。

(2) 当上下层的校验节点向没有删余的度为 (i,j) 的变量节点传递消息时，该消息的对数似然比的均值分别为：

$$m'^{l}=\sum_k\rho_k^{up}\phi^{-1}\left(\left(\frac{1}{\eta}\sum_{i\geqslant0,j\geqslant0}\frac{i}{i+j}\lambda_{i+j}\phi(m_{i,j}^{l-1})\right)^{k-1}\right)$$

$$n'^{l}=\sum_k\rho_k^{low}\phi^{-1}\left(\left(\frac{1}{1-\eta}\sum_{i\geqslant0,j\geqslant0}\frac{j}{i+j}\lambda_{i+j}\phi(n_{i,j}^{l-1})\right)^{k-1}\right)$$

上下层变量节点的均值更新过程如下：

假设 m'^{l} 和 n'^{l} 分别表示第 l 次迭代时，上层和下层的校验节点传给变量节点的对数似然比消息均值。第 l 次迭代时，度为 (i,j) ()变量节点传给上下层校验节点的对数似然比消息均值分别为[4]

$$m_{i,j}^{l}=\begin{cases}(i-1)m'^{l}+jn'^{l}+m_{u_0} & i\neq0,j\geqslant0\\ jn'^{l}+m_{u_0}^{l} & i=0,j\geqslant1\end{cases}\qquad(7)$$

$$n_{i,j}^{l}=\begin{cases}im'^{l}+(j-1)n'^{l}+m_{u_0} & i\neq0,j\geqslant1\\ (j-1)n'^{l}+m_{u_0}' & i=0,j\geqslant1\\ im'^{l}+m_{u_0} & i\neq0,j=0\end{cases}$$

若变量节点被删掉，则 $m_{u_0}(m_{u_0}')=0$；若变量节点为由源节点发送至目的节点的信息比特，则 $m_{u_0}=2/\sigma_{SD}^2$；若变量节点为中继节点发送至目的节点的信息比特，则 $m_{u_0}'=2/\sigma_{RD}^2$。第一次迭代时，校验节点的初始值 $m'^{(0)}=n'^{(0)}=0$。

因此，变量节点传给上下层校验节点的平均的消息均值分别为：

$$m^{l}=\frac{1}{\eta}\sum_{i\geqslant0,j\geqslant0}\frac{i}{i+j}\lambda_{i+j}m_{i,j}^{l}$$

$$n^{l}=\frac{1}{1-\eta}\sum_{i\geqslant0,j\geqslant0}\frac{j}{i+j}\lambda_{i+j}n_{i,j}^{l}$$

经过 L 次迭代后，码比特的平均消息均值为：

$$m_L=\eta m^L+(1-\eta)n^L$$

此时，网络 LDPC 码的被删余变量节点的恢复错误概率为：

$$P_e(v)=Q(\sqrt{m_L}/2)$$

其中

$$Q(x)=\frac{1}{\sqrt{2\pi}}\int_x^{\infty}e^{-t^2/2}\mathrm{d}t。$$

(C)1994-2023 China Academic Journal Electronic Publishing House. All rights reserved. http://www.cnki.net

3.3 网络 LDPC 码的速率兼容算法

由公式(3)和(4)可知，等效幸存邻居变量节点数 $\sum_{t=1}^{b} S_t \alpha_t$ 越小，更新得到的均值 m'^{l} 和 n'^{l} 的值越大，进而迭代后的变量节点 m_L 的均值也越大，同时由公式(12)得到的恢复错误概率越小。因此，在搜索节点时，需要寻找当前具有最小等效邻居的变量节点进行删余操作。与文献[2]设计的 LDPC 码的删余算法相似，所提出的网络 LDPC 码速率兼容算法主要包括分组和排序两个操作。

分组：

(1) 给定一个 $M \times N$ [D1]网络 LDPC 码的校验矩阵，初始化 $R_\infty = \{1,2,\cdots,M\}$，$G_\infty = \{1,2,\cdots,N\}$，$l=1$；[D2]

(2) 遍历集合 R_∞，找出行重最小的行集合 r；[D3]

(3) 遍历集合 G_∞，找出列重最小的列集合 c；[D4]

(4) 选出所有(2)(3)相交的[D5]元素的集合 $w = \{(r^*, c^*), r^* \in r, c^* \in c\}$，作为候选对；

(5) 在集合 w 中选出具有最小等效幸存邻居变量节点数的元素，记为 (r_j^*, c_k^*)。若有多对满足条件，随机选出其中一对，归[D6]入第 l 次迭代可以恢复的集合 G_l，[D7]更新 $R_\infty = R_\infty \setminus r_j^*$ 和 $G_\infty = G_\infty \setminus c_k^*$；

(6) 若集合 G_∞ 为空，停止迭代，否则跳至(7)；

(7) 若集合 R_∞ 不为空，跳至(2)；否则若步骤(5)中有多于一对满足条件，则 $l = l+1$，跳至(2)。

接下来计算最大可达码率[2]为：

$$R_{\max} = \frac{R_0}{1 - \sum_{j=1}^{K} \left| G_j \right| / n} \tag{13}$$

式中，R_0 是母码的码率，n_i 是母码的码长。

[D8]如果要设计码率为 R_j 的码子，需要删余的节点数为[2]：

$$np_j = \left\lfloor \frac{n(R_j - R_0)}{R_j} \right\rfloor$$

式中 i，$0 \leqslant j \leqslant M$。

组内排序：

(1) 给定一个 $M \times N$ 网络 LDPC 码的校验矩阵[D9]，初始化 $R_\infty = \{1,2,\cdots,M\}$，$l=1$，$j=1$，$P_0 = \phi$；$R_0 \leqslant R_1 \leqslant \cdots \leqslant R_M \leqslant R_{\max}$

(2) 若 $j > M$，停止迭代[D10]；否则，$0 \leqslant j \leqslant M$ $P_j = P_{j-1}$；

(3) $\Delta = np_j - \left| P_j \right|$；[D11]

(4) 若 $\Delta = 0$，$j = j+1$ [D12]，跳至(2[D3])；

(5) 根据集合 G_l 定义 $C_l = \{c_1^*, c_2^*, \cdots\}$，从 C_l 中选出列重最大的变量节点的集合 $c_{\max}^*$，并从 $c_{\max}^*$ 中找出具有最小数量的死校验节点[D14]的变量节点 $c_{\max}^{**}$。如果有多个满足条件，随机选出其中一个，归入排序的集合 P_j，更新 $P_j = P_j \bigcup \{c_{\max}^{**}\}$，$G_l = G_l \setminus \{c_{\max}^{**}\}$，$\Delta = \Delta - 1$，$R_\infty = R_\infty \setminus r_{\max}^{**}$；

(6) 若 G_l 为空，$l = l+1$，$R_\infty = \{1,2,\cdots,M\}$；

(7) 跳至(4)。

经过上述分组和组内排序操作，将 $G_l (1 < l < K)$ () 变量节点按照 l 从小到大删余，而在同一个 G_l 中，按照变量节点的列号从小到大删余，直到删掉 np_j 个节点。

4 仿真结果

仿真中两个源节点采用的 LDPC 码的码长均为 2048，码率均为 0.5，度分布为：$\lambda(x) = 0.23403x + 0.21242x^2 + 0.1469x^5 + 0.102840x^6 + 0.30381x^{19}$ 和 $\rho(x) = 0.71875x^7 + 0.28125x^8$。中继节点采用的 LDPC 码的校验比特数为 628。假设信道模型为理想加性高斯白噪声(AWGN)信道，源节点和中继节点均采用 BPSK 调制方式。中继节点与目的节点之间的信噪比固定为 5dB。中继节点可以正确译码得到两个源节点的发送数据。图 4 和图给出了母码经过本文所改进算法(intentional)、现有算法(original)[2]和随机删余(random)所得到的码率为 0.5、0.6 和 0.7 的网络 LDPC 子码的 BER 性能对比。

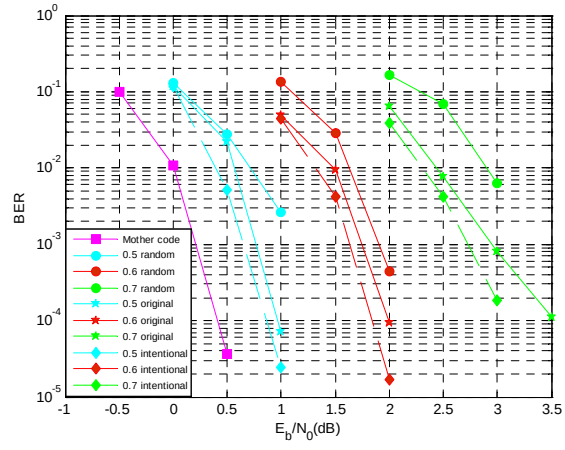


图 4 网络 LDPC 码的删余性能对比

由图 4 和图 5 可以看出，随着删余比特的增加，

(C)1994-2023 China Academic Journal Electronic Publishing House. All rights reserved. http://www.cnki.net

采用所提算法得到的网络 LDPC 码的性能增益也随之增加。当码率为 0.5， BER=10^{-3} 时，采用所提算法性能优于随机算法 0.45dB；当码率为 0.5，BER=10^{-4} 时，采用所提算法比文献[2]中算法的性能改善 0.15dB。在码率为 0.6， BER=10^{-3} 时，所提算法相对于随机算法性能增益为 0.3dB,相对于文献[2]中算法性能增益为 0.2dB。当码率为 0.7，SNR=3dB 时，所提算法的 BER 为 10^{-5} ，相比于随机算法的 10^{-3} 有了明显提升，而 BER=10^{-4} 时，所提算法比文献[2]中算法性能能增益改善 0.4 dB。

5 结论

文章首先介绍了网络 LDPC 码的结构及基本原理,然后针对其结构特性推导了译码恢复错误概率,并详述了适用于网络 LDPC 码的上下层变量节点和校验节点均值更新理论,接着介绍了网络 LDPC 码的速率兼容删余算法,最后对所设计的算法进行仿真,与现有算法相比，本文所提出的改进速率兼容算法在 BER=10^{-4} 时有 0.4dB 的性能增益。

参 考 文 献

[1] Hagenauer J. Rate-Compatible Punctured Convolutional Codes (RCPC codes) and Their Applications[J] . IEEE Trans on Communication, 1988, 36(4) : 389-400.

[2] J. Ha, J. Kim, D. Klinc, and S. W. McLaughlin, “Rate-Compatible Punctured Low-Density Parity-Check Codes With Short Block Lengths”, IEEE trans. Inform. Theory, vol. 52, no. 2, pp. 728-738, Feb. 2006.

[3] J. Ha, J. Kim, D. Klinc, and S. W. McLaughlin, “Rate-Compatible Puncturing of Low-Density Parity-Check Codes ”, IEEE trans. Inform. Theory, vol. 50, no. 11, pp. 2824-2836, NOV. 2004.

[4] Y. Li, G. H. Song, and L. L. Wang, “Design of joint network-low density parity check codes based on the EXIT charts”, IEEE Commun. Lett., vol. 13, no. 8, pp. 600-602, Aug. 2009.

(C)1994-2023 China Academic Journal Electronic Publishing House. All rights reserved. http://www.cnki.net

doi:10.3969/j.issn.1001-2400.2013.02.003

适用于网络 LDPC 码的速率兼容算法

王静怡[1,2]，李 颖[1,2]，孙 岳[1,2]

(1. 西安电子科技大学 综合业务网理论及关键技术国家重点实验室，陕西 西安 710071；
2. 电信科学研究院 无线移动通信国家重点实验室，北京 100083)

摘要：提出了一种可以获得最小比特错误概率的网络低密度奇偶校验(LDPC)码速率兼容删余算法，并推导了该算法的译码错误概率. 该算法基于网络 LDPC 码的结构特点，以达到译码最小比特错误概率为目标，在网络 LDPC 码的 Tanner 图上搜索出需要删余的变量节点，以获得最优的删余图样. 仿真结果表明，该算法比现有算法在 BER 为 10^{-4} 时有 0.4 dB 的性能增益.

关键词：多址接入中继网络；LDPC 码；网络 LDPC 码；速率兼容；删余

中图分类号：TN911.22 **文献标识码**：A **文章编号**：1001-2400(2013)02-0013-05

Rate-compatible network LDPC codes

WANG Jingyi[1,2], *LI Ying*[1,2], *SUN Yue*[1,2]

(1. State Key Lab. of Integrated Service Networks, Xidian Univ., Xi'an 710071, China; 2. State Key Lab. of Wireless Mobile Communications, China Academy of Telecommunication Technology, Beijing 100083, China)

Abstract: A rate-compatible puncturing algorithm for network LDPC codes is proposed to achieve the minimum error probability, and decoding error probability is derived. The algorithm for finding variable nodes to be deleted based on the tanner graph of network LDPC codes is proposed, which is aimed at minimizing the decoding error probability and optimizing the puncturing pattern. Simulation results illustrate that, at BER = 10^{-4}, the proposed rate-compatible network LDPC codes have a coding gain of about 0.4 dB compared with the codes obtained via the existing punctured methods.

Key Words: multi-access relay network; low-density parity-check (LDPC) codes; network LDPC code; rate-compatible; puncturing

由于无线移动信道具有衰落和时变特性，为最大限度地利用信道容量，可采用链路自适应技术，使信道编码速率、调制方式、信号功率等参数能够随信道质量的变化而变化. 链路自适应技术的基础是速率兼容纠错码的设计，其基本概念由文献[1]首次提出，速率兼容低密度奇偶校验(LDPC)码的设计则是近几年的研究热点. 文献[2-3]通过分组和排序操作，将 LDPC 码的变量节点按照迭代恢复次数进行分类，设计了 LDPC 码速率兼容删余算法，可以获得比随机删余更好的性能. 文献[4]首次提出了一种基于有限域上非零元素二进制镜像的缩短码构造方案，用来实现低码率的速率兼容多元 LDPC 码. 文献[5]研究了码率从 1/10 到 5/6 的灵活变化的非规则多元 LDPC 码比特级缩短算法. 文献[6]以多维累加交叉并行级联单奇偶校验码为母码，对奇偶校验比特按组删余，构建了一组速率兼容编码.

上述速率兼容算法都是针对点对点通信链路设计的. 然而，随着无线通信技术的发展和中继协作传输技术的引入，信道编码的设计也从点对点链路推广至无线中继网络. 对于多址接入中继网络，有多个节点同时

收稿日期：2012-06-09 网络出版时间：2012-11-16

基金项目：国家自然基金资助项目(61072064)；国家科技重大专项资助项目(2010ZX03003-003-03)；长江学者和创新团队发展计划资助项目(IRT0852)；中央高校科研业务费专项资金资助项目(K50510010026)

作者简介：王静怡(1984－)，女，西安电子科技大学博士研究生，E-mail：wangjy@stu.xidian.edu.cn.

网络出版地址：http://www.cnki.net/kcms/detail/61.1076.TN.20121116.0924.201302.16_009.html

(C)1994-2023 China Academic Journal Electronic Publishing House. All rights reserved. http://www.cnki.net

需要中继节点帮助转发数据,在中继节点设计有效的联合网络-信道编码算法,可在改善接收端性能的同时,有效提高转发效率. 文献[7]利用 LDPC 码,针对多址接入中继信道设计了一种网络 LDPC 码,并指出可以通过调整中继节点转发数据量来实现中继转发效率和接收端译码性能的有效折中. 与单个 LDPC 码相比,网络 LDPC 码的校验矩阵包括了源节点和中继节点所采用 LDPC 码的校验矩阵,因此其本质上可看做是一种多用户码. 另外,单个 LDPC 码的所有编码比特是在同一个信道中传输,所有编码比特受到相同的噪声干扰,网络 LDPC 码的编码比特则由对应的源节点和中继节点分别传输,不同传输链路将会受到不同的噪声干扰. 笔者将根据网络 LDPC 码的上述特性,设计相应的速率兼容算法.

1 适用于多址接入中继信道的网络 LDPC 码

由两个源节点、一个中继节点和一个目的节点构成的多址接入中继网络模型如图 1 所示. 两个源节点与目的节点之间的信息传输由广播发送和中继转发两个阶段完成. 在广播阶段,两个源节点分别向中继节点和目的节点广播发送编码序列 X_1 和 X_2;在中继转发阶段,中继节点首先对接收信号进行译码,得到两个源节点的估计数据,然后对译码得到的估计数据重新进行联合编码,并将编码序列 X_R 转发至目的节点. 目的节点则根据收到的信号进行联合译码,得到两个源节点的估计信息.

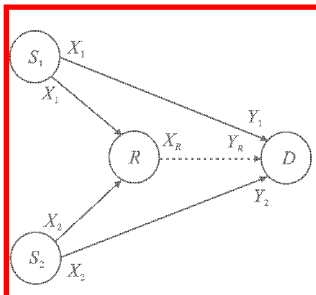


图 1 多址接入中继信道模型

目的节点将两个源节点和中继节点采用的 LDPC 码综合考虑,可得到如下校验矩阵:

$$\boldsymbol{H}=\begin{bmatrix}\boldsymbol{H}_1 & \boldsymbol{0} & \boldsymbol{0}\\ \boldsymbol{0} & \boldsymbol{H}_1 & \boldsymbol{0}\\ \boldsymbol{A} & \boldsymbol{B} & \boldsymbol{C}\end{bmatrix}, \tag{1}$$

其中,$\boldsymbol{H}_1$ 是源节点采用 LDPC 码的校验矩阵,$\boldsymbol{H}_3=[\boldsymbol{A},\boldsymbol{B},\boldsymbol{C}]$,是中继节点采用 LDPC 码的校验矩阵,$\boldsymbol{0}$ 是零矩阵. 由于式(1)中包含了源节点和中继节点所采用 LDPC 码的校验矩阵,并且中继节点是对两个源节点的数据进行联合编码,因此文献[7]称之为网络 LDPC 码,该码的 Tanner 图如图 2 所示.

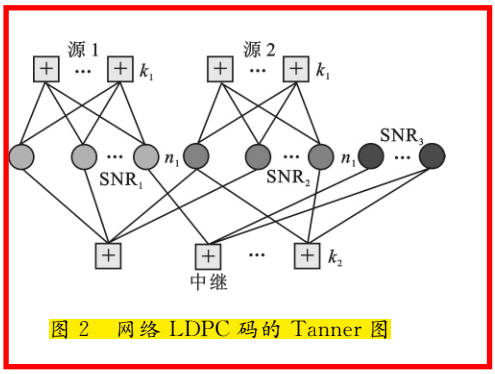


图 2 网络 LDPC 码的 Tanner 图

图 2 中网络 LDPC 码的 Tanner 图包含上下两层子图,其中上层子图包含 $2k_1$ 个校验节点,它们与变量节点的连接关系由 $\boldsymbol{H}_1$ 确定;下层子图包括 k_2 个校验节点,它们与变量节点的连接关系由式(1)中的 $\boldsymbol{H}_3$ 确定. 图中每个变量节点的度用(i,j)表示,其中 i 为变量节点与上层校验节点相连的边数,j 为变量节点与下层校验节点相连的边数. 用 d_c 和 d_c' 分别表示上层和下层校验节点的度数.

2 速率兼容网络 LDPC 码的设计

由图 2,网络 LDPC 码的变量节点包含两个源节点所采用的 LDPC 码的变量节点和中继节点所采用的联合 LDPC 码的变量节点,且不同变量节点通过不同的信道达到目的节点. 因此,需要考虑上述特点对删除变量节点恢复概率的影响,并由此设计适用于网络 LDPC 码的速率兼容算法.

2.1 几个定义

定义 1 若被删余的校验比特所对应的变量节点在迭代过程中接收到非零信息,则无论获得的信息正确与否,都称之为“恢复”[2].

定义 2 译码中第 n 次迭代时才恢复的被删除的变量节点称为 n 步恢复变量节点,用 n-SR 表示,而所有 n-SR 构成的集合则用 G_n 表示[2].

图 3 给出了一个包含 1-SR 节点、2-SR 节点的恢复树,其中竖线圆表示幸存的删余变量节点 S(v),横线圆表示未删余变量节点,方块表示校验节点.

(C)1994-2023 China Academic Journal Electronic Publishing House. All rights reserved. http://www.cnki.net

定义 3　如果一个一步恢复的删余变量节点至少与一个校验节点相连,且与这个校验节点相连的变量节点没有被完全删余掉,那么称这个校验节点为幸存校验节点[2]. 图 3 中的校验节点 S_1 和 S_2 即为幸存校验节点,而校验节点 D 则为死校验节点.

定义 4　幸存校验节点相连的其余未被删除的变量节点称为幸存变量节点.

由图 2 可见,网络 LDPC 码的编码比特是通过 3 个不同信道到达接收端的,因此,在设计网络 LDPC 码的删余算法时,不仅要考虑被删余变量节点的幸存邻居变量节点数,还要考虑每个幸存邻居变量节点受到的噪声大小. 下面,引入等效幸存变量节点数的概念.

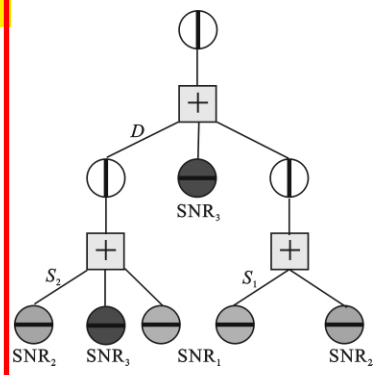


图 3　网络 LDPC 码的恢复树

定义 5　假设网络 LDPC 码所有编码比特在传输过程中受 K 种噪声干扰,其对应的噪声方差分别为 $\sigma_1^2>\sigma_2^2>\cdots>\sigma_K^2$,令每个受到噪声干扰最大(噪声功率为 σ_1^2)的幸存邻居变量节点的等效幸存邻居变量节点数为 1,则受其他噪声干扰的幸存邻居变量节点的等效幸存邻居变量节点数定义为

$$\alpha_i=\left\{\log\left(1-\varphi\left(\frac{2}{\sigma_i^2}\right)\right)\Big/\left[\log\left(1-\varphi\left(\frac{2}{\sigma_1^2}\right)\right)\right]\right\}\leqslant 1\quad,\quad i=1,2,\cdots,K\quad, \tag{2}$$

其中

$$\varphi(x)=\begin{cases}\dfrac{1}{(4\pi x)^{1/2}}\displaystyle\int_R\tanh\frac{u}{2}\exp\left(-\frac{(u-x)^2}{4x}\right)\mathrm{d}u\quad, & x>0\quad,\\ 0\quad, & x=0\quad.\end{cases}$$

2.2　译码恢复错误概率

将网络 LDPC 码的删余变量节点 v 的所有幸存邻居变量节点按照其所通过信道的噪声功率的大小分为 b 类,假设第 t 类的噪声功率为 $\sigma_t^2(t=1,2,\cdots,b)$,且 $\sigma_1^2>\sigma_2^2>\cdots>\sigma_b^2$,并设第 t 类包括 S_t 个变量节点,记为 $\{v_1^t,\cdots,v_s^t,\cdots,v_{S_t}^t\}$. 与 LDPC 码类似,首先估计每次迭代过程中删余网络 LDPC 码的每个变量节点的均值更新,并由此计算该节点的恢复错误概率.

由于网络 LDPC 码的译码同样包括变量节点更新和校验节点更新,但图 2 给出的 Tanner 图表明,网络 LDPC 码的校验节点更新实际上包括上层校验节点和下层校验节点更新. 下面将分析在迭代译码过程中,速率兼容删余的网络 LDPC 码的变量节点和校验节点的均值更新过程.

假设校验节点的度分布分别为 $\rho^{\mathrm{up}}(x)=\sum_{k=1}^{d_c}\rho_k^{\mathrm{up}}x^{k-1}$ 和 $\rho^{\mathrm{low}}(x)=\sum_{k=1}^{d_c'}\rho_k^{\mathrm{low}}x^{k-1}$;$\eta$ 是上层变量节点与校验节点相连的边数占总边数的比例;$\lambda_{i,j}$ 是与度为 (i,j) 的变量节点连接的边数占总边数的比例;$m_{i,j}^{l-1}$ 和 $n_{i,j}^{l-1}$ 分别表示第 $(l-1)$ 次迭代时,变量节点传给上下层的校验节点的对数似然比的均值. 第 l 次迭代时,上下层校验节点的均值更新过程如下:

(1) 当上下层的校验节点向被删余的度为 (i,j) 的变量节点 $v\in G_{l+1}$ 传递消息时,该消息的对数似然比的均值分别为

$$m'^{l}=\sum_k\rho_k^{\mathrm{up}}\varphi^{-1}\left\{\left[\frac{1}{\eta}\sum_{i\geqslant 0,j\geqslant 0}\frac{i}{i+j}\lambda_{i,j}\varphi(m_{i,j}^{l-1})\right]^{\sum_{t=1}^{b}S_t\alpha_t}\right\}\quad, \tag{3}$$

$$n'^{l}=\sum_k\rho_k^{\mathrm{low}}\varphi^{-1}\left\{\left[\frac{1}{1-\eta}\sum_{i\geqslant 0,j\geqslant 0}\frac{j}{i+j}\lambda_{i,j}\varphi(n_{i,j}^{l-1})\right]^{\sum_{t=1}^{b}S_t\alpha_t}\right\}\quad, \tag{4}$$

其中,α_t 表示每个幸存邻居变量节点 v_s^t 的等效幸存邻居变量节点数,S_t 表示与变量节点 v 相连的校验节点没有被删余的变量节点数,变量节点 v 的总等效幸存邻居变量节点数为 $\sum_{t=1}^{b}S_t\alpha_t$.

(2) 当上下层的校验节点向没有删余的度为 (i,j) 的变量节点 v 传递消息时,该消息的对数似然比的均值[7]分别为

$$m'^{l}=\sum_k\rho_k^{\mathrm{up}}\varphi^{-1}\left\{\left[\frac{1}{\eta}\sum_{i\geqslant 0,j\geqslant 0}\frac{i}{i+j}\lambda_{i,j}\varphi(m_{i,j}^{l-1})\right]^{k-1}\right\}\quad, \tag{5}$$

第61页,共397页
(C)1994-2023 China Academic Journal Electronic Publishing House. All rights reserved.　http://www.cnki.net

$$n'^{l}=\sum_{k}\rho_{k}^{\mathrm{low}}\varphi^{-1}\left\{\left[\frac{1}{1-\eta}\sum_{i\geqslant 0,j\geqslant 0}\frac{j}{i+j}\lambda_{i,j}\varphi(n_{i,j}^{l-1})\right]^{k-1}\right\}, \tag{6}$$

上下层变量节点的均值更新过程如下：

第 l 次迭代时，度为 (i,j) 的变量节点传给上下层校验节点的对数似然比消息均值[7]分别为

$$m_{i,j}^{l}=\begin{cases}(i-1)m'^{l}+jn'^{l}+m_{u_0}, & i\neq 0,\ j\geqslant 0,\\ jn'^{l}+m'_{u_0}, & i=0,\ j\geqslant 1,\end{cases} \tag{7}$$

$$n_{i,j}^{l}=\begin{cases}im'^{l}+(j-1)n'^{l}+m_{u_0}, & i\neq 0,\ j\geqslant 1,\\ (j-1)n'^{l}+m'_{u_0}, & i=0,\ j\geqslant 1,\\ im'^{l}+m_{u_0}, & i\neq 0,\ j=0.\end{cases} \tag{8}$$

若变量节点被删掉，则 $m_{u_0}(m'_{u_0})=0$；若变量节点为由源节点发送至目的节点的信息比特，则 $m_{u_0}=2/\sigma_{SD}^{2}$；若变量节点为中继节点发送至目的节点的信息比特，则 $m'_{u_0}=2/\sigma_{RD}^{2}$. 第 1 次迭代时，校验节点的初始值 $m'^{0}=n'^{0}=0$.

因此，变量节点传给上下层校验节点的平均的消息均值分别为

$$m^{l}=\frac{1}{\eta}\sum_{i\geqslant 0,j\geqslant 0}\frac{i}{i+j}\lambda_{i,j}m_{i,j}^{l}, \tag{9}$$

$$n^{l}=\frac{1}{1-\eta}\sum_{i\geqslant 0,j\geqslant 0}\frac{j}{i+j}\lambda_{i,j}n_{i,j}^{l}. \tag{10}$$

经过 L 次迭代后，码比特的平均消息均值为

$$m_{L}=\eta m^{L}+(1-\eta)n^{L}. \tag{11}$$

此时，网络 LDPC 码的被删余变量节点的恢复错误概率为

$$P_{e}(v)=Q\left[(m_{L}/2)^{1/2}\right], \tag{12}$$

其中 $Q(x)=\frac{1}{(2\pi)^{1/2}}\int_{x}^{\infty}\exp\left(-\frac{t^{2}}{2}\right)\mathrm{d}t$.

2.3 网络 LDPC 码的速率兼容算法

由式(3)和(4)可知，等效幸存邻居变量节点数 $\sum_{t=1}^{b}S_{t}\alpha_{t}$ 越小，更新得到的均值 m'^{l} 和 n'^{l} 的值越大，进而迭代后的变量节点 m_{L} 的均值也越大，同时由式(12)得到的恢复错误概率 $P_{e}(v)$ 越小. 因此，在搜索节点时，需要寻找当前具有最小等效邻居的变量节点进行删余操作. 与文献[2]设计的 LDPC 码的删余算法相似，所提出的网络 LDPC 码速率兼容算法主要包括分组和排序两个操作.

2.3.1 分组

将所有删余的变量节点按照迭代恢复次数分成 K 组 $G_{1},G_{2},\cdots,G_{K}$，其中 $G_{l}(1\leqslant l\leqslant K)$ 是经过 l 次迭代才能恢复的所有变量节点的集合.

(1) 给定一个 $M\times N$ 网络 LDPC 码的校验矩阵，初始化 $R_{\infty}=\{1,2,\cdots,M\}$，$G_{\infty}=\{1,2,\cdots,N\}$，$l=1$.

(2) 遍历集合 R_{∞}，找出行重最小的行集合 r.

(3) 遍历集合 G_{∞}，找出列重最小的列集合 c.

(4) 选出所有(2)和(3)相交的元素的集合，$w=\{(r^{*},c^{*}),r^{*}\in r,c^{*}\in c\}$，作为候选对.

(5) 在集合 w 中选出具有最小等效幸存邻居变量节点数的元素，记为 (r_{j}^{*},c_{k}^{*}). 若有多对满足条件，则随机选出其中一对，归入第 l 次迭代可以恢复的集合 G_{l}，更新 $R_{\infty}=R_{\infty}\setminus r_{j}^{*}$ 和 $G_{\infty}=G_{\infty}\setminus c_{k}^{*}$.

(6) 若集合 G_{∞} 为空，则停止迭代；否则，跳至(7).

(7) 若集合 R_{∞} 不为空，则跳至(2)；否则，若步骤(5)中有多于一对满足条件，则 $l=l+1$，跳至(2).

其中，$G_{\infty}(R_{\infty})$ 表示每次迭代后更新的列(行)的集合；$r(c)$ 表示第 l 次迭代时，在集合 $R_{\infty}(G_{\infty})$ 选出的行(列)重最小的行(列)集合；$G_{l}=\{(r_{1}^{*},c_{1}^{*}),(r_{2}^{*},c_{2}^{*}),\cdots\}$；$R_{\infty}=R_{\infty}\setminus r_{j}^{*}$ $(G_{\infty}=G_{\infty}\setminus c_{k}^{*})$ 表示集合 $R_{\infty}(G_{\infty})$ 去掉元素 $r_{j}^{*}(c_{k}^{*})$ 后的集合 $R_{\infty}(G_{\infty})$.

第62页，共397页
(C)1994-2023 China Academic Journal Electronic Publishing House. All rights reserved. http://www.cnki.net

计算最大可达码率[2] 为　　$R_{\max}=R_0\Big/\Big(1-\sum_{j=1}^{K}|G_j|/n\Big)$ ，　　(13)

其中，R_0 是母码的码率，n 是母码的码长.

在给定母码基础上，设计 Q 个码率的子码，对应码率记为 $R_0\leqslant R_1\leqslant\cdots\leqslant R_Q\leqslant R_{\max}$. 假设所设计码的码率为 R_j，需要删余的节点数为[2]

$$np_j=\lfloor n(R_j-R_0)/R_j\rfloor\quad,\quad 0\leqslant j\leqslant Q\quad.\tag{14}$$

2.3.2　组内排序

依次对 $G_l(1\leqslant l\leqslant K)$ 内的变量节点进行排序.

(1) 给定一个 $M\times N$ 网络 LDPC 码的校验矩阵，初始化 $R_\infty=\{1,2,\cdots,M\}$，$l=1$，$j=1$，$P_0=\varnothing$.

(2) 若 $j>Q$，则停止迭代；否则，$P_j=P_{j-1}$.

(3) $\Delta=np_j-|P_j|$.

(4) 若 $\Delta=0$，$j=j+1$，则跳至(2).

(5) 根据集合 G_l 定义 $C_l\xlongequal{\mathrm{d}}\{c_1^*,c_2^*,\cdots\}$，从 C_l 中选出列重最大的变量节点的集合 $c_{\max}^*$，并从 $c_{\max}^*$ 中找出具有最小数量的死校验节点的变量节点 $c_{\max}^{**}$. 如果有多个满足条件，则随机选出其中一个，归入排序的集合 P_j，更新 $P_j=P_j\bigcup\{c_{\max}^{**}\}$，$G_l=G_l\backslash\{c_{\max}^{**}\}$，$R_\infty=R_\infty\backslash r_{\max}^{**}$，$\Delta=\Delta-1$.

(6) 若 G_l 为空，$l=l+1$，则 $R_\infty=\{1,2,\cdots,M\}$.

(7) 跳至(4).

其中，(1)中的 $l=1$ 表示从 G_1 开始将各 G_l 内的变量节点排序，$j=1$ 表示初始码率为 R_1；(3) 计算需要删余 np_j 个节点，除了上次迭代删余的 $|P_j|$ 个节点外，本次还需要删余 Δ 个节点；(5) 中的集合 $c_{\max}$ 表示最大列重的变量节点的集合，同时意味着该集合包含的变量节点的幸存校验节点数最多；P_j 表示要达到码率 R_j，所需删余的变量节点的列集合；$r_{\max}^{**}$ 表示列为 $c_{\max}^{**}$ 的变量节点所在的行.

经过上述分组和组内排序操作，将 $G_l(1\leqslant l\leqslant K)$ 中的变量节点按照 l 从小到大删余，而在同一个 G_l 中，按照变量节点的列号从小到大删余，直到删掉 np_j 个节点.

3　仿真结果

仿真中两个信源节点采用的 LDPC 码的码率均为 0.5，度分布为

$$\lambda(x)=0.23403x+0.21242x^2+0.1469x^5+0.102840x^6+0.30381x^{19}$$

和

$$\rho(x)=0.71875x^7+0.28125x^8\quad.$$

根据文献[7]，假设所采用的网络 LDPC 码的度序列分布为：$\lambda_{0,2}=0.028043$，$\lambda_{2,0}=0.188139$，$\lambda_{2,1}=0.019382$，$\lambda_{2,2}=0.026283$，$\lambda_{3,0}=0.191239$，$\lambda_{3,1}=0.003360$，$\lambda_{3,2}=0.001150$，$\lambda_{6,0}=0.085989$，$\lambda_{6,1}=0.000980$，$\lambda_{6,2}=0.063446$，$\lambda_{7,0}=0.059576$，$\lambda_{7,2}=0.044374$，$\lambda_{20,0}=0.176218$，$\lambda_{20,1}=0.003570$，$\lambda_{20,2}=0.108251$，$\rho_6^{\mathrm{low}}=0.943049$，$\rho_7^{\mathrm{low}}=0.056951$.

假设两个源节点所采用 LDPC 码的码长均为 2 048，中继节点联合编码的 LDPC 码的校验比特数为 628，此时网络 LDPC 码(母码)的码率为 0.444. 根据式(14)，可以得到对该网络 LDPC 码进行删余获得的最大码率为 0.733. 利用文中所提算法对该网络 LDPC 码删余可以得到码率分别为 0.5、0.6 和 0.7 的子码. 利用文献[2]中的算法和随机删余也可得到同样码率的网络 LDPC 子码.

假设源节点和中继节点均采用 BPSK 调制方式，源节点与中继节点，源节点与目的节点，以及中继节点与目的节点之间的信道均为高斯白噪声信道，中继节点与目的节点之间的信噪比固定为 5 dB，且中继节点可以正确

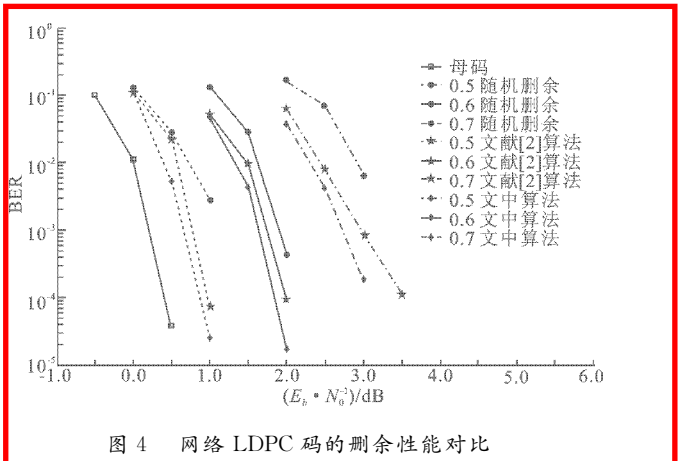


图 4　网络 LDPC 码的删余性能对比

(下转第 47 页)

第63页，共397页
(C)1994-2023 China Academic Journal Electronic Publishing House. All rights reserved.　http://www.cnki.net

scientific.net/AMR.311-313.2009.

[4] Bozorg M, Termeh F. Domains of PID Controller Coefficients which Guarantee Stability and Performance for LTI Ttime-delay [J]. Automaic, 2011, 47(9): 2122-2125.

[5] 杨莹，李俊民，陈国培. 一类广义混杂系统的随机稳定性及稳定化[J]. 西安电子科技大学学报, 2010, 37(5): 866-871.
Yang Ying, Li Junmin, Chen Guopei. Stochastic Stability and Stabilization for a Class of Singular Hybrid Systems[J]. Journal of Xidian University, 2010, 37(5): 866-871.

[6] 徐亚兰，陈建军. 压电柔性机械臂的轨迹跟踪控制[J]. 西安电子科技大学学报, 2008, 35(3): 504-507.
Xu Yalan, Chen Jianjun. Trajectory Tracking Control for the Flexible Link Robot Manipulator Using Piezoelectric Materious [J]. Journal of Xidian University, 2008, 35(3): 504-507.

（编辑：郭　华）

（上接第 17 页）

译出两个源节点的发送数据. 图 4 比较了 3 种不同算法得到的网络 LDPC 码在上述信道假设下的误比特性能，图中横坐标 E_b/N_0 表示源节点与目的节点之间链路的信噪比变化，且假设两个源节点与目的节点之间的链路是对称的.

由图 4 可以看出，随着删余比特的增加，采用所提算法得到的网络 LDPC 码的性能增益也随之增加. 当码率为 0.5，比特误码率(BER)为 10^{-3} 时，采用所提算法性能优于随机删余算法 0.45 dB；当码率为 0.5，BER 为 10^{-4} 时，采用所提算法比文献[2]中算法的性能改善 0.15 dB. 在码率为 0.6，BER 为 10^{-3} 时，所提算法相对于随机删余算法性能改善了 0.3 dB，相对于文献[2]中算法性能改善了 0.2 dB. 当码率为 0.7，SNR 为 3 dB 时，所提算法的 BER 为 10^{-5}，相比于随机删余算法的 10^{-3} 有了明显提升，而 BER 为 10^{-4} 时，所提算法比文献[2]中算法性能增益改善了 0.4 dB.

4　结 束 语

根据网络 LDPC 码的结构特点，以最小化恢复错误概率为目标，设计了一种网络 LDPC 码的速率兼容删余算法. 不同于已有的算法[2]，该算法利用被删余的变量节点的恢复原则和受到的噪声干扰大小设计了不同码率下的删余方案，在不增加系统复杂度的前提下，只需要一对编码译码器即可实现网络 LDPC 码的码率自适应. AWGN 信道下的仿真结果表明，在同等条件下，采用文中所提算法获得的速率兼容网络 LDPC 码比采用文献[2]中算法得到的速率兼容网络 LDPC 码有更好的性能.

参考文献：

[1] Hagenauer J. Rate-Compatible Punctured Convolutional Codes (RCPC codes) and Their Applications [J]. IEEE Trans on Communication, 1988, 36(4): 389-400.

[2] Ha J, Kim J, Klinc D, et al. Rate-Compatible Punctured Low-Density Parity-Check Codes with Short Block Lengths [J]. IEEE Trans on Inform Theory, 2006, 52(2): 728-738.

[3] Ha J, Kim J, Klinc D, et al. Rate-Compatible Puncturing of Low-Density Parity-Check Codes [J]. IEEE Trans on Inform Theory, 2004, 50(11): 2824-2836.

[4] Zhou Lin, Bai Baoming, Xu Ming. Design of Nonlinary Rate-compatible LDPC Codes Utilizing Bit-wise Shortening Method [J]. IEEE Communication Letters, 2010, 14(10): 963-965.

[5] 周林，白宝明，邵军虎，等. 多元 LDPC 码的速率兼容技术研究[J]. 西安电子科技大学学报, 2011, 38(1): 147-152.
Zhou Lin, Bai Baoming, Shao Junhu, et al. On Nonbinary Rate-compatible LDPC Codes [J]. Journal of Xidian University, 2011, 38(1): 147-152.

[6] 郭凯，陈彦辉，李建东. 一种对奇偶校验比特按组删余的速率兼容编码[J]. 西安电子科技大学学报, 2009, 36(5): 782-787.
Guo Kai, Chen Yanhui, Li Jiandong. Rate-compatible Codes Based on Puncturing Parity Check Bits in Group [J]. Journal of Xidian University, 2009, 36(5): 782-787.

[7] Li Y, Song G H, Wang L L. Analysis of the Joint Network LDPC Codes over Orthogonal Multi-Access Relay Channel [J]. IEEE Commun Lett, 2010, 14(2): 184-186.

（编辑：齐淑娟）

第64页，共397页
(C)1994-2023 China Academic Journal Electronic Publishing House. All rights reserved.　http://www.cnki.net

Optimal Design of the Joint Network LDPC Codes over Orthogonal Multi-Access Relay Channel

Jingyi Wang
State Key Lab of ISN
Xidian University
Xi'an, China
Email: wangjy@stu.xidian.edu.cn

Shuling Che
State Key Lab of ISN
Xidian University
Xi'an, China
Email: shlche@mail.xidian.edu.cn

Ying Li
and Junlong Wang
State Key Lab of ISN
Xidian University
Xi'an, China
Email:ying.lili1973@gmail.com

***Abstract*—Optimization of degree distribution of the joint network LDPC code for orthogonal multiple-access relay channel (MARC) is investigated in this paper. We first calculated the code capacity of the source-destination link of orthogonal MARC based on a Gaussian approximation,where two sources communicate with one destination in the presence of one relay. Then, a new generalized differential evolution algorithm is developed to iteratively improve the degree distribution of the joint network LDPC code. Simulation results show that, the gap between bit error rate (BER) performance of our designed codes and the decoding threshold is about 0.4dB, and that between the capacity limit and decoding threshold is less than 0.7dB at BER $= 10^{-6}$.**

***Index Terms*—Network LDPC Code; multi-access relay network; Gaussian approximation; differential evolution; capacity limit.**

I. Introduction

In wireless communications, cooperation relay networks[1][2][3] have recently attracted substantial research efforts with many promising techniques of improving performance in term of throughput, coverage or diversity gain. In relay networks, one or multiple relay nodes (RNs) to assist the sources in transmitting information.Optimal designs of Relay networks have attracted extensive attentions due to that they can increase the communication capacity. One of the earlier works on this subject is the application of LDPC code to the single-source single-relay networks [4]. To improve the performance of the single-source single-relay system, a class of bilayer LDPC codes is designed in[5][6].

Based on the principle of the bilayer LDPC codes, the authors proposed a class of the joint network LDPC code which helps the relay jointly re-encodes the messages from the two sources and sends the parity bits to the destination [7]. Moreover, the authors analyzed the capacity approaching ability of the joint network LDPC codes in [8]. In this paper, we study the problem of approaching capacity limit of a two-source single-relay multiple-access relay network with the joint network LDPC code, in which the two source-to-relay channels and the two source-to-destination channels are under the same channel parameters.Then, a new generalized differential evolution algorithm is developed to optimal the degree distribution of the joint network LDPC code.

The rest of this paper is organized as follows. Section II presents the system model and then describes the operation of the system throughout different stages of the cooperation strategy. Section III explains the optimum design method of degree distribution of the joint network LDPC code. Section IV presents simulation results, and Section VI concludes the paper.

II. System Model

Our system is a two-slot wireless relay network consisting of two sources, one relay and one destination, as shown in Fig.1.

In the first slot, sources $S_i(i = 1, 2)$ broadcast their LDPC coded signals $X_i(i = 1, 2)$, which are received by both relay R and destination D. We express the received bits as

$$Y_{S_i,R} = X_i + N_{S_i,R} \quad (1)$$

$$Y_{S_i,D} = X_i + N_{S_i,D} \quad (2)$$

where $i = 1, 2.X_i$ is the LDPC coded signal sent from source node S_i, while $Y_{S_i,R}$ and $Y_{S_i,D}$ are the corresponding received signal by the relay R and the destination D respectively. Finally, $N_{S_i,R}$ is a zero-mean additive Gaussian random variable with variance $\sigma^2_{S_i,R}$, and $N_{S_i,D}$ is a zero-mean additive Gaussian random variable with variance $\sigma^2_{S_i,D}$.

In the second slot, after decoding the received signals correctly, R jointly re-encodes the messages of the two sources and sends k_2 parity bits X_R to D. The received bits at the destination D is

$$Y_{R,D} = X_R + N_{R,D} \quad (3)$$

where X_R denotes the signal corresponding to the parity bits, and $N_{R,D}$ is a zero-mean additive Gaussian random variable with variance $\sigma^2_{R,D}$.

At last, the destination D can decode the information data of two sources by using the received signals Y_1, Y_2 and Y_R respectively from the two sources and relay. Therefore, X_1, X_2, and X_R can be treated as an equivalent super code which is called as the joint network LDPC code in [7]. The parity check matrix of the joint network LDPC code can be written as

$$\mathbf{H} = \begin{pmatrix} \mathbf{H_1} & \mathbf{0} & \mathbf{0} \\ \mathbf{0} & \mathbf{H_1} & \mathbf{0} \\ \mathbf{A} & \mathbf{B} & \mathbf{C} \end{pmatrix} \quad (4)$$

978-0-7695-4988-0/13 $26.00 © 2013 IEEE
DOI 10.1109/INCoS.2013.116

IEEE computer society

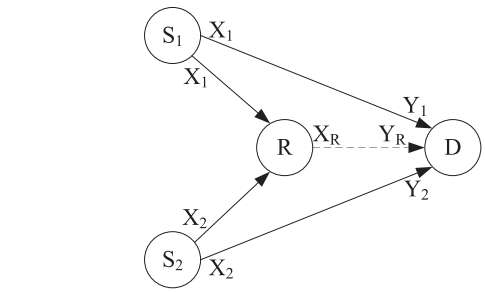


Fig. 1. The model of the joint network LDPC code based relaying scheme

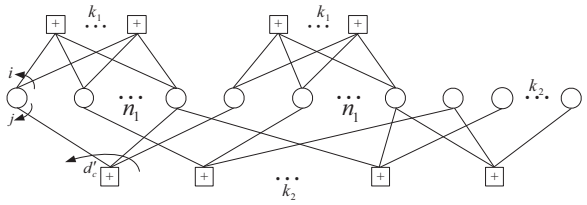


Fig. 2. Tanner graph of the joint network LDPC code

where $\mathbf{H_1}$ denotes the same parity-check matrix of the constituent codes at the two sources $S_i(i=1,2)$, $\mathbf{H_3}=(\mathbf{ABC})$ denotes the parity-check matrix generated by R, and $\mathbf{0}$ represents the all-zero matrix.

Assume that each source uses an (n_1, n_1-k_1) irregular LDPC code with code length n_1 and parity length k_1. According to [8], the Tanner graph of the joint network LDPC code is shown in Fig.2, where the upper sub-graph denotes the encoding at the sources and the lower sub-graph denots the encoding at the relay. This code includes $2k_1$ upper check nodes, k_2 lower check nodes and $2n_1+k_2$ variable nodes. A variable node is of degree (i,j), $1\le i\le d_v$ and $1\le i\le d_v^{'}$, where i (j) is its upper (lower) degree, and d_v $(d_v^{'})$ is its maximum upper (lower) degree. In addition, $\lambda_{i,j}$ represents the proportion of the number of edges connected to the variable nodes with the degree (i,j).

III. Optimization Of Degree Distribution

A. Preliminary

Definition 1: Decoding threshold of joint network LDPC code is defined as

$$\sigma^* = sup\{\sigma : \lim_{L\to+\infty} m_L > M\} \tag{5}$$

where L is the maximum iteration number, m_L denotes the mean value of the log-likelihood ratio (LLR) message of a code bit at L-th decoding iteration and M is the LLR mean value corresponding to the target error probability. Then with the knowledge in [8], $2m_L$ is the LLR variance value. When $\sigma<\sigma^*$, m_L will be greater than M, which means that the target error probability can be achieved. When $\sigma\ge\sigma^*$, the iterative decoding can not achieve the target error probability.

B. Calculation of decoding threshold σ^*_{SD}

Algorithm 1: Given degree distributions of the LDPC code at the sources, let σ_{SD} and σ_{RD} represent the channel parameters of source-destination link and relay-destination link respectively. We denote the target error probability as $P_e=10^{-6}(M=45)$ [8], and the maximum iteration number as L. Let $\Delta\sigma_{SD}$ denote a step length, and then algorithm 1 can be described as follows:

Step 1: Initialization

The initialized value of the average mean value of the LLR message output by the check node is $m^{'l}=n^{'l}=0$ (l is the iteration number, and $l=0$ in the first iteration)[8].

Step 2: Updating

When the iteration number $l<L$, update the mean values of the LLR messages at the variable node and the check node respectively, and then calculate the mean value (m_l) of the LLR message during this iteration using the method in [8]. If $m_l<M$, add the iteration number by 1 $(l=l+1)$, and continue Step 2. If $m_l\ge M$, $\sigma_{SD}=\sigma_{SD}+\Delta\sigma_{SD}$, and go to Step 1.

Step 3: Stopping criterion

If $l\ge L$ and $m_l<M$ during this iteration, stop the whole process, and the code capacity is defined as $\sigma^*_{SD}=\sigma_{SD}-\Delta\sigma_{SD}$. Otherwise, output the threshold value of channel parameter as $\sigma^*_{SD}=\sigma_{SD}$.

Using Algorithm 1, we can obtain the corresponding σ^*_{SD} from a given degree distribution of the upper layer LDPC code.

C. Optimal Design Of Degree Distribution Of The Lower Layer LDPC Code

Our goal is to search the optimal degree distribution of the network LDPC code, which can approach the capacity limit. Here we use differential evolution algorithm to optimal design of the network LDPC code sets.

Algorithm 2: Assume that N relay code sets of the network LDPC code structure are randomly generated, denoting their degree distributions of variable node as $\lambda_{i,j}(d), 0\le i\le d_v, 0\le j\le d_v^{'}, d=1,2,...N$. The degree of the lower check nodes is fixed as $d_c^{'}$.

Step 1: Initialization

Initialize that degree distribution as

$$C(d)=\{\lambda_{i,j}(d), 0\le i\le d_v, 0\le j\le d_v^{'}\}, d=1,2,\cdots,N. \tag{6}$$

Step 2: Performance estimation of code set

Calculate the code capacity $\sigma^*(d)$ of each code set $C(d)$ through the Algorithm 1, and search the optimal code set meeting $C^*=\arg\max_{1\le d\le N}\sigma^*(d)$. The degree distribution of the optimal code set corresponding to the maximum code capacity is $C^*=\{\lambda^*_{i,j}, 0\le i\le d_v, 0\le j\le d_v^{'}\}$.

Step 3: Code set updating

Select $\widetilde{N}$ code sets from $\{C(d)\}_{d=1}^{N}$ at random, and denote their degree distribution as $\widetilde{C}(k)=\{\lambda_{i,j}(k), 0\le i\le d_v, 0\le j\le d_v^{'}\}, k=1,2,\cdots,\widetilde{N}$. Then update the degree distribution of the code set: $C^*=C^*+\alpha\Sigma_{k=1}^{\widetilde{N}}(-1)^{k-1}\widetilde{C}(k)$, where $\alpha<1$ is the step length.

TABLE I
FOUR DIFFERENT PARAMETERS OF THE JOINT NETWORK LDPC CODES

Code Set	Code A	Code B	Code C	Code D
$d_v^{'}$	2	2	2	2
$d_c^{'}$	4	4	4	7
k_2	2814	4814	2814	2814
σ_{RD}	0.5	0.5	0.8	0.5
η	0.942065	0.904808	0.942065	0.902835
σ_{SD}^*	1.0568	1.0987	1.0393	1.1116
Threshold	0.15504dB	0.11512dB	0.20180dB	-0.22877dB
Capacity Limit	-0.24536dB	-0.51762dB	-0.14395dB	-0.24536dB
Gap	0.40040dB	0.63274dB	0.34575dB	0.01666dB

Step 4: Stopping criterion

If reaching the preset number of iteration and $m_l < M$, stop the iteration process. The degree distribution of the optimal code set is defined as $C^* = \{\lambda_{i,j}^*, 0 \le i \le d_v, 0 \le j \le d_v^{'}\}$; Otherwise, go to Step 3.

Remark: Restrictive conditions must be met for Step 1 and Step 3.

$$\begin{cases} \sum\limits_{i\ge 0, j\ge 0} \lambda_{i,j} = 1 \\ \lambda_i = \frac{1}{\eta} \sum\limits_{j\ge 0} \frac{i}{i+j} \lambda_{i,j} \\ \eta = \sum\limits_i \sum\limits_j \frac{i}{i+j} \lambda_{i,j} \\ d_c^{'} = \frac{1-\eta}{\sum\limits_j \frac{\lambda_{0,j}}{j}} \end{cases} \tag{7}$$

where η is the proportion of the total number of edges in the upper sub-graph. The total number of upper-layer edges of a source node is $E = \frac{n_1}{\sum\limits_{i\ge 2} \frac{\lambda_i}{i}} = \frac{k_1}{\sum\limits_{j\ge 2} \frac{\rho_j}{j}}$, and the total number of edges of the bilayer network LDPC code is $E^{'} = 2E + k_2 \cdot d_c^{'}$, so $\eta = \frac{2E}{E^{'}}$.

IV. SIMULATION RESULTS

Assume each source node employs an $(n_1, n_1 - k_1)$ LDPC code with $\lambda(x) = 0.23403x + 0.21242x^2 + 0.1469x^5 + 0.102840x^6 + 0.30381x^{19}$, and $\rho(x) = 0.71875x^7 + 0.28125x^8$, where $n_1 = 22164, k_1 = 11082$. $\text{SNR}_{RD} = 3\text{dB}$ and the two source-destination links are assumed to be symmetric. Using the Algorithm 1, four different parameters of the joint network LDPC codes, are obtained and listed in Table I, where σ_{RD}^2 represents the channel parameter between the relay-destination link.

Using the Algorithm 2, four optimal degree distributions of the joint network LDPC codes are given in Table II III IV.

The BER curves of four codes are illustrated in Fig.3. We see that the gap between the decoding threshold of four codes obtained by searching the maximum decoding threshold σ_{SD}^* and capacity limit is less than 0.7dB, and that between BER performance and decoding threshold is less than 0.4dB. Since the lower check degree of Code D is bigger and more information bits are contained in the check equation, it outperforms Code A by 0.2dB gains at BER $= 10^{-5}$. Another important observation is that Code B has a gain of about 0.15dB over Code A at BER $= 10^{-5}$ and the performance gain of Code D is about 0.1dB over Code B at BER $= 10^{-5}$. This indicates that increasing degrees of lower-layer check nodes is better than increasing the numbers of parity bits to improve system performance. When the noise variance between R-D link is increased, the system decoding performance will be reduced and Code A will have a gain of about 0.2dB over Code C at BER $= 10^{-5}$.

TABLE II
THE OPTIMAL DEGREE DISTRIBUTIONS OF CODE A

$\lambda_{i,j}$	$\lambda_{i,0}$	$\lambda_{i,1}$	$\lambda_{i,2}$
$i=2$	0.193815	0.00543635	0.04612661
$i=3$	0.171369	0.019109592	0.02409292
$i=6$	0.129299	0.006342408	0.00494214
$i=7$	0.09485	0.00008237	0.00259462
$i=20$	0.273877	0.000432436	0.00181212
$i=0$	0	0.0030528	0.02276564

TABLE III
THE OPTIMAL DEGREE DISTRIBUTIONS OF CODE B

$\lambda_{i,j}$	$\lambda_{i,0}$	$\lambda_{i,1}$	$\lambda_{i,2}$
$i=2$	0.07441004	0.20599344	0
$i=3$	0.19208258	0.0001582	0
$i=6$	0.13270189	0.00013842	0.00016819
$i=7$	0.09266986	0.00032638	0.00017797
$i=20$	0.27426244	0.00051525	0.0021752
$i=0$	0	0.0237937	0.0000099

TABLE IV
THE OPTIMAL DEGREE DISTRIBUTIONS OF CODE C

$\lambda_{i,j}$	$\lambda_{i,0}$	$\lambda_{i,1}$	$\lambda_{i,2}$
$i=2$	0.1206132	0	0
$i=3$	0.1001453	0.0000219	0
$i=6$	0.1860514	0.0002767	0.0000167
$i=7$	0.1964141	0.0002114	0.0000212
$i=20$	0.3858558	0.0003262	0.0000362
$i=0$	0	0.0041565	0.0206487

TABLE V
THE OPTIMAL DEGREE DISTRIBUTIONS OF CODE D

$\lambda_{i,j}$	$\lambda_{i,0}$	$\lambda_{i,1}$	$\lambda_{i,2}$
$i=2$	0.1112574	0.0136437	0.1818773
$i=3$	0.0917291	0.0876831	0.0571696
$i=6$	0.1322349	0.0003256	0.0001570
$i=7$	0.0926749	0.0000457	0.0000678
$i=20$	0.2740590	0.0001011	0.000217
$i=0$	0	0.0035171	0.0207269

V. CONCLUSION

In this paper, we employed differential evolution method to design degree distribution of the joint network LDPC code

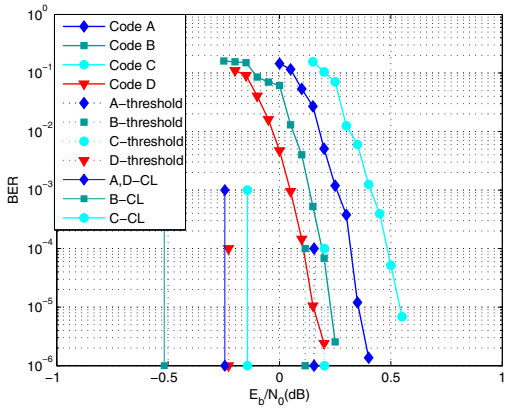


Fig. 3. Performance of the joint network LDPC codes

for a two-source single-relay system, under the assumption of symmetric AWGN channel. The performance of the new codes we designed have significant BER performance gain for a two-source single-relay system with symmetric channels.

ACKNOWLEDGMENT

This work was supported by NSFC(61072064) and NSFC(61101148).

REFERENCES

[1] T. Cover and A. E. Gamal, "Capacity theorems for the relay channel," *IEEE Trans. Inf. Theory.*, vol. 25, pp. 572-584, Sep. 1979.

[2] A. Nosratinia, T. E. Hunter, and A. Hedayat, "Cooperative Communication in Wireless Networks," *IEEE Communications Magazine.*, vol. 42, no. 10, pp.74-80, October 2004.

[3] J. Laneman, D. Tse, and G. Wornell, "Cooperative Diversity in Wireless Networks: Efficient Protocols and Outage Behavior," *IEEE Transactions on Information Theory.*, vol. 50, no. 12, pp. 3062-3080, December 2004.

[4] P. Razaghi and W. Yu, "Bilayer low-density parity-check codes for decode-and-forward in relay channels," *IEEE Trans. Inf. Theory.*, vol. 3, no. 10, pp. 3723-3739, Oct. 2007.

[5] M. H.Azmi, J. Yuan, J. Ning and H. Q.Huynh, "Improved Bilayer LDPC Code Using Irregular Check Node Degree Distribution ," *in Proc. IEEE Int'l Symposium on Information Theory.*, Toronto, Canada, July. 2008.

[6] J. P.Cances and V. Meghdadi, "Optimized Low Density Parity Check Codes Designs for Half Duplex Relay Channels," *IEEE Trans. Wireless Commun.*,vol. 8, no. 7, pp. 3390-3395, July. 2009.

[7] Y. Li, G. H. Song, and L. L. Wang, "Design of joint network-low density parity check codes based on the EXIT charts," *IEEE Commun. Lett.*, vol. 13, no. 8, pp. 600-602, Aug. 2009.

[8] Y. Li, G. H. Song, and L. L. Wang, "Analysis of the joint network LDPC codes over orthogonal multi-access relay channel," *IEEE Commun. Lett.*, vol. 14, no. 2, pp. 184-186, Feb. 2010.

Optimal design of joint network LDPC codes over orthogonal multiple-access relay channels

Jingyi Wang*, Shuling Che and Ying Li

State Key Laboratory of Integrated Service Networks (ISN),
Xidian University,
Xi'an 710071, China
Email: wangjy@stu.xidian.edu.cn
Email: shlche@mail.xidian.edu.cn
Email: ying.lili1973@gmail.com
*Corresponding author

Junlong Wang

Huawei Technologies Co. Ltd.,
Xi'an 710071, China
Email: 401834748@qq.com

Abstract: Optimisation of degree distribution for joint network LDPC code over orthogonal Multiple-Access Relay Channels (MARC) is investigated in this paper. We first use a differential evolution algorithm to optimise the degree distribution of the joint network LDPC code over orthogonal MARC based on Gaussian approximation. Then, using a modified differential evolution algorithm, we design a rate-compatible network LDPC code, which is equivalent to designing a single code with different Signal-to-Noise Ratio (SNR). Simulation results show that the gap between Bit Error Rate (BER) performance of the former algorithm and the decoding threshold is about 0.4 dB and that between the capacity limit and decoding threshold is less than 0.7 dB at $BER = 10^{-6}$. Simultaneously, the gap between BER performance of the latter algorithm and the decoding threshold is about 0.52 dB and that between the capacity limit and the decoding threshold is less than 0.46 dB at $BER = 10^{-7}$.

Keywords: network LDPC code; multiple-access relay network; Gaussian approximation; differential evolution; capacity limit.

Reference to this paper should be made as follows: Wang, J., Che, S., Li, Y. and Wang, J. (2016) 'Optimal design of joint network LDPC codes over orthogonal multiple-access relay channels', *Int. J. Grid and Utility Computing*, Vol. 7, No. 1, pp.68–74.

Biographical notes: Jingyi Wang is currently working towards the PhD degree in Communication and Information System at Xidian University. She received her Master's degree in Telecommunications Engineering from Xidian University in 2010. Her research interests include channel coding and network coding.

Shuling Che is currently an Associate Professor at the School of Telecommunications Engineering, Xidian University. She received her PhD in Communication and Information System from Xidian University in 2008. Her research interest includes channel coding.

Ying Li is currently a Professor at the School of Telecommunications Engineering, Xidian University. She received her PhD in Communication and Information System from Xidian University in 2005. Her research interests include channel coding, wireless network coding and MIMO theory.

Junlong Wang is currently working in Huawei Technologies Co. Ltd. He received his Master's degree in Communication and Information System from Xidian University in 2011.

This paper is a revised and expanded version of a paper entitled 'Optimal design of the joint network LDPC codes over orthogonal multi-access relay channel' presented at the '2013 5th International Conference on Intelligent Networking and Collaborative Systems', Xi'an, China, 9 September 2013.

Copyright © 2016 Inderscience Enterprises Ltd.

1 Introduction

In wireless communications (Shen et al., 2012), cooperation relay networks (Cover and Gamal, 1979; Nosratinia et al., 2004; Laneman et al., 2004) have recently attracted substantial research efforts with many promising techniques of improving performance in terms of throughput, coverage or diversity gain. In relay networks, one or multiple Relay Nodes (RNs) assist the sources in transmitting information. Optimal designs of relay networks have attracted extensive attentions owing to their ability to increase communication capacity. One of the earlier works on this subject dealt with the application of the LDPC code to single-source single-relay networks (Razaghi and Yu, 2007). To improve the performance of the single-source single-relay system, a class of bilayer LDPC codes is designed in Azmi et al. (2008) and Cances and Meghdadi (2009).

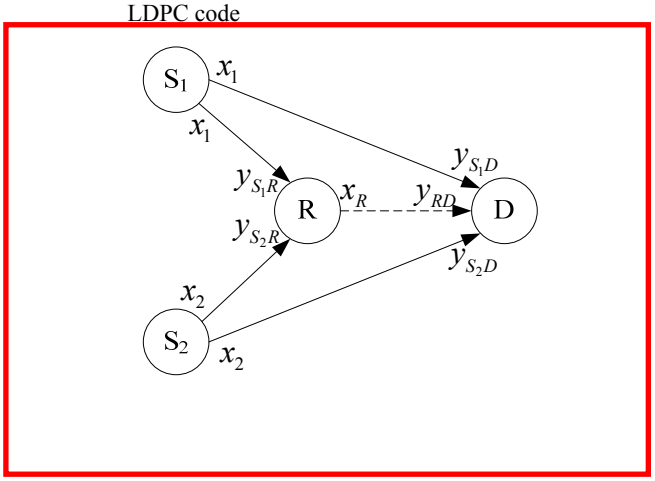
Based on the principle of the bilayer LDPC codes, the authors proposed a class of the joint network LDPC code with network coding (Zhang and Minier, 2013). And then it helps the relay to jointly re-encode the messages from the two sources and send the parity bits to the destination (Li et al., 2009). Moreover, Li et al. (2010) analysed the capacity approaching ability of the joint network LDPC codes. In this paper, we study two different methods of approaching capacity limit of two different transmission modes of a two-source single-relay system with joint network LDPC code, in which the first one requires the same code words transmitted at the two sources and the latter requires different code words transmitted at the two sources.

The rest of the paper is organised as follows. Section 2 presents the system model and then describes the operation of the system throughout different stages of the two cooperation strategies. Section 3 explains the design of two different optimisation methods. Numerical and simulation results are given in Section 4 and finally, the paper is concluded in Section 5.

2 System model

Our system is a two-slot wireless relay network consisting of two sources, one relay and one destination, as shown in Figure 1. Two different transmission modes of the system are described below, which are called Symmetry Cooperation Transmission (SCT) and Asymmetry Cooperation Transmission (ACT). The broadcast stage is followed by the cooperation stage.

Figure 1 Multi-access relay channel model with joint network LDPC code



2.1 The broadcast stage

In this stage, the sources S_i ($i=1,2$) broadcast their LDPC coded signals x_i ($i=1,2$), which are received by both relay R and destination D.

2.1.1 SCT mode

We express the received signals at the relay R and the destination D as follows:

$$y_{S_iR} = h_{S_iR}x_i + n_{S_iR} \tag{1}$$

$$y_{S_iD} = h_{S_iD}x_i + n_{S_iD} \tag{2}$$

where y_{S_iR} and y_{S_iD} are the corresponding received signal by R and D, respectively, h_{S_iR} and h_{S_iD} denote the associated channel gain and n_{S_iR} (n_{S_iD}) denotes a zero-mean Gaussian random variable with a variance $\sigma^2_{S_iR}$ ($\sigma^2_{S_iD}$).

2.1.2 ACT mode

We assume that $P^{(1)}_{S_i}$ ($i=1,2$) is the transmit power of S_i and $w^{(1)}_{S_i}$ ($i=1,2$) is a bit of an LDPC code transmitted by S_i in this stage. Then the received signals at R and D can be written as

$$y_{S_iR} = h_{S_iR}\cdot\sqrt{P^{(1)}_{S_i}}w^{(1)}_{S_i} + n_{S_iR} \tag{3}$$

$$y^{(1)}_{S_iD} = h^{(1)}_{S_iD}\cdot\sqrt{P^{(1)}_{S_i}}w^{(1)}_{S_i} + n^{(1)}_{S_iD} \tag{4}$$

where y_{S_iR}, h_{S_iR} and n_{S_iR} are as defined earlier, while $y^{(1)}_{S_iD}$, $h^{(1)}_{S_iD}$ and $n^{(1)}_{S_iD}$ are the corresponding parametric between S_i and D, where the superscript (1) represents the broadcast stage.

2.2 The cooperation stage

In this stage, after decoding the received signals correctly, R jointly re-encodes the messages of the two sources and sends parity bits x_R of the code words to D.

2.2.1 SCT mode

After x_i is decoded correctly, R jointly re-encodes the messages of the two sources and sends x_R to D. The received signal at D is

$$y_{RD} = h_{RD}x_R + n_{RD} \tag{5}$$

where y_{RD} and n_{RD} are the corresponding parametric between R and D.

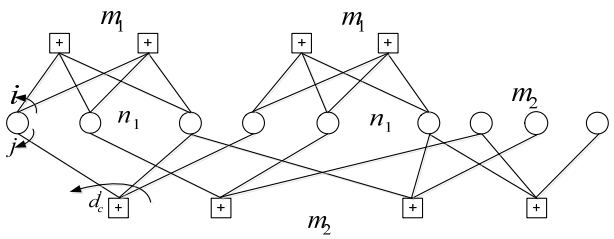
At last, D receives the signals y_{S_iD} and y_{RD}, respectively, from S_i and R. The parity check matrix of the joint network LDPC code can be written as

$$\mathbf{H} = \begin{pmatrix} \mathbf{H}_1 & \mathbf{0} & \mathbf{0} \\ \mathbf{0} & \mathbf{H}_1 & \mathbf{0} \\ \mathbf{A} & \mathbf{B} & \mathbf{C} \end{pmatrix} \tag{6}$$

where $\mathbf{H_1}$ denotes the same parity-check matrix of the constituent codes at the two sources S_i, $\mathbf{H_3} = (\mathbf{ABC})$ denotes the parity-check matrix generated by R and $\mathbf{0}$ represents the all-zero matrix.

Assume that each source uses an $(n_1, n_1 - m_1)$ irregular LDPC code with code length n_1 and parity length m_1. According to Li et al. (2010), the Tanner graph of the joint network LDPC code is shown in Figure 2, where the upper sub-graph denotes the encoding at the sources and the lower sub-graph denotes the encoding at the relay. This code includes $2m_1$ upper check nodes, m_2 lower check nodes and $2n_1 + m_2$ variable nodes. A variable node is of degree (i,j), $1 \le i \le d_v$ and $1 \le j \le d_v'$, where $i(j)$ is its upper (lower) degree and $d_v(d_v')$ is its maximum upper (lower) degree. In addition, $\lambda_{i,j}$ represents the proportion of the number of edges connected to the variable nodes with the degree (i,j).

Figure 2 The Tanner graph of the joint network LDPC code



2.2.2 ACT mode

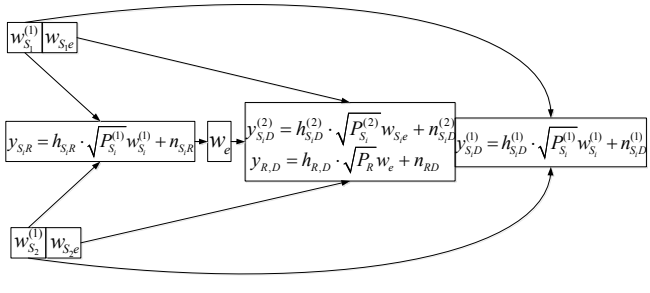
The source $S_i (i = 1,2)$ uses rate-compatible extension method from an entire LDPC code word $w_{S_i 2} = \left[w_{S_i}^{(1)}, w_{S_i e} \right]$ extended from the original code word $w_{S_i}^{(1)}$, and $w_{S_i e}$ carries additional parity-check bits as shown in Figure 3. R only generates two additional parity-check bits $w_{S_1 e}$ and $w_{S_2 e}$ from S_1 and S_2, respectively. Then network-coded code word $w_e = w_{S_1 e} \oplus w_{S_2 e}$. The received signals at D are

$$y_{S_i D}^{(2)} = h_{S_i D}^{(2)} \cdot \sqrt{P_{S_i}^{(2)}} w_{S_i e} + n_{S_i D}^{(2)} \tag{7}$$

$$y_{RD} = h_{RD} \cdot \sqrt{P_R} w_e + n_{RD} \tag{8}$$

where $P_{S_i 2}$ (P_R) is the transmit power of S_i (R) in the second stage. The other parameters were defined earlier, where the superscript (2) represents the cooperation stage.

Figure 3 Diagram of the multi-access relay channel model with joint network LDPC code



Then, D receives the signals $y_{S_i D}^{(1)}$ $\left(y_{S_i D}^{(2)} \right)$ and y_{RD}, respectively, from the two sources and the relay. First, D decodes y_{RD} and then obtains the network-coded code word $w_e = w_{S_1 e} \oplus w_{S_2 e}$. Second, D obtains $w_{S_1 e}$ and $w_{S_2 e}$ by iterative decoding with $y_{S_i D}^{(2)}$ and w_e. Different from the rate-compatible LDPC code designed in Li et al. (2009), the received SNR for $w_{S_i}^{(1)}$ and $w_{S_i e}$ are different. Using (4), (7) and (8), the SNR for the decoding of $w_{S_i}^{(1)}$ and $w_{S_i e}$ can be written, respectively, as

$$SNR_{S_i D} = \frac{\left| h_{S_i D}^{(1)} \right|^2 P_{S_i}^{(1)}}{N_0} \tag{9}$$

$$SNR'_{S_i D} = \frac{\left(h_{S_i D}^{(2)} \sqrt{P_{S_i}^{(2)}} + h_{RD} \sqrt{P_R} \right)^2}{N_0} \tag{10}$$

Finally, we decode $w_{S_1}^{(1)}$ and $w_{S_2}^{(1)}$ correctly by using the Belief Propagation (BP) iterative decoding algorithm with $w_{S_1 2} = \left[w_{S_1}^{(1)}, w_{S_1, e} \right]$ and $w_{S_2 2} = \left[w_{S_2}^{(1)}, w_{S_2, e} \right]$, respectively, at D.

3 Optimisation of degree distribution

3.1 SCT mode

3.1.1 Preliminary

Definition 1: *Decoding threshold of joint network LDPC code is defined as*

$$\sigma^* = \sup \left\{ \sigma : \lim_{L \to +\infty} m_L > M \right\} \tag{11}$$

where L is the maximum iteration number, m_L denotes the mean value of the Log-Likelihood Ratio (*LLR*) message of a code bit at the Lth decoding iteration and M is the *LLR* mean value corresponding to the target error probability.

Then with the knowledge in Li et al. (2010), $2m_L$ is the *LLR* variance value. When $\sigma < \sigma^*$, m_L will be greater than M, which means that the target error probability can be achieved. When $\sigma \ge \sigma^*$, the iterative decoding cannot achieve the target error probability.

3.1.2 Calculation of decoding threshold σ_{SD}^*

Algorithm 1: Given degree distribution of the LDPC code at the sources, let σ_{SD} and σ_{RD} represent the channel parameters of source–destination link and relay–destination link, respectively. We denote the target error probability as $P_e = 10^{-6}$ $(M = 45)$ and the maximum iteration number as L. Let $\Delta\sigma_{SD}$ denote a step length, and then Algorithm 1 can be described as follows.

- *Step 1: Initialisation.* The initialised value of the average mean value of the *LLR* message output by the check node is $m^{'l} = n^{'l} = 0$ (l is the iteration number and $l = 0$ in the first iteration) (Li et al., 2010).

- *Step 2: Updating.* When the iteration number $l < L$, update the mean values of the *LLR* messages at the variable node and the check node, and then calculate the mean value m_l of the *LLR* message during this iteration using the method in Li et al. (2010). If $m_l < M$, add the iteration number by 1 (l = l +1) and continue Step 2. If $m_l \geq M$, $\sigma_{SD} = \sigma_{SD} + \Delta\sigma_{SD}$, and go to Step 1.

- *Step 3: Stopping criterion.* If $l \geq L$ and $m_l < M$ during this iteration, stop the whole process, and the code capacity is defined as $\sigma^*_{SD} = \sigma_{SD} - \Delta\sigma_{SD}$. Otherwise, output the threshold value of channel parameter as $\sigma^*_{SD} = \sigma_{SD}$.

Using Algorithm 1, we can obtain the corresponding σ^*_{SD} from a given degree distribution of the upper layer LDPC code.

3.1.3 *Optimal design of the degree distribution of the lower layer LDPC code*

Our goal is to search the optimal degree distribution of the network LDPC code, which can approach the capacity limit. Here we use differential evolution algorithm to optimal design of the network LDPC code ensembles.

Algorithm 2. Assume that N relay code sets of the network LDPC code structure are randomly generated, denoting their degree distributions of variable node as $\lambda_{i,j}(d)$, $0 \leq i \leq d_v$, $0 \leq j \leq d'$, $d = 1,2,\ldots, N$. The degree of the lower check nodes is fixed as d'_c.

- *Step 1: Initialisation.* Initialise that degree distribution as

$$C(d) = \left\{\lambda_{i,j}(d), 0 \leq i \leq d_v, 0 \leq j \leq d'_v\right\}, d = 1,2,\ldots N \quad (12)$$

- *Step 2: Performance estimation of code sets.* Calculate the code capacity $\sigma^*(d)$ of each code set $C(d)$ through Algorithm 1, and search the optimal code ensemble meeting $C^* = \arg\max_{1\leq d\leq N}\sigma^*(d)$. The degree distribution of the optimal code ensemble corresponding to the maximum code capacity is $C^* = \left\{\lambda^*_{i,j}, 0 \leq i \leq d_v, 0 \leq j \leq d'_v\right\}$.

- *Step 3: Code set updating.* Select $\tilde{N}$ code sets from $\{C(d)\}_{d=1}^{N}$ at random and denote their degree distributions as $\tilde{C}(k) = \left\{\lambda_{i,j}(k), 0 \leq i \leq d_v, 0 \leq j \leq d'_v\right\}, k = 1,2,\ldots,\tilde{N}$. Then, update the degree distribution of the code ensemble: $C^* = C^* + \alpha\sum_{k=1}^{\tilde{N}}(-1)^{k-1}\tilde{C}(k)$, where $\alpha < 1$ is the step length.

- *Step 4: Stopping criterion.* If reaching the preset number of iteration and $m_l < M$, stop the iteration process. The degree distribution of the optimal code ensemble is defined as $C^* = \left\{\lambda^*_{i,j}, 0 \leq i \leq d_v, 0 \leq j \leq d'_v\right\}$; otherwise, go to Step 3.

Remark: *Restrictive conditions must be met for Steps 1 and 3:*

$$\begin{cases} \sum_{i\geq 0, j\geq 0}\lambda_{i,j} = 1 \\ \lambda_i = \frac{1}{\eta}\sum_{j\geq 0}\frac{i}{i+j}\lambda_{i,j} \\ \eta = \sum_i\sum_j\frac{i}{i+j}\lambda_{i,j} \\ d'_c = \frac{1-\eta}{\sum_j\frac{\lambda_{0,j}}{j}} \end{cases} \quad (13)$$

where η is the proportion of the total number of edges in the upper sub-graph. The total number of upper layer edges of a source node is $E = \frac{n_1}{\sum_{i\geq 2}\lambda_i/i} = \frac{k_1}{\sum_{j\geq 2}\rho_j/j}$ and the total number of edges of the bilayer network LDPC relay code is $E' = 2E + k_2 \cdot d'_c$, so $\eta = \frac{2E}{E'}$.

3.2 *ACT mode*

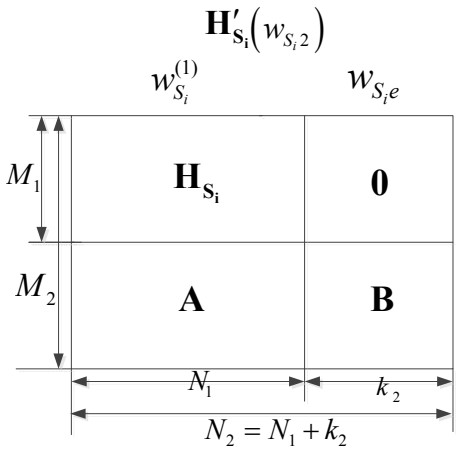
3.2.1 *Ensemble description of the joint network LDPC code*

We assume that R decodes the received signal from S_i correctly. The code rate R_1 of both S_1 and S_2 depends on $R_1 \leq C(SNR_{S_1R})$ and $R_1 \leq C(SNR_{S_2R})$, where $C(SNR_{S_iR})$ is the capacity when *SNR* of the channel between S_i and R is SNR_{S_iR}. Here we assume $R_1 = C(SNR_{S_1R}) = C(SNR_{S_2R})$.

In addition, the distance between S_i and D is farther than the distance between S_i and R, so the channel gain h_{S_iD} is smaller than h_{S_iR} and SNR_{S_iD} is smaller than SNR_{S_iR}. Here we assume $R_1 > C(SNR_{S_1D}) = C(SNR_{S_2D})$. And the capacity between the source and destination link is smaller than the capacity between the source and relay link. According to Shannon theorem, when the rate is greater than the channel capacity, the system cannot decode correctly after more iterations, so extra check bits are generated to help decode.

Figure 4 shows the extended parity-check matrix $\mathbf{H}'_{\mathbf{S}_i}(\mathbf{w}_{\mathbf{S}_i2})$, where $\mathbf{H}_{\mathbf{S}_i}$ denotes the parity-check matrix of the code word $w^{(1)}_{S_i}$ at the two sources $S_i(i = 1,2)$, w_{S_ie} denotes additional parity-check bits of the entire code word w_{S_i2} and $\mathbf{0}$ represents the all-zero matrix. The rate of the entire code word is $R_2 = \frac{N_1 - (k_1 + k_2)}{N_1 + k_2}$. We find a proper k_2, which must meet $R_2 \leq C(SNR_{S_1D}) = C(SNR_{S_2D})$.

Figure 4 Rate-compatible structure of the parity-check matrix for the relay code



R_1 and R_2 satisfy the following relationship:

$$R_1 = \frac{N_1 - k_1}{N_1} > R_2 = \frac{N_1 - (k_1 + k_2)}{N_1 + k_2} \tag{14}$$

As far as we know, the decoding performance depends on the parity-check matrix, while the degree distribution of the code ensembles determines parity-check matrix. So the design of the parity-check matrix $\mathbf{H}'_{\mathbf{S}_i}$ is equivalent to find the optimal degree distribution based on a given construction algorithm.

3.2.2 *Optimal design of the degree distribution of the joint network LDPC code*

According to the above analysis, when SNR_{S_iD} is given, we can determine the number of extra parity bits. In addition, D decodes the received information of S_i correctly; it is required to satisfy the formula

$$R_1 \le C\left(SNR_{S_iD}\right) + C\left(SNR'_{S_iD}\right) \tag{15}$$

When the transmit power and the channel gains are given, we can obtain the theoretical minimum SNR by (15). Our optimal goal is to find the relay extended code ensemble, whose threshold of SNR is approaching the theoretical extreme value.

Compared with the rate-compatible LDPC code of the single-source single-relay system, the two-source single-relay system uses the linear network-coded method at R, which achieves the same cooperative diversity to the single-source single-relay system and D decodes the received signal of S_1 and S_2 separately. Here the two-source single-relay system can be equal to two separate single-source single-relay systems for rate-compatible LDPC code. Therefore, we can use the algorithm in Cances and Meghdadi (2009) to optimise the design of the rate-compatible extended code ensemble of S_1 and S_2 separately, while linear network-coded is used at the relay.

4 Simulation results

4.1 *SCT mode*

Assume each source node employs an $(n_1, n_1 - m_1)$ LDPC code with $\lambda(x) = 0.23403x + 0.21242x^2 + 0.1469x^5 + 0.102840x^6 + 0.30381x^{19}$ and $\rho(x) = 0.71875x^7 + 0.28125x^8$, where $n_1 = 22164$ and $m_1 = 11082$. $SNR_{RD} = 3$ dB and the two source–destination links are assumed to be symmetric. Using Algorithm 1, four different parameters of the joint network LDPC codes are obtained and listed in Table 1, where σ_{RD}^2 represents the channel parameter between the relay and the destination link.

Table 1 Four optimal joint network LDPC codes

Code ensembles	*Code A*	*Code B*	*Code C*	*Code D*
d'_v	2	2	2	2
d'_c	4	4	4	7
k_2	2814	4814	2814	2814
σ_{RD}	0.5	0.5	0.8	0.5
η	0.942065	0.904808	0.942065	0.902835
σ^*_{SD}	1.0568	1.0987	1.0393	1.1116
Threshold (E_bN_0)	0.155039dB	0.115123dB	0.2018dB	–0.22877dB
Sum capacity (E_bN_0)	–0.24536dB	–0.517620dB	–0.143948dB	–0.24536dB
Gap	0.400399dB	0.632743dB	0.345748dB	0.01666dB

Using Algorithm 2, four optimal degree distributions of the joint network LDPC codes are given in Tables 2–5.

Table 2 Degree distributions of code A

$\lambda_{i,j}$	$\lambda_{i,0}$	$\lambda_{i,1}$	$\lambda_{i,2}$
$i = 2$	0.193815	0.00543635	0.04612661
$i = 3$	0.171369	0.019109592	0.02409292
$i = 6$	0.129299	0.006342408	0.00494214
$i = 7$	0.09485	8.2369E-05	0.00259462
$i = 20$	0.273877	0.000432436	0.00181212
$i = 0$	0	0.0030528	0.02276564

Table 3 Degree distributions of code B

$\lambda_{i,j}$	$\lambda_{i,0}$	$\lambda_{i,1}$	$\lambda_{i,2}$
$i = 2$	0.07441004	0.20599344	0
$i = 3$	0.19208258	0.00015819031	0
$i = 6$	0.1327018904	0.00013842	0.0001681903
$i = 7$	0.09266986	0.000326381	0.0001779641
$i = 20$	0.27426244	0.0005152496	0.0021751167
$i = 0$	0	0.0237936797	0.000009887

Table 4 Degree distributions of code C

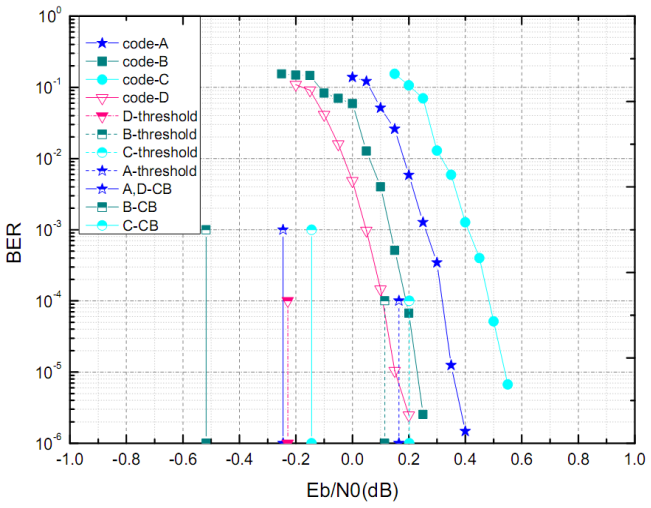
$\lambda_{i,j}$	$\lambda_{i,0}$	$\lambda_{i,1}$	$\lambda_{i,2}$
$i=2$	0.1206132872	0.0	0.0
$i=3$	0.1001453763	0.0000219458	0.0
$i=6$	0.1860514424	0.0002767963	0.000016798
$i=7$	0.1964141036	0.0002114936	0.0000212906
$i=20$	0.3858558271	0.0003262453	0.0000362551
i = 0	0.0	0.0041565109	0.0206487529

Table 5 Degree distributions of code D

$\lambda_{i,j}$	$\lambda_{i,0}$	$\lambda_{i,1}$	$\lambda_{i,2}$
$i=2$	0.1112574229	0.013643762	0.1818773738
$i=3$	0.09172912663	0.0876831253	0.0571696344
$i=6$	0.13223499235	0.00032560828	0.00015708008
$i=7$	0.092674986	4.568455E-05	6.788722E-05
$i=20$	0.274059093	0.00010113293	0.000217037
$i=0$	0	0.00351717946	0.02072694417

The BER curves of four codes are illustrated in Figure 5. We see that the gap between the decoding threshold of four codes obtained by searching the maximum decoding threshold σ_{SD}^{*} and capacity limit is less than 0.7 dB, and that between BER performance and decoding threshold is less than 0.4 dB. Since the lower check degree of Code D is bigger and more information bits are contained in the check equation, it outperforms Code A by 0.2 dB at $BER=10^{-5}$. Another important observation is that Code B has a gain of about 0.15 dB over Code A at $BER=10^{-5}$ and the performance gain of Code D is about 0.1 dB over Code B at $BER=10^{-5}$. This indicates that increasing the degrees of lower layer check nodes is better than increasing the numbers of parity bits to improve system performance. When the noise variances between the *R* and *D* link are increased, the system decoding performance will be reduced and Code A will have a gain of about 0.2 dB over Code C at $BER=10^{-5}$.

Figure 5 Performance of the joint network LDPC codes



4.2 ACT mode

Assume each source node employs LDPC code-1 and code-2 listed in Cances and Meghdadi (2009, Table 1). The two source–destination links are assumed to be symmetric. The distance between S_i and D is normalised to unity and d denotes the normalised distances between S_i and R. The channel gain $|h_{S_1D}|^2=|h_{S_2D}|^2=1$, $|h_{S_1R}|^2=|h_{S_2R}|^2=\frac{1}{d^{\alpha}}$ and $|h_{RD}|^2=\frac{1}{(1-d)^{\alpha}}$, where we assume that $\alpha=2$ is the path loss exponent and $d=0.25$. The power allocation among S_i and R is fixed as $P_{S_1}^{(1)}/2=P_{S_2}^{(1)}/2=P_{S_12}=P_{S_22}=P_R/2=P_T/8$, and $w_{S_i}^{(1)}$ and w_{S_i2} have the rate $R_1=1/2$ and $R_2=1/4$, respectively. Table 6 gives the optimum LDPC code ensemble of w_{S_i2} via the algorithm in Cances and Meghdadi (2009) and the network-coded method at the relay. And the node probability set of w_{S_12} is $h_1(2)=0.1978$, $h_1(i)=1$ for $i\in\{3,6,7,8,10,14,16,20,30,33\}$, the node probability set of w_{S_22} is $h_1(3)=0.1576$, $h_1(i)=1$ for $i\in\{2,4,7,8,10,14,16,20,30,33\}$, where $h_1(i)$ denotes the probability of a variable node that has a degree of *i* and falls in the region of region-1 (i.e. $\mathbf{H_1}$ and **A**, namely region-1; **0** and **B**, namely region-2.)

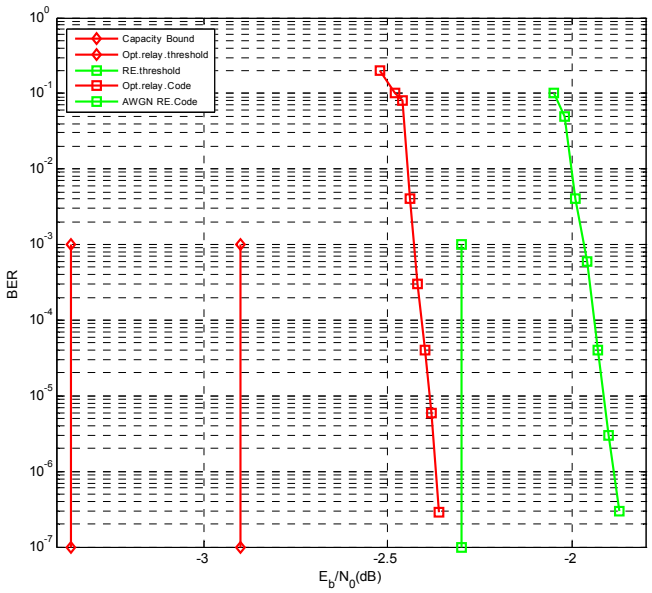
Table 6 Rate-compatible extended LDPC code ensembles

Code ensembles	*Extended code ensemble 1*	*Extended code ensemble 2*
λ_2	0.13370307136	0.06600453943
λ_3	0.02829823403	0.11086569074
λ_4	0.02371830093	0.07247855957
λ_5	0.00295003743	0.00422715433
λ_6	0.05593270965	0.03891266928
λ_7	0.00474956026	0.06403186741
λ_8	0.05605071114	0.03722942404
λ_9	0.11366862967	0.15231465261
λ_{10}	0.06932587957	0
λ_{11}	0.00125745345	0.00502688622
λ_{12}	0.00044250561	0
λ_{13}	0.00081494784	0
λ_{14}	0.00087763614	0.05326214450
λ_{15}	0.00027656601	0
λ_{16}	0.19417146355	0.13551266623
λ_{17}	0.20455190775	0
λ_{20}	0.00118001497	0.00411290691
λ_{22}	0.00186589867	0.16077657776
λ_{26}	0.00009587622	0
λ_{30}	0.10553758901	0.09505384861
ρ_8	0	0.22602708425
ρ_9	0.99563763215	0.77391198379

In simulations, the code lengths of $w_{S_i}^{(1)}$ and w_{S_i2} are $N_1=20000$ and $N_2=2N_1=40000$, respectively. We compare the BER performance between the optimum LDPC

code ensemble and the repetition code under the AWGN channel, when the repetition code has $w_{S_i e} = w_{S_i}^{(1)}$ and D receives $w_{S_i}^{(1)}$ from source S_i and R at the same time. Figure 6 shows the BER performance of the optimised relay code ensemble and the repetition code. It is seen that the relay code ensemble optimised via the algorithm in Cances and Meghdadi (2009) can achieve about 0.5 dB gain over the repetition scheme. The gap between the BER performance of the optimised relay code ensemble of the rate-compatible LDPC and the decoding threshold is about 0.52 dB, and the gap between the decoding threshold and the capacity limit is less than 0.46 dB.

Figure 6 The BER performance comparison between the optimised relay code and the repetition code



5 Conclusions

In this paper, we employed the differential evolution method to design degree distribution of different transmission modes of the joint network LDPC code for a two-source single-relay system. The performance of the new codes we designed showed significant BER performance gain for a two-source single-relay system with symmetric AWGN channels.

Acknowledgements

We are grateful to anonymous referees for their invaluable suggestions. This work is supported by the National Natural Science Foundation of China (Nos. 61072064, 61101148 and 61001131).

References

Azmi, M.H., Yuan, J., Ning, J. and Huynh, H.Q. (2008) 'Improved bilayer LDPC codes using irregular check node degree distribution', *Proceedings of the IEEE International Symposium on Information Theory*, 6–11 July, Toronto, Canada, pp.141–145.

Cances, J.P. and Meghdadi, V. (2009) 'Optimized low density parity check codes designs for half duplex relay channels', *IEEE Transactions on Wireless Communications*, Vol. 8, No. 7, pp.3390–3395.

Cover, T. and Gamal, A.E. (1979) 'Capacity theorems for the relay channel', *IEEE Transactions on Information Theory*, Vol. 25, pp.572–584.

Laneman, J., Tse, D. and Wornell, G. (2004) 'Cooperative diversity in wireless networks: efficient protocols and outage behavior', *IEEE Transactions on Information Theory*, Vol. 50, No. 12, pp.3062–3080.

Li, Y., Song, G.H. and Wang, L.L. (2009) 'Design of joint network-low density parity check codes based on the EXIT charts', *IEEE Communications Letters*, Vol. 13, No. 8, pp.600–602.

Li, Y., Song, G.H. and Wang, L.L. (2010) 'Analysis of the joint network LDPC codes over orthogonal multi-access relay channel', *IEEE Communications Letters*, Vol. 14, No. 2, pp.184–186.

Nosratinia, A., Hunter, T.E. and Hedayat, A. (2004) 'Cooperative communication in wireless networks', *IEEE Communications Magazine.*, Vol. 42, No. 10, pp.74–80.

Razaghi, P. and Yu, W. (2007) 'Bilayer low-density parity-check codes for decode-and-forward in relay channels', *Transactions on Information Theory*, Vol. 3, No. 10, pp.3723–3739.

Shen, Y., Pei, Q., Xu, Q. and Zhang, Z. (2012) 'The multimedia service session handoff method in heterogeneous wireless networks', *International Journal of Grid and Utility Computing*, Vol. 3, No. 1, pp.68–77.

Zhang, Y. and Minier, M. (2013) 'How network coding system constrains packet pollution attacks in wireless sensor networks', *International Journal of Grid and Utility Computing*, Vol. 4, Nos. 2–3, pp.197–203.

PAPER • **OPEN ACCESS**

Research on the changing trend of farmland area in China and its driving factors from 1996 to 2016

To cite this article: J Y Wang and X M Li 2018 *IOP Conf. Ser.: Mater. Sci. Eng.* **392** 062097

View the article online for updates and enhancements.

中文文章叫近20年，英文文章是1996 to 2016,文章完全一样

You may also like

- The 300 years cropland changes reflecting climate impacts and social resilience at the Yellow River–Huangshui River Valley, China
Qiong Chen, Liang Emlyn Yang, Jing Luo et al.
- Analysis and Research on the Value of Farmland Transfer Based on Environmental Protection Evaluation System
Zhenyu Zhang, Minghua Tian, Jianjun Li et al.
- High Standard Farmland Construction and Soil Conservation Evaluation
Jing Zhang and Lu Sun



This content was downloaded from IP address 219.144.164.16 on 16/11/2023 at 00:29

Research on the changing trend of farmland area in China and its driving factors from 1996 to 2016

J Y Wang [1] and X M Li[2*]

[1]Xi'an Shiyou University, Xi'an China, 710065

[2]Shaanxi Provincial Land Engineering Construction Group，Xi'an China, 710075

*Corresponding author: xmlisdc@126.com

Abstract. The paper was to research the changing trend of farmland area from 1996 to 2016. The original data of farmland area of China in these years were collected, data mining technology was used, and ARIMA model was chosen to predict each other between the two periods of 1996-2008 and 2008-2016, so the original farmland area data could be corrected and normalized. Then correlation analysis was used to study the driving factors. The trend research result showed, the farmland area decreased from 1996 to 2016, the decreasing rate was faster before 2004, and then it decreased slowly. The correlation analysis result showed, the added value proportion of primary industry, the total population, and the urban population were the most important driving factors, their coefficients were 0.959, -0.918 and -0.896 respectively. It could be concluded by the result that the industry configuration and the urbanization could affect the farmland area changing with the development of social economy.

1. Introduction

China is a great agricultural country, and the farmland is one very important resource which is related to food security. However, the vigorous demand for lands brings great challenge for farmland protection with the promotion of socialist modernization construction [1]. The research on farmland area change and its driving factors in China has always been one popular problem. The statement was refuted that China's cultivated land has been descending since 1957 based on the analysis of the actual change of the cultivated land area [2]. The farmland area changing trend, spatial characteristics and the driving factors in China for a period of time before 2007 were studied [3-5]. And in different scales such as the scale of province or in some part of China, the dynamic change trend of farmland was studied [6-8]. Since 1980s, with the development and application of 3S technology, many scholars studied the farmland change using the RS images such as Landsat TM images [9, 10]. And the analysis approaches in the study of the driving forces of land use change in large regions were explored by using digital satellite remote sensing data of China [11]. Not only the changes in China's cultivated land but also those in some provinces were analyzed based on remote sensing data such as Landsat TM/ETM+, NOAA, SPOT dataset [12, 13].

The statistic data sources of cultivated land in China are various, for example, the international organizations such as FAQ, WRI (the world resources institute), and different departments of China such as MLR (the ministry of land and resources), MOA (the ministry of agriculture), the bureau of statistics of PRC. However, the statistical data supplied by MLR are considered the most authoritative [14]. But the data from the MLR are not regularly entire in the demanded periods, and there was a jumping phenomenon with the farmland area from 2008 to 2009, that's because the data of 2008 was

Content from this work may be used under the terms of the Creative Commons Attribution 3.0 licence. Any further distribution of this work must maintain attribution to the author(s) and the title of the work, journal citation and DOI.
Published under licence by IOP Publishing Ltd

based on the first national land use survey, and the data of 2009 was based on the second national land use survey, that's seemly illogical. At present, most scholars analyze the farmland area change by the exiting data directly while ignoring the accuracy of the statistic data, or they just focused on some periods before 2008 or after 2009 evading the jumping years. Only a few scholars researched the farmland area in different historical periods [14, 15]. In this paper, the researched years included the years of before and after the second national land use survey. The method of data mining was introduced to analyze the relation between the two periods of the years before 2008 and the years after 2009, so the changing trend of China's farmland area could be reflected more scientifically. At the same time, the driving factors were studied based on data normalization. And this is not found in the present research, which could be useful for studying China's farmland changing trend.

2. Data and methods

2.1. Data acquisition

2.1.1. Data of farmland area in China

The farmland area of China, especially in the historical periods, has been hard for statistic for a long time. The national department of land management have been announcing the changing situation each year since 1986. In order to obtain the veracious statistical data of farmland in China, the first national land use survey was operated from 1984 to 1996. The survey result showed there was 1.95 billon mu (1 mu = 666.66 m^2) of farmland in China by the day of Oct.31 1996 [15], which was considered the most credible result at that time [16]. Then, the farmland area of each year from 1996 to 2008 can all be obtained from the statistical bulletin of the year.

In order to obtain more veracious statistical data of farmland, the second national land use survey was operated from 2007 to 2009. The survey result showed there was 2.03 billon mu of farmland in China by the year of 2009 [15]. And since then the land use change survey has been operated each year. And the farmland area from 2007 to 2016 can be obtained from the national service platform of land use survey result. Because new methods and technologies were applied with the second national land use survey, some farmlands which were not found in the first survey were found in the second survey, and there was a jumping phenomenon with the farmland area from 2008 to 2009, which would be specially researched after a while for analyzing the changing trend of farmland area.

2.1.2. Data of driving factors

Land is closely related to the human social and economic development. The national farmland change is influenced by the geographical and climate conditions, social and economic development, flood and waterlogging disaster and so on [1]. For researching the driving factors influencing the farmland changing, three kinds of factors were introduced for comparison and selection. One kind were the comprehensive factors reflecting the national economic development, and they were the gross national income (GNI), the gross domestic product (GDP), the primary industry added value and its ratio, the second industry added value and its ratio, the third industry added value and its ratio, the gross agricultural output value, per capita GDP, industrial added value, architectural added value. Another kind were special factors reflecting the level of urbanization, and they were the national population, the urban population, and the rural population. The third kind was the special factors reflecting the natural disaster, and they were the damage area and the grain yield. There were in total of 17 factors which were used for analysis [17]. And data of all factors for the recent 20 years could be obtained from the web site of the national bureau of statistics.

2.2. Study methods

In this paper, the national farmland area dada from 1996 to 2016 years were collected and analysed to study the changing trend, and the correlation analysis was operated to research the driving factors. While studying the changing trend of farmland from 1996 to 2016, according to the found jumping

phenomenon with the data from 2008 to 2009, the data mining technology was introduced. First, the farmland area of the year 2009 can be predicted with the data of 1996 to 2008. And the farmland area of the year 2008 can also be predicted reversely with the data of 2009 to 2016. Then, based on the predicted data and the practically collected data of the farmland of the years 2008 and 2009, the mathematical ratio relation between the farmland area of 2008 and 2009 could be analysed and obtained, so the jumping phenomenon could be solved with the ratio. At last, all the farmland data from 1996 to 2016 should be normalized for researching the changing trend more scientifically.

ARIMA (Autoregressive Integrated Moving Average) model was chosen for prediction with data mining, which was promoted by Box and Jenkins, it's a very famous and useful time-sequence forecast method, and that's just the needed one in this paper.

3. Analysis on the farmland area changing trend from 1996 to 2016

3.1. The analysis based on the original statistic data of farmland area

By collecting and analysing the original statistic data of farmland area for years of 1996-2016, the result showed that the national farmland area decreased year by year, as Figure1, and the decreasing speed was the most quick from 2000 to 2004. While the farmland area jumped from 1.826 billion mu in 2008 to 2.031 billion mu in 2009. And after 2009, the farmland area decreased very slowly.

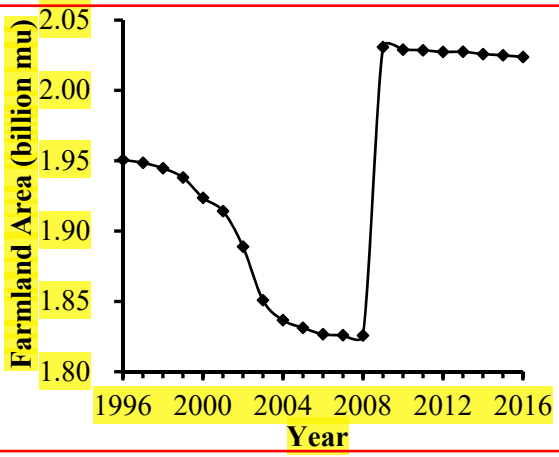


Figure 1. Changing Trend for Farmland Area of 1966-2016 Based on Original Statistic Data

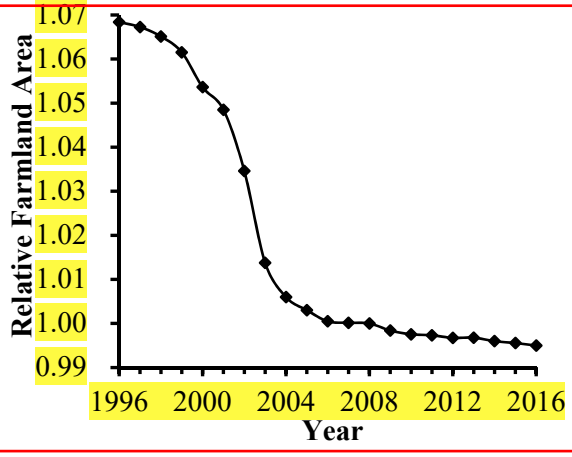


Figure 2. Changing Trend for Farmland Area of 1966-2016 Based on Revised Statistic Data

China finished the first national land use survey in 1996, and the second in 2009, so the jumping phenomenon just happened in the division years of the twice land use survey. Whether the national farmland increased by about 200 million mu in the year of 2009 or not should be studied deeply. And by reviewing literatures [14, 15, 18], it could be concluded that the main reason was that more advanced technologies were introduced while the second land use survey, so some farmlands lost of statistic in the first land use survey were found in the second time, and the accuracy of the statistic result was improved. In this paper, the farmland data for the recent 20 years were based on twice different land use survey and different technology conditions. We can easily studied the changing trend in each period before or after the second land use survey, while all the data of farmland area must be revised and normalized if we want to study the continual time-sequence changing trend from 1996 to 2016, then they might be comparable.

3.2. Revision of farmland area based on data mining technology

Data mining technology is much useful for time-sequence prediction, and by that, in this paper, the farmland area of the year 2009 was predicted with the farmland data of the years from 1996 to 2008, the ratio α between the farmland area of 2009 and that of 2008 could be obtained. And the farmland area of the year 2008 was also predicted reversely with the farmland data of the years from 2009 to

2016, the ratio β between the farmland area of 2009 and that of 2008 could also be obtained. Then, for reflecting the ratio more scientifically, we could get the ratio ρ by the average of α and β.

SPSS software was used for prediction in this paper, by analyzing and comparing, the model of ARIMA was used in both of the prediction and the reverse prediction. The model used while predicting the farmland area of the year 2009 was ARIMA(1,1,2) (r^2=0.975**), and the model used while predicting reversely the farmland area of the 2008 was ARIMA(1,1,4) (r^2=0.966**), both of the two models were significant in the level of 0.01, with that, the predicted farmland area of the year 2009 was 1820.08 million mu, the reversely predicted farmland area of the year 2008 was 2030.98 million mu, so we can get α=0.996899887, β=0.999895617, and then ρ=0.998397752, so we could use the ρ value as the revision ratio of the data of the two different periods.

3.3. Trend analysis based on the revised data of farmland area

All the original farmland area data were revised with the ratio ρ and normalized into relative values for reflecting the changing trend more scientifically. Based on the study of the previous paper, the relative farmland area of the years from 1996 to 2008 were calculated with the denominator of the farmland area of the year 2008, the relative farmland area of the years from 2009 to 2016 were calculated with the denominator of the farmland area of the year 2009 while revised by multiply the ratio ρ. Then the continual changing trend of farmland area from 1996 to 2016 could be obtained, shown as Figure 2, which showed the national farmland area decreased year by year. Before the 2004, the decreasing rate was faster, and after that the decreasing rate trends to be slower, especially after 2009, the farmland area trends to be stable.

4. Analysis on driving factors

A total of 17 factors were collected in this paper, and their descriptive statistical characters were shown in table 1. In order to study the driving factors, correlations between the farmland area and the factors were analysed, and then, by comparing the correlation coefficients shown as table 2. the driving factors could be chosen out.

Table 1. Descriptive Statistical Characters of All Factors from 1996 to 2016

Factors	*Min.*	*Max.*	*Ave.*	*Std.*	Factors	*Min.*	*Max.*	*Ave.*	*Std.*
x_1	7078	74114	30444.70	225956.60	x_{10}	589.8	5398	2287.2	16332.77
x_2	7181.4	74412.7	30571.87	226519.84	x_{11}	2953	24786	11653.28	79508.29
x_3	1387.8	6367.1	3124.07	17742.62	x_{12}	439.3	4952.2	1962.3	15992.73
x_4	8.556	19.325	12.11	3.28	x_{13}	122389	138271	131047.71	4702.17
x_5	3382.8	29623.6	13562.92	94949.58	x_{14}	37304	79298	58413.24	12989.27
x_6	39.810	47.559	45.33	2.00	x_{15}	58973	85085	72634.48	8313.40
x_7	2410.7	38422	13884.89	114605.84	x_{16}	43070	62144	52326.48	5812.06
x_8	33.569	51.634	42.56	4.47	x_{17}	21770	54688	41009.48	10706.30
x_9	1354	5928.8	2884.26	16570.35					

**In the table, x_1 means the gross national income (GNI), billion yuan; x_2 means the gross domestic product (GDP), billion yuan; x_3 means the primary industry added value, billion yuan; x_4 means the proportion of primary industry added value, %; x_5 means the second industry added value, billion yuan; x_6 means the proportion of second industry added value, %; x_7 means the third industry added value, billion yuan; x_8 means the proportion of third industry added value, %; x_9 means gross agricultural output value, billion yuan; x_{10} means per capita GDP, billion yuan; x_{11} means industrial added value, billion yuan; x_{12} means architectural added value, billion yuan; x_{13} means the national population, $*10^4$; x_{14} means the urban population, $*10^4$; x_{15} means the rural population, $*10^4$; x_{16} means the grain yield, $*10^4$ t; x_{17} means damage area, $*10^3$ ha; and the same as follows.*

Table 2. Correlation Coefficients between Original/Relative Farmland Area and Factors

	Original data	Relative data		Original data	Relative data
Relative data	-0.142	1.000	x_9	0.686	-0.709
x_1	0.649	-0.746	x_{10}	0.651	-0.749
x_2	0.652	-0.745	x_{11}	0.638	-0.784
x_3	0.663	-0.736	x_{12}	0.688	-0.716
x_4	-0.274	0.959	x_{13}	0.433	-0.918
x_5	0.647	-0.774	x_{14}	0.488	-0.896
x_6	-0.519	0.259	x_{15}	-0.518	0.880
x_7	0.649	-0.717	x_{16}	0.752	-0.524
x_8	0.433	-0.819	x_{17}	-0.514	0.708

As shown in table 2, the correlation coefficients between the original farmland area and the factors were poor because of the jumping phenomenon. However, by analyzing the correlations between the revised farmland area and the factors, we could find, the proportion of the first industry added value had the best correlation with the farmland area, its coefficient was up to 0.959. The national total population was secondary to it, and its correlation coefficient was -0.918, then the urban population and the rural population were secondary to that sequentially, which means the first industry added value, the national total population, the urban population and the rural population were the most important driving factors. According to the research result, we could conclude that it was mainly the national industry structure and the urbanization construction that influence the farmland changing.

5. Conclusion and discussion

Land has both of its own natural and social characters, and it's just all of the factors including society, economy, and policy factors that influence the statistics of farmland area for a long time. So it's difficult for a long-time changing trend research. The period studied in this paper was across twice national land use survey, and there happened to be a jumping phenomenon, but this couldn't reflect the boost of farmland area from 2008 to 2009. The reasons of the phenomenon were studied, that was mainly because RS, GIS and some other new technologies were applied in the second national land use survey, the survey and statistics were more standardized, so the accuracy was apparently promoted, which made the farmlands lost of statistics before found in the second land use survey. Therefore, in order to study the changing trend for a period across twice land use survey, the quantitative relation of the farmland area between the twice survey must be studied and obtained. In this paper, with data mining technology, revision and normalization of farmland area, the research result could reflect the changing trend more actually.

Research results showed China's farmland area decreased year by year from 1996 to 2016, especially before 2004, the decreasing rate was fast, and after that year the decreasing rate tended to be slow. As to the driving factors, it's the proportion of the primary industry added value in the aspect of the national industry structure and the national population, the urban population in the aspect of urbanization construction which were the main driving factors influencing the farmland changing. Because of the ecological restoration after the year of 1999, the farmland decreased rapidly [14, 19]. In 2004, the land management law was revised, which strengthened the protection and the requisition-compensation balance of farmland, and that's much useful for retaining farmland. In this paper, only the farmland area data from 1996 to 2016 were used to study the changing trend, and in present time, China pay much attention to farmland protection, not only including the quantity, but including the land quality with core of productivity in order to realize the protection of the trinity of quantity, quality and ecology [20]. In the future research, the changing trend of farmland area would be studied deeply.

The years of 1966 to 2016 were introduced in this paper to study the changing trend because the demand of statistical data for longer-time sequence was difficult to be satisfied. In future research, based on the collected statistical data, the data mining, remote sensing interpretation and some other methods would be applied to compensate the lack of some factors, so we wish we could obtain a longer time-sequence changing trend.

References

[1] Zhao Q G, Zhou S L, Wu S H and Ren K. 2006. Cultivated Land Resources and Strategies for Its Sustainable Utilization and Protection in China, *Acta Pedologica Sinica*,43(4): 662-72.
[2] Bi Y Y and Zheng Z Y. 2000. The Actual Changes of Cultivated Area Since The Founding of New China**,** *Resources Science*, 22(2): 8-12.
[3] Li X B. 1999. Change of arable land area in China during the past 20 years and its policy implications, *Journal of Natural Resources*, 14(4): 329-33.
[4] Cao Y G, Yuan C, Zhou W, Tao J and Hua R. 2008. Analysis on D iving Forces and Provincial Differences of Cultivated Land Change in China. *China Land Science*, 22(2): 17-22.
[5] Huang Z H and Wu C F. 2009. Empirical Study of Cultivated Land Change and Socio-economic Factors in China. *Journal of Natural Resources*. 24(2): 192-9.
[6] Yu T, Cao Y G and Xu J X. 2016. Driving Force of Cultivated Land Change in China Based on Different Scales. *Chinese Agricultural Science Bulletin*, 2016, 32(24): 194-8.
[7] Wu X, Wang S R, Shang H Y and Wang Z J. 2017. Analysis of Dynamic Change and Driving Forces of Cultivated Land in NingXia During The Past 18 Years. *Chinese Journal of Agricultural Resources and Regional Planning*. 38(8):98-104.
[8] Guo L Y, Wang D L and Wang J Y. 2012. Analysis of the Arable Land Change and Its Causes in the Eastern Coastal China Over the Last Decades. *Chinese Journal of Agricultural Resources and Regional Planning*. 33(1):6-10.
[9] Zhang G P, Liu J Y and Zhang Z X. 2003. Spatial-temporal Changes of Cropland in China for the Past 10 Years Based on Remote Sensing. *Acta Geographica Sinica*. 58(3): 323-32.
[10] Tian G J, Zhuang D F and Liu M L. 2003. The Spatial-temporal Dynamic Change of Cultivated Land in China in 1990s. *Advance in Earth Sciences*. 18(1): 30-6.
[11] Liu X H,Wang J F,Liu J Y, Liu M L and Meng B. 2005. Quantitative Analysis Approaches to the Driving Forces of Cultivated Land Changes on A National Scale.*Transactions of the Chinese Society of Agricultural Engineering*. 21(4):56-60.
[12] Xu L L, Li B L, Yuan Y C, Gao X Z, Liu H J and Dong G H. 2015. Changes in China's Cultivated Land and the Evaluation of Land Requisition-Compensation Balance Policy from 2000 to 2010. *Resources Science*. 37(8): 1543-51.
[13] Li J G, He C Y, Shi P J, Chen J, Gu Z H and Xu W. 2004. Change Process of Cultivated Land and Its Driving Forces in Northern China during 1983-2001. *Acta Geographica Sinica*. 59(2): 274-82.
[14] Feng Z M, Liu B Q and Yang Z. A Study of the Chaning Trend of Chines Cultivated Land Amount and Data Reconstructing:1949-2003. *Journal of Natural Resources*, 20(1): 35-43.
[15] Tan Y Z, He J, Yue W Z, Zhang L and Wang Q R. 2017. Spatial Pattern Change of the Cultivated Land before and after the Second National Land Survey in China. *Journal of Natural Resources*, 32(2): 186-97.
[16] Lin G C S, Ho S P S. 2003. China's land resources and land-use change: insights from the 1996 land survey. *Land Use Policy*, 20(2): 87-107.
[17] Fu Z Q, Cai Y L, Yang Y X and Dai E F. 2001. Research on the Relationship of Cultivated Land Change and Food Security in China. *Journal of Natural Resources*, 16(4): 313-9.
[18] Zhang Y Q and Yang Z S. 2013. Comparative Analysis of Two Investigations of Land Resource in China. *Scientific and Technological Management of Land and Resources*. 30(2): 100-4.
[19] Xu X L, Cai Y M, Zhang K L and Zheng W Y. 2005. Study on Dynamic Change of Cultivated Land Resources and Causes of the Changes. *China Population Resources and Environment.* 15(3): 75-9.
[20] Tan Y Z, Wu C F, Wang Q R, Zhou L Q and Yan D. 2005. The Change of Cultivated Land and Ecological Environment Effects Driven by the Policy of Dynamic Equilibrium of the Total Cultivated Land. *Journal of Natural Resources*. 20(5): 727-34.

第40卷，第8期
2019年8月
中国农业资源与区划
Chinese Journal of Agricultural Resources and Regional Planning
Vol. 40, No. 8, pp171-176
August, 2019

doi: 10.7621/cjarrp.1005-9121.20190821

中文文章叫近20年，英文文章是1996 to 2016, 文章完全一样

·资源利用·

近20年中国耕地数量变化趋势及其驱动因子分析*

王静怡[1]，李晓明[2※]

（1. 西安石油大学计算机学院，陕西西安 710065；2. 陕西省土地工程建设集团有限责任公司，西安 710075）

摘 要 【目的】研究“二调”前后近20年我国耕地面积的变化趋势及其影响因子，为促进耕地保护和土地资源的高效集约节约利用提供决策支撑。【方法】基于1996—2016年耕地数量的原始统计数据，利用数据挖掘技术选用ARIMA模型，基于两次全国土地调查时间段耕地数量数据进行相互预测和反推，即利用1996—2008年耕地数量数据预测2009年耕地数量，利用2009—2016年数据反推2008年耕地数量，从而实现数据的校正和比值归一化的目的，进一步研究近20年内我国耕地数量的变化趋势，并通过相关性分析研究遴选出其驱动因子。【结果】趋势研究结果表明，近20年内我国耕地数量呈现逐年递减的趋势，其中2004年之前递减速度较快，之后递减速度趋缓。相关性分析结果显示，第一产值增加值占比、年末总人口数，以及城镇人口数是影响耕地数量变化的重要驱动因子，其相关系数分别为0.959，-0.918，-0.896。【结论】从研究结果可以推论，我国在社会经济发展中的产业结构布局，以及城镇化建设进程对耕地数量变化产生了重要的影响。

关键词 数据挖掘 ARIMA模型 耕地数量 变化趋势 驱动因子

中图分类号：P96 **文献标识码**：A **文章编号**：1005-9121【2019】08171-06

0 引言

我国是一个农业大国，耕地资源直接关系到国家粮食安全问题，是确保“中国人的饭碗牢牢端在自己手中”的重要基础。同时，在加快推进我国社会主义现代化建设进程中，经济建设对土地的旺盛需求也对耕地保护带来了极大的挑战[1]。对于我国耕地的变化趋势及其影响驱动力的研究，一直都是一个热点问题，甚至有专家学者通过史册文献资料的查证对过去300年我国部分省区耕地资源数量变化及驱动因素进行了研究[2]。

目前，对于我国耕地变化趋势的研究，多基于对统计数据进行分析，从空间尺度上可以分为国家尺度和区域尺度的研究。其中，对于国家尺度上的研究，由于统计标准、技术手段等多种因素的限制，2008—2009年数据发生明显的跳跃式变化，所以绝大部分的研究均处于2008年之前的部分时间段内，如毕于运等[3]通过对我国建国至1996年实有耕地面积的收集整理研究分析了其变化分析；李秀彬[4]对1999年我国前20年耕地面积变化的总体趋势、空间特征和驱动因子进行了研究；曹银贵[5]研究分析了1996—2005年全国耕地变化的情况及其影响的主要因子；黄忠华、吴次芳等利用1978—2007年我国耕地、经济增长、城镇化、地方财政收入数据分析了社会经济因素对耕地变化的影响[6]。以上研究均将时间局限在2008年之前，而回避了2008—2009年耕地统计数据跳跃的现象，这不利于科学研究我国耕地的变化趋势和指导耕地保护工作。对于区域尺度，如省级，甚至市县级尺度，由于统计基数较小，受统计方法、技术标准等因素的影响不大，几乎各个省份区域都有专家对其耕地变化和驱动因子进行了大量研究，如郭丽英等[7]

收稿日期：2018-03-26

作者简介：王静怡（1984—），女，陕西榆林人，博士、讲师。研究方向：资源利用和数据科学

※通讯作者：李晓明（1983—），男，山东烟台人，博士、高级工程师，硕士生导师。研究方向：土地资源利用和遥感信息。Email: xmlisdc@126.com

* 资助项目：陕西省教育厅科研计划项目“无线MARC系统中联合网络—信道编码的优化设计研究”（18JK0626）

(C)1994-2022 China Academic Journal Electronic Publishing House. All rights reserved. http://www.cnki.net

分析了 1996—2008 年我国沿海地区耕地变化的基本态势、时空特征及其主导成因；吴霞等[8]选取 1997—2014 年宁夏耕地面积数据分析耕地面积变化趋势及其驱动因子；武江民等[9]专门针对甘肃兰州市研究其耕地动态变化与驱动力的定量关系。还有学者则基于基于国家、区域、省域、市县不同尺度研究了中国耕地变化的驱动力[10]；

20 世纪 80 年代以来，随着遥感等 3S 技术的发展应用，诸多学者开始不仅仅局限于统计数据的应用，开始借助遥感信息技术对耕地变化进行研究。如张国平、刘纪元等[11]利用中国资源环境数据库及遥感影像对 20 世纪 80 年代末至 2000 年的中国耕地时空变化进行了分析；田光进、庄大方等[12]通过对遥感图像解译研究 80 年代末与 90 年代末 10 年间耕地时空动态变化特征；刘旭华，王劲峰等使用中国 1987—1989 年和 2000 年两期土地利用遥感调查数据，探索定量化研究国家尺度土地利用变化的驱动力[13,14]；许丽丽等[15]基于中分辨率卫星遥感数据，深入分析了 2000—2010 年中国耕地变化及其空间差异，并对中国耕地占补平衡政策的实施效果进行了评估；李景刚等[16]选取 1983—2001 年 NOAA 等遥感数据分析了北方 13 省的耕地变化与驱动力。遥感信息技术的应用开拓了耕地变化研究的新途径，但是由于遥感解译的精度仍有待于进一步提高，所以一定程度上制约了对于耕地变化的研究。

多来以来，我国对于耕地数量的数据统计有多种来源，其中以国土资源部的统计数据被认为最权威[17]。由于遥感影像解译精度，与实地调查统计相比仍有一定差距，所以大部分学者仍采用统计数据进行研究，而且大多避开了数据有明显变化的过渡年份。目前仅有极少数学者对过渡年份前后时间段的统计数据变化一并进行了相关的分析[17,18]。针对两次全国土地调查的统计数据的跳跃式变化，文章研究提出了基于数据挖掘技术研究分析两个时间段的数量关系，以更科学地反映耕地数量的变化趋势，同时基于校正数值研究影响耕地变化的驱动因子，这在目前的研究中尚未见到，对于科学反映我国耕地变化趋势具有积极的意义。

1 数据与方法

1.1 数据获取

1.1.1 全国耕地数量数据

我国耕地数量，尤其是历史时期的耕地数量，长期以来难以确定。国家土地管理部门从 1986 年开始，每年统计并公布我国耕地的增减情况，虽然还有其他职能部门的统计数据，但仍以国土资源部的数据最为权威[17]。为准确掌握全国耕地数量，1984—1996 年国务院安排开展了全国第一次大规模的土地利用现状调查，数据成果统计到了 1996 年 10 月 31 日，结果表明，1996 年全国耕地面积约为 1.300 亿 hm^2（19.51 亿亩）[18]，这一统计数据被认为具有最高可信度[19]。随后，1996—2008 年耕地面积数据均可直接从统计公报中查得。

为进一步准确掌握耕地土地基础数据，国家于 2007 年 7 月 1 日起，启动了第二次全国土地调查，数据统计时间节点为 2009 年 12 月 31 日，统计结果显示 2009 年我国耕地面积为 1.354 亿 hm^2（20.31 亿亩）[18]。随后的每年都有二调变更调查，2007—2016 年每年的全国耕地面积都可以从国家土地调查成果服务平台直接查得。由于第二次全国土地调查采用的技术方法的改进等原因，2008 年与 2009 年的耕地数量存在“跳跃”现象，为科学分析耕地的变化趋势，这一现象问题在后文中进行了着重的研究处理。

1.1.2 驱动因子数据

土地与人类社会的经济发展密不可分，全国耕地变化是在地理背景制约下、社会经济条件、灾害等自然条件共同驱动下发生的[1]，为探索研究耕地变化的驱动因子，该文主要选取了 3 方面共 17 个因子指标做遴选分析：一方面是反映全国经济发展水平的综合类指标，包括国民总收入、国内生产总值、第一产业增加值及比例、第二产业增加值及比例、第三产业增加值及比例、人均国内生产总值、工业增加值、建筑业增加值、农业总产值；另一方面是反映社会城镇化水平的指标，包括年末总人口、城镇人口、乡村人口；还有第三方面是反映自然灾害的指标，包括受灾面积和粮食产量[20]。上述因子指标近 20 年的数据均

(C)1994-2022 China Academic Journal Electronic Publishing House. All rights reserved. http://www.cnki.net

直接从国家统计局网站查得。

1.2　研究方法

该文研究通过对近 20 年全国耕地数量数据的分析处理，研究其变化趋势，进而通过与选取的因子进行相关性分析，研究其变化的驱动因子。其中，在对 1996—2016 年耕地面积的数据分析中，针对 2008—2009 年数据的跳跃现象，通过数据挖掘，一方面利用 1996—2008 年数据预测 2009 年数据，另一方面利用 2009—2016 年数据反推 2008 年数据，基于上述两种相互预测或反推得出的数值，分析 2008 年和 2009 年耕地数量的数据比例关系，进而对 1996—2016 年耕地面积数据进行比值归一化，以探索研究耕地面积的变化趋势。

该文在数据挖掘预测中，通过遴选对比最终采用的为 ARIMA 模型，即自回归积分滑动平均模型(Autoregressive Integrated Moving Average Model)，是由博克思(Box)和詹金斯(Jenkins)提出的著名时间序列预测方法，主要是指将非平稳时间序列转化为平稳时间序列，然后将因变量仅对它的滞后值以及随机误差项的现值和滞后值进行回归所建立的模型，适用于该文的研究。

2　近 20 年耕地数量变化趋势分析

2.1　基于耕地数量原始统计数据的变化趋势及分析

通过对收集整理的 1996—2016 年耕地数量数据分析，如图 1，可以看出，1996—2008 年全国耕地面积逐年减少，其中以 2000—2004 年递减速度最快；2008—2009 年耕地面积数据出现跳跃，由 1.217 亿 hm^2(18.26 亿亩)增至 1.354 亿 hm^2(20.31 亿亩)；2009—2016 年耕地面积递减速度非常缓慢。

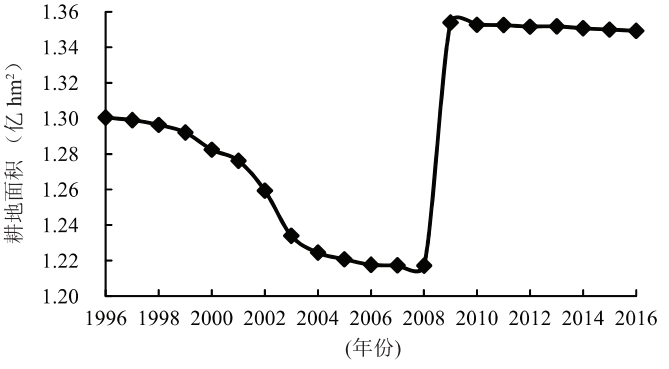


图 1　1996—2016 年基于原始统计数据的耕地数量变化趋势

1996 年国家完成了第一次大规模的土地利用现状调查；2009 年第二次全国土地利用现状调查完成。由此可见，2008—2009 年耕地面积数据的跳跃正是一调与二调数据的分界年份。全国耕地面积是否真的增多了约 0.14 亿 hm^2(2 亿亩)，经文献查阅分析[17,18,21]，主要原因在于二调采用了更为先进的技术手段，将以往少报的耕地面积统计入库，进一步提高了数据的准确度。所以，近 20 年全国耕地数量的统计数据是基于两次不同的技术水平，可直接分别研究各自时段内的变化趋势，但如果要研究连续 20 年时间段内的变化趋势，就须对两个时间段的数据进行校正，使之具有可对比性。

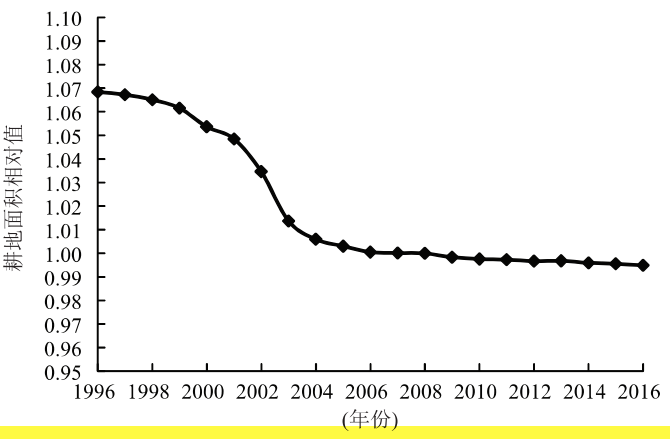


图 2　1996—2016 年基于校正后相对数据的耕地变化趋势

2.2　基于数据挖掘的耕地数量校正

数据挖掘技术在时间序列上具有强有力的预测功能，该文首先利用 1996—2008 年耕地数量数据，预测 2009 年的耕地数量，由此得出 2009 年与 2008 年耕地数量的比值关系 α；然后利用 2009—2016 年耕地数量数据，反推 2008 年的耕地数量，由此得出 2009 年与 2008 年耕地数量的比值关系 β；为更为科学地反映 2009 年与 2008 年耕地数量的比值关系，取利用正向预测与反向反推两种方法得出的 α 与 β 的算数平均值 ρ 作为实际的数量比值关系。

该文研究在预测过程中，利用 SPSS 软件，通过比较分析，在正向预测 2009 年数值和反向反推 2008

(C)1994-2022 China Academic Journal Electronic Publishing House. All rights reserved.　http://www.cnki.net

年数值中均选用 ARIMA 模型，其中正向预测选用的模型为 ARIMA（1，1，2）（$r^2=0.975^{**}$），反向反推选用的模型为 ARIMA（1，1，4）（$r^2=0.966^{**}$），两者均在 0.01 水平呈现显著性。由此，基于 1996—2008 年数据预测得出的 2009 年耕地数量为 1.213 387 亿 hm^2（18.200 8 亿亩），基于 2009—2016 年数据反推得出的 2008 年耕地数量为 1.353 987 亿 hm^2（20.309 8 亿亩），进一步可得出 $\alpha=996\ 899.887\ E-6$，$\beta=999\ 895.617\ E-6$，则 $\rho=998\ 397.752\ E-6$，由此推测 2009 年与 2008 年耕地数量的比值为998 397.752 E－6，即可为两个时间段数据的校正系数。

2.3 基于耕地数量校正相对值的变化趋势分析

为进一步客观的反映近 20 年的耕地数量变化趋势，对全部年份数据进行比值归一化及系数校正，在前文研究基础上，首先对 1996—2008 年全部原始耕地数量数据以 2008 年耕地数量为基数计算得到的比值即为其耕地数量相对值，对 2009—2016 年全部原始耕地数量数据以 2009 年耕地数量为基数计算得到的比值，再乘以校正系数 ρ，即为其相应年份的耕地数量相对值。由此可以得出 1996—2016 年耕地数量的变化趋势，如图 2 所示，可以看出，近 20 年全国耕地数量是呈现递减趋势的，其中 2004 年以前，递减速度较快，2004 年以后耕地数量递减速度较缓，尤其是 2006 年以后耕地数量递减速度趋于稳定。

3 耕地数量变化驱动因子分析

该文研究共收集了 1996—2016 年共 17 个因子指标，首先进行描述性特征统计，如表 1 所示；然后，通过分析耕地数量与各因子指标的相关性（表 2），进行对比分析，以此遴选出耕地数量变化的驱动因子。

表 1 1996—2016 年各因子指标的描述性统计特征

因子	最小值	最大值	平均值	标准差
国民总收入（亿元）	70 780	741 140	304 446.950	225 956.601
国内生产总值（亿元）	71 814	744 127	305 718.670	226 519.843
第一产业增加值（亿元）	13 878	63 671	31 240.710	17 742.619
第一产业增加值占比（%）	8.556	19.325	12.114	3.280
第二产业增加值（亿元）	33 828	296 236	135 629.240	94 949.577
第二产业增加值占比（%）	39.810	47.559	45.327	1.999
第三产业增加值（亿元）	24 107	384 220	138 848.860	114 605.836
第三产业增加值占比（%）	33.569	51.634	42.560	4.472
人均国内生产总值（亿元）	5 898	53 980	22 872	16 332.770
工业增加值（亿元）	29 530	247 860	116 532.760	79 508.293
建筑业增加值（亿元）	4 393	49 522	19 623	15 992.727
年末总人口（万人）	122 389	138 271	131 047.710	4 702.171
城镇人口（万人）	37 304	79 298	58 413.240	12 989.267
乡村人口（万人）	58 973	85 085	72 634.480	8 313.397
农业总产值（亿元）	13 540	59 288	28 842.620	16 570.347
粮食产量（万 t）	43 070	62 144	52 326.480	5 812.061
受灾面积（万 hm^2）	2 177	5 468.8	4 100.948 0	1 070.630

由表 2 可以看出，基于原始统计的耕地面积研究其与各因子指标的相关性，由于数据的跳跃不足以反映耕地变化的实际趋势，与各因子指标的相关性均不高。基于校正后的耕地数量的相对值，研究其与各因子指标的相关性，可以发现，与第一产值增加值占比的相关性最高，相关系数高达 0.959；与年末总人口的相关性次之，为负相关，系数为 －0.918，城镇人口和乡村人口与之的相关性也较高，即第一产业增加值占比，总人口以及城镇人口数量与耕地数量的变化相关性较好，是重要的驱动因子。由此，可以推论出国家产业结构布局调整、我国城镇化建设水平是影响我国耕地数量变化的重要因素条件。耕地作为第一产

(C)1994-2022 China Academic Journal Electronic Publishing House. All rights reserved. http://www.cnki.net

表 2　耕地面积与各因子的相关系数矩阵

	原始统计耕地面积	校正后耕地面积相对值		原始统计耕地面积	校正后耕地面积相对值
原始统计耕地面积	1	-0.142	人均国内生产总值	0.651	-0.749
校正后耕地面积相对值	-0.142	1	工业增加值	0.638	-0.784
国民总收入	0.649	-0.746	建筑业增加值	0.688	-0.716
国内生产总值	0.652	-0.745	年末总人口	0.433	-0.918
第一产业增加值	0.663	-0.736	城镇人口	0.488	-0.896
第一产业增加值占比	-0.274	0.959	乡村人口	-0.518	0.88
第二产业增加值	0.647	-0.774	农业总产值	0.686	-0.709
第二产业增加值占比	-0.519	0.259	粮食产量	0.752	-0.524
第三产业增加值	0.649	-0.717	受灾面积	-0.514	0.708

业的最重要的载体之一，与第一产业增加值密切正相关，我国产业结构中对于第一产业布局要求会直接诱使我国耕地的变化。而城镇化建设过程中，一方面由于城镇建设会直接占用大量的耕地，另一方面，城镇化建设中大量的农民人口直接进入城镇生活，或者进城务工而导致耕地撂荒，所以城镇化建设水平与耕地变化呈现密切的负相关。

4　结论与讨论

土地本身既有自然属性，又有社会属性，对于耕地数量的统计长期以来受社会、经济、政策等诸多因素的影响，导致难以对其进行长时间序列的趋势研究。该文研究的时间序列跨度全国两次土地调查的统计数据，两个时间阶段的数据具有明显的跳跃性，但并不代表 2009 年耕地数量真的比 2008 年大幅度增长。究其原因，主要是由于第二次全国土地调查中应用遥感等新方法、统一了标准，提高了调查的技术水平和准确度，使原来因少报、漏报、瞒报等各种原因未被统计到的耕地重新统计入库，所以要研究跨两个阶段的整体变化趋势，就必须研究建立其数值量化关系。该文通过数据挖掘，并对耕地数量进行校正和比值归一化，研究结果比较准确地反映了我国耕地变化趋势的实际情况。

研究结果表明，近 20 年，我国耕地数量呈现递减趋势，其中 2004 年以前递减速度较快，2004 年以后递减速度趋缓，我国产业结构布局方面，主要是第一产业增加值占比，以及我国人口总数方面，主要是城镇化人口数量是影响变化的主要驱动因子。由于 1999 年后开始生态退耕导致耕地数量迅速减少[17,22]，2004 年国家《土地管理法》修订后强调要加强耕地保护，实行占补平衡，对我国耕地的数量变化产生了积极作用。该文仅对近 20 年我国耕地数量的变化趋势进行了分析；现在国家加强耕地保护，不仅以数量为基础，更关注质量，以产能为核心，实现数量、质量和生态的三位一体保护[23]，下一步将对全国耕地质量的变化趋势进一步分析研究。同时，该文研究通过相关性分析研究提出了主要驱动因子，下一步还将进一步对驱动因子的贡献率进行量化分析研究。

该文研究仅对 1996—2016 年耕地数量的变化趋势进行了分析研究，由于对诸多指标因子数据统计的完整性需求，未对更长时间的耕地变化趋势进行研究。下一步，将在对统计数据分析的基础上，通过对遥感影像的数据挖掘，深入研究更长时间序列的变化趋势。

参考文献

[1] 赵其国，周生路，吴绍华，等. 中国耕地资源变化及其可持续利用与保护对策. 土壤学报，2006，43（4）：662－672.

[2] 葛全胜，戴君虎，何凡能，等. 过去 300 年中国部分省区耕地资源数量变化及驱动因素分析. 自然科学进展，2003，13（8）：825－832.

[3] 毕于运，郑振源. 建国以来中国实有耕地面积增减变化分析. 资源科学，2000，22（2）：8－12.

[4] 李秀彬. 中国近 20 年来耕地面积的变化及其政策启示. 自然资源学报，1999，14（4）：329－333.

(C)1994-2022 China Academic Journal Electronic Publishing House. All rights reserved.　http://www.cnki.net

[5] 曹银贵，袁春，周伟，等. 中国耕地变化的驱动因子及其省域差异分析. 中国土地科学，2008，22（2）：17－22.
[6] 黄忠华，吴次芳，杜雪君. 我国耕地变化与社会经济因素的实证分析. 自然资源学报，2009，24（2）：192－199.
[7] 郭丽英，王道龙，王介勇. 中国沿海地区耕地变化及其成因分析. 中国农业资源与区划，2012，33（1）：6－10.
[8] 吴霞，王世荣，尚红莺，等. 宁夏近 18 年来耕地面积动态变化及驱动力分析. 中国农业资源与区划，2017，38（8）：98－104.
[9] 武江民，赵学茂，党国锋. 甘肃兰州市耕地动态变化与驱动力关系定量研究. 干旱区资源与环境，2010，24（12）：33－38.
[10] 于天，曹银贵，许婧雪. 基于不同尺度的中国耕地变化驱动力研究进展. 中国农学通报，2016，32（24）：194－198.
[11] 张国平，刘纪远，张增祥. 近 10 年来中国耕地资源的时空变化分析. 地理学报，2003，58（3）：323－332.
[12] 田光进，庄大方，刘明亮. 近 10 年中国耕地资源时空变化特征. 地球科学进展，2003，18（1）：30－36.
[13] 刘旭华，王劲峰，刘纪远，等. 国家尺度耕地变化驱动力的定量分析方法. 农业工程学报，2005，21（4）：56－60.
[14] 刘旭华，王劲峰，刘明亮，等. 中国耕地变化驱动力分区研究. 中国科学 D 辑地球科学，2005，35（11）：1087－1095.
[15] 许丽丽，李宝林，袁烨城，等. 2000—2010 年中国耕地变化与耕地占补平衡政策效果分析. 资源科学，2015，37（8）：1543－1551.
[16] 李景刚，何春阳，史培军，等. 近 20 年中国北方 13 省的耕地变化与驱动力. 地理学报，2004，59（2）：274－282.
[17] 封志明，刘宝勤，杨艳昭. 中国耕地资源数量变化的趋势分析与数据重建：1949—2003. 自然资源学报，2005，20（1）：35－43.
[18] 谭永忠，何巨，岳文泽，等. 全国第二次土地调查前后中国耕地面积变化的空间格局. 自然资源学报，2017，32（2）：186－197.
[19] Lin G C S，HO S P S. China's land resources and land-use change：insights from the 1996 land survey. land Use Policy，2003，20（2）：87－107.
[20] 傅泽强，蔡运龙，杨友孝，等. 中国粮食安全与耕地资源变化的相关分析. 自然资源学报，2001，16（4）：313－319.
[21] 张雅琼，杨子生. 我国两次土地资源调查的对比分析. 国土资源科技管理，2013，30（2）：100－104.
[22] 徐宪立，蔡玉梅，张科利，等. 耕地资源动态变化及其影响因素分析. 中国人口·资源与环境，2005，15（3）：75－79.
[23] 谭永忠，吴次芳，王庆日，等. “耕地总量动态平衡”政策驱动下中国的耕地变化及其生态环境效应. 自然资源学报，2005，20（5）：727－734.

RESEARCH ON THE CHANGE TREND OF FARMLAND QUANTITY IN CHINA FOR RECENT 20 YEARS AND ITS DRIVING FACTORS*

Wang Jingyi[1], Li Xiaoming[2]※

(1. Xi'an Shiyou University, Xi'an, Shaanxi 710065, China;
2. Shaanxi Provincial Land Engineering Construction Group, Xi'an, Shaanxi 710075, China)

Abstract The research aims to research the changing trend of farmland quantity for recent 20 years before and after the second national land use survey. It could provide decision support for farmland protection and efficient use of land resources. The original data of farmland area from 1996 to 2016 were collected, data mining technology was introduced, and ARIMA model was chosen to predict the farmland quantity each other based on the farmland area of the twice land use survey, which meant to predict the farmland quantity of 2009 with the farmland quantity of the years from 1996 to 2008, and to predict the farmland quantity of 2008 inversely with the farmland quantity of the years from 2009 to 2016, so the original farmland area data could be corrected and normalized. Then the changing trend of farmland quantity for recent 20 years was studied furtherly and correlation analysis was used to study the driving factors. The trend research result showed, the farmland area decreased year by year for recent 20 years, the decreasing rate was faster before 2004, and then it decreased slowly. The correlation analysis result showed, the added value proportion of primary industry, the total population, and the urban population were the most important driving factors which influenced the farmland quantity change, their coefficients were 0.959, －0.918 and －0.896 respectively. It could be concluded by the result that the industry configuration and the urbanization could affect the farmland quantity with the development of social economy.

Keywords data mining; ARIMA model; farmland quantity; change trend; driving factors

(C)1994-2022 China Academic Journal Electronic Publishing House. All rights reserved. http://www.cnki.net

DOCTORAL DISSERTATION XIDIAN UNIVERSITY

西安電子科技大學

博士学位论文



无线中继系统中的信道编码技术研究

作者姓名 王静怡

指导教师姓名、职称 白宝明 李颖 教授

申请学位类别 工学博士

(C)1994-2022 China Academic Journal Electronic Publishing House. All rights reserved. http://www.cnki.net

学校代码 10701
分 类 号 TN911.22

学 号 1008110003
密 级 公开

西安电子科技大学

博士学位论文

无线中继系统中的信道编码技术研究

作者姓名： 王静怡

一级学科： 信息与通信工程

二级学科： 通信与信息系统

学位类别： 工学博士

指导教师姓名、职称： 白宝明 李颖 教授

学　　院： 通信工程学院

提交日期： 2016 年 4 月

(C)1994-2022 China Academic Journal Electronic Publishing House. All rights reserved. http://www.cnki.net

Study on Channel Codes in Wireless Relay Systems

A dissertation submitted to

XIDIAN UNIVERSITY

in partial fulfillment of the requirements

for the degree of Doctor of Philosophy

in Communications and Information Systems

By

Wang Jingyi

Supervisor: Bai Baoming Li Ying Professor

April 2016

(C)1994-2022 China Academic Journal Electronic Publishing House. All rights reserved. http://www.cnki.net

西安电子科技大学
学位论文独创性（或创新性）声明

秉承学校严谨的学风和优良的科学道德，本人声明所呈交的论文是我个人在导师指导下进行的研究工作及取得的研究成果。尽我所知，除了文中特别加以标注和致谢中所罗列的内容以外，论文中不包含其他人已经发表或撰写过的研究成果；也不包含为获得西安电子科技大学或其它教育机构的学位或证书而使用过的材料。与我一同工作的同事对本研究所做的任何贡献均已在论文中作了明确的说明并表示了谢意。

学位论文若有不实之处，本人承担一切法律责任。

本人签名：王静怡　　日　　期：2016.6.24

西安电子科技大学
关于论文使用授权的说明

本人完全了解西安电子科技大学有关保留和使用学位论文的规定，即：研究生在校攻读学位期间论文工作的知识产权属于西安电子科技大学。学校有权保留送交论文的复印件，允许查阅、借阅论文；学校可以公布论文的全部或部分内容，允许采用影印、缩印或其它复制手段保存论文。同时本人保证，结合学位论文研究成果完成的论文、发明专利等成果，署名单位为西安电子科技大学。

保密的学位论文在___年解密后适用本授权书。

本人签名：王静怡　　导师签名：李颖

日　　期：2016.6.24　　日　　期：2016.6.24

(C)1994-2022 China Academic Journal Electronic Publishing House. All rights reserved.　http://www.cnki.net

摘要

随着无线通信技术的快速发展，如何提高信息的传输速率、改善系统的纠错性能等问题受到越来越多人的关注。中继传输技术的出现扩大了通信网络的覆盖范围，获得了额外的空间分集增益，提高了系统资源利用率和网络的容量。因此，设计适合于中继网络的差错控制编码技术是近年来无线通信领域的研究热点之一。本文针对几种典型的中继网络结构，研究了相应的差错控制编码传输方案。本文的主要工作概括如下：

针对包含两个源节点、一个中继节点和一个目的节点的中继系统模型，提出了一种速率兼容网络 LDPC 码的删余算法，并推导了该算法的译码错误概率。该算法基于网络 LDPC 码的结构特点，以最小化比特错误概率为目标，在网络 LDPC 码的 Tanner 图上搜索出需要删余的变量节点，以获得最优的删余图样。另外，本文还采用改进的差分进化算法对网络 LDPC 码的度分布进行优化。仿真结果表明，所提算法可以提供很好的纠错性能。

针对包含多个源节点、多个中继节点和一个目的节点的中继系统模型，研究了基于 RS 码和 LDPC 码的中继传输策略，提出了一种基于 RS 编码的混合译码转发策略。该策略引入了一个决定中继是否转发信息的阈值，只有当中继译码后的信息比特的对数似然比大于该阈值时，该信息比特才会被转发。基于最小化比特错误概率，分别对独立协作和混合协作两种策略研究了最佳阈值的优化方法。仿真结果显示，所提方法可有效改善多址接入中继网络在高斯信道和衰落信道的性能。

针对包含一个源节点、一个中继节点和一个目的节点的三节点中继信道，基于半速率可逆码原理，设计了一种 II 型 HARQ 构造的双层 LDPC 码，提出了相应的联合译码方法，并对其译码阈值进行了分析。在该设计方法中，中继节点首先采用半速率可逆 LDPC 码进行编码。随后，中继节点对编码后的校验位进行高码率编码。在高斯中继信道下，与已有的基于传统方式构造的双层 LDPC 码相比，所设计的双层 LDPC 码可以明显降低系统的错误概率。

关 键 词：多址接入中继信道，双层网络 LDPC 码，速率兼容 LDPC 码，中继出错，半速率可逆码

(C)1994-2022 China Academic Journal Electronic Publishing House. All rights reserved. http://www.cnki.net

ABSTRACT

How to increase the transmission rate and improve the error-correcting performance of system have attracted more and more attentions with the rapid development of wireless communication. With the emergence of the relay technology, the coverage of communication network is extended, extra spatial diversity gain is achieved and the network capacity is also increased. Therefore, the design of error control coding scheme for wireless relay communication has been one of the focuses recently. Based on several typical relay network models, the corresponding transmission schemes are studied. The main results of this dissertation are summarized as follows:

For the relay channel with two source nodes, one relay node and one destination node, this dissertation proposes a kind of puncturing algorithm for the rate-compatible network low-density parity-check (LDPC) codes, and derives the expression of decoding error probability. To minimize the decoding error probability, an algorithm of selecting variable nodes to be deleted is proposed. Moreover, an improved differential evolution algorithm is used to optimize the degree distribution of the proposed network LDPC code. Simulation results show that the proposed algorithms can provide good error-correcting performance.

For the relay channel consisting of multiple source nodes, multiple relay nodes and one destination node, this dissertation studies the relay transmission scheme based on Reed-Solomon (RS) code and LDPC code. In order to combat the effects of error propagation in error-prone multiple-user multiple-relay (MUMR) wireless networks, a threshold based decode-and-forward (DF) relaying strategy is proposed. That means the relay node only forwards those bits whose log-likelihood ratios (LLRs) are larger than this threshold. Furthermore, this dissertation investigates the optimization of the threshold by minimizing the bit error rate (BER). Both separated cooperation and combined cooperation strategies are discussed. Simulation results indicate that the proposed strategy can effectively decrease the error probability of the system over both additive white Gaussian noise (AWGN) channel and fading channel.

For the DF relay channel with one source node, one relay node and one destination node, this dissertation proposes a type-Ⅱ hybrid automatic repeat-request (HARQ) based bilayer LDPC code by employing a half-rate invertible LDPC code, designs a joint decoding algorithm and analyzes the decoding threshold. In the proposed code, the relay node first encodes the message with a half-rate invertible LDPC code, and then encodes

(C)1994-2022 China Academic Journal Electronic Publishing House. All rights reserved. http://www.cnki.net

the coded parity check bits with a high rate LDPC code. Compared with the classic bilayer LDPC code, the designed bilayer LDPC code can significantly decrease the error probability of system.

Keywords: multiple access relay channel (MARC), bilayer-network low-density parity-check (LDPC) code, rate-compatible LDPC, relay error, half-rate invertible code

(C)1994-2022 China Academic Journal Electronic Publishing House. All rights reserved. http://www.cnki.net

插图索引

图 1.1 三节点中继系统模型 3
图 1.2 分布式 Turbo 码 7
图 1.3 双层 LDPC 码的 Tanner 图 8
图 1.4 蝶形拓扑图 9
图 1.5 自适应协作编码 10
图 1.6 5 个用户的 ANCC 网络模型 11
图 1.7 中继节点的编码框图 12
图 2.1 多址接入中继信道模型 17
图 2.2 正交多址接入信道模型 18
图 2.3 基于网络编码的正交多址接入信道模型 18
图 2.4 非正交的多址接入中继信道模型 19
图 2.5 蜂窝移动通信系统框图 20
图 2.6 两源多址接入中继系统框图 22
图 2.7 两源 MARC 的两种场景模型 26
图 2.8 场景 1：两源 MARC 的可达速率上界和可达速率（$P_1 = P_2 = P_r$=10dB） 27
图 2.9 场景 2：两源 MARC 的可达速率上界和可达速率（$P_1 = P_2 = P_r$=10dB） 28
图 2.10 场景 1：两源 MARC 的可达速率上界和可达速率（$P_1 = P_2 = P_r$=10dB） 28
图 2.11 场景 2：两源 MARC 的可达速率上界和可达速率（$P_1 = P_2 = P_r$=10dB） 29
图 3.1 多址接入中继系统框图 33
图 3.2 网络 LDPC 码的 Tanner 图 33
图 3.3 网络 LDPC 码的恢复树 34
图 3.4 AWGN 信道下网络 LDPC 码的删余性能对比 42
图 3.5 瑞利衰落信道下网络 LDPC 码的删余性能对比 43
图 3.6 AWGN 信道下网络 LDPC 码的性能 45
图 4.1 M 个源节点和 N 个中继节点组成的系统框图 49
图 4.2 单独协作时中继节点的操作流程框图 50
图 4.3 联合协作时中继节点的操作流程框图 51
图 4.4 AWGN 信道下的误码性能 59
图 4.5 瑞利衰落信道下的误码性能 59
图 5.1 半双工模式下的三节点多址接入中继系统的结构框图 63
图 5.2 中继节点的编译码方案 63

(C)1994-2022 China Academic Journal Electronic Publishing House. All rights reserved. http://www.cnki.net

图 5.3 目的节点的编译码方案 64
图 5.4 双层 LDPC 码的构造图 68
图 5.5 双层 LDPC 码的 Tanner 图 69
图 5.6 目的节点的译码器结构 70
图 5.7 双层 LDPC 码等效的四层 Tanner 图 73
图 5.8 AWGN 信道下双层 LDPC 码的误码性能仿真图 76
图 5.9 AWGN 信道下双层 LDPC 码的误码性能仿真图 77

(C)1994-2022 China Academic Journal Electronic Publishing House. All rights reserved. http://www.cnki.net

表格索引

表 3.1　双层网络 LDPC 码的四个码集 44
表 3.2　双层网络 LDPC 码 A 的码集 44
表 3.3　双层网络 LDPC 码 B 的码集 44
表 3.4　双层网络 LDPC 码 C 的码集 45
表 3.5　双层网络 LDPC 码 D 的码集 45

(C)1994-2022 China Academic Journal Electronic Publishing House. All rights reserved.　http://www.cnki.net

符号对照表

符号	符号名称
$\min\{x,y\}$	取 x,y 中较小的数
$\sup\{A\}$	取集合 A 的上确界
A^c	集合 A 的补集
$\|u\|$	随机变量 u 的基数限
$A \subset B$	集合 A 包含于集合 B
$\max\{x,y\}$	取 x,y 中较大的数
$GF(q)$	q 进制域
$\mathcal{N}(\mu,\sigma^2)$	均值为 μ，方差为 σ^2 的实高斯分布
$A \backslash B$	集合 A 中去掉集合 B
$a \in A$	元素 a 属于集合 A
$\lfloor a \rfloor$	a 下取整
$p(\cdot)$	条件概率密度函数
$sign(\cdot)$	符号函数
$\|x\|$	x 的绝对值
erfc（·）	误差补函数
$F_A(x)$	变量 A 的概率累积分布函数
$f_A(x)$	变量 A 的概率密度分布函数
$\Pr\{A\}$	事件 A 的概率
$\Pr\{A \text{ and } B\}$	事件 A 和事件 B 同时发生的概率

(C)1994-2022 China Academic Journal Electronic Publishing House. All rights reserved. http://www.cnki.net

缩略语对照表

缩略语	英文全称	中文对照
2D	Two Dimensions	二维
3D	Three Dimensions	三维
2G	2th Generation	第二代移动通信系统
3G	3th Generation	第三代移动通信系统
4G	4th Generation	第四代移动通信系统
5G	5th Generation	第五代移动通信系统
AF	Amplify-and-forward	放大转发
ARQ	Automatic Repeat-request	自动重传请求
AWGN	Additive White Gaussian Noise	加性高斯白噪声
BC	Broadcast	广播
BCH	Bose Ray-Chaudhri Hocquenghem	BCH 码
BER	Bit Error Rate	比特错误概率
BF	Bit- Flipping	比特翻转
BP	Belief Propagation	置信传播
BPSK	Binary Phase Shift Keying	二进制相位键控
BSC	Binary Symmetric Channel	二进制对称信道
CF	Compress-and-forward	压缩转发
C-MARC	Constrained-MARC	受限多址接入中继信道
DF	Decode-and-forward	译码转发
EXIT	Extrinsic Information Transform Chart	外信息转移图
FEC	Forward-error-control	前向差错控制
HARQ	Hybrid Automatic Repeat-request	混合自动重传请求
LDPC	Low-Density Parity-Check	低密度奇偶校验码
LLR	Log-Likelihood Ratio	对数似然比
LR	Likelihood Ratio	似然比
LTE	Long Term Evolution	长期演进
MAC	Multiple-access mode	多址接入
MARC	Multiple Access Relay Channel	多址接入中继信道
MIMO	Multiple-input Multiple-output	多输入多输出
MUMR	Multi-User Multi-Relay	多用户多中继

(C)1994-2022 China Academic Journal Electronic Publishing House. All rights reserved. http://www.cnki.net

MDS	Maximum Distance Separable	最大距离可分码
NAK	Negative Acknowledgment	否定应答
pdf	probability density function	概率密度函数
RM	Reed Muller	RM 码
RS	Reed Solomon	RS 码
SNR	Signal-to-Noise Ratio	信噪比
TDMA	Time Division Multiple Access	时分多址

(C)1994-2022 China Academic Journal Electronic Publishing House. All rights reserved. http://www.cnki.net

目录

摘要 I
ABSTRACT III
插图索引 V
表格索引 VII
符号对照表 IX
缩略语对照表 XI
目录 XIII
第一章 绪论 1
1.1 研究背景 1
1.2 中继系统的发展与演进 2
1.2.1 系统模型 2
1.2.2 中继系统的容量 3
1.2.3 中继系统的主要研究 4
1.3 中继系统的编码设计研究现状 6
1.3.1 信道编码协作方案 6
1.3.2 网络编码协作方案 8
1.3.3 联合网络-信道编码协作方案 12
1.4 本文的研究内容及结构安排 14
第二章 多址接入中继系统模型及传输策略 17
2.1 多址接入中继信道模型 17
2.1.1 正交多址接入中继信道模型 18
2.1.2 非正交多址接入中继信道模型 19
2.2 多址接入中继信道的容量域 20
2.2.1 正交多址接入中继信道的容量 20
2.2.2 非正交多址接入中继信道的容量 21
2.2.3 非正交多址接入中继信道的仿真结果 25
2.3 本章小结 29
第三章 适用于 MARC 的速率兼容网络 LDPC 码设计 31
3.1 引言 31
3.2 适用于 MARC 的网络 LDPC 码 32
3.3 速率兼容网络 LDPC 码的设计 34

(C)1994-2022 China Academic Journal Electronic Publishing House. All rights reserved. http://www.cnki.net

3.3.1 几个定义 34
3.3.2 译码恢复错误概率 35
3.3.3 速率兼容网络 LDPC 码的删余算法 37
3.4 基于差分进化的网络 LDPC 码的设计 39
3.4.1 网络 LDPC 码的门限值分析 39
3.4.2 网络 LDPC 码的度分布的优化设计 40
3.5 性能分析 41
3.5.1 速率兼容网络 LDPC 码的性能分析 41
3.5.2 基于差分进化的网络 LDPC 码的性能分析 43
3.6 本章小节 46
第四章 基于分布式 RS 码的中继转发策略设计 47
4.1 引言 47
4.2 MARC 下基于混合 DF 策略的方案 48
4.2.1 系统模型 48
4.2.2 基于混合 DF 策略的编译码方案 49
4.2.3 基于网络编码的 RS 码设计 52
4.3 转发策略的设计 55
4.3.1 基于转发的阈值 55
4.3.2 阈值优化 56
4.4 仿真结果 58
4.5 本章小节 60
第五章 MARC 的一种半速率可逆码的设计 61
5.1 引言 61
5.2 半双工多址接入中继系统 62
5.2.1 系统模型 62
5.2.2 编译码方案 63
5.2.3 传输速率的分析 64
5.3 基于半速率可逆码的双层 LDPC 码的设计 65
5.3.1 半速率可逆码 65
5.3.2 基于半速率可逆码构造双层 LDPC 码 68
5.3.3 基于双层 LDPC 码的目的端译码器结构 70
5.4 采用半速率可逆码的双层 LDPC 码阈值分析 72
5.5 仿真结果 76
5.6 结论 78

(C)1994-2022 China Academic Journal Electronic Publishing House. All rights reserved. http://www.cnki.net

第六章　结束语 79
附录 81
附录 A 81
附录 B 82
附录 C 82
参考文献 85
致谢 97
作者简介 99

(C)1994-2022 China Academic Journal Electronic Publishing House. All rights reserved.　http://www.cnki.net

第一章 绪论

本章首先简单介绍了无线通信的发展现状，以及面临的主要问题；其次介绍了无线中继系统的码设计的研究现状；并详细阐述了中继系统中常见的几种编码方案；最后给出了本文的结构安排和作者在攻读博士学位期间所取得的研究成果。

1.1 研究背景

早期的通信是指各种总线技术、局域网技术等有线网络的使用。但随着射频技术、集成电路技术的发展，无线通信的实现变得越来越容易，数据传输速度也越来越快，并且逐渐取代有线网络。无线通信的研究可以追溯到 1895 年马可尼发明的无线电系统，而后诞生了大量实现快速无线通信的方法，特别是 1948 年 shannon 提出的信息论，更是从理论上为无线通信的发展奠定了坚实的基础。经过第一、二代低速移动通信后，如今的无线移动通信与以前提供语音电话业务为主的 2G 移动通信系统不同，3G 和 4G 时代的无线移动通信更多地提供高速率的多媒体业务和 Internet 网等，因此通信系统的发展必须采取一些更先进的通信技术来进一步扩大系统的容量、提高信息的传输速率和增加信道的利用率[1]。从理论上讲，提高通信网络的信道容量是解决这些问题的关键。提高网络的信道容量不仅可以解决无线网络的频谱资源紧缺和多径衰落问题，还增加了网络覆盖率和提高传输效率。

未来的无线通信技术的发展和演进将面临着大容量和高速率的挑战，在这样的形势下多输入多输出（Multiple-input Multiple-output, MIMO）技术[2]应运而生。MIMO 技术的出现可以使系统达到空间复用增益和空间分集增益，从而化解了无线通信系统中大容量需求和有限频谱资源之间的矛盾，抵抗多径衰落的影响。该技术具有极高的频谱利用率，能在不增加频谱带宽的情况下成倍地提高无线通信系统的容量，且大大增强了通信信道的可靠性，是这一代无线通信系统（Beyond 3G/4G）采用的核心技术之一。但是随着研究的进一步深入，MIMO 技术的移动终端受体积、功率及硬件复杂度等因素的制约，使得多天线技术很难在实际中应用。1998 年，Sendonaris 等[3]人提出了一种新的空间分集技术，即协作 MIMO（Cooperative MIMO）。协作 MIMO 是在多用户通信环境下的单天线用户共享其终端的天线，从而在用户和基站之间建立多条

(C)1994-2022 China Academic Journal Electronic Publishing House. All rights reserved. http://www.cnki.net

研究方向之一。

然而，协作 MIMO 技术在用户之间的距离较远时，传输速率仍受到制约。为了解决小区内和小区间的干扰问题以及扩大通信网络的覆盖范围，中继技术被引入到了无线协作通信系统中。中继技术的出现最早可以追溯到 20 世纪七十年代早期 Cover 和 Gamal[4]研究的关于中继信道的信息理论。他们针对图 1.1 所示的一个三节点网络进行容量及性能分析，将中继系统分解为一个广播信道和一个多址接入信道（分别从源节点和目的节点来看）。他们的研究得出几种特殊情况下的中继信道的容量和通用中继信道容量的上下界，从而为协作中继技术的研究奠定了理论基础，促进了协作通信技术的进一步发展[2,3,5]。传统的中继节点一般只能用来转发用户的信息，经常采用频分、时分的方式来同时转发多个用户的信息，这样大大降低了资源的利用率。2005 年 Yeung 等[6]人提出了网络编码，该技术可以使得中继节点先对接收到的信息进行一定的处理后再转发出去，有效地提高了通信网络的吞吐量，同时也解决了无线通信网络中的中继传输的瓶颈问题。随着用户需求的驱动，对于传输技术和网络容量等技术在内的 5G 关键技术提出了极大的挑战。

目前，网络编码已被证明是可以逼近网络容量理论传输极限的有效方法，具有确定拓扑图结构的网络编码已受到国内外学者们广泛的关注。由于无线链路的不可靠性和物理层广播特性等都非常适合采用有线网络的网络编码技术，用来解决传统路由以及跨层设计等技术所无法解决的难题，同时也提高网络的性能。而在实际的无线通信网络中，由于信道具有衰落性，需要通过信道编码来保证通信的可靠性。鉴于两者技术的种种优势，可以将两者有机的结合起来进一步提高通信系统的性能。目前，中继系统中的编码协作技术主要包括基于信道编码的编码协作技术、基于网络编码的编码协作技术以及基于网络编码和信道编码联合设计的编码协作技术等。

1.2 中继系统的发展与演进

1.2.1 系统模型

一个三节点的无线中继系统的信道模型[7]如图 1.1 所示，其中源节点 $\mathcal{S}$ 的发送信号 X，中继节点 $\mathcal{R}$ 的接收信号 Y_1，目的节点 $\mathcal{D}$ 的接收信号 Y_2，中继节点 $\mathcal{R}$ 对接收到的 Y_1 先进行处理后再发送信号 X_1。最后，目的节点 $\mathcal{D}$ 接收到的信号为 Y。假设信号同时受到信道的衰减和噪声的影响。

中继传输模式可以分为两类：半双工传输和全双工传输。全双工传输是指中继节点发送数据的同时也能够接收数据，两者同步进行，这好像平时打电话一样，说话的一方同时也能够听到对方的声音。而半双工传输是指在一个时间段内只有其中一个动作在发生，中继节点不能同时发送和接收数据。本文研究的中继节点均假设为半双工

(C)1994-2022 China Academic Journal Electronic Publishing House. All rights reserved. http://www.cnki.net

传输模式，即中继节点在同一频段内不能同时发送和接收数据。

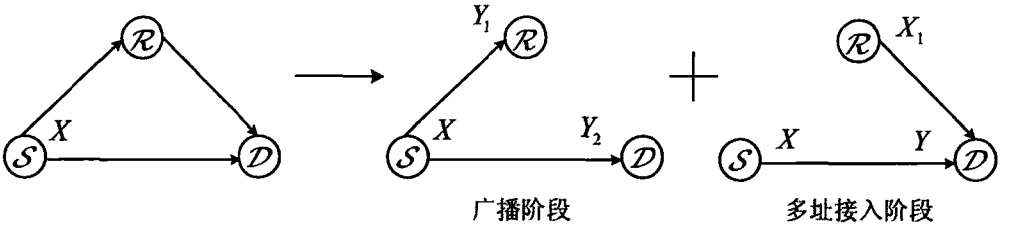


图1.1 三节点中继系统模型

从图 1.1 可以看出，一个三节点的中继通信系统的传输过程可以看作是一个广播阶段和一个多址接入阶段的结合。在第一个传输时隙时，源节点$\mathcal{S}$发送信号X到中继节点$\mathcal{R}$和目的节点$\mathcal{D}$，这个阶段可以看作是广播阶段。在第二个传输阶段，中继节点$\mathcal{R}$发送信号X_1，源节点$\mathcal{S}$发送信号X，目的节点$\mathcal{D}$对两个信道接收到的信息Y进行联合处理，这个阶段可以看作是多址接入阶段。这样的三节点中继系统模型是所有带有中继信道模型的典型。

1.2.2 中继系统的容量

中继信道可以看作是广播信道（X到Y_1与Y_2）和多址接入信道（X到X_1与Y）的组合。早在 1971 年，Meulen 开始研究了中继信道的容量问题[8]。后来在 1977 年，他又对多种中继信道进行研究和总结[9]。针对离散无记忆高斯中继信道，Cover 等在 1979 年通过构造随机编码方式得到三节点中继信道的可达码率集的上确界[4]。使用“最大流最小割”定理，可以得到如下一般意义的无记忆高斯中继信道容量上限：

$$C \le \sup_{p(x,x_1)} \min\left\{I\left(X,X_1;Y\right),I\left(X;Y,Y_1|X_1\right)\right\} \tag{1-1}$$

考虑一族中继信道模型，它们的中继接收端都优于最终接收端Y。此时式（1-1）中最大流最小割上界是可达的。可以得到一种被称为物理退化中继信道的容量：

$$C = \sup_{p(x,x_1)} \min\left\{I\left(X,X_1;Y\right),I\left(X;Y_1|X_1\right)\right\} \tag{1-2}$$

其中，式（1-2）比 Meulen[8]在 1971 年提出的退化中继信道容量有了很大的改善。随后，Gamal 等[10]在 1982 年把 Cover 研究的单中继信道容量的结果推广到了多中继网络中，研究了包含多个中继节点的半确定性中继信道的容量。之后，由于信息论方面

(C)1994-2022 China Academic Journal Electronic Publishing House. All rights reserved. http://www.cnki.net

的研究成果没有太多深入，所以从20世纪80年代开始研究中继信道容量的成果逐渐变少。

信息论发展的同时，信道编码理论也随之创立，具有高纠错能力的码的构造方法及对应的高效译码算法的设计成为人们研究的热点。如在20世纪中期RM码、RS码为代表的分组码，以及拓扑结构的编码主要是由网格图或树状图表示的卷积码等被发明。1993年Turbo码被提出，这种编码方式具有类随机性的特性以及足够的结构信息，使得其很好的应用了编码定理中的随机性编译码条件和最佳译码算法，并且获得了几乎接近香农理论极限的译码性能，立即在国内外通信界引起了研究Turbo码的热潮[11]。除Turbo码之外，低密度奇偶校验（Low-Density Parity-Check, LDPC）码是另一类逼近香农限的编码方式。LDPC码是由Gallager[12]于19世纪60年代初期首次提出的。不幸的是，这一重大的发现被编码界忽视了大约20年，直到1981年Tanner在一次偶然的工作中从图的角度提出了一种对LDPC码最全新的解释。可是，Tanner[13-15]的工作再一次被忽视了长达14年。直到19世纪末一些编码界研究人员才开始研究图编码和一些迭代译码算法。他们的研究使得当初Gallager的发现才得到进一步的研究和推广。采用置信传播迭代译码算法的长LDPC码已经被证明能够获得逼近香农限的误码性能。1998年空时编码被正式提出[16]等。这些信道编码的提出进一步推动了中继信道容量的深入研究。Anders等[17,18]人研究了中继信道的容量上下界和功率分配问题。2005年，Karmer等[19]研究了中继衰落信道的容量。随后，Cover于2007年分析了一类确定性高斯中继信道容量。受益于前人科研工作的启发，本文也考虑了无线传输过程中的一些中继节点的特性。对于中继节点传输需要的时间和消耗的能量本文没有过多提及和解决。

在分析研究三节点中继信道容量的同时，广播中继信道、多址接入中继信道以及MIMO中继信道的容量也得到了进一步深入[20-29]。信道编码技术被引入到中继系统中，涌现出许多协作编码方式。Hunte等[30,31]在2002年率先在协作中继系统中引入了信道编码技术，中继节点只需要转发用户发来信息的校验部分，而不是完全地重复转发。基于Turbo码、卷积码、分组码以及LDPC码等编码方式也出现了许多编码协作的研究成果[32-35]。近年来，随着人们对协作中继技术的深入研究，许多新的将已有方法相互融合而成的混合协作中继策略和协议随之产生。2009年，Li等[36,37]研究了LDPC码与网络编码相结合的技术，并给出了正交多址接入中继信道下的阈值和容量。

1.2.3 中继系统的主要研究

第一，资源分配。中继系统中引入了一个中间节点进行信息处理与转发。虽然降低了系统的错误概率，但是消耗了额外的带宽、功率和时隙等系统资源。为了降低系统的复杂度和提高系统资源利用率，多种对用户的发送功率进行优化分配[38,39]的算法

(C)1994-2022 China Academic Journal Electronic Publishing House. All rights reserved. http://www.cnki.net

被提出。根据中断概率最小[40]、传输能量消耗最少[41,42]以及系统容量最大[43]等设计准则对中继系统中的用户和中继节点的发送功率进行合理地优化分配。Larsson 等[44]人研究了功率、带宽和时隙等无线网络资源的的联合优化分配问题。为了满足人们对通信多媒体日益增长的质量需求，Jia 等[45]人对中继系统地功率分配进行了 cross-layer 设计，从而得到更好的系统性能。

上述技术中大都是假设通信信道是固定不变的，但是随着无线通信的飞速发展，信道状态实时在变，现有的固定功率分配方法已经不是最优选择。根据通信系统的实时多变性，近年来学者们研究了很多更加合理地功率分配方法[46-51]。每个中继系统都将面临着关于发送信号的功率分配问题，这一关键因素将成为中继通信系统中资源分配研究的热点之一。

第二，中继节点的选择和管理策略。中继节点的选择是指中继系统中源节点如何选择与其中一个或多个中继节点进行协作通信[52-54]。中继节点管理是指规定多长时间通信结束后需要重新选择中继节点进行通信[55]。由于蜂窝通信系统与无线自组织（ad hoc）通信网络的结构不同，所以中继节点的选择和管理方法也并不相同，可以分为集中式方案[56,57]和分布式方案[58,59]。集中式选择方案是指系统中所有节点之间交换信息集中到一个指定的网络节点处，由该节点控制节点间进行正常通信。分布式选择方案是指系统中局部节点间进行信息交换通信，没有中心控制节点的选择。

对于蜂窝通信系统来说，所有的用户都要和基站进行通信，基站已知所有通信信道间的信道状态信息。因此，采用集中式方法对所有中继节点进行统一的选择和管理。基站可以确定一个性能指标（所有用户的平均信噪比值最大[60]或者所有用户的消耗总能量最小[61]等优化准则）对各中继节点进行选择，从而使得系统性能达到最优。

对于无线 ad hoc 通信网络和无线遥感网络来说，网络中不存在一个中心节点控制，各节点间的通信需要采用一种分布式选择协议方式来完成通信。每个用户在任意时间点按照一定的准则（中断概率和系统容量等[62,63]）决定与其它哪个用户进行通信。特别指出，在中继节点的选择过程中可以和用户的多种资源分配联合起来进行优化设计，比如用户间噪声的影响、小区的范围大小以及基站的位置等[64-66]。

第三，跨层设计。现阶段通信的发展要求在传统协作协议的基础上提供各种自适应能力。为了提高整个系统的性能，需要各协议间能够有效的协作。中继系统的跨层设计主要包含两方面内容：一方面是协作分集和链路层的自动重传请求（Automatic Repeat-request: ARQ）相结合[67-72]，另一方面是协作分集和网络层的路由相结合[73-75]。前者可以有效地减小网络中的重传和传输次数，有效地提高系统的频谱效率。后者可以有效地增加多跳网络中的网络容量、减少用户间的干扰和减少能量受限的影响。

(C)1994-2022 China Academic Journal Electronic Publishing House. All rights reserved. http://www.cnki.net

1.3 中继系统的编码设计研究现状

现如今，中继系统的编码策略有很多种，本节主要从信道编码技术、网络编码技术、联合信道编码与网络编码设计技术等方面进行详细介绍，其中包括得分布式 Turbo 码、自适应中继编码以及双层 LDPC 码等在中继系统中得到了广泛的研究和应用。同时，本文的工作也从这些经典的编码策略出发来研究中继系统的码设计。

1.3.1 信道编码协作方案

中继系统的编码技术发展是编码与协作通信技术有机结合的过程，中继节点对数据进行处理主要包括译码、编码及转发三大类步骤，即源节点的信号经过纠错编码后广播给中继节点和目的节点，中继节点对收到的信号进行纠错译码恢复出源节点发来的信号，并将信号重新编码后转发给目的节点；目的节点对来自源节点和中继节点的信号进行合并处理，得到源节点的原始信息。目前大部分研究从两个角度展开：单用户中继系统和多用户中继系统。

单用户中继信道模型是研究中继系统的典型模型，其它的中继系统的模型都是由单用户中继系统推广得到的。根据中继节点个数不同，可以分为单中继信道模型和多中继信道模型。针对单源单中继信道模型，2003 年 Zhao 等[76]最早提出了分布式 Turbo 码的思想。2005 年，Cao 等[77]提出了在中继信道模型下串行 LDPC 码的设计方案。接着，Wen 等[78]提出了并行 LDPC 码在中继信道模型下的设计准则。2006 年，Hu 等[79]提出了在半双工模式下中继信道中 LDPC 码的设计方案，并通过高斯近似等优化方法对码的度分布序列进行优化。2007 年，Yu 等[80]提出了双层 LDPC 码。上述研究假定的都是理想化的中继系统模型，无线通信的实际应用中，由于通信的信道状态和传输的比特不同，研究的模型也相对复杂些。针对比特重要性不同，Hausl 等[81]提出了中继系统中的分等级设计思想。2009 年，Sediq 等[82]提出了不同信道下自适应信息合并优化策略，经证实，采用此策略可以极大地提高系统的性能。针对单源多中继信道模型，以 LDPC 码为例。2007 年，Li 等[83]提出了 LDPC 码在多中继信道下的改进的优化密度进化算法。

较早研究多用户中继信道模型下的编码技术是从 2005 年开始。在 2009 年，针对 LTE-advanced 4G 的多用户中继系统模型，Cao 等[84]通过采用一类满秩的编码矩阵以及扩频信息来研究多用户协作的译码性能。随后在 2010 年，针对多用户中继系统，Youssef 等[85]提出了一种改进型的分布式类 Turbo 码的设计方案，并获得了很大的性能增益。2012 年，基于多维空间的映射和编码理论的基本思想，黄英等[86]设计了两种适用于多用户单中继系统模型的中继编码矩阵，计算机仿真结果表明两种设计方案均可获得额外的性能增益。

(C)1994-2022 China Academic Journal Electronic Publishing House. All rights reserved. http://www.cnki.net

接下来首先重点介绍分布式 Turbo 码的基本原理框图，如图 1.2 所示。首先源节点 $\mathcal{S}$ 将一个码字 $c=[c_1\ c_2]$ 分成两部分进行传输，第一时隙时，源节点 $\mathcal{S}$ 将第一部分 c_1（通常采用递归卷积码）广播发送给中继节点和目的节点，中继节点 $\mathcal{R}$ 对接收到的信息进行卷积译码、交织、重新编码等处理后，产生的 c_2 被发送给目的节点。目的节点在两个时隙共收到两个码字组成并行级联码，这样就构成了一个 Turbo 码，并且码的两部分经历了两种独立的信道，目的节点利用两部分独立的码字进行迭代译码。结果显示，利用这些简单的分量码可以获得编码增益和分集增益。

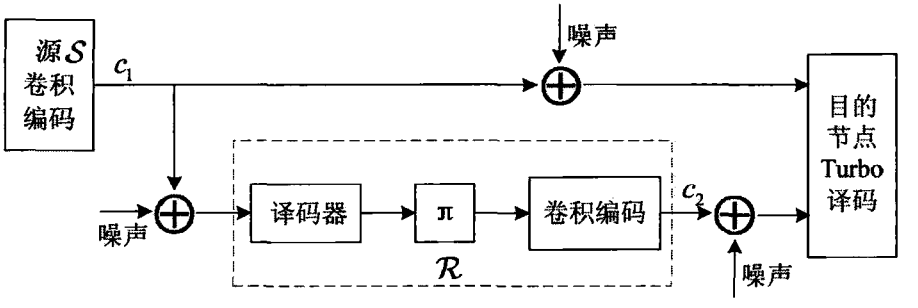


图1.2 分布式 Turbo 码

为了进一步提高分布式 Turbo 码的性能，Li 等[87]提出了软中继的分布式 Turbo 码，仿真结果表明，这种编码方式在高信噪比时可以达到包含两跳的分布式中继网络的中断概率界。后来，Sneessens[88]提出了一种改进的分布式 Turbo 中继传输方案，编译码原理如图 1.3 所示。如果中继节点 $\mathcal{R}$ 不能正确译码时，它在发送自己消息的同时还会将源节点到中继节点的信道状态信息或者信道衰落系数 h_{sr} 一起发送给目的节点，则目的节点利用 h_{sr} 可以估计出源节点到中继节点信道的误码率 p_e，并联合 p_e 进行迭代译码。与传统的 Turbo 码的译码器不同的是，该码中采用的两个分量码的输出并不是直接被当作另一个译码器的先验概率，而是通过一个转移概率后到达分量译码器的，其中的转移概率即为 p_e：

$$p(u'|u)=\begin{cases}1-p_e & if\ u'=u\\ p_e & if\ u'\neq u\end{cases} \tag{1-3}$$

$$p(u')=\sum_{u=0,1}p(u'|u)p(u) \tag{1-4}$$

其中，变量 u 和 u' 分别表示源节点和中继节点发送的信息比特位。当 $p_e=0$ 时，$p(u')=p(u)$，即表示分量译码器 1 的可以直接作为分量译码器 2 的先验概率输入，

(C)1994-2022 China Academic Journal Electronic Publishing House. All rights reserved. http://www.cnki.net

这样的译码器即变为普通 Turbo 译码器。可知，这样的译码算法可以认为是最普通的译码算法，通常所用的 Turbo 译码是其中的一种特殊例子。

其次重点介绍第二种编码设计方案。Razaghi 等[80]提出的双层 LDPC 码，他们根据 Cover 的逼近中继容量限的构造思想，构造了双层 LDPC。他们针对典型的三节点中继信道，如图 1.1 所示。首先假设源节点到中继节点的信道是无错的，其次中继节点将译出的正确信息重新编码，而后发送校验位到目的节点，整个过程和 Cover 理论中的中继节点发送码字的块号相对应。其中校验位是由一个新的码字编码产生并进行传输，并且假设目的节点可以成功译出中继节点发来的这些校验位，这也和 Cover 理论中的目的节点能够正确译出块号相对应。

主要工作是首先源节点采用 LDPC 码，其次利用密度进化方法来优化中继节点的编码方案。这种码对应的 Tanner 图，如图 1.3 所示，其中上层子图是传统的 LDPC 码的结构图，即源节点采用的(n,k_1)LDPC 码，下层子图为中继编码的结构图，k_2表示中继节点所产生的校验位比特。文中采用的这种码的密度进化方法，被称为双层密度进化算法。关于这种码的优化算法及新的构造法，我们将在第五章中详细研究。

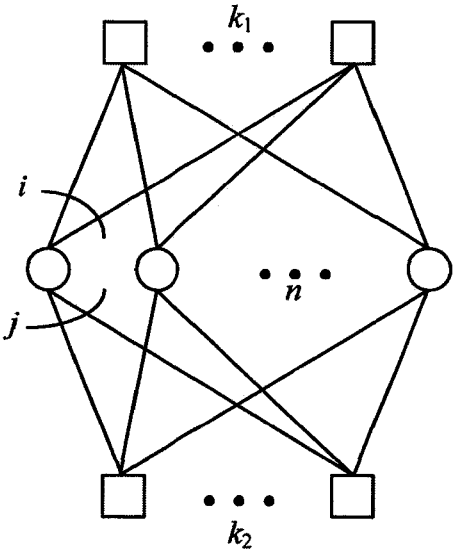


图1.3 双层 LDPC 码的 Tanner 图

1.3.2 网络编码协作方案

网络编码技术是一种融合了路由和编码的新型的信息传输技术，其基本思想是处于网络中间的节点可以对接收到的信息进行编码或者处理后转发给下一阶段节点。Ahlswede 等以蝶型拓扑图（如图 1.4）为例，研究了网络编码技术可以进一步提高网络的容量，并很大程度上提高了信息的传输效率。

(C)1994-2022 China Academic Journal Electronic Publishing House. All rights reserved. http://www.cnki.net

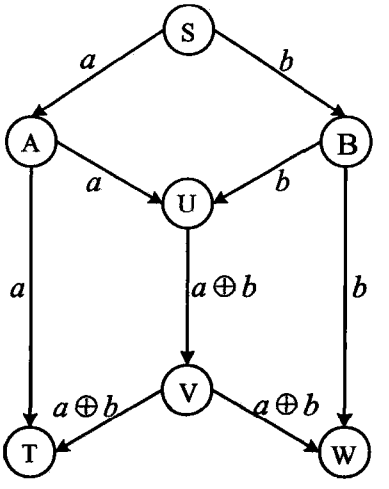


图1.4 蝶形拓扑图

2000 年，Cai 等[89]将纠错编码[90]的原理应用到多用户中继系统中，产生了网络纠错码。随后，Li 等[91,92]借助于线性编码技术的简单性和实用性，提出了一种线性网络编码，并得到具有最大流量码率的线性码。他们的工作奠定了网络编码技术研究的基础，启发了更多的人们去研究网络编码及其相关技术。

网络编码是一种富有创新性的技术，多用户中继系统是满足多用户通信的代表性模型。两者有机的结合不仅可以提高系统的吞吐量和增加系统的分集增益，而且在对抗小区干扰和提高网络覆盖面积等方面具有很好的性能优势。早期的网络编码仅被应用在两用户单中继系统中[93]。后来，Peng 等[94]学者研究了物理层网络编码在多用户单中继系统中的应用。在多用户中继系统中，中继节点对来自多个源节点的信息分别进行译码，而后对信息进行硬判决编码和软信息合并等处理，最后发送给目的节点。如果源节点到中继节点的信道状况好时，中继节点会对接收到来自源节点的信息直接进行译码判决后，将模二和发送到目的节点[95]；否则中继节点对接收到来自源节点的信息进行软信息合并，并发送到目的节点[96]。在中继节点处进行网络编码，可以有效地提高系统的资源利用率和系统的吞吐量，同时可以提高系统的频谱效率。

网络编码技术被广泛地应用在中继系统中是一种很自然的研究趋势，但是关于网络编码技术早期的研究都是基于二进制网络编码的原理[97,98]，由于其传输效率（如：误帧率、能量效率[99]等）不是最优的。后来 Ayanoglu 等[100]提出了一种适用于多用户单中继系统的分级网络编码方案，其中链路损失问题被视作为删除信道。假设源节点独立或者相关的情况下，Yeung 等[101]人研究了最佳的同步多层分级网络编码方案。Wang 等[102]在 2008 年提出了复数域网络编码（Complex Field Network Coding，CFNC）技术的思想，每个源节点将各自的数据与复数域上的一个加权因子相乘后发送给中继节点，中继节点通过多用户检测方法来恢复各源节点发来的信息，并采用网络编码后将它们转发出去。该技术可以获得 1/2 符号/信源/时隙的吞吐量，同时还能够获得满

(C)1994-2022 China Academic Journal Electronic Publishing House. All rights reserved. http://www.cnki.net

分集增益。在慢衰落信道模型下，以提高数据传输效率为目的，Xiao 等[103]人研究了非二进制网络编码在多用户多中继系统中的性能情况，通过仿真结果可以得出该方案可以获得一个全分集阶数。

下面重点阐述一种自适应网络编码协作（Adaptive Network Coded Cooperation, ANCC）技术在中继系统中的应用。首先介绍一种协作分集方案[30]，如图 1.5 所示。两个源节点互为对方的中继节点，在第一个时隙时两个源节点分别广播各自的数据包 1，此时源 1 和源 2 都收到了对方的数据。如果源 1 和源 2 都能正确译出对方的消息，在第二个时隙时，各自将发送对方的一个冗余信息数据包 2，否则将发送各自的数据包 2，这样相当于一种新的分布式编码。这个传输过程可以保证从它们各自发来的信息是正确的，通过仿真可知，即使两个源节点间的信息质量很差时，系统的性能依然会有很大的提升。

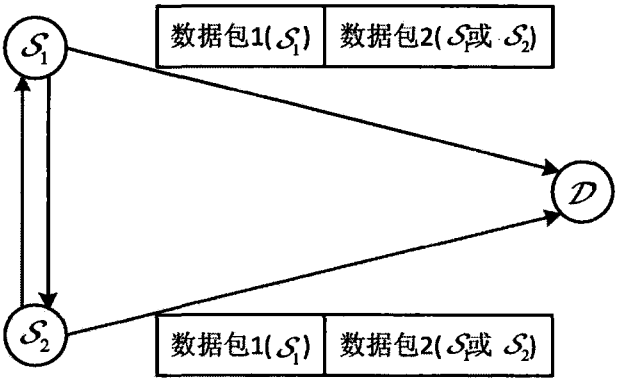


图1.5 自适应协作编码

Bao 等[104]通过将 LDPC 码的因子图与网络拓扑图相融合，提出了一种 ANCC 方案。自适应，顾名思义就是中继节点根据信道的状态信息不同选择不同的协作方案。由于基于因子图的码与基于网络的码相对应，通过对设计校验矩阵来选择中继节点，从而抵抗无线信道的衰落特性。试验表明 ANCC 的性能优于重复码大约几十 dB 的增益。如图 1.6 所示。基本传输过程如下：假设网络中有五个移动用户，每个用户都有一个分组需要发送，同时也作为别的用户的中继节点，转发其它用户的信息。整个过程分两个阶段进行:第一阶段五个用户将各自的分组分别广播出去。如果采用半双工模式，每个用户在不同的时隙发送信息。如果采用全双工模式，每个用户间可以采用时分、频分或码分等正交复用方式发送信息，避免不同的用户间的相互干扰。第二阶段每个用户从各自正确接收到的分组（不一定全部正确接收）中随机的挑选出部分分组做异或运算，各自作为中继节点将分组转发出去。

如果上面选择的部分分组数很小，则整个过程可以构成了一个随机低密度生成矩阵(Low Density Generator Matrix, LDGM)码，LDGM是LDPC的其中一种码，该码不

(C)1994-2022 China Academic Journal Electronic Publishing House. All rights reserved. http://www.cnki.net

但校验矩阵中包含1的个数少，而且它的生成矩阵包含1的个数也很少。上面的信息传输过程中第一个阶段发送的就是LDGM码的信息比特，第二个阶段发送的是其校验比特。译码可将整个传输过程看成一个大的LDPC码进行迭代译码，也可以先进行网络LDPC译码然后再进行信道译码。

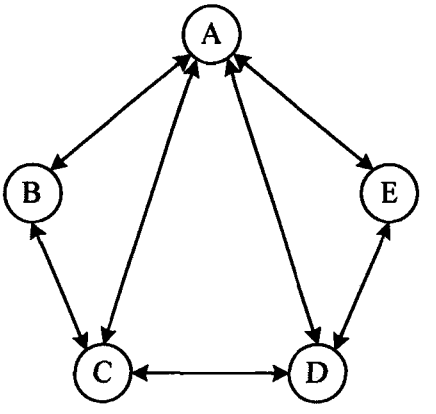


图1.6 5个用户的ANCC网络模型

用户个数和选择的分组数的大小对系统影响很大，用户很多时则LDGM的码长很长可以获得的分集增益也变大。选择的分组数越小则编译码的复杂度会越低，同时也可以避免长度为4的环，从而在接收端就可以使用基于置信传播的迭代译码。但是分组的减小会出现严重的错误平层效应，所以分组的选择要根据具体要求而定。

通常噪声很大的固定路由的协作效率很低，但是自适应动态路由的协作效率大大提高，这时ANCC能够获得很高的协作效率。这是因为当噪声很大时，中继节点转发的分组在很大程度上是错误的。

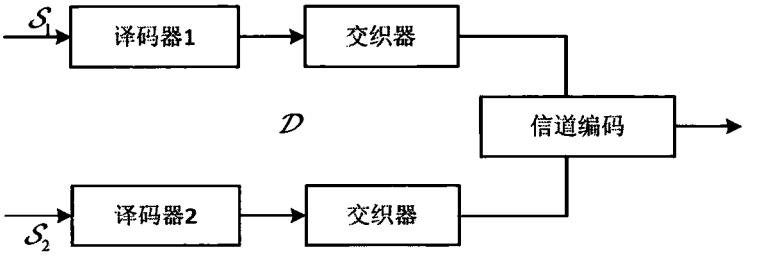
由于LDGM码本身的校验矩阵的右半部分是一个单位阵，根据置信传播的迭代译码算法，这样会严重的影响码的性能。所以当用户采用时分复用方式发送信息时，可以使用性能更好的下三角低密度校验码(LT-LDPC)，虽然该码的生成矩阵不一定是低密度的，但该码有着更低的误码率和更小的错误平层效应。

这时，Bao又将ANCC推广得到了GANCC(generalized adaptive network coded cooperation)[105]。它与ANCC的区别在于第二阶段每个用户从各自正确接收到的分组中随机的选取部分分组不在进行异或运算而是交织(每个分组所用的交织器不同，为降低每个节点的存储量使用代数交织，ANCC中不交织)，之后再进行网络编码操作。交织不仅可以去除信道的相关性，同时也减少长度为4的环，进而降低了系统的错误概率。实验表明GANCC可比ANCC获得更多的增益时间和空间分集。

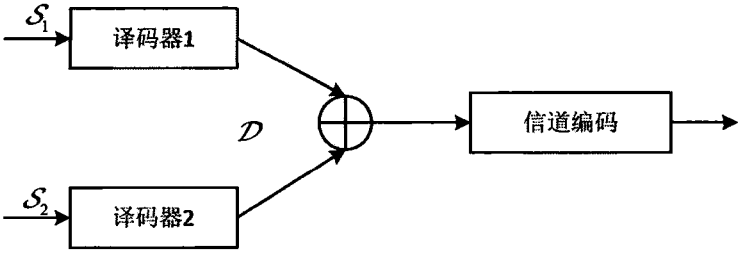
(C)1994-2022 China Academic Journal Electronic Publishing House. All rights reserved. http://www.cnki.net

1.3.3 联合网络-信道编码协作方案

无线通信的发展过程中，网络编码与信道编码的结合是中继系统中的又一研究热点。两者相结合的技术不仅可以增加系统的吞吐量，还可以提高抗噪声的性能。早期的研究大多集中在源节点和目的节点有直接链路和没有直接链路两种模型，如图 1.7 中的（a）和（b）。



(a) 联合信道和网络编码



(b) 分离信道和网络编码

图1.7 中继节点的编码框图

2006 年，Song 等[106]提出了网络编码与信道编码的分离定理，即网络编码可以发挥自己的独特作用使通信网络达到最大流量，信道编码可以保证每条独立信道传输信息的可靠性，将两者的设计方案分开进行。与此同时，针对双向中继信道模型，Hausl 等[107]研究了网络编码与 Turbo 编码的联合编译码设计方案。目前，研究网络编码和信道编码大多数都是基于两者的联合设计，大致可以分为两种：嵌套编码[108,109]和混合编码[110,111]。

嵌套编码：对于一个两源单中继的多址接入网络来说，中继节点采用与源节点相同的编码来构造嵌套编码，如图 1.7（a）所示，本质上是中继节点将源节点的信息重新编码后，再进行异或运算后发送给目的节点。但是从纠错码的理论角度看，重复码相当于一类纠错码，若中继采用与源节点不同的编码方式来构造嵌套码可能获得更好的性能。Hausl 等[108,109]利用 LDPC 码来构造嵌套码。前者采用了 LDPC 码搭建了窃套码，但是没有一个系统的设计方法。在大规模的通信网络中，由于中继节点接收到

(C)1994-2022 China Academic Journal Electronic Publishing House. All rights reserved. http://www.cnki.net

的信息中包含有多个源节点的信息，如何能够合理的对这些信息进行有效的编码，保证目的节点的性能不会减少太多，是目前窃套码需要解决的另一个问题。另外，窃套码的整体码率是所有子码码率之和，一般情况下要求每个子码的码率要小于 1/2。针对多源多中继的多址接入网络来说，中继节点会接收到来自多个源节点的信息，同时一个源节点发送信息到多个中继节点，这就要求多源多中继的网络编码与信道编码的联合设计，这个问题在本文第四章详细研究。

混合编码：针对两源单中继的多址接入中继网络来说，Hausl 和 Dupraz 等[110,111]人提出了采用一种混合编码方式来实现网络编码与信道编码的联合设计，如图 1.7(b)所示，即中继节点对来自不同源节点的信息进行交错编码，而后将编码后的信息转发出去。2007 年，Razaghi 等[112]提出了一种双层 LDPC 编码方案，中继节点根据源节点采用的 LDPC 码的特点设计出相应的 LDPC 码的度序列，目的节点进行联合迭代译码并获得逼近容量限的译码性能。2009 年，Li 等[36]给出了双层 LDPC 编码的基于 EXIT 图的度优化算法，并获得了很好的误码性能。

如图 1.8 所示的两源单中继的多址接入中继信道模型。第一个时隙时移动台 1 广播信息到中继节点和基站，第二时隙移动台 2 广播信息到中继节点和基站，第三时隙中继节点将两路信息译码再进行网络编码后转发出去。目的节点收到三路信息后进行联合译码。三个时隙的时间长短并不相同。与通常的多址接入中继信道模型相比，这种采用时分复用技术的模型性能不是最优的。由于它采用的是半双工中继节点和非对称的约束条件，在实际的系统中很容易实现。

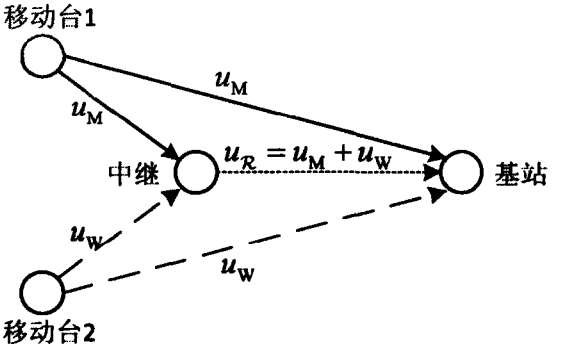


图 1.8 联合网络-信道编码的多址接入中继信道模型

文中基于 Turbo 码提出了一种联合网络-信道编码的设计方法，并且研究了如何合理分配三个时隙的发送时间。首先与分布式 Turbo 码进行对比。其次研究了编码调制的中断概率，并推导了多址接入中继信道(Multiple Access Relay Channel, MARC)模型中采用更高码率的码所能够获得的分集增益。最后，结果表明联合网络-信道编码相对于独立网络-信道编码技术，可以使得中继节点在发送时获得有效的冗余。

(C)1994-2022 China Academic Journal Electronic Publishing House. All rights reserved. http://www.cnki.net

其次针对双向（Two-way）中继信道模型，如图 1.9 所示。两终端通过一个中继协作通信，这种系统可以用在协作通信的移动台与基站之间的上行链路和下行链路。第一个时隙时移动台发送信息到中继节点，第二个时隙基站发送信息到中继节点，第三时隙中继节点将两路进行异或运算的网络编码后广播出去。

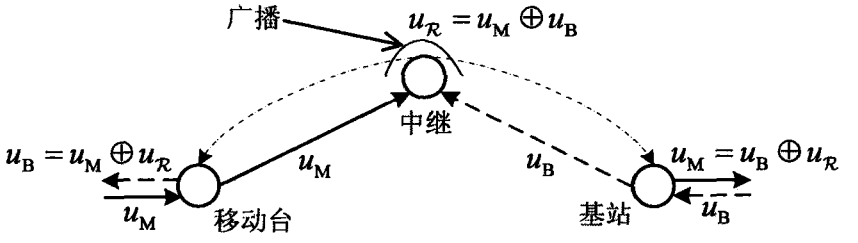


图 1.9 联合网络-信道编码的双向中继信道模型

文中提出了一种改进联合网络-信道编码的设计方法，并且研究了最佳分配三个时隙的发送时间。首先在上行链路和下行链路不等的速率下设计的码。其次推导了时间分配的闭合界表达式以及对称双向中继信道的译码转发模式下的可达速率。在此基础上与分布式 Turbo 码进行了对比。最后，结果表明改进的联合网络-信道编码相对于独立网络-信道编码技术，可以获得速率增益和很高的吞吐量。

目前，将网络编码与信道编码技术相结合的成果明显改善了系统的性能，但是这种结合技术会消耗很多额外的网络资源，比如：功率、码字、时间、空间和频率等。因此，在多址接入中继信道中采用联合网络编码和信道编码技术会损失系统的吞吐率，降低频谱利用率，必须采用一种合适的方法加以改善。这个问题的研究详见第三章，提出了一种速率兼容网络 LDPC 码的删余方案。中继节点只需要将源节点的部分信息用于转发，很好的弥补了消耗系统资源这一缺点。

1.4 本文的研究内容及结构安排

在“新一代宽带无线移动通信网”国家科技重大专项“IMT-Advanced 开放性关键技术研究”课题（2009ZX03003-011，2009ZX03003-003-03）、国家自然科学基金项目（61072064）、973 计划项目“高谱效高能效调制信号设计与编码调制理论研究”课题和长江学者和创新团队发展计划（IRT0852）资助下，本文针对无线中继系统中信道编码技术进行了深入研究，主要研究成果如下：

首先基于两源单中继信道中网络 LDPC 码的结构特点，提出了一种可以获得最小比特错误概率的速率兼容网络 LDPC 码删余算法,并推导了该算法的译码错误概率；随后采用一种差分进化算法对网络 LDPC 码的度分布进行优化；其次在多源多中继信道中，为了降低易错中继节点的错误传播，提出了一种基于 RS 编码的混合译码转发

(C)1994-2022 China Academic Journal Electronic Publishing House. All rights reserved. http://www.cnki.net

策略。最后，基于半速率可逆码的特性，在半双工译码转发模式的三节点中继系统中，提出了一种采用叠加组合的方法构造双层 LDPC 码。全文共分为六章，现将具体内容安排如下：

第一章介绍了中继系统的发展背景和本文研究的选题意义，详细阐述了几种常见的中继系统的编码设计方案及论文主要内容的章节安排。

第二章首先介绍了多址接入中继系统的信道模型，其次详细分析了两类多址接入中继信道的容量，然后给出了它们的仿真结果及性能分析。

第三章针对两源单中继信道，提出了一种可以获得最小比特错误概率的速率兼容网络 LDPC 码删余算法,并推导了该算法的译码错误概率。该算法以网络 LDPC 码的结构特点为基础，以达到最小化译码比特错误概率为目标，在网络 LDPC 码的因子图上搜索出需要删除的变量节点，从而获得最优的删余图样。其次采用差分进化算法对网络 LDPC 码的度分布进行优化，获得最优的码集。最后，给出仿真结果。

第四章针对多源多中继易错无线中继信道，提出了一种基于 RS 编码的混合译码转发策略。该策略引入了一个决定中继节点是否转发信息的阈值。当中继译码后的信息比特的对数似然比大于该阈值时，该信息比特才会被转发。否则该信息比特被丢弃。在此基础上，以最小化比特错误概率为优化目标，分别对独立协作和混合协作两种策略通过优化方法设计了最佳阈值。仿真结果表明，不管是在高斯信道还是在瑞利衰落信道下，该方法可提高系统的误码性能。

第五章针对单源单中继信道，以半速率可逆 LDPC 码的Ⅱ型 HARQ 的特点为基础，采用叠加组合方法构造的一种双层 LDPC 码，并通过高斯近似密度进化方法对其译码阈值进行了研究分析。从计算机的仿真结果可以看出，同已有的基于传统方式构造的双层 LDPC 码相比，这种应用半速率可逆 LDPC 码的Ⅱ型 HARQ 构造的双层 LDPC 码可以使误码性能获得较大的提高。

最后，对整篇论文的研究内容进行了总结，并指明了后续的研究方向。

(C)1994-2022 China Academic Journal Electronic Publishing House. All rights reserved. http://www.cnki.net

(C)1994-2022 China Academic Journal Electronic Publishing House. All rights reserved. http://www.cnki.net

第二章 多址接入中继系统模型及传输策略

本章首先描述了多址接入中继系统的信道模型-四节点中继信道，研究了两种信道模型下的几种重要的传输协议下的信道容量域。最后，给出了几种重要传输协议下的计算机性能仿真结果。

2.1 多址接入中继信道模型

研究协作通信和中继传输系统的模型大部分拘泥于一个源节点、一个中继节点和一个目的节点的单个链路的通信网络。本文的主要研究重点是多址接入中继信道。多址接入信道是未来无线通信的基础模型。多址接入中继系统中的大量节点间的通信使用共同的通信信道，每个源节点和中继节点都可以向目的节点发送信息。最早 MARC 是由 Kramer 等[113]人在 2000 年提出的。文中针对多源单中继单目的节点的信道模型，构造了一个虚拟多天线阵列，为整个系统增加了空间分集增益。

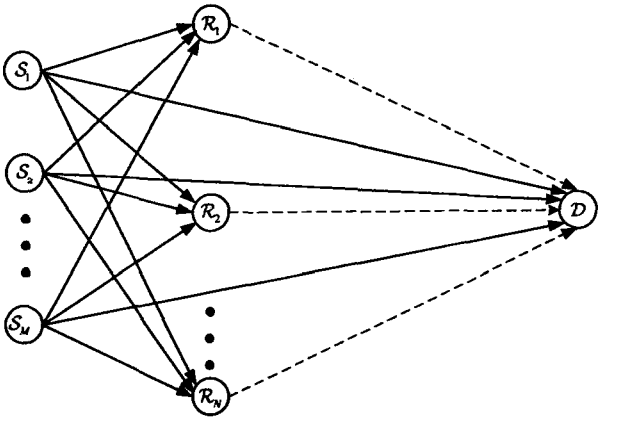


图2.1 多址接入中继信道模型

目前研究的多址接入中继信道模型如图 2.1 所示，包含 M 个源节点 $\mathcal{S}_1,\mathcal{S}_2,\cdots,\mathcal{S}_M$、$N$ 个中继节点 $\mathcal{R}_1,\mathcal{R}_2,\cdots,\mathcal{R}_N$ 和一个目的节点 $\mathcal{D}$。首先，源节点 $\mathcal{S}_i\left(i=1,2,\cdots,M\right)$ 广播信息到中继节点 $\mathcal{R}_j\left(j=1,2,\cdots,N\right)$ 和目的节点 $\mathcal{D}$。其次，中继节点 $\mathcal{R}_j$ 对接收到的信息进行处理后转发给目的节点 $\mathcal{D}$。最后，目的节点 $\mathcal{D}$ 对直接链路的信息与中继节点转发来的信息进行联合处理，中继节点 $\mathcal{R}_j$ 实现了提高空间分集增益的目的。根据源节点和中继节点对信号的发送时间和频率的不同，多址接入中继信道模型的传输方式可以分为两种类型。

(C)1994-2022 China Academic Journal Electronic Publishing House. All rights reserved. http://www.cnki.net

2.1.1 正交多址接入中继信道模型

一种基于 TDMA 系统的正交多址接入信道模型如图 2.2 所示，包含两个源节点 $\mathcal{S}_1,\mathcal{S}_2$、一个中继节点 $\mathcal{R}$ 和一个目的节点 $\mathcal{D}$。两个源节点在一个中继节点的协助下与目的节点进行通信，为了避免信道间的干扰，同一时隙只能发送一个源节点的信息。针对图 2.2 所示的模型，需要四个时隙完成通信。第一时隙，源节点 $\mathcal{S}_1$ 向中继节点 $\mathcal{R}$ 和目的节点 $\mathcal{D}$ 广播信息。第二时隙，源节点 $\mathcal{S}_2$ 向中继节点 $\mathcal{R}$ 和目的节点 $\mathcal{D}$ 广播信息。第三、四时隙，中继节点 $\mathcal{R}$ 分别转发源节点 $\mathcal{S}_1(\mathcal{S}_2)$ 的信息给目的节点 $\mathcal{D}$。

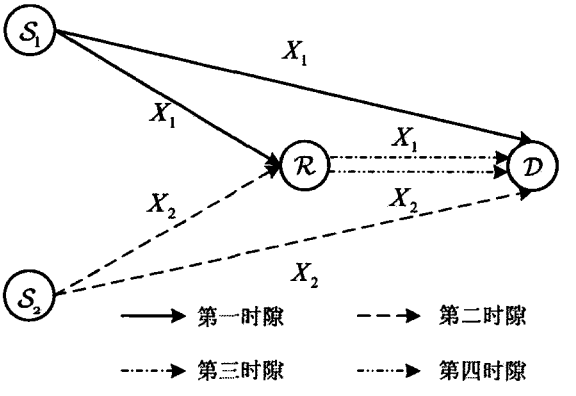


图2.2 正交多址接入信道模型

采用上述这种传统的正交多址接入中继信道，各信道之间没有干扰，可以有效的提高目的节点的性能。但是中继节点的这种转发方式需要为每个源节点分配独立的资源，随着源节点数目的增多，中继节点转发的效率随之降低。为了解决这一问题，中继采用了网络编码技术，可以有效的提高中继的转发效率，并提出了基于网络编码的正交多址中继信道模型。

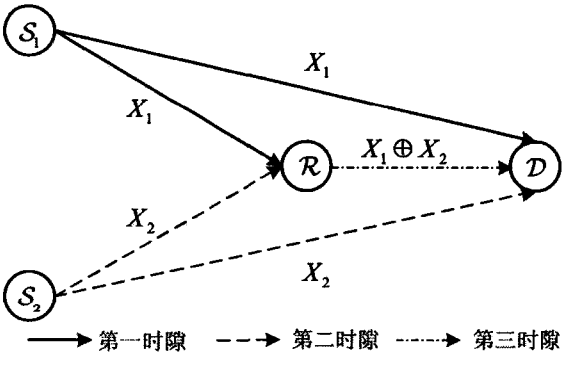


图2.3 基于网络编码的正交多址接入信道模型

如图 2.3 所示，基于网络编码的正交多址接入中继信道模型包含两个源节点 $\mathcal{S}_1,\mathcal{S}_2$、

(C)1994-2022 China Academic Journal Electronic Publishing House. All rights reserved. http://www.cnki.net

一个中继节点$\mathcal{R}$和一个目的节点$\mathcal{D}$。这个信息传输过程需要三个时隙完成：第一、二时隙，源节点$\mathcal{S}_1(\mathcal{S}_2)$分别向中继节点$\mathcal{R}$和目的节点$\mathcal{D}$广播信息，并且中继节点$\mathcal{R}$对接收到的两个源节点$\mathcal{S}_1(\mathcal{S}_2)$的信息进行网络编码；第三时隙，中继节点$\mathcal{R}$将网络编码后的信息转发给目的节点$\mathcal{D}$，目的节点$\mathcal{D}$根据三条链路发来的信息进行译码恢复出源节点信息。显然，采用网络编码的多址接入中继系统中的传输效率提高了25%。

2.1.2 非正交多址接入中继信道模型

基于非正交多址接入的中继信道通用模型如图2.4所示，包含两个源节点$\mathcal{S}_1,\mathcal{S}_2$、一个中继节点$\mathcal{R}$和一个目的节点$\mathcal{D}$。本模型的传输信息时隙可分为两个：第一个时隙为源节点$\mathcal{S}_1,\mathcal{S}_2$同时向中继节点$\mathcal{R}$和目的节点$\mathcal{D}$广播信息，中继节点$\mathcal{R}$和目的节点$\mathcal{D}$将接收到的两个源节点$\mathcal{S}_1,\mathcal{S}_2$发来的叠加信息；第二时隙，中继节点$\mathcal{R}$对叠加的信息进行处理后转发给目的节点$\mathcal{D}$，目的节点$\mathcal{D}$根据三条链路发来的信息恢复出源节点的信息。与传统的正交多址接入信道模型相比较，采用非正交的多址接入中继系统的传输效率能提高50%。

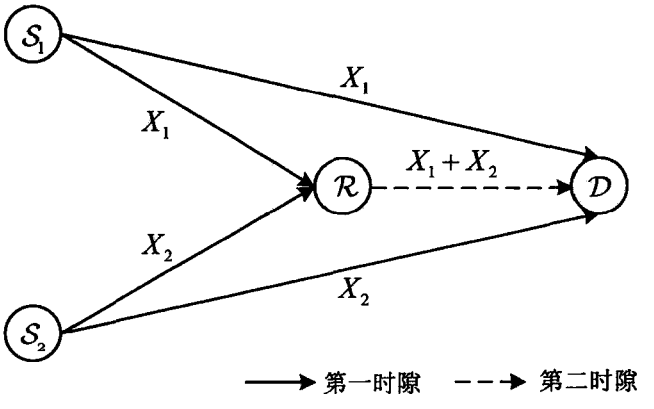


图2.4 非正交的多址接入中继信道模型

本节介绍的两大类多址接入中继信道模型，中继节点传输均采用半双工传输模式。中继节点采用全双工的传输模式也可以得到类似的结论。再者，中继节点处可以根据传输方案的不同，从放大转发（Amplify-and-forward, AF）、压缩转发（Compress-and-forward, CF）和译码转发（Decode-and-forward, DF）等角度来分析系统的容量。

(C)1994-2022 China Academic Journal Electronic Publishing House. All rights reserved. http://www.cnki.net

2.2 多址接入中继信道的容量域

2.2.1 正交多址接入中继信道的容量

针对两用户正交多址接入中继信道模型，Hausl 等[114]人研究分析其信道容量如下。

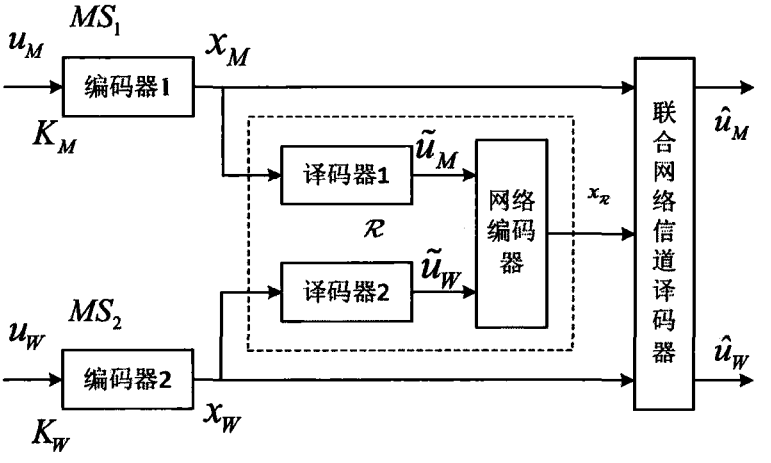


图2.5 蜂窝移动通信系统框图

如图 2.5 所示的蜂窝移动通信系统中，假设两个移动端 MS_1 和 MS_2 分别发送被分割成长度为 K_M 和 K_W 的统计独立的比特数据包 u_M 和 u_W 到基站。不失一般性，假设 $K_M \geq K_W$。信息比特数据包 u_M 和 u_W 经过编码调制后分别输出包含 M_M 和 M_W 个符号的数据块 x_M 和 x_W。第一个时隙时 MS_1 以功率为 P 向中继和基站广播包含 M_M 个符号的数据包；第二个时隙时 MS_2 以功率为 P 向中继和基站广播包含 M_M 个符号的数据包。第三个时隙时中继以功率为 P 向基站发送经过信息处理后的包含 M_R 个符号的数据包 x_R。整个系统总的发送符号数为 $M = M_M + M_W + M_R$。假定 MS_1 的速率 $R_M = K_M/M$，MS_2 的速率 $R_W = K_W/M$，系统总的速率为 $R = R_M + R_W = (K_M + K_W)/M$。假设整个系统所有的信道均为瑞利块衰落信道，所有的接收数据包表示如下：

$$y_{MR} = h_{MR} \cdot x_M + z_{MR} \quad (MS_1 \text{发送}) \tag{2-1}$$

$$y_{MB} = h_{MB} \cdot x_M + z_{MB} \quad (MS_1 \text{发送}) \tag{2-2}$$

$$y_{WR} = h_{WR} \cdot x_W + z_{WR} \quad (MS_2 \text{发送}) \tag{2-3}$$

$$y_{WB} = h_{WB} \cdot x_W + z_{WB} \quad (MS_2 \text{发送}) \tag{2-4}$$

$$y_{RB} = h_{RB} \cdot x_R + z_{RB} \quad (\text{中继发送}) \tag{2-5}$$

(C)1994-2022 China Academic Journal Electronic Publishing House. All rights reserved. http://www.cnki.net

其中，$h_i = a_i \cdot \sqrt{P_r(d_i)/P}$，$i \in \{MR, MB, WR, WB, RB\}$，$E\left[|a_i|^2\right]=1$。平均信噪比$\rho_i = P_r(d_i)/(N_0 \cdot W)$，瞬时信噪比$\gamma_i = |a_i|^2 \cdot \rho_i$，五条路径的信噪比之间的关系取决于节点间的距离$d_i$和路径衰减指数$n$。

在时分多址接入中继系统模型中，当中继节点采用译码转发模式且各发送端发送的时间最佳分配时，译码转发的可达速率需满足以下五个约束不等式的条件，基站可以正确译出两个移动台的数据，如下：

$$K_M \le M_M \cdot C(\gamma_{MR}) \tag{2-6}$$

$$K_W \le M_W \cdot C(\gamma_{WR}) \tag{2-7}$$

$$K_M \le M_M \cdot C(\gamma_{MB}) + M_R \cdot C(\gamma_{RB}) \tag{2-8}$$

$$K_W \le M_W \cdot C(\gamma_{WB}) + M_R \cdot C(\gamma_{RB}) \tag{2-9}$$

$$K_M + K_W \le M_M \cdot C(\gamma_{MB}) + M_W \cdot C(\gamma_{WB}) + M_R \cdot C(\gamma_{RB}) \tag{2-10}$$

其中，$C(\gamma_i) = \log_2\left(1 + |a_i|^2 \rho_i\right)$表示点对点通信时高斯信道的容量。

2.2.2 非正交多址接入中继信道的容量

Sankarana 等[115]人针对两类非正交多址接入信道模型的容量进行分析，主要结果如下：

一个高斯多址接入中继信道模型由M个源节点，一个中继节点，以及一个目的节点组成的。其中$M+1$个输入节点表示为$X_{ki}(k=1,2,\ldots,M+1)$，i表示发送第i个符号，整个系统共发送n次符号，中继节点和目的节点接收到的信号分别为$Y_{M+1,i}$和$Y_{M+2,i}$：

$$Y_{M+1,i} = \left(\sum_{k=1}^{M} h_{M+1,ki} X_{ki}\right) + Z_{M+1,i} \tag{2-11}$$

$$Y_{M+2,i} = \left(\sum_{k=1}^{M} h_{M+2,ki} X_{ki}\right) + Z_{M+2,i} \tag{2-12}$$

其中，$Z_{ji}\left(j \in \{M+1, M+2\}\right)$表示复高斯噪声，其实部和虚部都服从均值为 0，方差为 1/2 的独立同分布的随机变量，且$E\left(|Z_{ji}|^2\right)=1$。第$k$个源节点和中继节点的发送功率满足约束条件：$\sum_{i=1}^{n} E\left(|X_{ki}|^2\right)/n \le P_k$。$h_{j,ki}$表示第$k$个节点向第$j$个节点发送第$i$个符号时的信道衰落系数，且第$j$个节点已知信道状态信息。

(C)1994-2022 China Academic Journal Electronic Publishing House. All rights reserved. http://www.cnki.net

以上模型中中继节点发送和接收信号是同时进行，即称为全双工的 MARC。但是，在实际的无线通信过程中，中继节点的发送和接收会受到物理或者实际通信环境的约束，不能同时进行发送和接收信号，即为半双工的 MARC，也简称受限-MARC（constrained-MARC, C-MARC）。

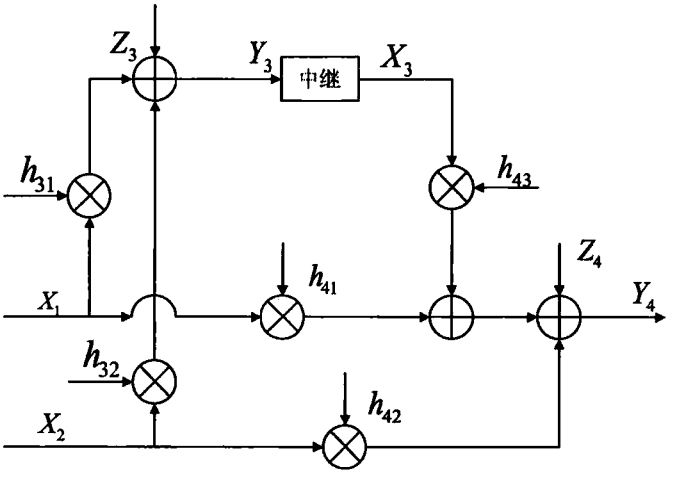


图2.6 两源多址接入中继系统框图

如图2.6所示，由两个源节点，一个中继节点和一个目的节点构成的高斯C-MARC框图。假设中继节点的接收和发送信息的总时隙为 1，其中接收信息占用时隙比α，发送信息时隙比$1-\alpha$。中继节点接收n_1个符号，发送$n-n_1$个符号，且$n_1/n=\alpha$。C-MARC 接收阶段的输出信号表达式即为式（2-11）（2-12），其中$i\in[1,n_1]$。C-MARC 发送阶段的输出信号表达式为：

$$Y_{M+1,i}=0 \tag{2-13}$$

$$Y_{M+2,i}=\left(\sum_{k=1}^{M+1}h_{M+2,ki}X_{ki}\right)+Z_{M+2,i} \tag{2-14}$$

其中，$i\in[n_1+1,n]$。噪声Z_{ji}和信道衰落系数的定义与式（2-11）（2-12）相同。

一般情况下，一个连续的块中不能同时存在接收和发送两个信道状态。MARC 直接退化成 C-MARC，只需额外满足约束：

$$\text{当}\ X_{M+1}\neq 0\text{时，}\ Y_{M+1}=0 \tag{2-15}$$

其中，在α时隙时，$X_{M+1}=0$。这样，MARC 的理论推导可以直接应用在 C-MARC 模型下。

(C)1994-2022 China Academic Journal Electronic Publishing House. All rights reserved. http://www.cnki.net

当目的节点译码错误概率小于ε（ε是无穷小的正数）时，速率集合$(R_1,R_2,\cdots,R_M)$是可达的，且容量域是可达速率集的闭集。MARC 和 C-MARC 的容量域的外界可以通过著名的割集定理得到。内界可以通过构造码和计算可达速率得到。

首先采用割集定理得到 **MARC 的可达速率外界**：

令$G\subset S=\{1,2,\cdots,M\}$。定义$\mathbf{X}_{(G)}=\{X_i:i\in G\}$、$\mathbf{Y}=(Y_{M+1},Y_{M+2})$和$G^C$表示集合$G$在集合$S$中的补集，包含$M$个源节点的 MARC 的容量区域是速率集$(R_1,\cdots,R_M)$的并集所构成集合的子集需满足约束条件：

$$\sum_{i\in G}R_i\le\min\left\{I\left(\mathbf{X}_{(G)};\mathbf{Y}\middle|\mathbf{X}_{(G^C)},X_{M+1},U\right),I\left(\mathbf{X}_{(G)},X_{M+1};Y_{M+2}\middle|\mathbf{X}_{(G^C)},U\right)\right\}\tag{2-16}$$

任意的$G\subset S$。其中速率的并集遍历所有输入分布：$p(u,\mathbf{x},x_{M+1})=p(u)\cdot\left(\prod_{i=1}^{M}p(x_i|u)\right)\cdot p(x_{M+1}|u,\mathbf{x})$，其中$\mathbf{x}\triangleq(x_1,x_2,\cdots,x_M)$，$|u|\le 2^{M+1}$-2。随机变量$U$的基数限采用 Csiszar 等[116]人的研究结果推论得到。

译码转发模型下的可达速率区域：

经典单源单中继信道[4]中采用的编码策略可以直接扩展到 MARC 模型中得到各种可达速率策略。在译码转发模式下，中继节点对源节点的信息译码后转发给目的节点，并协助目的节点联合两路信息进行联合译码处理。该译码转发模式下的速率集$(R_1,\cdots,R_M)$可达域[117]：

$$\sum_{i\in G}R_i\le\min\left\{I\left(\mathbf{X}_{(G)};Y_{M+1}\middle|\bar{\mathbf{V}},\mathbf{X}_{(G^C)}\right),I\left(\mathbf{X}_{(G)},X_{M+1};Y_{M+2}\middle|\bar{\mathbf{X}}_{(G^C)}\right)\right\}\tag{2-17}$$

任意的$G\subset S$。其中，$\bar{\mathbf{X}}_{(G^C)}\triangleq\left(\mathbf{V}_{(G^C)},\mathbf{X}_{(G^C)}\right)$，$\bar{\mathbf{V}}\triangleq\left(\mathbf{V}_{(S)},X_{M+1}\right)$。辅助的随机变量$V_i$满足分布$\left(\prod_{i=1}^{M}p(v_i)p(x_i|v_i)\right)\cdot p(x_{M+1}|\mathbf{v})$，其中$\mathbf{v}=(v_1,v_2,\ldots,v_M)$。上式右边括号里第一个界保证中继节点可以正确译出源节点的各块信息，第二个界保证目的节点联合源节点和中继节点发来的信息进行正确译码。在式（2-16）中增加一个时分随机变量可以证明上式。

压缩转发模型下的可达速率区域：

中继节点将压缩后的M个源节点的信息转发给目的节点[4]。目的节点首先译出来自中继节点的信息得到$\hat{Y}_{M+1}$，而后利用$\hat{Y}_{M+1}$和来自源节点的信息Y_{M+2}译出源节点的信息，该模式下的速率集$(R_1,\cdots,R_M)$可达域：

$$\sum_{i\in G}R_i\le I\left(\mathbf{X}_{(G)};\hat{Y}_{M+1},\mathbf{Y}_{M+2}\middle|X_{M+1},\mathbf{X}_{(G^C)}\right)\tag{2-18}$$

(C)1994-2022 China Academic Journal Electronic Publishing House. All rights reserved. http://www.cnki.net

$$I\left(X_{M+1};Y_{M+2}\right)\geq I\left(\hat{Y}_{M+1};Y_{M+1}\middle|Y_{M+2},X_{M+1}\right) \tag{2-19}$$

其中，X_i，（$i\in[1,M+1]$）是独立的，$\hat{Y}_{M+1}$是关于Y_{M+1}和X_{M+1}的概率函数。式（2-19）的右边表示：在中继节点处源节点的编码速率$I\left(\hat{Y}_{M+1};Y_{M+1}\middle|Y_{M+2},X_{M+1}\right)$的上界为中继节点到目的节点的可达速率$I(X_{M+1};Y_{M+2})$。

其次采用割集定理得到**C-MARC 的可达速率区域的外界**：

中继节点分别在时隙α和$1-\alpha$时接收和发送信息，$M+2$个节点处均已知收发信道状态信息。令$\mathbf{X}\triangleq\left(X_1,X_2,...,X_M\right)$，$\bar{\alpha}\triangleq 1-\alpha$，$\alpha\in[0,1]$和$\overline{\mathbf{X}}_{(\cdot)}\triangleq\left(X_{M+1},\mathbf{X}_{(\cdot)}\right)$。包含$M$个源节点的 C-MARC 的速率界是速率集$\left(R_1,\cdots,R_M\right)$的并集所构成集合的子集需满足约束条件：

$$\sum_{i\in G}R_i\leq\max_{\alpha}\min\begin{pmatrix}\alpha I\left(\mathbf{X}_{(G)};\mathbf{Y}\middle|\mathbf{X}_{(G^c)},U\right)+\bar{\alpha}I\left(\mathbf{X}_{(G)};Y_{M+2}\middle|\overline{\mathbf{X}}_{(G^c)},U\right),\\ \alpha I\left(\mathbf{X}_{(G)};Y_{M+2}\middle|\mathbf{X}_{(G^c)},U\right)+\bar{\alpha}I\left(\overline{\mathbf{X}}_{(G)};Y_{M+2}\middle|\mathbf{X}_{(G^c)},U\right)\end{pmatrix} \tag{2-20}$$

任意的$G\subset S$，在时隙α和$1-\alpha$内，其联合概率分别遍历$p(u)\cdot\prod_{i=1}^{M}p\left(x_i\middle|u\right)$和$p(u)\cdot\prod_{i=1}^{M}p\left(x_i\middle|u\right)\cdot p\left(x_{M+1}\middle|u,x_1,x_2,...,x_M\right)$，且$|u|\leq 2^{M+1}-2$。与式（2-16）相同，随机变量$U$的基数限采用 Csiszar 等人[116]的研究结果推论得到。

译码转发模式下 C-MARC 的可达速率区域：

接收状态时，中继节点译出接收到的信息。发送状态时，中继节点与源节点共同协助目的节点进行译码。与全双工 MARC 不同，当中继节点的发送信息时，源节点不发送新信息，而是协助目的节点译出接收到的信息。因此，对于任意的$G\subset S$，和速率限满足：

$$\sum_{i\in G}R_i\leq\max_{\alpha}\min\left(\alpha I\left(\mathbf{X}_{(G)};Y_{M+1}\middle|\mathbf{X}_{(G^c)}\right),\alpha I\left(\mathbf{X}_{(G)};Y_{M+2}\middle|\mathbf{X}_{(G^c)}\right)+\bar{\alpha}I\left(\overline{\mathbf{X}}_{(G)};Y_{M+2}\middle|\mathbf{X}_{(G^c)}\right)\right) \tag{2-21}$$

其中，$X_i,i\in[1,M+1]$是独立的。

部分译码转发模式下 C-MARC 的可达速率区域：

在部分译码转发模式下，源节点除了与中继节点进行协作外，源节点还发送新的信息给目的节点。因此，中继节点和目的节点进行可靠译码时，速率集的所有组合的可达速率区域界满足：

(C)1994-2022 China Academic Journal Electronic Publishing House. All rights reserved. http://www.cnki.net

$$\sum_{i\in G} R_i \le \max_{\alpha} \min \begin{pmatrix} \alpha I\left(\mathbf{X}_{(G)}; Y_{M+1} \middle| \mathbf{X}_{(G^c)}\right) + \overline{\alpha} I\left(\mathbf{X}_{(G)}; Y_{M+2} \middle| \overline{\mathbf{X}}_{(G^c)}, \mathbf{V}\right), \\ \alpha I\left(\mathbf{X}_{(G)}; Y_{M+2} \middle| \mathbf{X}_{(G^c)}\right) + \overline{\alpha} I\left(\overline{\mathbf{X}}_{(G)}; Y_{M+2} \middle| \hat{\mathbf{X}}_{(G^c)}\right) \end{pmatrix} \tag{2-22}$$

其中 $\hat{\mathbf{X}}_{(\cdot)} \triangleq \left(\mathbf{V}_{(\cdot)}, \mathbf{X}_{(\cdot)}\right)$，$\mathbf{V} \triangleq \mathbf{V}_{(S)}$，且$\left(V_i, X_i\right)$和$i \in [1, M]$相互独立，$\mathrm{X} \to \mathrm{V} \to X_{M+1}$构成马尔可夫链。

压缩转发模式下 C-MARC 的可达速率区域：

接收状态时，中继节点对接收到的信息进行压缩。发送状态时，中继节点转发压缩后的信息给目的节点。另外，发送状态时，源节点同时也向目的节点发送新的信息。因此，目的节点可靠译码时满足的可达速率区域界：

$$\sum_{i\in G} R_i \le \max_{\alpha} \left(\alpha I\left(\mathbf{X}_{(G)}; \mathbf{Y}_d \middle| \mathbf{X}_{(G^c)}\right) + (1-\alpha) I\left(\mathbf{X}_{(G)}; Y_{M+2} \middle| \overline{\mathbf{X}}_{(G^c)}\right) \right) \tag{2-23}$$

其中，$X_i, i \in [1, M+1]$独立的，且满足约束：$\overline{\alpha} I\left(X_{M+1}; Y_{M+2}\right) \ge \alpha I\left(\hat{Y}_{M+1}; Y_{M+1} \middle| Y_{M+2}\right)$其中$\hat{Y}_{M+1}$是辅助随机变量，表示中继节点处的压缩信息且$Y_d \triangleq \left(\hat{Y}_{M+1}, Y_{M+2}\right)$。

放大转发模式下 C-MARC 的可达速率区域：

与 MARC 相同，源节点在每个状态时总发送新信息，中继节点发送信息是其接收信息的放大值，即$X_{M+1,i} = cY_{M+1,i-1}$，其中$Y_{M+1,i-1}$表示中继节点发送第$i-1$个符号，$X_{M+1,i}$表示中继节点接收第i个符号，放大系数c满足中继节点处的功率约束。此策略仅适用于$\alpha = 1/2$的情形。单用户速率限直接扩展到 C-MARC 模型中的可达速率限[118]：

$$\sum_{i\in G} R_i \le \frac{1}{2} I\left(\mathbf{X}_{(G)}^1, \mathbf{X}_{(G)}^2; \mathbf{Y}_{M+2} \middle| \mathbf{X}_{(G^c)}^1, \mathbf{X}_{(G^c)}^2\right) \tag{2-24}$$

存在分布$p\left(x_{(S)}^1, x_{(S)}^2\right)$，其中$\mathbf{Y}_{M+2} \triangleq \left[Y_{M+2}^1 Y_{M+2}^2\right]^T$表示目的节点在第一、二个时间符号内接收的一个信号向量，$\mathbf{X}_{(G)}^j = \left\{X_i^j : i \in G\right\}$表示在第$j, j \in [1,2]$个时间符号内发送集合$G$内来自源节点的符号集合。

2.2.3 非正交多址接入中继信道的仿真结果

不失一般性，如图 2.7 所示，以两种典型的模型为例来说明上述策略的性能。场景 1 是假设两个源节点关于中继节点和目的节点是对称的，场景 2 是两个源节点与目的节点的距离为单位 1，且在同一水平线上。假设两个源节点和中继节点的信噪比为 10dB，路径衰落指数$\gamma = 2$，所有对数函数的底为 2。

(C)1994-2022 China Academic Journal Electronic Publishing House. All rights reserved. http://www.cnki.net

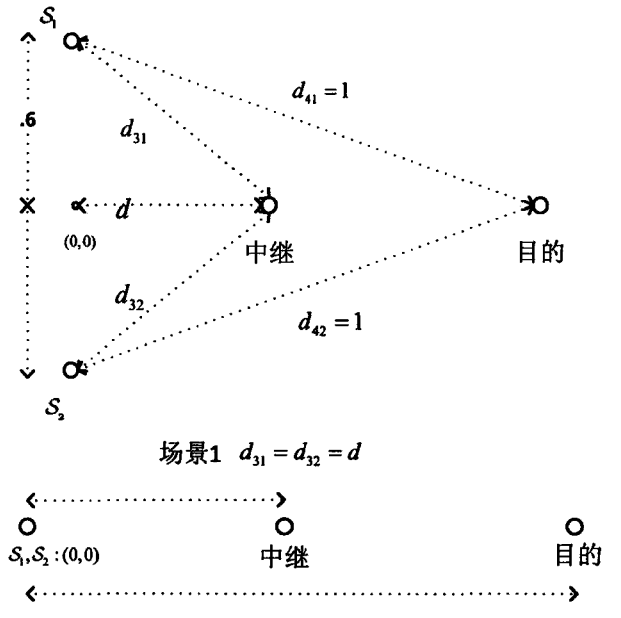


图2.7 两源 MARC 的两种场景模型

1）MARC 模型

MARC 模型下的三种策略的和速率外界分别在场景 1 和场景 2 的情况下的仿真结果如图 2.8，2.9 所示。图中包含直接链路 MARC 和速率限的仿真结果。M 个源节点的 MARC 在译码转发模式下的可达速率限：

$$\sum_{i\in G}R_i \le \max_{\{\beta_i\}_{i\in G}} \min\left\{C\left(\sum_{i\in G}\beta_i P_i^r\right), C\left(\sum_{i\in G}P_i^d + P_r^d + 2\sum_{i\in G}\sqrt{\bar{\beta}_i\beta_{ri}P_i^d P_r^d}\right)\right\} \tag{2-25}$$

其中，$\beta_{ri}=(1-\beta_i)P_i/\sum_{i\in G}(1-\beta_i)P_i$ 是中继节点协作第 i 个源节点时的功率分配系数，$\beta_i=(1-\bar{\beta}_i)$ 是第 i 个源节点在多址接入阶段发送新信息时的功率分配系数。相应的源节点和中继节点的信息分别表示为

$$X_i=\sqrt{\beta_i P_i}V_{i0}+\sqrt{\bar{\beta}_i P_i}V_i \qquad i\in[1,M] \tag{2-26}$$

$$X_{M+1}=\sum_{i\in G}\sqrt{\beta_{ri}P_{M+1}}V_i+\sqrt{\left(1-\sum_{i\in G}\beta_{ri}\right)P_{M+1}}V_{M+1} \tag{2-27}$$

其中，$\{V_{i0}\}_{i=1}^{M}$ 和 $\{V_i\}_{i=1}^{M+1}$ 是相互独立的均值为 0，方差为 1 的复高斯循环对称的随机变量。$P_i^d=P_i/d_{M+2,i}^r$ 和 $P_i^r=P_i/d_{M+1,i}^r$ 分别表示目的节点和中继节点接收到来自源节点 i 的信息功率。$P_r^d=P_{M+1}/d_{M+2,M+1}^r$ 表示目的节点接收到来自中继节点的信息功率。场景

(C)1994-2022 China Academic Journal Electronic Publishing House. All rights reserved. http://www.cnki.net

1 和场景 2 最佳的系数 $\beta_1 = \beta_2 = \beta$。

图 2.8 是在场景 1 时各策略的性能图，当中继节点无限接近目的节点时，CF 策略可以达到无错误的可达速率。因为量化信号的失真会随着中继到目的节点的可靠性的增加而降低。目的节点根据两个信道输出值得到式（2-16）的可达速率上限。与单用户模型相似，当中继节点靠近目的节点时，AF 的性能与 DF 相同。AF 的性能损失是由于中继节点接收到的噪声放大的原因。当中继节点远离目的节点时，由于 AF 策略的性能线低于直接链路的多址接入速率限，导致中继节点到目的节点的高速率信道的优点会丢失。相反，中继节点靠近源节点时，DF 策略的性能达到最大。源节点与中继节点间的高容量信道使源节点与中继节点最大化协助从而帮助目的节点译码。当目的节点的可达速率大于源节点与中继节点的最大速率时，DF 策略中的最佳的 $\beta = 1$。

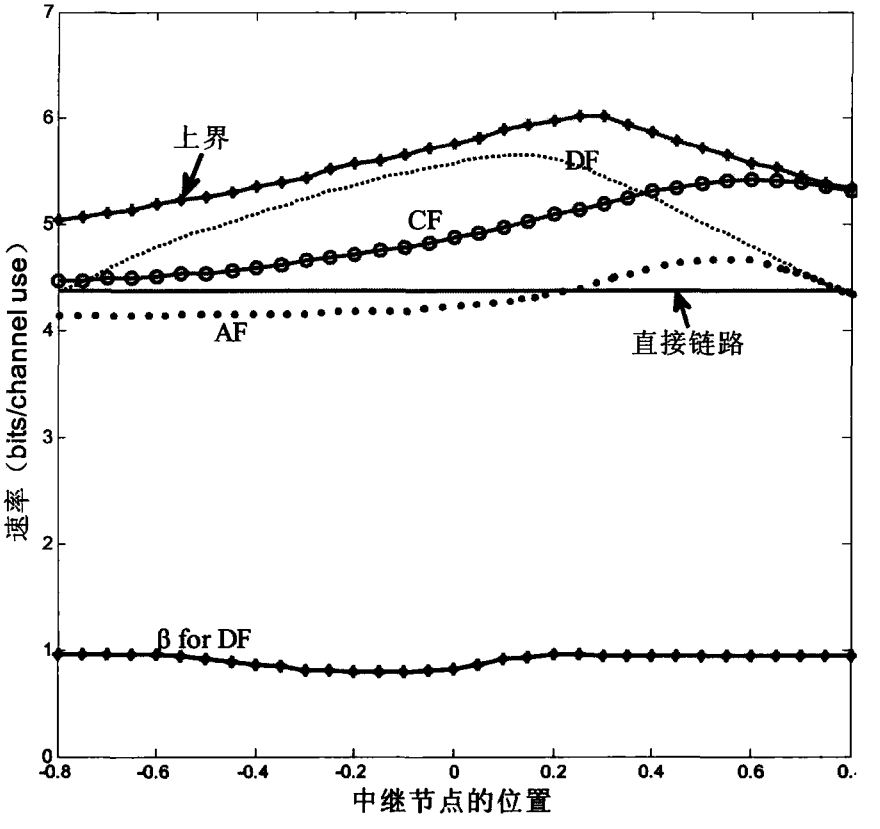


图2.8 场景 1：两源 MARC 的可达速率上界和可达速率（$P_1 = P_2 = P_r$=10dB）

图 2.9 是在场景 2 时各策略的性能图，当中继节点无限靠近两源节点时，DF 策略可以接近可达速率上界。当中继节点与源节点近时，信道模型变成物理退化的高斯 MARC，此时，DF 策略获得容量限。最后，当中继节点与源节点间的距离小于其与目的节点的距离甚至不在两者之间时，DF 和 CF 的可达速率大于直接链路的和速率。

总之，给定中继节点位置时，这里研究如何选择合理的协作策略来获得最大的可达速率。

(C)1994-2022 China Academic Journal Electronic Publishing House. All rights reserved. http://www.cnki.net

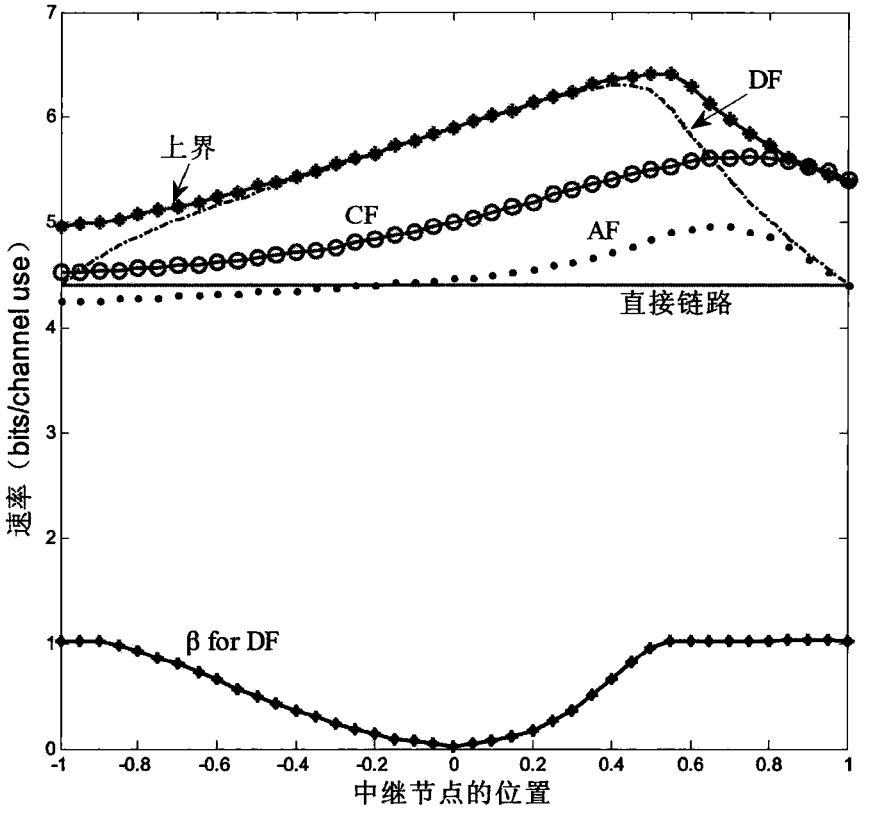


图2.9 场景 2：两源 MARC 的可达速率上界和可达速率（$P_1 = P_2 = P_r$=10dB）

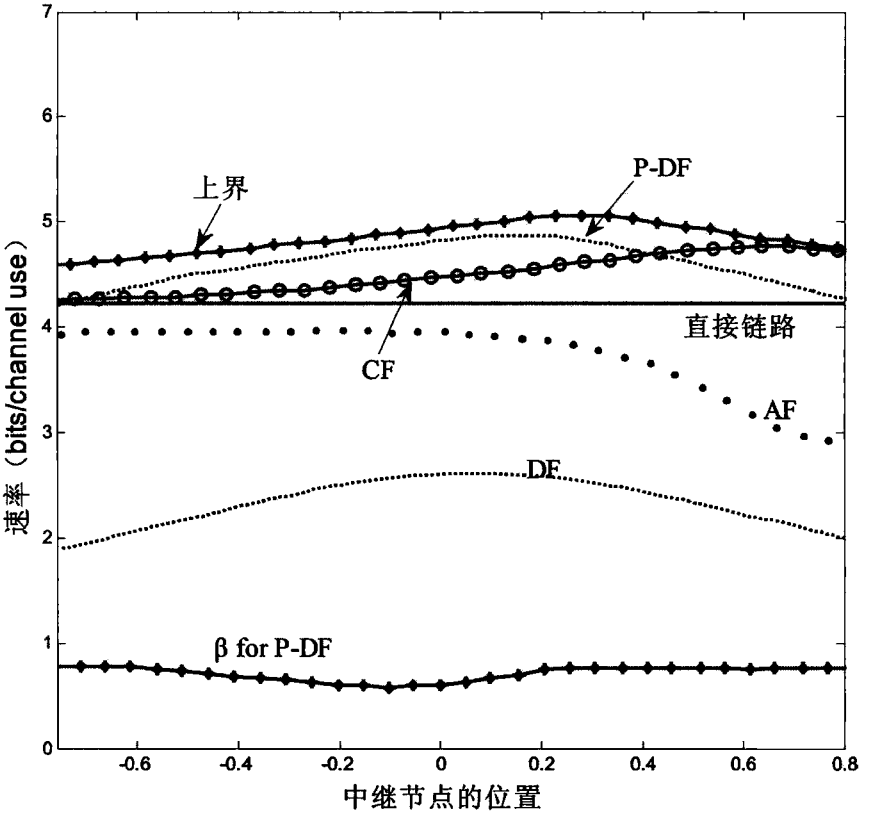


图2.10 场景 1：两源 MARC 的可达速率上界和可达速率（$P_1 = P_2 = P_r$=10dB）

(C)1994-2022 China Academic Journal Electronic Publishing House. All rights reserved. http://www.cnki.net

2）C-MARC 模型

C-MARC 模型在图 2.7 所示的两种场景下的各策略性能仿真图如图 2.10、2.11 所示。为了比较简单起见，假设 CF 策略、DF 策略、P-DF 策略和 AF 策略中 $\alpha=1$。

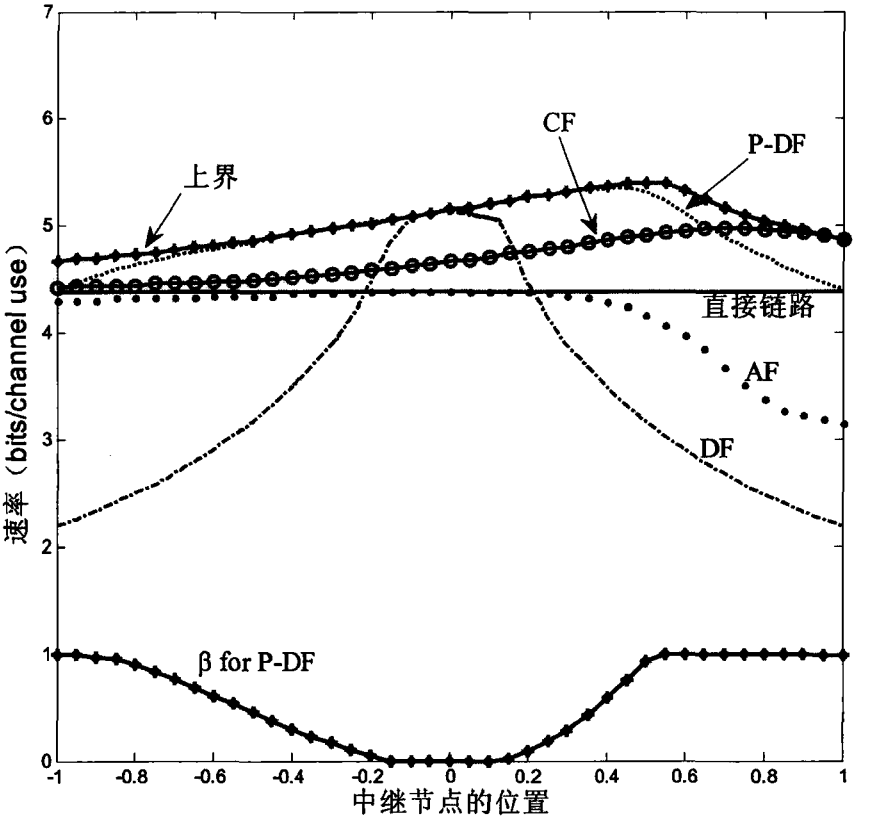


图2.11　场景 2：两源 MARC 的可达速率上界和可达速率（$P_1=P_2=P_r$=10dB）

两种场景下，当中继节点接近目的节点时，CF 策略逼近上界。在场景 2 的情况下，退化高斯 C-MARC 的中继节点和源节点的距离很近时，P-DF 策略和 DF 策略可以达到容量限。如图 2.10、2.11 中所示，除了源节点到中继节点的距离很近以外，式（2-21）中的 DF 策略的可达速率小于式（2-22）中 P-DF 的可达速率，原因是在时隙 $1-\alpha$ 时 DF 策略中的源节点与中继节点的协作严格受限。最佳的 β 线衡量的是 P-DF 策略中在时隙 $1-\alpha$ 时每个源节点发送新信息时分配的功率系数。由于 CF 策略和 AF 策略在时隙 $1-\alpha$ 时源节点不发送新的信息，所以 $\beta_1=\beta_2=1$。

2.3 本章小结

本章主要介绍了多址接入中继系统的信道模型，根据发送信息的频率和时间不同将其分为两种模型分别进行详细研究，并给出了两种信道模型下的几种重要的传输协议下的信道容量域。最后，给出了几种重要传输协议下的计算机性能仿真结果。

(C)1994-2022 China Academic Journal Electronic Publishing House. All rights reserved.　http://www.cnki.net

(C)1994-2022 China Academic Journal Electronic Publishing House. All rights reserved. http://www.cnki.net

第三章 适用于MARC的速率兼容网络LDPC码设计

本章分析了无线移动信道中衰落和时变等带来的信道容量的减少，首先提出了一种可以获得最小比特错误概率的速率兼容网络 LDPC 码的删余算法,并推导了该算法的译码错误概率。该算法以网络 LDPC 码的结构特点为基础，以达到最小化译码比特错误概率为目标，在网络 LDPC 码的因子图上搜索出需要删除的变量节点，从而获得最优的删余图样。其次基于网络双层网络 LDPC 码的中继节点编码方法，利用差分进化算法来优化设计中继码集。最后，给出了在高斯信道和衰落信道下的计算机仿真结果。

3.1 引言

由于无线移动信道的衰落和时变特性，为了最大限度地利用信道容量，可以采用链路自适应技术，使信道编码速率、调制方式和信号功率等参数能够随信道质量的变化而变化。链路自适应技术的基础是速率兼容纠错码的设计，其基本概念由 Hagenauer 等[119]首次提出，并且速率兼容 LDPC 码的设计是近几年来的研究热点之一。后来，Ha 和 Kim 等[120,121]人通过分组和排序操作，将 LDPC 码的变量节点按照迭代恢复次数进行分类，设计了 LDPC 码速率兼容删余算法，可以获得比随机删余更好的性能。与之不同的是，周林等[122]人首次提出了一种基于有限域上非零元素二进制镜像的缩短码构造方案，用来实现低码率的速率兼容多元 LDPC 码，并研究了码率从1/10到5/6灵活变化的非规则多元 LDPC 码比特级缩短算法[123]。郭等[124]人以多维累加交叉并行级联单奇偶校验码为母码，对奇偶校验比特按组删余，构建了一组速率兼容编码。

上述速率兼容算法都是针对点对点通信链路设计的。然而，随着无线通信技术的发展以及中继协作传输技术的引入，信道编码的设计也逐渐从点对点链路推广至无线中继网络。对于多址接入中继网络，有多个节点同时需要中继节点帮助转发数据，在中继节点设计有效的联合网络-信道编码算法，可在改善接收端性能的同时有效提高转发效率。李等[37]人利用 LDPC 码，针对多址接入中继信道设计了一种网络 LDPC 码，并指出可以通过调整中继节点转发数据量来实现中继转发效率和接收端译码性能的有效折中。但是，文章没有给出具体实现算法，本章将在此基础上，研究了速率兼容网络 LDPC 码的算法设计以及网络 LDPC 码的优化设计。

与单个 LDPC 码的校验矩阵相比，网络 LDPC 码的校验矩阵同时包含了源节点和中继节点所采用 LDPC 码的校验矩阵，因此其本质上可被视为一种多用户码。另外，单个 LDPC 码的所有编码比特位是在同一个信道中传输的，所有编码比特位受到相同

(C)1994-2022 China Academic Journal Electronic Publishing House. All rights reserved. http://www.cnki.net

的噪声干扰，而网络 LDPC 码的编码比特位则由对应的源节点和中继节点分别进行传输，不同传输信道将会受到不同的噪声干扰。本章将根据网络 LDPC 码的上述特点，设计出相应的速率兼容算法。

本章的第二小节给出了适用于多址接入中继信道的网络 LDPC 码的模型、Tanner 图及对应的校验矩阵，第三小节介绍了速率兼容网络 LDPC 码的设计方案，第四小节介绍了基于差分进化的网络 LDPC 码优化算法，第五节给出了高斯信道和瑞利信道下，速率兼容网络 LDPC 码设计方案的仿真结果和性能分析，最后给出本章的小节。

3.2 适用于 MARC 的网络 LDPC 码

考虑包含两个源节点和一个中继节点的多址接入中继信道的模型如图 2.3 所示，即两个源节点到中继节点和目的节点的信道条件相同，且它们采用相同的编码方案，系统结构框图如图 3.1 所示，两个源节点$\mathcal{S}_1$（$\mathcal{S}_2$）与目的节点$\mathcal{D}$之间的信息传输由广播发送和中继转发两个阶段完成。在广播阶段，两个源节点$\mathcal{S}_1$（$\mathcal{S}_2$）分别向中继节点$\mathcal{R}$和目的节点$\mathcal{D}$广播发送编码序列X_1和X_2；中继节点和目的节点接收信号分别为：

$$Y_{\mathcal{S}_i,\mathcal{R}} = X_i + N_{\mathcal{S}_i,\mathcal{R}} \tag{3-1}$$

$$Y_{\mathcal{S}_i,\mathcal{D}} = X_i + N_{\mathcal{S}_i,\mathcal{D}} \tag{3-2}$$

其中，$i=1,2$。X_i表示源节点i的 LDPC 编码符号。$Y_{\mathcal{S}_i,\mathcal{R}}$和$Y_{\mathcal{S}_i,\mathcal{D}}$分别表示中继节点和目的节点的接收信号形式。$N_{\mathcal{S}_i,\mathcal{R}}$表示均值为零方差为$\sigma^2_{\mathcal{S}_i,\mathcal{R}}$的高斯随机变量。$N_{\mathcal{S}_i,\mathcal{D}}$表示均值为零方差为$\sigma^2_{\mathcal{S}_i,\mathcal{D}}$的高斯随机变量。

在中继转发阶段，中继节点首先对接收信号进行译码，得到两个源节点的估计数据，然后对译码得到的估计数据重新进行联合编码，得到编码序列$X_{\mathcal{R}}$，并将编码序列$X_{\mathcal{R}}$的校验位$P(X_{\mathcal{R}})$转发至目的节点$\mathcal{D}$。目的节点的接收信号：

$$Y_{\mathcal{R},\mathcal{D}} = P(X_{\mathcal{R}}) + N_{\mathcal{R},\mathcal{D}} \tag{3-3}$$

其中，$P(X_{\mathcal{R}})$表示中继节点重新编码后产生的校验位。$N_{\mathcal{R},\mathcal{D}}$表示均值为零方差为$\sigma^2_{\mathcal{R},\mathcal{D}}$的高斯随机变量。

目的节点$\mathcal{D}$则根据收到的信号$Y_{\mathcal{S}_i,\mathcal{D}}$和$Y_{\mathcal{R},\mathcal{D}}$进行联合译码，得到两个源节点的估计信息。因此，目的节点处X_1、X_2和$P(X_{\mathcal{R}})$被看作是一个等效叠加码。

(C)1994-2022 China Academic Journal Electronic Publishing House. All rights reserved. http://www.cnki.net

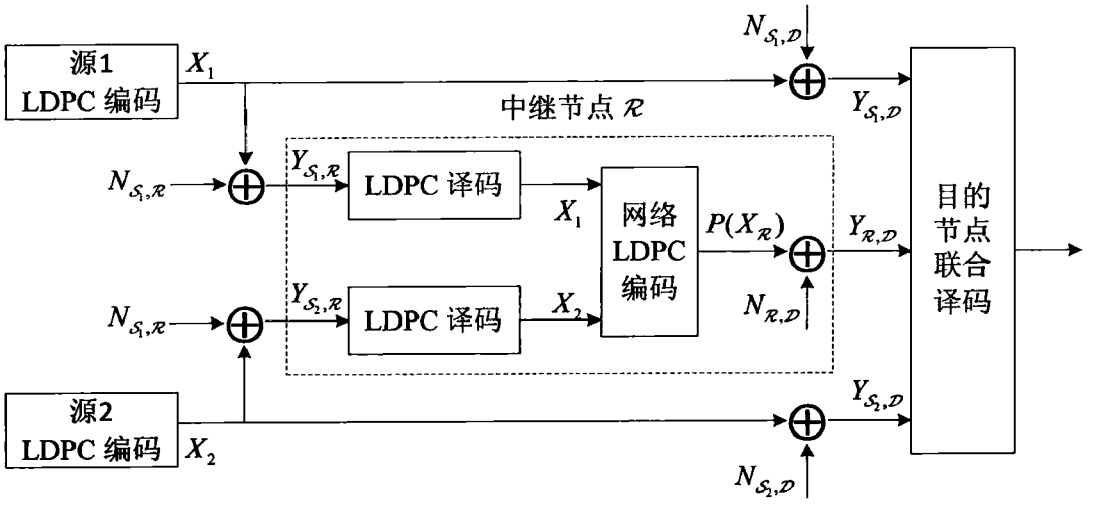


图3.1 多址接入中继系统框图

目的节点将两个源节点和中继节点采用的 LDPC 码综合考虑，可得到如下校验矩阵：

$$\mathbf{H}=\begin{pmatrix}\mathbf{H}_1 & \mathbf{0} & \mathbf{0}\\ \mathbf{0} & \mathbf{H}_1 & \mathbf{0}\\ \mathbf{A} & \mathbf{B} & \mathbf{C}\end{pmatrix} \tag{3-4}$$

其中，$\mathbf{H}_1$ 是源节点采用 LDPC 码的校验矩阵，$\mathbf{H}_3=(\mathbf{A}\,\mathbf{B}\,\mathbf{C})$ 是中继节点采用 LDPC 码的校验矩阵，$\mathbf{0}$ 是零矩阵。由于式(3-4)中包含了源节点和中继节点所采用 LDPC 码的校验矩阵，并且中继节点是对两个源节点的数据进行联合编码，因此被称之为网络 LDPC 码[37]，该码相对应的 Tanner 图，如图 3.2 所示。

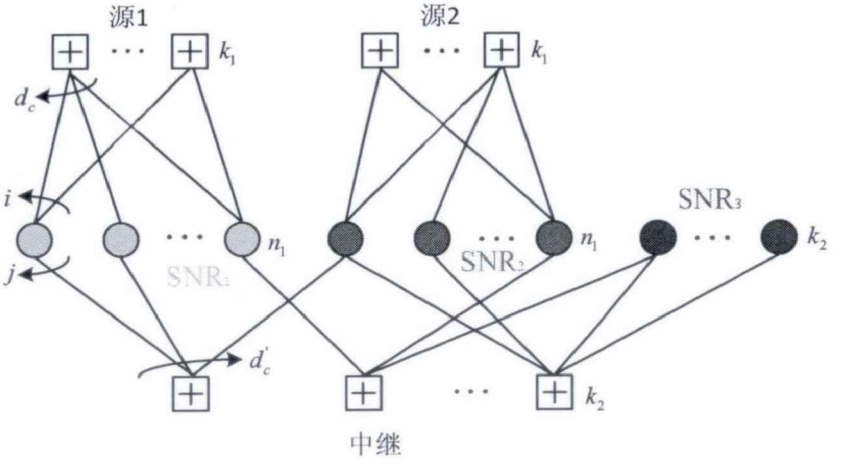


图3.2 网络 LDPC 码的 Tanner 图

由图 3.2，网络 LDPC 码的 Tanner 图中包含上下两层子图，其中上层子图包含 $2k_1$

(C)1994-2022 China Academic Journal Electronic Publishing House. All rights reserved. http://www.cnki.net

个校验节点，它们与变量节点的连接关系由式（3-26）中的$\mathbf{H}_1$确定；下层子图包括k_2个校验节点，它们与变量节点的连接关系由式（3-26）中的$\mathbf{H}_3$确定。图中每个变量节点的度用(i,j)表示，其中i表示变量节点与上层校验节点相连的边数，j表示变量节点与下层校验节点相连的边数，用d_c和d_c'分别表示上层和下层校验节点的度数。

3.3 速率兼容网络 LDPC 码的设计

由图 3.2，网络 LDPC 码的变量节点包含两个源节点所采用的 LDPC 码的变量节点和中继节点所采用的联合 LDPC 码的变量节点，且不同变量节点通过不同信道到达目的节点。因此，需要考虑上述特点对删除变量节点恢复概率的影响，并由此设计适用于网络 LDPC 码的速率兼容算法。

3.3.1 几个定义

定义 1（恢复）：若被删余的校验比特所对应的变量节点在迭代过程中接收到非零信息，则无论获得的信息正确与否，都称之为“恢复”[120]。

定义 2（n 步恢复变量节点）：译码中第 n 次迭代时才恢复的被删除的变量节点称为 n 步恢复变量节点，用 n-SR 表示，而所有 n-SR 构成的集合则用G_n表示[120]。

图 3.3 给出了一个包含 1-SR 节点、2-SR 节点的恢复树，其中竖线圆表示幸存的删余变量节点$S(v)$，横线圆表示未删余变量节点，方块表示校验节点。

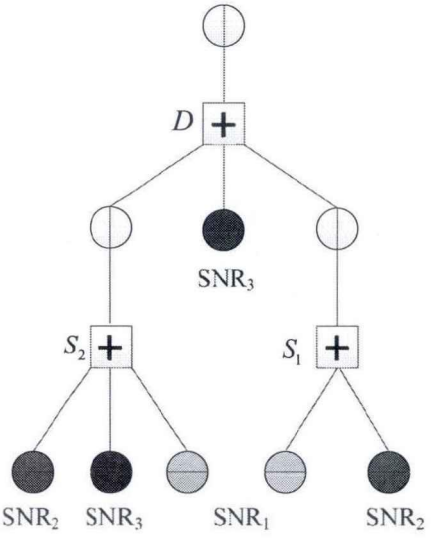


图3.3 网络 LDPC 码的恢复树

定义 3(幸存校验节点)：如果一个一步恢复的删余变量节点至少与一个校验节点相连，且与这个校验节点相连的变量节点没有被完全删余掉，那么称这个校验节点为

(C)1994-2022 China Academic Journal Electronic Publishing House. All rights reserved. http://www.cnki.net

幸存校验节点[120]。图 3.3 中的校验节点S_1和S_2即为幸存校验节点，而校验节点D则为死校验节点。

定义 4(幸存变量节点)：与幸存校验节点相连的其余未被删除的变量节点称为幸存变量节点。

由图 3.2 可见，网络 LDPC 码的编码比特是通过三个不同信道到达接收端的，因此，在设计网络 LDPC 码的删余算法时，不仅要考虑被删余变量节点的幸存邻居变量节点数，还要考虑每个幸存邻居变量节点受到的噪声大小。下面，我们引入等效幸存变量节点数的概念。

定义 5（等效幸存邻居变量节点数）：假设网络 LDPC 码所有编码比特在传输过程中受K种噪声干扰，其对应的噪声方差分别为$\sigma_1^2 > \sigma_2^2 > \cdots > \sigma_K^2$，令每个受到噪声干扰最大（噪声功率为$\sigma_1^2$）的幸存邻居变量节点的等效幸存邻居变量节点数为 1，则受其它噪声干扰的幸存邻居变量节点的等效幸存邻居变量节点数定义为

$$\alpha_i = \frac{\log\left[1-\phi\left[\frac{2}{\sigma_i^2}\right]\right]}{\log\left[1-\phi\left[\frac{2}{\sigma_1^2}\right]\right]} \le 1, i = 1,2,\cdots K. \tag{3-5}$$

其中

$$\phi(x)=\begin{cases}\dfrac{1}{\sqrt{4\pi x}}\int_R \tanh\dfrac{u}{2}e^{\frac{(u-x)^2}{4x}}du & x>0\\ 0 & x=0\end{cases}。$$

3.3.2 译码恢复错误概率

将网络LDPC码的删余变量节点v的所有幸存邻居变量节点按照其所通过信道的噪声功率的大小分为b类，假设第t类的噪声功率为$\sigma_t^2(t=1,2,\cdots,b)$，且$\sigma_1^2 > \sigma_2^2 > \cdots > \sigma_b^2$，并设第$t$类包括$S_t$个变量节点，记为$\{v_1^t,\cdots,v_s^t,\cdots,v_{S_t}^t\}$。与 LDPC 码类似，首先估计每次迭代过程中删余网络 LDPC 码的每个变量节点的均值更新，并由此计算该节点的恢复错误概率。

由于网络 LDPC 码的译码同样包括变量节点更新和校验节点更新，但图 3.2 给出的 Tanner 图表明，网络 LDPC 码的校验节点更新实际上包括上层校验节点和下层校验节点更新。下面，我们将分析在迭代译码过程中，速率兼容删余的网络 LDPC 码的变量节点和校验节点的均值更新过程。

假设校验节点的度分布分别为$\rho^{up}(x)=\sum_{k=1}^{d_c}\rho_k^{up}x^{k-1}$和$\rho^{low}(x)=\sum_{k=1}^{d_c}\rho_k^{low}x^{k-1}$，$\eta$是上层

(C)1994-2022 China Academic Journal Electronic Publishing House. All rights reserved. http://www.cnki.net

变量节点与校验节点相连的边数占总边数的比例，$\lambda_{i,j}$是与度(i,j)的变量节点连接的边数占总边数的比例。$m_{i,j}^{l-1}$和$n_{i,j}^{l-1}$分别表示第$(l-1)$次迭代时，变量节点传给上下层的校验节点的对数似然比的均值。第l次迭代时，上下层校验节点的均值更新过程如下：

（1）当上下层的校验节点向被删余的度为(i,j)的变量节点$v\in G_{l+1}$传递消息时，该消息的对数似然比的均值分别为:

$$m'^{l}=\sum_{k}\rho_{k}^{up}\phi^{-1}\left(\left(\frac{1}{\eta}\sum_{i\geq 0,j\geq 0}\frac{i}{i+j}\lambda_{i+j}\phi\left(m_{i,j}^{l-1}\right)\right)^{\sum_{i=1}^{b}S_i\alpha_i}\right) \tag{3-6}$$

$$n'^{l}=\sum_{k}\rho_{k}^{low}\phi^{-1}\left(\left(\frac{1}{1-\eta}\sum_{i\geq 0,j\geq 0}\frac{j}{i+j}\lambda_{i+j}\phi\left(n_{i,j}^{l-1}\right)\right)^{\sum_{i=1}^{b}S_i\alpha_i}\right) \tag{3-7}$$

其中，α_t表示每个幸存邻居变量节点v_s^t的等效幸存邻居变量节点数，S_t表示与变量节点v相连的校验节点没有被删余的变量节点数，变量节点v的总等效幸存邻居变量节点数为$\sum_{t=1}^{b}S_t\alpha_t$。

（2）当上下层的校验节点向没有删余的度为(i,j)的变量节点v传递消息时，该消息的对数似然比的均值[37]分别为：

$$m'^{l}=\sum_{k}\rho_{k}^{up}\phi^{-1}\left(\left(\frac{1}{\eta}\sum_{i\geq 0,j\geq 0}\frac{i}{i+j}\lambda_{i+j}\phi\left(m_{i,j}^{l-1}\right)\right)^{k-1}\right) \tag{3-8}$$

$$n'^{l}=\sum_{k}\rho_{k}^{low}\phi^{-1}\left(\left(\frac{1}{1-\eta}\sum_{i\geq 0,j\geq 0}\frac{j}{i+j}\lambda_{i+j}\phi\left(n_{i,j}^{l-1}\right)\right)^{k-1}\right) \tag{3-9}$$

上下层变量节点的均值更新过程如下：

第l次迭代时，度为(i,j)的变量节点传给上下层校验节点的对数似然比消息均值[37]分别为：

$$m_{i,j}^{l}=\begin{cases}(i-1)m'^{l}+jn'^{l}+m_{u_0} & i\neq 0,j\geq 0\\ jn'^{l}+m_{u_0}' & i=0,j\geq 1\end{cases} \tag{3-10}$$

(C)1994-2022 China Academic Journal Electronic Publishing House. All rights reserved. http://www.cnki.net

$$n_{i,j}^{l}=\begin{cases} im^{'l}+(j-1)n^{'l}+m_{u_0} & i\neq 0, j\geq 1 \\ (j-1)n^{'l}+m_{u_0}^{'} & i=0, j\geq 1 \\ im^{'l}+m_{u_0} & i\neq 0, j=0 \end{cases} \tag{3-11}$$

若变量节点被删掉，则$m_{u_0}(m_{u_0}^{'})=0$；若变量节点为由源节点发送至目的节点的信息比特，则$m_{u_0}=2/\sigma_{SD}^2$；若变量节点为中继节点发送至目的节点的信息比特，则$m_{u_0}^{'}=2/\sigma_{RD}^2$。第一次迭代时，校验节点的初始值$m^{'0}=n^{'0}=0$。

因此，变量节点传给上下层校验节点的平均的消息均值分别为：

$$m^{l}=\frac{1}{\eta}\sum_{i\geq 0,j\geq 0}\frac{i}{i+j}\lambda_{i,j}m_{i,j}^{l} \tag{3-12}$$

$$n^{l}=\frac{1}{1-\eta}\sum_{i\geq 0,j\geq 0}\frac{j}{i+j}\lambda_{i,j}n_{i,j}^{l} \tag{3-13}$$

经过L次迭代后，码比特的平均消息均值为：

$$m_L=\eta m^{L}+(1-\eta)n^{L} \tag{3-14}$$

此时，网络LDPC码的被删余变量节点的恢复错误概率为：

$$P_e(v)=Q\left(\sqrt{m_L/2}\right), \tag{3-15}$$

其中

$$Q(x)=\frac{1}{\sqrt{2\pi}}\int_x^{\infty}e^{-t^2/2}dt\text{。}$$

3.3.3 速率兼容网络LDPC码的删余算法

由公式（3-28）和（3-29）可知，等效幸存邻居变量节点数$\sum_{t=1}^{b}S_t\alpha_t$越小，更新得到的均值$m^{'}$和$n^{'}$的值越大，进而迭代后的变量节点$m_L$的均值也越大，同时由公式（3-37）得到的恢复错误概率$P_e(v)$越小。因此，在搜索节点时，需要寻找当前具有最小等效邻居的变量节点进行删余操作。与Ha等[120]设计的LDPC码的删余算法相似，所提出的网络LDPC码速率兼容算法主要包括分组和排序两个操作。

(C)1994-2022 China Academic Journal Electronic Publishing House. All rights reserved. http://www.cnki.net

分组：将所有删余的变量节点按照迭代恢复次数分成 K 组 $G_1,\cdots,G_K$，其中 $G_l(1\le l\le K)$ 是经过 l 次迭代才能恢复的所有变量节点的集合。

（1）给定一个 $M\times N$ 网络 LDPC 码的校验矩阵，初始化 $R_\infty=\{1,2,\cdots,M\}$，$G_\infty=\{1,2,\cdots,N\}$，$l=1$；

（2）遍历集合 R_∞，找出行重最小的行集合 r；

（3）遍历集合 G_∞，找出列重最小的列集合 c；

（4）选出所有（2）（3）相交的元素的集合 $w=\{(r^*,c^*),r^*\in r,c^*\in c\}$，作为候选对；

（5）在集合 w 中选出具有最小等效幸存邻居变量节点数的元素，记为 (r_j^*,c_k^*)。若有多对满足条件，随机选出其中一对，归入第 l 次迭代可以恢复的集合 G_l，更新 $R_\infty=R_\infty\setminus r_j^*$ 和 $G_\infty=G_\infty\setminus c_k^*$；

（6）若集合 G_∞ 为空，停止迭代，否则跳至（7）；

（7）若集合 R_∞ 不为空，跳至（2）；否则若步骤（5）中有多于一对满足条件，则 $l=l+1$，跳至（2）。

其中，R_∞（G_∞）表示每次迭代后更新的行（列）的集合；r（c）表示第 l 次迭代时，在集合 R_∞（G_∞）选出的行（列）重最小的行（列）集合；$G_l=\{(r_1^*,c_1^*),(r_2^*,c_2^*),\cdots\}$；$R_\infty=R_\infty\setminus r_j^*$（$G_\infty=G_\infty\setminus c_k^*$）表示集合 R_∞（G_∞）去掉元素 r_j^*（c_k^*）后的集合 R_∞（G_∞）。

接下来计算最大可达码率[120]为：

$$R_{\max}=\frac{R_0}{1-\sum_{j=1}^{K}\left|G_j\right|\Big/n} \tag{3-16}$$

其中，R_0 是母码的码率，n 是母码的码长。

在给定母码基础上，设计 Q 个码率的子码，对应码率记为 $R_0\le R_1\le\cdots\le R_Q\le R_{\max}$。假设所设计码的码率为 R_j，需要删余的节点数为[120]：

$$np_j=\left\lfloor\frac{n(R_j-R_0)}{R_j}\right\rfloor \tag{3-17}$$

其中，$0\le j\le Q$。

组内排序：依次对 $G_l,1\le l\le K$ 内的变量节点进行排序。

（1）给定一个 $M\times N$ 网络 LDPC 码的校验矩阵，初始化 $R_\infty=\{1,2,\cdots,M\}$，$l=1$，$j=1$，$P_0=\phi$；

（2）若 $j>Q$，停止迭代；否则，$P_j=P_{j-1}$；

（3）$\Delta=np_j-\left|P_j\right|$；

（4）若 $\Delta=0$，$j=j+1$，跳至（2）；

(C)1994-2022 China Academic Journal Electronic Publishing House. All rights reserved. http://www.cnki.net

（5）根据集合G_l定义$C_l=\{c_1^*,c_2^*,\cdots\}$,从$C_l$中选出列重最大的变量节点的集合$c_{\max}^*$，并从$c_{\max}^*$中找出具有最小数量的死校验节点的变量节点$c_{\max}^{**}$。如果有多个满足条件，随机选出其中一个，归入排序的集合P_j，更新$P_j=P_j\cup\{c_{\max}^{**}\}$,$G_l=G_l\setminus\{c_{\max}^{**}\}$,$R_\infty=R_\infty\setminus r_{\max}^{**}$,$\Delta=\Delta-1$；

（6）若G_l为空，$l=l+1$，$R_\infty=\{1,2,\cdots,M\}$；

（7）跳至（4）。

其中，（1）中的$l=1$表示从G_1开始将各G_l内的变量节点排序，$j=1$表示初始码率为R_1；（3）计算需要删余np_j个节点，除了上次迭代删余的$|P_j|$个节点外，本次还需要删余Δ个节点；（5）中的集合$c_{\max}$表示最大列重的变量节点的集合，同时意味着该集合包含的变量节点的幸存校验节点数最多；P_j表示要达到码率R_j所需删余的变量节点的列集合；$r_{\max}^{**}$表示列为$c_{\max}^{**}$的变量节点所在的行。

经过上述分组和组内排序操作，将G_l（$1\le l\le K$）中的变量节点按照l从小到大删余，而在同一个G_l中，按照变量节点的列号从小到大删余，直到删掉np_j个节点。

3.4 基于差分进化的网络LDPC码的设计

本小节主要研究多址接入信道下网络LDPC度分布的优化算法。首先介绍了源节点到目的节点直接链路上的信道参数的门限值，也称为码容量。其次，基于网络LDPC码的结构特点设计了一种新的差分进化来优化网络LDPC码的度分布。

3.4.1 网络LDPC码的门限值分析

（1） 网络LDPC码的译码阈值定义:

$$\sigma^*=\sup\left\{\sigma:\lim_{l\to+\infty}m_l>M\right\} \tag{3-18}$$

其中，σ表示信道质量参数，l表示译码过程中的迭代次数，m_l表示第l次迭代译码时一个码比特的对数似然比（Log-likelihood ratio, LLR）的平均均值，M表示目标错误概率所对应的LLR的均值。同时可以得出码比特的LLR方差值为$2m_l$。当$\sigma<\sigma^*$，且$m_l>M$时，该码在第l次迭代时可以获得目标译码错误概率。当$\sigma\ge\sigma^*$时，该码通过迭代译码是达不到目标错误概率的。

（2） 码容量σ_{SD}^*的计算方法

算法1：已知两个源节点采用的LDPC码的度分布，假设σ_{SD}和σ_{RD}分别表示源节点到目的节点链路以及中继节点到目的节点链路的信道质量参数。定义目标错误概率[37]$P_e=10^{-6}(M=45)$，最大迭代次数为L，迭代步长为$\Delta\sigma_{SD}$。计算码容量的步骤：

(C)1994-2022 China Academic Journal Electronic Publishing House. All rights reserved. http://www.cnki.net

1）初始化

校验节点输出的LLR均值初始化值为$m^{'l}=n^{'l}=0$。迭代次数$l=0$。

2）更新

当迭代次数$l<L$时，采用双层网络LDPC码的消息均值迭代算法[37]，变量节点的消息均值和校验节点的消息均值进行交替更新，计算出变量节点的LLR的消息均值m_l，若$m_l<M$时，迭代次数$l=l+1$，继续进行步骤2）。否则，当$m_l\geq M$时，$\sigma_{SD}=\sigma_{SD}+\Delta\sigma_{SD}$,返回到步骤1。

3）停止准则

在迭代过程中，当$l\geq L$且$m_l<M$时，整个迭代过程结束。此时信道的码容量表示为$\sigma^*_{SD}=\sigma_{SD}-\Delta\sigma_{SD}$。否则，信道的码容量为$\sigma^*_{SD}=\sigma_{SD}$。

根据算法1，可以获得信道的码容量所对应的网络LDPC码的度分布优化算法。

3.4.2 网络LDPC码的度分布的优化设计

通过搜索来优化度分布的终极目标就是寻找到最能逼近容量限的网络LDPC码的度分布。这里采用差分进化算法对双层网络LDPC码的度分布进行优化设计。

算法2：已知两个源节点采用的(n_1,k_1)的LDPC码，码率为R_1,度分布为$\left\{\{\lambda_i\}_{i=1}^{d_v},\{\rho_j\}_{j=1}^{d_c}\right\}$。随机生成$N$个基于网络LDPC码结构的中继码的码集合，并且每个中继码的校验比特位为k_2,即图3.2中的下层子图包含的k_2个校验节点。综上所述，可知网络LDPC码的总码长为$n_2=2n_1+k_2$，下层子图的校验节点的度数为$d_c^{'}$。寻找最优度分布步骤如下：

1）初始化

中继码的度分布初始化为：

$$C(d)=\left\{\lambda_{i,j}(d),0\leq i\leq d_v,0\leq j\leq d_v^{'}\right\},d=1,2,\cdots,N. \tag{3-19}$$

2）码集的性能分析

利用前一小节的算法1可以计算出每个码集$C(d)$对应的码容量$\sigma^*(d)$，且搜索到最优的码集$C^*=\arg\max_{1\leq d\leq N}\sigma^*(d)$。最大的码容量对应的最优码集的度分布为$C^*=\left\{\lambda^*_{i,j},0\leq i\leq d_v,0\leq j\leq d_v^{'}\right\}$。

3）码集的更新

从码集$\{C(d)\}_{d=1}^{N}$中随机选出$\tilde{N}$个码集，它们的度分布表示为：$\tilde{C}(k)=\left\{\lambda_{i,j}(k),0\leq i\leq d_v,0\leq j\leq d_v^{'}\right\},k=1,2,\cdots,\tilde{N}$。而后更新码集的度分布，表示为：$C(d)=C^*+\alpha\sum_{k=1}^{\tilde{N}}(-1)^{k-1}\tilde{C}(k)$，其中$\alpha$表示更新时的步长。

4）停止准则

(C)1994-2022 China Academic Journal Electronic Publishing House. All rights reserved. http://www.cnki.net

如果迭代次数等于预设最大迭代次数，且 $m_l < M$，停止迭代。得到最优码集的度分布：$C^* = \left\{\lambda_{i,j}^*, 0 \le i \le d_v, 0 \le j \le d_v^{'}\right\}$；否则，跳至步骤 2）。

上述优化步骤 1）和步骤 3）必须满足如下条件：

$$\begin{cases} \sum\limits_{i\ge 0, j\ge 0} \lambda_{i,j} = 1 \\ \eta = \sum\limits_{i}\sum\limits_{j} \dfrac{i}{i+j}\lambda_{i,j} \\ \lambda_i = \dfrac{1}{\eta}\sum\limits_{j\ge 0} \dfrac{i}{i+j}\lambda_{i,j} \\ d_c^{'} = \dfrac{1-\eta}{\sum\limits_{j} \dfrac{\lambda_{0,j}}{j}} \end{cases} \tag{3-20}$$

其中，η 表示图 3.2 中上层子图的变量节点连接的边数占上下两层的总边数的比例。上层子图的变量节点所连接的总数为 $E = n_1 / \sum_{i\ge 2} \lambda_i / i = k_1 / \sum_{j\ge 2} \rho_j / j$，整个双层网络 LDPC 码的总边数为 $E' = 2E + k_2 \cdot d_c^{'}$，因此 $\eta = 2E/E'$。

3.5 性能分析

3.5.1 速率兼容网络 LDPC 码的性能分析

考虑到无线通信中信道的多样性，本小节主要研究了两种信道下的速率兼容网络 LDPC 码的性能。仿真中两个源节点都采用码率为 0.5 的 LDPC 码，码长均为 2048，度分布表示为：$\lambda(x) = 0.23403x + 0.21242x^2 + 0.1469x^5 + 0.102840x^6 + 0.30381x^{19}$ 和 $\rho(x) = 0.71875x^7 + 0.28125x^8$。根据李等人研究结果[37]，假设所采用的网络 LDPC 码的度序列分布为：$\lambda_{0,2} = 0.028043$，$\lambda_{2,0} = 0.188139$，$\lambda_{2,1} = 0.019382$，$\lambda_{2,2} = 0.026283$，$\lambda_{3,0} = 0.191239$，$\lambda_{3,1} = 0.003360$，$\lambda_{3,2} = 0.001150$，$\lambda_{6,0} = 0.085989$，$\lambda_{6,1} = 0.000980$，$\lambda_{6,2} = 0.063446$，$\lambda_{7,0} = 0.059576$，$\lambda_{7,2} = 0.044374$，$\lambda_{20,0} = 0.176218$，$\lambda_{20,1} = 0.003570$，$\lambda_{20,2} = 0.108251$，$\rho_6^{low} = 0.943049$，$\rho_7^{low} = 0.056951$。

假设源节点和中继节点均采用 BPSK 调制方式，中继节点联合编码的 LDPC 码的校验比特数为 628，此时网络 LDPC 码(Mother code)的码率为 0.444。根据式（3-16），可以得到对该网络 LDPC 码进行删余获得的最大码率为 0.733。利用本文所提算法对该网络 LDPC 码删余可以得到码率分别为 0.5、0.6 和 0.7 的子码。利用 Ha 等[120]人研究的算法和随机删余也可得到同样码率的网络 LDPC 子码。

在 AWGN 信道下，假设源节点与中继节点，源节点与目的节点，以及中继节点与目的节点之间的信道均为高斯白噪声信道，中继节点与目的节点之间的信噪比固定

(C)1994-2022 China Academic Journal Electronic Publishing House. All rights reserved. http://www.cnki.net

为 5dB，且中继节点可以正确译出两个源节点的发送数据。图 3.4 比较了三种不同算法得到的网络 LDPC 码在上述信道假设下的误比特性能，图中横坐标 E_b / N_0 表示源节点与目的节点之间链路的信噪比变化，且假设两源节点与目的节点间的链路是对称的。

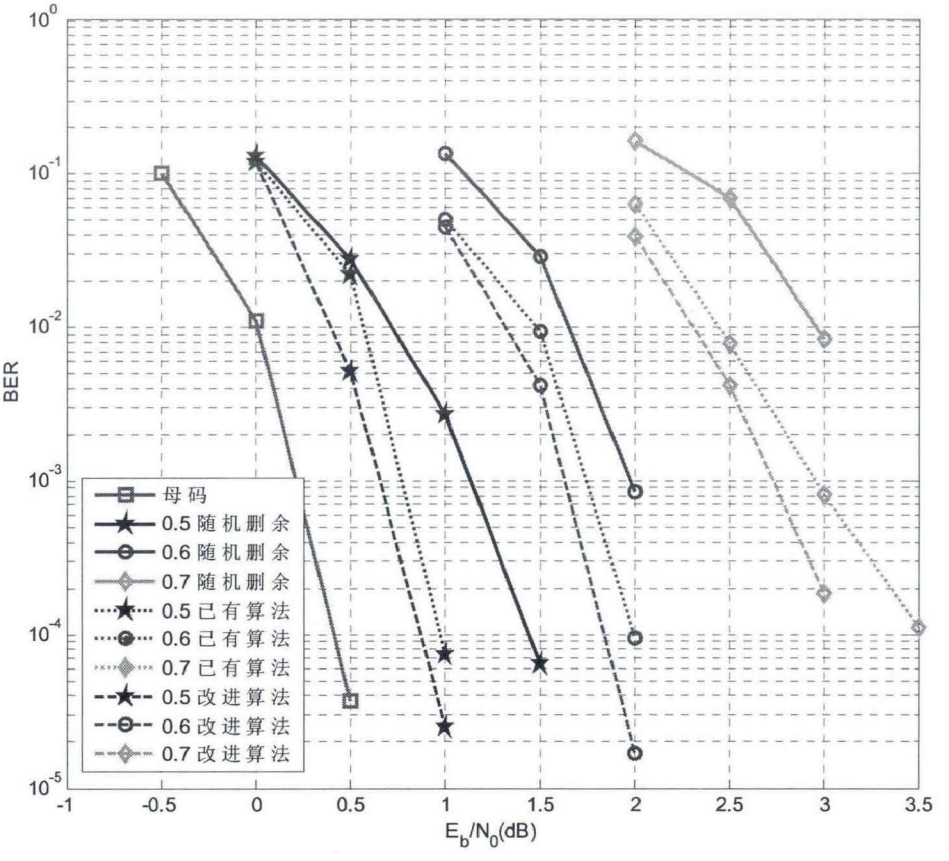


图3.4 AWGN 信道下网络 LDPC 码的删余性能对比

图 3.4 显示，随着删余比特的增加，采用所提目标速率兼容算法得到的网络 LDPC 码的性能增益也随之增加。当码率为 0.5，BER=10^{-3} 时，采用改进算法性能优于随机删余算法 0.45dB；当码率为 0.5，BER=10^{-4} 时，采用所提改进算法比 Ha 等[120]人提出已有算法的性能改善 0.15dB。在码率为 0.6，BER=10^{-3} 时，所提改进算法相对于随机删余算法性能增益为 0.3dB，相对于已有算法性能增益为 0.2dB。当码率为 0.7，SNR=3dB 时，所提改进算法的 BER 为 10^{-5}，相比于随机删余算法的 10^{-3} 有了明显提升，而 BER=10^{-4} 时，所提改进算法比 Ha 等[120]人研究的已有算法性能增益改善 0.4dB。

在瑞利衰落信道下，假设源节点与中继节点，源节点与目的节点，以及中继节点与目的节点之间的信道均为瑞利衰落信道，中继节点与目的节点之间的信噪比固定为 30dB，且中继节点可以正确译出两个源节点的发送数据。图 3.5 比较了三种不同算法得到的网络 LDPC 码在上述信道假设下的误比特性能，图中横坐标 E_b / N_0 表示源节点与目的节点之间链路的信噪比变化，且假设两个源节点与目的节点间的链路是对称的。

(C)1994-2022 China Academic Journal Electronic Publishing House. All rights reserved. http://www.cnki.net

图 3.5 显示，随着删余比特的增加，采用改进算法得到的网络 LDPC 码的性能增益随之增加。当码率为 0.5 时，随着信噪比的增加，采用改进算法比 Ha 等[120]人提出的算法的性能改善越来越好；当 BER=10^{-4} 时，采用改进算法性能优于已有删余算法 4dB。在码率为 0.6，BER=10^{-4} 时，采用改进算法相对于已有算法性能增益为 2dB。当码率为 0.7，BER=10^{-4} 时，采用改进算法相比于已有算法的 10^{-4} 有了明显提升。整个图显示，随着信噪比的增加，删余后的网络 LDPC 码的性能会与原母码的差距越来越大。

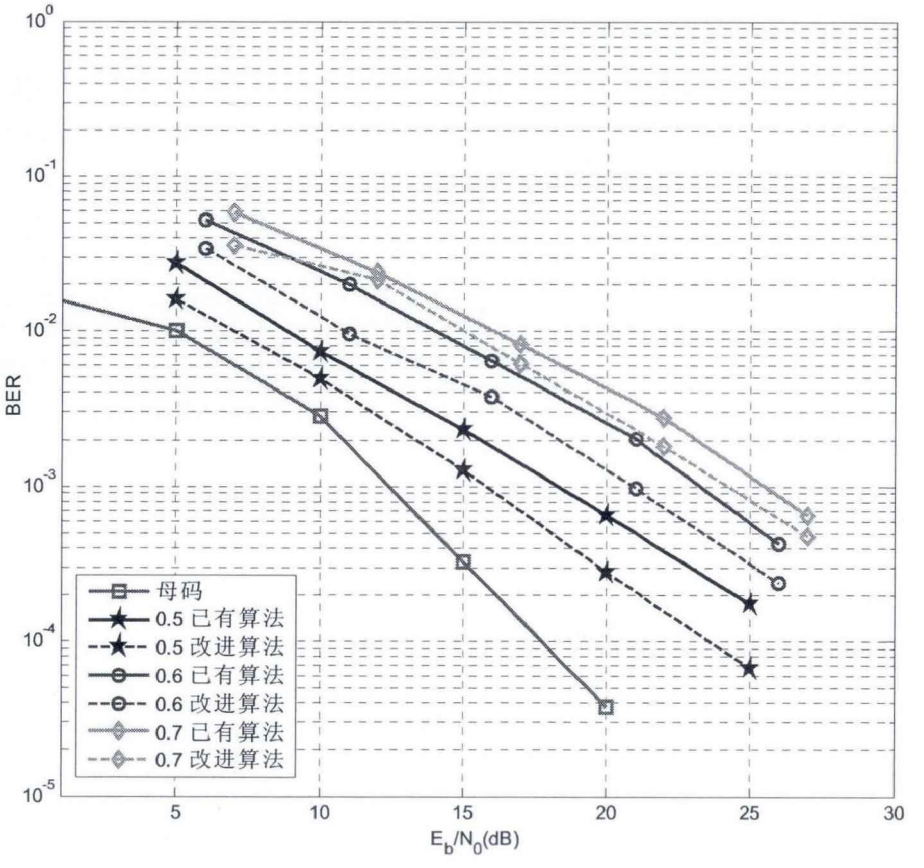


图3.5 瑞利衰落信道下网络 LDPC 码的删余性能对比

3.5.2 基于差分进化的网络 LDPC 码的性能分析

在 AWGN 信道下，假设两个源节点均采用（22164，11082）的 LDPC 码，其度分布表示为：$\lambda(x)=0.23403x+0.21242x^2+0.1469x^5+0.102840x^6+0.30381x^{19}$ 和 $\rho(x)=0.71875x^7+0.28125x^8$。根据李等[37]人研究结果，假设所采用的网络 LDPC 码的度序列分布为：$\lambda_{0,2}=0.028043$，$\lambda_{2,0}=0.188139$，$\lambda_{2,1}=0.019382$，$\lambda_{2,2}=0.026283$，$\lambda_{3,0}=0.191239$，$\lambda_{3,1}=0.003360$，$\lambda_{3,2}=0.001150$，$\lambda_{6,0}=0.085989$，$\lambda_{6,0}=0.085989$，$\lambda_{6,1}=0.000980$，$\lambda_{6,2}=0.063446$，$\lambda_{7,0}=0.059576$，$\lambda_{7,2}=0.044374$，$\lambda_{20,0}=0.176218$，$\lambda_{20,1}=0.003570$，$\lambda_{20,2}=0.108251$，$\rho_6^{low}=0.943049$，$\rho_7^{low}=0.056951$。中继节点与目的节点之间的信噪比固定为 3dB，且中继节点可以正确译出两个源节点的发送数据。

(C)1994-2022 China Academic Journal Electronic Publishing House. All rights reserved. http://www.cnki.net

假设两个源节点与目的节点之间的链路是对称的。利用上一小节的算法 1 搜索到四个不同参数的最优码集，如表 1 所示。表中 σ_{RD} 表示源节点到目的节点的信道质量参数。

表3.1 双层网络 LDPC 码的四个码集

码集	码 A	码 B	码 C	码 D
d_v'	2	2	2	2
d_c'	4	4	4	7
k_2	2814	4814	2814	2814
σ_{RD}	0.5	0.5	0.8	0.5
η	0.942065	0.904808	0.942065	0.902835
σ_{SD}^*	1.0568	1.0987	1.0393	1.1116
阈值(EbN_0)	0.155039dB	0.115123dB	0.2018dB	-0.22877dB
容量限(EbN_0)	-0.24536dB	-0.517620dB	-0.143948dB	-0.24536dB
差值	0.400399dB	0.632743dB	0.345748dB	0.01666dB

使用上一小节的算法 2，搜索到不同参数下的四种码的最优度分布，结果如表 2，3，4 和 5 所示。

表3.2 双层网络 LDPC 码 A 的码集

$\lambda_{i,j}$	$\lambda_{i,0}$	$\lambda_{i,1}$	$\lambda_{i,2}$
$i=2$	0.193815	0.00543635	0.04612661
$i=3$	0.171369	0.019109592	0.02409292
$i=6$	0.129299	0.006342408	0.00494214
$i=7$	0.09485	0.000082369	0.00259462
$i=20$	0.273877	0.000432436	0.00181212
$i=0$	0	0.0030528	0.02276564

表3.3 双层网络 LDPC 码 B 的码集

$\lambda_{i,j}$	$\lambda_{i,0}$	$\lambda_{i,1}$	$\lambda_{i,2}$
$i=2$	0.07441004	0.20599344	0
$i=3$	0.19208258	0.0001581903	0
$i=6$	0.1327018904	0.00013842	0.0001681903
$i=7$	0.09266986	0.000326381	0.0001779641
$i=20$	0.27426244	0.0005152496	0.0021751167
$i=0$	0	0.0237936797	0.000009887

(C)1994-2022 China Academic Journal Electronic Publishing House. All rights reserved. http://www.cnki.net

表3.4 双层网络 LDPC 码 C 的码集

$\lambda_{i,j}$	$\lambda_{i,0}$	$\lambda_{i,1}$	$\lambda_{i,2}$
$i=2$	0.12061328722	0.0	0.0
$i=3$	0.10014537635	0.00002194583	0.0
$i=6$	0.18605144239	0.00027679631	0.0000167976
$i=7$	0.19641410356	0.00021149360	0.00002129058
$i=20$	0.38585582714	0.00032624525	0.00003625514
$i=0$	0.0	0.00415651089	0.02064875289

表3.5 双层网络 LDPC 码 D 的码集

$\lambda_{i,j}$	$\lambda_{i,0}$	$\lambda_{i,1}$	$\lambda_{i,2}$
$i=2$	0.1112574229	0.013643762	0.1818773738
$i=3$	0.09172912663	0.0876831253	0.0571696344
$i=6$	0.13223499235	0.00032560828	0.00015708008
$i=7$	0.092674986	4.568455E-05	6.788722E-05
$i=20$	0.274059093	0.00010113293	0.000217037
$i=0$	0	0.00351717946	0.02072694417

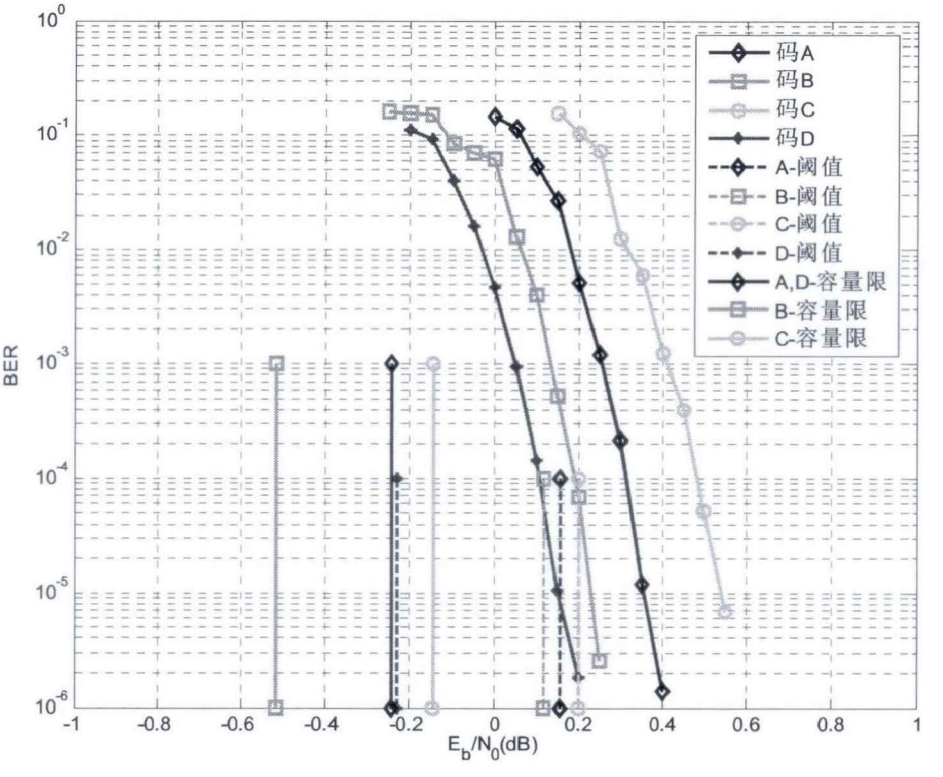


图3.6 AWGN 信道下网络 LDPC 码的性能

(C)1994-2022 China Academic Journal Electronic Publishing House. All rights reserved. http://www.cnki.net

图 3.6 给出了四个最优度分布的网络 LDPC 码的误码率曲线。从图中可以看出，通过搜索四个码的最大译码阈值可以分别得到的四个译码阈值与容量限相差小于 0.7dB，且它们的误码率性能与译码阈值相差小于 0.4dB。由于码 D 的校验节点的度数大于码 A 的，在其它条件相同的情况下，码 D 的校验方程中包含的信息位就会多于码 A，导致在 BER=10^{-5} 时，码 A 的性能优于码 D 大概 0.2dB。在 BER=10^{-5} 时，码 B 的性能优于码 A 大约 0.15dB，码 D 的性能优于码 B 大概 0.1dB。后者是由于增加下层校验节点的度数比增加校验比特个数更能提高系统的性能。随着源节点到目的节点链路的噪声方差的变大，系统的误码性能随着降低，码 A 相比于码 C 大概有 0.2dB 性能增益。

3.6 本章小节

本章首先根据网络 LDPC 码的结构特点，以最小化恢复错误概率为目标，设计了一种网络 LDPC 码的速率兼容删余算法。不同于 Ha 等[120]人研究的算法，该算法利用被删余的变量节点的恢复原则和受到的噪声干扰大小设计了不同码率下的删余方案，在不增加系统复杂度的前提下，只需要一对编码译码器即可实现网络 LDPC 码的码率自适应。计算机仿真结果表明，在同等条件下，采用本文所提算法获得的速率兼容网络 LDPC 码比采用 Ha 等[120]人研究的算法得到的速率兼容 LDPC 码有更好的性能。其次，基于差分进化算法优化网络 LDPC 码的中继码集，通过仿真分析可知，基于双层网络 LDPC 码的中继最优码集得到的系统误码性能与译码阈值之间的差距约为 0.4dB，译码阈值与容量限之间的差距小于 0.6dB。

(C)1994-2022 China Academic Journal Electronic Publishing House. All rights reserved. http://www.cnki.net

第四章 基于分布式RS码的中继转发策略设计

为了降低多用户多中继（Multi-User Multi-Relay, MUMR）易错无线网络中的错误影响，本章提出了一种基于RS编码的混合译码转发策略。该策略引入了一个决定中继是否转发信息的阈值。当中继译码后的信息比特的对数似然比大于该阈值时，该信息比特才会被转发。否则该比特被丢弃。基于最小化比特错误概率，分别对独立协作和混合协作两种策略通过优化方法设计了最佳阈值。最后，给出了在高斯信道和瑞利衰落信道下该策略的性能仿真结果。

4.1 引言

近年来，人们对无线协作中继网络[125-127]的研究逐渐加大，提出了许多新技术来提高其在吞吐量，覆盖范围或分集增益等方面的性能。中继传输是其中一种提高分集增益和覆盖范围的方法。在中继网络中，一个或多个中继节点被用来协作源节点进行信息传输。

在译码转发协作网络中，潜在的错误传播降低了点对点网络的性能。因此，人们提出了大量的方法来减少误差传播所带来的影响[128-131]。Zhao 等[128]人中提出了一种分布式 Turbo 码的译码转发方法。随后，Sneessens 和 Li 等[129,130]人在中继节点上将该方法扩展为软编码来均衡中继上的误差和错误比特。Khuong 等[131]人研究了在中继节点处计算所接收到的比特的 LLR，如果该比特的 LLR 低于其阈值，则中继将不再转发该比特到目的节点。该方法在一定程度上避免了中继译码错误传播到目的节点。

相对于 MIMO 系统，协作通信系统的另一个缺点是其低吞吐量。为了提高系统的吞吐量，人们提出了网络编码[132,133]。早期的网络编码方案仅适用于两用户单中继网络[134]，且推导出了准确的比特错误概率。Peng 等[135]人研究了物理层网络编码在多用户单中继网络中的应用，但这并不是多中继网络中的最优方案。此外，Hausl 和 Xiao 等[134-136]人还研究了一个有限域网络编码的特例-二进制网络编码。但是其传输效率（如：误帧率，能量效率[137]等）不是最优的。后来，Ayanoglu 等[138]人提出了多源单中继有线网络中线性有限域网络编码的设计。但是多源多中继无线网络中网络编码的设计并未涉及到。Yeung 等[139]人研究了没有考虑信道错误影响的独立或相关源节点的对称多层分级编码的最佳化设计。Maric 等[140]人研究了高斯信道下的模拟网络编码，并证明了接收到的能量增长不受限时，该研究所得到的码在一定范围内能逼近割集限。2010 年，Xiao 等[141]人又研究了在快衰落信道下的协作网络中的获得短暂分集增益的非二元网络编码，并没有涉及到该码的误码率性能等方面的研究。

(C)1994-2022 China Academic Journal Electronic Publishing House. All rights reserved. http://www.cnki.net

综上所述，目前大部分无线中继网络都是假设中继无差错传输或者可以完全正确纠正错误的条件下应用网络编码技术。然而，中继上没有任何纠错方案（如 ARQ）是不符合实际应用的，这样的错误会进一步扩散到所有的目的节点处。基于此，本章在中继节点处设置一个可靠的阈值来控制错误的传播。通过计算来自于源节点的每个比特的 LLR，将基于最大距离可分码（MDS）的非二进制网络编码应用于 $M\left(M\geq 2\right)$ 用户 $N\left(N\geq 1\right)$ 中继的无线网络中。本章研究了不同信道模型及中继信道下采用不同 LLR 阈值的多种方案。

4.2 MARC 下基于混合 DF 策略的方案

包含多个中继节点的多址接入中继系统中，中继节点处理信息的方案对系统性能有重要的影响。本节首先给出了多址接入中继系统的信道模型，然后介绍了该系统模型下基于混合 DF 策略的编译码方案以及基于网络编码的 RS 编码设计方案。

4.2.1 系统模型

考虑包括 M 个源节点 $\mathcal{S}_i\left(i=1,2,\cdots,M\right)$，$N$ 个中继节点 $\mathcal{R}_j\left(j=1,2,\cdots,N\right)$ 和一个目的节点 $\mathcal{D}$ 构成的多用户多中继网络模型，如图 2.1 所示。已有的中继传输模式主要有 AF、DF 和 CF 模式等。由于 DF 模式充分考虑到源节点到中继节点信道的可靠性，可以获得比其它两种模式更高的性能增益，本章重点研究 DF 模式。假设每个节点配备一根天线，且采用半双工模式。整个系统的 M 个源节点和一个目的节点之间的传输由广播发送和中继转发两个阶段完成。

在第一时隙中，M 个源节点 $\mathcal{S}_i$ 以码率为 $R_i\left(i=1,2,\cdots,M\right)$ 分别向 N 个中继节点 $\mathcal{R}_j$ 和一个目的节点 $\mathcal{D}$ 广播发送编码序列 $X_i^t\left(i=1,2,\cdots,M\right)$，其中上标 t 表示时间，得到：

$$\begin{aligned} Y_{\mathcal{S}_i,\mathcal{D}}^t &= h_{\mathcal{S}_i,\mathcal{D}}^t X_i^t + N_{\mathcal{S}_i,\mathcal{D}}^t \\ Y_{\mathcal{S}_i,\mathcal{R}_j}^t &= h_{\mathcal{S}_i,\mathcal{R}_j}^t X_i^t + N_{\mathcal{S}_i,\mathcal{R}_j}^t \end{aligned} \tag{4-1}$$

其中，$Y_{\mathcal{S}_i,\mathcal{D}}^t$ 和 $Y_{\mathcal{S}_i,\mathcal{R}_j}^t$ 分别为中继节点 $\mathcal{R}_j$ 和目的节点 $\mathcal{D}$ 接收到的相应信号，$N_{\mathcal{S}_i,\mathcal{D}}^t$ 和 $N_{\mathcal{S}_i,\mathcal{R}_j}^t$ 为零均值加性高斯白噪声随机变量，其方差分别为 $\sigma_{\mathcal{S}_i,\mathcal{D}}^2$ 和 $\sigma_{\mathcal{S}_i,\mathcal{R}_j}^2$。$h_{\mathcal{S}_i,\mathcal{D}}^t$ 和 $h_{\mathcal{S}_i,\mathcal{R}_j}^t$ 为相关的信道系数，其下标表示具体的信道。

(C)1994-2022 China Academic Journal Electronic Publishing House. All rights reserved. http://www.cnki.net

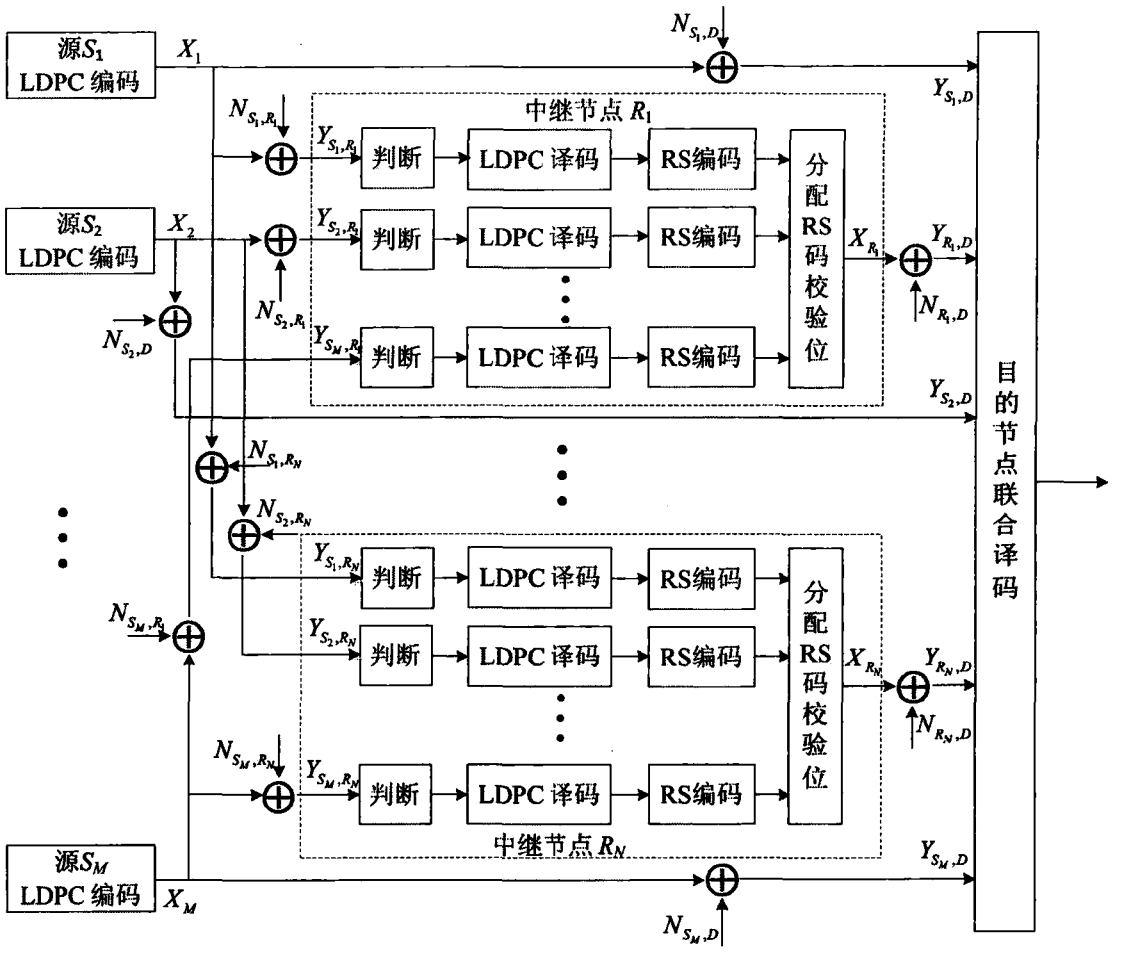


图4.1 M 个源节点和 N 个中继节点组成的系统框图

在第二个时隙中，中继节点 $\mathcal{R}_j$ 计算由各个源节点 $\mathcal{S}_i$ 发送的比特 LLR，如果某个比特 LLR 小于预先设置的阈值，则中继节点 $\mathcal{R}_j$ 将丢弃该比特，不转发其到目的节点 $\mathcal{D}$。随后，中继节点 $\mathcal{R}_j$ 对选出的比特位进行重新编码并将编码序列转发到目的节点 $\mathcal{D}$。令 $X'_{\mathcal{R}_j}$ 为中继节点 $\mathcal{R}_j$ 所发送的重新编码序列，则目的节点 $\mathcal{D}$ 接收到的信号为：

$$Y^t_{\mathcal{R}_j,\mathcal{D}} = h_{\mathcal{R}_j,\mathcal{D}} X^t_{\mathcal{R}_j} + N^t_{\mathcal{R}_j,\mathcal{D}} \tag{4-2}$$

其中，$Y^t_{\mathcal{R}_j,\mathcal{D}}$ 为目的节点 $\mathcal{D}$ 接收到来自于中继节点 $\mathcal{R}_j$ 的信号。$N^t_{\mathcal{R}_j,\mathcal{D}}$ 为零均值加性高斯白噪声，方差为 $\sigma^2_{\mathcal{R}_j,\mathcal{D}}$。中继节点 $\mathcal{R}_j$ 转发的编码序列 $X^t_{\mathcal{R}_j}$ 表示所转发的比特符号。为了简化起见，以下公式中省略上标 t。

4.2.2 基于混合 DF 策略的编译码方案

本章对中继节点转发信息的研究，制定了两种方案。第一种方案是各个中继节点与各源节点之间进行单独协作，每个中继节点独立确定第 i 个源节点的比特是否被转

(C)1994-2022 China Academic Journal Electronic Publishing House. All rights reserved. http://www.cnki.net

发。第二种方案是各个中继节点与所有源节点同时进行协作，只有当来自所有源节点的比特 LLR 都大于阈值时，该中继节点才对这些比特信息进行重新编码并转发它们到目的节点。整个系统的结构框图如图 4.1 所示，下面主要从两方面详细介绍信息传输过程中的编译码方案。

首先，M 个源节点同时对各自长度为 k 的原始信息进行 LDPC 编码，得到码字 (n,k)。而后将各自的编码序列调制后分别广播发送到 N 个中继节点和目的节点处。

其次，目的节点接收到 M 个源节点的信息后，首先对它们进行 LDPC 译码，并将译码后的每个源节点的信息等分成两部分，且把信息的表示形式从域 GF(2) 转换到 $GF(2^q)$，并保存这些信息。各中继节点在处理信息时，首先判断是否需要转发来自各源节点的信息时，其选择过程可分为两种情况如下：

第一，单独协作

各中继节点的检测和处理信息过程如图 4.2 所示，各中继节点首先判断接收到的 M 个源节点的信息比特 LLR 是否小于预设阈值，若是，则此中继节点不转发该源节点的任何信息。若否，中继节点对接收到的各源节点的信息分别进行 LDPC 译码，并将译码后的信息等分成两部分，而后对它们分别进行域 $GF(2^q)$ 上的 RS 编码，得到 $2M$ 个 RS 码。随后将这些 RS 码对应的校验位依次平均分配到 N 个中继节点处。若其中一些中继节点还同时接收到了别的中继节点分配给的相同源节点的信息，此时该中继节点将对同一源节点的所有信息进行最大比合并后，将所有源节点的信息校验位调制后同时转发给目的节点。

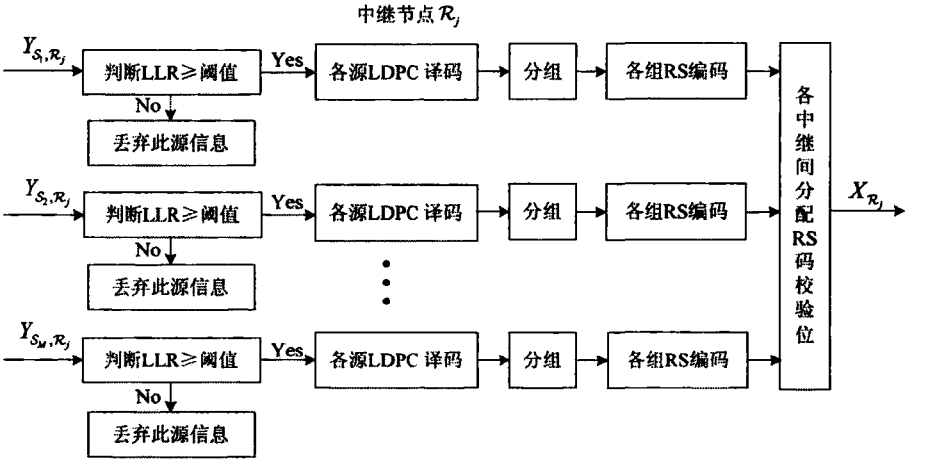


图4.2 单独协作时中继节点的操作流程框图

第二，联合协作

各中继节点的检测和处理信息过程如图 4.3 所示，各中继节点首先判断接收到的 M 个源节点的信息比特 LLR 与预设阈值的大小，若其中任意一个源节点 S_i 的信息比

(C)1994-2022 China Academic Journal Electronic Publishing House. All rights reserved. http://www.cnki.net

特 LLR 小于预设阈值，则此中继节点将不转发任何源节点的信息给目的节点，此时目的节点处只能通过直接链路得到 LDPC 译码后的源节点的原始信息。否则，所有的源节点的信息比特 LLR 都同时大于预设阈值时，中继节点对接收到的所有源节点的信息分别进行 LDPC 译码，将译码后的信息等分成两部分分别进行域 $GF(2^q)$ 上的 RS 编码，得到 $2M$ 个 RS 码。随后将这些码对应的校验位依次平均分配到 N 个中继节点处。若其中一些中继节点还同时接收到了别的中继节点分配给的相同源节点的信息，此时该中继节点将对这一源节点的所有信息进行最大比合并后，将所有源节点的信息校验位调制后同时转发给目的节点。

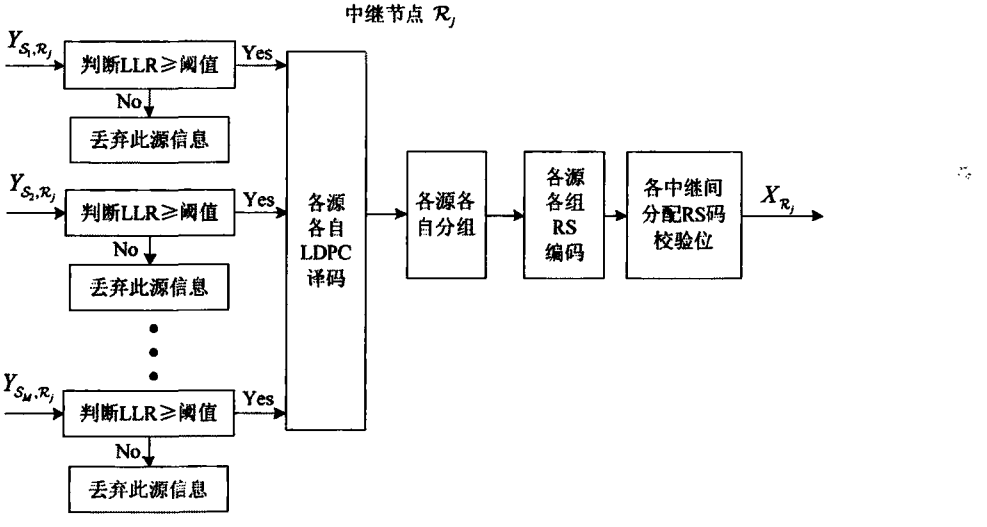


图4.3 联合协作时中继节点的操作流程框图

最后，如果目的节点同时接收到了来自源节点的信息时，首先对中继节点发来的信息的校验位部分进行解调，而后将它们与直接链路的信息合成 $2M$ 个完整的 RS 码，并且对这些 RS 码分别进行译码。

对比上述两种方案：

第一种单独协作方案中，每个源节点的信息分别经过中继节点判断选择后被转发给目的节点。各源节点之间没有任何约束和限制，整个传输过程中都是各自通过的信道质量好坏来决定该源节点的信息是否被转发。该方案有效地提高了系统的资源利用率，但是会造成整个系统很复杂，中继节点需要处理的信息杂乱，没有秩序。

第二种联合协作方案中，每个源节点的信息必须同时满足条件后中继节点才能将其选择后转发给目的节点。各源节点之间相互制约，整个传输过程中所有源节点的信道质量好坏共同决定其中一个源节点的信息是否被转发。该方案会浪费额外的系统资源，但是会使得整个系统有条不紊，中继节点的选择和管理相对容易。

(C)1994-2022 China Academic Journal Electronic Publishing House. All rights reserved. http://www.cnki.net

4.2.3 基于网络编码的RS码设计

在中继节点$\mathcal{R}_j$上，所传输信号$X_{\mathcal{R}_j}$表示为：

$$X_{\mathcal{R}_j}=\sum_{i=1}^{M} g_{i,j}\hat{X}_{i,j} \tag{4-3}$$

其中，$\hat{X}_j=\left[\hat{X}_{1,j}\hat{X}_{2,j}\cdots\hat{X}_{M,j}\right]$表示中继节点$\mathcal{R}_j$对源节点信息估值，$g_{i,j}$表示中继节点所采用的网络编码系数，$g_{i,j}=0$表示中继节点$\mathcal{R}_j$不转发第$i$个源节点信息到目的节点。

令

$$\mathbf{P}=\begin{bmatrix} g_{1,1} & g_{1,2} & \cdots & g_{1,N} \\ g_{2,1} & g_{2,2} & \cdots & g_{2,N} \\ \vdots & & & \vdots \\ g_{M,1} & g_{M,2} & \cdots & g_{M,N} \end{bmatrix} \tag{4-4}$$

其中，矩阵$\mathbf{P}$表示N个中继节点所采用的网络编码方案，将其与$M\times M$单位矩阵相组合，得到：

$$\begin{aligned}\mathbf{G}&=\begin{bmatrix} g_{1,1} & g_{1,2} & \cdots & g_{1,N} & 1 & 0 & \cdots & 0 \\ g_{2,1} & g_{2,2} & \cdots & g_{2,N} & 0 & 1 & \cdots & 0 \\ \vdots & & & \vdots & & & \ddots & \\ g_{M,1} & g_{M,2} & \cdots & g_{M,N} & 0 & 0 & 0 & 1 \end{bmatrix} \\ &=\left[\mathbf{P}\quad \mathbf{I}_{M\times M}\right]\end{aligned} \tag{4-5}$$

显然，$\mathbf{G}$表示长度为$M+N$的RS码的生成矩阵，即网络编码矩阵$\mathbf{P}$可通过RS码原理进行设计。其中，RS码采用Berlekamp译码算法如下：

令待发送的码多项式为：

$$v(x)=v_0+v_1x+\cdots+v_{n-1}x^{n-1} \tag{4-6}$$

相对应的接收多项式为：

$$r(x)=r_0+r_1x+\cdots+r_{n-1}x^{n-1} \tag{4-7}$$

则接收信道中的错误多项式为：

(C)1994-2022 China Academic Journal Electronic Publishing House. All rights reserved. http://www.cnki.net

$$e(x)=r(x)-v(x)=e_0+e_1x+\cdots e_{n-1}x^{n-1} \tag{4-8}$$

其中，系数$e_i=r_i-v_i$是属于$GF(q)$中的一个符号。假设在错误多项式$e(x)$中在位置$x^{j_1},x^{j_2},\cdots,x^{j_v}$处包含$v$个错误（这些位置的分量是非零的），且$0\le j_1<j_2<\cdots<j_v\le n-1$。得出：

$$e(x)=e_{j_1}x^{j_1}+e_{j_2}x^{j_2}+\cdots+e_{j_v}x^{j_v} \tag{4-9}$$

其中，$e_{j_1},e_{j_2},\cdots,e_{j_v}$表示错误数值。为了确定错误多项式$e(x)$，必须同时已知错误位置$x^{j_i}$和错误数值$e_{j_i}$，即必须找到$v$对$\left(x^{j_i},e_{j_i}\right)$。

若需要对q进制RS码进行译码，首先需要计算校正子$(S_1,S_2,\cdots,S_{2t})$，并且这些校正子也是$GF(q^m)$上个一个$2t$维向量。其中$S_i=r(\alpha^i)$，$1\le i\le 2t$。

由于$r(x)=v(x)+e(x)$，可以得出：

$$S_i=v(\alpha^i)+e(\alpha^i)=e(\alpha^i) \tag{4-10}$$

又因为式（4-9）和式（4-10），得出一组方程，表示出错误位置和错误数值与接收多项式$r(x)$的校正子之间的关系式：

$$\begin{aligned}
S_1&=e_{j_1}\alpha^{j_1}+e_{j_2}\alpha^{j_2}+\cdots+e_{j_v}\alpha^{j_v}\\
S_2&=e_{j_1}\alpha^{2j_1}+e_{j_2}\alpha^{2j_2}+\cdots+e_{j_v}\alpha^{2j_v}\\
&\vdots\\
S_{2t}&=e_{j_1}\alpha^{2tj_1}+e_{j_2}\alpha^{2tj_2}+\cdots+e_{j_v}\alpha^{2tj_v}
\end{aligned} \tag{4-11}$$

令

$$\beta_i\triangleq\alpha^{j_i}\text{和}\delta_i\triangleq e_{j_i},\ 1\le i\le v$$

上面两个式子分别表示错误位置数和错误数值。通过应用β_i和δ_i的定义，可以把式（4-11）的方程组表换成如下表达式：

$$\begin{aligned}
S_1&=\delta_1\beta_1+\delta_2\beta_2+\cdots+\delta_v\beta_v\\
S_2&=\delta_1\beta_1^2+\delta_2\beta_2^2+\cdots+\delta_v\beta_v^2\\
&\vdots\\
S_{2t}&=\delta_1\beta_1^{2t}+\delta_2\beta_2^{2t}+\cdots+\delta_v\beta_v^{2t}
\end{aligned} \tag{4-12}$$

(C)1994-2022 China Academic Journal Electronic Publishing House. All rights reserved. http://www.cnki.net

其次，由校正子分量$S_1,S_2,\cdots,S_{2t}$确定错误位置多项式$\sigma(x)$。

令错误位置多项式$\sigma(x)$为：

$$\sigma(x)=(1-\beta_1 x)(1-\beta_2 x)\cdots(1-\beta_v x)=\sigma_0+\sigma_1 x+\sigma_2 x^2+\cdots+\sigma_v x^v \tag{4-13}$$

其中，$\sigma_0=1$。错误位置多项式$\sigma(x)$中根的倒数就是错误位置数。由式（4-12）和式（4-13），可以得到下面一组方程组，用来表示$\sigma(x)$的系数σ_i与校正子分量S_i之间的关系组：

$$\begin{aligned}
&S_{v+1}+\sigma_1 S_v+\sigma_2 S_{v-1}+\cdots+\sigma_v S_1=0\\
&S_{v+2}+\sigma_1 S_{v+1}+\sigma_2 S_v+\cdots+\sigma_v S_2=0\\
&\vdots\\
&S_{2t}+\sigma_1 S_{2t-1}+\sigma_2 S_{2t-2}+\cdots+\sigma_v S_{2t-v}=0
\end{aligned} \tag{4-14}$$

这些方程称为广义牛顿恒等式。计算的目标就是找到上面这些系数满足这些广义牛顿恒等式的最低次数多项式$\sigma(x)$。若找到$\sigma(x)$，就可以确定错误位置和错误数值。

通过 Berlekamap[142]研究中知道 Berlekamp 算法是通过$2t$次迭代计算出错误位置多项式$\sigma(x)$。在第μ步迭代时，确定最低次数多项式为：

$$\sigma^{(\mu)}(\mathrm{x})=\sigma_0^{(\mu)}+\sigma_1^{(\mu)}x+\cdots+\sigma_{l_\mu}^{(\mu)}x^{l_\mu}$$

使得其系数满足下面$\mu-l_\mu$个恒等式为：

$$\begin{aligned}
&S_{l_\mu+1}+\sigma_1^{(\mu)}S_{l_\mu}+\cdots+\sigma_{l_\mu}^{(\mu)}S_1=0\\
&S_{l_\mu+2}+\sigma_1^{(\mu)}S_{l_\mu+1}+\cdots+\sigma_{l_\mu}^{(\mu)}S_2=0\\
&\vdots\\
&S_\mu+\sigma_1^{(\mu)}S_{\mu-1}+\cdots+\sigma_{l_\mu}^{(\mu)}S_{\mu-l_\mu}=0
\end{aligned} \tag{4-15}$$

继续上述迭代步骤，直至$2t$步完成。第$2t$步时，可以得到：$\sigma(x)=\sigma^{(2t)}(x)$。如果错误多项式$e(x)$中的错误数目没超过能纠错的数目$t$时，此时得到的错误位置多项式就是真正的错误位置多项式。这种情形下，错误位置多项式$\sigma(x)$的系数满足式（4-15）的广义牛顿恒等式方程组。

接下来通过将$GF(q^m)$中的元素一一代入$\sigma(x)$来确定$\sigma(x)$在$GF(q^m)$中的根。若$\sigma(\alpha^i)=0$，则α^i就是$\sigma(x)$的根，且$\alpha^{-i}=\alpha^{q^m-1-i}$就是错误位置数。这种方法是全范围

(C)1994-2022 China Academic Journal Electronic Publishing House. All rights reserved. http://www.cnki.net

尝试法。也可以用 Chien[143]搜索法来完成这个步骤。

4.3 转发策略的设计

假定源节点和中继节点没有采用信道编码，根据 Khuong 等[131]人研究中的讨论原理，我们研究了中继节点的转发策略，如果比特 LLR 低于预设阈值，则中继节点保持不变，不会转发任何源节点的信息，否则，将会发送源节点信息网络编码后的符号。为了得到最小的 BER，本章研究了两种译码转发协作方式下的最佳阈值。

4.3.1 基于转发的阈值

假设源节点采用 BPSK 调制，$\Lambda_{x_i}^{j}$ 表示中继节点 $\mathcal{R}_j$ 计算来自第 i 个源节点的比特 LLR，得到：

$$\begin{aligned}\Lambda_{x_i}^{j} &= \ln\frac{p\left(x_i=1\middle|y_{S_i,R_j},h_{S_i,R_j}\right)}{p\left(x_i=-1\middle|y_{S_i,R_j},h_{S_i,R_j}\right)}=\ln\frac{p\left(y_{S_i,R_j}\middle|x_i=1,h_{S_i,R_j}\right)}{p\left(y_{S_i,R_j}\middle|x_i=-1,h_{S_i,R_j}\right)}\\ &=2\frac{y_{S_i,R_j}h_{S_i,R_j}}{\sigma_{S_i,R_j}^{2}}\end{aligned} \tag{4-16}$$

其中，$p(\cdot)$表示条件概率密度函数，$\Lambda_{x_i}^{j}$ 表示硬判决值，且其值代表比特的可靠性，$\mathcal{R}_j$ 估计的原始数据为：

$$\hat{x}_i^{j}=sign(\Lambda_{x_i}^{j}) \tag{4-17}$$

其中，$sign(\cdot)$ 为符号函数，则中继节点 $\mathcal{R}_j$ 处的瞬时 BER 为：

$$P_{e-S_i,R_j}=\frac{1}{1+e^{\left|\Lambda_{x_i}^{j}\right|}} \tag{4-18}$$

令 P_{eT} 为预设阈值，且 $P_{e-S_i,R_j}\le P_{eT}$，否则中继节点不会转发估算的比特 $\hat{x}_i^{j}$ 到目的节点。

根据（4-18）式，可得：

$$P_{e-S_i,R_j}=\frac{1}{1+e^{\left|\Lambda_{x_i}^{j}\right|}}\le P_{eT}$$

或

(C)1994-2022 China Academic Journal Electronic Publishing House. All rights reserved. http://www.cnki.net

$$\left|\Lambda_{x_i}^{j}\right| \geq \ln\left(\frac{1}{P_{eT}}-1\right)=\Lambda_0 \tag{4-19}$$

从式(4-16)-(4-19)中，$\Lambda_{x_i}^{j}$提供了最大后验概率的可靠信息，可以将错误概率降至最低。

4.3.2 阈值优化

（1）单独协作的优化

在单独协作中，中继节点$\mathcal{R}_j$将估计来自每个源节点的信息，若比特的LLR大于预设阈值，中继节点转发存储的信息至目的节点，否则，中继节点在第二个时隙中保持不变。转发的信号表示为：

$$X_{\mathcal{R}_j}=\sum_{i=1}^{M} g_{i,j}\hat{X}_{i,j} \tag{4-20}$$

其中，$g_{i,j}=0$即$\left|\Lambda_{x_i}^{j}\right|<\Lambda_{\mathcal{S}_i 0}$，$g_{i,j}\neq 0$即$\left|\Lambda_{x_i}^{j}\right|\geq\Lambda_{\mathcal{S}_i 0}$，$\Lambda_{\mathcal{S}_i 0}$为集合$\mathcal{S}_i$的阈值。

单独协作时，令$P_{S_i e}^{sep}$为目的节点的平均BER，最佳阈值$\Lambda_{S_i 0}^{opt}$可由$P_{S_i e}^{sep}$的最小值来确定，即为：

$$\min_{\Lambda_{S_i 0}} \quad P_{S_i e}^{sep} \tag{4-21}$$

$$s.t. \quad \Lambda_{S_i 0}>0 \tag{4-22}$$

这是一个线性规划问题，应用概率分布函数得到最佳值$\Lambda_{S_i 0}^{opt}$。

目的节点得到的错误信号有两种可能，一种是在直接链路中产生，另一种是中继节点转发比特到目的节点链路中产生，由于这两种情况是相互独立的，因此，可得：

$$P_{S_i e}^{sep}=P_{S_i e}^{1}+P_{S_i e}^{2} \tag{4-23}$$

其中，$P_{S_i e}^{1}$和$P_{S_i e}^{2}$分别为第一、二种可能时得到的错误概率，由下式计算得出：

$$P_{S_i e}^{1}=P_{S_i}^{(SD)}\cdot Pr\left[\left|\Lambda_{x_i}\right|<\Lambda_{S_i 0}\right] \tag{4-24}$$

$$\begin{aligned} P_{S_i e}^{2} &= Pr\left[\hat{X}_{i,j}=1\middle|X_i=-1,\left|\Lambda_{x_i}\right|\geq\Lambda_{S_i 0}\right] \\ &= P_{S_i}^{(MAC)}\cdot\left(1-P_{S_i,\mathcal{R}_j}^{e}\right)+P_{S_i}^{(X)}\cdot P_{S_i,\mathcal{R}_j}^{e} \end{aligned} \tag{4-25}$$

(C)1994-2022 China Academic Journal Electronic Publishing House. All rights reserved. http://www.cnki.net

其中，$P_{S_i}^{(SD)}$表示源节点到目的节点信道传输的错误概率，$P_{S_i}^{(MAC)}$为假定中继正确译码时源节点到目的节点信道和中继节点到目的节点信道产生的错误概率。$P_{S_i}^{(X)}$为假定中继译码错误时源节点到目的节点信道和中继节点到目的节点信道产生的错误概率。$P_{S_i,\mathcal{R}_j}^{e}$为中继节点$\mathcal{R}_j$对源节点$\mathcal{S}_i$的信息译码错误的概率，$Pr\left[\left|\Lambda_{x_i}\right|<\Lambda_{S_i0}\right]$和$P_{S_i,\mathcal{R}_j}^{e}$的计算参见附录B。

根据式(4-20)-(4-25)，计算出最佳的阈值将误码率降至最小，最佳阈值$\Lambda_{S_i0}^{opt}$可表示为：

$$\Lambda_{S_i0}^{opt}=\log\left(\frac{P_{S_i}^{(X)}-P_{S_i}^{(MAC)}}{P_{S_i}^{(SD)}}-1\right) \tag{4-26}$$

（2）联合协作

该方案中，中继节点$\mathcal{R}_j$估计来自每个源节点的信息，若所有源节点的比特LLR同时大于预设阈值，中继节点$\mathcal{R}_j$转发存储信息到目的节点$\mathcal{D}$；否则，不转发。转发信号表示为：

$$X_{\mathcal{R}_j}=\begin{cases}\sum_{i=1}^{M}g_{i,j}\hat{X}_{i,j}, & \left|\Lambda_{x_i}\right|>\Lambda_{S_i0}\quad for\ all\ i\\ 0, & otherwise\end{cases} \tag{4-27}$$

其中，Λ_{S_i0}为中继节点$\mathcal{R}_j$转发源节点$\mathcal{S}_i$的比特阈值集。

联合协作时，令P_e^{com}为目的节点的平均BER，最佳阈值集$\Lambda_{S_10}^{opt},\Lambda_{S_20}^{opt},\cdots,\Lambda_{S_M0}^{opt}$可由$P_e^{com}$最小值来确定，具体表示为：

$$\min_{\Lambda_{S_10},\Lambda_{S_20},\cdots,\Lambda_{S_M0}} \quad P_e^{com} \tag{4-28}$$

$$s.t.\quad \Lambda_{S_i0}>0,\quad i=1,2,\cdots,M \tag{4-29}$$

令$T_{S_1,S_2,\cdots,S_M}^{e}$表示各中继节点处的译码错误，$T_{S_1,S_2,\cdots,S_M}^{c}$表示各中继节点处的译码正确，$T_{S_1,S_2,\cdots,S_M}^{x}$表示中继节点保持不变，不会转发任何源节点的信息。假设：集合P定义为$P=\left\{\mathrm{sgn}\left(\Lambda_{x_1}\right)\neq x_1,\mathrm{sgn}\left(\Lambda_{x_2}\right)\neq x_2,\cdots,\mathrm{sgn}\left(\Lambda_{x_M}\right)\neq x_M\right\}$，$U\in P$且$U\neq\varnothing$；集合$Q$定义为$Q=\left\{\left|\Lambda_{x_1}\right|<\Lambda_{S_1,0},\left|\Lambda_{x_2}\right|<\Lambda_{S_2,0},\cdots,\left|\Lambda_{x_M}\right|<\Lambda_{S_M,0}\right\}$，$V\in Q$且$V\neq\varnothing$。集合$T$定义为$T=\left\{\left|\Lambda_{x_1}\right|>\Lambda_{S_1,0},\left|\Lambda_{x_2}\right|>\Lambda_{S_2,0},\cdots,\left|\Lambda_{x_M}\right|>\Lambda_{S_M,0}\right\}$；$T_{S_1,S_2,\cdots,S_M}^{e}$，$T_{S_1,S_2,\cdots,S_M}^{c}$和$T_{S_1,S_2,\cdots,S_M}^{x}$概率函数可以表示为：

(C)1994-2022 China Academic Journal Electronic Publishing House. All rights reserved. http://www.cnki.net

$$\begin{aligned}\Pr\left[T^{e}_{\mathcal{S}_1,\mathcal{S}_2,\cdots,\mathcal{S}_M}\right]&=\Pr\left[U|T\right]\\ \Pr\left[T^{c}_{\mathcal{S}_1,\mathcal{S}_2,\cdots,\mathcal{S}_M}\right]&=1-\Pr\left[U|T\right]\\ \Pr\left[T^{x}_{\mathcal{S}_1,\mathcal{S}_2,\cdots,\mathcal{S}_M}\right]&=\Pr\left[V\right]\end{aligned} \tag{4-30}$$

因此，目的节点的误码率为：

$$P_e^{com}=P^{(SD)}_{\mathcal{S}_1,\mathcal{S}_2,\cdots,\mathcal{S}_M}\Pr\left[T^{x}_{\mathcal{S}_1,\mathcal{S}_2,\cdots,\mathcal{S}_M}\right]+P^{(MAC)}_{\mathcal{S}_1,\mathcal{S}_2,\cdots,\mathcal{S}_M}\Pr\left[T^{c}_{\mathcal{S}_1,\mathcal{S}_2,\cdots,\mathcal{S}_M}\right]+P^{(X)}_{\mathcal{S}_1,\mathcal{S}_2,\cdots,\mathcal{S}_M}\Pr\left[T^{e}_{\mathcal{S}_1,\mathcal{S}_2,\cdots,\mathcal{S}_M}\right] \tag{4-31}$$

其中，$P^{(SD)}_{\mathcal{S}_1,\mathcal{S}_2,\cdots,\mathcal{S}_M}$ 表示源节点到目的节点直接链路发生错误的概率，$P^{(MAC)}_{\mathcal{S}_1,\mathcal{S}_2,\cdots,\mathcal{S}_M}$ 表示中继节点译码正确时源节点到目的节点和中继节点到目的节点链路发生错误的概率，$P^{(X)}_{\mathcal{S}_1,\mathcal{S}_2,\cdots,\mathcal{S}_M}$ 表示中继节点译码错误时源节点和中继节点到目的节点链路发生错误的概率。$\Pr\left[T^{x}_{\mathcal{S}_1,\mathcal{S}_2,\cdots,\mathcal{S}_M}\right]$，$\Pr\left[T^{c}_{\mathcal{S}_1,\mathcal{S}_2,\cdots,\mathcal{S}_M}\right]$和$\Pr\left[T^{e}_{\mathcal{S}_1,\mathcal{S}_2,\cdots,\mathcal{S}_M}\right]$的计算过程详见附录 C。

通过数值积分来估计表达式得到 P_e^{com} 的所有变量，从而得到一个的集合 $\Lambda_{\mathcal{S}_1,0},\Lambda_{\mathcal{S}_2,0}\cdots,\Lambda_{\mathcal{S}_M,0}$。最后，通过数值优化（如梯度下降法）算法得到 P_e^{com} 最小时的最佳阈值集合 $\Lambda^{opt}_{\mathcal{S}_1 0},\Lambda^{opt}_{\mathcal{S}_2 0},\cdots,\Lambda^{opt}_{\mathcal{S}_M 0}$。

4.4 仿真结果

仿真中，假设多址接入中继信道的模型中包含四个源节点，四个中继节点和一个目的节点，且采用正交信道，BPSK 调制。四个源节点均采用(3824,1912)的 LDPC 码，且度分布 $\lambda(x)=0.21606x+0.1576x^2+0.154x^4+0.01848x^5+0.04312x^6+0.41074x^{18}$，$\rho(x)=x^8$。假设在GF($2^8$)上的 RS 码，最小多项式 $p(X)=1+X^2+X^3+X^4+X^8$。下面分别对没有预设阈值、有预设阈值和最佳化阈值三种情况进行仿真。

当 $SNR_{\mathcal{S}_i,\mathcal{R}_j}=SNR_{\mathcal{S}_i,\mathcal{D}},N_{\mathcal{R}_j,\mathcal{D}}=0.3$ 时，由图 4.4 可以看出，在 AWGN 信道下，随着信噪比的增加，采用文中研究方案得到的系统性能增益随之增加。采用单独协作方案比无阈值方案的性能明显改善，当 BER $=10^{-5}$ 时，采用单独协作方案性能优于无阈值方案 0.13dB；当 $P_{eT}=10^{-1},10^{-2}$ 时，联合协作方案和单独协作方案的性能趋于一致；当 $E_b/N_0<1.5$ dB 时，最佳化阈值联合协作方案与阈值 $P_{eT}=10^{-2}$ 的联合协作方案并无明显差异，当大于这个信噪比之后，前者性能比后者有了明显提升。从整个性能图看，单独协作方案优于联合协作方案，且最佳化阈值的两种方案接近于中继正确译码时的性能。

(C)1994-2022 China Academic Journal Electronic Publishing House. All rights reserved. http://www.cnki.net

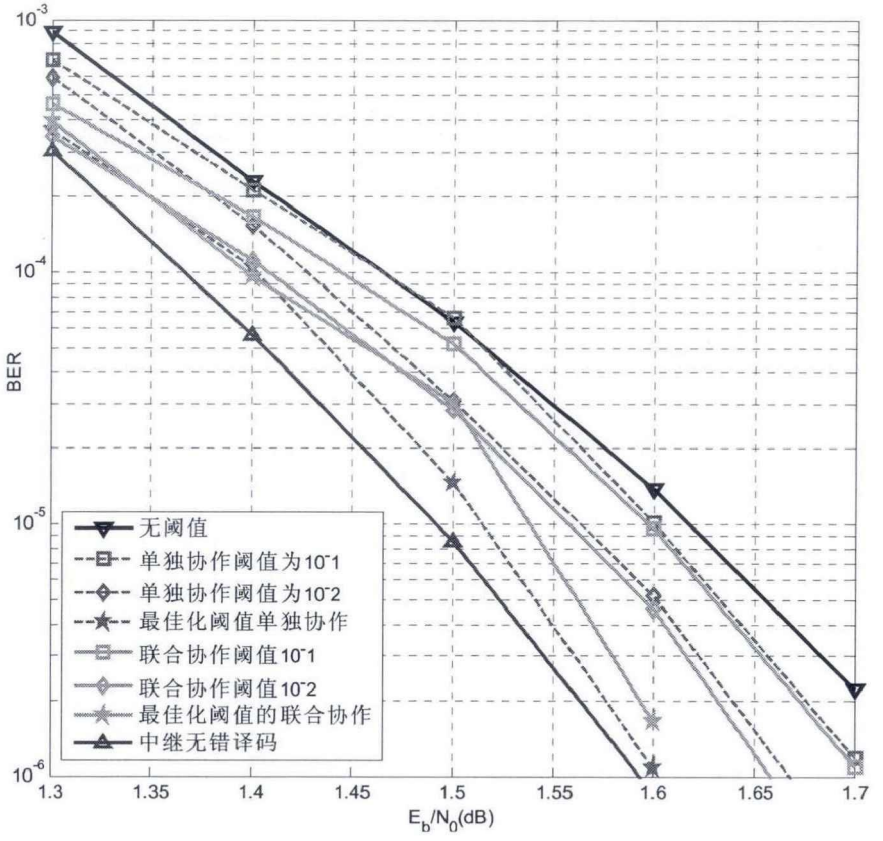


图4.4 AWGN信道下的误码性能

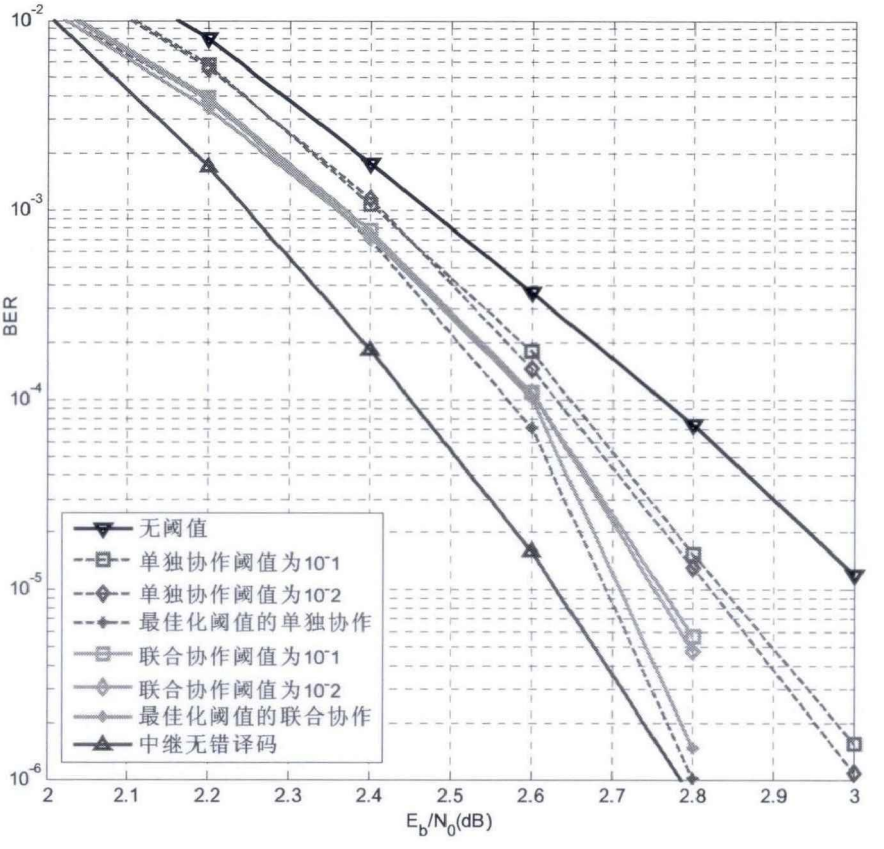


图4.5 瑞利衰落信道下的误码性能

(C)1994-2022 China Academic Journal Electronic Publishing House. All rights reserved. http://www.cnki.net

仿真中，采用瑞利衰落信道，且信道系数满足 $E\left[\left|h_{S_i,\mathcal{R}_j}\right|^2\right]=E\left[\left|h_{S_i,\mathcal{D}}\right|^2\right]=E\left[\left|h_{\mathcal{R}_j,\mathcal{D}}\right|^2\right]=1$，$SNR_{S_i,\mathcal{R}_j}=SNR_{S_i,\mathcal{D}}+2$，$N_{\mathcal{R}_j,\mathcal{D}}=0.3$，由图 4.5 可以看出，随着信噪比的增加，采用文中阈值方案得到的系统性能增益随之增加。当 $\mathrm{BER}=10^{-5}$ 时，采用单独协作方案性能优于无阈值方案 0.3dB；当 $E_b/N_0<0.6\,\mathrm{dB}$ 时，各阈值的联合协作方案性能并无差异，但大于这个信噪比之后，最佳化阈值联合协作方案性能明显优于阈值为 $P_{eT}=10^{-1},10^{-2}$ 的联合协作方案。从整个性能图看，单独协作方案优于联合协作方案，且最佳化阈值的两种方案接近于中继正确译码时的性能。

4.5 本章小节

针对多源多中继网络中的中继错误传播的信道模型，设计了整个系统的信息传输过程中的编译码算法，同时提出了一种基于 RS 码的混合译码转发策略。该策略中根据比特的可靠性引入了一个阈值，中继采用该阈值来确定是否转发信息。此外，本章还通过最小化误码率推导出最佳化阈值，并分别适应于单独协作方案和联合协作方案中。仿真结果表示，在同等条件下，采用最佳化阈值协作比无阈值协作方案有更好的性能。

(C)1994-2022 China Academic Journal Electronic Publishing House. All rights reserved. http://www.cnki.net

第五章 MARC 的一种半速率可逆码的设计

在译码转发模式下的多址接入中继系统中，可以采用好的编码技术来提高系统的误码性能。本章针对多址接入中继系统的特点，采用组合叠加的方法，提出了一种基于半速率可逆码的II型 HARQ 构造的双层 LDPC 码，并对其译码阈值进行了分析。从仿真结果可以看出，同已有的基于传统方式构造的双层 LDPC 码相比，这种应用半速率可逆码的II型 HARQ 构造的双层 LDPC 码可以使误码性能获得较大的提高。

5.1 引言

随着无线通信技术的发展，人们对通信的可靠性要求越发强烈。但是，实际通信中多径衰落和时分多变等问题仍然会给提高无线通信质量带来挑战。为了解决现有蜂窝无线网络中的这些问题引入了协作中继。无线通信系统中采用了中继能很大程度上提高信道的容量、减少功率的损耗和提供额外的分集增益，从而增加系统的可靠性。为了解决干扰的进一步延伸，人们集中的研究了半双工信道。半双工中继信道的传输过程可以分成两步模式：广播模式是源节点发送信息给中继节点和目的节点，多址接入模式是源节点和中继节点同时发送信息给目的节点。显然，两种模式的传输过程的信噪比和数据速率都不同，导致两种模式下设计的码逼近容量限变得很困难。Zheng 和 Duman 等[144,145]提出了采用 Turbo 码的设计方案来达到译码转发中继信道的容量。后来，Ha 和 Hu 等[146,147]应用删余的方法在不同速率时设计 LDPC 码，这一改进方案使得源节点到中继节点和中继节点到目的节点链路获得了最佳的 LDPC 码。从此，如何提高中继系统的性能方面，LDPC 码受到了越来越多的关注。为了提高单源单中继系统的性能，Razaghi 等[148]提出了一种双层 LDPC 码。该技术采用了加长和删余两种结构来设计双层 LDPC 码，且双层 LDPC 码的 Tanner 图包含上下两层校验节点。为了最佳化逼近容量通过搜索下层图节点（对应于源节点到目的节点链路）的度分布来优化设计 LDPC 码，从而构造源节点到目的节点的整个最优码。可是，整个码在最优化时采用置信传播算法（Belief Propagation, BP）的每一步都需要考虑错误概率密度函数实现起来很复杂。为了简化这个算法，Clakrabarti 等[149]提出了采用信息均值更新来最佳化半双工中继系统中的 LDPC 码。他们只是单独最佳化源节点到中继节点链路或者中继节点到目的节点的链路。因为最佳化整体链路的缺陷在于仿真结果和 SNR 预期阈值会有一定的差距。为了克服上述困难，引入了高斯近似优化方法。因为该方法把处理均值的密度进化的多维问题减少到一维问题，这样可以采用线性规划工具来优化码的性能。后来，Cances 等[150]人研究了在半双工中继系统中采用信息均值更新

(C)1994-2022 China Academic Journal Electronic Publishing House. All rights reserved. http://www.cnki.net

与高斯近似同步最佳化非规则 LDPC 码，并提出了一种联合码最佳化源节点到中继节点链路和中继节点到目的节点链路，从而设计码的性能逼近容量理论限。基于现有的双层LDPC码的原理，本章提出了一种新的基于半速率可逆LDPC码的II型HARQ[151]来构造双层 LDPC 码。

一般来说，纠错能力较强的码可以解决大多数的错误类型，从而大大降低重传次数，有利于提高系统的吞吐量；另一角度，这样的码往往编码效率很低，妨碍了传输速率的提高，同时复杂度也很大，许多场景下难以实现。针对中继系统中平均数据传输速率较低的问题，提出的基于半速率可逆LDPC码的II型HARQ的双层LDPC码，可以在一定程度上解决上述编码效率和传输速度之间的矛盾。理论分析及仿真结果表明，这种新的双层 LDPC 码可以很好地提高系统的误码性能。

5.2 半双工多址接入中继系统

5.2.1 系统模型

考虑一个包含一个源节点$\mathcal{S}$、一个中继节点$\mathcal{R}$和一个目的节点$\mathcal{D}$构成的三节点多址接入中继信道模型如图 1.1 所示。该系统采用半双工模式，节点不能同时接收和发送信息。假设连续的两个时隙量化为t和$1-t$。第一个时隙时，即为广播（Broadcast，BC）模式阶段，源节点$\mathcal{S}$发送信息给中继节点$\mathcal{R}$和目的节点$\mathcal{D}$。第二个时隙时，即为多址接入（Multiple-access, MAC）模式阶段，源节点$\mathcal{S}$和中继节点$\mathcal{R}$同时发送信息给目的节点$\mathcal{D}$。整个系统结构框图如图 5.1 所示，接收节点所有接收信息表达式如下：

$$\begin{aligned} V_1 &= h_{SR}X_1 + N_{SR} \\ Y_1 &= h_{SD}X_1 + N_{D_1} \\ Y_2 &= h_{SD}X_2 + h_{RD}X_{\mathcal{R}} + N_{D_2} \end{aligned} \tag{5-1}$$

其中，标记 1 和 2 表示两个独立的时隙。h_{SR}表示源节点与中继节点间的信道衰落指数，N_{SR}表示在 BC 阶段源节点到中继节点信道的高斯白噪声，且服从$N\left(0,\sigma_{SR}^2\right)$分布。其它两式中的符号相似。各节点的功率约束[145]满足：

$$t\cdot P_{S_1} + (1-t)\cdot\left(P_{S_2} + P_{\mathcal{R}_2}\right) \le P \tag{5-2}$$

其中，$P_{S_1} = E\left[X_1^2\right]$表示在 BC 阶段源节点的发送功率，$P_{S_2}$和$P_{\mathcal{R}_2}$的定义相似。$P$代表整个系统总的发送功率。协作中继策略中面临的挑战是中继节点必须在SNR_1时，

(C)1994-2022 China Academic Journal Electronic Publishing House. All rights reserved. http://www.cnki.net

译出来自源节点的码字。目的节点必须在 $SNR_2 < SNR_1$ 时，译出来自源节点的码字，此时必须借助于在多址接入模式下来自中继节点的边信息。

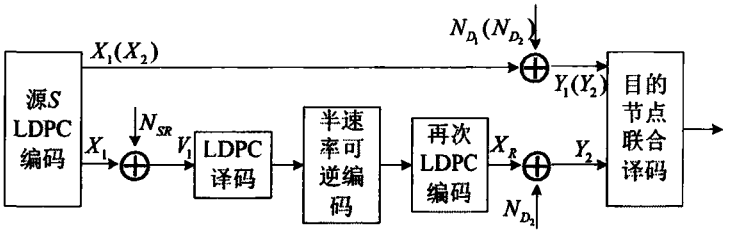


图5.1 半双工模式下的三节点多址接入中继系统的结构框图

5.2.2 编译码方案

在数据传输系统中有两种技术用来控制传输差错[151]：前向纠错控制（forward-error-control, FEC）方法和自动请求重传(automatic-repeat-request, ARQ)方法。FEC 系统中采用的是纠错码。ARQ 系统中采用一个检错能力强的码。FEC 和 ARQ 两种差错控制方法各自具有优缺点，如果适当的结合这两种差错控制方法，则 FEC 和 ARQ 缺点都被克服了。其中，Ⅰ型混合 ARQ 方法采用的码必须能纠正一定错误集合并同时具有检测能力，从而需要很多的校验位。这就增加了每次传送和重传的额外开销。当信道无损时这样做显然是一种浪费。为了克服这个缺点，提出了一种自适应方案，即第二类混合（Ⅱ型 Hybrid）ARQ 方法，简称Ⅱ型 HARQ。在此基础上，本章设计的编译码方案如下。

首先，源节点 $\mathcal{S}$ 将长度为 k 的原始信息 I 经过 LDPC 编码后得到 (n,k) 的 LDPC 码字 (I,Q)。随后，源节点 $\mathcal{S}$ 将其编码序列 (I,Q) 广播发送给中继节点 $\mathcal{R}$ 和目的节点 $\mathcal{D}$ 处。

其次，目的节点 $\mathcal{D}$ 首先将接收到的码字 $(\tilde{I},\tilde{Q})$ 进行 LDPC 译码，检测无误，则此信息传输成功，本次传输结束。否则，目的节点 $\mathcal{D}$ 将 $\tilde{I}$ 保存到缓存中，并反馈 NAK 给中继节点 $\mathcal{R}$。中继节点处编译码框图如图 5.2 所示。中继节点 $\mathcal{R}$ 收到 NAK 后，首先将前一时隙接收到的信息部分 I 进行的 LDPC 编码得到码字 $(I,P(I))$，再将校验部分 $P(I)$ 进行 C_0 方式的 LDPC 编码得到码字 $(P(I),Q^1)$ 并发送给目的节点 $\mathcal{D}$。

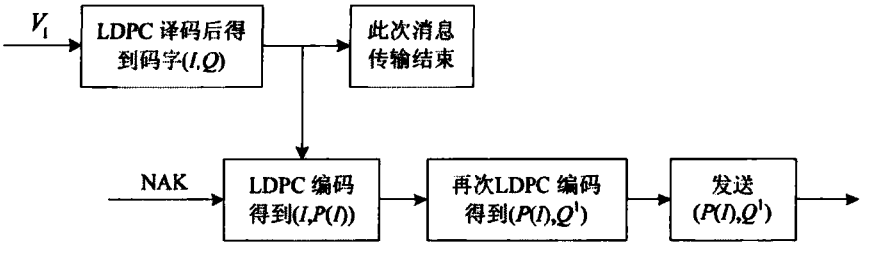


图5.2 中继节点的编译码方案

(C)1994-2022 China Academic Journal Electronic Publishing House. All rights reserved. http://www.cnki.net

最后，目的节点$\mathcal{D}$对信息进行最后的译码，如图5.3所示。目的节点首先对接收到的$\left(\tilde{P}(I),\tilde{Q}^{1}\right)$进行LDPC译码，检测无误，则经过可逆过程可直接恢复出信息部分I，传输成功，本次传输结束；若有错，则将校验部分$\tilde{P}(I)$和之前收到的信息部分$\tilde{I}$合成$\left(\tilde{I},\tilde{P}(I)\right)$，尝试纠错。若错误可以纠正，则信息部分$I$得以正确恢复，传输成功，本次传输结束；否则，目的节点将信息部分$\tilde{I}$从缓存中清除，将校验部分$\tilde{P}(I)$保存到缓存中，并反馈NAK给源节点$\mathcal{S}$。源节点$\mathcal{S}$收到NAK后再次广播发送原始码字(I,Q)，目的节点$\mathcal{D}$重复上述过程直至收到的信息无误。为了简化起见，本文假设如果需要重传码字，不管正确与否，不再传输该码字。

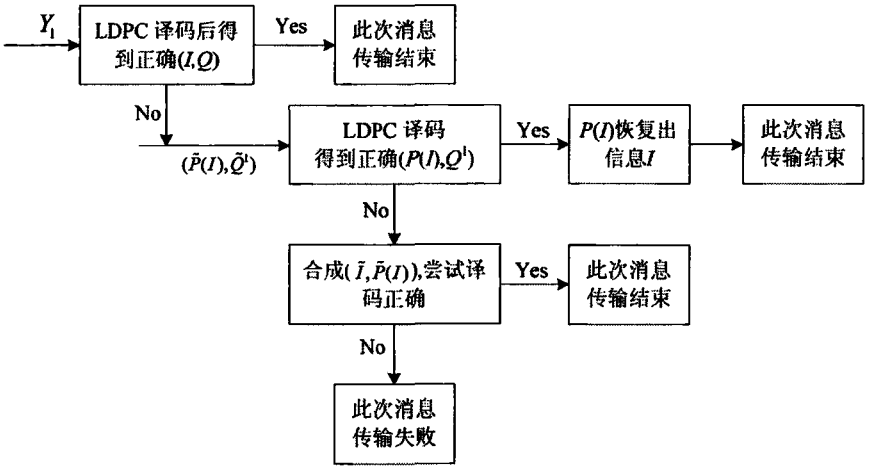


图5.3 目的节点的编译码方案

5.2.3 传输速率的分析

在半双工信道模型下，采用译码转发协议的可达速率[149]如下：

$$R_{DF}=\sup_{0\le t\le 1}\min\left\{tI\left(X_1;V\right)+\left(1-t\right)I\left(X_2;Y_2\middle|W_2\right),tI\left(X_1;Y_1\right)+\left(1-t\right)I\left(X_2,W_2;Y_2\right)\right\} \quad (5\text{-}3)$$

从式（5-3）可以得出，只有当源节点到中继节点的链路比源节点到目的节点链路的信道质量好时，译码转发下的中继通信相当于直接链路的通信。接下来设计的码可以达到预期的速率。假设整个码字符号共N个，其中tN个符号用于BC阶段发送，$(1-t)N$个符号用于MAC阶段发送。根据Cover的规则[4]，DF协议下的码的传输过程如下：

1- 在BC阶段的编码：源节点将原始信息编成tN长的码字C_{SR_1}及速率如下：

$$R_{SR_1}=I(X_1;V_1) \quad (5\text{-}4)$$

(C)1994-2022 China Academic Journal Electronic Publishing House. All rights reserved. http://www.cnki.net

2- 在 BC 阶段的译码：源节点发送码字 C_{SR_1} 经过高斯信道后，到达中继节点和目的节点。由于 R_{SR_1} 小于源节点到中继节点链路的容量，中继节点可以正确译出源节点的码字 C_{SR_1}。该阶段目的节点只是存储接收到的码字以便在 MAC 阶段的最后一步译码使用。

3- 在 MAC 阶段的编码：目的节点没有译码，但储存了 $tNI(X_1;Y_1)$ 个比特信息，还需要 $tN\left(I(X_1;V_1)-I(X_1;Y_1)\right)$ 个额外的比特信息来可靠的译出 C_{SR_1}。源节点和中继节点发送这些额外比特时码字 C_{RD_2} 速率：

$$R_{RD_2}=\frac{t}{1-t}\left(I(X_1;V_1)\text{-}I(X_1;Y_1)\right) \tag{5-5}$$

在 MAC 模式下，源节点和中继节点发送相同的信息，因此源节点不发送新的信息。与 Clakrabarti 等[149]研究结果相比，这里没有码字 C_{SD_2}。虽然此方案不是最优的，但是很大程度上简化了双层 LDPC 码的设计复杂度。

4- 在 MAC 阶段最后一步译码：目的节点首先译出码字 C_{RD_2}，而后借助 C_{RD_2} 译出 BC 阶段的 C_{SR_1}。这时码字 C_{RD_2} 中的信息位被用来当作 C_{SR_1} 的校验位。

5.3 基于半速率可逆码的双层 LDPC 码的设计

针对典型的三节点网络模型，Yu 等[148]最早构造了一种双层 LDPC 码结构。这种结构分别通过删余或延长得到两种不同的双层 LDPC 码。基于 Lin 等[151]提出的一种采用半速率可逆码的 II 型 HARQ，本章采用一种叠加组合的方式构造一种双层 LDPC 码，构造过程如图 5.4 所示。本小节首先介绍了半速率可逆码的特性，在此基础上构造了一种新的双层 LDPC 码，并对其结构进行详细分析。

5.3.1 半速率可逆码

半速率的意思是一个码字的信息位长度和校验位长度相同，即码率为 1/2。一个码被称为可逆的充要条件是一个码字的校验位已知的情况下，对应的信息位可以经过一个可逆的过程唯一确定。由于其具有可逆性，便于数据准确恢复。在重传过程中，若校验部分被成功接收（即没有检测出错误），则原始消息就可以通过可逆过程重新构造，而没有必要经过很复杂的译码过程来恢复。同时，这种求逆的过程还可以减少重传的概率。例如，若接收到的消息包含的错误数多于其纠错能力而收到的校验部分中却没有错误，则根据接收到的消息和校验位是无法恢复出原始消息的，从而需要再次重传。然后，对于无错的校验部分来说，可以通过可逆过程很快的恢复出原始消息，从而避免了再次重传。下面，详细介绍一类半速率可逆分组码[151]。

(C)1994-2022 China Academic Journal Electronic Publishing House. All rights reserved. http://www.cnki.net

令C是一个$n-k\le k$的(n,k)循环码。$g(\mathrm{X})$是C的生成多项式：

$$g(X)=1+\mathrm{g}_1X+g_2X^2+\cdots+g_{n-k-1}X^{n-k-1}+X^{n-k} \tag{5-6}$$

码多项式：

$$v(X)=v_0+v_1X+v_2X^2+\cdots+v_{n-1}X^{n-1} \tag{5-7}$$

其中，前k个高阶位系数$v_{n-k},v_{n-k+1},\cdots,v_{n-1}$和$k$个信息位相对应，$n-k$个低阶位系数$v_0,v_1,\cdots+v_{n-k-1}$是与校验位相对应。码字集合$C$中有$2^{n-k}$个码字其前$2k-n$个高阶分量$v_{2(n-k)},v_{2(n-k)+1},\cdots,v_{n-1}$为零。如果将$2k-n$个高阶零分量从这些码字中去掉，可以得到长为$2(n-k)$的$2^{n-k}$个向量集合，即构成了一个半速率$(2n-2k,n-k)$缩短循环码$C_1$。这个缩短码和码$C$具有一样的纠错能力。

令待编码信息多项式为：

$$u(X)=u_0+u_1X+\cdots+u_{n-k-1}X^{n-k-1} \tag{5-8}$$

$X^{n-k}u(X)$除以生成多项式$g(X)$，得到：

$$X^{n-k}u(X)=a(X)\mathrm{g}(X)+b(X) \tag{5-9}$$

其中，$a(X)$和$b(X)$分别是商式和余式。所以，得到$u(X)$的码字多项式：

$$w(X)=b(X)+X^{n-k}u(X) \tag{5-10}$$

其中，$b(X)$是校验部分。下面证明码字C_1的可逆性。

令$u_1(X)$和$u_2(X)$是两个不同的待编码信息。$X^{n-k}u_1(X)$和$X^{n-k}u_2(X)$分别除以生成多项式$g(X)$得到：

$$X^{n-k}u_1(X)=a_1(X)\mathrm{g}(X)+b_1(X) \tag{5-11}$$

$$X^{n-k}u_2(X)=a_2(X)\mathrm{g}(X)+b_2(X) \tag{5-12}$$

则$u_1(X)$和$u_2(X)$的码字分别为：

(C)1994-2022 China Academic Journal Electronic Publishing House. All rights reserved. http://www.cnki.net

$$w_1(X)=b_1(X)+X^{n-k}u_1(X) \tag{5-13}$$

$$w_2(X)=b_2(X)+X^{n-k}u_2(X) \tag{5-14}$$

假设$b_1(X)=b_2(X)=b(X)$,将式（5-11）和式（5-12）相加得到：

$$\left[u_1(X)+u_2(X)\right]X^{n-k}=\left[a_1(X)+a_2(X)\right]\mathrm{g}(X) \tag{5-15}$$

其中，$g(X)$和X^{n-k}互质，$u_1(X)+u_2(X)$能被$g(X)$除尽。这个不可能，因为$u_1(X)+u_2(X)\neq 0$且其次数小于$n-k$，但是$g(X)$的次数为$n-k$。所以，$b_1(X)\neq b_2(X)$。

上述证明校验部分$b(X)$是唯一的，即原始消息$u(X)$和其校验部分$b(X)$是一一对应的。所以，已知$b(X)$，$u(X)$可以唯一确定。

若已知校验部分$b(X)$，是如何恢复出原始消息$u(X)$。如下：

首先，将式（5-9）两边同乘以X^k：

$$X^n u(X)=a(X)\mathrm{g}(X)X^k+b(X)X^k \tag{5-16}$$

整理式（5-16），得到：

$$u(X)\left(X^n+1\right)+u(X)=a(X)\mathrm{g}(X)X^k+b(X)X^k \tag{5-17}$$

其中$g(X)$可以被$u(X)$整除，式（5-17）变换为：

$$b(X)X^k=\left[u(X)h(X)+a(X)X^k\right]g(X)+u(X) \tag{5-18}$$

其中，$h(X)=\left(X^n+1\right)/g(X)$。从式（5-18）可以看出，消息$u(X)$就是$b(X)X^k$除以生成多项式$g(X)$所得到的余式。这个过程可以把$g(X)$作为反馈连接的除法电路来实现。已知校验部分$b(X)$，得到消息$u(X)$的过程称为求逆过程。

Lin 等[152]人基于有限几何理论首次提出了一种代数、系统的 LDPC 码的构造方法。这类有限几何 LDPC 码具有性能好的最小距离，且它们的 Tanner 图没有短环。这类码可以通过各类译码方法来译码，且获得很好的误码性能。再者，这些码是循环和准循环的码。所以，这些码具有半速率可逆性。本章将码率为 1/2 的 LDPC 码作为半速率可逆码来研究。

(C)1994-2022 China Academic Journal Electronic Publishing House. All rights reserved. http://www.cnki.net

5.3.2 基于半速率可逆码构造双层 LDPC 码

II 型 HARQ 方法的思想是用于纠错的校验位仅在需要时才发送给接收端[153-155]。这种类型的方法中采用两种线性码，一种是用于检错的高码率(n,k)码C_0，另一种是用于纠错的半速率可逆$(2k,k)$码C_1。此方法的重要特点是校验重传以便根据半速率可逆码C_1进行纠错。由于C_1的可逆性，可以通过求逆从校验方程中唯一地重新恢复出原始消息，因此校验部分含有和原消息相同的信息量。结果使得每次传输和重传的开销减少到(n,k)码C_0检错时所需的$n-k$个校验位，这是任何一个 ARQ 方法所必须具备的。在前一节设计的编译码方案基础上，本章采用组合叠加的方法构造一种基于半速率可逆码的II型HARQ的新结构双层 LDPC 码，步骤如下：

在广播阶段，源节点$\mathcal{S}$经过C_0方式的 LDPC 编码后得到(n,k)的 LDPC 码字，该码作为双层 LDPC 码的第一层，如图 5.4 左图所示。此时采用C_0方式的 LDPC 编码的校验矩阵为$\mathbf{H}_1$。随后，源节点$\mathcal{S}$将其编码序列广播发送给中继节点$\mathcal{R}$和目的节点$\mathcal{D}$处。

多址接入阶段，目的节点$\mathcal{D}$首先将接收到的码字进行C_0方式 LDPC 译码，经检测有误时，目的节点$\mathcal{D}$请求中继节点$\mathcal{R}$发送信息。中继节点$\mathcal{R}$首先对前一时隙接收到的信息部分,即图 5.4 中竖线阴影的变量节点，进行C_1方式的 LDPC 编码得到码字，该码字作为双层 LDPC 码的第二层左半部分，如图 5.4 右下子图所示。此时采用C_1方式的 LDPC 编码的校验矩阵为$\mathbf{H}_2$。而后，再将此 LDPC 码字的校验部分，即图 5.5 下子图横线阴影的校验节点，进行C_0方式的 LDPC 编码得到码字，该码字作为双层 LDPC 码的第二层右半部分，如图 5.5 右上子图所示。此时采用C_0方式的 LDPC 编码的校验矩阵为$\mathbf{H}_3$。

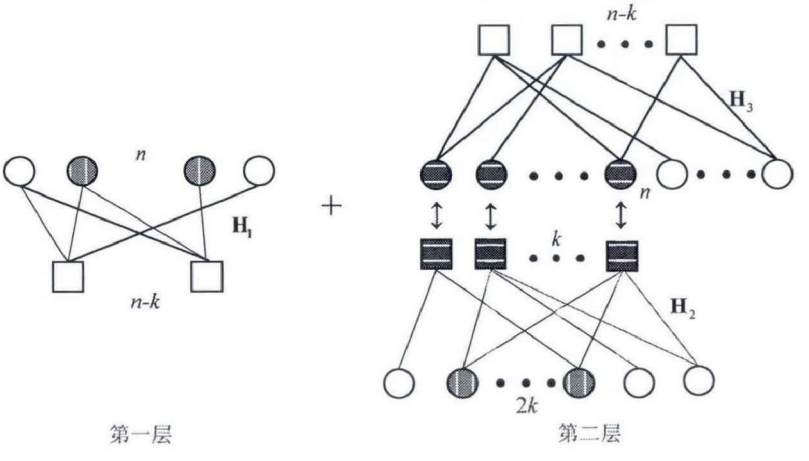


图5.4 双层 LDPC 码的构造图

综上步骤，在整个传输过程中，三个编码信息X_1，X_2和$X_{\mathcal{R}}$被看作三个同等的码

(C)1994-2022 China Academic Journal Electronic Publishing House. All rights reserved. http://www.cnki.net

构成一个双层 LDPC 码。对应的校验矩阵：

$$\mathbf{H}=\begin{pmatrix}\mathbf{H}_1 & \mathbf{0} & \mathbf{0}\\ \mathbf{0} & \mathbf{H}_2 & \mathbf{0}\\ \mathbf{0} & \mathbf{0} & \mathbf{H}_3\end{pmatrix}=\begin{pmatrix}\mathbf{P}_1 & \mathbf{I}_1 & \mathbf{0} & \mathbf{0}\\ \mathbf{0} & \mathbf{I}_2 & \mathbf{P}_2 & \mathbf{0}\\ \mathbf{0} & \mathbf{0} & \mathbf{I}_3 & \mathbf{P}_3\end{pmatrix} \tag{5-19}$$

其中，$\mathbf{H}_1=[\mathbf{P}_1\ \mathbf{I}_1]$是源节点采用$C_0$方式的 LDPC 编码的校验矩阵。$\mathbf{H}_2=[\mathbf{I}_2\ \mathbf{P}_2]$是中继节点采用$C_1$方式的半速率可逆编码的校验矩阵。$\mathbf{H}_3=[\mathbf{I}_3\ \mathbf{P}_3]$是在 MAC 阶段中继节点采用$C_0$方式的 LDPC 编码的校验矩阵。$\mathbf{0}$表示全零矩阵。

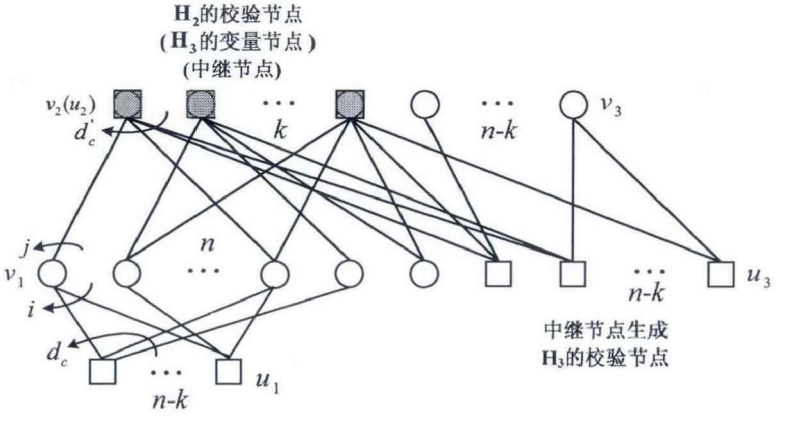


图5.5 双层 LDPC 码的 Tanner 图

根据 Yu 等[148]人的研究结论，上述双层 LDPC 码的 Tanner 图如图 5.5 所示，其中上下两层的子图是由式（5-19）矩阵中的三行确定。图中可以看出，变量节点v_1的度分布$\lambda_{i,j}(i\geq 2,j\geq 0)$是分上下两层，上层的度数$j$表示该变量节点$v_1$在上层子图中连接的边的个数，下层的度数$i$表示该变量节点$v_1$在下层子图中连接的边的个数，且度分布满足：$\sum_{i\geq 2,j\geq 0}\lambda_{i,j}=1$。阴影的变量（校验）节点同时参与了中继节点处$\mathbf{H}_2$和$\mathbf{H}_3$两个校验矩阵的编码。另外$\eta$表示与变量节点$v_1$相连上层的边数占上下两层所有总边数的比例，假设双层 LDPC 码的变量节点v_1上下层校验节点的度分布相对集中分布，上层的k个校验节点的度数为$d_c^{'}$，下层的$n-k$个校验节点的最大度数为d_c，得到:

$$\eta=\frac{kd_c^{'}}{(n-k)\dfrac{1}{\int_0^1\rho(x)\mathrm{d}x}+kd_c^{'}} \tag{5-20}$$

(C)1994-2022 China Academic Journal Electronic Publishing House. All rights reserved. http://www.cnki.net

5.3.3 基于双层 LDPC 码的目的端译码器结构

上述的双层 LDPC 码在构造中，如果采用的半速率可逆码的校验部分$P(I)$在目的节点处被成功译码，仅需要一个简单的可逆过程就可以完全恢复出原始信息位I，而不需要经过复杂的译码过程。同时，由于码C_1的可逆性减少了重传的概率。当校验部分$P(I)$有误时，合并$(\tilde{I},\tilde{P}(I))$进行联合译码，最佳的译码方式是以双层 LDPC 的结构为基础，把三部分编码信息联合起来做迭代译码，三个独立的译码器相互传递 LLR 信息，目的节点处的译码器结构如图 5.6 所示，包含三个变量节点译码器（V_1ND,V_2ND,V_3ND）、上层校验节点译码器（上层 C_2ND，上层 C_3ND）和下层校验节点译码器（下层 C_1ND，下层 C_3ND）。

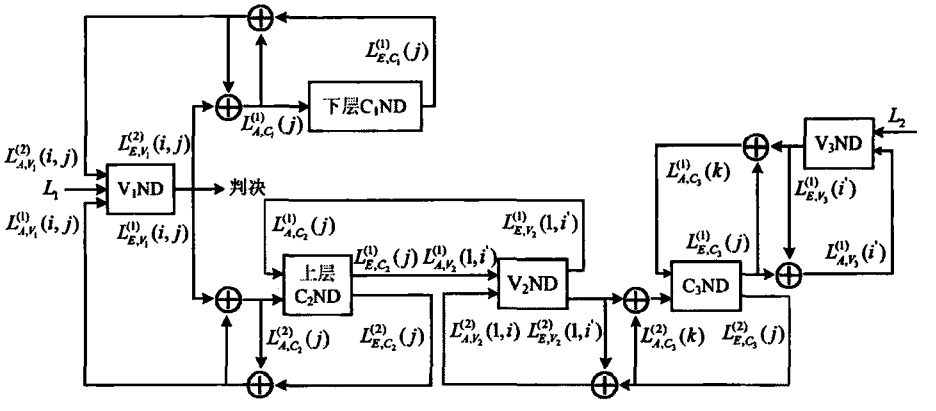


图5.6 目的节点的译码器结构

整个双层 LDPC 码的译码过程即为：所有的变量节点的译码器和上下层的校验节点译码器之间迭代进行消息的更新。每次迭代过程中，目的节点首先从多址接入阶段接收到的信息进行译码，并更新变量节点和校验节点的信息，并分别输出更新信息给其它相连的节点，结合广播阶段接收到的信息进行联合消息的更新，所有的变量节点和校验节点更新完一次信息后，则会判断变量节点 V_1ND 的更新信息，如果正确译码，则译码结束。否则进入下一次迭代过程。

变量节点的消息更新：

（a）当$i\neq 0$时，从度为(i,j)的 V_1ND 输出到下层 C_1ND 的 LLR 消息为：

$$L_{E,V_1}^{(1)}(i,j)=L_1+\sum_{k\neq i}L_{A,V_1}^{(1)}(k,j)+\sum_{k}L_{A,V_1}^{(2)}(i,k) \tag{5-21}$$

其中，L_1是从源节点到目的节点信道接收到的消息初始值的 LLR,且$L_1\sim N(2/\sigma_{SD}^2,4/\sigma_{SD}^2)$；从度为$(i,j)$的 V_1ND 输出到上层 C_2ND 的 LLR 消息为：

(C)1994-2022 China Academic Journal Electronic Publishing House. All rights reserved. http://www.cnki.net

$$L_{E,V_1}^{(2)}(i,j)=L_1+\sum_{k}L_{A,V_1}^{(1)}(k,j)+\sum_{k\neq j}L_{A,V_1}^{(2)}(i,k) \tag{5-22}$$

其中，若$i=0$时，$L_{E,V_1}^{(1)}(i,j)=0$。而输入上层 C_2ND 的 LLR 消息为：

$$L_{E,V_1}^{(2)}(i,j)=\sum_{k\neq j}L_{A,V_1}^{(2)}(i,k) \tag{5-23}$$

（b）从度为$(1,i')$的 V_2ND 输出到下层 C_2ND 的 LLR 消息为：

$$L_{E,V_2}^{(1)}(1,i')=\sum_{k}L_{A,V_2}^{(2)}(1,k) \tag{5-24}$$

其中，V_2ND 没有经过信道传输，信道初始值为 0；从度为$(1,i')$的 V_2ND 输出到上层 C_3ND 的 LLR 消息为：

$$L_{E,V_2}^{(2)}(1,i')=L_{A,V_2}^{(1)}(k,j)+\sum_{k\neq i'}L_{A,V_2}^{(2)}(1,k) \tag{5-25}$$

（c）从度为(i')的 V_3ND 输出到下层 C_3ND 的 LLR 消息为：

$$L_{E,V_3}^{(1)}(i')=L_2+\sum_{k\neq i'}L_{A,V_3}^{(1)}(k) \tag{5-26}$$

其中，L_2 是中继节点到目的节点信道接收到的消息初始值的 LLR,且 $L_2\sim N(2/\sigma_{RD}^2,4/\sigma_{RD}^2)$。

校验节点的消息更新：

（a） 下层 C_1ND 的消息更新：

$$L_{E,C_1}^{(1)}(i)=2\tanh^{-1}\left(\prod_{k\neq i}\tanh\left(\frac{L_{A,C_1}^{(1)}(k)}{2}\right)\right) \tag{5-27}$$

（b）上层 C_2ND 的消息更新：

$$L_{E,C_2}^{(2)}(j)=2\tanh^{-1}\left(\prod_{k\neq j}\tanh\left(\frac{L_{A,C_2}^{(1)}(k)}{2}\right)\times\tanh\left(\frac{L_{A,C_2}^{(1)}(j)}{2}\right)\right) \tag{5-28}$$

(C)1994-2022 China Academic Journal Electronic Publishing House. All rights reserved. http://www.cnki.net

（c）下层 C_2ND 的消息更新：

$$L_{E,C_2}^{(1)}(j)=2\tanh^{-1}\left(\prod_k \tanh\left(\frac{L_{A,C_2}^{(2)}(k)}{2}\right)\right) \tag{5-29}$$

（d）上层 C_3ND 的消息更新：

$$L_{E,C_3}^{(2)}(j)=2\tanh^{-1}\left(\prod_{k\neq j} \tanh\left(\frac{L_{A,C_3}^{(2)}(k)}{2}\right)\times\prod_k \tanh\left(\frac{L_{A,C_3}^{(1)}(k)}{2}\right)\right) \tag{5-30}$$

（e）下层 C_3ND 的消息更新：

$$L_{E,C_3}^{(1)}(j)=2\tanh^{-1}\left(\prod_{k\neq j} \tanh\left(\frac{L_{A,C_3}^{(1)}(k)}{2}\right)\times\prod_k \tanh\left(\frac{L_{A,C_3}^{(2)}(k)}{2}\right)\right) \tag{5-31}$$

通过式(5-21)~(5-31)的计算，我们就可以完成一次迭代译码的消息更新过程。

5.4 采用半速率可逆码的双层 LDPC 码阈值分析

Razaghi 等[148]人研究提出了使用跟踪消息错误概率函数的密度进化方法来优化双层 LDPC 码。由于这个概率密度函数是一个多维函数，计算量大。为了简化运算，本章采用更新消息的均值[156]来优化问题。该方法充分利用了双层 LDPC 码结构的消息的度分布接近于高斯近似。相比于传统非规则 LDPC 码，双层 LDPC 码的结构有很多新特性。将双层 LDPC 码的 Tanner 图等价为一个四层 Tanner 图，如图 5.7 所示。变量节点 v_2 的上层的最大度数 i' 表示该变量节点 v_2 在上层子图中连接的边的个数，下层的度数 1 表示该变量节点 v_2 在下层子图中与校验节点 u_2 一一对应的。变量节点 v_3 的最大度为 i' 表示该变量节点 v_3 在上层子图中与校验节点连接的边的个数。校验节点 u_3 的度数分为 $d_c^{v_2}$ 和 $d_c^{v_3}$，度数 $d_c^{v_2}$ 表示该校验节点 u_3 与变量节点 v_2 相连的边数，度数 $d_c^{v_3}$ 表示该校验节点与变量节点 v_3 相连的边数。其它节点度数的定义如图 5.5。双层密度进化分为：下层节点传输给上层节点的对应上层子图消息的均值，上层节点传输给下层节点对应下层子图消息的均值。使用 $m_v^{(1),(l)}$ 表示第 l 次迭代时变量节点 v 输入下层校验节点更新消息的均值，$m_v^{(2),(l)}$ 表示第 l 次迭代时变量节点 v 输入上层校验节点更新消息的均值。同样，$m_u^{(1),(l)}$ 表示第 l 次迭代时下层校验节点 u 输出的更新消息的均值，$m_u^{(2),(l)}$ 表示第 l 次迭代时上层校验节点 u 输出的更新消息的均值。根据 BP 算法变量节点消息更新规则[156]，可得：

(C)1994-2022 China Academic Journal Electronic Publishing House. All rights reserved. http://www.cnki.net

$$m_{v_1,i,j}^{(1),(l)} = m_{u0} + (i-1)\cdot m_{u_1}^{(1),(l-1)} + j\cdot m_{u_2}^{(2),(l-1)} \tag{5-32}$$

$$m_{v_1,i,j}^{(2),(l)} = m_{u0} + i\cdot m_{u_1}^{(1),(l-1)} + (j-1)\cdot m_{u_2}^{(2),(l-1)} \tag{5-33}$$

$$m_{v_2,1,i'}^{(1),(l)} = i'\cdot m_{u_3}^{(v_2),(l-1)} \tag{5-34}$$

$$m_{v_2,1,i'}^{(2),(l)} = (i'-1)\cdot m_{u_3}^{(v_2),(l-1)} + m_{u_2}^{(1),(l-1)} \tag{5-35}$$

$$m_{v_3,0,i'}^{(2),(l)} = m_{u0}' + (i'-1)\cdot m_{u_3}^{(v_3),(l-1)} \tag{5-36}$$

其中，m_{u0}表示信道的 LLR 均值，$m_{u0}=2/\sigma_c^2$，且σ_c^2是信道的噪声方差。$m_{v_1,i,j}^{(1),(l)}$表示度为(i,j)的变量节点v_1输出到下层校验节点的消息均值，$m_{v_1,i,j}^{(2),(l)}$表示度为(i,j)的变量节点v_1输出到上层校验节点的消息均值。$m_{v_2,1,i'}^{(1),(l)}$表示度为$(1,i')$的变量节点v_2输出到下层校验节点的消息均值，$m_{v_2,1,i'}^{(2),(l)}$表示度为$(1,i')$的变量节点v_2输出到上层校验节点的消息均值。m_{u0}'表示信道的 LLR 均值，$m_{u0}'=2/\sigma_c'^2$，且$\sigma_c'^2$是信道的噪声方差。$m_{v_3,0,i'}^{(2),(l)}$表示度为i'的变量节点v_3输出到上层校验节点的消息均值。

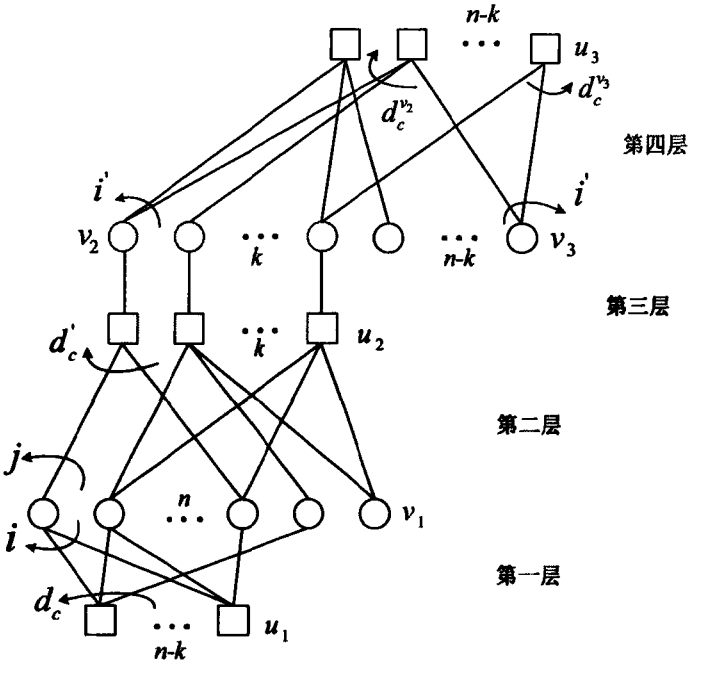


图5.7 双层 LDPC 码等效的四层 Tanner 图

校验节点的消息更新的均值：

(C)1994-2022 China Academic Journal Electronic Publishing House. All rights reserved. http://www.cnki.net

$$m_{u_1}^{(1),(l)}=\sum_{j_1\geq 0}\rho_{j_1}\phi^{-1}\left(1-\left(1-\sum_{i\geq 0,j\geq 0}\lambda_{i,j}\phi(\mathrm{m}_{v_1,i,j}^{(1),(l)})\right)^{j_1-1}\right) \tag{5-37}$$

$$m_{u_2}^{(2),(l)}=\sum_{j_1\geq 0}\rho_{j_1}\phi^{-1}\left(1-\left(1-\sum_{i\geq 0,j\geq 0}\lambda_{i,j}\phi(\mathrm{m}_{v_1,i,j}^{(1),(l)})\right)^{j_1-1}\left(1-\phi(\mathrm{m}_{v_2}^{(1),(l)})\right)\right) \tag{5-38}$$

$$m_{u_2}^{(1),(l)}=\sum_{j_1\geq 0}\rho_{j_1}\phi^{-1}\left(1-\left(1-\sum_{i\geq 0,j\geq 0}\lambda_{i,j}\phi(\mathrm{m}_{v_1,i,j}^{(1),(l)})\right)^{j_1}\right) \tag{5-39}$$

$$m_{u_3}^{(v_2),(l)}=\sum_{j_1\geq 0}\rho_{j_1}\sum_{j_2\geq 0}\rho_{j_2}\phi^{-1}\left(1-\left(1-\sum_{i\geq 0,j\geq 0}\lambda_{i,j}\phi(\mathrm{m}_{v_2,1,i}^{(2),(l)})\right)^{j_1-1}\left(1-\sum_{i\geq 0,j\geq 0}\lambda_{i,j}\phi(\mathrm{m}_{v_3,0,i}^{(2),(l)})\right)^{j_2}\right) \tag{5-40}$$

$$m_{u_3}^{(v_3),(l)}=\sum_{j_1\geq 0}\rho_{j_1}\sum_{j_2\geq 0}\rho_{j_2}\phi^{-1}\left(1-\left(1-\sum_{i\geq 0,j\geq 0}\lambda_{i,j}\phi(\mathrm{m}_{v_2,1,i}^{(2),(l)})\right)^{j_1}\left(1-\sum_{i\geq 0,j\geq 0}\lambda_{i,j}\phi(\mathrm{m}_{v_3,0,i}^{(2),(l)})\right)^{j_2-1}\right) \tag{5-41}$$

其中，$m_{u_1}^{(1),(l)}$表示第l次迭代时下层校验节点u_1输出的更新消息的均值，$m_{u_2}^{(2),(l)}$表示第l次迭代时上层校验节点u_2向变量节点v_1输出的更新消息的均值。$m_{u_2}^{(1),(l)}$表示第l次迭代时下层校验节点u_2向变量节点v_2输出的更新消息的均值，$m_{u_3}^{(v_2),(l)}$表示上层校验节点u_3向变量节点v_2输出的更新消息的均值。$m_{u_3}^{(v_3),(l)}$表示上层校验节点u_3向变量节点v_3输出的更新消息的均值。定义

$$\phi(x)=\begin{cases}1-\dfrac{1}{\sqrt{4\pi x}}\displaystyle\int_R\tanh\left(\frac{u}{2}\right)\exp\left(-\frac{(u-x)^2}{4x}\right), & x>0\\ 1, & x=0\end{cases}$$

根据式（5-32）（5-33），得到度为(i,j)的变量节点v_1的消息更新后的均值：

$$\begin{aligned}m_{v_1}^{(l)}&=\sum_{i\geq 2,j\geq 0}\lambda_{i,j}\cdot\left(\frac{i}{i+j}m_{v_1,i,j}^{(1),(l)}+\frac{j}{i+j}m_{v_1,i,j}^{(2),(l)}\right)\\&=\sum_{i\geq 2,j\geq 0}\lambda_{i,j}\cdot\left(\frac{i}{i+j}\cdot g_{i,j}\left(m_{v_1,i,j}^{(1),(l-1)},m_{v_1,i,j}^{(2),(l-1)}\right)+\frac{j}{i+j}\cdot h_{i,j}\left(m_{v_1,i,j}^{(1),(l-1)},m_{v_1,i,j}^{(2),(l-1)}\right)\right)\end{aligned} \tag{5-42}$$

其中，

(C)1994-2022 China Academic Journal Electronic Publishing House. All rights reserved. http://www.cnki.net

$$g_{i,j}\left(m_{v_1,i,j}^{(1),(l-1)},m_{v_1,i,j}^{(2),(l-1)}\right)$$
$$=\phi\left(m_{u0}+(i-1)\cdot\sum_{j_1\geq 0}\rho_{j_1}\phi^{-1}\left(1-\left[1-m_{v_1,i,j}^{(1),(l-1)}\right]^{j_1-1}\right)+j\cdot\phi^{-1}\left(1-\left[1-m_{v_1,i,j}^{(2),(l-1)}\right]^{d_c'-1}\right)\right)$$

$$h_{i,j}\left(m_{v_1,i,j}^{(1),(l-1)},m_{v_1,i,j}^{(2),(l-1)}\right)$$
$$=\phi\left(m_{u0}+i\cdot\sum_{j_1\geq 0}\rho_{j_1}\phi^{-1}\left(1-\left[1-m_{v_1,i,j}^{(1),(l-1)}\right]^{j_1-1}\right)+(j-1)\phi^{-1}\left(1-\left[1-m_{v_1,i,j}^{(2),(l-1)}\right]^{d_c'-1}\right)\right)$$

度为(i,j)的变量节点v_1的消息均值也可以通过上下两层的变量节点的连接边的比例$1-\eta$和η组合得到：

$$m_{v_1,i,j}^{(l)}=(1-\eta)m_{v_1,i,j}^{(1),(l)}+\eta m_{v_1,i,j}^{(2),(l)} \tag{5-43}$$

根据和积算法中的高斯近似理论[152]，成功译码必须满足条件：

$$\sum_{i\geq 2,j\geq 0}\lambda_{i,j}\cdot\left(\frac{i}{i+j}\cdot g_{i,j}\left(m_{v_1,i,j}^{(1),(l)},m_{v_1,i,j}^{(2),(l)}\right)+\frac{j}{i+j}\cdot h_{i,j}\left(m_{v_1,i,j}^{(1),(l)},m_{v_1,i,j}^{(2),(l)}\right)\right)$$
$$<(1-\eta)m_{v_1,i,j}^{(1),(l)}+\eta m_{v_1,i,j}^{(2),(l)} \tag{5-44}$$

上式近似线性的，可以应用在线性规划问题中。

若已知源节点到中继节点的变量节点v_1的度分布λ_i，校验节点的度d_c'，得到：

$$m_v^{(l)}=\sum_i\lambda_i\cdot\phi\left(m_{u0}+(i-1)\cdot\sum_{j_1\geq 0}\rho_{j_1}\phi^{-1}\left(1-\left[1-m_v^{(l-1)}\right]^{j_1-1}\right)\right) \tag{5-45}$$

在 BP 译码迭代过程中，高斯近似密度进化满足收敛条件：

$$m_v^{(l+1)}=\sum_i\lambda_i\cdot\phi\left(m_{u0}+(i-1)\cdot\sum_{j_1\geq 0}\rho_{j_1}\phi^{-1}\left(1-\left[1-m_v^{(l)}\right]^{j_1-1}\right)\right)<m_v^{(l)} \tag{5-46}$$

整个译码迭代过程中只需要判断变量节点v_1的均值迭代情况。给定源节点到中继节点的信噪比SNR_{SR}，采用式（5-32）-（5-46）迭代估计出双层 LDPC 码的译码阈值。经过L次迭代后，双层 LDPC 码中变量节点v_1的错误概率。

(C)1994-2022 China Academic Journal Electronic Publishing House. All rights reserved. http://www.cnki.net

$$P_e = \frac{1}{2} erfc\left(\sqrt{m_{v_1,i,j}^{(L)}/4}\right) \tag{5-45}$$

其中，当 $m_{v_1,i,j}^{(L)}$ 无穷大时，$P_e \to 0$。

5.5 仿真结果

为了便于同 Cances 等人[150]研究中的双层 LDPC 码-E(B)进行比较，本节仿真中，假设 $h_{SR}^2 = 1.1509, h_{RD}^2 = 1.4489, h_{SD}^2 = 2.2963$，归一化 $\sigma_D^2 = \sigma_R^2 = 1$，$SNR_{RD} = SNR_{SD} + 1$，总码长 $N = 10000$。目标速率 $R = 0.4405$。源节点采用（5000，4405）的 LDPC 码 C_0，度分布为 $\lambda(x)=0.0497x+0.4678x^2+0.0341x^5+0.056x^6+0.2684x^8+0.1240x^9$ 和 $\rho(x) = 0.84331x^{34} + 0.13633x^{35} + 0.00672x^{70} + 0.01364x^{71}$。中继节点采用半速率可逆码（8810，4405）的 LDPC 码 C_1，且度数分布表示为 $d_c^{'} = 9$ 和 $\lambda(x) = 0.2161x + 0.1574x^2 + 0.1543x^4 + 0.0185x^5 + 0.0432x^6 + 0.4105x^{18}$。

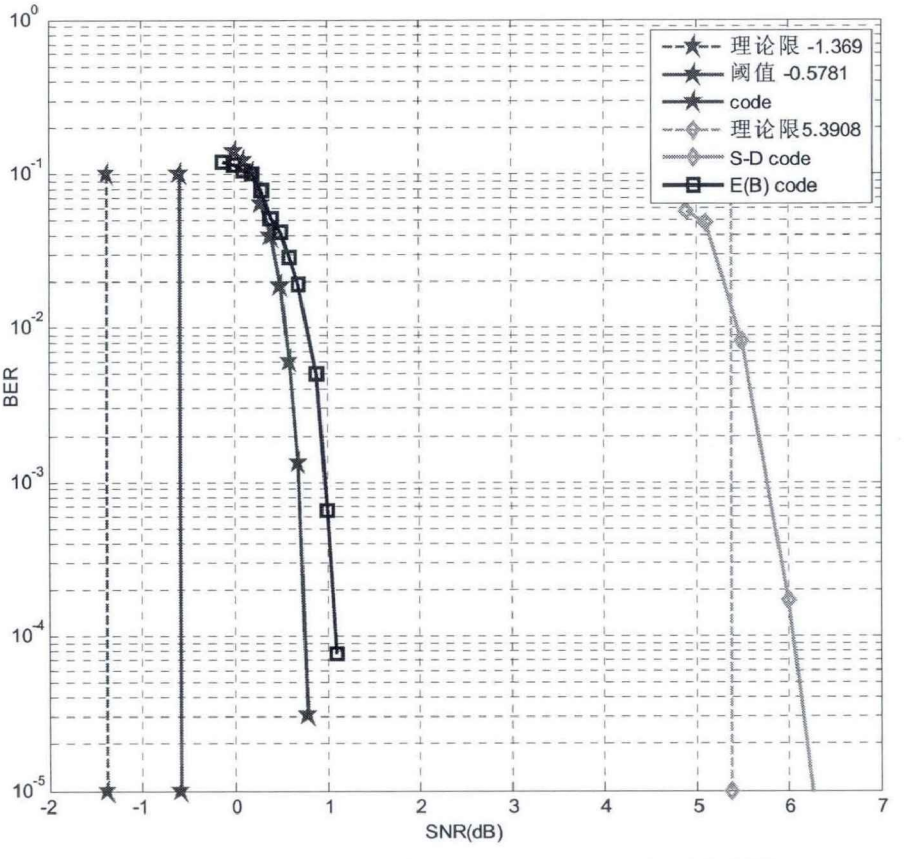


图5.8 AWGN 信道下双层 LDPC 码的误码性能仿真图

图 5.8 给出了在 AWGN 信道时，采用 BPSK 调制对两种不同的双层 LDPC 码的

(C)1994-2022 China Academic Journal Electronic Publishing House. All rights reserved. http://www.cnki.net

误码性能进行仿真的结果。Cances 等[150]人研究的传统双层 LDPC 码仿真中假设在 MAC 阶段中继节点发送给目的节点的校验位部分是可以正确译码的，考虑到实际应用，本文将目的节点两阶段接收到的所有信息进行联合译码。从图中可以看出，采用半速率可逆码的双层 LDPC 码的误码性能在所示的信噪比范围内明显优于 Cances 等[150]人研究的传统双层 LDPC 码，信噪比越高，误码性能提高越明显。这是由于在高信噪比时，只需要源节点到中继节点直接链路上传输信息位部分即可，因而其传输效率明显变高。在低信噪比时，由于基于半速率可逆码的 II 型 HARQ 构造的双层 LDPC 码随着重传次数的增加，纠错能力会不断地增强，但是这样会导致编码效率变低阻碍了性能的提高。所以，低信噪比时，性能没有明显提升。并且该码得到的系统误码性能与译码阈值之间的差距约为 0.5dB，译码阈值与容量限之间的差距小于 1.2dB。

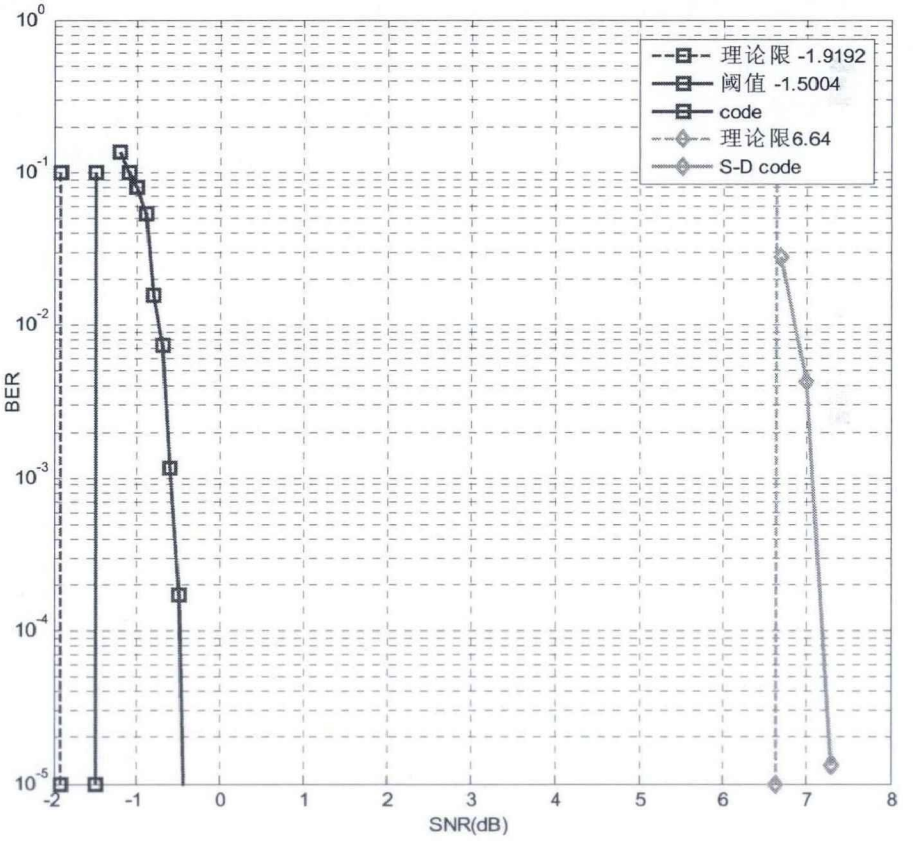


图5.9 AWGN 信道下双层 LDPC 码的误码性能仿真图

图 5.9 给出了在 AWGN 信道时，另一组参数下的双层 LDPC 码的性能。假设 $h_{SR}^2=1.1560, h_{RD}^2=1.4533, h_{SD}^2=2.3120$，归一化 $\sigma_D^2=\sigma_R^2=1$，$SNR_{RD}=SNR_{SD}+1$，总码长 $N=10000$。目标速率 $R=0.4687$。源节点采用（5000，4687）的 LDPC 码 C_0，度分布为 $\lambda(x)=0.02876x+0.47969x^2+0.05277x^5+0.07166x^6+0.23915x^8+0.12797x^9$ 和 $\rho(x)=0.64428x^{64}+0.21202x^{65}+0.03537x^{94}+0.108334x^{96}$。中继节点采用半速率可逆

(C)1994-2022 China Academic Journal Electronic Publishing House. All rights reserved. http://www.cnki.net

码（9374，4687）的 LDPC 码 C_1，且度数分布表示为 $d_c^{'}=9$ 和 $\lambda(x)=0.2161x+0.1574x^2+0.1543x^4+0.0185x^5+0.0432x^6+0.4105x^{18}$。采用 BPSK 调制。考虑到实际应用，本文将目的节点两阶段接收到的所有信息进行联合译码。从图中可以看出，信噪比越高，采用这组参数构造的双层 LDPC 码的误码性能提高越明显。并且该码的误码率性能与译码阈值之间的差距约为 1dB，译码阈值与容量限之间的差距小于 0.5dB。

5.6 结论

本章提出了一种基于半速率可逆码的Ⅱ型 HARQ 的双层 LDPC 码来提高系统误码性能的方法。该方法在重传过程中，校验位和信息位可以交替传输，从而更有效地提高了信息的传输效率。校验位在目的节点处被成功译码，仅需要一个简单的可逆过程就可以完全恢复出原始信息位，而不需要经过复杂的译码过程，避免了再次重传。因此，这种方法中的信息部分和校验部分拥有相同的信息含量，使得每次传输和重传的开销减少到检错码 $C_0\left(n,k\right)$ 中检错部分 $n-k$ 个比特，极大地提高了编码效率。

(C)1994-2022 China Academic Journal Electronic Publishing House. All rights reserved. http://www.cnki.net

第六章 结束语

Meulen 等在 1968 年提出三节点中继信道模型以来，大多数的研究都是通过共用单个用户的天线，形成了一个虚拟的单天线 MIMO 系统。这样，中继系统不仅抑制小区间和小区内的干扰，同时也增加网络的覆盖率、提高了信息的传输速率，对它的研究已经成为无线通信领域一个重要的研究热点。随着技术的进一步发展，国内外许多学者提出了关于中继系统的研究成果，比如：如何提升系统的容量，增加系统的带宽以及资源分配等问题都做了很深入的研究。同时，信道编码技术也取得了举世瞩目的成果，它能有效地提高系统的误码性能，降低译码的错误概率，从而提高了信息的传输效率。将现有的信道编码技术如何合理的应用到中继系统，并设计出很好的信道编码传输方案，将成为无线通信界的一个研究焦点。现有的基于信道编码的中继系统在实际无线通信应用中主要存在中继出错、如何选择中继通信，处理多条路径信噪比不同的等方面的问题，因此怎样能进一步提高中继系统中信道编码技术的性能称为本论文研究的主要目标。

针对上述问题，本文对中继系统的研究背景、容量以及现有的编码技术方案做了较为系统的介绍和分析，主要是对多址接入中继系统的编码设计和传输方案等进行了深入研究，并取得以下成果：

（1） 针对两源单中继系统的模型，提出了一种可以获得最小比特错误概率的网络 LDPC 码速率兼容删余算法,并推导了该算法的译码错误概率。该算法基于网络 LDPC 码的结构特点，以达到译码最小比特错误概率为目标，在网络 LDPC 码的 Tanner 图上搜索出需要删余的变量节点，以获得最优的删余图样。其次，采用改进的差分进化算法对网络 LDPC 码的度分布进行优化。仿真结果表明，改进的算法比现有算法具有明显的性能增益优势，有效地降低了系统的误码率。

（2） 针对多源多中继（Multi-User Multi-Relay, MUMR）系统模型中的中继节点出错这一问题展开研究，提出了一种基于 RS 编码的混合译码转发策略。该策略引入了一个决定中继是否转发信息的阈值。当中继译码后的信息比特的对数似然比大于该阈值时，该信息比特才会被转发。基于最小化比特错误概率，分别对独立协作和混合协作两种策略通过优化方法设计了最佳阈值。仿真结果表明，该方法与假设中继正确译码的系统性能差距极小。

（3） 针对译码转发模式下的三节点中继系统，基于半速率可逆 LDPC 码的 II 型 HARQ，采用叠加组合的方法，构造一种新型结构的双层 LDPC 码，并通过高斯近似密度进化算法对其译码阈值进行了分析。从仿真结果可以看出，同已有的基于传统方式构造的双层 LDPC 码相比，这种基于半速率可逆 LDPC 码的 II 型 HARQ 构造的双

(C)1994-2022 China Academic Journal Electronic Publishing House. All rights reserved. http://www.cnki.net

层 LDPC 码可以使误码性能获得较大的提高。

无线中继通信系统中需要学习和研究的内容相当广泛，本文虽然取得了一点研究成果，但是其实际应用还处于初级阶段。联合网络-信道编码和中继系统的研究内容还很多，就本论文来说，还有很多内容有待于进一步研究，主要包含：

（1） 在研究两源单中继系统的模型时，只是研究了单纯的高斯信道和衰落信道下 BPSK 调制时所提算法的性能。因此，以后可以考虑两种信道下多进制调制时所提算法的误码性能。更进一步设计多源多中继系统模型下，如何设计速率兼容网络 LDPC 码以及它的删余算法等。而且本文考虑的信道都是对称信道，以后可以设计非对称信道下的情况。实际无线通信中，各节点的处理器结构及译码算法不尽相同，完全同步的假设有些勉强。如何把时延等问题考虑进去，设计出更加实用的方案是一个很考验的工作。

（2） 在研究多源多中继系统模型时，假设的是正交信道，如果是非正交信道，信道间的干扰怎么处理，以及用户间的信息泄露和窃听等方面可以作为研究点。文中是采用 RS 码进行设计的，如果换成另外一种信道编码，也许会有更好的误码性能，现有的研究中，还没有采用过这种方式的设计。

（3） 在研究译码转发模式下三节点中继系统时，利用半速率可逆 LDPC 码的可逆性设计了双层 LDPC 码。在半双工传输模式下分析其译码阈值等。为了增强实用性，可以结合 5G 的关键技术同时同频全双工传输模式下分析并设计双层 LDPC 码。为了获得更好的性能，可以采用一些分析码的工具，比如：密度进化、EXIT 图等进一步优化其性能，是未来这个技术研究中一个很好的方向。

总之，由于作者的水平一般，论文中的缺陷和不足在所难免，敬请各位评审老师和专家批评指正。

(C)1994-2022 China Academic Journal Electronic Publishing House. All rights reserved. http://www.cnki.net

附录

附录 A

假设一个点到点的信道中，源节点发送信号比特 x，目的节点接收到的信号 $y=x+n$，其中 n 是均值为 0，方差为 1 的随机变量。目的节点接收到的比特 LLR：$\Lambda=2y/\sigma^2$。当 $|\Lambda|=\Lambda$ 时，$x=1$ 或者 $x=-1$。不妨设 $x=1$。由于 n 的概率密度函数：

$$f_n(a)=\frac{1}{\sqrt{2\pi}\sigma}\exp\left(-\frac{a^2}{2\sigma^2}\right) \tag{A-1}$$

因此，y 的概率密度函数为：

$$f_n(y)=\frac{1}{\sqrt{2\pi}\sigma}\exp\left(-\frac{(y-1)^2}{2\sigma^2}\right) \tag{A-2}$$

Λ 的概率密度函数 ：

$$f_\Lambda(\Lambda)=\frac{1}{\sqrt{2\pi}*\frac{2}{\sigma}}\exp\left(-\frac{\left(\Lambda-\frac{2}{\sigma^2}\right)^2}{2*\frac{4}{\sigma^2}}\right)=\frac{\sigma}{2\sqrt{2\pi}}\exp\left(-\frac{\sigma^2\left(\Lambda-\frac{2}{\sigma^2}\right)^2}{8}\right) \tag{A-3}$$

因此，$|\Lambda|$ 的概率密度函数：

$$\begin{aligned} f_{|\Lambda|}(\Lambda)=\left(F_{|\Lambda|}(\Lambda)\right)' &= \left(\frac{\sigma}{2\sqrt{2\pi}}\int_{-\Lambda}^{\Lambda}\exp\left(-\frac{\sigma^2\left(\Lambda-\frac{2}{\sigma^2}\right)^2}{8}\right)d\Lambda\right)' \\ &=\frac{\sigma\left(e^{-\Lambda}+1\right)}{2\sqrt{2\pi}}\exp\left(-\frac{\left(\sigma^2\Lambda-2\right)^2}{8\sigma^2}\right) \end{aligned} \tag{A-4}$$

其中，$F_{|\Lambda|}(\Lambda)$ 是 $|\Lambda|$ 累计分布函数。

(C)1994-2022 China Academic Journal Electronic Publishing House. All rights reserved. http://www.cnki.net

附录 B

根据概率论知识，得到

$$\begin{aligned}\Pr\left[\left|\Lambda_{x_i}\right|<\Lambda_{S_i0}\right]&=\int_0^{\Lambda_{S_i0}} f_{\left|\Lambda_{x_i}\right|}(\Lambda)d\Lambda\\&=\int_0^{\Lambda_{S_i0}}\frac{\sigma_{S_i,R_j}\left(e^{-\Lambda}+1\right)}{2\sqrt{2\pi}}\exp\left(-\frac{\left(\sigma_{S_i,R_j}^2\Lambda-2\right)^2}{8\sigma_{S_i,R_j}^2}\right)d\Lambda\\&=\frac{1}{2}erf\left(\frac{\sigma_{S_i,R_j}^2\Lambda_{S_i0}+2}{2\sqrt{2}\sigma_{S_i,R_j}}\right)+\frac{1}{2}erf\left(\frac{\sigma_{S_i,R_j}^2\Lambda_{S_i0}-2}{2\sqrt{2}\sigma_{S_i,R_j}}\right)\end{aligned}\tag{B-1}$$

$$\begin{aligned}\Pr\left[\epsilon\left\|\Lambda_{x_i}\right|\geq\Lambda_{S_i0}\right]&=\int_{\Lambda_{S_i0}}^{\infty}P_{e-S_iR_j}\cdot f_{\left|\Lambda_{x_i}\right|}(\Lambda)d\Lambda\\&=\int_{\Lambda_{S_i0}}^{\infty}\frac{1}{1+e^{\Lambda}}\cdot\frac{\sigma_{S_i,R_j}\left(e^{-\Lambda}+1\right)}{2\sqrt{2\pi}}\exp\left(-\frac{\left(\sigma_{S_i,R_j}^2\Lambda-2\right)^2}{8\sigma_{S_i,R_j}^2}\right)d\Lambda\\&=\frac{1}{2}erfc\left(\frac{\sigma_{S_i,R_j}^2\Lambda_{S_i0}+2}{2\sqrt{2}\sigma_{S_i,R_j}}\right)\end{aligned}\tag{B-2}$$

其中， ϵ 表示中继将符号 X_i 判断错误。

附录 C

基于式（4-30）的定义，得到 $T_{S_1S_2\cdots S_M}^x$， $T_{S_1S_2\cdots S_M}^c$ 和 $T_{S_1S_2\cdots S_M}^e$ 的概率：

$$\begin{aligned}&\Pr\left[T_{S_1S_2\cdots S_M}^x\right]=\Pr\left[\left|\Lambda_{x_1}\right|\leq\Lambda_{S_1,0}\cup\left|\Lambda_{x_2}\right|\leq\Lambda_{S_2,0}\cup\cdots\cup\left|\Lambda_{x_M}\right|\leq\Lambda_{S_M,0}\right]\\&=\sum_{i=1,2,\cdots M}\Pr\left(\left|\Lambda_{x_i}\right|\leq\Lambda_{S_i,0}\right)-\sum_{i\neq j\in[1,2,\cdots M]}\Pr\left(\left|\Lambda_{x_i}\right|\leq\Lambda_{S_i,0}\right)\Pr\left(\left|\Lambda_{x_j}\right|\leq\Lambda_{S_j,0}\right)\\&+\sum_{i\neq j\neq k\in[1,2,\cdots M]}\Pr\left(\left|\Lambda_{x_i}\right|\leq\Lambda_{S_i,0}\right)\Pr\left(\left|\Lambda_{x_j}\right|\leq\Lambda_{S_j,0}\right)\cdot\Pr\left(\left(\left|\Lambda_{x_k}\right|\leq\Lambda_{S_k,0}\right)\right)\\&-\cdots-\Pr\left(\left|\Lambda_{x_1}\right|<\Lambda_{S_1,0}\right)\Pr\left(\left|\Lambda_{x_2}\right|<\Lambda_{S_2,0}\right)\cdots\Pr\left(\left|\Lambda_{x_1}\right|<\Lambda_{S_M,0}\right)\end{aligned}\tag{C-1}$$

$$\Pr\left[T_{S_1S_2\cdots S_M}^e\right]=1-\Pr\left[T_{S_1S_2\cdots S_M}^c\right]$$

(C)1994-2022 China Academic Journal Electronic Publishing House. All rights reserved. http://www.cnki.net

$$
\begin{aligned}
\Pr\left[T^{c}_{S_1S_2\cdots S_M}\right] &= \Pr\left[\operatorname{sgn}\left(\Lambda_{x_1}\right)=x_1,\operatorname{sgn}\left(\Lambda_{x_2}\right)=x_2,\cdots\operatorname{sgn}\left(\Lambda_{x_M}\right)=x_M,\right.\\
&\qquad \left.\left|\Lambda_{x_1}\right|>\Lambda_{S_1,0},\left|\Lambda_{x_2}\right|>\Lambda_{S_2,0},\cdots\left|\Lambda_{x_M}\right|>\Lambda_{S_M,0}\right]\\
&= \Pr\left[\operatorname{sgn}(\Lambda_{x_1})=x_1\left|\Lambda_{x_1}\right|>\Lambda_{S_1,0}\right]\cdot\Pr\left[\operatorname{sgn}(\Lambda_{x_2})=x_2\left|\Lambda_{x_2}\right|>\Lambda_{S_2,0}\right]\\
&\quad\cdots\Pr\left[\operatorname{sgn}(\Lambda_{x_M})=x_M\left|\Lambda_{x_M}\right|>\Lambda_{S_M,0}\right]\\
&= \left(1-\int_{\Lambda_{S_1,0}}^{\infty}\frac{f_{|\Lambda_1|}(\Lambda)}{1+e^{\Lambda}}d\Lambda\right)\left(1-\int_{\Lambda_{S_2,0}}^{\infty}\frac{f_{|\Lambda_2|}(\Lambda)}{1+e^{\Lambda}}d\Lambda\right)\\
&\quad\cdots\left(1-\int_{\Lambda_{S_M,0}}^{\infty}\frac{f_{|\Lambda_M|}(\Lambda)}{1+e^{\Lambda}}d\Lambda\right)
\end{aligned}
\tag{C-2}
$$

其中最后一个等式是由于

$$
\Pr\left[\operatorname{sgn}(\Lambda_{x_i})\neq x_i\left|\Lambda_{x_i}\right.\right]=\frac{1}{1+e^{|\Lambda_{x_i}|}} \tag{C-3}
$$

证明见 Sang 等[157]人的研究结果。

(C)1994-2022 China Academic Journal Electronic Publishing House. All rights reserved. http://www.cnki.net

(C)1994-2022 China Academic Journal Electronic Publishing House. All rights reserved. http://www.cnki.net

参考文献

[1] PROAKIS J G. Digital communications[M]. 4th ed. London: McGraw-Hill Companies, Inc., 2001.

[2] SENDONARIS A, ERKIP E, AAZHANG B. User cooperation diversity – part I: system description [J]. IEEE Trans on Comm., 2003, 51 (11): 1927-1938.

[3] LANEMAN J N, TSE D N C, WORNELL G W. Cooperative diversity in wireless networks: Efficient protocols and outage behavior [J]. IEEE Trans. Inf. Theory, 2004, 50(12): 3062-3080.

[4] COVER T, GAMAL A E. Capacity theorems for the relay channel [J]. IEEE Transactions on Information Theory, 1979, 25(5): 572-584.

[5] SENDONARIS A, ERKIP E, AAZHANG B. User cooperation diversity Part Ⅱ: System description [J]. IEEE Transactions on Communications, 2003, 51(11): 1939-1948.

[6] YEUNG R W, LI SY R, CAI N, et al. Network coding theory. Foundation and Trends in Communications and Information Technology [J]. 2005, 2(45):241-381.

[7] VAN DER MEULEN E C. Transmission of information in A T-terminal discrete memoryless channel [D]. Berkeley: Univ. of California. 1968.

[8] VAN DER MEULEN E C. Three-terminal communication channels [J]. Adv. Appl. Probab., 1971, 3(1): 120-154.

[9] VAN DER MEULEN E C. A survey of multi-way channels in information theory: 1961-1977 [J]. IEEE Trans. Inform. Theory, 1977, 23(6): 1-37.

[10] GAMAL A, AREF M. The capacity of the semideterministic relay channel [J]. IEEE Trans. Inform. Theory, 1982, 28(3): 536.

[11] BERROU C, GLAVIEUX A, THITIMAJSHIMA P. Near Shannon limit error-correcting coding and decoding: Turbo-codes: Proc. IEEE International Conference on Communications, 1993 [C]. USA: IEEE, 1993.

[12] GALLAGER R G. Low-density Parity-Check Codes [M]. Cambridge. MA: M. I. T. Press, 1963.

[13] MACKAY D J C, NEAL R M. Good codes based on very sparse matrices: Proc. Cryptography and Coding. 5th IMA Conf., C. Boyd, Ed. 1995 [C]. Berlin: Springer, 1995.

[14] MACKAY D J C, NEAL R M. Near Shannon limit performance of low density parity check codes [J]. Electron. Lett, 1996, 32(18): 1645-1646.

[15] RICHARDSON T J, URBANKE R L. The capacity of low-density parity-check codes under message-passing decoding [J]. IEEE Trans. Inf. Theory, 2001, 47(2): 599-618.

[16] TAROKH V, SESHADRI N, CALDERBANK A R. Space-time codes for high data rate wireless communication: performance criterion and code construction [J]. IEEE Trans. Inform. Theory, 1998, 44: 744-765.

(C)1994-2022 China Academic Journal Electronic Publishing House. All rights reserved. http://www.cnki.net

[17] ANDERS H-M. On the capacity of wireless relaying: 2002 IEEE 56th vehicular technology conference proceedings. Piscataway, NJ [C]. USA: IEEE, 2002.

[18] ANDERS H-M, ZHANG J S. Capacity bounds and power allocation for wireless relay channels [J]. IEEE Transactions on Information Theory, 2005, 51(6): 2020-2040.

[19] KRAMER G, GASTPAR M, GUPTA P. Cooperative strategies and capacity theorems for relay networks [J]. IEEE Trans. Inform. Theory, 2005, 51(9): 3037-3063.

[20] SATO H. Information transmission through a channel with relay [D]. Manoa: University of Hawaii, 1976.

[21] THOMAS J A. Feedback can at most double Gaussian multiple access channel capacity [J]. IEEE Trans. Inform. Theory, 1987, 33(5): 711-716.

[22] ZHANG Z. Partial converse for a relay channel [J]. IEEE Trans. Inform. Theory, 1988, 34(5): 1106-1110.

[23] CHENG R S, VERDU S. Gaussian multiaccess channels with ISI: Capacity region and multiuser waterfilling [J]. IEEE Transactions on Information Theory, 1993, 39(3): 773-785.

[24] RHEE W, JOHN M. Ergodic capacity of multi-antenna gaussian multiple access channels: the 35th Asilomar Conference on Signals Systems and Computers, 2001 [C]. USA: IEEE, 2001.

[25] CAIRE G, SHAMAI S. On the achievable throughput of a multi-antenna gaussian broadcast channel [J]. IEEE Transactions on Information Theory, 2003, 49(7): 1691-1706.

[26] JINDAL N, VISHWANATH S, DUALITY. Achievable rates and sum-rate capacity of gaussian MIMO broadcast channels [J]. IEEE Transactions on Information Theory, 2003, 49(10): 2658-2668.

[27] WANG B, ZHANG J, HOST-MADSEN A. On the capacity of MIMO relay channels, IEEE Trans. Inform. Theory [J]. 2005, 51(1): 21-43.

[28] TANG T, CHAE C B, HEATH R W. On achievable sum rates of a multiuser MIMO relay channel: Proc. IEEE International Symposium on Information Theory，2006 [C]. USA: IEEE, 2006.

[29] KHOJASTEPOUR M A. Capacity bounds for MIMO shared relay channel with half-duplex constraint: Proc. IEEE International Symposium on Information Theory, 2008 [C]. USA: IEEE, 2008.

[30] HUNTER T E, ARIA N. Cooperation diversity through coding: IEEE International Symposium on Information Theory – Proceedings. Piscataway, 2002 [C]. USA: IEEE, 2002.

[31] HUNTER T E, ARIA N. Coded cooperation under slow fading, fast fading, and power control: Conference Record of the ThirtySixth Asilomar Conference on Signals Systems and Computers. Piscataway, NJ [C]. USA: IEEE, 2002.

[32] LI Y, VUCETIC B, TANG Y, et al, Practical distributed Turbo coding through soft information

(C)1994-2022 China Academic Journal Electronic Publishing House. All rights reserved. http://www.cnki.net

relaying: IEEE 16th International Symposium on Personal, Indoor and Mobile Radio Communications, 2005 [C]. USA: IEEE, 2005.

[33] HUA K, JANG W M, NGUYEN L. Convolutional Coding in Cooperative Relay Systems with Spread Spectrum: Fourth International Conference on Networked Computing and Advanced Information Management, 2008 [C].USA:IEEE, 2008.

[34] CHAKRABARTI A, DE BAYNAST A, SABHARWAL A, et al. Low density parity check codes for the relay channel [J]. IEEE J. Select. Areas Commun., 2007, 25(2): 280-291.

[35] HU J, DUMAN T M. Low density parity check codes over wireless relay channels [J]. IEEE Trans. Wireless Commun., 2007, 6(9): 3384-3394.

[36] LI Y, SONG G H, WANG L L. Design of joint network-low density parity check codes based on the EXIT Charts [J]. IEEE Commun. Lett., 2009, 13(8): 600-602.

[37] LI Y, SONG G H, WANG L L. Analysis of the joint network LDPC codes over orthogonal multi-access relay channel [J]. IEEE Commun. Lett., 2010, 14(2): 184-186.

[38] TSAI Y, LIN L C. Optimal power allocation for decode-and-forward cooperative diversity under an outage performance constraint [J]. IEEE Commun. Lett., 2010, 14(10): 945-947.

[39] BHARADIA D, BANSAL G, KALIGINEEDI P, et al. Relay and power allocation schemes for OFDM-based cognitive radio systems [J]. IEEE Trans. Wireless Commun.,2011, 10(9): 2812-2817.

[40] ELFITURI M, HAMOUDA W, GHRAYEB A. Outage probability analysis of distributed coded cooperation for relay channeld: Proc. IEEE Symposium on Personal, Indoor and Mobile R adio Communications, 2007 [C].USA: IEEE, 2007.

[41] ZHENG G, ZHANG Y, JI C, et al. A stochastic optimization approach for joint relay assignment and power allocation in orthogonal amplify-and-forward cooperative wireless networks [J]. IEEE Trans. Wireless Commun., 2011, 10(12): 4091-4099.

[42] HASNA M O, ALOUINI M. Optimal power allocation for relayed transmissions over rayleigh fading channels [J]. IEEE Trans. Wireless Communication, 2004, 3(6): 1999-2004.

[43] KANG X, LIANG Y C, GARG H K. Fading cognitive multiple access channels: outage capacity regions and optimal power allocation [J]. IEEE Trans. Wireless Commun., 2010, 9(7): 2382-2391.

[44] LARSSON E G, CAO Y. Collaborative transmit diversity with adaptive radio resource and power allocation [J]. IEEE Comm. Letters, 9(6): 511-513.

[45] JIA T, XI Z. Cross-layer resource allocation over wireless relay networks for quality of service provisioning [J]. IEEE Journal on Selected Areas in Communications, 2007, 25(4): 645-656.

[46] RIIHONEN T, WERNER S, WICHMAN R. Hybrid full-duplex half-duplex relaying with transmit power adaptation [J]. IEEE Trans. Wireless Commun., 2011, 10(9): 3074-3085.

(C)1994-2022 China Academic Journal Electronic Publishing House. All rights reserved. http://www.cnki.net

[47] ZHAO H, SU W. Cooperative wireless multicast: performance analysis and power/location optimization [J]. IEEE Trans. Wireless Commun., 2010, 9(6): 2088-2100.

[48] YANG Y, GE J, JI Y, et al. Performance analysis and instantaneous power allocation for two-way opportunistic amplify-andforward relaying [J]. Institution of Engineering and Technology, 2011, 5(10): 1430-1439.

[49] LI L, ZHOU X, XU H, et al. Simplified relay selection and power allocation in cooperative cognitive radio systems [J]. IEEE Trans. Wireless Commun., 2011, 10(1): 33-36.

[50] YANG Y, GE J, GAO Y. Power allocation for two-way opportunistic amplify-and-forward relaying over Nakagami-m channels [J]. IEEE Trans. Wireless Commun., 2011, 10(7): 2063-2068.

[51] YAN Z, ZHANG X, WANG W. Exact outage performance of cognitive relay networks with maximum transmit power limits [J]. IEEE Commun. Lett., 2011, 15(12): 1317-1319.

[52] COSTA D, AISSA S. Amplify-and-forward relaying in channel-noise-assisted cooperative networks with relay se lection [J]. IEEE Commun. Lett., 2010, 14(7): 608 -610.

[53] SUN L, MCKAY M R. Opportunistic relaying for MIMO wireless communication: relay selection and capacity scaling laws [J]. IEEE Trans. Wireless Commun., 2011, 10(6): 1786-1797.

[54] LEE I H, KIM D. Outage performance of opportunistic cooperation in amplify-and-forward relaying systems with relay selection [J]. IEEE Commun. Lett., 2012, 16(2): 224-227.

[55] BERES E, ADVE R. Optimal relay-subset selection and time-allocation in decode-and-forward cooperative networks: Proc. IEEE Global Telecommunications Conference, 2009 [C]. USA: IEEE, 2009.

[56] IBRAHIM A S, SADEK A K, SU W, et al. Relay selection in multi-node cooperative communications: when to cooperate and whom to cooperate with ? :GLOBECOM - IEEE Global Telecommunications Conference. Piscataway, NJ [C], USA: IEEE, 2006.

[57] MADAN R, MEHTA N B, MOLISCH A F, et al. Energy-efficient cooperative relaying over fading channels with simple relay selection. IEEE Transactions on Wireless Communications [J].2008, 7(8): 3013-3025.

[58] BLETSAS A, KHISTI A, REED D P, et al. A simple cooperative diversity method based on network path selection [J]. IEEE Journal on Selected Areas in Communications, 2006, 24(3): 659-672.

[59] ELZBIETA B, RAVIRAJ A. On selection cooperation in distributed networks: 2006 40th Annual Conference on Information Sciences and Systems. Piscataway, NJ [C]. USA: IEEE, 2006.

[60] LEE S, HAN M, HONG D. Average SNR and ergodic capacity analysis for opportunistic DF relaying with outage over rayleigh fading channels [J]. IEEE Trans.Wireless Commun., 2009, 8(6): 2807-2812.

(C)1994-2022 China Academic Journal Electronic Publishing House. All rights reserved. http://www.cnki.net

[61] KE F, FENG S, ZHUANG H. Relay selection and power allocation for cooperative network based on energy pricing [J]. IEEE Commun. Lett., 2010, 14(5): 396-398.

[62] ZOU Y, ZHENG B, ZHU J. Outage analysis of opportunistic cooperation over rayleigh fading channels [J]. IEEE Trans. Wireless Commun., 2009, 8(6): 3077-3085.

[63] XU Y, WU P, DING L, et al. Capacity analysis of selection cooperation in wireless ad-hoc networks [J]. IEEE Commun. Lett., 2011, 15(11): 1212-1214.

[64] SIMIC L, BERBER S M, SOWERBY K W. Partner choice and power allocation for energy efficient cooperation in wireless sensor networks: Proc of IEEE ICC, May 2008 [C].USA: IEEE, 2008.

[65] CHOI B G, BAE S J, CHEON K, et al. Relay selection and resource allocation schemes for effective utilization of relay zones in relay-based cellular networks [J]. IEEE Commun. Lett., 2011, 15(4): 407-409.

[66] HADZI-VELKOV Z, ZLATANOV N. Outage rates and outage durations of opportunistic relaying systems [J]. IEEE Commun. Lett., 2010, 14(2): 148-150.

[67] CHIAROTTO D, SIMEONE O, ZORZI M. Spectrum leasing via cooperative opportunistic routing techniques [J]. IEEE Trans. Wireless Commun., 2011, 10(9): 2960-2970.

[68] LEE S, SU W, BATALAMA S, et al. Cooperative decode-and-forward ARQ relaying: performance analysis and power optimization [J]. IEEE Trans. Wireless Commun., 2010, 9(8): 2632-2642.

[69] DEHNIE S, TOMASIN S. Detection of selfish nodes in networks using CoopMAC protocol with ARQ [J]. IEEE Trans. Wireless Commun., 2010, 9(7): 2328-2337.

[70] HASSAN S A, INGRAM M A. The benefit of co-locating groups of nodes in cooperative line networks [J]. IEEE Commun. Lett., 2012, 16(2): 234-237.

[71] LEE S, SU W, Batalama S, et al. Cooperative decode-and-forward ARQ relaying: performance analysis and power optimization [J]. IEEE Trans. Wireless Commun., 2010, 9(8): 2632-2642.

[72] DEHNIE S, TOMASIN S. Detection of selfish nodes in networks using CoopMAC protocol with ARQ [J]. IEEE Trans. Wireless Commun., 2010, 9(7): 2328-2337.

[73] IBRAHIM A S, HAN Z, RAY K J. Distributed energy-efficient cooperative routing in wireless networks: Proc. of IEEE GLOBECOM, 2007 [C]. USA: IEEE, 2007.

[74] CHIAROTTO D, SIMEONE O, ZORZI M. Spectrum leasing via cooperative opportunistic routing techniques [J]. IEEE Trans. Wireless Commun., 2011, 10(9): 2960-2970.

[75] SHIH C F, LIAO W, CHAO H L. Joint Routing and Spectrum Allocation for Multi-Hop Cognitive Radio Networks with Route Robustness Consideration [J]. Wireless Communications IEEE Transactions on, 2011, 10(9): 2940-2949.

(C)1994-2022 China Academic Journal Electronic Publishing House. All rights reserved. http://www.cnki.net

[76] ZHAO B, VALENTI M C. Distributed Turbo Codes: Towards the Capacity of the Relay Channel: IEEE Vehicular Technology Conference (VTC-Fall), 2003 [C]. USA: IEEE, 2004.

[77] CAO Y, VOJCIC B. Cooperative coding using serial concatenated convolutional codes: Proc. IEEE Wireless Communications and Networking Conference, 2005 [C].USA : IEEE, 2005.

[78] WEN H, ZHOU L, ZHANG Z. Cooperative coding using parallel concatenated LDPC codes: Proc. IEEE Information Theory Workshop, 2006 [C].USA : IEEE, 2006.

[79] HU J, DUMAN T. Low density parity check codes over half-duplex relay channels: Proc. IEEE International Symposium on Information Theory, Seattle, 2006 [C]. USA : IEEE, 2006.

[80] RAZAGHI P, YU W. Bilayer low-density parity-check codes for decode-and-forward in relay channels [J]. IEEE Transactions on Information Theory, 2007, 53(10): 3723-3739.

[81] HAUSL C, HAGENAUER J. Relay communication with hierarchical modulation [J]. IEEE Commun. Lett., 2007, 11(1): 64-66.

[82] SEDIQ A B, YANIKOMEROGLU H. Performance analysis of soft-bit maximal ratio combining in cooperative relay networks [J]. IEEE Trans. Wireless Commun., 2009, 8(10): 4934-4939.

[83] LI C, KHOJASTEPOUR M, YUE G, et al. LDPC code design for half-duplex relay networks: Proc. IEEE International Conference on Acoustics, Speech and Signal Processing, 2007 [C].USA : IEEE, 2007.

[84] CAO L, ZHANG J, KANNO N. Relay-coded multi-user cooperative communications for uplink lte-advanced 4G Systems.WiCOM, 2009 [C]. USA, IEEE, 2009.

[85] YOUSSEF R, ALEXANDRE G I A. Distributed Turbo-like codes for multi-user cooperative relay networks, ICC, 2010 [C]. USA: IEEE, 2010.

[86] 黄英，雷菁，魏急波，等. 基于多用户协同的中继编码设计[J]. 电子学报，2012, 40(10): 1971-1975.

[87] LI Y, VUCETIC B, WONG T F, et al. Distributed turbo coding with soft information relaying in multihop relay networks [J]. IEEE Journal on Selected Areas in Communications, 2006, 24(11): 2040-2050.

[88] SNEESSENS H H, LOUVEAUX J, VANDENDORPE L. Turbo-coded decode-and-forward strategy resilient to relay errors, ICASSP, 2008 [C]. USA : IEEE, 2008.

[89] CAI N, YEUNG R. Network coding and error correction: Proc. IEEE Information Theory Workshop, 2002 [C]. USA: IEEE, 2002.

[90] 王新梅, 肖国镇. 纠错码一原理与方法（修订版）[M], 西安：西安电子科技大学出版社, 2001.

[91] LI S Y, YEUNG R, CAI N. Linear network coding [J]. IEEE Trans. Inform. Theory, 2003, 49(2): 371-381.

[92] LI S Y, CAI N, YEUNG R. On theory of linear network coding: Proc. IEEE International

(C)1994-2022 China Academic Journal Electronic Publishing House. All rights reserved. http://www.cnki.net

Symposium on Information Theory, 2005 [C]. USA: IEEE, 2010.

[93] HAUSL C, SCHRECKENBACH F, OIKONOMIDIS I, et al. Iterative network and channel decoding on a Tanner graph: Proc. 2005 IEEE Allerton Conf. Commun., Control, Comput, 2005 [C]. USA: IEEE, 2005.

[94] PENG Y C, YOUSEFI S, KIM I M. On error analysis and distributed phase steering for wireless network coding over fading channels [J]. IEEE Transactions on Wireless Communications, 2009, 8(11): 5639-5649.

[95] KATTI S, RAHUL H, HU W, et al. XORs in the air: practical wireless network coding [J]. IEEE/ACM Transactions on Networking, 2008, 16(3): 497-510.

[96] YANG S, KOETTER R. Network coding over a noisy relay: a belief propagation approach: Proc. IEEE International Symposium on Information Theory, 2007 [C]. USA: IEEE, 2007.

[97] OECHTERING T, BOCHE H. Piggyback a common message on half-duplex bidirectional relaying [J]. IEEE Trans. Wireless Commun.,2008, 7(2): 3394-3406.

[98] XIAO M, AULIN T. Optimal decoding and performance analysis of a noisy channel network with network coding [J]. IEEE Trans. Commun., 2009,57: 1402-1412.

[99] XIAO M, SKOGLUND M. Multiple-user cooperative communications based on linear network coding [J]. IEEE Trans. Commun., 2010, 58: 3345-3351.

[100] AYANOLU E, GITLIN C L, MAZO J E. Diversity coding for transparent self-healing and fault-tolerant communication networks [J]. IEEE Trans. Commun., 1993, 41: 1677-1686.

[101] YEUNG R, ZHANG Z. On symmetrical multilevel diversity coding [J]. IEEE Trans. Inf. Theory, 1999, 45(2): 609-617.

[102] WANG T, GIANNAKIS G B. Complex Field Network Coding for Multiuser Cooperative Communications [J]. IEEE Journal on Selected Areas in Communications, 2008, 26(3): 561-571.

[103] XIAO M, KLIEWER J, SKOGLUND M. Design of Network Codes for Multiple-user Multiple-Relay Wireless Networks [J]. IEEE Trans. Commun., 2012, 60(12): 3755-3766.

[104] BAO X, LI J. A unified channel-cetwork coding treatment for user cooperation in wireless ad-hoc networks: Proc. IEEE International Symposium on Information Theory, 2006 [C]. USA: IEEE, 2006.

[105] BAO X, LI J. Generalized adaptive network coded cooperation (GANCC): a unified framework for network coding and channel coding [J], IEEE Trans. Commun., 2011, 59(11): 2934-2938.

[106] SONG L, YEUNG R W, CAI N. A separation theorem for single-source network coding [J]. IEEE Trans. On Inf. Theory, 2006, 52(5): 1861-1871.

[107] HAUSL C, HAGENAUER J. Iterative network and channel decoding for the two-way relay channel: Proc. ICC, 2006 [C]. USA: IEEE, 2006.

(C)1994-2022 China Academic Journal Electronic Publishing House. All rights reserved. http://www.cnki.net

[108] HAUSL C, SCHRECKENBACH F, OIKONMIDIS I. Iterative network and channel decoding on a tanner graph: Proc.43rd Allerton. Conf. on Communications, Control, and Computing, 2005 [C]. USA: IEEE, 2005.

[109] XUE F, SANDHU S. PHY-layer network coding for broadcast channel with side information: ITW 2007, California, 2007 [C]. USA: IEEE, 2007.

[110] HAUSL C, DUPRAZ P. Joint network-channel coding for the multiple access relay channel: SECON'06, 2006 [C]. USA: IEEE, 2006.

[111] NGUYEN H T, NGUYEN H H, LE-NGOC T. A joint network-channel coding scheme for relay-based communications: CCECE 2007 [C]. USA: IEEE, 2007.

[112] RAZAGHI P, YU W. Bilayer low-density parity-check codes for decode-and-forward in relay channels [J], IEEE Trans. Inform. Theory, 2007, 53(10): 3723-3739.

[113] KRAMER G, VAN WIJINGAARDEN A J. On the white Gaussian multiple access relay channel: Proc. IEEE International Symp. Inf. Theory, 2000 [C]. USA: IEEE, 2000.

[114] HAUSL C, DUPRAZ P. Joint Network-channel coding for wireless relay networks [D]. Munich: Institute for Communications Engineering (LNT), Munich University of Technology (TUM), 2008.

[115] SANKARANARAYANAN L, KRAMER G, MANDAYAM N B. Hierarchical sensor networks: capacity bounds and cooperative strategies using the multiple-access relay channel model: IEEE SECON 2004[C]. USA: IEEE, 2004.

[116] CSISZAR L, KÖRNER J. Information theory: coding theorems for discrete memoryless systems [M]. New York: Academic Press, 1981.

[117] KRAMER G, GUPTA P, GASTPAR M. Information-theoretic multi-hopping for relay networks: International Zurich Seminar on Communications, ETH Zurich, Switzerland, 2004 [C]. USA: IEEE, 2004.

[118] NABAR R U, BÖLCSKEI H, KNEUBÜHLER F W. Fading relay channels: Performance limits and space-time signal design [J]. IEEE JSAC,2004, 22(6): 1099-1109.

[119] HAGENAUER J. Rate-compatible punctured convolutional codes (RCPC codes) and their applications [J]. IEEE Trans on Communication, 1988, 36(4) : 389-400.

[120] HA J, KIM J, KLINC D, et al. Rate-compatible punctured low-density parity-check codes with short block lengths [J]. IEEE trans. Inform. Theory, 2006, 52(2): 728-738.

[121] HA J, KIM J, KLINC D, et al. Rate-compatible puncturing of low-density parity-check codes [J], IEEE trans. Inform. Theory, 2004, 50(11): 2824-2836.

[122] ZHOU L, BAI B M, XU M. Design of Nonlinary Rate-compatible LDPC Codes Utilizing Bit-wise Shortening Method [J] . IEEE Communication Letters, 2010, 14(10): 963-965.

(C)1994-2022 China Academic Journal Electronic Publishing House. All rights reserved. http://www.cnki.net

[123] 周林, 白宝明, 邵军虎, 等. 多元LDPC码的速率兼容技术研究 [J]. 西安电子科技大学学报, 2011, 38(1): 147-152.

[124] 郭凯, 陈彦辉, 李建东. 一种对奇偶校验比特按组删余的速率兼容编码 [J]. 西安电子科技大学学报, 2009, 36(5): 782-787.

[125] COVER T, GAMAL A E. Capacity theorems for the relay channel [J]. IEEE Trans. Inf. Theory, 1979, 25: 572-584.

[126] NOSRATINIA A, HUNTER T E, HEDAYAT A. Cooperative Communication in Wireless Networks [J]. IEEE Communications Magazine, 2004, 42(10): 74-80.

[127] LANEMAN J, TSE D, WORNELL G. Cooperative Diversity in Wireless Networks: Efficient Protocols and Outage Behavior [J]. IEEE Transactions on Information Theory, 2004, 50(12): 3062-3080.

[128] ZHAO B, VALENTI M C. Distributed Turbo Codes: Towards the Capacity of the Relay Channel: IEEE Vehicular Technology Conference (VTC-Fall), 2003 [C]. USA: IEEE, 2004.

[129] SNEESSENS H H, LOUVEAUX J, VANDENDORPE L. Turbo-coded decode-and-forward strategy resilient to relay errors: Proc. IEEE Int. Conf. Acoustics, Speech and Signal Processing ICASSP 2008 [C]. USA: IEEE, 2008.

[130] LI Y, VUCETIC B, WONG T, et al. Distributed Turbo Coding with Soft Information Relaying in Multihop Relay Networks [J]. IEEE Journal on Selected Areas in Communications, 2006, 24(11): 2040-2050.

[131] KHUONG H V, KONG, H Y. LLR-based decode-and-forward protocol for relay networks and closed-form ber expressions [J]. IE-ICE Trans.Fundamentals, 2006, E89A: 1832-1841.

[132] LI S, YEUNG R W, CAI N. Linear network coding [J]. IEEE Trans. Inf. Theory, 2003, 49(2): 371-381.

[133] KOETTER R, MDARD M. An algebraic approach to network coding [J]. IEEE/ACM Trans. Netw., 2003, 11(5): 782-795.

[134] HAUSL C, SCHRECKENBACH F, OIKONOMIDIS I, et al. Iterative network and channel decoding on a Tanner graph: Proc. 2005 IEEE Allerton Conf. Commun., Control, Comput.2005 [C]. USA: IEEE, 2005.

[135] PENG A Y C, YOUSEFI S, KIM L M. On error analysis and distributed phase steering for wireless network coding over fading channels [J]. IEEE Trans. Wireless Commun., 2009, 8(11): 5639-5649.

[136] XIAO M, AULIN T. Optimal decoding and performance analysis of a noisy channel network with network coding [J]. IEEE Trans. Commun.,2009, 57: 1402-1412.

[137] XIAO M, SKOGLUND M. Multiple-user cooperative communications based on linear network

(C)1994-2022 China Academic Journal Electronic Publishing House. All rights reserved. http://www.cnki.net

coding [J]. IEEE Trans. Commun., 2010, 58: 3345-3351.

[138] AYANOGLU E, CHIH-LIN I, GITLIN R D, et al. Diversity coding for transparent self-healing and fault-tolerant communication networks [J]. IEEE Transactions on Communications, 1993, 41(11): 1677-1686.

[139] YEUNG R W, ZHANG Z. On symmetrical multilevel diversity coding [J]. Information Theory IEEE Transactions on, 1999, 45(2): 609-621.

[140] MARIC I, GOLDSMITH A, MEDARD M. Analog network coding in the high-snr regime, Wireless Network Coding Conference, 2010 [C]. USA: IEEE, 2010.

[141] XIAO M, SKOGLUND M. Multiple-user cooperative communications based on linear network coding [J]. IEEE Transactions on Communications, 2010, 58(12): 3345-3351.

[142] BERLEKAMAP E R. Algebraic coding theory [M]. New York: McGrw-Hill, 1968.

[143] CHIEN R. Cyclic decoding procedures for Bose-Chaudhuri-Hocquenghem codes [J]. Information Theory IEEE Transactions on, 1964, 10(4): 357-363.

[144] ZHENG Z, DUMAN T M. Capacity approaching Turbo coding for half duplex relaying: Proc. International Symposium Inform. Theory, 2005 [C]. USA: IEEE, 2005.

[145] ZHENG Z, DUMAN T M. Capacity-approaching Turbo coding and iterative decoding for relay channels [J]. IEEE Trans. Commun., 2005, 53(11): 1895-1905.

[146] HA J, KIM J, MCLAUGHLIN S W. Rate-compatible puncturing of low-density parity-check codes [J]. IEEE Trans. Inform. Theory, 2004, 50(11): 2824-2836.

[147] HU J, DUMAN T M. Low density parity check codes over wireless relay channels [J]. IEEE Trans. Wireless Commun., 2007, 6: 3384-3394.

[148] RAZAGHI P, YU W. Bilayer low-density parity-check codes for decode-and-forward in relay channels [J]. IEEE Transactions on Information Theory, 2007, 53(10): 3723-3739.

[149] CHAKRABARTI A, DE BAYNAST A, SABHARWAL A, et al. Low density parity check codes for the relay channel [J]. IEEE J. Select. Areas Commun., 2007, 25: 280-291.

[150] CANCES J P, MEGHDADI V. Optimized low density parity check codes designs for half duplex relay channels [J]. IEEE Transactions on Wireless Communications, 2009, 8(7): 3390-3395.

[151] LIN S, YU P S. A hybrid arq scheme with parity retransmission for error control of satellite channels [J]. IEEE Transactions on Communications, 1982, 30(7): 1701-1719.

[152] KOU Y, LIN S, FOSSORIER M. Low density parity check codes based on finite geometries: a rediscovery: Proc. IEEE Intl. Symp. Inform. Theory, 2000 [C]. USA: IEEE, 2000.

[153] MANDELBAUM D M. An adaptive-feedback coding scheme using incremental redundancy [J]. IEEE Transactions on Information Theory, 1974, 20(3): 388-389.

[154] METZNER J J. Improvements in block-retransmission schemes [J]. Communications IEEE

(C)1994-2022 China Academic Journal Electronic Publishing House. All rights reserved. http://www.cnki.net

Transactions on, 1979, 27(2): 524-532.

[155] ANCHETA T C. Convolutional parity check automatic repeat request: IEEE Intl. Symp. Inform. Theory, 1979 [C]. USA: IEEE, 1979.

[156] CHUNG S Y, RICHARDSON T J, URBANKE R L. Analysis of sum-product decoding of low-density parity-check codes using a Gaussian approximation [J]. IEEE Transactions on Information Theory, 2001, 47(2): 657-670.

[157] KIM S W, KIM E Y. Optimum receive antenna selection minimizing error probability: WCNC2003 [C]. USA: IEEE, 2003.

(C)1994-2022 China Academic Journal Electronic Publishing House. All rights reserved. http://www.cnki.net

(C)1994-2022 China Academic Journal Electronic Publishing House. All rights reserved. http://www.cnki.net

致谢

问道于西电，九载即逝，叹时光之荏苒。拙作新成，感慨油然，借此片方，畅吐心声，聊表谢忱。

吾之恩师李颖先生，治学严谨，学识渊博，行端表正，身体力行。乍入师门，懵懂愚钝，先生于吾之学业，循循善诱，言传身教以授业解惑也。文之选题、资料、撰写、以至定稿，皆得先生悉心指导。先生于吾，犹如长风之于鲲鹏，非其托举而不能翱翔九天也，铭记师恩，谢无尽焉。其夫郭君旭东，温恭和蔼，平易近人，与先生天作之合也。二君于吾之生活，关怀备至，事无巨细。其子亮，生性活泼，尝解吾辈之沉闷也。祝先生阖家幸福，工作顺利。

有良师谓白宝明者，翩翩鸿儒，利物不争，其学术造诣之高深，举止谈吐之幽默，为吾辈效法之楷模也。先生于吾求学间，指导良多，受益匪浅；更有良师谓林舒者，信道编码之泰斗，先生身居加州，不辞舟车劳顿，远洋来华，以其学识博吾辈之孤陋，蔚为大家矣。祝白林二君身体安康，万事顺意。并有益友刁君秋菊，温文尔雅，倍具才华，尝解吾之心垒，情比姐妹，身在彼岸，多自珍重，祝福婚姻美满，事业有成。

另有信道编码室之师者，谓孙蓉、刘景伟、孙岳、刘景美、郑贱平、车书玲、童胜、李卓、邢丽娟、王云江；有友者，谓邵军虎、林伟、周林、施玉晨、崔俊云、宋光辉、张博、李勇、李琪、岳婧，同游学于信道编码之宇海，切磋之谊，当为后生所追忆也。

同门博士者，谓苏玉萍、谓刘洋、谓吴道龙、谓杨伟强、谓于晓璞、谓刘雷、谓池育浩、谓刘敬敏、谓吕治国，谓孟茁，谓郝伟旭，朝夕相处、同畅于食堂饭馆以大快朵颐，并行于操场林荫以追逐嬉戏，峥嵘岁月，永生铭记。诸君各擅所长，皆菁英栋梁之才也，更于拙作之锤炼期，倾力相助，屡得金石珠玉之言，方得玉成。同门之谊，堪比手足，吾甚幸哉。

另有硕期之同窗者，谓周宁、李海强、张元龙、吴华、王丽丽、路姗，皆古道热肠之士，尝逗趣于吾之低落时，鼓励于吾之消沉时，手援于吾之急难时。聚散无常，盛况难再，祝福诸君生活幸福。并有同门硕士者，谓侯伟、王军龙、程浪涛、张冠荣、马葳、周微、顾嘉辉、李琳、武丽琴、宋宣霈、张景鹏、马琰、齐赞、高耀龙、董兰、张茜、刘红、皮爱霞、高原、李京娥、马建民、曲莉莉、杨依灿、张辉，八仙过海，神通各异，朝气蓬勃，课题组气氛活跃之源也，期诸君学业有成、光耀师门。

有妹若淑雅，有弟若登峰者，相伴成长，嬉笑怒骂，皆成亲情，有汝幸甚。外婆高寿，尝嘘寒问暖，于吾之琐事，无不挂怀，祝外婆笑口常开，永享天伦。有舅谓李非、谓李雷，职海奔波，尝导吾以得安身立命之本，更示吾以康庄之通途，祝二君骏

(C)1994-2022 China Academic Journal Electronic Publishing House. All rights reserved. http://www.cnki.net

业肇兴，生活美满。各路亲朋，不曾一一道出，感恩有汝，吾甚幸哉。

特感恩于吾之父母，赐吾以生命，含辛茹苦，养吾成年，教吾成人。求学路漫漫，高堂泪沾襟，其默默关怀催吾负重而前行。今出师而立，必常怀乌鸟之情、反哺之心，供奉赡养，自当不在话下。并感恩于吾之公婆，待吾如己出，顾吾生活于无微，让吾任性于无度，以成家和事兴之气也。惟祈父母公婆安康顺意、福寿延绵。

至此，尤感恩于吾夫李君晓明，离鲁弃吴而入秦，与吾相识相知而相爱，终成眷属以成天公之美意也。风雨同舟，携手相伴，一生有汝，此生无憾。爱女奔奔，天之垂赐，一咿一嚶皆慰吾心，其乐融融。怜其年纪尚幼，每欲起身而不放，尝紧抱于吾身，奈何战鼓雷雷而闪退，不觉潸然而泪下也。谨以此文赠予爱女，愿其平安、健康、快乐，茁壮成长。

恩长笔短，尚有诸君未曾一一表出，在此一并谢过，言辞有尽，谢意无穷。最后，再以吾之诚意，拜谢于恩师、双亲、夫君及诸亲朋好友。人生须臾间，吾辈定当励志以奋发，上孝父母，下教子女，与诸君共勉。

丙申年四月于陕西西安高新

(C)1994-2022 China Academic Journal Electronic Publishing House. All rights reserved. http://www.cnki.net

作者简介

1. 基本情况

王静怡，女，陕西榆林人，1984 年 5 月出生，西安电子科技大学通信工程学院通信与信息系统专业 2010 级博士研究生。

2. 教育背景

2002.08～2006.07 西安邮电大学，本科，专业：通信工程
2007.08～2010.03 西安电子科技大学，硕士研究生，专业：通信与信息系统
2010.03～ 今　　西安电子科技大学，博士研究生，专业：通信与信息系统

3. 攻读博士学位期间的研究成果

3.1 发表学术论文

[1] Jingyi Wang, Shuling Che，Ying Li and Junlong Wang. Optimal Design of Joint Network LDPC Codes over Orthogonal Multiple-Access Relay Channel [J]. Int. J. Grid Util. Comput,UK.,2016,7(2): 68-74.(EI:20160201779608)

[2] Jingyi Wang, Ying Li，Daolong Wu and Baoming Bai. A Distributed RS code based hybrid Forward strategy for Multiple-Access Relay Channel [J]. Cluster Computing.(EI 已录用)

[3] 王静怡，李颖，孙岳. 适用于网络 LDPC 码的速率兼容算法 [J]. 西安电子科技大学学报，2013, 40(2): 13-17.（EI:20131816300822）;

[4] Jingyi Wang, Shuling Che, Ying Li and Junlong Wang. Optimal Design of the Joint Network LDPC Codes over Orthogonal Multi-Access Relay Channel. 2013 5th International Conference on Intelligent. 2013 [C]. USA: IEEE, 2013. (EI:20135117090330)

3.2 参与科研项目及获奖

[1] 新一代宽带无线移动通信国家工信部科技重大专项,面向 IMT-Advanced 协作中继的网络编码技术, 2010 年 1 月-2013 年 12 月,已结题,中继系统中的网络编码设计。

(C)1994-2022 China Academic Journal Electronic Publishing House. All rights reserved. http://www.cnki.net

[2] 新一代宽带无线移动通信国家工信部科技重大专项, IMT-Advanced 开放性关键技术研究, 2007 年 1 月-2010 年 12 月,已结题,信道编码调制与网络编码。

[3] 国家 973 计划项目，高移动性宽带无线通信网络重点理论基础研究，2012 年 1 月-2016 年 8 月，未结题，高能效调制信号设计与编码调制理论

[4] 国家自然科学基金，无线中继网络中的联合信道-网络编码理论与技术研究，2011 年 1 月-2013 年 12 月，已结题，网络编码与信道编码的联合设计。

(C)1994-2022 China Academic Journal Electronic Publishing House. All rights reserved. http://www.cnki.net

附录6

尊敬的陕西省科技厅：

本人是西安石油大学教师，本人实名举报我校王静怡老师存在多处涉嫌学术不端情况，王静怡老师在学术研究以及职称评审中学术不端、违反公平竞争的基本原则，并且王静怡老师主持科技厅在研项目一项，因此，本人向科技厅实名举报。

举报材料的内容包括王静怡老师的学习、工作经历、承担科研项目情况、项目申报及成果发表中涉嫌存在学术不端的情况。

1.王静怡老师的教育经历为本、硕、博均为通信工程。具体学习经历为：

2010/03~2016/06，西安电子科技大学，通信与信息系统，博士

2007/09~2010/03，西安电子科技大学，通信与信息系统，硕士

2002/09~2006/07，西安邮电大学，通信工程，学士

具体工作经历为：

2016/07~至今，西安石油大学计算机学院，教师

2.王静怡老师主持的 3 项科研项目及相应项目的研究内容为：

（1）无线 MARC 系统中联合网络-信道编码的优化设计研究（18JK0626），陕西省教育厅基础研究项目，2018.01-2021.04，2 万，结题

研究内容：本项目针对无线通信应用中多址接入中继信道（MARC）模型，研究联合网络-信道编码的优化设计方法。通过对理想信道下半速率可逆码和速率兼容网络 LDPC 码删余算法的优化设计，基于 RS 码和 LDPC 码的中继混合译码转发策略，研究非理想信道下适用于多源 MARC 系统的最佳阈值优化方法，以改善目的节点的比特错误概率（Bit Error Ratio,BER）性能。通过本项目的研究，将会为联合网络-信道编码优化设计提供理论支撑，研究成果可应用于未来无线通信系统中。研究内容包含以下三点：①提出一种叠加 LDPC 编码方法，设计新型高斯近似密度进化算法。②系统研究联合网络-信道编码理论及设计算法。③充分利用信道统计特性设计软输出迭代译码算法。

（2）基于信息物理融合的智能油田监控系统关键技术研究（2020GY-038），陕西省科技厅重点研发计划项目一般项目-工业领域，2019.01-2020.12/2020.01-2021.12，5 万，在研

研究内容：本研究基于信息物理融合，拟采用信道编码、干扰消除等无线通信相关技术建立智能油田监控系统，以更好满足油田现场对数据采集、远程传输和实时控制等应用需求。具体为：首先，针对油田信息物理监控系统安全威胁，以保障系统安全运行为目的，提出安全防护措施；然后，针对油田信息物理系统的数据传输可靠性问题，基于信道编码、干扰消除和中继技术分别设计传输方案，并进一步对所提方案不同阶段以及不同通信模型的性能展开深入研究，以改善不同传输方案下系统的可靠性能；最后，采用 BP 神经网络的数据训练方法对采集到的数据流进行实时监测，提高预警的时效性。

（3）基于遥感大数据的汾渭平原空气质量时空特征及其驱动力研究与模拟（62002286），国家自然科学基金委员会青年基金项目，2021.01-2023.12，1/1，24 万，在研

研究内容：未知。

3. 王静怡在省科技厅项目申请、实施中存在的涉嫌学术不端行为分别有：

（1）项目申请中列入申请书的论文 7 篇中有 6 篇存在涉嫌重复发表及 1 篇提供虚假信息。

王静怡老师在基于信息物理融合的智能油田监控系统关键技术研究

（2020GY-038）项目申报中列入申请书的论文有：

[1] Jingyi Wang*, Shuling Che, Ying Li and Junlong Wang, Optimal design of Joint network LDPC Codes over Orthogonal Multiple-Access Relay Channel. International Journal of Grid and Utility Computing, UK., 2016, 7(2): 68-74.

[2] Jingyi Wang*, Ying Li, Daolong Wu and Baoming Bai. A distributed RS code based hybrid forward strategy for MARC. Gummi Fasern Kunstst, 2016, 69(14): 706-713.

[3] 王静怡, 李晓明*. 近 20a 中国耕地数量变化趋势及其驱动因子分析. 中国农业资源与划分. 2018.（已录用，等待刊出）

[4] 王静怡*, 李颖, 孙岳. 适用于网络 LDPC 码的速率兼容算法. 西安电子科技大学学报,2013, 40(2): 13-17.

[5] Jingyi Wang, Xiaoming Li*.Research on the changing trend of farmland area in China and its driving factors from 1996 to 2016. IOP Conference Series: Earth and Environmental Science(EES), 6 月 22 日~24 日, 珠海, 中国, 2018.

[6] Jingyi Wang*, Shuling Che, Ying Li and Junlong Wang. Optimal design of the joint network LDPC codes for half-duplex coopreative multi-Access relay channel. 2013 5th International Conference on Intelligent. 2013. USA: IEEE, 622-625.

[7] 王静怡*, 李颖, 孙岳. 速率兼容网络 LDPC 码的设计. 第十七届全国青年通信学术年会, 7 月 29 日~31 日, 秦皇岛, 中国, 2013

列入申请书的论文存在 6 篇次重复表及 1 篇提供虚假信息的涉嫌学术不端情况：①文章[1]和文章[6]属于英文一稿双发，文章[6]2013 年发表，文章[1]2016 年发表。文章[1]首页虽有标注了文章[1]为文章[6]的改写和扩展，但两篇文章整体内容、结构、图表以及结论雷同，且整段整段的文字写法均完全一样，雷同率至少超过 60%以上，属于明显不符合成果发表规范。

另文章[6]“Optimal design of the joint network LDPC codes for half-duplex coopreative multi-Access relay channel”在 EI 数据库中经过检索不存在，后通过文章发表时间、页码范围搜索发现文章[6]可能为：

Jingyi Wang, Shuling Che, Ying Li, Optimal design of the Joint network LDPC Codes over Orthogonal Multiple-Access Relay Channel. 2013 5th International Conference on Intelligent Networking and Collaborative Systems, 2013. XI’AN: IEEE, 622-625。另于王静怡 2016 年 4 月博士论文末尾攻读博士期间论文成果（博士论文 99 页）未发现会议论文“Optimal design of the joint network LDPC codes for half-duplex coopreative multi-Access relay channel”而是会议论文“Optimal design of the Joint network LDPC Codes over Orthogonal Multiple-Access Relay Channel”。由此可见王静怡老师为避免论文同名易被发现一稿双发，将文章[6]名称由“Optimal design of the Joint network LDPC Codes over Orthogonal Multiple-Access Relay Channel”篡改成了“Optimal design of the joint network LDPC codes for half-duplex coopreative multi-Access relay channel”，但在文章[1]的首页王静怡老师准确写出 2013 年会议论文名称为“Optimal design of the Joint network LDPC Codes over Orthogonal Multiple-Access Relay Channel”。王静怡将会议名称由“2013 5th International Conference on Intelligent Networking and Collaborative Systems”改为了“2013 5th International Conference on Intelligent”，会议举办地由

“XI’AN”改为了“USA”，可见此番篡改论文名称、会议名称、会议举办地属于刻意为之。

②文章[5]和[3]属于中英文一稿双发，文章[5]英文先于 2018 年在国内举办的国际会议发表，文章[3]为 2019 年在国内中文期刊发表。文章[3]中对文章之前已经发表情况未做任何说明，也没有引用[5]。王静怡第一次重复发表始于 2013 年，2016 年第二次重复发表时在文章[1]的首页还标注了此论文曾经发表，此次为改写扩展的说明。但在 2019 年第三次重复发表时，却在文章[3]中对文章[5]曾经发表过没有做任何说明，这说明王静怡重复发表是明知故犯。为了避免被易于发现一稿双发，文章[5]的名字“Research on the changing trend of farmland area in China and its driving factors **from 1996 to 2016**”在文章[3]再次重复发表时改成了“**近 20 年**中国耕地数量变化趋势及其驱动因子分析 ”。文章[3]在文章[5]的 20 篇参考文献基础上仅增加了 3 篇参考文献，文章[5]和[3]雷同率超过 90%，文章[3]和[5]整体内容、结构、图表以及结论高度雷同，仅仅在第一部分介绍部分有少量差异，其余均雷同，雷同率超过 90%。

③文章[4]和[7]属于中文一稿双发。文章[4]于 2013 年 4 月于西安电子科技大学学报上发表，文章[7]于 2013 年 7 月底在会议上发表。文章[4]和[7]完全雷同。

（2）基于信息物理融合的智能油田监控系统关键技术研究（2020GY-038）项目执行中，王静怡老师在成果发表中存在研究成果与项目申请书研究内容不一致、滥标项目号等问题。

截止目前，标注省基金（2020GY-038）论文总计有 9 篇，其中文章[8]研究土地盐碱化与项目申请书研究内容完全不一致，为一作非通讯作者论文；文章[9]为一般期刊，文章[10]为国内举办的国际会议论文，仅这 2 篇论文与项目申请书研究内容一致；文章[11]-[12]为标注省基金（2020GY-038）王静怡老师有署名论文 2 篇，论文内容与项目申请书研究内容不一致；文章[13]-[16]为标注省基金（2020GY-038）王静怡老师无署名论文 4 篇，论文内容与项目申请书研究内容不一致。在基于信息物理融合的智能油田监控系统关键技术研究（2020GY-038）项目执行已 4 年的时间里，在标注省基金（2020GY-038）的 9 篇论文中，仅有 1 篇会议论文和 1 篇一般期刊论文属于王静怡老师一作，其他 7 篇论文内容均与（2020GY-038）申请书研究内容不一致。

一作非通讯作者的论文：

[8]Wang Jingyi, Li Xiaoming*.Comparison on quantitative inversion of characteristic ions in salinized soils with hyperspectral based on support vector regression and partial least squares regression[J].European Journal of Remote Sensing, 2020, 53 (1): 340-348.(标注国家自然科学基金青年基金项目 620022860，陕西省科技厅重点研发计划项目 2020GY-038，陕西省教育厅基础研究项目 18JK0626）权威期刊，根据王静怡博士论文致谢（博士论文 98 页）判断通信作者李晓明疑为王静怡丈夫，其研究方向恰为土地整治

标注省基金的一作论文：

[9]王静怡,孙旭华,卜宏博，付旭.一种面向油田的信息物理融合系统模型[J].石化技术,2020,27(08):28+74.一般期刊（标注陕西省教育厅基础研究项目 18JK0626,陕西省科技厅重点研发计划项目 2020GY-038）

[10]Wang Jingyi*,Guo Jiahang,Cheng Xia, Zhao Rui.Research on Safety and Reliability of Intelligent oilfield monitoring system based on Cyber-Physical System[C],2021 IEEE 6th International Conference on Intelligent Computing and

Signal Processing（ICSP）,pp:921-924.（标注陕西省教育厅基础研究项目 18JK0626, 陕西省科技厅重点研发计划项目 2020GY-038）

标注省基金的参与署名论文：

[11]Hu Hongtao*, Zhang Qian,Wang Jingyi*. Detection of Key Targets in Video Logging Based on Convolutional Neural Network,2021 IEEE 6th International Conference on Computer and Communication Systems,pp:254-257.（标注陕西省科技厅重点研发计划项目 2020GY-038）

[12]Hu Hongtao*, Wang Kang, Wang Jingyi.Application of Deep Residual Network in Fault Diagnosis of Wellbore[C],2021 IEEE 6th International Conference on Intelligent Computing and Signal Processing, pp:1036-1039.（标注陕西省科技厅重点研发计划项目 2020GY-038）

标注省基金的未参与署名论文：

[13]王康. 深度学习在视频测井井筒检测中的应用研究[D].西安石油大学,2022（硕士论文）.（标注陕西省科技厅重点研发计划项目 2020GY-038）

[14]袁凯涛,焦卫华,周亚茹,张瑞;张仙伟.基于数据挖掘算法低渗透油田水淹井治理效果建模[J].粘接,2021,48(12):83-87+92.（标注陕西省科技厅重点研发计划项目 2020GY-038）一般期刊

[15]张仙伟,邢佳瑶.双最小二乘支持向量数据描述[J].西安科技大学学报,2021,41(03):559-565.（标注陕西省科技厅重点研发计划项目 2020GY-038）核心期刊

[16]张仙伟,尚俊倩,张鑫.基于物联网的抽油机参数分析与故障诊断[J].西安石油大学学报(自然科学版),2020,35(05):47-53.（标注陕西省科技厅重点研发计划项目 2020GY-038）核心期刊

参考国科金监处〔2022〕73 号关于对唐永永等发表的论文存在**重复发表**、篡改数据和未经同意使用他人署名等问题并**在项目申请材料中存在虚假信息**的处理决定、国科金监处〔2022〕75 号关于对张义平等发表的论文存在伪造、篡改图片和**重复发表**等问题的处理决定、关于对张开飞等发表的论文存在抄袭、**重复发表**及擅自使用他人署名等问题并在**项目申请书中存在虚假信息**处理结果的通报等相关处理案例，王静怡在陕西省科技厅项目申报、执行过程中存在 10 年内三次连续重复发表和申请材料中存在虚假信息等情况，请陕西省科技厅核查处理。

综上，在基于信息物理融合的智能油田监控系统关键技术研究（2020GY-038）项目申请中，王静怡老师在申请书中提交的作为工作基础的 7 篇论文中 6 篇涉嫌重复发表，并且为了避免被发现重复发表，1 篇论文名称、会议名称、会议举办地信息均不正确。王静怡在研究成果发表中 3 次重复发表，并且在先的重复发表（2016 年第二次重复发表）还在论文首页对重复发表做了所谓的解释说明，在后发生的重复发表（2019 年第三次重复发表）却故意隐瞒已经发表的事实。这属于明知故犯的学术不端。在项目（2020GY-038）执行中，王静怡老师在成果发表过程中存在恶意重复发表（文章[5]和[3]，在[3]故意隐瞒[5]已经发表的事实），提供虚假信息，在与项目申请书研究内容不一致的成果中标注项目号（2020GY-038）等一系列学术不端情况。王静怡老师在国基金项目申请、执行过程中也同样存在和科技厅、教育厅项目类似的问题（一作发表的成果与项目申请书研究内容不一致，列入研究基础的论文 6 篇次涉嫌重复发表，提供

虚假信息，参与或不参与署名的与项目申请书研究内容不一致的成果标注基金号等问题），因国基金项目与科技厅无关，在此不再详述。王静怡老师的涉嫌学术不端行为，在 2023 年西安石油大学职称评审期间（2023/11/3-2023/12/1），本人已经实名向西安石油大学纪委及人事处举报，西安石油大学纪委及人事处转交科技处，科技处转交计算机学院调查，计算机学院包庇纵容，职能部门推诿搪塞。在此，恳请省科技厅相关部门本着对财政经费执行效率、科研风气、学术道德负责的态度，发现一起、查处一起，做到事实清楚、程序合法，公平公正的调查处理。

附件：数据库下载的文章及王静怡博士论文电子版

此致

敬礼

2023 年 12 月 12 日

为节省页面，王静怡博士论文电子版此处不再重复列出，详见本文总第89-204页

Optimal design of joint network LDPC codes over orthogonal multiple-access relay channels

Jingyi Wang*, Shuling Che and Ying Li

State Key Laboratory of Integrated Service Networks (ISN),
Xidian University,
Xi'an 710071, China
Email: wangjy@stu.xidian.edu.cn
Email: shlche@mail.xidian.edu.cn
Email: ying.lili1973@gmail.com
*Corresponding author

Junlong Wang

Huawei Technologies Co. Ltd.,
Xi'an 710071, China
Email: 401834748@qq.com

Abstract: Optimisation of degree distribution for joint network LDPC code over orthogonal Multiple-Access Relay Channels (MARC) is investigated in this paper. We first use a differential evolution algorithm to optimise the degree distribution of the joint network LDPC code over orthogonal MARC based on Gaussian approximation. Then, using a modified differential evolution algorithm, we design a rate-compatible network LDPC code, which is equivalent to designing a single code with different Signal-to-Noise Ratio (SNR). Simulation results show that the gap between Bit Error Rate (BER) performance of the former algorithm and the decoding threshold is about 0.4 dB and that between the capacity limit and decoding threshold is less than 0.7 dB at $BER = 10^{-6}$. Simultaneously, the gap between BER performance of the latter algorithm and the decoding threshold is about 0.52 dB and that between the capacity limit and the decoding threshold is less than 0.46 dB at $BER = 10^{-7}$.

Keywords: network LDPC code; multiple-access relay network; Gaussian approximation; differential evolution; capacity limit.

Reference to this paper should be made as follows: Wang, J., Che, S., Li, Y. and Wang, J. (2016) 'Optimal design of joint network LDPC codes over orthogonal multiple-access relay channels', *Int. J. Grid and Utility Computing*, Vol. 7, No. 1, pp.68–74.

Biographical notes: Jingyi Wang is currently working towards the PhD degree in Communication and Information System at Xidian University. She received her Master's degree in Telecommunications Engineering from Xidian University in 2010. Her research interests include channel coding and network coding.

Shuling Che is currently an Associate Professor at the School of Telecommunications Engineering, Xidian University. She received her PhD in Communication and Information System from Xidian University in 2008. Her research interest includes channel coding.

Ying Li is currently a Professor at the School of Telecommunications Engineering, Xidian University. She received her PhD in Communication and Information System from Xidian University in 2005. Her research interests include channel coding, wireless network coding and MIMO theory.

Junlong Wang is currently working in Huawei Technologies Co. Ltd. He received his Master's degree in Communication and Information System from Xidian University in 2011.

This paper is a revised and expanded version of a paper entitled 'Optimal design of the joint network LDPC codes over orthogonal multi-access relay channel' presented at the '2013 5th International Conference on Intelligent Networking and Collaborative Systems', Xi'an, China, 9 September 2013.

Copyright © 2016 Inderscience Enterprises Ltd.

1 Introduction

In wireless communications (Shen et al., 2012), cooperation relay networks (Cover and Gamal, 1979; Nosratinia et al., 2004; Laneman et al., 2004) have recently attracted substantial research efforts with many promising techniques of improving performance in terms of throughput, coverage or diversity gain. In relay networks, one or multiple Relay Nodes (RNs) assist the sources in transmitting information. Optimal designs of relay networks have attracted extensive attentions owing to their ability to increase communication capacity. One of the earlier works on this subject dealt with the application of the LDPC code to single-source single-relay networks (Razaghi and Yu, 2007). To improve the performance of the single-source single-relay system, a class of bilayer LDPC codes is designed in Azmi et al. (2008) and Cances and Meghdadi (2009).

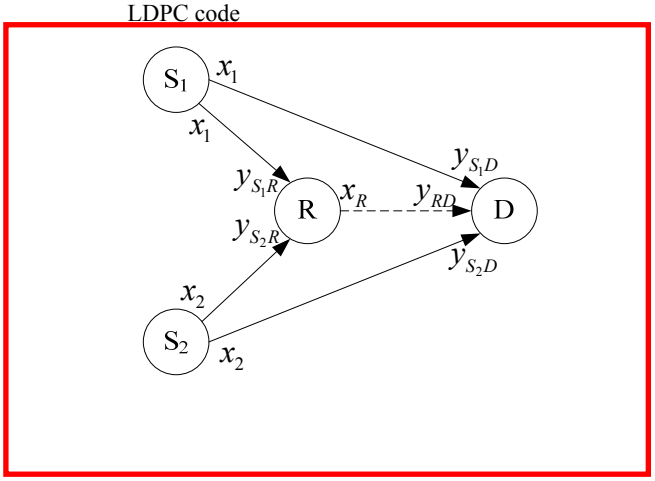
Based on the principle of the bilayer LDPC codes, the authors proposed a class of the joint network LDPC code with network coding (Zhang and Minier, 2013). And then it helps the relay to jointly re-encode the messages from the two sources and send the parity bits to the destination (Li et al., 2009). Moreover, Li et al. (2010) analysed the capacity approaching ability of the joint network LDPC codes. In this paper, we study two different methods of approaching capacity limit of two different transmission modes of a two-source single-relay system with joint network LDPC code, in which the first one requires the same code words transmitted at the two sources and the latter requires different code words transmitted at the two sources.

The rest of the paper is organised as follows. Section 2 presents the system model and then describes the operation of the system throughout different stages of the two cooperation strategies. Section 3 explains the design of two different optimisation methods. Numerical and simulation results are given in Section 4 and finally, the paper is concluded in Section 5.

2 System model

Our system is a two-slot wireless relay network consisting of two sources, one relay and one destination, as shown in Figure 1. Two different transmission modes of the system are described below, which are called Symmetry Cooperation Transmission (SCT) and Asymmetry Cooperation Transmission (ACT). The broadcast stage is followed by the cooperation stage.

Figure 1 Multi-access relay channel model with joint network LDPC code



2.1 The broadcast stage

In this stage, the sources S_i ($i=1,2$) broadcast their LDPC coded signals x_i ($i=1,2$), which are received by both relay R and destination D.

2.1.1 SCT mode

We express the received signals at the relay R and the destination D as follows:

$$y_{S_iR} = h_{S_iR}x_i + n_{S_iR} \tag{1}$$

$$y_{S_iD} = h_{S_iD}x_i + n_{S_iD} \tag{2}$$

where y_{S_iR} and y_{S_iD} are the corresponding received signal by R and D, respectively, h_{S_iR} and h_{S_iD} denote the associated channel gain and n_{S_iR} (n_{S_iD}) denotes a zero-mean Gaussian random variable with a variance $\sigma^2_{S_iR}$ ($\sigma^2_{S_iD}$).

2.1.2 ACT mode

We assume that $P^{(1)}_{S_i}$ ($i=1,2$) is the transmit power of S_i and $w^{(1)}_{S_i}$ ($i=1,2$) is a bit of an LDPC code transmitted by S_i in this stage. Then the received signals at R and D can be written as

$$y_{S_iR} = h_{S_iR}\cdot\sqrt{P^{(1)}_{S_i}}w^{(1)}_{S_i} + n_{S_iR} \tag{3}$$

$$y^{(1)}_{S_iD} = h^{(1)}_{S_iD}\cdot\sqrt{P^{(1)}_{S_i}}w^{(1)}_{S_i} + n^{(1)}_{S_iD} \tag{4}$$

where y_{S_iR}, h_{S_iR} and n_{S_iR} are as defined earlier, while $y^{(1)}_{S_iD}$, $h^{(1)}_{S_iD}$ and $n^{(1)}_{S_iD}$ are the corresponding parametric between S_i and D, where the superscript (1) represents the broadcast stage.

2.2 The cooperation stage

In this stage, after decoding the received signals correctly, R jointly re-encodes the messages of the two sources and sends parity bits x_R of the code words to D.

2.2.1 SCT mode

After x_i is decoded correctly, R jointly re-encodes the messages of the two sources and sends x_R to D. The received signal at D is

$$y_{RD} = h_{RD}x_R + n_{RD} \tag{5}$$

where y_{RD} and n_{RD} are the corresponding parametric between R and D.

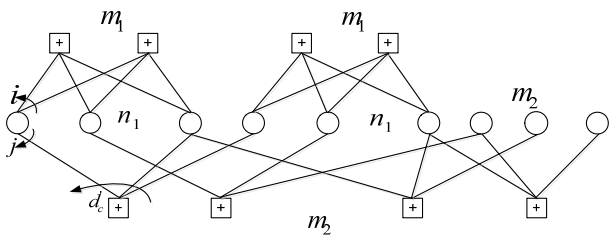
At last, D receives the signals y_{S_iD} and y_{RD}, respectively, from S_i and R. The parity check matrix of the joint network LDPC code can be written as

$$\mathbf{H} = \begin{pmatrix} \mathbf{H}_1 & \mathbf{0} & \mathbf{0} \\ \mathbf{0} & \mathbf{H}_1 & \mathbf{0} \\ \mathbf{A} & \mathbf{B} & \mathbf{C} \end{pmatrix} \tag{6}$$

where $\mathbf{H_1}$ denotes the same parity-check matrix of the constituent codes at the two sources S_i, $\mathbf{H_3} = (\mathbf{ABC})$ denotes the parity-check matrix generated by R and $\mathbf{0}$ represents the all-zero matrix.

Assume that each source uses an $(n_1, n_1 - m_1)$ irregular LDPC code with code length n_1 and parity length m_1. According to Li et al. (2010), the Tanner graph of the joint network LDPC code is shown in Figure 2, where the upper sub-graph denotes the encoding at the sources and the lower sub-graph denotes the encoding at the relay. This code includes $2m_1$ upper check nodes, m_2 lower check nodes and $2n_1 + m_2$ variable nodes. A variable node is of degree (i,j), $1 \le i \le d_v$ and $1 \le j \le d_v'$, where $i(j)$ is its upper (lower) degree and $d_v(d_v')$ is its maximum upper (lower) degree. In addition, $\lambda_{i,j}$ represents the proportion of the number of edges connected to the variable nodes with the degree (i,j).

Figure 2 The Tanner graph of the joint network LDPC code



2.2.2 ACT mode

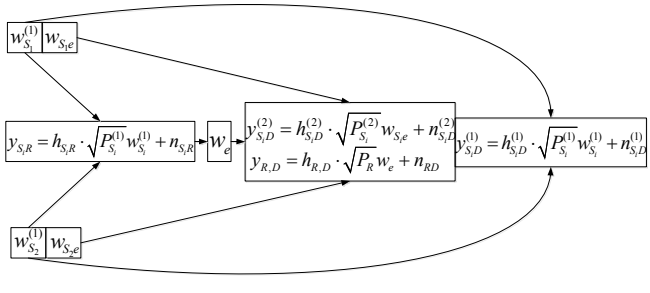
The source $S_i (i = 1,2)$ uses rate-compatible extension method from an entire LDPC code word $w_{S_i 2} = \left[w_{S_i}^{(1)}, w_{S_i e} \right]$ extended from the original code word $w_{S_i}^{(1)}$, and $w_{S_i e}$ carries additional parity-check bits as shown in Figure 3. R only generates two additional parity-check bits $w_{S_1 e}$ and $w_{S_2 e}$ from S_1 and S_2, respectively. Then network-coded code word $w_e = w_{S_1 e} \oplus w_{S_2 e}$. The received signals at D are

$$y_{S_i D}^{(2)} = h_{S_i D}^{(2)} \cdot \sqrt{P_{S_i}^{(2)}} w_{S_i e} + n_{S_i D}^{(2)} \tag{7}$$

$$y_{RD} = h_{RD} \cdot \sqrt{P_R} w_e + n_{RD} \tag{8}$$

where $P_{S_i 2}$ (P_R) is the transmit power of S_i (R) in the second stage. The other parameters were defined earlier, where the superscript (2) represents the cooperation stage.

Figure 3 Diagram of the multi-access relay channel model with joint network LDPC code



Then, D receives the signals $y_{S_i D}^{(1)}$ $\left(y_{S_i D}^{(2)} \right)$ and y_{RD}, respectively, from the two sources and the relay. First, D decodes y_{RD} and then obtains the network-coded code word $w_e = w_{S_1 e} \oplus w_{S_2 e}$. Second, D obtains $w_{S_1 e}$ and $w_{S_2 e}$ by iterative decoding with $y_{S_i D}^{(2)}$ and w_e. Different from the rate-compatible LDPC code designed in Li et al. (2009), the received SNR for $w_{S_i}^{(1)}$ and $w_{S_i e}$ are different. Using (4), (7) and (8), the SNR for the decoding of $w_{S_i}^{(1)}$ and $w_{S_i e}$ can be written, respectively, as

$$SNR_{S_i D} = \frac{\left| h_{S_i D}^{(1)} \right|^2 P_{S_i}^{(1)}}{N_0} \tag{9}$$

$$SNR'_{S_i D} = \frac{\left(h_{S_i D}^{(2)} \sqrt{P_{S_i}^{(2)}} + h_{RD} \sqrt{P_R} \right)^2}{N_0} \tag{10}$$

Finally, we decode $w_{S_1}^{(1)}$ and $w_{S_2}^{(1)}$ correctly by using the Belief Propagation (BP) iterative decoding algorithm with $w_{S_1 2} = \left[w_{S_1}^{(1)}, w_{S_1,e} \right]$ and $w_{S_2 2} = \left[w_{S_2}^{(1)}, w_{S_2,e} \right]$, respectively, at D.

3 Optimisation of degree distribution

3.1 SCT mode

3.1.1 Preliminary

Definition 1: *Decoding threshold of joint network LDPC code is defined as*

$$\sigma^* = \sup \left\{ \sigma : \lim_{L \to +\infty} m_L > M \right\} \tag{11}$$

where L is the maximum iteration number, m_L denotes the mean value of the Log-Likelihood Ratio (*LLR*) message of a code bit at the Lth decoding iteration and M is the *LLR* mean value corresponding to the target error probability.

Then with the knowledge in Li et al. (2010), $2m_L$ is the *LLR* variance value. When $\sigma < \sigma^*$, m_L will be greater than M, which means that the target error probability can be achieved. When $\sigma \ge \sigma^*$, the iterative decoding cannot achieve the target error probability.

3.1.2 Calculation of decoding threshold σ_{SD}^*

Algorithm 1: Given degree distribution of the LDPC code at the sources, let σ_{SD} and σ_{RD} represent the channel parameters of source–destination link and relay–destination link, respectively. We denote the target error probability as $P_e = 10^{-6}$ $(M = 45)$ and the maximum iteration number as L. Let $\Delta\sigma_{SD}$ denote a step length, and then Algorithm 1 can be described as follows.

- *Step 1: Initialisation.* The initialised value of the average mean value of the *LLR* message output by the check node is $m^{'l} = n^{'l} = 0$ (l is the iteration number and $l = 0$ in the first iteration) (Li et al., 2010).

- *Step 2: Updating.* When the iteration number $l < L$, update the mean values of the *LLR* messages at the variable node and the check node, and then calculate the mean value m_l of the *LLR* message during this iteration using the method in Li et al. (2010). If $m_l < M$, add the iteration number by 1 (l = l +1) and continue Step 2. If $m_l \geq M$, $\sigma_{SD} = \sigma_{SD} + \Delta\sigma_{SD}$, and go to Step 1.

- *Step 3: Stopping criterion.* If $l \geq L$ and $m_l < M$ during this iteration, stop the whole process, and the code capacity is defined as $\sigma^*_{SD} = \sigma_{SD} - \Delta\sigma_{SD}$. Otherwise, output the threshold value of channel parameter as $\sigma^*_{SD} = \sigma_{SD}$.

Using Algorithm 1, we can obtain the corresponding σ^*_{SD} from a given degree distribution of the upper layer LDPC code.

3.1.3 *Optimal design of the degree distribution of the lower layer LDPC code*

Our goal is to search the optimal degree distribution of the network LDPC code, which can approach the capacity limit. Here we use differential evolution algorithm to optimal design of the network LDPC code ensembles.

Algorithm 2. Assume that N relay code sets of the network LDPC code structure are randomly generated, denoting their degree distributions of variable node as $\lambda_{i,j}(d)$, $0 \leq i \leq d_v$, $0 \leq j \leq d'$, $d = 1,2,\ldots, N$. The degree of the lower check nodes is fixed as d'_c.

- *Step 1: Initialisation.* Initialise that degree distribution as

$$C(d) = \left\{\lambda_{i,j}(d), 0 \leq i \leq d_v, 0 \leq j \leq d'_v\right\}, d = 1,2,\ldots N \quad (12)$$

- *Step 2: Performance estimation of code sets.* Calculate the code capacity $\sigma^*(d)$ of each code set $C(d)$ through Algorithm 1, and search the optimal code ensemble meeting $C^* = \arg\max_{1\leq d\leq N}\sigma^*(d)$. The degree distribution of the optimal code ensemble corresponding to the maximum code capacity is $C^* = \left\{\lambda^*_{i,j}, 0 \leq i \leq d_v, 0 \leq j \leq d'_v\right\}$.

- *Step 3: Code set updating.* Select $\tilde{N}$ code sets from $\{C(d)\}_{d=1}^{N}$ at random and denote their degree distributions as $\tilde{C}(k) = \left\{\lambda_{i,j}(k), 0 \leq i \leq d_v, 0 \leq j \leq d'_v\right\}, k = 1,2,\ldots,\tilde{N}$. Then, update the degree distribution of the code ensemble: $C^* = C^* + \alpha\sum_{k=1}^{\tilde{N}}(-1)^{k-1}\tilde{C}(k)$, where $\alpha < 1$ is the step length.

- *Step 4: Stopping criterion.* If reaching the preset number of iteration and $m_l < M$, stop the iteration process. The degree distribution of the optimal code ensemble is defined as $C^* = \left\{\lambda^*_{i,j}, 0 \leq i \leq d_v, 0 \leq j \leq d'_v\right\}$; otherwise, go to Step 3.

Remark: *Restrictive conditions must be met for Steps 1 and 3:*

$$\begin{cases} \sum_{i\geq 0, j\geq 0}\lambda_{i,j} = 1 \\ \lambda_i = \frac{1}{\eta}\sum_{j\geq 0}\frac{i}{i+j}\lambda_{i,j} \\ \eta = \sum_i\sum_j\frac{i}{i+j}\lambda_{i,j} \\ d'_c = \frac{1-\eta}{\sum_j\frac{\lambda_{0,j}}{j}} \end{cases} \quad (13)$$

where η is the proportion of the total number of edges in the upper sub-graph. The total number of upper layer edges of a source node is $E = \frac{n_1}{\sum_{i\geq 2}\lambda_i/i} = \frac{k_1}{\sum_{j\geq 2}\rho_j/j}$ and the total number of edges of the bilayer network LDPC relay code is $E' = 2E + k_2 \cdot d'_c$, so $\eta = \frac{2E}{E'}$.

3.2 *ACT mode*

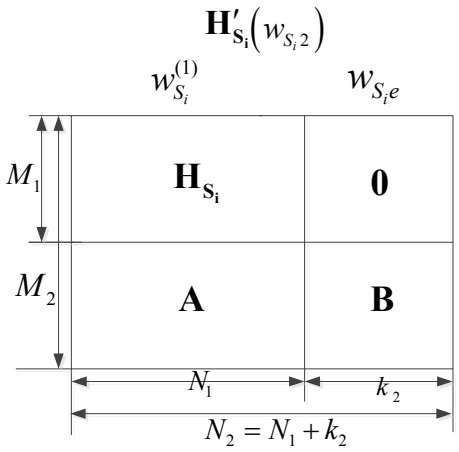
3.2.1 *Ensemble description of the joint network LDPC code*

We assume that R decodes the received signal from S_i correctly. The code rate R_1 of both S_1 and S_2 depends on $R_1 \leq C(SNR_{S_1R})$ and $R_1 \leq C(SNR_{S_2R})$, where $C(SNR_{S_iR})$ is the capacity when *SNR* of the channel between S_i and R is SNR_{S_iR}. Here we assume $R_1 = C(SNR_{S_1R}) = C(SNR_{S_2R})$.

In addition, the distance between S_i and D is farther than the distance between S_i and R, so the channel gain h_{S_iD} is smaller than h_{S_iR} and SNR_{S_iD} is smaller than SNR_{S_iR}. Here we assume $R_1 > C(SNR_{S_1D}) = C(SNR_{S_2D})$. And the capacity between the source and destination link is smaller than the capacity between the source and relay link. According to Shannon theorem, when the rate is greater than the channel capacity, the system cannot decode correctly after more iterations, so extra check bits are generated to help decode.

Figure 4 shows the extended parity-check matrix $\mathbf{H}'_{\mathbf{S}_i}(\mathbf{w}_{\mathbf{S}_i2})$, where $\mathbf{H}_{\mathbf{S}_i}$ denotes the parity-check matrix of the code word $w^{(1)}_{S_i}$ at the two sources $S_i(i = 1,2)$, w_{S_ie} denotes additional parity-check bits of the entire code word w_{S_i2} and $\mathbf{0}$ represents the all-zero matrix. The rate of the entire code word is $R_2 = \frac{N_1 - (k_1 + k_2)}{N_1 + k_2}$. We find a proper k_2, which must meet $R_2 \leq C(SNR_{S_1D}) = C(SNR_{S_2D})$.

Figure 4 Rate-compatible structure of the parity-check matrix for the relay code



R_1 and R_2 satisfy the following relationship:

$$R_1 = \frac{N_1 - k_1}{N_1} > R_2 = \frac{N_1 - (k_1 + k_2)}{N_1 + k_2} \tag{14}$$

As far as we know, the decoding performance depends on the parity-check matrix, while the degree distribution of the code ensembles determines parity-check matrix. So the design of the parity-check matrix $\mathbf{H}'_{\mathbf{S}_i}$ is equivalent to find the optimal degree distribution based on a given construction algorithm.

3.2.2 *Optimal design of the degree distribution of the joint network LDPC code*

According to the above analysis, when SNR_{S_iD} is given, we can determine the number of extra parity bits. In addition, D decodes the received information of S_i correctly; it is required to satisfy the formula

$$R_1 \le C\left(SNR_{S_iD}\right) + C\left(SNR'_{S_iD}\right) \tag{15}$$

When the transmit power and the channel gains are given, we can obtain the theoretical minimum SNR by (15). Our optimal goal is to find the relay extended code ensemble, whose threshold of SNR is approaching the theoretical extreme value.

Compared with the rate-compatible LDPC code of the single-source single-relay system, the two-source single-relay system uses the linear network-coded method at R, which achieves the same cooperative diversity to the single-source single-relay system and D decodes the received signal of S_1 and S_2 separately. Here the two-source single-relay system can be equal to two separate single-source single-relay systems for rate-compatible LDPC code. Therefore, we can use the algorithm in Cances and Meghdadi (2009) to optimise the design of the rate-compatible extended code ensemble of S_1 and S_2 separately, while linear network-coded is used at the relay.

4 Simulation results

4.1 *SCT mode*

Assume each source node employs an $(n_1, n_1 - m_1)$ LDPC code with $\lambda(x) = 0.23403x + 0.21242x^2 + 0.1469x^5 + 0.102840x^6 + 0.30381x^{19}$ and $\rho(x) = 0.71875x^7 + 0.28125x^8$, where $n_1 = 22164$ and $m_1 = 11082$. $SNR_{RD} = 3$ dB and the two source–destination links are assumed to be symmetric. Using Algorithm 1, four different parameters of the joint network LDPC codes are obtained and listed in Table 1, where σ_{RD}^2 represents the channel parameter between the relay and the destination link.

Table 1 Four optimal joint network LDPC codes

Code ensembles	*Code A*	*Code B*	*Code C*	*Code D*
d'_v	2	2	2	2
d'_c	4	4	4	7
k_2	2814	4814	2814	2814
σ_{RD}	0.5	0.5	0.8	0.5
η	0.942065	0.904808	0.942065	0.902835
σ^*_{SD}	1.0568	1.0987	1.0393	1.1116
Threshold (E_bN_0)	0.155039dB	0.115123dB	0.2018dB	–0.22877dB
Sum capacity (E_bN_0)	–0.24536dB	–0.517620dB	–0.143948dB	–0.24536dB
Gap	0.400399dB	0.632743dB	0.345748dB	0.01666dB

Using Algorithm 2, four optimal degree distributions of the joint network LDPC codes are given in Tables 2–5.

Table 2 Degree distributions of code A

$\lambda_{i,j}$	$\lambda_{i,0}$	$\lambda_{i,1}$	$\lambda_{i,2}$
$i = 2$	0.193815	0.00543635	0.04612661
$i = 3$	0.171369	0.019109592	0.02409292
$i = 6$	0.129299	0.006342408	0.00494214
$i = 7$	0.09485	8.2369E-05	0.00259462
$i = 20$	0.273877	0.000432436	0.00181212
$i = 0$	0	0.0030528	0.02276564

Table 3 Degree distributions of code B

$\lambda_{i,j}$	$\lambda_{i,0}$	$\lambda_{i,1}$	$\lambda_{i,2}$
$i = 2$	0.07441004	0.20599344	0
$i = 3$	0.19208258	0.00015819031	0
$i = 6$	0.1327018904	0.00013842	0.0001681903
$i = 7$	0.09266986	0.000326381	0.0001779641
$i = 20$	0.27426244	0.0005152496	0.0021751167
$i = 0$	0	0.0237936797	0.000009887

Table 4 Degree distributions of code C

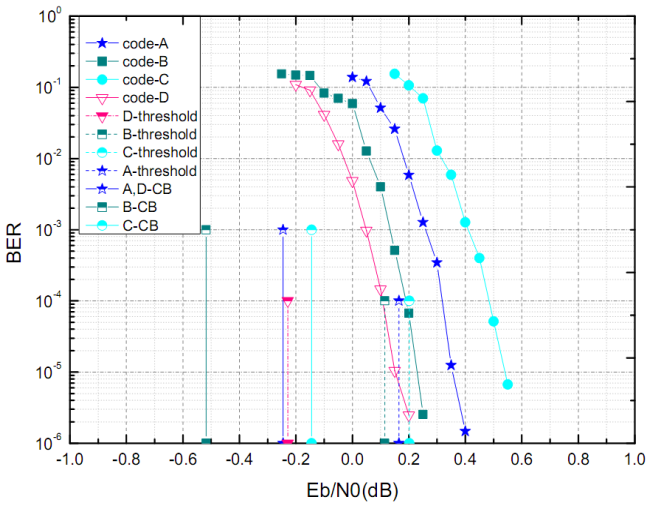
$\lambda_{i,j}$	$\lambda_{i,0}$	$\lambda_{i,1}$	$\lambda_{i,2}$
$i=2$	0.1206132872	0.0	0.0
$i=3$	0.1001453763	0.0000219458	0.0
$i=6$	0.1860514424	0.0002767963	0.000016798
$i=7$	0.1964141036	0.0002114936	0.0000212906
$i=20$	0.3858558271	0.0003262453	0.0000362551
i = 0	0.0	0.0041565109	0.0206487529

Table 5 Degree distributions of code D

$\lambda_{i,j}$	$\lambda_{i,0}$	$\lambda_{i,1}$	$\lambda_{i,2}$
$i=2$	0.1112574229	0.013643762	0.1818773738
$i=3$	0.09172912663	0.0876831253	0.0571696344
$i=6$	0.13223499235	0.00032560828	0.00015708008
$i=7$	0.092674986	4.568455E-05	6.788722E-05
$i=20$	0.274059093	0.00010113293	0.000217037
$i=0$	0	0.00351717946	0.02072694417

The BER curves of four codes are illustrated in Figure 5. We see that the gap between the decoding threshold of four codes obtained by searching the maximum decoding threshold σ_{SD}^{*} and capacity limit is less than 0.7 dB, and that between BER performance and decoding threshold is less than 0.4 dB. Since the lower check degree of Code D is bigger and more information bits are contained in the check equation, it outperforms Code A by 0.2 dB at $BER=10^{-5}$. Another important observation is that Code B has a gain of about 0.15 dB over Code A at $BER=10^{-5}$ and the performance gain of Code D is about 0.1 dB over Code B at $BER=10^{-5}$. This indicates that increasing the degrees of lower layer check nodes is better than increasing the numbers of parity bits to improve system performance. When the noise variances between the *R* and *D* link are increased, the system decoding performance will be reduced and Code A will have a gain of about 0.2 dB over Code C at $BER=10^{-5}$.

Figure 5 Performance of the joint network LDPC codes



4.2 ACT mode

Assume each source node employs LDPC code-1 and code-2 listed in Cances and Meghdadi (2009, Table 1). The two source–destination links are assumed to be symmetric. The distance between S_i and D is normalised to unity and d denotes the normalised distances between S_i and R. The channel gain $|h_{S_1D}|^2=|h_{S_2D}|^2=1$, $|h_{S_1R}|^2=|h_{S_2R}|^2=\frac{1}{d^{\alpha}}$ and $|h_{RD}|^2=\frac{1}{(1-d)^{\alpha}}$, where we assume that $\alpha=2$ is the path loss exponent and $d=0.25$. The power allocation among S_i and R is fixed as $P_{S_1}^{(1)}/2=P_{S_2}^{(1)}/2=P_{S_12}=P_{S_22}=P_R/2=P_T/8$, and $w_{S_i}^{(1)}$ and w_{S_i2} have the rate $R_1=1/2$ and $R_2=1/4$, respectively. Table 6 gives the optimum LDPC code ensemble of w_{S_i2} via the algorithm in Cances and Meghdadi (2009) and the network-coded method at the relay. And the node probability set of w_{S_12} is $h_1(2)=0.1978$, $h_1(i)=1$ for $i\in\{3,6,7,8,10,14,16,20,30,33\}$, the node probability set of w_{S_22} is $h_1(3)=0.1576$, $h_1(i)=1$ for $i\in\{2,4,7,8,10,14,16,20,30,33\}$, where $h_1(i)$ denotes the probability of a variable node that has a degree of *i* and falls in the region of region-1 (i.e. $\mathbf{H_1}$ and **A**, namely region-1; **0** and **B**, namely region-2.)

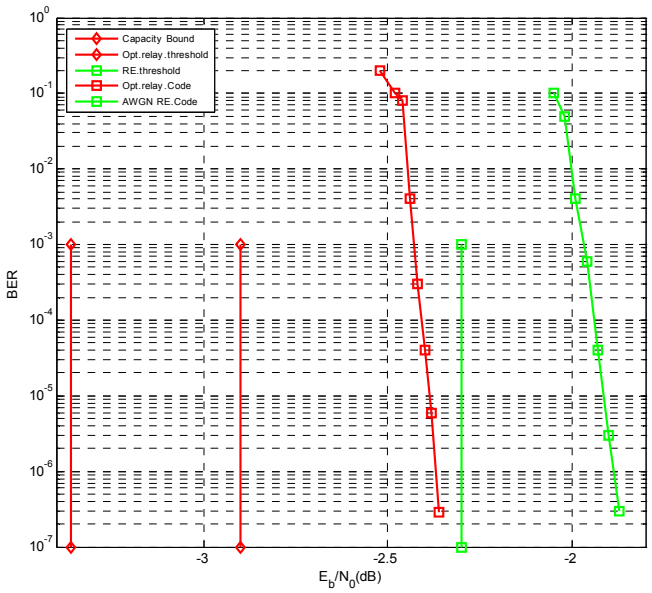
Table 6 Rate-compatible extended LDPC code ensembles

Code ensembles	*Extended code ensemble 1*	*Extended code ensemble 2*
λ_2	0.13370307136	0.06600453943
λ_3	0.02829823403	0.11086569074
λ_4	0.02371830093	0.07247855957
λ_5	0.00295003743	0.00422715433
λ_6	0.05593270965	0.03891266928
λ_7	0.00474956026	0.06403186741
λ_8	0.05605071114	0.03722942404
λ_9	0.11366862967	0.15231465261
λ_{10}	0.06932587957	0
λ_{11}	0.00125745345	0.00502688622
λ_{12}	0.00044250561	0
λ_{13}	0.00081494784	0
λ_{14}	0.00087763614	0.05326214450
λ_{15}	0.00027656601	0
λ_{16}	0.19417146355	0.13551266623
λ_{17}	0.20455190775	0
λ_{20}	0.00118001497	0.00411290691
λ_{22}	0.00186589867	0.16077657776
λ_{26}	0.00009587622	0
λ_{30}	0.10553758901	0.09505384861
ρ_8	0	0.22602708425
ρ_9	0.99563763215	0.77391198379

In simulations, the code lengths of $w_{S_i}^{(1)}$ and w_{S_i2} are $N_1=20000$ and $N_2=2N_1=40000$, respectively. We compare the BER performance between the optimum LDPC

code ensemble and the repetition code under the AWGN channel, when the repetition code has $w_{S_i e} = w_{S_i}^{(1)}$ and D receives $w_{S_i}^{(1)}$ from source S_i and R at the same time. Figure 6 shows the BER performance of the optimised relay code ensemble and the repetition code. It is seen that the relay code ensemble optimised via the algorithm in Cances and Meghdadi (2009) can achieve about 0.5 dB gain over the repetition scheme. The gap between the BER performance of the optimised relay code ensemble of the rate-compatible LDPC and the decoding threshold is about 0.52 dB, and the gap between the decoding threshold and the capacity limit is less than 0.46 dB.

Figure 6 The BER performance comparison between the optimised relay code and the repetition code



5 Conclusions

In this paper, we employed the differential evolution method to design degree distribution of different transmission modes of the joint network LDPC code for a two-source single-relay system. The performance of the new codes we designed showed significant BER performance gain for a two-source single-relay system with symmetric AWGN channels.

Acknowledgements

We are grateful to anonymous referees for their invaluable suggestions. This work is supported by the National Natural Science Foundation of China (Nos. 61072064, 61101148 and 61001131).

References

Azmi, M.H., Yuan, J., Ning, J. and Huynh, H.Q. (2008) 'Improved bilayer LDPC codes using irregular check node degree distribution', *Proceedings of the IEEE International Symposium on Information Theory*, 6–11 July, Toronto, Canada, pp.141–145.

Cances, J.P. and Meghdadi, V. (2009) 'Optimized low density parity check codes designs for half duplex relay channels', *IEEE Transactions on Wireless Communications*, Vol. 8, No. 7, pp.3390–3395.

Cover, T. and Gamal, A.E. (1979) 'Capacity theorems for the relay channel', *IEEE Transactions on Information Theory*, Vol. 25, pp.572–584.

Laneman, J., Tse, D. and Wornell, G. (2004) 'Cooperative diversity in wireless networks: efficient protocols and outage behavior', *IEEE Transactions on Information Theory*, Vol. 50, No. 12, pp.3062–3080.

Li, Y., Song, G.H. and Wang, L.L. (2009) 'Design of joint network-low density parity check codes based on the EXIT charts', *IEEE Communications Letters*, Vol. 13, No. 8, pp.600–602.

Li, Y., Song, G.H. and Wang, L.L. (2010) 'Analysis of the joint network LDPC codes over orthogonal multi-access relay channel', *IEEE Communications Letters*, Vol. 14, No. 2, pp.184–186.

Nosratinia, A., Hunter, T.E. and Hedayat, A. (2004) 'Cooperative communication in wireless networks', *IEEE Communications Magazine.*, Vol. 42, No. 10, pp.74–80.

Razaghi, P. and Yu, W. (2007) 'Bilayer low-density parity-check codes for decode-and-forward in relay channels', *Transactions on Information Theory*, Vol. 3, No. 10, pp.3723–3739.

Shen, Y., Pei, Q., Xu, Q. and Zhang, Z. (2012) 'The multimedia service session handoff method in heterogeneous wireless networks', *International Journal of Grid and Utility Computing*, Vol. 3, No. 1, pp.68–77.

Zhang, Y. and Minier, M. (2013) 'How network coding system constrains packet pollution attacks in wireless sensor networks', *International Journal of Grid and Utility Computing*, Vol. 4, Nos. 2–3, pp.197–203.

Univ. . Vol. 69, № 14, 706 - 713, 2016

A Distributed RS code based hybrid Forward strategy for MARC

Jingyi Wang*, Ying Li, Daolong Wu, Baoming Bai

State Key Lab. of ISN, Xidian University, Xi'an, China

Abstract: To combat the effects of error propagation in error-prone multiple-user multiple-relay (MUMR) wireless networks, a Reed-Solomon (RS) code based hybrid decoded-and-forward (DF) strategy is proposed. In this paper, we introduce a proposed hybrid DF strategy for the MUMR wireless networks. We propose a threshold to analyse and only forwards those bits whose log-likelihood ratios (LLRs) are larger than this threshold. Furthermore, we investigate the optimization of the threshold by minimizing the bit error rate (BER), and this technique is applied to separated cooperation and combined cooperation, respectively. Both separated cooperation and combined cooperation strategy are discussed in the optimization of the threshold. Using the suggested design guidelines in this paper, we show that the performance gap for different scenarios between the MUMR wireless networks with error-free relay and that with the proposed scheme is only 0.01dB at BER=10-6 over both additive white Gaussian noise (AWGN) channel and fading channel. In addition, the effectiveness of our proposed method in mitigating error propagation in error-prone MUMR wireless networks, which demonstrates that the proposed scheme may have potential use in MUMR wireless networks.

Keywords: network coding; relaying strategies; RS code; error propagation; threshold

1. Introduction

Cooperative wireless relay networks [1-3] have recently attracted substantial research efforts. Many promising techniques are proposed to improve the performance in terms of throughput, coverage or diversity gain. In relay networks, one or multiple relay nodes (RNs) can be used to assist the sources in transmitting information. Early works on cooperative communications suggested three types of relay transmission protocol [3]: amplify-and-forward (AF), decode-and-forward (DF) and compress-and-forward (CF).

For practical DF cooperative networks, the potential error propagation limits the attainable end-to-end performance. Hence, various methods have been proposed to mitigate the effects of error propagation imposed by the RNs [4-7]. In [4], authors introduced a distributed turbo-code for the DF scheme. This approach was then extended by [5] and [6] to soft re-encoding at the relay in order to cope with erroneous or unreliable bits at the relay. Authors in [7] proposed to calculate the log-likelihood ratio (LLR) of received bits at the relay. If the LLR of a bit falls below a predetermined threshold, the relay blocks the bit and does not forward it to the destination. This method can avoid errors propagation to the destination in some extent.

Another limitation of cooperative communication systems is their low throughput as compared to that of MIMO systems. To increase the throughput of such networks, network coding was proposed to reduce the traffic in such networks [8,9]. Although the application of network coding to relay networks seems to be natural and beneficial, of which earlier schemes only used in two-user one-relay networks [10]. The design of network coding rarely applied in multiple-user single-relay (MUMR) networks. In [11], physical-layer network coding was studied to multiple-user single-relay networks, which is not optimal for network with multiple relays. Moreover, previous work[10-12] studied binary network coding which represented a special case of general finite field network coding. However, binary network coding is generally not optimal for multiple-user multiple-relay (MUMR) wireless networks in terms of transmission efficiency e.g., frame error rate, energy efficiency [13]. Most of the network coding theory applied to wireless networks based on the assumption that the data is delivered with error-free or all error can be corrected by error correcting coding scheme. However, such an assumption without any error checking schemes (such as ARQ) is impractical as error will propagate to all terminals. So we adopt a reliable threshold at the relays to control error propagation. By calculating LLR values for the bits sent from the sources, the relays apply non-binary network coding based on maximum distance separable codes (MDS) to MUMR wireless networks with arbitrary M ($M \geq 2$) users and N ($N \geq 1$) relays. In this paper, we study different scenarios of source-relay channels, as well as different schemes of applying the LLR threshold at the relays. The results show that separated cooperation has better performance than combined cooperation using optimal threshold.

The rest of this paper is organized as follows. Section 2 presents the system model and then describes the operation of the system throughout different slots of the cooperation strategy. Section 3 analyses the

performance of the system, as well as optimizes the threshold with minimum end-to-end BER as a target. Section 4 presents simulation results, and the paper is concluded in Section 5.

2. System Description

2.1 System Model

The wireless relay network with orthogonal channels consists of *M* sources S_i $(i=1,2,\cdots,M)$, *N* relays R_j $(j=1,2,\cdots,N)$ and one destination D, as shown in Fig.1. The transmission between the *M* sources and the destination will be implemented through two slots.

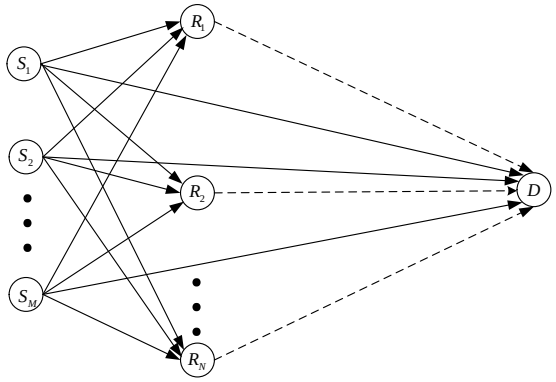


Fig.1 Wireless network with *M* sources and *N* relays

In the first slot, the *M* sources broadcast their coded symbol X_i^t ($i=1,2,\cdots,M$) with rate R_i ($i=1,2,\cdots,M$) to the *N* relays and the destination D, where the superscript *t* represents time throughout this paper. Then we have

$$Y_{S_i,D}^t = h_{S_i,D}^t X_i^t + N_{S_i,D}^t \tag{1}$$

$$Y_{S_i,R_j}^t = h_{S_i,R_j}^t X_i^t + N_{S_i,R_j}^t \tag{2}$$

where $Y_{S_i,D}^t$ and Y_{S_i,R_j}^t are the corresponding signal received by the relay R_j and the destination D respectively, $N_{S_i,D}^t$ and N_{S_i,R_j}^t are the zero-mean additive Gaussian random variables with variance $\sigma_{S_i,D}^2$ and σ_{S_i,R_j}^2 respectively. $h_{S_i,D}^t$ and h_{S_i,R_j}^t are the associated fading, with subscripts indicating the specific channel.

In the second slot, the relay R_j calculates the LLR values of the bits sent from all the sources. If the LLR of a bit falls below a predetermined threshold, the relay R_j blocks the bit and does not forward it to the destination. After this process, the relay R_j re-encodes the selected bits and forwards the encoded sequence to the destination. Let $X_{R_j}^t$ be the coded symbol transmitted by the relay R_j. The received signal at the destination is

$$Y_{R_j,D}^t = h_{R_j,D} X_{R_j}^t + N_{R_j,D}^t \tag{3}$$

where $Y_{R_j,D}^t$ is the received signal at the destination D from the relay R_j, $N_{R_j,D}^t$ is a zero-mean additive Gaussian random variable with variance $\sigma_{R_j,D}^2$.

In this paper, we consider two forwarding schemes. The first scheme is that the relays cooperate with each source individually. In this scheme, each relay determines which users bits can be forwarded independently. The second scheme is that the relays cooperate with all the *M* sources. To be more specific, only when all the LLR values of all the *M* sources are larger than the threshold, can the relay re-encode these bits and forward them to the destination. No matter which scheme is employed, the forwarded symbol $X_{R_j}^t$ is the coded symbol of the

selected bits. A detailed discussion will be given in the next section. The superscript t will be omitted in the following formula for simplicity.

2.1 RS code based Network Coding Scheme

In the relay R_j, the transmitted signal $X_{R_j}^t$ can be written as

$$X_{R_j} = \sum_{i=1}^{M} g_{i,j} \hat{X}_{i,j} \tag{4}$$

where $\hat{X}_j = \left[\hat{X}_{1,j} \hat{X}_{2,j} \cdots \hat{X}_{M,j} \right]$ is the estimation of the source messages at the relay R_j. And $g_{i,j}$ is the network coding coefficient used at the relay R_j. $g_{i,j} = 0$ means that the relay node R_j will not forward to the i-th source.

Let

$$\mathbf{P} = \begin{bmatrix} g_{1,1} & g_{1,2} & \cdots & g_{1,N} \\ g_{2,1} & g_{2,2} & \cdots & g_{2,N} \\ \vdots & & & \vdots \\ g_{M,1} & g_{M,2} & \cdots & g_{M,N} \end{bmatrix} \tag{5}$$

where the matrix $\mathbf{P}$ defines the network coding scheme used by the N relays. Combining $\mathbf{P}$ with an $M \times M$ identity matrix, we can have

$$\begin{aligned} \mathbf{G} &= \begin{bmatrix} g_{1,1} & g_{1,2} & \cdots & g_{1,N} & 1 & 0 & \cdots & 0 \\ g_{2,1} & g_{2,2} & \cdots & g_{2,N} & 0 & 1 & \cdots & 0 \\ \vdots & & & \vdots & & & \ddots & \\ g_{M,1} & g_{M,2} & \cdots & g_{M,N} & 0 & 0 & 0 & 1 \end{bmatrix} \\ &= \left[\mathbf{P} \quad \mathbf{I}_{M \times M} \right] \end{aligned} \tag{6}$$

Apparently, $\mathbf{G}$ is a generator matrix of a RS code with length $M+N$. In other words, the network coding matrix $\mathbf{P}$ can be designed via the help of RS coding theory.

3. Forward Strategy

In this section, we assume that no channel coding is used by the source and the relays. Based on the principle discussed in [7], we study the forward strategy at the relays. If the LLR of the bit is below the preset threshold, the relays stay silent and transmit nothing. Otherwise, the network coded symbols are sent. We calculate optimum decoding threshold for two possible scenarios to obtain minimum BER.

3.1 Threshold based forwarding

Assume BPSK modulation is employed by the sources. Let $\Lambda_{x_i}^j$ denote the LLR of the bit of the i-th user at R_j. We have

$$\begin{aligned} \Lambda_{x_i}^j &= \ln \frac{p\left(x_i = 1 \middle| y_{S_i,R_j}, h_{S_i,R_j} \right)}{p\left(x_i = -1 \middle| y_{S_i,R_j}, h_{S_i,R_j} \right)} = \ln \frac{p\left(y_{S_i,R_j} \middle| x_i = 1, h_{S_i,R_j} \right)}{p\left(y_{S_i,R_j} \middle| x_i = -1, h_{S_i,R_j} \right)} \\ &= 2 y_{S_i,R_j} h_{S_i,R_j} \Big/ \sigma_{S_i,R_j}^2 \end{aligned} \tag{7}$$

where $p(\cdot)$ indicates the conditional probability density function. It is well-known that the sign of $\Lambda_{x_i}^j$ is the hard decision value, and the magnitude is a good measure of the reliability of the bit. R_j estimates the original data as

$$\hat{x}_i^j = sign\left(\Lambda_{x_i}^j \right) \tag{8}$$

where $sign(\cdot)$ is the signature function. The instantaneous BER in terms of $\Lambda_{x_i}^j$ at the R_j can be computed by

$$P_{e-S_i,R_j} = \frac{1}{1+e^{\left|\Lambda_{x_i}^j\right|}} \tag{9}$$

Let P_{eT} be the pre-determined threshold, which means that the relay does not forward the estimated bit $\hat{x}_i^j$ to the destination unless $P_{e-S_i,R_j} \le P_{eT}$. According to (9), we have

$$P_{e-S_i,R_j} = \frac{1}{1+e^{\left|\Lambda_{x_i}^j\right|}} \le P_{eT}$$

or

$$\left|\Lambda_{x_i}^j\right| \ge \ln\left(\frac{1}{P_{eT}} - 1\right) = \Lambda_0 \tag{10}$$

From (7)-(10), $\Lambda_{x_i}^j$ provides the reliable information of the maximum a-posteriori probability decision, which minimizes the error probability.

3.2 Optimization of Threshold

3.2.1 Optimization for separated Cooperation

In the separated cooperation, the relay R_j will evaluate the quality of the received signal from each user. If the LLR exceeds in the preset threshold, the relay decodes and forwards the restored data to D. Otherwise, it keeps silent in the second slot. The transmitted signal can be written as

$$X_{R_j} = \sum_{i=1}^{M} g_{i,j}\hat{X}_{i,j} \tag{11}$$

where $g_{i,j} = 0$ if $\left|\Lambda_{x_i}^j\right| < \Lambda_{S_i 0}$, and $g_{i,j} \ne 0$ if $\left|\Lambda_{x_i}^j\right| \ge \Lambda_{S_i 0}$, $\Lambda_{S_i 0}$ is the threshold of set of S_i.

Let $P_{S_i e}^{sep}$ be the average BER at the destination when separated cooperation is employed. The optimal threshold $\Lambda_{S_i 0}^{opt}$ will be determined by minimizing $P_{S_i e}^{sep}$. More specifically, we have

$$\min_{\Lambda_{S_i 0}} \quad P_{S_i e}^{sep} \tag{12}$$

$$s.t. \quad \Lambda_{S_i 0} > 0 \tag{13}$$

This is a linear programming problem. We use the following probability distribution function to obtain the optimum $\Lambda_{S_i 0}^{opt}$.

There are two events causing the erroneous signal at D. One is that the relay stays silent and an error happens in direct transmission. The other is that the relay forwards the bit to the destination and an error still happens. Since the two events are mutually exclusive, $P_{S_i e}^{sep}$ can be written as

$$P_{S_i e}^{sep} = P_{S_i e}^1 + P_{S_i e}^2 \tag{14}$$

where $P_{S_i e}^1$ and $P_{S_i e}^2$ are the error probabilities corresponding to the first and second event, respectively. They can be computed by

$$P_{S_i e}^1 = P_{S_i}^{(SD)} Pr\left[\left|\Lambda_{x_i}\right| < \Lambda_{S_i 0}\right] \tag{15}$$

$$\begin{aligned} P_{S_i e}^2 &= Pr\left[\hat{X}_{i,j} = 1 \middle| X_i = -1, \left|\Lambda_{x_i}\right| \ge \Lambda_{S_i 0}\right] \\ &= P_{S_i}^{(MAC)}\left(1 - P_{S_i,R_j}^e\right) + P_{S_i}^{(X)} \cdot P_{S_i,R_j}^e \end{aligned} \tag{16}$$

where $P_{S_i}^{(SD)}$ indicates the bit error probability that an error happens in the source-destination link, $P_{S_i}^{(MAC)}$ is the bit error probability that an error happens when the destination decodes by using the signals from both $S_i - D$ link and $R_j - D$ link, $P_{S_i}^{(X)}$ is the bit error probability that an error happens when the destination decodes by using the signals from both $S_i - D$ link and $R_j - D$ link. P_{S_i,R_j}^{e} is the error probability that the R_j decodes messages from the S_i unsuccessfully..

Based on (11)-(16), we can easily compute optimum thresholds to minimize the error probability. It is shown that the optimal thresholds $\Lambda_{S_i 0}^{opt}$ in the case of separated cooperation can be expressed as

$$\Lambda_{S_i 0}^{opt} = \log\left(\frac{P_{S_i}^{(X)} - P_{S_i}^{(MAC)}}{P_{S_i}^{(SD)}} - 1 \right) \tag{17}$$

3.2.2 Combined Cooperation

In this method, R_j evaluates the quality of the received signals from each user. If each LLR satisfies the preset requirement simultaneously, the relay R_j decodes and forwards the restored data to D. Otherwise, the output is null when one of them is null. The transmitted signal can be written as

$$X_{R_j} = \begin{cases} \sum_{i=1}^{M} g_{i,j} \hat{X}_{i,j}, & \left|\Lambda_{x_i}\right| > \Lambda_{S_i 0} \quad \textit{for all } i \\ 0, & \textit{otherwise} \end{cases} \tag{18}$$

where $\Lambda_{S_i 0}$ is the threshold set for forwarding the bits of S_i at the relay R_j.

Let P_e^{com} be the average BER at the destination when combined cooperation is employed. The optimal thresholds $\Lambda_{S_1 0}^{opt}, \Lambda_{S_2 0}^{opt}, \cdots, \Lambda_{S_M 0}^{opt}$ will be determined by minimizing P_e^{com}. More specifically, we have

$$\min_{\Lambda_{S_1 0}, \Lambda_{S_2 0}, \cdots, \Lambda_{S_M 0}} P_e^{com} \tag{19}$$

$$s.t. \quad \Lambda_{S_i 0} > 0, \quad i = 1, 2, \cdots, M. \tag{20}$$

Let $T_{S_1 S_2 \cdots S_M}^{e}$ denotes the event that the bit of S_i is decoded incorrectly at the relays, $T_{S_1 S_2 \cdots S_M}^{c}$ denotes the event that the bit of S_i is decoded correctly at the relays and $T_{S_1 S_2 \cdots S_M}^{x}$ denotes the event that the nulled bit of S_i at the relays. Assume $P = \left\{ \text{sgn}\left(\Lambda_{x_1}\right) \neq x_1, \text{sgn}\left(\Lambda_{x_2}\right) \neq x_2, \cdots \text{sgn}\left(\Lambda_{x_M}\right) \neq x_M \right\}$, $U \in P$ and $U \neq \varnothing$; $T = \left\{ \left|\Lambda_{x_1}\right| > \Lambda_{S_1,0}, \left|\Lambda_{x_2}\right| > \Lambda_{S_2,0}, \cdots \left|\Lambda_{x_M}\right| > \Lambda_{S_M,0} \right\}$; $Q = \left\{ \left|\Lambda_{x_1}\right| < \Lambda_{S_1,0}, \left|\Lambda_{x_2}\right| < \Lambda_{S_2,0}, \cdots \left|\Lambda_{x_1}\right| < \Lambda_{S_M,0} \right\}$, $V \in Q$ and $V \neq \varnothing$ respectively. The probabilities of $T_{S_1 S_2 \cdots S_M}^{e}$, $T_{S_1 S_2 \cdots S_M}^{e}$ and $T_{S_1 S_2 \cdots S_M}^{x}$ can be defined as

$$\begin{aligned} \Pr\left[T_{S_1 S_2 \cdots S_M}^{e} \right] &= \Pr\left[U \middle| T \right] \\ \Pr\left[T_{S_1 S_2 \cdots S_M}^{c} \right] &= 1 - \Pr\left[U \middle| T \right] \\ \Pr\left[T_{S_1 S_2 \cdots S_M}^{x} \right] &= \Pr\left[V \right] \end{aligned} \tag{21}$$

Consequently, the bit error probability at D is expressed as

$$P_e^{com} = P_{S_1 S_2 \cdots S_M}^{(SD)} \Pr\left[T_{S_1 S_2 \cdots S_M}^{x} \right] + P_{S_1 S_2 \cdots S_M}^{(MAC)} \Pr\left[T_{S_1 S_2 \cdots S_M}^{c} \right] + P_{S_1 S_2 \cdots S_M}^{(X)} \Pr\left[T_{S_1 S_2 \cdots S_M}^{e} \right] \tag{22}$$

where $P_{S_1S_2\cdots S_M}^{(SD)}$ indicates the bit error probability that an error happens in the source-destination link, $P_{S_1S_2\cdots S_M}^{(MAC)}$ is the bit error probability that an error happens when the destination decodes by using the signals from both $S_i - D$ link and $R - D$ link, $P_{S_1S_2\cdots S_M}^{(X)}$ is the bit error probability that an error happens in the cooperative transmission from S_i and R_j to D.

By using numerical integration to evaluate the expressions, we obtain all the elements of P_e^{com}; allowing us to obtain their numerical values for a specific ($\Lambda_{S_1 0}, \Lambda_{S_2 0}\cdots, \Lambda_{S_M 0}$) set. Finally, by using a numerical optimization algorithm (such as gradient descent), we can obtain the optimal set of ($\Lambda_{S_1 0}, \Lambda_{S_2 0}\cdots, \Lambda_{S_M 0}$) (denoted as ($\Lambda_{S_1 0}^{opt}, \Lambda_{S_2 0}^{opt}\cdots, \Lambda_{S_M 0}^{opt}$), respectively) optimized for minimize P_e^{com}.

4. Simulation Results

We study an example with four users, four relays and orthogonal channels among sources and relays. Assuming that each source node employs a (3824,1912) irregular LDPC code with degree distribution $\lambda(x) = 0.21606x + 0.1576x^2 + 0.154x^4 + 0.01848x^5 + 0.04312x^6 + 0.41074x^{18}$, $\rho(x) = x^8$. We assume the RS code coefficients are in the finite field $\mathrm{GF}\left(2^8\right)$, which is constructed based on the minimal polynomial $p\left(X\right) = 1 + X^2 + X^3 + X^4 + X^8$. We simulated all thresholding types in addition to the cases of without any thresholding , with the preset thresholding, with the optimal thresholding at the relays.

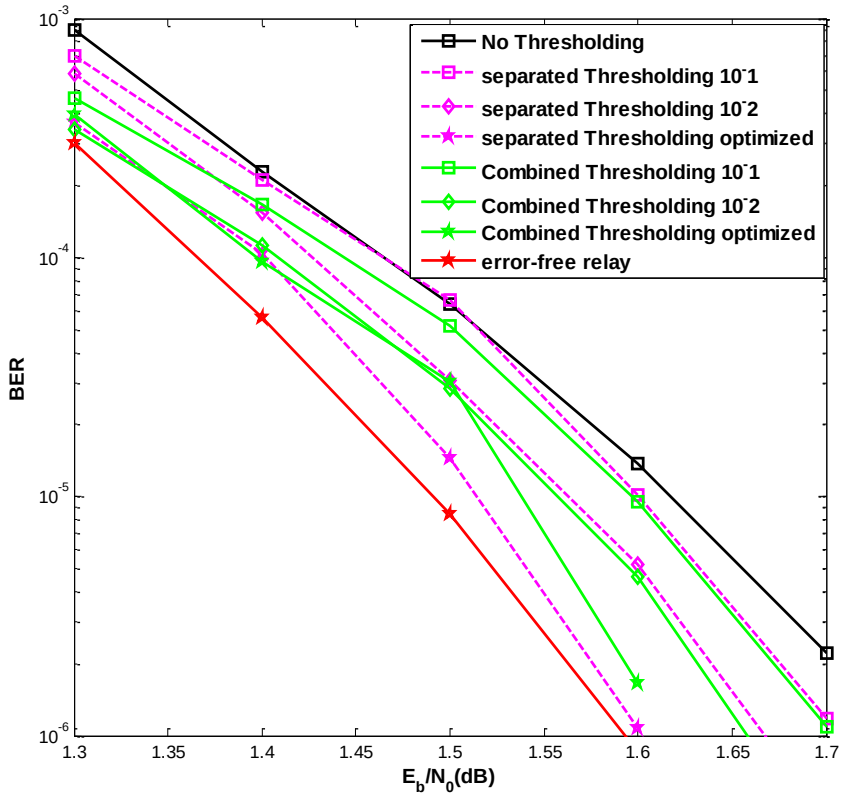


Fig.2 BER performance over AWGN channel

The results are depicted in Fig.2 for $SNR_{S_i,R_j} = SNR_{D,R_j}$, $N_{R_j,D} = 0.3$ over AWGN channel. We can see that the significant gain that separate thresholds provides over no thresholding at the relays, with the performance of separate thresholds displaying a gain of more than 0.18 dB at $\mathrm{BER} = 10^{-6}$ over no thresholding. Although we see a matching performance of combined thresholding and separate thresholding for $P_{eT} = 10^{-1}, 10^{-2}$. For $E_b / N_0 < 1.5\,\mathrm{dB}$, we find no difference between combined thresholding optimized and combined thresholding

$P_{eT}=10^{-2}$, but after that point we see that P_D^e using combined thresholding optimized is better than $P_{eT}=10^{-2}$. Finally we notice that the performance of combined thresholding performs worse than separate thresholds.

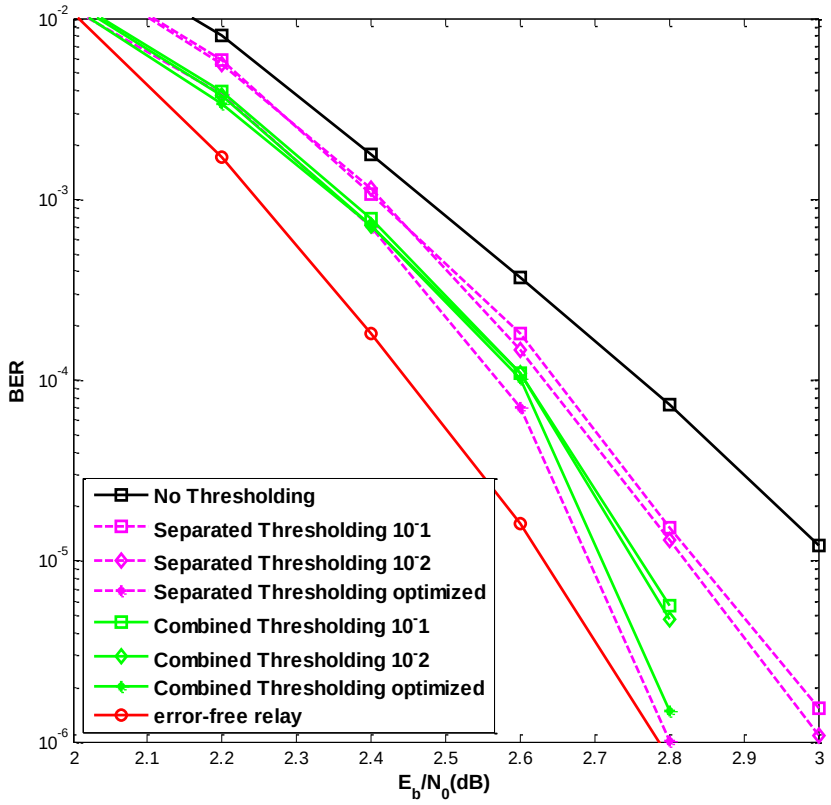


Fig.3 BER performance over Rayleigh fading channel

The results for the case are depicted in Fig.3 for $SNR_{S_i,R_j}=SNR_{D,R_j}+2$, $N_{R_j,D}=0.3$. Throughout the simulations, the channel is assumed that Rayleigh fading channel with $E\left[\left|h_{S_i,R_j}\right|^2\right]=E\left[\left|h_{S_i,D}\right|^2\right]=E\left[\left|h_{R_j,D}\right|^2\right]=1$. We can see that the significant gain that optimized thresholdes provides over no thresholding at the relays, with the performance of separated thresholds displaying a gain of more than 0.3dB and combined thresholds more than 0.2dB at BER $=10^{-5}$ over no thresholding. We see a matching performance of separated thresholding and combined thresholding for $P_{eT}=10^{-1}, P_{eT}=10^{-2}$. For $E_b/N_0<0.6$ dB, we find no difference of combined thresholding for all cases, but after that point we notice that the performance of combined thresholding optimized becomes better than $P_{eT}=10^{-1}, P_{eT}=10^{-2}$. However, we notice that the performance of separated thresholding for thresholding optimized performs better than $P_{eT}=10^{-1}, P_{eT}=10^{-2}$. We see that P_D^e using separated thresholding optimized performs better gain than other thresholds (where the performance without thresholding is significantly worse).

5. Conclusion

In this paper, a RS code based hybrid DF strategy at the relays has been proposed to mitigate error propagation in MUMR wireless networks. Our proposed technique relies on finding the reliability of bits at the relays, which can used to block the forwarding of unreliable bits. In addition, the optimal threshold derivation is derived to minimize bit error ratio (BER), and this technique is applied to separated cooperation and combined cooperation, respectively. Simulation results show that 0.01dB performance improvement with the proposed scheme in MUMR wireless networks at BER equal to 10-6 could be obtained when our proposed method was employed over both an AWGN channel and a fading channel. Applying the achieved guidelines, the noticeable performance improvement compared to of MUMR wireless networks with no the optimal threshold. This large performance gain could be achieved at the cost of slightly increased computational complexity. In terms of complexity it was shown that the performance of the optimal threshold for the separated cooperation was close to the combined cooperation while reducing the computational complexity of the LLR of the bit. In this paper, the effectiveness of our proposed method in mitigating error propagation in error-prone MUMR wireless

networks, which demonstrates that the proposed scheme may have potential use in MUMR wireless networks. However, their use in these specific scenarios needs further detailed analysis.

Acknowledgements

The authors acknowledge the 973 Program (2012CB316100).

References

[1] T. Cover and A. E. Gamal. “Capacity theorems for the relay channel”. IEEE Tran. Inf. Theory, 1979. 25, pp. 572-584.
[2] A. Nosratinia, T. E. Hunter, and A. Hedayat. “Cooperative Communication in Wireless Networks,” IEEE Communications Magazine, 2004, 42(10), pp. 74-80.
[3] J. Laneman, D. Tse, and G. Wornell. “Cooperative Diversity in Wireless Networks: Efficient Protocols and Outage Behavior”. IEEE Transactions on Information Theory, 2004, 50(12), pp. 3062-3080.
[4] B. Zhao and M.C. Valenti. “Distributed turbo codes diversity for the Relay Channel”. IEE Electronics Letters, 2003, 39(10), pp. 786-787.
[5] H. H. Sneessens, J. Louveaux, and L. Vandendorpe. “Turbo-coded decode-and-forward strategy resilient to relay errors”. in Proc. IEEE Int. Conf. Acoustics, Speech and Signal Processing ICASSP 2008, 2008, pp. 3213-3216.
[6] Y. Li, B. Vucetic, T. Wong, and M. Dohler. “Distributed Turbo Coding with Soft Information Relaying in Multihop Relay Networks”. IEEE Journal on Selected Areas in Communications, 2006, 24(11), pp. 2040-2050.
[7] H. V. Khuong and H. Y. Kong. “LLR-based decode-and-forward protocol for relay networks and closed-form ber expressions,” IE-ICE Tran. Fundamentals, 2006, 89, pp. 1832-1841.
[8] S. Li, R. W. Yeung, and N. Cai. “Linear network coding”. IEEE Tran. Inf. Theory, 2003, 49(2), pp. 371-381.
[9] R. Koetter and M. Mdard. “An algebraic approach to network coding”. IEEE/ACM Tran. Netw., 2003, pp. 782-795.
[10] C. Hausl, and J. Hagenauer, “Iterative network and channel decoding for the two-way relay channel”. in Proc. IEEE International Conference on Communication, 2006, 4, pp. 1568-1573.
[11] A. Y. C. Peng, S. Yousefi, and L. M. Kim, “On error analysis and distributed phase steering for wireless network coding over fading channels,” IEEE Tran. Wireless Commun, 2009, 8(11), pp. 5639-5649.
[12] M. Xiao and T. Aulin, “Optimal decoding and performance analysis of a noisy channel network with network coding,” IEEE Trans. Commun., 2009, 57, pp. 1402-1412.
[13] M. Xiao and M. Skoglund, “Multiple-user cooperative communications based on linear network coding,” IEEE Trans. Commun, 2010, 58, pp. 3345-3351.
[14] S. Y. Li, R. Yeung, and N. Cai, “Linear network coding”, IEEE Trans. Inform. Theory, 2003, 49(2), pp.371-381.
[15] S.W. Kim and E.Y. Kim, “Optimum receive antenna selection minimizing error probability,” WCNC2003, 2003, 1, pp.441-447.

第40卷，第8期
2019年8月
中国农业资源与区划
Chinese Journal of Agricultural Resources and Regional Planning
Vol. 40, No. 8, pp171-176
August, 2019

doi: 10.7621/cjarrp.1005-9121.20190821

中文文章叫近20年，英文文章是1996 to 2016, 文章完全一样

·资源利用·

近20年中国耕地数量变化趋势及其驱动因子分析*

王静怡[1]，李晓明[2※]

（1. 西安石油大学计算机学院，陕西西安 710065；2. 陕西省土地工程建设集团有限责任公司，西安 710075）

摘 要 [目的] 研究“二调”前后近20年我国耕地面积的变化趋势及其影响因子，为促进耕地保护和土地资源的高效集约节约利用提供决策支撑。[方法] 基于1996—2016年耕地数量的原始统计数据，利用数据挖掘技术选用ARIMA模型，基于两次全国土地调查时间段耕地数量数据进行相互预测和反推，即利用1996—2008年耕地数量数据预测2009年耕地数量，利用2009—2016年数据反推2008年耕地数量，从而实现数据的校正和比值归一化的目的，进一步研究近20年内我国耕地数量的变化趋势，并通过相关性分析研究遴选出其驱动因子。[结果] 趋势研究结果表明，近20年内我国耕地数量呈现逐年递减的趋势，其中2004年之前递减速度较快，之后递减速度趋缓。相关性分析结果显示，第一产值增加值占比、年末总人口数，以及城镇人口数是影响耕地数量变化的重要驱动因子，其相关系数分别为0.959，-0.918，-0.896。[结论] 从研究结果可以推论，我国在社会经济发展中的产业结构布局，以及城镇化建设进程对耕地数量变化产生了重要的影响。

关键词 数据挖掘 ARIMA模型 耕地数量 变化趋势 驱动因子

中图分类号：P96 文献标识码：A 文章编号：1005-9121[2019]08171-06

0 引言

我国是一个农业大国，耕地资源直接关系到国家粮食安全问题，是确保“中国人的饭碗牢牢端在自己手中”的重要基础。同时，在加快推进我国社会主义现代化建设进程中，经济建设对土地的旺盛需求也对耕地保护带来了极大的挑战[1]。对于我国耕地的变化趋势及其影响驱动力的研究，一直都是一个热点问题，甚至有专家学者通过史册文献资料的查证对过去300年我国部分省区耕地资源数量变化及驱动因素进行了研究[2]。

目前，对于我国耕地变化趋势的研究，多基于对统计数据进行分析，从空间尺度上可以分为国家尺度和区域尺度的研究。其中，对于国家尺度上的研究，由于统计标准、技术手段等多种因素的限制，2008—2009年数据发生明显的跳跃式变化，所以绝大部分的研究均处于2008年之前的部分时间段内，如毕于运等[3]通过对我国建国至1996年实有耕地面积的收集整理研究分析了其变化分析；李秀彬[4]对1999年我国前20年耕地面积变化的总体趋势、空间特征和驱动因子进行了研究；曹银贵[5]研究分析了1996—2005年全国耕地变化的情况及其影响的主要因子；黄忠华、吴次芳等利用1978—2007年我国耕地、经济增长、城镇化、地方财政收入数据分析了社会经济因素对耕地变化的影响[6]。以上研究均将时间局限在2008年之前，而回避了2008—2009年耕地统计数据跳跃的现象，这不利于科学研究我国耕地的变化趋势和指导耕地保护工作。对于区域尺度，如省级，甚至市县级尺度，由于统计基数较小，受统计方法、技术标准等因素的影响不大，几乎各个省份区域都有专家对其耕地变化和驱动因子进行了大量研究，如郭丽英等[7]

收稿日期：2018-03-26

作者简介：王静怡（1984—），女，陕西榆林人，博士、讲师。研究方向：资源利用和数据科学

※通讯作者：李晓明（1983—），男，山东烟台人，博士、高级工程师，硕士生导师。研究方向：土地资源利用和遥感信息。Email: xmlisdc@126.com

* 资助项目：陕西省教育厅科研计划项目“无线MARC系统中联合网络—信道编码的优化设计研究”（18JK0626）

(C)1994-2022 China Academic Journal Electronic Publishing House. All rights reserved. http://www.cnki.net

分析了 1996—2008 年我国沿海地区耕地变化的基本态势、时空特征及其主导成因；吴霞等[8]选取 1997—2014 年宁夏耕地面积数据分析耕地面积变化趋势及其驱动因子；武江民等[9]专门针对甘肃兰州市研究其耕地动态变化与驱动力的定量关系。还有学者则基于基于国家、区域、省域、市县不同尺度研究了中国耕地变化的驱动力[10]；

20 世纪 80 年代以来，随着遥感等 3S 技术的发展应用，诸多学者开始不仅仅局限于统计数据的应用，开始借助遥感信息技术对耕地变化进行研究。如张国平、刘纪元等[11]利用中国资源环境数据库及遥感影像对 20 世纪 80 年代末至 2000 年的中国耕地时空变化进行了分析；田光进、庄大方等[12]通过对遥感图像解译研究 80 年代末与 90 年代末 10 年间耕地时空动态变化特征；刘旭华，王劲峰等使用中国 1987—1989 年和 2000 年两期土地利用遥感调查数据，探索定量化研究国家尺度土地利用变化的驱动力[13,14]；许丽丽等[15]基于中分辨率卫星遥感数据，深入分析了 2000—2010 年中国耕地变化及其空间差异，并对中国耕地占补平衡政策的实施效果进行了评估；李景刚等[16]选取 1983—2001 年 NOAA 等遥感数据分析了北方 13 省的耕地变化与驱动力。遥感信息技术的应用开拓了耕地变化研究的新途径，但是由于遥感解译的精度仍有待于进一步提高，所以一定程度上制约了对于耕地变化的研究。

多来以来，我国对于耕地数量的数据统计有多种来源，其中以国土资源部的统计数据被认为最权威[17]。由于遥感影像解译精度，与实地调查统计相比仍有一定差距，所以大部分学者仍采用统计数据进行研究，而且大多避开了数据有明显变化的过渡年份。目前仅有极少数学者对过渡年份前后时间段的统计数据变化一并进行了相关的分析[17,18]。针对两次全国土地调查的统计数据的跳跃式变化，文章研究提出了基于数据挖掘技术研究分析两个时间段的数量关系，以更科学地反映耕地数量的变化趋势，同时基于校正数值研究影响耕地变化的驱动因子，这在目前的研究中尚未见到，对于科学反映我国耕地变化趋势具有积极的意义。

1 数据与方法

1.1 数据获取

1.1.1 全国耕地数量数据

我国耕地数量，尤其是历史时期的耕地数量，长期以来难以确定。国家土地管理部门从 1986 年开始，每年统计并公布我国耕地的增减情况，虽然还有其他职能部门的统计数据，但仍以国土资源部的数据最为权威[17]。为准确掌握全国耕地数量，1984—1996 年国务院安排开展了全国第一次大规模的土地利用现状调查，数据成果统计到了 1996 年 10 月 31 日，结果表明，1996 年全国耕地面积约为 1.300 亿 hm^2（19.51 亿亩）[18]，这一统计数据被认为具有最高可信度[19]。随后，1996—2008 年耕地面积数据均可直接从统计公报中查得。

为进一步准确掌握耕地土地基础数据，国家于 2007 年 7 月 1 日起，启动了第二次全国土地调查，数据统计时间节点为 2009 年 12 月 31 日，统计结果显示 2009 年我国耕地面积为 1.354 亿 hm^2（20.31 亿亩）[18]。随后的每年都有二调变更调查，2007—2016 年每年的全国耕地面积都可以从国家土地调查成果服务平台直接查得。由于第二次全国土地调查采用的技术方法的改进等原因，2008 年与 2009 年的耕地数量存在“跳跃”现象，为科学分析耕地的变化趋势，这一现象问题在后文中进行了着重的研究处理。

1.1.2 驱动因子数据

土地与人类社会的经济发展密不可分，全国耕地变化是在地理背景制约下、社会经济条件、灾害等自然条件共同驱动下发生的[1]，为探索研究耕地变化的驱动因子，该文主要选取了 3 方面共 17 个因子指标做遴选分析：一方面是反映全国经济发展水平的综合类指标，包括国民总收入、国内生产总值、第一产业增加值及比例、第二产业增加值及比例、第三产业增加值及比例、人均国内生产总值、工业增加值、建筑业增加值、农业总产值；另一方面是反映社会城镇化水平的指标，包括年末总人口、城镇人口、乡村人口；还有第三方面是反映自然灾害的指标，包括受灾面积和粮食产量[20]。上述因子指标近 20 年的数据均

(C)1994-2022 China Academic Journal Electronic Publishing House. All rights reserved. http://www.cnki.net

直接从国家统计局网站查得。

1.2　研究方法

该文研究通过对近 20 年全国耕地数量数据的分析处理，研究其变化趋势，进而通过与选取的因子进行相关性分析，研究其变化的驱动因子。其中，在对 1996—2016 年耕地面积的数据分析中，针对 2008—2009 年数据的跳跃现象，通过数据挖掘，一方面利用 1996—2008 年数据预测 2009 年数据，另一方面利用 2009—2016 年数据反推 2008 年数据，基于上述两种相互预测或反推得出的数值，分析 2008 年和 2009 年耕地数量的数据比例关系，进而对 1996—2016 年耕地面积数据进行比值归一化，以探索研究耕地面积的变化趋势。

该文在数据挖掘预测中，通过遴选对比最终采用的为 ARIMA 模型，即自回归积分滑动平均模型(Autoregressive Integrated Moving Average Model)，是由博克思(Box)和詹金斯(Jenkins)提出的著名时间序列预测方法，主要是指将非平稳时间序列转化为平稳时间序列，然后将因变量仅对它的滞后值以及随机误差项的现值和滞后值进行回归所建立的模型，适用于该文的研究。

2　近 20 年耕地数量变化趋势分析

2.1　基于耕地数量原始统计数据的变化趋势及分析

通过对收集整理的 1996—2016 年耕地数量数据分析，如图 1，可以看出，1996—2008 年全国耕地面积逐年减少，其中以 2000—2004 年递减速度最快；2008—2009 年耕地面积数据出现跳跃，由 1.217 亿 hm^2(18.26 亿亩)增至 1.354 亿 hm^2(20.31 亿亩)；2009—2016 年耕地面积递减速度非常缓慢。

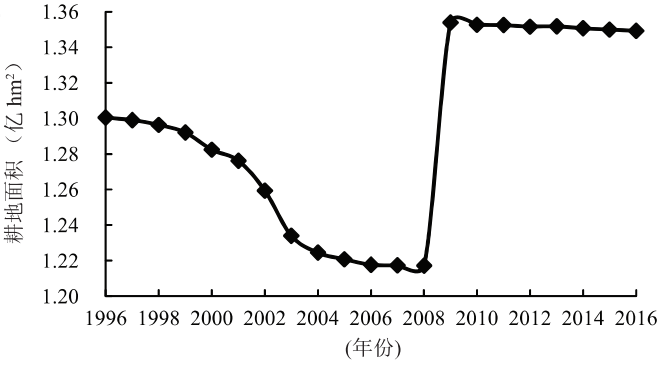


图 1　1996—2016 年基于原始统计数据的耕地数量变化趋势

1996 年国家完成了第一次大规模的土地利用现状调查；2009 年第二次全国土地利用现状调查完成。由此可见，2008—2009 年耕地面积数据的跳跃正是一调与二调数据的分界年份。全国耕地面积是否真的增多了约 0.14 亿 hm^2(2 亿亩)，经文献查阅分析[17,18,21]，主要原因在于二调采用了更为先进的技术手段，将以往少报的耕地面积统计入库，进一步提高了数据的准确度。所以，近 20 年全国耕地数量的统计数据是基于两次不同的技术水平，可直接分别研究各自时段内的变化趋势，但如果要研究连续 20 年时间段内的变化趋势，就须对两个时间段的数据进行校正，使之具有可对比性。

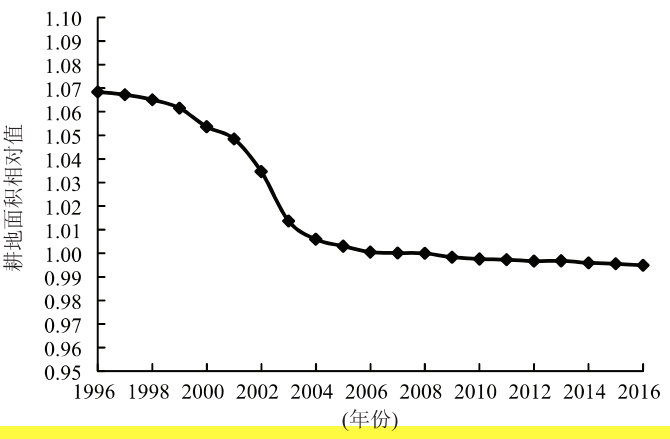


图 2　1996—2016 年基于校正后相对数据的耕地变化趋势

2.2　基于数据挖掘的耕地数量校正

数据挖掘技术在时间序列上具有强有力的预测功能，该文首先利用 1996—2008 年耕地数量数据，预测 2009 年的耕地数量，由此得出 2009 年与 2008 年耕地数量的比值关系 α；然后利用 2009—2016 年耕地数量数据，反推 2008 年的耕地数量，由此得出 2009 年与 2008 年耕地数量的比值关系 β；为更为科学地反映 2009 年与 2008 年耕地数量的比值关系，取利用正向预测与反向反推两种方法得出的 α 与 β 的算数平均值 ρ 作为实际的数量比值关系。

该文研究在预测过程中，利用 SPSS 软件，通过比较分析，在正向预测 2009 年数值和反向反推 2008

(C)1994-2022 China Academic Journal Electronic Publishing House. All rights reserved.　http://www.cnki.net

年数值中均选用 ARIMA 模型，其中正向预测选用的模型为 ARIMA（1，1，2）（$r^2=0.975^{**}$），反向反推选用的模型为 ARIMA（1，1，4）（$r^2=0.966^{**}$），两者均在 0.01 水平呈现显著性。由此，基于 1996—2008 年数据预测得出的 2009 年耕地数量为 1.213 387 亿 hm^2（18.200 8 亿亩），基于 2009—2016 年数据反推得出的 2008 年耕地数量为 1.353 987 亿 hm^2（20.309 8 亿亩），进一步可得出 $\alpha=996\ 899.887\ E-6$，$\beta=999\ 895.617\ E-6$，则 $\rho=998\ 397.752\ E-6$，由此推测 2009 年与 2008 年耕地数量的比值为998 397.752 E－6，即可为两个时间段数据的校正系数。

2.3 基于耕地数量校正相对值的变化趋势分析

为进一步客观的反映近 20 年的耕地数量变化趋势，对全部年份数据进行比值归一化及系数校正，在前文研究基础上，首先对 1996—2008 年全部原始耕地数量数据以 2008 年耕地数量为基数计算得到的比值即为其耕地数量相对值，对 2009—2016 年全部原始耕地数量数据以 2009 年耕地数量为基数计算得到的比值，再乘以校正系数 ρ，即为其相应年份的耕地数量相对值。由此可以得出 1996—2016 年耕地数量的变化趋势，如图 2 所示，可以看出，近 20 年全国耕地数量是呈现递减趋势的，其中 2004 年以前，递减速度较快，2004 年以后耕地数量递减速度较缓，尤其是 2006 年以后耕地数量递减速度趋于稳定。

3 耕地数量变化驱动因子分析

该文研究共收集了 1996—2016 年共 17 个因子指标，首先进行描述性特征统计，如表 1 所示；然后，通过分析耕地数量与各因子指标的相关性（表 2），进行对比分析，以此遴选出耕地数量变化的驱动因子。

表 1 1996—2016 年各因子指标的描述性统计特征

因子	最小值	最大值	平均值	标准差
国民总收入（亿元）	70 780	741 140	304 446.950	225 956.601
国内生产总值（亿元）	71 814	744 127	305 718.670	226 519.843
第一产业增加值（亿元）	13 878	63 671	31 240.710	17 742.619
第一产业增加值占比（%）	8.556	19.325	12.114	3.280
第二产业增加值（亿元）	33 828	296 236	135 629.240	94 949.577
第二产业增加值占比（%）	39.810	47.559	45.327	1.999
第三产业增加值（亿元）	24 107	384 220	138 848.860	114 605.836
第三产业增加值占比（%）	33.569	51.634	42.560	4.472
人均国内生产总值（亿元）	5 898	53 980	22 872	16 332.770
工业增加值（亿元）	29 530	247 860	116 532.760	79 508.293
建筑业增加值（亿元）	4 393	49 522	19 623	15 992.727
年末总人口（万人）	122 389	138 271	131 047.710	4 702.171
城镇人口（万人）	37 304	79 298	58 413.240	12 989.267
乡村人口（万人）	58 973	85 085	72 634.480	8 313.397
农业总产值（亿元）	13 540	59 288	28 842.620	16 570.347
粮食产量（万 t）	43 070	62 144	52 326.480	5 812.061
受灾面积（万 hm^2）	2 177	5 468.8	4 100.948 0	1 070.630

由表 2 可以看出，基于原始统计的耕地面积研究其与各因子指标的相关性，由于数据的跳跃不足以反映耕地变化的实际趋势，与各因子指标的相关性均不高。基于校正后的耕地数量的相对值，研究其与各因子指标的相关性，可以发现，与第一产值增加值占比的相关性最高，相关系数高达 0.959；与年末总人口的相关性次之，为负相关，系数为 －0.918，城镇人口和乡村人口与之的相关性也较高，即第一产业增加值占比，总人口以及城镇人口数量与耕地数量的变化相关性较好，是重要的驱动因子。由此，可以推论出国家产业结构布局调整、我国城镇化建设水平是影响我国耕地数量变化的重要因素条件。耕地作为第一产

(C)1994-2022 China Academic Journal Electronic Publishing House. All rights reserved. http://www.cnki.net

表 2　耕地面积与各因子的相关系数矩阵

	原始统计耕地面积	校正后耕地面积相对值		原始统计耕地面积	校正后耕地面积相对值
原始统计耕地面积	1	-0.142	人均国内生产总值	0.651	-0.749
校正后耕地面积相对值	-0.142	1	工业增加值	0.638	-0.784
国民总收入	0.649	-0.746	建筑业增加值	0.688	-0.716
国内生产总值	0.652	-0.745	年末总人口	0.433	-0.918
第一产业增加值	0.663	-0.736	城镇人口	0.488	-0.896
第一产业增加值占比	-0.274	0.959	乡村人口	-0.518	0.88
第二产业增加值	0.647	-0.774	农业总产值	0.686	-0.709
第二产业增加值占比	-0.519	0.259	粮食产量	0.752	-0.524
第三产业增加值	0.649	-0.717	受灾面积	-0.514	0.708

业的最重要的载体之一，与第一产业增加值密切正相关，我国产业结构中对于第一产业布局要求会直接诱使我国耕地的变化。而城镇化建设过程中，一方面由于城镇建设会直接占用大量的耕地，另一方面，城镇化建设中大量的农民人口直接进入城镇生活，或者进城务工而导致耕地撂荒，所以城镇化建设水平与耕地变化呈现密切的负相关。

4　结论与讨论

土地本身既有自然属性，又有社会属性，对于耕地数量的统计长期以来受社会、经济、政策等诸多因素的影响，导致难以对其进行长时间序列的趋势研究。该文研究的时间序列跨度全国两次土地调查的统计数据，两个时间阶段的数据具有明显的跳跃性，但并不代表 2009 年耕地数量真的比 2008 年大幅度增长。究其原因，主要是由于第二次全国土地调查中应用遥感等新方法、统一了标准，提高了调查的技术水平和准确度，使原来因少报、漏报、瞒报等各种原因未被统计到的耕地重新统计入库，所以要研究跨两个阶段的整体变化趋势，就必须研究建立其数值量化关系。该文通过数据挖掘，并对耕地数量进行校正和比值归一化，研究结果比较准确地反映了我国耕地变化趋势的实际情况。

研究结果表明，近 20 年，我国耕地数量呈现递减趋势，其中 2004 年以前递减速度较快，2004 年以后递减速度趋缓，我国产业结构布局方面，主要是第一产业增加值占比，以及我国人口总数方面，主要是城镇化人口数量是影响变化的主要驱动因子。由于 1999 年后开始生态退耕导致耕地数量迅速减少[17,22]，2004 年国家《土地管理法》修订后强调要加强耕地保护，实行占补平衡，对我国耕地的数量变化产生了积极作用。该文仅对近 20 年我国耕地数量的变化趋势进行了分析；现在国家加强耕地保护，不仅以数量为基础，更关注质量，以产能为核心，实现数量、质量和生态的三位一体保护[23]，下一步将对全国耕地质量的变化趋势进一步分析研究。同时，该文研究通过相关性分析研究提出了主要驱动因子，下一步还将进一步对驱动因子的贡献率进行量化分析研究。

该文研究仅对 1996—2016 年耕地数量的变化趋势进行了分析研究，由于对诸多指标因子数据统计的完整性需求，未对更长时间的耕地变化趋势进行研究。下一步，将在对统计数据分析的基础上，通过对遥感影像的数据挖掘，深入研究更长时间序列的变化趋势。

参考文献

[1] 赵其国，周生路，吴绍华，等. 中国耕地资源变化及其可持续利用与保护对策. 土壤学报，2006，43（4）：662－672.

[2] 葛全胜，戴君虎，何凡能，等. 过去 300 年中国部分省区耕地资源数量变化及驱动因素分析. 自然科学进展，2003，13（8）：825－832.

[3] 毕于运，郑振源. 建国以来中国实有耕地面积增减变化分析. 资源科学，2000，22（2）：8－12.

[4] 李秀彬. 中国近 20 年来耕地面积的变化及其政策启示. 自然资源学报，1999，14（4）：329－333.

(C)1994-2022 China Academic Journal Electronic Publishing House. All rights reserved.　http://www.cnki.net

[5] 曹银贵，袁春，周伟，等. 中国耕地变化的驱动因子及其省域差异分析. 中国土地科学，2008，22（2）：17－22.
[6] 黄忠华，吴次芳，杜雪君. 我国耕地变化与社会经济因素的实证分析. 自然资源学报，2009，24（2）：192－199.
[7] 郭丽英，王道龙，王介勇. 中国沿海地区耕地变化及其成因分析. 中国农业资源与区划，2012，33（1）：6－10.
[8] 吴霞，王世荣，尚红莺，等. 宁夏近 18 年来耕地面积动态变化及驱动力分析. 中国农业资源与区划，2017，38（8）：98－104.
[9] 武江民，赵学茂，党国锋. 甘肃兰州市耕地动态变化与驱动力关系定量研究. 干旱区资源与环境，2010，24（12）：33－38.
[10] 于天，曹银贵，许婧雪. 基于不同尺度的中国耕地变化驱动力研究进展. 中国农学通报，2016，32（24）：194－198.
[11] 张国平，刘纪远，张增祥. 近 10 年来中国耕地资源的时空变化分析. 地理学报，2003，58（3）：323－332.
[12] 田光进，庄大方，刘明亮. 近 10 年中国耕地资源时空变化特征. 地球科学进展，2003，18（1）：30－36.
[13] 刘旭华，王劲峰，刘纪远，等. 国家尺度耕地变化驱动力的定量分析方法. 农业工程学报，2005，21（4）：56－60.
[14] 刘旭华，王劲峰，刘明亮，等. 中国耕地变化驱动力分区研究. 中国科学 D 辑地球科学，2005，35（11）：1087－1095.
[15] 许丽丽，李宝林，袁烨城，等. 2000—2010 年中国耕地变化与耕地占补平衡政策效果分析. 资源科学，2015，37（8）：1543－1551.
[16] 李景刚，何春阳，史培军，等. 近 20 年中国北方 13 省的耕地变化与驱动力. 地理学报，2004，59（2）：274－282.
[17] 封志明，刘宝勤，杨艳昭. 中国耕地资源数量变化的趋势分析与数据重建：1949—2003. 自然资源学报，2005，20（1）：35－43.
[18] 谭永忠，何巨，岳文泽，等. 全国第二次土地调查前后中国耕地面积变化的空间格局. 自然资源学报，2017，32（2）：186－197.
[19] Lin G C S，HO S P S. China´s land resources and land-use change：insights from the 1996 land survey. land Use Policy，2003，20（2）：87－107.
[20] 傅泽强，蔡运龙，杨友孝，等. 中国粮食安全与耕地资源变化的相关分析. 自然资源学报，2001，16（4）：313－319.
[21] 张雅琼，杨子生. 我国两次土地资源调查的对比分析. 国土资源科技管理，2013，30（2）：100－104.
[22] 徐宪立，蔡玉梅，张科利，等. 耕地资源动态变化及其影响因素分析. 中国人口·资源与环境，2005，15（3）：75－79.
[23] 谭永忠，吴次芳，王庆日，等. “耕地总量动态平衡”政策驱动下中国的耕地变化及其生态环境效应. 自然资源学报，2005，20（5）：727－734.

RESEARCH ON THE CHANGE TREND OF FARMLAND QUANTITY IN CHINA FOR RECENT 20 YEARS AND ITS DRIVING FACTORS*

Wang Jingyi[1], Li Xiaoming[2]※

（1. Xi´an Shiyou University，Xi´an，Shaanxi 710065，China；
2. Shaanxi Provincial Land Engineering Construction Group，Xi´an，Shaanxi 710075，China）

Abstract The research aims to research the changing trend of farmland quantity for recent 20 years before and after the second national land use survey. It could provide decision support for farmland protection and efficient use of land resources. The original data of farmland area from 1996 to 2016 were collected，data mining technology was introduced，and ARIMA model was chosen to predict the farmland quantity each other based on the farmland area of the twice land use survey，which meant to predict the farmland quantity of 2009 with the farmland quantity of the years from 1996 to 2008，and to predict the farmland quantity of 2008 inversely with the farmland quantity of the years from 2009 to 2016，so the original farmland area data could be corrected and normalized. Then the changing trend of farmland quantity for recent 20 years was studied furtherly and correlation analysis was used to study the driving factors. The trend research result showed，the farmland area decreased year by year for recent 20 years，the decreasing rate was faster before 2004，and then it decreased slowly. The correlation analysis result showed，the added value proportion of primary industry，the total population，and the urban population were the most important driving factors which influenced the farmland quantity change，their coefficients were 0.959，－0.918 and －0.896 respectively. It could be concluded by the result that the industry configuration and the urbanization could affect the farmland quantity with the development of social economy.

Keywords data mining；ARIMA model；farmland quantity；change trend；driving factors

(C)1994-2022 China Academic Journal Electronic Publishing House. All rights reserved. http://www.cnki.net

doi:10.3969/j.issn.1001-2400.2013.02.003

适用于网络 LDPC 码的速率兼容算法

王静怡[1,2]，李 颖[1,2]，孙 岳[1,2]

(1. 西安电子科技大学 综合业务网理论及关键技术国家重点实验室，陕西 西安 710071；
2. 电信科学研究院 无线移动通信国家重点实验室，北京 100083)

摘要：提出了一种可以获得最小比特错误概率的网络低密度奇偶校验(LDPC)码速率兼容删余算法，并推导了该算法的译码错误概率. 该算法基于网络 LDPC 码的结构特点，以达到译码最小比特错误概率为目标，在网络 LDPC 码的 Tanner 图上搜索出需要删余的变量节点，以获得最优的删余图样. 仿真结果表明，该算法比现有算法在 BER 为 10^{-4} 时有 0.4 dB 的性能增益.

关键词：多址接入中继网络；LDPC 码；网络 LDPC 码；速率兼容；删余

中图分类号：TN911.22 **文献标识码**：A **文章编号**：1001-2400(2013)02-0013-05

Rate-compatible network LDPC codes

WANG Jingyi[1,2], *LI Ying*[1,2], *SUN Yue*[1,2]

(1. State Key Lab. of Integrated Service Networks, Xidian Univ., Xi'an 710071, China; 2. State Key Lab. of Wireless Mobile Communications, China Academy of Telecommunication Technology, Beijing 100083, China)

Abstract: A rate-compatible puncturing algorithm for network LDPC codes is proposed to achieve the minimum error probability, and decoding error probability is derived. The algorithm for finding variable nodes to be deleted based on the tanner graph of network LDPC codes is proposed, which is aimed at minimizing the decoding error probability and optimizing the puncturing pattern. Simulation results illustrate that, at BER = 10^{-4}, the proposed rate-compatible network LDPC codes have a coding gain of about 0.4 dB compared with the codes obtained via the existing punctured methods.

Key Words: multi-access relay network; low-density parity-check (LDPC) codes; network LDPC code; rate-compatible; puncturing

由于无线移动信道具有衰落和时变特性，为最大限度地利用信道容量，可采用链路自适应技术，使信道编码速率、调制方式、信号功率等参数能够随信道质量的变化而变化. 链路自适应技术的基础是速率兼容纠错码的设计，其基本概念由文献[1]首次提出，速率兼容低密度奇偶校验(LDPC)码的设计则是近几年的研究热点. 文献[2-3]通过分组和排序操作，将 LDPC 码的变量节点按照迭代恢复次数进行分类，设计了 LDPC 码速率兼容删余算法，可以获得比随机删余更好的性能. 文献[4]首次提出了一种基于有限域上非零元素二进制镜像的缩短码构造方案，用来实现低码率的速率兼容多元 LDPC 码. 文献[5]研究了码率从 1/10 到 5/6 的灵活变化的非规则多元 LDPC 码比特级缩短算法. 文献[6]以多维累加交叉并行级联单奇偶校验码为母码，对奇偶校验比特按组删余，构建了一组速率兼容编码.

上述速率兼容算法都是针对点对点通信链路设计的. 然而，随着无线通信技术的发展和中继协作传输技术的引入，信道编码的设计也从点对点链路推广至无线中继网络. 对于多址接入中继网络，有多个节点同时

收稿日期：2012-06-09 网络出版时间：2012-11-16
基金项目：国家自然基金资助项目(61072064)；国家科技重大专项资助项目(2010ZX03003-003-03)；长江学者和创新团队发展计划资助项目(IRT0852)；中央高校科研业务费专项资金资助项目(K50510010026)
作者简介：王静怡(1984－)，女，西安电子科技大学博士研究生，E-mail：wangjy@stu.xidian.edu.cn.
网络出版地址：http://www.cnki.net/kcms/detail/61.1076.TN.20121116.0924.201302.16_009.html

(C)1994-2023 China Academic Journal Electronic Publishing House. All rights reserved. http://www.cnki.net

需要中继节点帮助转发数据,在中继节点设计有效的联合网络-信道编码算法,可在改善接收端性能的同时,有效提高转发效率. 文献[7]利用 LDPC 码,针对多址接入中继信道设计了一种网络 LDPC 码,并指出可以通过调整中继节点转发数据量来实现中继转发效率和接收端译码性能的有效折中. 与单个 LDPC 码相比,网络 LDPC 码的校验矩阵包括了源节点和中继节点所采用 LDPC 码的校验矩阵,因此其本质上可看做是一种多用户码. 另外,单个 LDPC 码的所有编码比特是在同一个信道中传输,所有编码比特受到相同的噪声干扰,网络 LDPC 码的编码比特则由对应的源节点和中继节点分别传输,不同传输链路将会受到不同的噪声干扰. 笔者将根据网络 LDPC 码的上述特性,设计相应的速率兼容算法.

1 适用于多址接入中继信道的网络 LDPC 码

由两个源节点、一个中继节点和一个目的节点构成的多址接入中继网络模型如图 1 所示. 两个源节点与目的节点之间的信息传输由广播发送和中继转发两个阶段完成. 在广播阶段,两个源节点分别向中继节点和目的节点广播发送编码序列 X_1 和 X_2;在中继转发阶段,中继节点首先对接收信号进行译码,得到两个源节点的估计数据,然后对译码得到的估计数据重新进行联合编码,并将编码序列 X_R 转发至目的节点. 目的节点则根据收到的信号进行联合译码,得到两个源节点的估计信息.

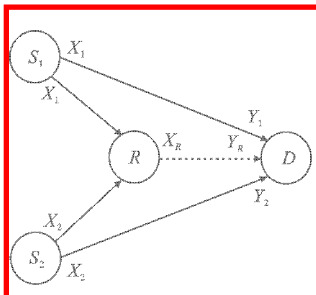


图 1 多址接入中继信道模型

目的节点将两个源节点和中继节点采用的 LDPC 码综合考虑,可得到如下校验矩阵:

$$\boldsymbol{H}=\begin{bmatrix}\boldsymbol{H}_1 & \boldsymbol{0} & \boldsymbol{0}\\ \boldsymbol{0} & \boldsymbol{H}_1 & \boldsymbol{0}\\ \boldsymbol{A} & \boldsymbol{B} & \boldsymbol{C}\end{bmatrix}, \tag{1}$$

其中,$\boldsymbol{H}_1$ 是源节点采用 LDPC 码的校验矩阵,$\boldsymbol{H}_3=[\boldsymbol{A},\boldsymbol{B},\boldsymbol{C}]$,是中继节点采用 LDPC 码的校验矩阵,$\boldsymbol{0}$ 是零矩阵. 由于式(1)中包含了源节点和中继节点所采用 LDPC 码的校验矩阵,并且中继节点是对两个源节点的数据进行联合编码,因此文献[7]称之为网络 LDPC 码,该码的 Tanner 图如图 2 所示.

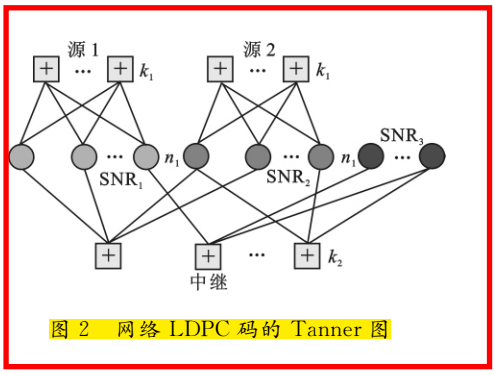


图 2 网络 LDPC 码的 Tanner 图

图 2 中网络 LDPC 码的 Tanner 图包含上下两层子图,其中上层子图包含 $2k_1$ 个校验节点,它们与变量节点的连接关系由 $\boldsymbol{H}_1$ 确定;下层子图包括 k_2 个校验节点,它们与变量节点的连接关系由式(1)中的 $\boldsymbol{H}_3$ 确定. 图中每个变量节点的度用(i,j)表示,其中 i 为变量节点与上层校验节点相连的边数,j 为变量节点与下层校验节点相连的边数. 用 d_c 和 d'_c 分别表示上层和下层校验节点的度数.

2 速率兼容网络 LDPC 码的设计

由图 2,网络 LDPC 码的变量节点包含两个源节点所采用的 LDPC 码的变量节点和中继节点所采用的联合 LDPC 码的变量节点,且不同变量节点通过不同的信道达到目的节点. 因此,需要考虑上述特点对删除变量节点恢复概率的影响,并由此设计适用于网络 LDPC 码的速率兼容算法.

2.1 几个定义

定义 1 若被删余的校验比特所对应的变量节点在迭代过程中接收到非零信息,则无论获得的信息正确与否,都称之为“恢复”[2].

定义 2 译码中第 n 次迭代时才恢复的被删除的变量节点称为 n 步恢复变量节点,用 n-SR 表示,而所有 n-SR 构成的集合则用 G_n 表示[2].

图 3 给出了一个包含 1-SR 节点、2-SR 节点的恢复树,其中竖线圆表示幸存的删余变量节点 S(v),横线圆表示未删余变量节点,方块表示校验节点.

(C)1994-2023 China Academic Journal Electronic Publishing House. All rights reserved. http://www.cnki.net

定义 3　如果一个一步恢复的删余变量节点至少与一个校验节点相连,且与这个校验节点相连的变量节点没有被完全删余掉,那么称这个校验节点为幸存校验节点[2]. 图 3 中的校验节点 S_1 和 S_2 即为幸存校验节点,而校验节点 D 则为死校验节点.

定义 4　幸存校验节点相连的其余未被删除的变量节点称为幸存变量节点.

由图 2 可见,网络 LDPC 码的编码比特是通过 3 个不同信道到达接收端的,因此,在设计网络 LDPC 码的删余算法时,不仅要考虑被删余变量节点的幸存邻居变量节点数,还要考虑每个幸存邻居变量节点受到的噪声大小. 下面,引入等效幸存变量节点数的概念.

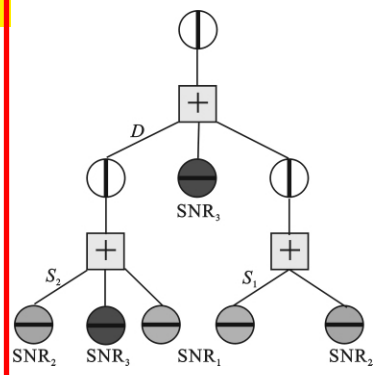


图 3　网络 LDPC 码的恢复树

定义 5　假设网络 LDPC 码所有编码比特在传输过程中受 K 种噪声干扰,其对应的噪声方差分别为 $\sigma_1^2>\sigma_2^2>\cdots>\sigma_K^2$,令每个受到噪声干扰最大(噪声功率为 σ_1^2)的幸存邻居变量节点的等效幸存邻居变量节点数为 1,则受其他噪声干扰的幸存邻居变量节点的等效幸存邻居变量节点数定义为

$$\alpha_i=\left\{\log\left(1-\varphi\left(\frac{2}{\sigma_i^2}\right)\right)\Big/\left[\log\left(1-\varphi\left(\frac{2}{\sigma_1^2}\right)\right)\right]\right\}\leqslant 1\quad,\quad i=1,2,\cdots,K\quad, \tag{2}$$

其中

$$\varphi(x)=\begin{cases}\dfrac{1}{(4\pi x)^{1/2}}\displaystyle\int_R\tanh\frac{u}{2}\exp\left(-\frac{(u-x)^2}{4x}\right)\mathrm{d}u\quad, & x>0\quad,\\ 0\quad, & x=0\quad.\end{cases}$$

2.2　译码恢复错误概率

将网络 LDPC 码的删余变量节点 v 的所有幸存邻居变量节点按照其所通过信道的噪声功率的大小分为 b 类,假设第 t 类的噪声功率为 $\sigma_t^2(t=1,2,\cdots,b)$,且 $\sigma_1^2>\sigma_2^2>\cdots>\sigma_b^2$,并设第 t 类包括 S_t 个变量节点,记为 $\{v_1^t,\cdots,v_s^t,\cdots,v_{S_t}^t\}$. 与 LDPC 码类似,首先估计每次迭代过程中删余网络 LDPC 码的每个变量节点的均值更新,并由此计算该节点的恢复错误概率.

由于网络 LDPC 码的译码同样包括变量节点更新和校验节点更新,但图 2 给出的 Tanner 图表明,网络 LDPC 码的校验节点更新实际上包括上层校验节点和下层校验节点更新. 下面将分析在迭代译码过程中,速率兼容删余的网络 LDPC 码的变量节点和校验节点的均值更新过程.

假设校验节点的度分布分别为 $\rho^{\mathrm{up}}(x)=\sum_{k=1}^{d_c}\rho_k^{\mathrm{up}}x^{k-1}$ 和 $\rho^{\mathrm{low}}(x)=\sum_{k=1}^{d_c'}\rho_k^{\mathrm{low}}x^{k-1}$;$\eta$ 是上层变量节点与校验节点相连的边数占总边数的比例;$\lambda_{i,j}$ 是与度为 (i,j) 的变量节点连接的边数占总边数的比例;$m_{i,j}^{l-1}$ 和 $n_{i,j}^{l-1}$ 分别表示第 $(l-1)$ 次迭代时,变量节点传给上下层的校验节点的对数似然比的均值. 第 l 次迭代时,上下层校验节点的均值更新过程如下:

(1) 当上下层的校验节点向被删余的度为 (i,j) 的变量节点 $v\in G_{l+1}$ 传递消息时,该消息的对数似然比的均值分别为

$$m^{\prime l}=\sum_k\rho_k^{\mathrm{up}}\varphi^{-1}\left\{\left[\frac{1}{\eta}\sum_{i\geqslant 0,j\geqslant 0}\frac{i}{i+j}\lambda_{i,j}\varphi(m_{i,j}^{l-1})\right]^{\sum_{t=1}^{b}S_t\alpha_t}\right\}\quad, \tag{3}$$

$$n^{\prime l}=\sum_k\rho_k^{\mathrm{low}}\varphi^{-1}\left\{\left[\frac{1}{1-\eta}\sum_{i\geqslant 0,j\geqslant 0}\frac{j}{i+j}\lambda_{i,j}\varphi(n_{i,j}^{l-1})\right]^{\sum_{t=1}^{b}S_t\alpha_t}\right\}\quad, \tag{4}$$

其中,α_t 表示每个幸存邻居变量节点 v_s^t 的等效幸存邻居变量节点数,S_t 表示与变量节点 v 相连的校验节点没有被删余的变量节点数,变量节点 v 的总等效幸存邻居变量节点数为 $\sum_{t=1}^{b}S_t\alpha_t$.

(2) 当上下层的校验节点向没有删余的度为 (i,j) 的变量节点 v 传递消息时,该消息的对数似然比的均值[7]分别为

$$m^{\prime l}=\sum_k\rho_k^{\mathrm{up}}\varphi^{-1}\left\{\left[\frac{1}{\eta}\sum_{i\geqslant 0,j\geqslant 0}\frac{i}{i+j}\lambda_{i,j}\varphi(m_{i,j}^{l-1})\right]^{k-1}\right\}\quad, \tag{5}$$

(C)1994-2023 China Academic Journal Electronic Publishing House. All rights reserved.　http://www.cnki.net

$$n^{'l}=\sum_k \rho_k^{\text{low}}\varphi^{-1}\left\{\left[\frac{1}{1-\eta}\sum_{i\geqslant 0,j\geqslant 0}\frac{j}{i+j}\lambda_{i,j}\varphi(n_{i,j}^{l-1})\right]^{k-1}\right\}. \tag{6}$$

上下层变量节点的均值更新过程如下:

第 l 次迭代时,度为(i,j) 的变量节点传给上下层校验节点的对数似然比消息均值[7]分别为

$$m_{i,j}^{l}=\begin{cases}(i-1)m^{'l}+jn^{'l}+m_{u_0}, & i\neq 0,\ j\geqslant 0,\\ jn^{'l}+m'_{u_0}, & i=0,\ j\geqslant 1,\end{cases} \tag{7}$$

$$n_{i,j}^{l}=\begin{cases}im^{'l}+(j-1)n^{'l}+m_{u_0}, & i\neq 0,\ j\geqslant 1,\\ (j-1)n^{'l}+m'_{u_0}, & i=0,\ j\geqslant 1,\\ im^{'l}+m_{u_0}, & i\neq 0,\ j=0.\end{cases} \tag{8}$$

若变量节点被删掉,则 $m_{u_0}(m'_{u_0})=0$;若变量节点为由源节点发送至目的节点的信息比特,则 $m_{u_0}=2/\sigma_{SD}^2$;若变量节点为中继节点发送至目的节点的信息比特,则 $m'_{u_0}=2/\sigma_{RD}^2$. 第 1 次迭代时,校验节点的初始值 $m^{'0}=n^{'0}=0$.

因此,变量节点传给上下层校验节点的平均的消息均值分别为

$$m^{l}=\frac{1}{\eta}\sum_{i\geqslant 0,j\geqslant 0}\frac{i}{i+j}\lambda_{i,j}m_{i,j}^{l}, \tag{9}$$

$$n^{l}=\frac{1}{1-\eta}\sum_{i\geqslant 0,j\geqslant 0}\frac{j}{i+j}\lambda_{i,j}n_{i,j}^{l}. \tag{10}$$

经过 L 次迭代后,码比特的平均消息均值为

$$m_L=\eta m^{L}+(1-\eta)n^{L}. \tag{11}$$

此时,网络 LDPC 码的被删余变量节点的恢复错误概率为

$$P_e(v)=Q\left[(m_L/2)^{1/2}\right], \tag{12}$$

其中 $$Q(x)=\frac{1}{(2\pi)^{1/2}}\int_x^{\infty}\exp\left(-\frac{t^2}{2}\right)\mathrm{d}t.$$

2.3 网络 LDPC 码的速率兼容算法

由式(3)和(4)可知,等效幸存邻居变量节点数 $\sum_{t=1}^{b}S_t\alpha_t$ 越小,更新得到的均值 $m^{'l}$ 和 $n^{'l}$ 的值越大,进而迭代后的变量节点 m_L 的均值也越大,同时由式(12)得到的恢复错误概率 $P_e(v)$ 越小. 因此,在搜索节点时,需要寻找当前具有最小等效邻居的变量节点进行删余操作. 与文献[2]设计的 LDPC 码的删余算法相似,所提出的网络 LDPC 码速率兼容算法主要包括分组和排序两个操作.

2.3.1 分组

将所有删余的变量节点按照迭代恢复次数分成 K 组 $G_1,G_2,\cdots,G_K$,其中 $G_l(1\leqslant l\leqslant K)$ 是经过 l 次迭代才能恢复的所有变量节点的集合.

(1) 给定一个 $M\times N$ 网络 LDPC 码的校验矩阵,初始化 $R_\infty=\{1,2,\cdots,M\}$,$G_\infty=\{1,2,\cdots,N\}$,$l=1$.

(2) 遍历集合 R_∞,找出行重最小的行集合 r.

(3) 遍历集合 G_∞,找出列重最小的列集合 c.

(4) 选出所有(2)和(3)相交的元素的集合,$w=\{(r^*,c^*),r^*\in r,c^*\in c\}$,作为候选对.

(5) 在集合 w 中选出具有最小等效幸存邻居变量节点数的元素,记为(r_j^*,c_k^*). 若有多对满足条件,则随机选出其中一对,归入第 l 次迭代可以恢复的集合 G_l,更新 $R_\infty=R_\infty\backslash r_j^*$ 和 $G_\infty=G_\infty\backslash c_k^*$.

(6) 若集合 G_∞ 为空,则停止迭代;否则,跳至(7).

(7) 若集合 R_∞ 不为空,则跳至(2);否则,若步骤(5)中有多于一对满足条件,则 $l=l+1$,跳至(2).

其中,$G_\infty(R_\infty)$ 表示每次迭代后更新的列(行)的集合;$r(c)$ 表示第 l 次迭代时,在集合 $R_\infty(G_\infty)$ 选出的行(列)重最小的行(列)集合;$G_l=\{(r_1^*,c_1^*),(r_2^*,c_2^*),\cdots\}$;$R_\infty=R_\infty\backslash r_j^*$ $(G_\infty=G_\infty\backslash c_k^*)$ 表示集合 $R_\infty(G_\infty)$ 去掉元素 $r_j^*(c_k^*)$ 后的集合 $R_\infty(G_\infty)$.

第234页,共397页
(C)1994-2023 China Academic Journal Electronic Publishing House. All rights reserved. http://www.cnki.net

计算最大可达码率[2] 为

$$R_{\max}=R_0\Big/\Big(1-\sum_{j=1}^{K}|G_j|\Big/n\Big)\quad,\tag{13}$$

其中,R_0 是母码的码率,n 是母码的码长.

在给定母码基础上,设计 Q 个码率的子码,对应码率记为 $R_0\leqslant R_1\leqslant\cdots\leqslant R_Q\leqslant R_{\max}$. 假设所设计码的码率为 R_j,需要删余的节点数为[2]

$$np_j=\lfloor n(R_j-R_0)/R_j\rfloor\quad,\quad 0\leqslant j\leqslant Q\quad.\tag{14}$$

2.3.2　组内排序

依次对 $G_l(1\leqslant l\leqslant K)$ 内的变量节点进行排序.

(1) 给定一个 $M\times N$ 网络 LDPC 码的校验矩阵,初始化 $R_\infty=\{1,2,\cdots,M\}$,$l=1$,$j=1$,$P_0=\varnothing$.

(2) 若 $j>Q$,则停止迭代;否则,$P_j=P_{j-1}$.

(3) $\Delta=np_j-|P_j|$.

(4) 若 $\Delta=0$,$j=j+1$,则跳至(2).

(5) 根据集合 G_l 定义 $C_l\overset{\mathrm{d}}{=\!=}\{c_1^*,c_2^*,\cdots\}$,从 C_l 中选出列重最大的变量节点的集合 $c_{\max}^*$,并从 $c_{\max}^*$ 中找出具有最小数量的死校验节点的变量节点 $c_{\max}^{**}$. 如果有多个满足条件,则随机选出其中一个,归入排序的集合 P_j,更新 $P_j=P_j\bigcup\{c_{\max}^{**}\}$,$G_l=G_l\backslash\{c_{\max}^{**}\}$,$R_\infty=R_\infty\backslash r_{\max}^{**}$,$\Delta=\Delta-1$.

(6) 若 G_l 为空,$l=l+1$,则 $R_\infty=\{1,2,\cdots,M\}$.

(7) 跳至(4).

其中,(1)中的 $l=1$ 表示从 G_1 开始将各 G_l 内的变量节点排序,$j=1$ 表示初始码率为 R_1;(3) 计算需要删余 np_j 个节点,除了上次迭代删余的 $|P_j|$ 个节点外,本次还需要删余 Δ 个节点;(5) 中的集合 $c_{\max}$ 表示最大列重的变量节点的集合,同时意味着该集合包含的变量节点的幸存校验节点数最多;P_j 表示要达到码率 R_j,所需删余的变量节点的列集合;$r_{\max}^{**}$ 表示列为 $c_{\max}^{**}$ 的变量节点所在的行.

经过上述分组和组内排序操作,将 $G_l(1\leqslant l\leqslant K)$ 中的变量节点按照 l 从小到大删余,而在同一个 G_l 中,按照变量节点的列号从小到大删余,直到删掉 np_j 个节点.

3　仿真结果

仿真中两个信源节点采用的 LDPC 码的码率均为 0.5,度分布为

$$\lambda(x)=0.23403x+0.21242x^2+0.1469x^5+0.102840x^6+0.30381x^{19}$$

和

$$\rho(x)=0.71875x^7+0.28125x^8\quad.$$

根据文献[7],假设所采用的网络 LDPC 码的度序列分布为:$\lambda_{0,2}=0.028043$,$\lambda_{2,0}=0.188139$,$\lambda_{2,1}=0.019382$,$\lambda_{2,2}=0.026283$,$\lambda_{3,0}=0.191239$,$\lambda_{3,1}=0.003360$,$\lambda_{3,2}=0.001150$,$\lambda_{6,0}=0.085989$,$\lambda_{6,1}=0.000980$,$\lambda_{6,2}=0.063446$,$\lambda_{7,0}=0.059576$,$\lambda_{7,2}=0.044374$,$\lambda_{20,0}=0.176218$,$\lambda_{20,1}=0.003570$,$\lambda_{20,2}=0.108251$,$\rho_6^{\mathrm{low}}=0.943049$,$\rho_7^{\mathrm{low}}=0.056951$.

假设两个源节点所采用 LDPC 码的码长均为 2 048,中继节点联合编码的 LDPC 码的校验比特数为 628,此时网络 LDPC 码(母码)的码率为 0.444. 根据式(14),可以得到对该网络 LDPC 码进行删余获得的最大码率为 0.733. 利用文中所提算法对该网络 LDPC 码删余可以得到码率分别为 0.5、0.6 和 0.7 的子码. 利用文献[2]中的算法和随机删余也可得到同样码率的网络 LDPC 子码.

假设源节点和中继节点均采用 BPSK 调制方式,源节点与中继节点,源节点与目的节点,以及中继节点与目的节点之间的信道均为高斯白噪声信道,中继节点与目的节点之间的信噪比固定为 5 dB,且中继节点可以正确

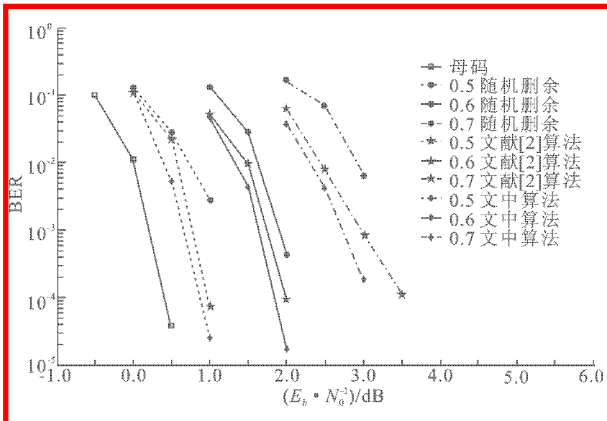


图 4　网络 LDPC 码的删余性能对比

(下转第 47 页)

(C)1994-2023 China Academic Journal Electronic Publishing House. All rights reserved.　http://www.cnki.net

scientific.net/AMR.311-313.2009.

[4] Bozorg M, Termeh F. Domains of PID Controller Coefficients which Guarantee Stability and Performance for LTI Ttime-delay [J]. Automaic, 2011, 47(9): 2122-2125.

[5] 杨莹，李俊民，陈国培. 一类广义混杂系统的随机稳定性及稳定化[J]. 西安电子科技大学学报，2010，37(5)：866-871.
Yang Ying, Li Junmin, Chen Guopei. Stochastic Stability and Stabilization for a Class of Singular Hybrid Systems[J]. Journal of Xidian University, 2010, 37(5): 866-871.

[6] 徐亚兰，陈建军. 压电柔性机械臂的轨迹跟踪控制[J]. 西安电子科技大学学报，2008，35(3)：504-507.
Xu Yalan, Chen Jianjun. Trajectory Tracking Control for the Flexible Link Robot Manipulator Using Piezoelectric Materious [J]. Journal of Xidian University, 2008, 35(3): 504-507.

（编辑：郭　华）

（上接第 17 页）

译出两个源节点的发送数据. 图 4 比较了 3 种不同算法得到的网络 LDPC 码在上述信道假设下的误比特性能，图中横坐标 E_b/N_0 表示源节点与目的节点之间链路的信噪比变化，且假设两个源节点与目的节点之间的链路是对称的.

由图 4 可以看出，随着删余比特的增加，采用所提算法得到的网络 LDPC 码的性能增益也随之增加. 当码率为 0.5，比特误码率(BER)为 10^{-3} 时，采用所提算法性能优于随机删余算法 0.45 dB；当码率为 0.5，BER 为 10^{-4} 时，采用所提算法比文献[2]中算法的性能改善 0.15 dB. 在码率为 0.6，BER 为 10^{-3} 时，所提算法相对于随机删余算法性能改善了 0.3 dB，相对于文献[2]中算法性能改善了 0.2 dB. 当码率为 0.7，SNR 为 3 dB 时，所提算法的 BER 为 10^{-5}，相比于随机删余算法的 10^{-3} 有了明显提升，而 BER 为 10^{-4} 时，所提算法比文献[2]中算法性能增益改善了 0.4 dB.

4　结 束 语

根据网络 LDPC 码的结构特点，以最小化恢复错误概率为目标，设计了一种网络 LDPC 码的速率兼容删余算法. 不同于已有的算法[2]，该算法利用被删余的变量节点的恢复原则和受到的噪声干扰大小设计了不同码率下的删余方案，在不增加系统复杂度的前提下，只需要一对编码译码器即可实现网络 LDPC 码的码率自适应. AWGN 信道下的仿真结果表明，在同等条件下，采用文中所提算法获得的速率兼容网络 LDPC 码比采用文献[2]中算法得到的速率兼容网络 LDPC 码有更好的性能.

参考文献：

[1] Hagenauer J. Rate-Compatible Punctured Convolutional Codes (RCPC codes) and Their Applications [J]. IEEE Trans on Communication, 1988, 36(4): 389-400.

[2] Ha J, Kim J, Klinc D, et al. Rate-Compatible Punctured Low-Density Parity-Check Codes with Short Block Lengths [J]. IEEE Trans on Inform Theory, 2006, 52(2): 728-738.

[3] Ha J, Kim J, Klinc D, et al. Rate-Compatible Puncturing of Low-Density Parity-Check Codes [J]. IEEE Trans on Inform Theory, 2004, 50(11): 2824-2836.

[4] Zhou Lin, Bai Baoming, Xu Ming. Design of Nonlinary Rate-compatible LDPC Codes Utilizing Bit-wise Shortening Method [J]. IEEE Communication Letters, 2010, 14(10): 963-965.

[5] 周林，白宝明，邵军虎，等. 多元 LDPC 码的速率兼容技术研究[J]. 西安电子科技大学学报，2011，38(1)：147-152.
Zhou Lin, Bai Baoming, Shao Junhu, et al. On Nonbinary Rate-compatible LDPC Codes [J]. Journal of Xidian University, 2011, 38(1): 147-152.

[6] 郭凯，陈彦辉，李建东. 一种对奇偶校验比特按组删余的速率兼容编码[J]. 西安电子科技大学学报，2009，36(5)：782-787.
Guo Kai, Chen Yanhui, Li Jiandong. Rate-compatible Codes Based on Puncturing Parity Check Bits in Group [J]. Journal of Xidian University, 2009, 36(5): 782-787.

[7] Li Y, Song G H, Wang L L. Analysis of the Joint Network LDPC Codes over Orthogonal Multi-Access Relay Channel [J]. IEEE Commun Lett, 2010, 14(2): 184-186.

（编辑：齐淑娟）

(C)1994-2023 China Academic Journal Electronic Publishing House. All rights reserved.　http://www.cnki.net

PAPER • OPEN ACCESS

Research on the changing trend of farmland area in China and its driving factors from 1996 to 2016

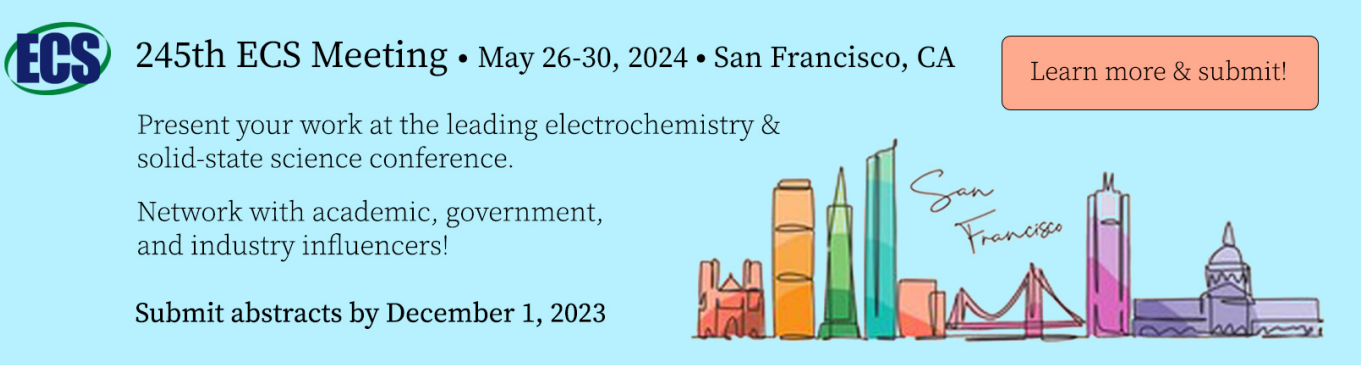
To cite this article: J Y Wang and X M Li 2018 *IOP Conf. Ser.: Mater. Sci. Eng.* **392** 062097

View the article online for updates and enhancements.

中文文章叫近20年，英文文章是1996 to 2016,文章完全一样

You may also like

- The 300 years cropland changes reflecting climate impacts and social resilience at the Yellow River–Huangshui River Valley, China
Qiong Chen, Liang Emlyn Yang, Jing Luo et al.
- Analysis and Research on the Value of Farmland Transfer Based on Environmental Protection Evaluation System
Zhenyu Zhang, Minghua Tian, Jianjun Li et al.
- High Standard Farmland Construction and Soil Conservation Evaluation
Jing Zhang and Lu Sun



This content was downloaded from IP address 219.144.164.16 on 16/11/2023 at 00:29

IOP Conf. Series: Materials Science and Engineering **392** (2018) 062097 doi:10.1088/1757-899X/392/6/062097

Research on the changing trend of farmland area in China and its driving factors from 1996 to 2016

J Y Wang [1] and X M Li[2*]

[1]Xi'an Shiyou University, Xi'an China, 710065

[2]Shaanxi Provincial Land Engineering Construction Group，Xi'an China, 710075

*Corresponding author: xmlisdc@126.com

Abstract. The paper was to research the changing trend of farmland area from 1996 to 2016. The original data of farmland area of China in these years were collected, data mining technology was used, and ARIMA model was chosen to predict each other between the two periods of 1996-2008 and 2008-2016, so the original farmland area data could be corrected and normalized. Then correlation analysis was used to study the driving factors. The trend research result showed, the farmland area decreased from 1996 to 2016, the decreasing rate was faster before 2004, and then it decreased slowly. The correlation analysis result showed, the added value proportion of primary industry, the total population, and the urban population were the most important driving factors, their coefficients were 0.959, -0.918 and -0.896 respectively. It could be concluded by the result that the industry configuration and the urbanization could affect the farmland area changing with the development of social economy.

1. Introduction

China is a great agricultural country, and the farmland is one very important resource which is related to food security. However, the vigorous demand for lands brings great challenge for farmland protection with the promotion of socialist modernization construction [1]. The research on farmland area change and its driving factors in China has always been one popular problem. The statement was refuted that China's cultivated land has been descending since 1957 based on the analysis of the actual change of the cultivated land area [2]. The farmland area changing trend, spatial characteristics and the driving factors in China for a period of time before 2007 were studied [3-5]. And in different scales such as the scale of province or in some part of China, the dynamic change trend of farmland was studied [6-8]. Since 1980s, with the development and application of 3S technology, many scholars studied the farmland change using the RS images such as Landsat TM images [9, 10]. And the analysis approaches in the study of the driving forces of land use change in large regions were explored by using digital satellite remote sensing data of China [11]. Not only the changes in China's cultivated land but also those in some provinces were analyzed based on remote sensing data such as Landsat TM/ETM+, NOAA, SPOT dataset [12, 13].

The statistic data sources of cultivated land in China are various, for example, the international organizations such as FAQ, WRI (the world resources institute), and different departments of China such as MLR (the ministry of land and resources), MOA (the ministry of agriculture), the bureau of statistics of PRC. However, the statistical data supplied by MLR are considered the most authoritative [14]. But the data from the MLR are not regularly entire in the demanded periods, and there was a jumping phenomenon with the farmland area from 2008 to 2009, that's because the data of 2008 was

Content from this work may be used under the terms of the Creative Commons Attribution 3.0 licence. Any further distribution of this work must maintain attribution to the author(s) and the title of the work, journal citation and DOI.
Published under licence by IOP Publishing Ltd

based on the first national land use survey, and the data of 2009 was based on the second national land use survey, that's seemly illogical. At present, most scholars analyze the farmland area change by the exiting data directly while ignoring the accuracy of the statistic data, or they just focused on some periods before 2008 or after 2009 evading the jumping years. Only a few scholars researched the farmland area in different historical periods [14, 15]. In this paper, the researched years included the years of before and after the second national land use survey. The method of data mining was introduced to analyze the relation between the two periods of the years before 2008 and the years after 2009, so the changing trend of China's farmland area could be reflected more scientifically. At the same time, the driving factors were studied based on data normalization. And this is not found in the present research, which could be useful for studying China's farmland changing trend.

2. Data and methods

2.1. Data acquisition

2.1.1. Data of farmland area in China

The farmland area of China, especially in the historical periods, has been hard for statistic for a long time. The national department of land management have been announcing the changing situation each year since 1986. In order to obtain the veracious statistical data of farmland in China, the first national land use survey was operated from 1984 to 1996. The survey result showed there was 1.95 billon mu (1 mu = 666.66 m^2) of farmland in China by the day of Oct.31 1996 [15], which was considered the most credible result at that time [16]. Then, the farmland area of each year from 1996 to 2008 can all be obtained from the statistical bulletin of the year.

In order to obtain more veracious statistical data of farmland, the second national land use survey was operated from 2007 to 2009. The survey result showed there was 2.03 billon mu of farmland in China by the year of 2009 [15]. And since then the land use change survey has been operated each year. And the farmland area from 2007 to 2016 can be obtained from the national service platform of land use survey result. Because new methods and technologies were applied with the second national land use survey, some farmlands which were not found in the first survey were found in the second survey, and there was a jumping phenomenon with the farmland area from 2008 to 2009, which would be specially researched after a while for analyzing the changing trend of farmland area.

2.1.2. Data of driving factors

Land is closely related to the human social and economic development. The national farmland change is influenced by the geographical and climate conditions, social and economic development, flood and waterlogging disaster and so on [1]. For researching the driving factors influencing the farmland changing, three kinds of factors were introduced for comparison and selection. One kind were the comprehensive factors reflecting the national economic development, and they were the gross national income (GNI), the gross domestic product (GDP), the primary industry added value and its ratio, the second industry added value and its ratio, the third industry added value and its ratio, the gross agricultural output value, per capita GDP, industrial added value, architectural added value. Another kind were special factors reflecting the level of urbanization, and they were the national population, the urban population, and the rural population. The third kind was the special factors reflecting the natural disaster, and they were the damage area and the grain yield. There were in total of 17 factors which were used for analysis [17]. And data of all factors for the recent 20 years could be obtained from the web site of the national bureau of statistics.

2.2. Study methods

In this paper, the national farmland area dada from 1996 to 2016 years were collected and analysed to study the changing trend, and the correlation analysis was operated to research the driving factors. While studying the changing trend of farmland from 1996 to 2016, according to the found jumping

phenomenon with the data from 2008 to 2009, the data mining technology was introduced. First, the farmland area of the year 2009 can be predicted with the data of 1996 to 2008. And the farmland area of the year 2008 can also be predicted reversely with the data of 2009 to 2016. Then, based on the predicted data and the practically collected data of the farmland of the years 2008 and 2009, the mathematical ratio relation between the farmland area of 2008 and 2009 could be analysed and obtained, so the jumping phenomenon could be solved with the ratio. At last, all the farmland data from 1996 to 2016 should be normalized for researching the changing trend more scientifically.

ARIMA (Autoregressive Integrated Moving Average) model was chosen for prediction with data mining, which was promoted by Box and Jenkins, it's a very famous and useful time-sequence forecast method, and that's just the needed one in this paper.

3. Analysis on the farmland area changing trend from 1996 to 2016

3.1. The analysis based on the original statistic data of farmland area

By collecting and analysing the original statistic data of farmland area for years of 1996-2016, the result showed that the national farmland area decreased year by year, as Figure1, and the decreasing speed was the most quick from 2000 to 2004. While the farmland area jumped from 1.826 billion mu in 2008 to 2.031 billion mu in 2009. And after 2009, the farmland area decreased very slowly.

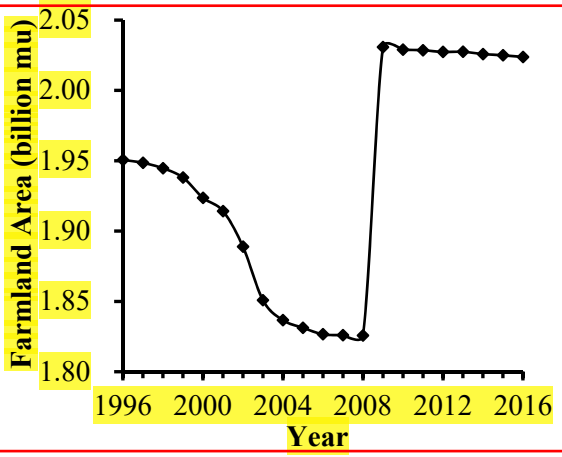


Figure 1. Changing Trend for Farmland Area of 1966-2016 Based on Original Statistic Data

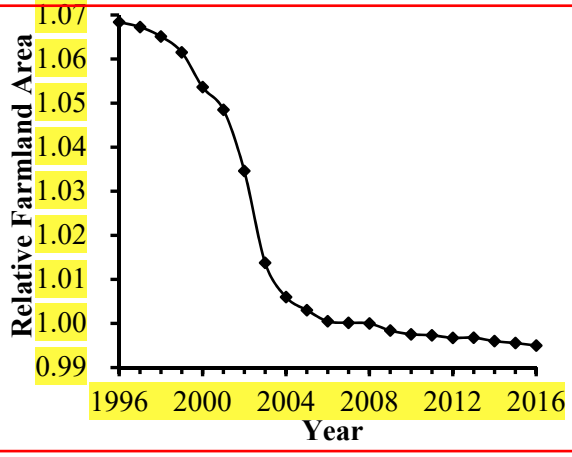


Figure 2. Changing Trend for Farmland Area of 1966-2016 Based on Revised Statistic Data

China finished the first national land use survey in 1996, and the second in 2009, so the jumping phenomenon just happened in the division years of the twice land use survey. Whether the national farmland increased by about 200 million mu in the year of 2009 or not should be studied deeply. And by reviewing literatures [14, 15, 18], it could be concluded that the main reason was that more advanced technologies were introduced while the second land use survey, so some farmlands lost of statistic in the first land use survey were found in the second time, and the accuracy of the statistic result was improved. In this paper, the farmland data for the recent 20 years were based on twice different land use survey and different technology conditions. We can easily studied the changing trend in each period before or after the second land use survey, while all the data of farmland area must be revised and normalized if we want to study the continual time-sequence changing trend from 1996 to 2016, then they might be comparable.

3.2. Revision of farmland area based on data mining technology

Data mining technology is much useful for time-sequence prediction, and by that, in this paper, the farmland area of the year 2009 was predicted with the farmland data of the years from 1996 to 2008, the ratio α between the farmland area of 2009 and that of 2008 could be obtained. And the farmland area of the year 2008 was also predicted reversely with the farmland data of the years from 2009 to

2016, the ratio β between the farmland area of 2009 and that of 2008 could also be obtained. Then, for reflecting the ratio more scientifically, we could get the ratio ρ by the average of α and β.

SPSS software was used for prediction in this paper, by analyzing and comparing, the model of ARIMA was used in both of the prediction and the reverse prediction. The model used while predicting the farmland area of the year 2009 was ARIMA(1,1,2) (r^2=0.975**), and the model used while predicting reversely the farmland area of the 2008 was ARIMA(1,1,4) (r^2=0.966**), both of the two models were significant in the level of 0.01, with that, the predicted farmland area of the year 2009 was 1820.08 million mu, the reversely predicted farmland area of the year 2008 was 2030.98 million mu, so we can get α=0.996899887, β=0.999895617, and then ρ=0.998397752, so we could use the ρ value as the revision ratio of the data of the two different periods.

3.3. Trend analysis based on the revised data of farmland area

All the original farmland area data were revised with the ratio ρ and normalized into relative values for reflecting the changing trend more scientifically. Based on the study of the previous paper, the relative farmland area of the years from 1996 to 2008 were calculated with the denominator of the farmland area of the year 2008, the relative farmland area of the years from 2009 to 2016 were calculated with the denominator of the farmland area of the year 2009 while revised by multiply the ratio ρ. Then the continual changing trend of farmland area from 1996 to 2016 could be obtained, shown as Figure 2, which showed the national farmland area decreased year by year. Before the 2004, the decreasing rate was faster, and after that the decreasing rate trends to be slower, especially after 2009, the farmland area trends to be stable.

4. Analysis on driving factors

A total of 17 factors were collected in this paper, and their descriptive statistical characters were shown in table 1. In order to study the driving factors, correlations between the farmland area and the factors were analysed, and then, by comparing the correlation coefficients shown as table 2. the driving factors could be chosen out.

Table 1. Descriptive Statistical Characters of All Factors from 1996 to 2016

Factors	*Min.*	*Max.*	*Ave.*	*Std.*	Factors	*Min.*	*Max.*	*Ave.*	*Std.*
x_1	7078	74114	30444.70	225956.60	x_{10}	589.8	5398	2287.2	16332.77
x_2	7181.4	74412.7	30571.87	226519.84	x_{11}	2953	24786	11653.28	79508.29
x_3	1387.8	6367.1	3124.07	17742.62	x_{12}	439.3	4952.2	1962.3	15992.73
x_4	8.556	19.325	12.11	3.28	x_{13}	122389	138271	131047.71	4702.17
x_5	3382.8	29623.6	13562.92	94949.58	x_{14}	37304	79298	58413.24	12989.27
x_6	39.810	47.559	45.33	2.00	x_{15}	58973	85085	72634.48	8313.40
x_7	2410.7	38422	13884.89	114605.84	x_{16}	43070	62144	52326.48	5812.06
x_8	33.569	51.634	42.56	4.47	x_{17}	21770	54688	41009.48	10706.30
x_9	1354	5928.8	2884.26	16570.35					

**In the table, x_1 means the gross national income (GNI), billion yuan; x_2 means the gross domestic product (GDP), billion yuan; x_3 means the primary industry added value, billion yuan; x_4 means the proportion of primary industry added value, %; x_5 means the second industry added value, billion yuan; x_6 means the proportion of second industry added value, %; x_7 means the third industry added value, billion yuan; x_8 means the proportion of third industry added value, %; x_9 means gross agricultural output value, billion yuan; x_{10} means per capita GDP, billion yuan; x_{11} means industrial added value, billion yuan; x_{12} means architectural added value, billion yuan; x_{13} means the national population, *10^4; x_{14} means the urban population, *10^4; x_{15} means the rural population, *10^4; x_{16} means the grain yield, *10^4 t; x_{17} means damage area, *10^3 ha; and the same as follows.*

Table 2. Correlation Coefficients between Original/Relative Farmland Area and Factors

	Original data	Relative data		Original data	Relative data
Relative data	-0.142	1.000	x_9	0.686	-0.709
x_1	0.649	-0.746	x_{10}	0.651	-0.749
x_2	0.652	-0.745	x_{11}	0.638	-0.784
x_3	0.663	-0.736	x_{12}	0.688	-0.716
x_4	-0.274	0.959	x_{13}	0.433	-0.918
x_5	0.647	-0.774	x_{14}	0.488	-0.896
x_6	-0.519	0.259	x_{15}	-0.518	0.880
x_7	0.649	-0.717	x_{16}	0.752	-0.524
x_8	0.433	-0.819	x_{17}	-0.514	0.708

As shown in table 2, the correlation coefficients between the original farmland area and the factors were poor because of the jumping phenomenon. However, by analyzing the correlations between the revised farmland area and the factors, we could find, the proportion of the first industry added value had the best correlation with the farmland area, its coefficient was up to 0.959. The national total population was secondary to it, and its correlation coefficient was -0.918, then the urban population and the rural population were secondary to that sequentially, which means the first industry added value, the national total population, the urban population and the rural population were the most important driving factors. According to the research result, we could conclude that it was mainly the national industry structure and the urbanization construction that influence the farmland changing.

5. Conclusion and discussion

Land has both of its own natural and social characters, and it's just all of the factors including society, economy, and policy factors that influence the statistics of farmland area for a long time. So it's difficult for a long-time changing trend research. The period studied in this paper was across twice national land use survey, and there happened to be a jumping phenomenon, but this couldn't reflect the boost of farmland area from 2008 to 2009. The reasons of the phenomenon were studied, that was mainly because RS, GIS and some other new technologies were applied in the second national land use survey, the survey and statistics were more standardized, so the accuracy was apparently promoted, which made the farmlands lost of statistics before found in the second land use survey. Therefore, in order to study the changing trend for a period across twice land use survey, the quantitative relation of the farmland area between the twice survey must be studied and obtained. In this paper, with data mining technology, revision and normalization of farmland area, the research result could reflect the changing trend more actually.

Research results showed China's farmland area decreased year by year from 1996 to 2016, especially before 2004, the decreasing rate was fast, and after that year the decreasing rate tended to be slow. As to the driving factors, it's the proportion of the primary industry added value in the aspect of the national industry structure and the national population, the urban population in the aspect of urbanization construction which were the main driving factors influencing the farmland changing. Because of the ecological restoration after the year of 1999, the farmland decreased rapidly [14, 19]. In 2004, the land management law was revised, which strengthened the protection and the requisition-compensation balance of farmland, and that's much useful for retaining farmland. In this paper, only the farmland area data from 1996 to 2016 were used to study the changing trend, and in present time, China pay much attention to farmland protection, not only including the quantity, but including the land quality with core of productivity in order to realize the protection of the trinity of quantity, quality and ecology [20]. In the future research, the changing trend of farmland area would be studied deeply.

The years of 1966 to 2016 were introduced in this paper to study the changing trend because the demand of statistical data for longer-time sequence was difficult to be satisfied. In future research, based on the collected statistical data, the data mining, remote sensing interpretation and some other methods would be applied to compensate the lack of some factors, so we wish we could obtain a longer time-sequence changing trend.

References

[1] Zhao Q G, Zhou S L, Wu S H and Ren K. 2006. Cultivated Land Resources and Strategies for Its Sustainable Utilization and Protection in China, *Acta Pedologica Sinica*,43(4): 662-72.
[2] Bi Y Y and Zheng Z Y. 2000. The Actual Changes of Cultivated Area Since The Founding of New China**,** *Resources Science*, 22(2): 8-12.
[3] Li X B. 1999. Change of arable land area in China during the past 20 years and its policy implications, *Journal of Natural Resources*, 14(4): 329-33.
[4] Cao Y G, Yuan C, Zhou W, Tao J and Hua R. 2008. Analysis on D iving Forces and Provincial Differences of Cultivated Land Change in China. *China Land Science*, 22(2): 17-22.
[5] Huang Z H and Wu C F. 2009. Empirical Study of Cultivated Land Change and Socio-economic Factors in China. *Journal of Natural Resources*. 24(2): 192-9.
[6] Yu T, Cao Y G and Xu J X. 2016. Driving Force of Cultivated Land Change in China Based on Different Scales. *Chinese Agricultural Science Bulletin*, 2016, 32(24): 194-8.
[7] Wu X, Wang S R, Shang H Y and Wang Z J. 2017. Analysis of Dynamic Change and Driving Forces of Cultivated Land in NingXia During The Past 18 Years. *Chinese Journal of Agricultural Resources and Regional Planning*. 38(8):98-104.
[8] Guo L Y, Wang D L and Wang J Y. 2012. Analysis of the Arable Land Change and Its Causes in the Eastern Coastal China Over the Last Decades. *Chinese Journal of Agricultural Resources and Regional Planning*. 33(1):6-10.
[9] Zhang G P, Liu J Y and Zhang Z X. 2003. Spatial-temporal Changes of Cropland in China for the Past 10 Years Based on Remote Sensing. *Acta Geographica Sinica*. 58(3): 323-32.
[10] Tian G J, Zhuang D F and Liu M L. 2003. The Spatial-temporal Dynamic Change of Cultivated Land in China in 1990s. *Advance in Earth Sciences*. 18(1): 30-6.
[11] Liu X H,Wang J F,Liu J Y, Liu M L and Meng B. 2005. Quantitative Analysis Approaches to the Driving Forces of Cultivated Land Changes on A National Scale.*Transactions of the Chinese Society of Agricultural Engineering*. 21(4):56-60.
[12] Xu L L, Li B L, Yuan Y C, Gao X Z, Liu H J and Dong G H. 2015. Changes in China's Cultivated Land and the Evaluation of Land Requisition-Compensation Balance Policy from 2000 to 2010. *Resources Science*. 37(8): 1543-51.
[13] Li J G, He C Y, Shi P J, Chen J, Gu Z H and Xu W. 2004. Change Process of Cultivated Land and Its Driving Forces in Northern China during 1983-2001. *Acta Geographica Sinica*. 59(2): 274-82.
[14] Feng Z M, Liu B Q and Yang Z. A Study of the Chaning Trend of Chines Cultivated Land Amount and Data Reconstructing:1949-2003. *Journal of Natural Resources*, 20(1): 35-43.
[15] Tan Y Z, He J, Yue W Z, Zhang L and Wang Q R. 2017. Spatial Pattern Change of the Cultivated Land before and after the Second National Land Survey in China. *Journal of Natural Resources*, 32(2): 186-97.
[16] Lin G C S, Ho S P S. 2003. China's land resources and land-use change: insights from the 1996 land survey. *Land Use Policy*, 20(2): 87-107.
[17] Fu Z Q, Cai Y L, Yang Y X and Dai E F. 2001. Research on the Relationship of Cultivated Land Change and Food Security in China. *Journal of Natural Resources*, 16(4): 313-9.
[18] Zhang Y Q and Yang Z S. 2013. Comparative Analysis of Two Investigations of Land Resource in China. *Scientific and Technological Management of Land and Resources*. 30(2): 100-4.
[19] Xu X L, Cai Y M, Zhang K L and Zheng W Y. 2005. Study on Dynamic Change of Cultivated Land Resources and Causes of the Changes. *China Population Resources and Environment.* 15(3): 75-9.
[20] Tan Y Z, Wu C F, Wang Q R, Zhou L Q and Yan D. 2005. The Change of Cultivated Land and Ecological Environment Effects Driven by the Policy of Dynamic Equilibrium of the Total Cultivated Land. *Journal of Natural Resources*. 20(5): 727-34.

Optimal Design of the Joint Network LDPC Codes over Orthogonal Multi-Access Relay Channel

Jingyi Wang
State Key Lab of ISN
Xidian University
Xi'an, China
Email: wangjy@stu.xidian.edu.cn

Shuling Che
State Key Lab of ISN
Xidian University
Xi'an, China
Email: shlche@mail.xidian.edu.cn

Ying Li
and Junlong Wang
State Key Lab of ISN
Xidian University
Xi'an, China
Email:ying.lili1973@gmail.com

***Abstract*—Optimization of degree distribution of the joint network LDPC code for orthogonal multiple-access relay channel (MARC) is investigated in this paper. We first calculated the code capacity of the source-destination link of orthogonal MARC based on a Gaussian approximation,where two sources communicate with one destination in the presence of one relay. Then, a new generalized differential evolution algorithm is developed to iteratively improve the degree distribution of the joint network LDPC code. Simulation results show that, the gap between bit error rate (BER) performance of our designed codes and the decoding threshold is about 0.4dB, and that between the capacity limit and decoding threshold is less than 0.7dB at BER $= 10^{-6}$.**

***Index Terms*—Network LDPC Code; multi-access relay network; Gaussian approximation; differential evolution; capacity limit.**

I. Introduction

In wireless communications, cooperation relay networks[1][2][3] have recently attracted substantial research efforts with many promising techniques of improving performance in term of throughput, coverage or diversity gain. In relay networks, one or multiple relay nodes (RNs) to assist the sources in transmitting information.Optimal designs of Relay networks have attracted extensive attentions due to that they can increase the communication capacity. One of the earlier works on this subject is the application of LDPC code to the single-source single-relay networks [4]. To improve the performance of the single-source single-relay system, a class of bilayer LDPC codes is designed in[5][6].

Based on the principle of the bilayer LDPC codes, the authors proposed a class of the joint network LDPC code which helps the relay jointly re-encodes the messages from the two sources and sends the parity bits to the destination [7]. Moreover, the authors analyzed the capacity approaching ability of the joint network LDPC codes in [8]. In this paper, we study the problem of approaching capacity limit of a two-source single-relay multiple-access relay network with the joint network LDPC code, in which the two source-to-relay channels and the two source-to-destination channels are under the same channel parameters.Then, a new generalized differential evolution algorithm is developed to optimal the degree distribution of the joint network LDPC code.

The rest of this paper is organized as follows. Section II presents the system model and then describes the operation of the system throughout different stages of the cooperation strategy. Section III explains the optimum design method of degree distribution of the joint network LDPC code. Section IV presents simulation results, and Section VI concludes the paper.

II. System Model

Our system is a two-slot wireless relay network consisting of two sources, one relay and one destination, as shown in Fig.1.

In the first slot, sources $S_i(i = 1, 2)$ broadcast their LDPC coded signals $X_i(i = 1, 2)$, which are received by both relay R and destination D. We express the received bits as

$$Y_{S_i,R} = X_i + N_{S_i,R} \quad (1)$$

$$Y_{S_i,D} = X_i + N_{S_i,D} \quad (2)$$

where $i = 1, 2.X_i$ is the LDPC coded signal sent from source node S_i, while $Y_{S_i,R}$ and $Y_{S_i,D}$ are the corresponding received signal by the relay R and the destination D respectively. Finally, $N_{S_i,R}$ is a zero-mean additive Gaussian random variable with variance $\sigma^2_{S_i,R}$, and $N_{S_i,D}$ is a zero-mean additive Gaussian random variable with variance $\sigma^2_{S_i,D}$.

In the second slot, after decoding the received signals correctly, R jointly re-encodes the messages of the two sources and sends k_2 parity bits X_R to D. The received bits at the destination D is

$$Y_{R,D} = X_R + N_{R,D} \quad (3)$$

where X_R denotes the signal corresponding to the parity bits, and $N_{R,D}$ is a zero-mean additive Gaussian random variable with variance $\sigma^2_{R,D}$.

At last, the destination D can decode the information data of two sources by using the received signals Y_1, Y_2 and Y_R respectively from the two sources and relay. Therefore, X_1, X_2, and X_R can be treated as an equivalent super code which is called as the joint network LDPC code in [7]. The parity check matrix of the joint network LDPC code can be written as

$$\mathbf{H} = \begin{pmatrix} \mathbf{H_1} & \mathbf{0} & \mathbf{0} \\ \mathbf{0} & \mathbf{H_1} & \mathbf{0} \\ \mathbf{A} & \mathbf{B} & \mathbf{C} \end{pmatrix} \quad (4)$$

978-0-7695-4988-0/13 $26.00 © 2013 IEEE
DOI 10.1109/INCoS.2013.116

IEEE computer society

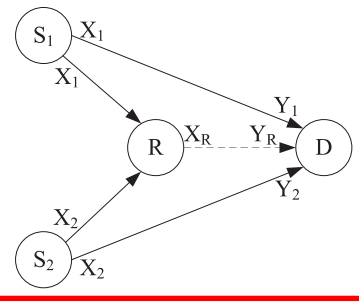


Fig. 1. The model of the joint network LDPC code based relaying scheme

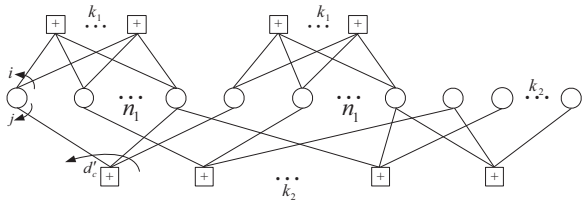


Fig. 2. Tanner graph of the joint network LDPC code

where $\mathbf{H_1}$ denotes the same parity-check matrix of the constituent codes at the two sources $S_i(i=1,2)$, $\mathbf{H_3}=(\mathbf{ABC})$ denotes the parity-check matrix generated by R, and $\mathbf{0}$ represents the all-zero matrix.

Assume that each source uses an (n_1, n_1-k_1) irregular LDPC code with code length n_1 and parity length k_1. According to [8], the Tanner graph of the joint network LDPC code is shown in Fig.2, where the upper sub-graph denotes the encoding at the sources and the lower sub-graph denots the encoding at the relay. This code includes $2k_1$ upper check nodes, k_2 lower check nodes and $2n_1+k_2$ variable nodes. A variable node is of degree (i,j), $1\le i\le d_v$ and $1\le i\le d_v^{'}$, where i (j) is its upper (lower) degree, and d_v $(d_v^{'})$ is its maximum upper (lower) degree. In addition, $\lambda_{i,j}$ represents the proportion of the number of edges connected to the variable nodes with the degree (i,j).

III. Optimization Of Degree Distribution

A. Preliminary

Definition 1: Decoding threshold of joint network LDPC code is defined as

$$\sigma^* = sup\{\sigma : \lim_{L\to+\infty} m_L > M\} \tag{5}$$

where L is the maximum iteration number, m_L denotes the mean value of the log-likelihood ratio (LLR) message of a code bit at L-th decoding iteration and M is the LLR mean value corresponding to the target error probability. Then with the knowledge in [8], $2m_L$ is the LLR variance value. When $\sigma<\sigma^*$, m_L will be greater than M, which means that the target error probability can be achieved. When $\sigma\ge\sigma^*$, the iterative decoding can not achieve the target error probability.

B. Calculation of decoding threshold σ^*_{SD}

Algorithm 1: Given degree distributions of the LDPC code at the sources, let σ_{SD} and σ_{RD} represent the channel parameters of source-destination link and relay-destination link respectively. We denote the target error probability as $P_e=10^{-6}(M=45)$ [8], and the maximum iteration number as L. Let $\Delta\sigma_{SD}$ denote a step length, and then algorithm 1 can be described as follows:

Step 1: Initialization

The initialized value of the average mean value of the LLR message output by the check node is $m^{'l}=n^{'l}=0$ (l is the iteration number, and $l=0$ in the first iteration)[8].

Step 2: Updating

When the iteration number $l<L$, update the mean values of the LLR messages at the variable node and the check node respectively, and then calculate the mean value (m_l) of the LLR message during this iteration using the method in [8]. If $m_l<M$, add the iteration number by 1 $(l=l+1)$, and continue Step 2. If $m_l\ge M$, $\sigma_{SD}=\sigma_{SD}+\Delta\sigma_{SD}$, and go to Step 1.

Step 3: Stopping criterion

If $l\ge L$ and $m_l<M$ during this iteration, stop the whole process, and the code capacity is defined as $\sigma^*_{SD}=\sigma_{SD}-\Delta\sigma_{SD}$. Otherwise, output the threshold value of channel parameter as $\sigma^*_{SD}=\sigma_{SD}$.

Using Algorithm 1, we can obtain the corresponding σ^*_{SD} from a given degree distribution of the upper layer LDPC code.

C. Optimal Design Of Degree Distribution Of The Lower Layer LDPC Code

Our goal is to search the optimal degree distribution of the network LDPC code, which can approach the capacity limit. Here we use differential evolution algorithm to optimal design of the network LDPC code sets.

Algorithm 2: Assume that N relay code sets of the network LDPC code structure are randomly generated, denoting their degree distributions of variable node as $\lambda_{i,j}(d), 0\le i\le d_v, 0\le j\le d_v^{'}, d=1,2,...N$. The degree of the lower check nodes is fixed as $d_c^{'}$.

Step 1: Initialization

Initialize that degree distribution as

$$C(d)=\{\lambda_{i,j}(d), 0\le i\le d_v, 0\le j\le d_v^{'}\}, d=1,2,\cdots,N. \tag{6}$$

Step 2: Performance estimation of code set

Calculate the code capacity $\sigma^*(d)$ of each code set $C(d)$ through the Algorithm 1, and search the optimal code set meeting $C^*=\arg\max_{1\le d\le N}\sigma^*(d)$. The degree distribution of the optimal code set corresponding to the maximum code capacity is $C^*=\{\lambda^*_{i,j}, 0\le i\le d_v, 0\le j\le d_v^{'}\}$.

Step 3: Code set updating

Select $\widetilde{N}$ code sets from $\{C(d)\}_{d=1}^{N}$ at random, and denote their degree distribution as $\widetilde{C}(k)=\{\lambda_{i,j}(k), 0\le i\le d_v, 0\le j\le d_v^{'}\}, k=1,2,\cdots,\widetilde{N}$. Then update the degree distribution of the code set: $C^*=C^*+\alpha\Sigma_{k=1}^{\widetilde{N}}(-1)^{k-1}\widetilde{C}(k)$, where $\alpha<1$ is the step length.

TABLE I
FOUR DIFFERENT PARAMETERS OF THE JOINT NETWORK LDPC CODES

Code Set	Code A	Code B	Code C	Code D
$d_v^{'}$	2	2	2	2
$d_c^{'}$	4	4	4	7
k_2	2814	4814	2814	2814
σ_{RD}	0.5	0.5	0.8	0.5
η	0.942065	0.904808	0.942065	0.902835
σ_{SD}^*	1.0568	1.0987	1.0393	1.1116
Threshold	0.15504dB	0.11512dB	0.20180dB	-0.22877dB
Capacity Limit	-0.24536dB	-0.51762dB	-0.14395dB	-0.24536dB
Gap	0.40040dB	0.63274dB	0.34575dB	0.01666dB

Step 4: Stopping criterion

If reaching the preset number of iteration and $m_l < M$, stop the iteration process. The degree distribution of the optimal code set is defined as $C^* = \{\lambda_{i,j}^*, 0 \le i \le d_v, 0 \le j \le d_v^{'}\}$; Otherwise, go to Step 3.

Remark: Restrictive conditions must be met for Step 1 and Step 3.

$$\begin{cases} \sum\limits_{i\ge 0, j\ge 0} \lambda_{i,j} = 1 \\ \lambda_i = \frac{1}{\eta} \sum\limits_{j\ge 0} \frac{i}{i+j} \lambda_{i,j} \\ \eta = \sum\limits_i \sum\limits_j \frac{i}{i+j} \lambda_{i,j} \\ d_c^{'} = \frac{1-\eta}{\sum\limits_j \frac{\lambda_{0,j}}{j}} \end{cases} \tag{7}$$

where η is the proportion of the total number of edges in the upper sub-graph. The total number of upper-layer edges of a source node is $E = \frac{n_1}{\sum\limits_{i\ge 2} \frac{\lambda_i}{i}} = \frac{k_1}{\sum\limits_{j\ge 2} \frac{\rho_j}{j}}$, and the total number of edges of the bilayer network LDPC code is $E^{'} = 2E + k_2 \cdot d_c^{'}$, so $\eta = \frac{2E}{E^{'}}$.

IV. SIMULATION RESULTS

Assume each source node employs an $(n_1, n_1 - k_1)$ LDPC code with $\lambda(x) = 0.23403x + 0.21242x^2 + 0.1469x^5 + 0.102840x^6 + 0.30381x^{19}$, and $\rho(x) = 0.71875x^7 + 0.28125x^8$, where $n_1 = 22164, k_1 = 11082$. $\text{SNR}_{RD} = 3\text{dB}$ and the two source-destination links are assumed to be symmetric. Using the Algorithm 1, four different parameters of the joint network LDPC codes, are obtained and listed in Table I, where σ_{RD}^2 represents the channel parameter between the relay-destination link.

Using the Algorithm 2, four optimal degree distributions of the joint network LDPC codes are given in Table II III IV.

The BER curves of four codes are illustrated in Fig.3. We see that the gap between the decoding threshold of four codes obtained by searching the maximum decoding threshold σ_{SD}^* and capacity limit is less than 0.7dB, and that between BER performance and decoding threshold is less than 0.4dB. Since the lower check degree of Code D is bigger and more information bits are contained in the check equation, it outperforms Code A by 0.2dB gains at BER $= 10^{-5}$. Another important observation is that Code B has a gain of about 0.15dB over Code A at BER $= 10^{-5}$ and the performance gain of Code D is about 0.1dB over Code B at BER $= 10^{-5}$. This indicates that increasing degrees of lower-layer check nodes is better than increasing the numbers of parity bits to improve system performance. When the noise variance between R-D link is increased, the system decoding performance will be reduced and Code A will have a gain of about 0.2dB over Code C at BER $= 10^{-5}$.

TABLE II
THE OPTIMAL DEGREE DISTRIBUTIONS OF CODE A

$\lambda_{i,j}$	$\lambda_{i,0}$	$\lambda_{i,1}$	$\lambda_{i,2}$
$i=2$	0.193815	0.00543635	0.04612661
$i=3$	0.171369	0.019109592	0.02409292
$i=6$	0.129299	0.006342408	0.00494214
$i=7$	0.09485	0.00008237	0.00259462
$i=20$	0.273877	0.000432436	0.00181212
$i=0$	0	0.0030528	0.02276564

TABLE III
THE OPTIMAL DEGREE DISTRIBUTIONS OF CODE B

$\lambda_{i,j}$	$\lambda_{i,0}$	$\lambda_{i,1}$	$\lambda_{i,2}$
$i=2$	0.07441004	0.20599344	0
$i=3$	0.19208258	0.0001582	0
$i=6$	0.13270189	0.00013842	0.00016819
$i=7$	0.09266986	0.00032638	0.00017797
$i=20$	0.27426244	0.00051525	0.0021752
$i=0$	0	0.0237937	0.0000099

TABLE IV
THE OPTIMAL DEGREE DISTRIBUTIONS OF CODE C

$\lambda_{i,j}$	$\lambda_{i,0}$	$\lambda_{i,1}$	$\lambda_{i,2}$
$i=2$	0.1206132	0	0
$i=3$	0.1001453	0.0000219	0
$i=6$	0.1860514	0.0002767	0.0000167
$i=7$	0.1964141	0.0002114	0.0000212
$i=20$	0.3858558	0.0003262	0.0000362
$i=0$	0	0.0041565	0.0206487

TABLE V
THE OPTIMAL DEGREE DISTRIBUTIONS OF CODE D

$\lambda_{i,j}$	$\lambda_{i,0}$	$\lambda_{i,1}$	$\lambda_{i,2}$
$i=2$	0.1112574	0.0136437	0.1818773
$i=3$	0.0917291	0.0876831	0.0571696
$i=6$	0.1322349	0.0003256	0.0001570
$i=7$	0.0926749	0.0000457	0.0000678
$i=20$	0.2740590	0.0001011	0.000217
$i=0$	0	0.0035171	0.0207269

V. CONCLUSION

In this paper, we employed differential evolution method to design degree distribution of the joint network LDPC code

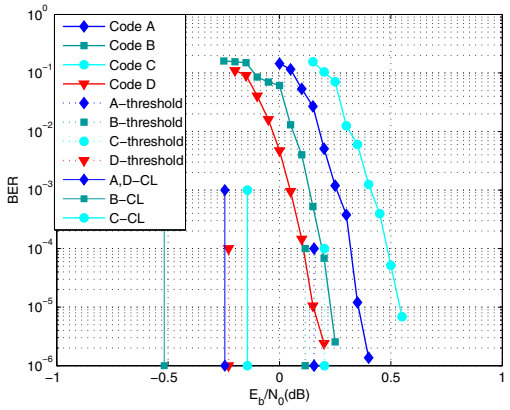


Fig. 3. Performance of the joint network LDPC codes

for a two-source single-relay system, under the assumption of symmetric AWGN channel. The performance of the new codes we designed have significant BER performance gain for a two-source single-relay system with symmetric channels.

ACKNOWLEDGMENT

This work was supported by NSFC(61072064) and NSFC(61101148).

REFERENCES

[1] T. Cover and A. E. Gamal, "Capacity theorems for the relay channel," *IEEE Trans. Inf. Theory.*, vol. 25, pp. 572-584, Sep. 1979.

[2] A. Nosratinia, T. E. Hunter, and A. Hedayat, "Cooperative Communication in Wireless Networks," *IEEE Communications Magazine.*, vol. 42, no. 10, pp.74-80, October 2004.

[3] J. Laneman, D. Tse, and G. Wornell, "Cooperative Diversity in Wireless Networks: Efficient Protocols and Outage Behavior," *IEEE Transactions on Information Theory.*, vol. 50, no. 12, pp. 3062-3080, December 2004.

[4] P. Razaghi and W. Yu, "Bilayer low-density parity-check codes for decode-and-forward in relay channels," *IEEE Trans. Inf. Theory.*, vol. 3, no. 10, pp. 3723-3739, Oct. 2007.

[5] M. H.Azmi, J. Yuan, J. Ning and H. Q.Huynh, "Improved Bilayer LDPC Code Using Irregular Check Node Degree Distribution ," *in Proc. IEEE Int'l Symposium on Information Theory.*, Toronto, Canada, July. 2008.

[6] J. P.Cances and V. Meghdadi, "Optimized Low Density Parity Check Codes Designs for Half Duplex Relay Channels," *IEEE Trans. Wireless Commun.*,vol. 8, no. 7, pp. 3390-3395, July. 2009.

[7] Y. Li, G. H. Song, and L. L. Wang, "Design of joint network-low density parity check codes based on the EXIT charts," *IEEE Commun. Lett.*, vol. 13, no. 8, pp. 600-602, Aug. 2009.

[8] Y. Li, G. H. Song, and L. L. Wang, "Analysis of the joint network LDPC codes over orthogonal multi-access relay channel," *IEEE Commun. Lett.*, vol. 14, no. 2, pp. 184-186, Feb. 2010.

The Design of Rate Compatible Network LDPC Codes

Jingyi Wang，Ying Li，Yue Sun，
State Key Lab. of Integrated Service Networks, Xidian Univ., Xi'an , China

Abstract: This paper studies the design of rate compatible network LDPC codes and proposes a rate-compatible puncturing algorithm, which can obtain the minimum error probability. First, based on the structure of network LDPC codes, the recovery error probability is derived. Then an algorithm of finding variable nodes to be deleted based on the tanner graph of network LDPC codes is proposed, which is aimed at minimizing the decoding error probability and optimizing the puncturing pattern. Simulation results show that the proposed methods of rate-compatible network-LDPC codes have 0.4dB of gain at $BER=10^{-4}$ in error performance compare to the existing punctured methods.

Keywords: multi-access relay channel; Network-LDPC code; rate-compatible; puncturing

速率兼容网络 LDPC 码的设计

王静怡，，李颖，孙岳
西安电子科技大学　综合业务网理论及关键技术国家重点实验室，西安，中国，710071

摘　要：本文研究了网络 LDPC 码的速率兼容算法设计，提出了一种可以获得最低译码错误概率的速率兼容删余算法。首先针对网络 LDPC 码的结构特点，推导了译码恢复错误概率，并基于网络 LDPC 码的 Tanner 图搜索需要删余的变量节点，并以达到最小译码错误概率为目标，获得最优的删余图样。仿真结果表明，与采用现有算法获得的网络 LDPC 码相比，采用所提的改进速率兼容算法获得的网络 LDPC 码的性能在 $BER=10^{-4}$ 时有 0.4 个 dB 的性能增益。

关键词：多址接入信道；网络 LDPC 码；速率兼容；删余

1　引言

无线通信系统中采用中继协作传输技术，可以获取额外的分集增益，从而改善系统性能。但是，对于多址接入中继网络，有多个节点同时需要中继节点帮助转发数据，传统的译码转发或者放大转发模式，会使得中继转发效率降低。因此，通过在中继节点设计有效的联合网络-信道编码算法，在改善接收端性能的同时提高转发效率，是目前的研究热点之一。文献[4]利用低密度奇偶校验(LDPC)码，针对多址接入中继信道设计了一种网络 LDPC 码，并指出可以通过调整中继节点转发数据量来实现中继转发效率和接收端译码性能的有效折中。但是，文中并没有给出具体实现算法，本文将在此基础上，研究适用于网络 LDPC 码的速率兼容算法。

速率兼容码的概念由文献[1]首次提出，文中研究了速率兼容卷积码的设计。删余是实现速率兼容的一种常用方法，即通过将低码率母码中的某些编码比特删余来获取高码率码。速率兼容 LDPC 码的设计是近几年研究热点，文献[2，3]通过分组和排序操作，将 LDPC 码的变量节点按照迭代恢复次数进行分类，设计了 LDPC 码速率兼容删余算法。

资助信息：国家自然基金项目(61072064)；国家科技重大专项(2010ZX03003-003-03)；长江学者和创新团队发展计划资助(IRT0852)；中央高校科研业务费专项资金项目(K50510010026).

(C)1994-2023 China Academic Journal Electronic Publishing House. All rights reserved.　http://www.cnki.net

2 适用于多址接入中继信道的网络 LDPC 码

由两个源节点和一个中继节点构成的多址接入中继网络模型如图 1 所示，两个源节点与目的节点之间的信息传输由广播发送和中继转发两个阶段完成。在广播阶段，两个源节点分别向中继节点和目的节点广播发送编码序列 X_1 和 X_2；在中继转发阶段，中继节点首先对接收信号进行译码，得到两个源节点的估计数据，然后对译码得到的估计数据重新进行联合编码，并将编码序列 X_R 转发至目的节点。目的节点则根据收到的信号进行联合译码，得到两个源节点的估计信息。

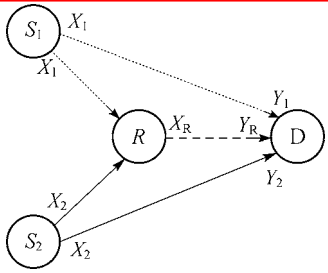


图 1　多址接入中继信道模型

在目的节点端将两个源节点和中继节点采用的 LDPC 码综合考虑，得到如下校验矩阵

$$\boldsymbol{H}=\begin{pmatrix}\boldsymbol{H}_1 & \boldsymbol{0} & \boldsymbol{0}\\ \boldsymbol{0} & \boldsymbol{H}_1 & \boldsymbol{0}\\ \boldsymbol{A} & \boldsymbol{B} & \boldsymbol{C}\end{pmatrix} \qquad (0)$$

式中，$\boldsymbol{H}_1$ 是源节点采用 LDPC 码的校验矩阵，$\boldsymbol{H}_3=(\boldsymbol{A}\quad \boldsymbol{B}\quad \boldsymbol{C})$ 是中继节点采用 LDPC 码的校验矩阵和 $\boldsymbol{0}$ 是零矩阵。由于式(1)中包括了源节点和中继节点所采用 LDPC 码的校验矩阵，并且中继节点是对两个源节点的数据进行联合编码，因此文献[4]称之为网络 LDPC 码，该码的 Tanner 图如图 2 所示。

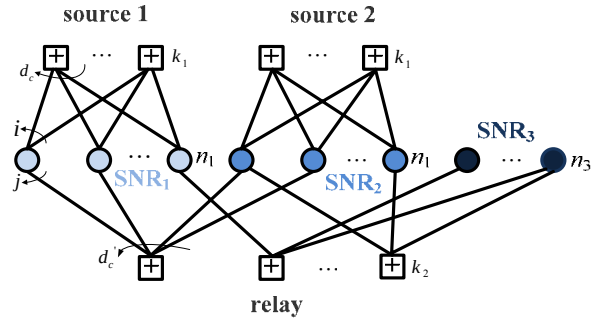


图 2　网络 LDPC 码的 Tanner 图

由图 2，网络 LDPC 码的 Tanner 图中包含上下两层子图，其中上层子图包含 $2k_1$ 个校验节点，它们与变量节点连接关系由式(1)中的 $\boldsymbol{H}_1$ 确定；下层子图包括 k_2 个校验节点，它们与变量节点的连接关系由式(1)中的 $\boldsymbol{H}_3$ 确定。图中每个变量节点的度用 (i,j) 表示，其中 i 为变量节点与上层校验节点相连的边数，j 为变量节点与下层校验节点相连的边数，d_c 和 d_c' 分别表示上层和下层校验节点的度数。

3 速率兼容网络 LDPC 码的设计

3.1 几个定义

定义 1(n 步恢复变量节点)：第 n 次迭代译码时才可以恢复的被删除的变量节点称为 n 步恢复变量节点，用 n-SR 表示。n-SR 的集合用群 G_n 表示。

定义 2(幸存校验节点)：如果一个一步恢复的删余变量节点至少与一个校验节点相连，且与这个校验节点相连的其它变量节点没有都被删余掉，那么这个校验节点就是幸存校验节点。图 3 中的校验节点 S_1 和 S_2 即为幸存校验节点。相反，校验节点 D 即为死校验节点。

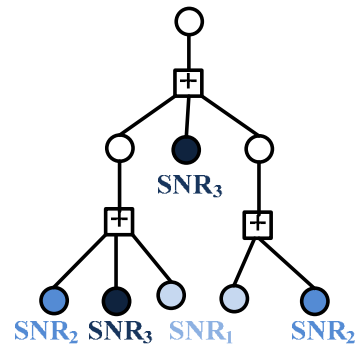


图 3　网络 LDPC 码的恢复树(横线圆表示幸存的变量节点 $S(v)$，竖线圆表示删掉的变量节点)

定义 3(幸存变量节点)：与幸存校验节点相连的其它没有被删除的变量节点称为幸存变量节点。

定义 4(等效幸存邻居变量节点数)：假设网络 LDPC 码所有编码比特在传输过程中受 K 种噪声干扰，对应噪声方差分别为 $\sigma_1^2>\sigma_2^2>\cdots>\sigma_K^2$，令每个受到噪声干扰最大(噪声功率为 σ_1^2)的幸存邻居变量节点的等效幸存邻居变量节点数为 1，则受其他噪声干扰的幸存邻居变量节点的等效幸存邻居变量节点数定义为

$$\alpha_i=\left(\log\left[1-\phi\left[\frac{2}{\sigma_i^2}\right]\right]\Big/\log\left[1-\phi\left[\frac{2}{\sigma_1^2}\right]\right]\right)\leqslant 1 \qquad ()$$

(C)1994-2023 China Academic Journal Electronic Publishing House. All rights reserved.　http://www.cnki.net

式中，$i=1,2,\cdots,K$。

$$\phi(x)=\begin{cases}\dfrac{1}{\sqrt{4\pi x}}\displaystyle\int_R \tanh\frac{u}{2}e^{-\frac{(u-x)^2}{4x}}su & x>0\\ 0 & x=0\end{cases}。$$

3.2 译码恢复错误概率

将网络 LDPC 码的删余变量节点 v 的所有幸存邻居变量节点按照其所通过信道的噪声功率的大小分为 b 类，假设第 t 类的噪声功率为 $\sigma_t^2(t=1,2,\cdots,b)$，且 $\sigma_1^2>\sigma_2^2>\cdots>\sigma_b^2$,并设第 t 类包括 S_t 个变量节点，记为 $\{v_1^t,\cdots,v_s^t,\cdots v_{S_t}^t\}$。与 LDPC 码类似，首先估计每次迭代过程中网络 LDPC 码的每个变量节点的均值更新，并由此计算该节点的恢复错误概率。

$\rho^{up}(x)=\sum_{k=1}^{d_c}\rho_k^{up}x^{k-1}$ $\rho^{low}(x)=\sum_{k=1}^{d_c'}\rho_k^{low}x^{k-1}$ 假设校验节点的度分布分别为 $\rho^{up}(x)=\sum_{k=1}^{d_c}\rho_k^{up}x^{k-1}$ 和 $\rho^{low}(x)=\sum_{k=1}^{d_c'}\rho_k^{low}x^{k-1}$，其中 η 是上层变量节点与校验节点相连的边数占总边数的比例，$\lambda_{i,j}$ 是与度为 (i,j) 的变量节点连接的边数占总边数的比例。$m_{i,j}^{l-1}$ 和 $n_{i,j}^{l-1}$ 分别表示第 $(l-1)$ 次迭代时，变量节点传给上下层的校验节点的对数似然比的均值。第 l 次迭代时，上下层校验节点的均值更新过程如下：

$$m'^{l}=\sum_k\rho_k^{up}\phi^{-1}\left(\left(\frac{1}{\eta}\sum_{i\geqslant0,j\geqslant0}\frac{i}{i+j}\lambda_{i+j}\phi(m_{i,j}^{l-1})\right)^{\sum_{t=1}^{b}S_t\alpha_t}\right)$$

$$n'^{l}=\sum_k\rho_k^{low}\phi^{-1}\left(\left(\frac{1}{1-\eta}\sum_{i\geqslant0,j\geqslant0}\frac{j}{i+j}\lambda_{i+j}\phi(n_{i,j}^{l-1})\right)^{\sum_{t=1}^{b}S_t\alpha_t}\right)\quad()(1)$$

当上下层的校验节点向被删余的度为 (i,j) 变量节点 $v\in G_{l+1}$ 传递消息时，该消息的对数似然比的均值分别为:

$$m'^{l}=\sum_k\rho_k^{up}\phi^{-1}\left(\left(\frac{1}{\eta}\sum_{i\geqslant0,j\geqslant0}\frac{i}{i+j}\lambda_{i+j}\phi(m_{i,j}^{l-1})\right)^{\sum_{t=1}^{b}S_t\alpha_t}\right)$$

$$n'^{l}=\sum_k\rho_k^{low}\phi^{-1}\left(\left(\frac{1}{1-\eta}\sum_{i\geqslant0,j\geqslant0}\frac{j}{i+j}\lambda_{i+j}\phi(n_{i,j}^{l-1})\right)^{\sum_{t=1}^{b}S_t\alpha_t}\right)$$

其中，α_t 表示每个幸存邻居变量节点的等效幸存邻居变量节点数，S_t 表示与变量节点 v 相连的校验节点没有被删余的变量节点数，变量节点 m_L v 的总等效幸存邻居变量节点数为 $\sum_{t=1}^{b}S_t\alpha_t$。

(2) 当上下层的校验节点向没有删余的度为 (i,j) 的变量节点传递消息时，该消息的对数似然比的均值分别为：

$$m'^{l}=\sum_k\rho_k^{up}\phi^{-1}\left(\left(\frac{1}{\eta}\sum_{i\geqslant0,j\geqslant0}\frac{i}{i+j}\lambda_{i+j}\phi(m_{i,j}^{l-1})\right)^{k-1}\right)$$

$$n'^{l}=\sum_k\rho_k^{low}\phi^{-1}\left(\left(\frac{1}{1-\eta}\sum_{i\geqslant0,j\geqslant0}\frac{j}{i+j}\lambda_{i+j}\phi(n_{i,j}^{l-1})\right)^{k-1}\right)$$

上下层变量节点的均值更新过程如下：

假设 m'^{l} 和 n'^{l} 分别表示第 l 次迭代时，上层和下层的校验节点传给变量节点的对数似然比消息均值。第 l 次迭代时，度为 (i,j) ()变量节点传给上下层校验节点的对数似然比消息均值分别为[4]

$$m_{i,j}^{l}=\begin{cases}(i-1)m'^{l}+jn'^{l}+m_{u_0} & i\neq0,j\geqslant0\\ jn'^{l}+m_{u_0}^{'} & i=0,j\geqslant1\end{cases}\qquad(7)$$

$$n_{i,j}^{l}=\begin{cases}im'^{l}+(j-1)n'^{l}+m_{u_0} & i\neq0,j\geqslant1\\ (j-1)n'^{l}+m_{u_0}^{'} & i=0,j\geqslant1\\ im'^{l}+m_{u_0} & i\neq0,j=0\end{cases}$$

若变量节点被删掉，则 $m_{u_0}(m_{u_0}^{'})=0$；若变量节点为由源节点发送至目的节点的信息比特，则 $m_{u_0}=2/\sigma_{SD}^2$；若变量节点为中继节点发送至目的节点的信息比特，则 $m_{u_0}^{'}=2/\sigma_{RD}^2$。第一次迭代时，校验节点的初始值 $m'^{(0)}=n'^{(0)}=0$。

因此，变量节点传给上下层校验节点的平均的消息均值分别为：

$$m^{l}=\frac{1}{\eta}\sum_{i\geqslant0,j\geqslant0}\frac{i}{i+j}\lambda_{i+j}m_{i,j}^{l}$$

$$n^{l}=\frac{1}{1-\eta}\sum_{i\geqslant0,j\geqslant0}\frac{j}{i+j}\lambda_{i+j}n_{i,j}^{l}$$

经过 L 次迭代后，码比特的平均消息均值为：

$$m_L=\eta m^L+(1-\eta)n^L$$

此时，网络 LDPC 码的被删余变量节点的恢复错误概率为：

$$P_e(v)=Q(\sqrt{m_L/2})$$

其中

$$Q(x)=\frac{1}{\sqrt{2\pi}}\int_x^{\infty}e^{-t^2/2}\mathrm{d}t。$$

(C)1994-2023 China Academic Journal Electronic Publishing House. All rights reserved. http://www.cnki.net

3.3 网络 LDPC 码的速率兼容算法

由公式(3)和(4)可知，等效幸存邻居变量节点数 $\sum_{t=1}^{b} S_t \alpha_t$ 越小，更新得到的均值 m'^{l} 和 n'^{l} 的值越大，进而迭代后的变量节点 m_L 的均值也越大，同时由公式(12)得到的恢复错误概率越小。因此，在搜索节点时，需要寻找当前具有最小等效邻居的变量节点进行删余操作。与文献[2]设计的 LDPC 码的删余算法相似，所提出的网络 LDPC 码速率兼容算法主要包括分组和排序两个操作。

分组：

(1) 给定一个 $M \times N$ [D1]网络 LDPC 码的校验矩阵，初始化 $R_\infty = \{1,2,\cdots,M\}$，$G_\infty = \{1,2,\cdots,N\}$，$l=1$；[D2]

(2) 遍历集合 R_∞，找出行重最小的行集合 r；[D3]

(3) 遍历集合 G_∞，找出列重最小的列集合 c；[D4]

(4) 选出所有(2)(3)相交的[D5]元素的集合 $w = \{(r^*, c^*), r^* \in r, c^* \in c\}$，作为候选对；

(5) 在集合 w 中选出具有最小等效幸存邻居变量节点数的元素，记为 (r_j^*, c_k^*)。若有多对满足条件，随机选出其中一对，归[D6]入第 l 次迭代可以恢复的集合 G_l，[D7]更新 $R_\infty = R_\infty \setminus r_j^*$ 和 $G_\infty = G_\infty \setminus c_k^*$；

(6) 若集合 G_∞ 为空，停止迭代，否则跳至(7)；

(7) 若集合 R_∞ 不为空，跳至(2)；否则若步骤(5)中有多于一对满足条件，则 $l = l+1$，跳至(2)。

接下来计算最大可达码率[2]为：

$$R_{\max} = \frac{R_0}{1 - \sum_{j=1}^{K} \left| G_j \right| / n} \tag{13}$$

式中，R_0 是母码的码率，n_i 是母码的码长。

[D8]如果要设计码率为 R_j 的码子，需要删余的节点数为[2]：

$$np_j = \left\lfloor \frac{n(R_j - R_0)}{R_j} \right\rfloor$$

式中 i，$0 \leqslant j \leqslant M$。

组内排序：

(1) 给定一个 $M \times N$ 网络 LDPC 码的校验矩阵[D9]，初始化 $R_\infty = \{1,2,\cdots,M\}$，$l=1$，$j=1$，$P_0 = \phi$；$R_0 \leqslant R_1 \leqslant \cdots \leqslant R_M \leqslant R_{\max}$

(2) 若 $j > M$，停止迭代[D10]；否则，$0 \leqslant j \leqslant M$ $P_j = P_{j-1}$；

(3) $\Delta = np_j - \left| P_j \right|$；[D11]

(4) 若 $\Delta = 0$，$j = j+1$ [D12]，跳至(2[D3])；

(5) 根据集合 G_l 定义 $C_l = \{c_1^*, c_2^*, \cdots\}$，从 C_l 中选出列重最大的变量节点的集合 $c_{\max}^*$，并从 $c_{\max}^*$ 中找出具有最小数量的死校验节点[D14]的变量节点 $c_{\max}^{**}$。如果有多个满足条件，随机选出其中一个，归入排序的集合 P_j，更新 $P_j = P_j \bigcup \{c_{\max}^{**}\}$，$G_l = G_l \setminus \{c_{\max}^{**}\}$，$\Delta = \Delta - 1$，$R_\infty = R_\infty \setminus r_{\max}^{**}$；

(6) 若 G_l 为空，$l = l+1$，$R_\infty = \{1,2,\cdots,M\}$；

(7) 跳至(4)。

经过上述分组和组内排序操作，将 $G_l (1 < l < K)$ () 变量节点按照 l 从小到大删余，而在同一个 G_l 中，按照变量节点的列号从小到大删余，直到删掉 np_j 个节点。

4 仿真结果

仿真中两个源节点采用的 LDPC 码的码长均为 2048，码率均为 0.5，度分布为：$\lambda(x) = 0.23403x + 0.21242x^2 + 0.1469x^5 + 0.102840x^6 + 0.30381x^{19}$ 和 $\rho(x) = 0.71875x^7 + 0.28125x^8$。中继节点采用的 LDPC 码的校验比特数为 628。假设信道模型为理想加性高斯白噪声(AWGN)信道，源节点和中继节点均采用 BPSK 调制方式。中继节点与目的节点之间的信噪比固定为 5dB。中继节点可以正确译码得到两个源节点的发送数据。图 4 和图给出了母码经过本文所改进算法(intentional)、现有算法(original)[2]和随机删余(random)所得到的码率为 0.5、0.6 和 0.7 的网络 LDPC 子码的 BER 性能对比。

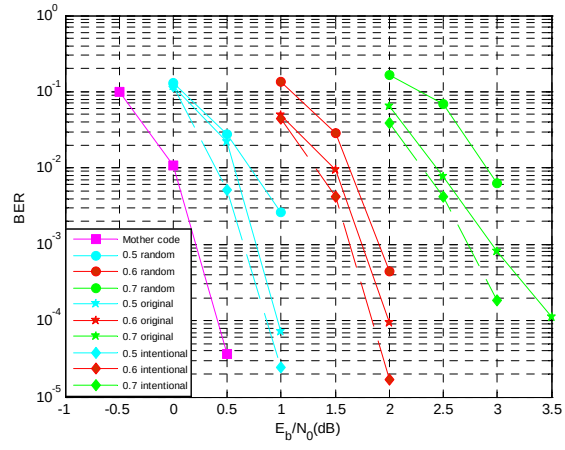


图 4 网络 LDPC 码的删余性能对比

由图 4 和图 5 可以看出，随着删余比特的增加，

(C)1994-2023 China Academic Journal Electronic Publishing House. All rights reserved. http://www.cnki.net

采用所提算法得到的网络 LDPC 码的性能增益也随之增加。当码率为 0.5， BER=10^{-3} 时，采用所提算法性能优于随机算法 0.45dB；当码率为 0.5，BER=10^{-4} 时，采用所提算法比文献[2]中算法的性能改善 0.15dB。在码率为 0.6， BER=10^{-3} 时，所提算法相对于随机算法性能增益为 0.3dB,相对于文献[2]中算法性能增益为 0.2dB。当码率为 0.7，SNR=3dB 时，所提算法的 BER 为 10^{-5} ，相比于随机算法的 10^{-3} 有了明显提升，而 BER=10^{-4} 时，所提算法比文献[2]中算法性能能增益改善 0.4 dB。

5 结论

文章首先介绍了网络 LDPC 码的结构及基本原理,然后针对其结构特性推导了译码恢复错误概率,并详述了适用于网络 LDPC 码的上下层变量节点和校验节点均值更新理论,接着介绍了网络 LDPC 码的速率兼容删余算法,最后对所设计的算法进行仿真,与现有算法相比，本文所提出的改进速率兼容算法在 BER=10^{-4} 时有 0.4dB 的性能增益。

参 考 文 献

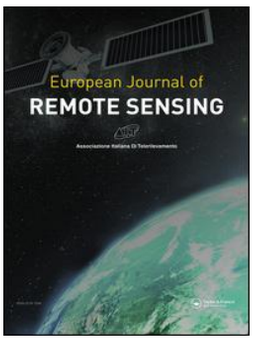
[1] Hagenauer J. Rate-Compatible Punctured Convolutional Codes (RCPC codes) and Their Applications[J] . IEEE Trans on Communication, 1988, 36(4) : 389-400.

[2] J. Ha, J. Kim, D. Klinc, and S. W. McLaughlin, “Rate-Compatible Punctured Low-Density Parity-Check Codes With Short Block Lengths”, IEEE trans. Inform. Theory, vol. 52, no. 2, pp. 728-738, Feb. 2006.

[3] J. Ha, J. Kim, D. Klinc, and S. W. McLaughlin, “Rate-Compatible Puncturing of Low-Density Parity-Check Codes ”, IEEE trans. Inform. Theory, vol. 50, no. 11, pp. 2824-2836, NOV. 2004.

[4] Y. Li, G. H. Song, and L. L. Wang, “Design of joint network-low density parity check codes based on the EXIT charts”, IEEE Commun. Lett., vol. 13, no. 8, pp. 600-602, Aug. 2009.

(C)1994-2023 China Academic Journal Electronic Publishing House. All rights reserved. http://www.cnki.net



European Journal of Remote Sensing

ISSN: (Print) (Online) Journal homepage: https://www.tandfonline.com/loi/tejr20

Comparison on quantitative inversion of characteristic ions in salinized soils with hyperspectral based on *support vector regression* and *partial least squares regression*

Jingyi Wang & Xiaoming Li

To cite this article: Jingyi Wang & Xiaoming Li (2020) Comparison on quantitative inversion of characteristic ions in salinized soils with hyperspectral based on *support vector regression* and *partial least squares regression* , European Journal of Remote Sensing, 53:1, 340-348, DOI: 10.1080/22797254.2020.1854622

To link to this article: https://doi.org/10.1080/22797254.2020.1854622

© 2020 The Author(s). Published by Informa UK Limited, trading as Taylor & Francis Group.

Published online: 09 Dec 2020.

Submit your article to this journal

Article views: 23

View related articles

View Crossmark data

Full Terms & Conditions of access and use can be found at
https://www.tandfonline.com/action/journalInformation?journalCode=tejr20

EUROPEAN JOURNAL OF REMOTE SENSING
2020, VOL. 53, NO. 1, 340–348
https://doi.org/10.1080/22797254.2020.1854622

Taylor & Francis
Taylor & Francis Group

OPEN ACCESS Check for updates

Comparison on quantitative inversion of characteristic ions in salinized soils with hyperspectral based on *support vector regression* and *partial least squares regression*

Jingyi Wang[a] and Xiaoming Li[b]

[a]College of Computer Science, Xi'an Shiyou University, Xi'an, China; [b]Key Laboratory of Degraded and Unused Land Consolidation Engineering, Ministry of Natural Resources, Xi'an, China

ABSTRACT

This study aimed to investigate quantitative inversion of salt ions. Now, most research on hyperspectral characters in salinized soils focus on quantitative inversion of salt content, but few on ions. Original hyperspectral data were collected and calculated average as reflectance (R), the logarithm of the reciprocal of R (Log(1/R)) and continual removed reflectance (R_{cr}) were also used. Correlations between salt content and ions were calculated, three ions were chosen as characteristic. SVR and PLSR methods were used to derive inversion models. Results showed both methods provided accurate measurement. For modeling precision, no matter which hyperspectral characters based on, inversion models derived with SVR were more accurate than PLSR. For test precision, inversion models derived with SVR were also more accurate. Inversion model of Cl^- based on R was the most accurate, followed by that based on R_{cr}, while the inversion model of K^+ based on R_{cr} was the most accurate. All the inversion models of Na^+ based on R, Log(1/R) and R_{cr} had good test precision. In conclusion, the accuracy of the quantitative inversion model with SVR was higher than PLSR, the best hyperspectral characters for inversion models were chosen, making a useful diagnostic tool for soil salinity.

ARTICLE HISTORY
Received 29 December 2019
Revised 19 November 2020
Accepted 19 November 2020

KEYWORDS
Quantitative inversion; soil salinization ions; hyperspectral data; characteristic bands

Introduction

Soil salinization is a global problem for resource and environment, being one of the most important barriers for land productivity. The area of salinized soils in China is about 3 600 × 10^4 ha, distributed in the regions of Shaanxi, Gansu, Ningxia, Qinghai, Xinjiang, and the east coastal areas (Yang, 2008). The national strategy to guarantee food safety intends to maintain the area of farmland in these regions, as well as to ensure no decrease in farmland quality. This requires soil salinization to be addressed early and warned and controlled adequately. Traditional methods of monitoring soil salinization consist of collecting soil samples and analyzing them in laboratory. While the precision of such methods is adequate, it is time-consuming and labor-intensive, making it hard to monitor a large area of land. As the electromagnetic technology was introduced, it enabled quick diagnosis of soil salinization at medium scales (Li et al., 2010). However, using this technology to monitor on a large scale is difficult. The development of remote sensing technology and particularly the application of hyperspectral technology that provide high resolution and abundant spectrum information enabled the quantitative inversion of salinization characters (Yao et al., 2013a). Remote sensing also enabled the realization of whole cover RS monitoring from the point scale to regional scale.

Soil salinization results from some conditions including land hydrologic, climatic, geologic, terrain conditions, and the human activities. And the spectral responses for salinized soil are closely related with its physical and chemical characteristics (Zhu et al., 2017). A number of national and international research have been conducted on quantitative inversion and monitoring for soil salinization with spectral characters. Some studies focused on the mining of hyperspectral data, extracting the hyperspectral characters having the best correlations with soil salt information, such as reflectance (R) (Duan et al., 2017), reciprocal of reflectance (1/R) (Yao et al., 2013a), logarithm of the reciprocal of reflectance (Log(1/R)), continual removed reflectance (R_{cr}) (Ding et al., 2012), and derivative transformations (J. Wang et al., 2009; D. Zhang et al., 2014), allowing them to derive the quantitative inversion models. Other studies focused on methods for deriving inversion models, such as multiple regression (Kelimu et al., 2016), support vector regression (SVR), partial least square regression (PLSR) (Dai et al., 2015; Qu et al., 2009), and artificial neutral networks (J. Wang et al., 2009). Some scholars used fused hyperspectral data and other primary data (such as electromagnetic data) to derive quantitative

CONTACT Xiaoming Li xmlihyc@126.com Key Laboratory of Degraded and Unused Land Consolidation Engineering, Ministry of Natural Resources, Xi'an, China

© 2020 The Author(s). Published by Informa UK Limited, trading as Taylor & Francis Group.
This is an Open Access article distributed under the terms of the Creative Commons Attribution License (http://creativecommons.org/licenses/by/4.0/), which permits unrestricted use, distribution, and reproduction in any medium, provided the original work is properly cited.

inversion models (Yao et al., 2013b, 2013a), while others applied the quantitative models with remote sensing image interpretation on larger scales (Kelimu et al., 2016). Recently, most researchers focus on the quantitative inversion of the total salt content using hyperspectral data, and only few scholars studied the quantitative inversion of salt ions (Dai et al., 2015; Liu et al., 2016; H. J. Wang et al., 2018). Furthermore, this specific research was limited to only one method to derive the inversion model. In this paper, quantitative inversion models of salt ions were derived using two different methods (SVR and PLSR), based on hyperspectral transformation data. The accuracy of each method was compared to indicate which would make the most useful diagnostic tool for soil salinization detection and monitoring at large regional scales.

Data and methods

Data collection

The study area was located in a typical salinized field where the soil type is *arenosols* by WRB classification in Dingbian County, north of Shaanxi province, which is shown in Figure 1. The soil salinization in this area is so severe that it has become one of the most serious limitations for agriculture, the crops are hard to grow. To empirically study the quantitative inversion of soil salinization, a large range of soil salinization is needed. Therefore, 70 sample points over different grades of salinization were selected randomly by viewing soil salt accumulation but not just by equal distance. All sampling points consisted of bare soil with no vegetation cover. 42 and 28 sample points were used to derive the inversion models and for precision testing, respectively. On each sample point, the hyperspectral data was collected first; then, the topsoil (0 ~ 10 cm) was sampled separately.

The hyperspectral data of reflectance were collected outdoors between 11:00, 14:00, using a FieldSpec 4 HR by ASD. The sampling intervals of the spectrum were 1.4 nm with a band wavelength of 350–1000 nm and 2 nm with the band wavelength of 1001–2500 nm; the resampling interval was 1 nm. The spectrum average was defined as 10, denoting that the reflectance was collected 10 times for each sample point.

Calibration was performed in the field before each measurement, using a whiteboard. Hyperspectral data were collected 10 times on each sample point. Additionally, some pretreatments were made in laboratory: the spectral data were loaded in the ViewSpecPro software, abnormal data were eliminated, and the average values were calculated as the hyperspectral characteristic values for a given sample point. In this paper, the hyperspectral characters of reflectance (R), the logarithm of the reciprocal of reflectance ($\mathrm{Log}(1/R)$), and the continual removed reflectance (R_{cr}) were used for the quantitative inversion; the former two characters were extracted directly using the ViewSpecPro software, whereas R_{cr} was obtained with the ENVI software.

After gathering the spectral data, the topsoil (0 ~ 10 cm) was sampled at each point to measure the salinization variables. All the soil samples were taken back to the laboratory, naturally air-dried, grinded, and sieved through a 2-mm mesh screen. Then, soil extract liquid (the soil/water ratio is 1/5) was made. Subsequently, the salinization characteristics, including the total content of soil salt and eight salinization ions (Ca^{2+}, Mg^{2+}, K^{+}, Na^{+}, SO_4^{2-}, Cl^{-}, CO_3^{2-}, HCO_3^{-}), were obtained through sample analysis (Lu, 1999): gravimetric method was used to determine the total content of soil salt, EDTA titration method was used to determine Ca^{2+} and Mg^{2+}, spectrophotometer was used to determine K^{+} and Na^{+}, EDTA indirect complexometric titration method was used to determine SO_4^{2-}, silver nitrate titration method was used to determine Cl^{-}, and double indicators neutralization titration method was used to determine CO_3^{2-} and HCO_3^{-}.

Methods

A correlation analysis between the total salt content and the eight salinization ions was performed, and the salinization characteristic ions were identified by selecting the high correlation coefficients. For the quantitative inversion of salinization characteristic ions, the correlations between the characteristic ionic content and the hyperspectral characters were analyzed, and the characteristic bands were selected using a correlation coefficient extreme method (Zhu et al., 2017) to derive the inversion models.

The PLSR and SVR methods were used to derive quantitative inversion models. Comparing with the traditional multiple regression method, the PLSR method combined all the advantages of a principal component analysis, typical correlation analysis, and multiple line regression and can be used to derive models even when there are strong correlations among variables and the number of the samples is less than the number of variables, so its precision is better than the traditional regression method (Q. Zhang et al., 2018). On the other hand, Support Vector Regression (SVR) is an application of support vector machine (SVM) to the regression problem, namely, to find a regression plane that minimizes the distance of all the data of a set from the plane (Liang et al., 2013). The SVR function can be expressed as:

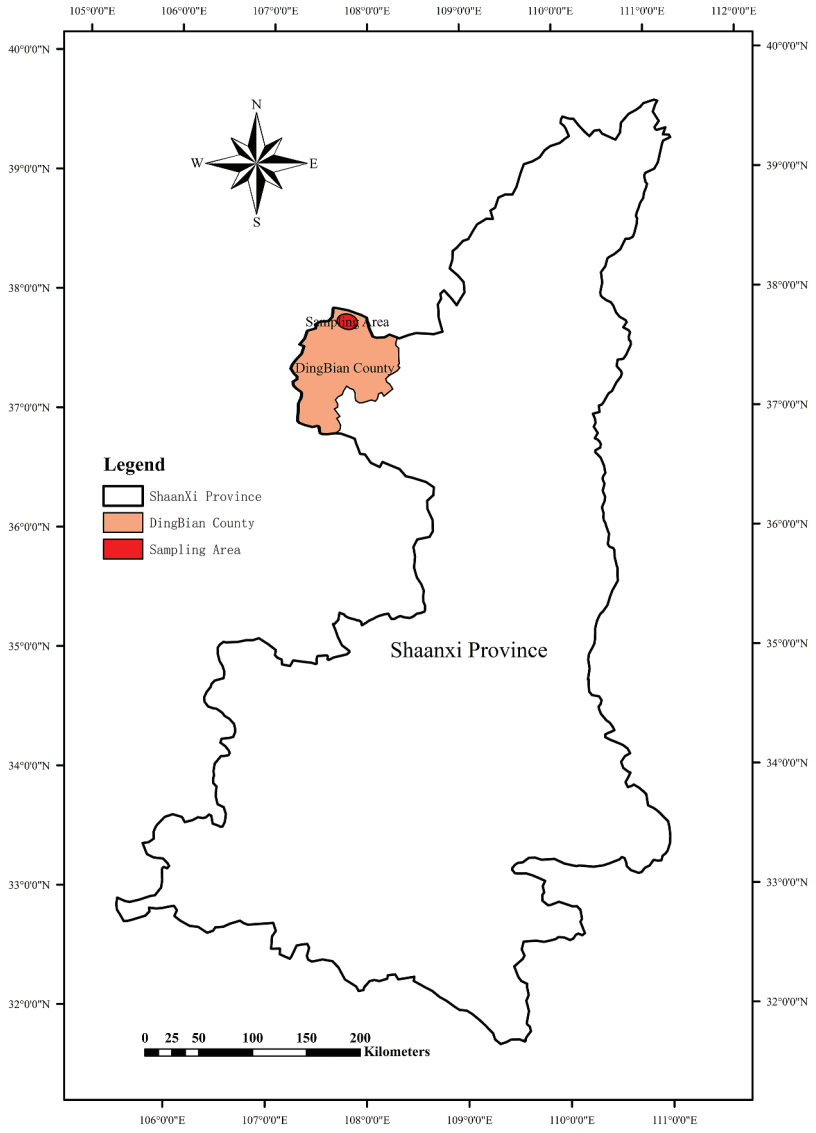


Figure 1. Location of the study area in Shaanxi Province.

$$f(x) = \sum_{i=1}^{N} \left(a_i - a_i^*\right) \cdot k(x, x_i) + b$$

where N is the number of samples, $(a_i \_ a_i^*)$ is the Lagrange multiplier, $k\ (x,\ x_i)$ is the kernel function, and b is the bias term.

For each method, the model precision was compared. All the calculations were realized with Matlab software, and the *PLSR* order in the toolbox and the *libsvm tool* by Chih-Chung Chang and Chih-Jen Lin were used to derive the models. To test the precision of quantitative inversion calculations, both the modeling precision and the test precision were compared. The determination coefficient (r^2) and the root mean square error (RMSE) were compared to determine modeling precision, while the correlations and RMSE between the predicted and the measured value with the test samples were compared to determine test precision.

Results and Discussion

Salinization characteristic ions

The summary statistics of the eight ions and the total salt content are shown in Table 1 The total salt content was from 1.050 g/kg to 29.380 g/kg, and its mean value was 7.690 g/kg, which meant the salinity level in the study area was serious. And that just could explain why the ration of seeding lack in the study area was high, and even nearly bare in some places. As to why the salinity is so serious, the study area is one of the main producing areas for lake salt, and the water in soil contents much soluble salt. When the water moves upwards, especially in the seasons of spring and autumn, the salt could move together, and accumulate on the top soil under the impact of strong evaporation. By the statistical data such as chorography, the salinity of Dingbian County could reach up to 50 g/kg, and even more.

The results of the correlation analysis between the total salt content and eight salinization ions showed

Table 1. Summary statistics for eight salinization ions and the total salt content (TS).

Variables	Sample Quantity (*n*)	Minimum (g/kg)	Maximum (g/kg)	Mean (g/kg)	Standard Deviation (*Std.*)
Ca^{2+}	70	0.050	0.330	0.089	0.057
Mg^{2+}	70	0.010	0.500	0.121	0.099
K^{+}	70	0.017	0.081	0.037	0.018
Na^{+}	70	0.115	0.787	0.362	0.168
SO_4^{2-}	70	0.070	0.226	0.161	0.045
Cl^{-}	70	0.011	0.694	0.174	0.177
CO_3^{2-}	70	0.001	0.002	0.002	0.001
HCO_3^{-}	70	0.003	0.020	0.013	0.004
TS	70	1.050	29.380	7.690	6.942

that the correlation coefficients of K^{+}, Na^{+}, and Cl^{-} are strong (Table 2), the correlation coefficients of Pearson were 0.861**, 0.953** and 0.987**, respectively, and the correlations were all significant at 0.01 level (2-tailed). It could be concluded that the salinization in our study area was caused by chlorides of potassium and sodium, and the characteristic ions should be K^{+}, Na^{+}, and Cl^{-}.

Table 2. Correlations among total content of soil salt (TS) and salt ions.

	Ca^{2+}	Mg^{2+}	K^{+}	Na^{+}	SO_4^{2-}	Cl^{-}	CO_3^{2-}	HCO_3^{-}	TS
Ca^{2+}	1.000								
Mg^{2+}	0.136	1.000							
K^{+}	0.219	0.777	1.000						
Na^{+}	−0.287	0.661	0.808	1.000					
SO_4^{2-}	−0.429	0.339	0.341	0.517	1.000				
Cl^{-}	−0.109	0.702	0.840	0.954	0.306	1.000			
CO_3^{2-}	−0.330	0.246	0.224	0.447	0.217	0.436	1.000		
HCO_3^{-}	−0.067	−0.182	−0.091	−0.079	−0.061	−0.071	−0.242	1.000	
TS	−0.093	0.776	0.861	0.953	0.340	0.987	0.427	−0.126	1.000

Table 3. Descriptive statistical characteristics of hyperspectral characters for Cl^{-} ion (*n*= 42).

Hyperspectral Character	Band	Min	Max	Mean	*Std.*	*Var.*
R	B465	0.070	1.023	0.282	0.306	0.094
	B1365	0.213	1.264	0.509	0.270	0.073
	B1407	0.188	1.251	0.488	0.274	0.075
	B2210	0.203	1.303	0.510	0.275	0.075
	B2353	0.202	1.296	0.501	0.275	0.076
Log(1/R)	B356	−0.110	1.470	0.889	0.450	0.202
	B1365	−0.195	0.676	0.332	0.212	0.045
	B1406	−0.200	0.727	0.353	0.226	0.051
	B2211	−0.227	0.693	0.331	0.223	0.050
	B2353	−0.228	0.698	0.340	0.227	0.051
R_{cr}	B495	0.743	1.000	0.883	0.073	0.005
	B762	0.804	1.000	0.982	0.045	0.002
	B1371	0.681	0.995	0.899	0.077	0.006
	B2140	0.559	1.000	0.896	0.115	0.013
	B2277	0.535	0.998	0.918	0.122	0.015

Table 4. Descriptive statistical characteristics of hyperspectral characters for K^{+} ion (*n*= 42).

Hyperspectral Character	Band	Min	Max	Mean	*Std.*	*Var.*
R	B486	0.076	1.030	0.292	0.304	0.092
	B1366	0.204	1.234	0.509	0.270	0.073
	B1406	0.188	1.254	0.489	0.274	0.075
	B2211	0.204	1.306	0.510	0.275	0.076
	B2336	0.204	1.272	0.503	0.269	0.072
Log(1/R)	B439	−0.137	1.207	0.736	0.388	0.150
	B1363	−0.206	0.682	0.325	0.215	0.046
	B1406	−0.200	0.727	0.353	0.226	0.051
	B2211	−0.227	0.693	0.331	0.223	0.050
	B2336	−0.218	0.692	0.336	0.224	0.050
R_{cr}	B508	0.764	1.000	0.889	0.066	0.004
	B764	0.802	1.000	0.981	0.046	0.002
	B1371	0.681	0.995	0.899	0.077	0.006
	B2140	0.559	1.000	0.896	0.115	0.013
	B2275	0.536	1.000	0.917	0.121	0.015

Table 5. Descriptive statistical characteristics of hyperspectral characters for Na^+ ion (n= 42).

Hyperspectral Character	Band	Min	Max	Mean	*Std.*	*Var.*
R	B491	0.077	1.035	0.295	0.304	0.092
	B1365	0.213	1.264	0.509	0.270	0.073
	B1406	0.188	1.254	0.489	0.274	0.075
	B2211	0.204	1.306	0.510	0.275	0.076
	B2353	0.202	1.296	0.501	0.275	0.076
Log(1/R)	B354	−0.110	1.475	0.892	0.451	0.203
	B1365	−0.195	0.676	0.332	0.212	0.045
	B1406	−0.200	0.727	0.353	0.226	0.051
	B2211	−0.227	0.693	0.331	0.223	0.050
	B2353	−0.228	0.698	0.340	0.227	0.051
R_{cr}	B495	0.743	1.000	0.883	0.073	0.005
	B764	0.802	1.000	0.981	0.046	0.002
	B1371	0.681	0.995	0.899	0.077	0.006
	B2141	0.560	0.999	0.897	0.114	0.013
	B2275	0.536	1.000	0.917	0.121	0.015

Characteristic bands for ions

The correlations between ionic content and *R* are shown in Figure 2. For the Cl^- ion, for example, the correlations are well within the band range of 350~550 nm. With the band wavelength increasing, the correlation coefficients decreased, but there were two peaks between 1350~1450 nm and 2150~2450 nm, shown on the coefficient curve. In the range from 1750 nm to 2000 nm, the correlation coefficients changed significantly, as this band range was mainly the absorption zone of water vapor, which was more sensitive to water (D. Zhang et al., 2014), meaning the curve jumped significantly, suggesting this band range was not adaptive for quantitative inversion. Given the rule of the correlation coefficient extreme, the bands at 465 nm, 1365 nm, 1407 nm, 2210 nm, and 2353 nm were chosen as the characteristic bands, and the reflectance (*R*) of these bands was used to derive the quantitative inversion model of the ion Cl^-. The correlations between Cl^- content and its reciprocal of reflectance (Log(1/*R*)) are shown in Figure 3, and the coefficient curve indicates that their correlation is negative. With the band wavelength increasing, the correlation coefficients decreased on the whole, their correlations being the strongest between 350 and 550 nm, with peaks in the curve in the band ranges of 1350~1450 nm, 2150~2450 nm, and 2150~2450 nm. Given the rule of correlation coefficient extreme, the bands at 356 nm, 1365 nm, 1406 nm, 2211 nm, and 2353 nm were chosen as characteristic bands, and the reciprocal of reflectance

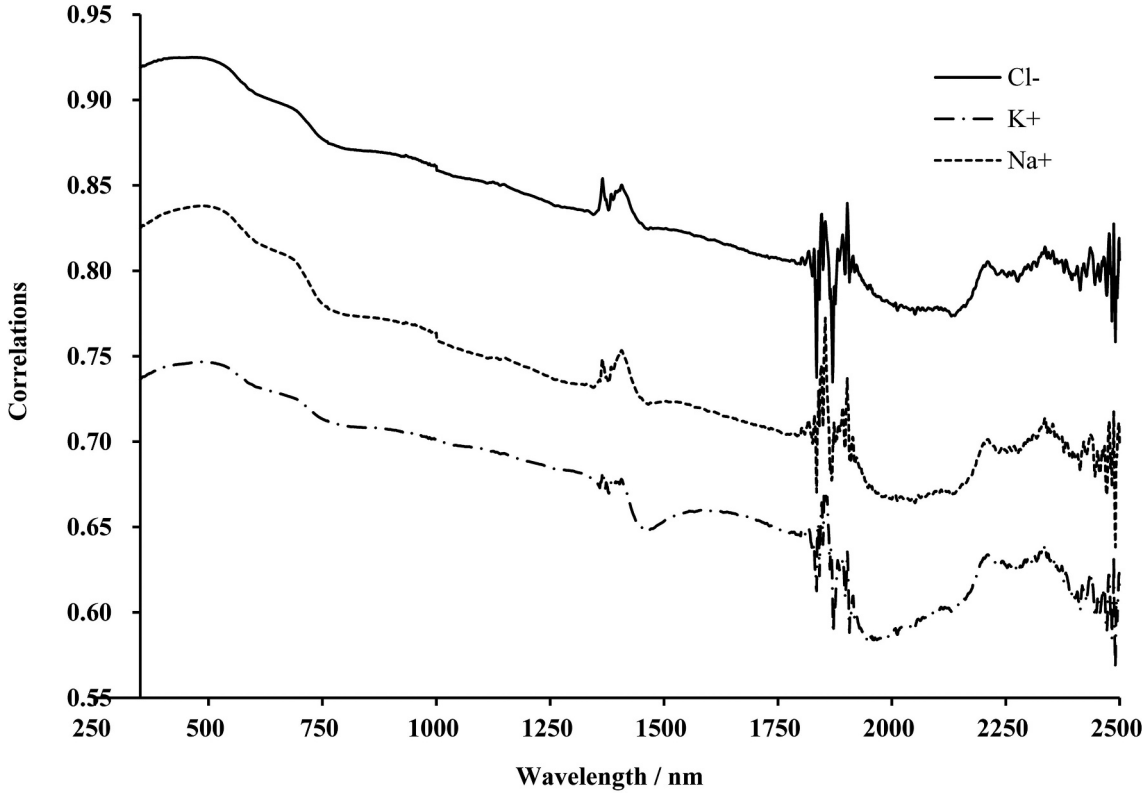


Figure 2. Correlations between reflectance (R) and characteristic ions.

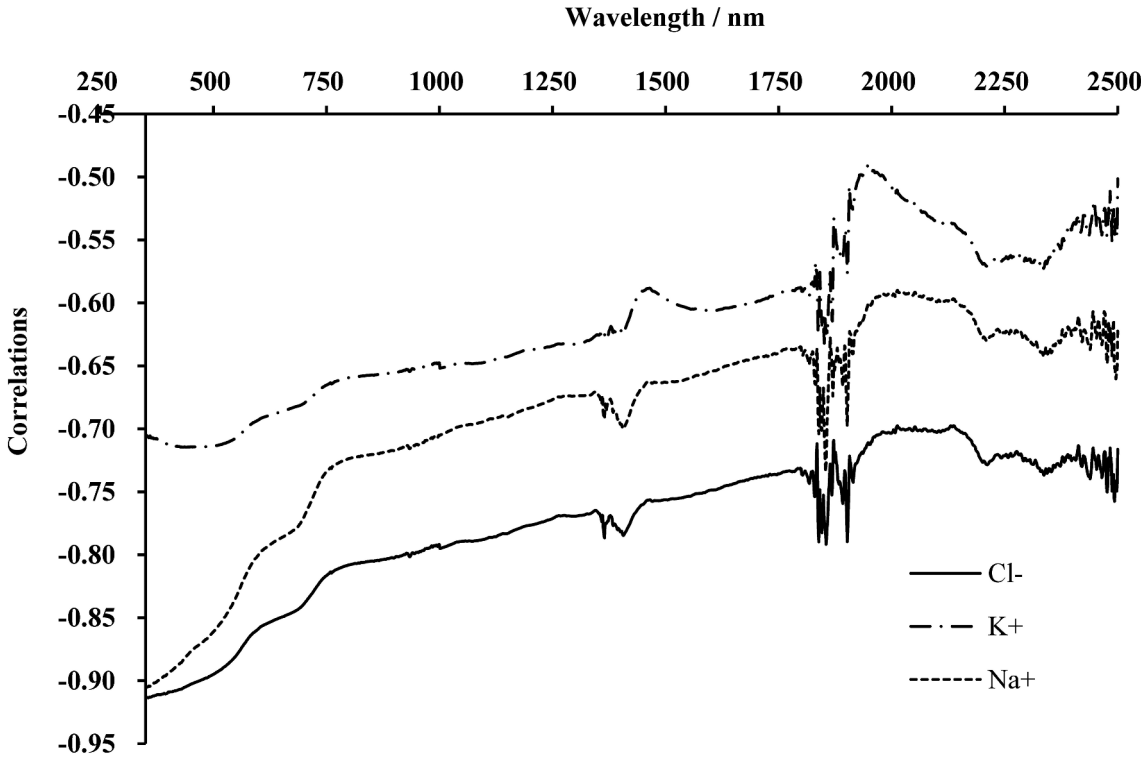


Figure 3. Correlations between Log(1/R) and characteristic ions.

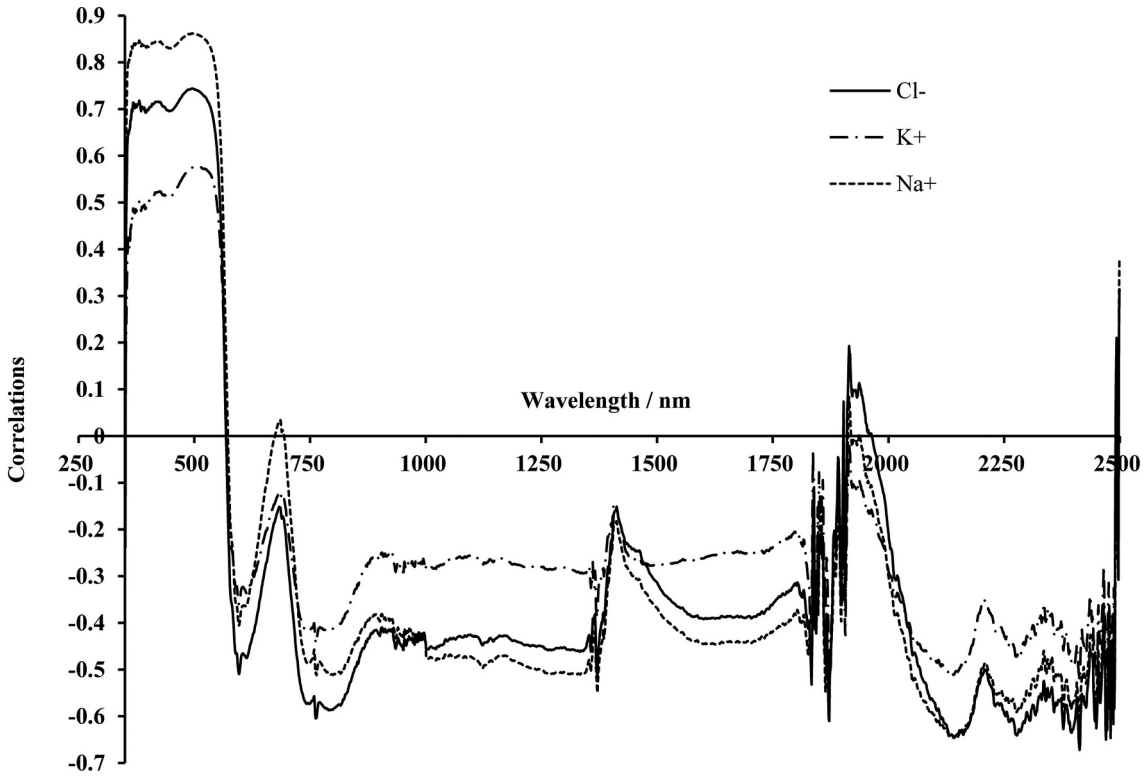


Figure 4. Correlations between R_{cr} and characteristic ions.

(Log(1/R)) of these bands was used to derive the quantitative inversion model of the Cl^- ion. The correlations between Cl^- content and its continual removed reflectance (R_{cr}) are shown in Figure 4. Given the rule of the correlation coefficient extreme, the bands of 495 nm, 762 nm, 1371 nm, 2140 nm, and 2277 nm were chosen as characteristic bands, the continual removed reflectance (R_{cr}) of these bands

was used to derive the quantitative inversion model for the Cl^- ion.

Similarly, for the ion of K^+, the characteristic bands of R were 486 nm, 1366 nm, 1406 nm, 2211 nm, and 2336 nm; the characteristic bands of Log(1/R) were 439 nm, 1363 nm, 1406 nm, 2211 nm, and 2336 nm; and the characteristic bands of R_{cr} were 508 nm, 764 nm, 1371 nm, 2140 nm, and 2275 nm. Finally, for the ion of Na^+, the characteristic bands of R were 491 nm, 1365 nm, 1406 nm, 2211 nm, and 2353 nm; the characteristic bands of Log(1/R) were 354 nm, 1365 nm, 1406 nm, 2211 nm, and 2353 nm; and the characteristic bands of R_{cr} were 495 nm, 764 nm, 1371 nm, 2141 nm, and 2275 nm.

Quantitative inversion for characteristic ions and precision test

The descriptive statistical characteristics of all the hyperspectral characters for the ions of Cl^-, K^+, and Na^+ were shown in Tables 3–5 respectively. And the modeling precisions for the quantitative inversion models calculated using each method are shown in Table 6. For the quantitative inversion models of the ions of Cl^-, K^+, and Na^+, with the same hyperspectral character variables, the models derived with SVR had higher r^2 and smaller RMSE than those derived with PLSR, suggesting higher precision by the former method. The models derived using R, R_{cr}, and R_{cr} provided the best modeling precision for Cl^-, K^+, and Na^+, respectively. In summary, the models derived with SVR showed higher modeling precision than those derived with PLSR.

Based on the 28 testing samples, the correlations between the predicted values and measured values were compared. The resulting test precisions are shown in Table 7. For the quantitative inversion models of the ion Cl^-, with the same hyperspectral character variables, the RMSE between the predicted values and measured values was smaller, and the slope k of the trend line was nearer to 1 with SVR than with PLSR, this suggests that test precision with the former method was higher, and the model derived with R had the best test precision. For the quantitative inversion models of the ion K^+, with the same hyperspectral character variables, the RMSE between the predicted values and measured values was smaller, and the slope k of the trend line was nearer to 1 with SVR than with PLSR. This suggests that the test precision of the former method was better, and the model derived with R_{cr} had the best test precision. For the quantitative inversion models of the ion Na^+, with the same hyperspectral character variables, the RMSE between the predicted values and measured values with SVR was smaller than that with PLSR, and the slope k of the trend lines was nearly the same nearer to 1, but the coefficients of determination r^2 were higher with SVR

Table 6. The modeling precisions of inversion models based on hyperspectral characters (n= 42).

			R	Log(1/R)	R_{cr}
Cl^-	SVR	RMSE	0.0483	0.0496	0.0533
		r^2	0.9414	0.9397	0.9328
	PLSR	RMSE	0.0539	0.0665	0.0851
		r^2	0.9249	0.8856	0.8214
K^+	SVR	RMSE	0.0119	0.0070	0.0065
		r^2	0.6458	0.8827	0.8929
	PLSR	RMSE	0.0125	0.0124	0.0144
		r^2	0.5811	0.5885	0.4501
Na^+	SVR	RMSE	0.05430	0.0528	0.0459
		r^2	0.9140	0.9194	0.9342
	PLSR	RMSE	0.0710	0.0565	0.0603
		r^2	0.8420	0.9001	0.8861

Table 7. The test precision of the inversion models based on hyperspectral characters (n= 28).

			R	Log(1/R)	R_{cr}
Cl^-	SVR	RMSE	0.0791	0.0797	0.0829
		$y = kx + b$	$y = 1.191x + 0.0066$	$y = 1.2146x + 0.0174$	$y = 0.962x+0.0355$
		r^2	0.8566	0.8983	0.7413
	PLSR	RMSE	0.0824	0.1004	0.0888
		$y = kx + b$	$y = 1.1924x + 0.002$	$y = 1.395x - 0.0109$	$y = 0.752x + 0.0544$
		r^2	0.8349	0.8789	0.6183
K^+	SVR	RMSE	0.0116	0.0102	0.0097
		$y = kx + b$	$y = 0.8559x + 0.0123$	$y = 0.8991x + 0.0078$	$y = 0.9239x + 0.0041$
		r^2	0.6641	0.6703	0.6610
	PLSR	RMSE	0.0186	0.0117	0.0124
		$y = kx + b$	$y = 0.7668x + 0.0104$	$y = 0.8192x + 0.0114$	$y = 0.3161x + 0.024$
		r^2	0.6792	0.5752	0.2661
Na^+	SVR	RMSE	0.0738	0.0769	0.0718
		$y = kx + b$	$y = 1.0526x + 0.0013$	$y = 1.1706x-0.0289$	$y = 1.1502x - 0.0063$
		r^2	0.8234	0.8384	0.8326
	PLSR	RMSE	0.0838	0.0841	0.0903
		$y = kx + b$	$y = 0.9786x + 0.0232$	$y = 1.1619x - 0.0225$	$y = 0.9137x + 0.0478$
		r^2	0.7028	0.8700	0.7902

than those with PLSR. It could be concluded that the test precision for the former method was higher, and all the models derived with R, Log(1/R), and R_{cr} had good test precision. In summary, the models derived with SVR showed higher test precision than those derived with PLSR, and that was just accordant to the modeling precision.

Conclusions

This study demonstrated the strong correlations between the total soil salinity and ionic content for K^+, Na^+, and Cl^-, which were chosen as characteristic ions. The hyperspectral characters of R, Log(1/R), and R_{cr} were analyzed to calculate the quantitative inversion of characteristic ions, and the precisions were higher, possibly because salinized soils are more sensitive to absorption and reflectance characters of the spectrum: the more severe the salinization, the higher the reflectance. Hyperspectral data have high resolution, which can reflect the detailed characters of the soil salinization, such as salt ionic content. This, in turn, allows the quantitative inversion of characteristic ions based on hyperspectral characters.

The inversion models derived with SVR had better precision including modeling precision and test precision than those derived with PLSR. The SVR method is based on the statistical learning theory and the minimum structure risk principle, which could provide the best compromise between model complexity and learning ability; hence, its precision is higher than PLSR.

The precisions of the inversion models for characteristic ions based on different hyperspectral characters were different, which indicated that different ions had different sensitive hyperspectral characters. Among the quantitative inversion models derived with SVR, the model for Cl^- derived with the variable of R showed the highest precision, followed by R_{cr}; in addition, both of the models for the two positive ions K^+ and Na^+ derived with the variable of R_{cr} showed the highest precision.

In this paper, the quantitative inversion models were derived with different hyperspectral characters based on different methods, and the precisions were analyzed and compared, which aimed to improve the precision of the quantitative inversion for salinization characteristic ions. The results of this study are particularly relevant for accurate, efficient prevention and recovery of salinized land. Furthermore, on the foundation of the inversion models, they could also be merged with large-scale RS images and big data to improve the efficiency and accuracy of assessment and monitoring of soil salinization on the next study.

Disclosure statement

No potential conflict of interest was reported by the authors.

Funding

This work was supported by the National Natural Science Foundation of China (62002286), the National Natural Science Foundation of Shaanxi Province (2020GY-038) and the Scientific Research Program from Education Department of Shaanxi Provincial Government (18JK0626).

References

Dai, X. J., Zhang, Y. L., Peng, J., Luo, H. P., & Xiang, H. Y. (2015). Prediction and validation of water-soluble salt ions content using hyperspectral data. *Transactions of the Chinese Society of Agricultural Engineering*, *31*(22), 139–145. doi:10.11975/j.issn.1002-6819.2015.22.019

Ding, J. L., Wu, M. C., Liu, H. X., & Li, Z. G. (2012). Study on the soil salinization monitoring based on synthetical hyperspectral index. *Spectroscopy and Spectral Analysis*, *32*(7), 1918–1922. doi:10.3964/j.issn.1000-0593(2012)07-1918-05

Duan, P. C., Xiong, H. G., Li, R. R., & Zhang, L. (2017). A quantitative analysis of the reflectance of the saline soil under different disturbance extent. *Spectroscopy and Spectral Analysis*, *37*(2), 571–576. doi:10.3964/j.issn.1000-0593(2017)02-0571-06

Kelimu, A., Tiyip, T., Zhang, D., & Nurmemet, I. (2016). Calibration and validation of soil salinity estimation model based on measured hyperspectral and Aster image. *Transactions of the Chinese Society of Agricultural Engineering*, *32*(12), 144–150. doi:10.11975/j.issn.1002-6819.2016.12.021

Li, X. M., Yang, J. S., Liu, M. X., Liu, G. M., & Yao, R. J. (2010). Spatial heterogeneity of soil salinity in typical arid area based on electromagnetic induction. *Transactions of the Chinese Society of Agricultural Engineering*, *26*(12), 97–101. doi: 10.3969/j.issn.1002-6819.2010.12.016

Liang, D., Guang, Q. S., Huang, W. J., Huang, L. S., & Yang, G. J. (2013). Remote sensing inversion of leaf area index based on support vector machine regression in winter wheat. *Transactions of the Chinese Society of Agricultural Engineering*, *29*(7), 117–123. doi: 10.3969/j.issn.1002-6819.2013.07.015

Liu, Y. Q., Chen, H. Y., Wang, R. Y., Chang, C. Y., & Chen, Z. (2016). Quantitative analysis of soil salt and its main ions based on visible/near infrared spectroscopy in estuary area of yellow river. *Scientia Agricultura Sinica*, *49*(10), 1925–1935. doi: 10.3864/j.issn.0578-1752.2016.10.009

Lu, R. K. (1999). *Analysis methods of soil agrochemistry*. China Agricultural Science and Technology Press.

Qu, Y. H., Duan, X. L., Gao, H. Y., Chen, A. P., An, Y. Q., Song, J. L., Zhou, H. M., & He, T. (2009). Quantitative retrieval of soil salinity using hyperspectral data in the region of inner mongolia hetao irrigation district. *Spectroscopy and Spectral Analysis*, *29*(5), 1362–1366. doi:10.3964/j.issn.1000-0593(2009)05-1362-05

Wang, H. J., Jiang, T. C., Yunger, J. A., Li, Y. L., Tian, T., & Wang, J. G. (2018). Hyperspectral inverse model for soil salt ions based on support vector machine. *Transactions of the Chinese Society for Agricultural Machinery*, *49*, 263–270. doi:10.6041/j.issn.1000-1298.2018.05.031

Wang, J., Liu, X. N., Huang, F., Tang, J. L., & Zhao, L. B. (2009). Salinity forecasting of saline soil based on ANN and hyperspectral remote sensing. *Transactions of the Chinese Society of Agricultural Engineering*, *25*(12), 161–166. doi:10.3969/j.issn.1002-6819.2009.12.029

Yang, J. S. (2008). Development and prospect of the research on salt-affected soils in China. *Acta Pedologica Sinica*, *45*(5), 837–845. doi:10.3321/j.issn:0564-3929.2008.05.010

Yao, Y., Ding, J. L., Kelimu, A., Zhang, F., & Lei, L. (2013b). Research on remote sensing monitoring of soil salinization based on measured hyperspectral and EM38 data. *Spectroscopy and Spectral Analysis*, *33*(7), 1917–1921. doi:10.3964/j.issn.1000-0593(2013)07-1917-05

Yao, Y., Ding, J. L., Zhang, F., Zhao, Z. L., & Jiang, H. N. (2013a). Research on model of soil salinization monitoring based on hyperspectral index and EM38. *Spectroscopy and Spectral Analysis*, *33*(6), 1658–1664. doi: 10.3964/j.issn.1000-0593(2013)06-1658-07

Zhang, D., Tiyip, T., Zhang, F., & Kelimu, A. (2014). Application of fractional differential in preprocessing hyperspectral data of saline soil. *Transactions of the Chinese Society of Agricultural Engineering*, *30*(24), 151–160. doi: 10.3969/j.issn.1002-6819.2014.24.018

Zhang, Q., Zhou, B. B., Li, M. J., Wei, Q. P., & Han, Z. H. (2018). Multivariate analysis between meteorological factor and fruit quality of Fuji apple at different locations in China. *Journal of Integrative Agriculture*, *17*(6), 1338–1347. https://doi.org/10.1016/S2095-3119(17)61826-4

Zhu, Y., Shen, G. R., Wang, Z. J., Lu, S. M., Zhi, Y. E., & Xiang, Q. Q. (2017). Soil salt content and its spectral characteristics during microbial remediation processes. *Spectroscopy and Spectral Analysis*, *37*(5): 1507-1513. doi: 10.3964/j.issn.1000-0593(2017)05-1507-07

一种面向油田的信息物理融合系统模型

王静怡　孙旭华　卜宏博　付旭

西安石油大学　陕西　西安　710065

摘要：信息物理融合系统（CPS）是一种汇集了计算、通信和物理等功能为一体监控实体世界的庞大物理计算机系统。针对大数据流背景下油田安全生产的需求，本文构建具有油田生产监测以及控制功能的油田信息物理融合系统模型，并给出了涉及到的数据模型。该系统的构建对于及时发现停井或产量下降等故障和降低损失具有重要的作用。

关键词：CPS　信息采集　实时控制

A model of information physical fusion system for oil field

Wang Jingyi，Sun Xuhua，Bu Hongbo，Fu Xu

Xi'an University of Petroleum，Shanxi Xi'an 710065

Abstract：The Cyber-Physical System （CPS） is a huge physical computer system that integrates functions such as computing，communication，and physics to monitor the physical world. In view of the demand for safe production of oilfield in the context of the big data flow，an oilfield information physical system is constructed with production monitoring and controlling. Furthermore，the data model of this system is given. The construction of this system plays an important role in the timely detection of faults such as stopping wells or decreasing production in time and reducing losses.

Keywords：CPS；information acquisition；timely control

随着电子、计算机与自动控制技术的发展，物理世界与信息系统相结合的速度越来越快。在此背景下，产生了信息物理融合系统（CPS）。目前，CPS已在各领域的应用越来越广泛，比如国防、医疗、工业生产等。施等[1]研究了CPS与能源系统相融合的能源互联网技术。曹[2]研究了基于信息物理融合的猪舍系统。张[3]研究了如何构建具有监控功能的煤矿CPS系统。善[4]把信息物理融合系统引入到电力系统中。本文拟采用智能设备、数据计算、控制等技术，给出一个基于CPS的智能油田实时监控系统模型，并建立数据模型。

1　油田CPS系统模型与架构设计

针对油田现场生产数据安全、传输可靠和事故处理等问题，给出了基于信息物理融合技术的油田生产监控系统模型。如图1所示。

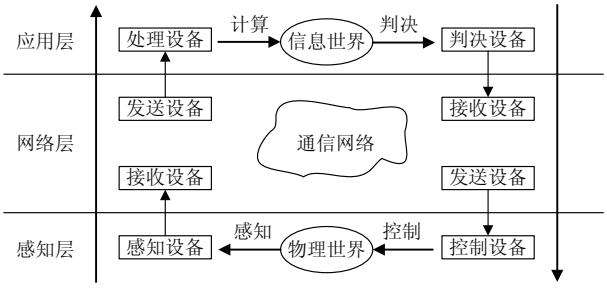


图1　基于信息物理融合的智能油田监控系统模型

（1）感知控制层：智能感知设备主要负责采集数据，并通过传输设备传递给网络层。同时，通过控制设备实时监控温度、油压、套压、载荷、排量和电力等抽油机的参数变化。

（2）网络层：数据的可靠通信才能保障整个网络的正常运行。设计安全可靠的网络层也是该系统的一个关键技术。

（3）应用层：该层的处理设备能够借助先进技术对采集数据进行实时分析，并在必要时发出控制指令，实现智能设备的远程监控。

2　数据模型

油田CPS监控系统的感知层主要通过智能设备将抽油机的数据实时采集后转化为计算机能够识别的信息，然后通过网络层传送到应用层。在整个传输数据的过程中，需要采用的数据模型如下：

（1）感知层主要采用兼有感知和控制功能的物理设备来完成数据采集、实时监控和针对感知到的物理环境做出反馈。感知层中客观存在的各种物理实体（智能设备）及所处的环境都属于物理对象，将其抽象为4个元素，分别表示：

被监测物理对象所在的位置、所属的油井编号、油井内部的设备编号和被监测物理对象时的时间。其中被监测物理对象的属性包含温度、油压、套压、载荷、排量和电力等6个属性值。

（2）网络层是连接信息世界和物理世界的媒介，主要实现数据资源共享和传输；按照传递数据的方向可分为上行和下行，上行表示源节点将数据向信息处理中心传送。下行表示网络节点向信息监控中心传送数据。该层的数据抽象成5个元素，分别为：上行传输数据的传感器的编号、传感器向无线网络发送的数

项目：陕西省重点研发计划项目+基于信息物理融合的智能油田监控系统关键技术研究+2020GY-038；
陕西省教育厅专项计划项目+无线MARC系统中联合网络-信道编码的优化设计研究+18JK0626；
教育部高等教育司2018年大学生创新创业训练项目+偏远地区数字油田监控系统的数据传输方法研究+201810705040。

（下转第74页）

第263页，共397页
(C)1994-2023 China Academic Journal Electronic Publishing House. All rights reserved.　http://www.cnki.net

时由于静液柱压差较大且钻井泵排量在2m³/min时循环压力较致使发生失返性漏失，采用0.8m³/min的排量替浆时由于水泥浆自身具有一定的堵漏性能且黏度、失水等性能调节较好，产生塞流顶替致使漏层被封堵最终水泥浆返出地面，且前期大排量顶替很好的保证的下部未漏失段固井质量。

3.2 英36-5井基本情况

英36-5井在二开钻进过程中采用1.25 g/cm³泥浆密度且提高黏度（最高156s）的方式进行钻井，但甲方要求本开次244.5mm套管固井采用设计规定的1.88g/cm³的水泥浆进行固井。在固井施工过程中大概水泥浆出套管35m³时井口返出迅速减小至失返，判断为遇到断层由于泥浆与水泥浆静液柱压差较大产生漏失，为保证顶替效率保证下层固井质量，现场将替注排量由2m³/min降低至1.5m³/min井口仍然失返，决定碰压后环空关井侯凝8h后进行井口反挤施工，反挤水泥40t。电测显示中部漏层处固井质量差，下部及顶部固井质量优质，试压合格满足三开钻进全部要求。

原因分析：该井泥浆密度与水泥浆密度差值较大，水泥浆在环空上返时随着高度增加静液柱压力增大造成较薄弱的断层处发生较大漏失，反挤施工时上层再次发生漏失造成水泥浆未能衔接成功。

4 水泥浆配方改进及应用

英36-5井的最大的难题仍是固井时严重漏失。常规水泥浆体系很难解决固井过程中的漏失，在反挤水泥时即便提高水泥浆附加量，仍然不能保证水泥浆返高。于是在水泥浆中加入堵漏材料和早强材料，使水泥具有较好的堵漏效果，快速的封固漏失通道，解决后续反挤过程中的漏失问题。

4.1 速凝水泥浆性能

速凝水泥浆体系的特点是在流动度变化不大的情况下，初始稠度提高，而初凝时间减少，在反挤时，较高的初始稠度使其在进入地层后能迅速封堵漏失地层，极短的初凝时间使其能快速凝固减少漏失量的同时有效封固漏失地层，保证水泥浆返高达到设计要求的同时确保了在候凝期间水泥浆的防气窜能力。

4.2 速凝水泥浆体系在反挤时的应用情况

英10-1-B6上井二开钻井过程中一直存在漏失，套管鞋处地破试验未成功。由于英36-5井反挤未达到全井封固的要求，判断是水泥浆稠化时间太长，在反挤后，大部分水泥浆仍从裂缝处漏失，导致虽然反挤水泥浆，但最终结果仍不理想。因此本次施工结束8h后挤入速凝水泥浆8m³，经电测结果显示水泥返高基本到地面全井质量合格。

4.3 加入早强剂对水泥返高的影响

从中10-1-B6上井水泥返高来看，相对于英36-5井有明显的提高，说明速凝水泥浆确实如设想一样能减少漏失，提高水泥返高。但即便如此，水泥浆量特别是反挤时的水泥浆用量对最后的水泥返高也有明显的影响。

5 结束语

对于像清海油田英东油田这类漏失严重区块，使用常规水泥浆体系很难解决在固井时的漏失问题。对于漏失量相对较小的井可采取优化水泥浆体系和优选施工排量和顶替方式最后关环空侯凝的方式来减少漏失保证固井返高。而漏失较严重的井由于速凝水泥浆体系较高的成本使其很难在初次固井时大量使用，因此正注反挤是一种较为较为经济且实用的手段，在反挤过程中使用速凝水泥浆体系，既能保证水泥浆返高，又能降低固井成本，具有较好的应用前景。

参考文献

[1] 张建平,张健,万建中 . 沁南潘河煤层气田空气钻井和固井技术 [J]. 天然气工业,2011.31.

（上接第28页）

据、该下行发送的数据、下行发送数据对应的编号和该无线网络发送数据的时间。

（3）应用层主要是通过大量的数据业务模型进行集成，且将判决信息反馈到生产现场进而完成生产的实时监控，从而有效地提高数据的利用率。信息处理中心接收到的数据抽象成3个元素，分别为数据来源的油井号、数据的属性和接收数据所对应的时间。

系统将信息处理中心接收到的6个被监测物理对象作为网络的输入。不同的数据组合对应不同的设备状态，从而建立实时监控架构。

3 结束语

本文将信息物理融合系统应用到油田生产中，给出了具有控制功能的油田信息物理融合系统模型，并对构建过程中涉及到的数据模型进行阐述。该系统的提出可以节省油田的运行成本，为推动未来数字化油田建设奠定了理论基础。

参考文献

[1] 施陈博,苗权,陈启鑫 . 基于 CPS 的能源互联网技术与应用 [J]. 清华大学学报 :自然科学学报,2016,56（9）:930-936.

[2] 曹振丽 . 1 种面向猪舍的信息物理融合系统模型 [J]. 江苏农业科学,2017,45（5）:193-196.

[3] 张文 . 煤矿信息物理融合系统的模型与技术研究 [J]. 物联网技术,2018,1 :97-98.

[4] 善金鹏 . 分布式发电信息物理融合系统架构研究 [J]. 电力信息与通信技术,2019,17（3）:73-78.

作者简介

王静怡（1984-）,女,汉,博士,讲师,研究方向 :数字油田,计算机、通信相关技术。

第264页,共397页
(C)1994-2023 China Academic Journal Electronic Publishing House. All rights reserved. http://www.cnki.net

2021 IEEE 6th International Conference on Intelligent Computing and Signal Processing (ICSP 2021)

Research on Safety and Reliability of Intelligent oilfield monitoring system based on Cyber-Physical System

Jingyi Wang*, Jiahang Guo, Xia Cheng and Rui Zhao
School of Computer Science
Xi'an Shiyou University
Xi'an 710065, China
jywang@xsyu.edu.cn

2021 6th International Conference on Intelligent Computing and Signal Processing (ICSP) | 978-1-6654-0413-6/20/$31.00 ©2021 IEEE | DOI: 10.1109/ICSP51882.2021.9408733

***Abstract*—The intelligent oilfield monitoring system based on cyber-physical fusion technology realizes the five functions including calculation, communication, precise control, remote coordination and autonomy. In order to solve the problems of security threat, remote transmission and real-time control of the oilfield production data, an optimization scheme of data safety and reliability of oilfield production monitoring system is given, which ensures that the oilfield information monitoring center can collect data and process it in time.**

Keywords- CPS; timely control; Intelligent oilfield; Safety and Reliabilityinsert

I. INTRODUCTION

With the development of computer, communication and control technology, the integration speed of the physical world and information system is becoming faster and faster. The physical world facing human beings is developing towards networking and informatization. The integration of the physical world and information world will be the trend of scientific and technological development in the future. In the context, the concept of Cyber-Physical System (CPS) was proposed.

At present, CPS has been widely used in various fields around the world, such as defense [1], medical [2-3], aerospace [4-5] and other fields. At the same time, CPS-related technologies have been applied in autonomous driving, robotic application, intelligent building and so on, and are becoming the foundation of various large-scale industrial systems [6]. Shi et al. [7] studied the energy Internet technology that integrates CPS with the energy field, which will reconstruct the energy industry value chain system. Liu et al. [8] analyzed and built the event model of the cyber-physical system based on the target method, and applied it to the adaptive cruise control system. Cui et al. [9] proposed a data fusion method based on a large amount of real data and the experimental results show that the method can accurately detect the traffic conditions of highways. Cao et al. [10] abstracted the event information of time and space into a cyber-physical fusion model and applied the model to breeding agriculture. Zhang et al. [11] studied how to build a coal mine CPS system with monitoring function, and analyzed the information acquisition, calculation and collaborative control technologies for coal mine cyber-physical systems. Shan et al. [12] proposed a distributed generation cyber-physical system architecture scheme including two-way communication network, grid situation awareness, multi-source big data processing and multi-source collaborative optimization control, and analyzed the key technologies involved in the Distributed Generation Cyber-Physical System (DGCPS) architecture in detail. Zhang et al. [13] studied that CPS has high openness, but higher openness will inevitably have potential safety hazards. There are hidden dangers in more and more CPS, such as smart grid, smart transportation system, medical system, intelligent oilfield system and so on. Therefore, safety problem has become one of the key factors that determine whether CPS can be widely used [14]. Wang et al. [15] gave a real-time monitoring system model of intelligent oilfield based on CPS, but it did not involve safe and reliable measures of the system. In this paper, the safety and reliability measures of the intelligent oilfield monitoring system based on cyber-physical fusion technology are given in combination with the related technology of communication and computer, so as to improve the operability of the system.

II. SYSTEM DESCRIPTION

In this section, a communication structure diagram of the oilfield is described first, and then an intelligent oilfield monitoring system based on cyber-physical system is given [15].

A. A communication structure diagram of the oilfield

Large-scale oilfields in China are distributed in remote areas, and the communication equipment in the oilfield is scattered and cumbersome. The traditional operation mode is facing with great impact and challenge, and it will inevitably disappear gradually and withdraw from the operation mode of oilfield production. At the same time, the rapid industrialization process in China has promoted the vigorous development of communication and sensor technology. These advanced technologies undoubtedly provide technical support for unmanned oil well inspection and provide a new opportunity to improve the backward production method of the oil industry. Therefore, people pay more and more attention to the environment of oilfield, and must take real-time monitoring and detecting measures to the operating environment of oilfield. A communication structure model of oilfield is shown in Figure 1. The wireless ZigBee instrumentation equipment can be used as a sensor node to collect current, temperature, pressure, load, displacement and other data. After processing the data collected by each wireless ZigBee sensor, the wellhead controller broadcasts it to the information-controlling center.

978-1-6654-0413-6/21/$31.00 ©2021 IEEE

Authorized licensed use limited to: East Carolina University. Downloaded on June 20,2021 at 10:25:23 UTC from IEEE Xplore. Restrictions apply.

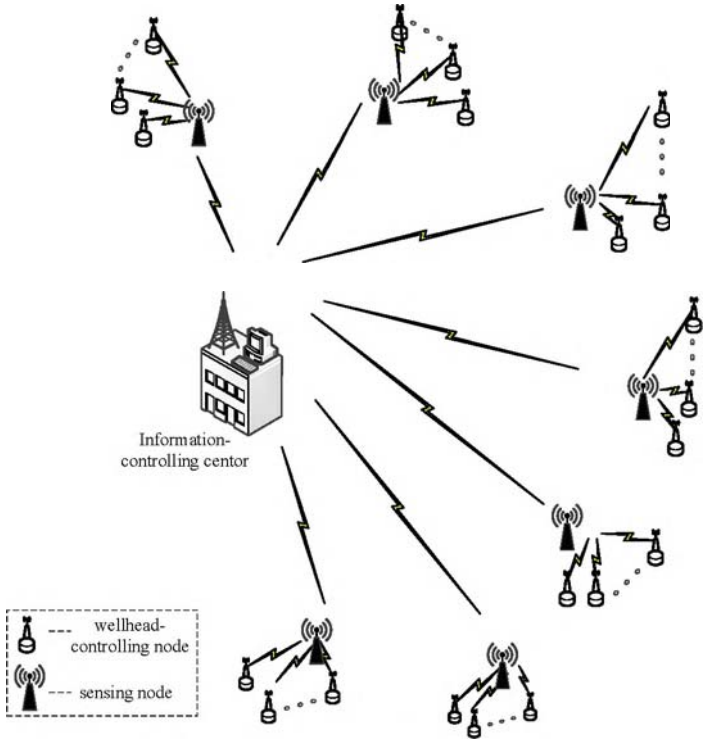


Figure 1. A communication topology diagram of the oilfield.

B. *An intelligent oilfield monitoring system model based on cyber-physical system*

Now, the Internet of Things technology has been promoted in the safe production of oil fields, and the production and construction of oil fields are gradually changing from digital to intelligent. After the concepts of Internet of Things, cloud computing and so on, big data and cyber-physical system have been proposed and attracted serious concern and recognition in the field of the information. What follows is that they become the inevitable trend of information development in the future. Cyber-physical system is a networked computer system that monitors entities in the physical world and integrates communication, computing and control capabilities. By establishing the physical process and computing platform of the model, the production process can be promoted, which helps the staff to understand the system status better and achieve better control ultimately. An intelligent oilfield monitoring system model based on cyber-physical fusion technology is shown in Figure 2 [15].

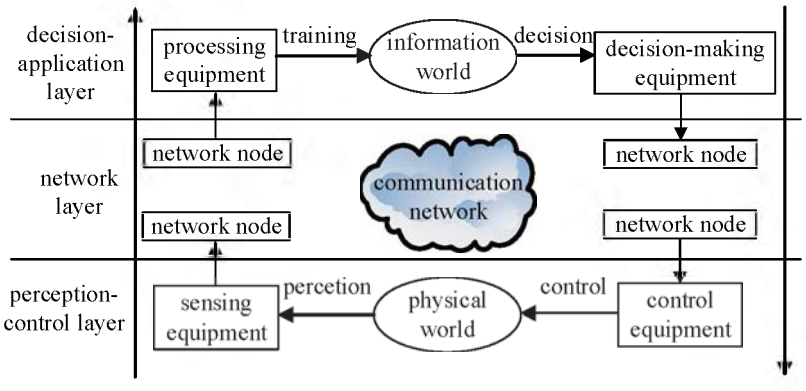


Figure 2. An intelligent oilfield monitoring system model based on cyber-physical fusion technology

The intelligent sensing equipment in the perception control layer is mainly responsible for collecting data and transmitting it to the network layer through the transmission equipment. At the same time, the control equipment monitors the change of

Authorized licensed use limited to: East Carolina University. Downloaded on June 20,2021 at 10:25:23 UTC from IEEE Xplore. Restrictions apply.

temperature, oil pressure, casing pressure, load, displacement and power in real time. The main function of the network layer is to transmit collected data and share resources. It is a network that realizes interconnection and interoperability between all layers. The safe and reliable transmission technology of this layer can guarantee the normal operation of the whole network. The application layer is the interface between the Cyber-physical system and the staff. The processing equipment at this layer can analyze the collected data in real time with the help of advanced technology, and issue control instructions when necessary to realize the remote monitoring of intelligent equipment. The oilfield cyber-physical system ensures that the oil wells in the oil field can communicate with each other, coordinate operation and share information under the support of the network protocol. Additional decision-making and control components are added to ensure that the staff can better implement the control.

III. Safety Measures

The system structure of the oilfield monitoring system based on cyber-physical system consists of three layers. The physical equipment of each layer is connected to the internet, and the physical equipment is inevitably attacked by unauthorized data. The corresponding solutions are presented for each layer of security threats.

- The intelligent collection, transmission and monitoring equipment of the perception control layer are generally relatively open and can be moved at any time, so it is easy to invade or intercept the data collected in the oil field during the transmission process. Oilfield data is easy to be tampered with, added or deleted or stolen by attackers, so there are incorrect data in the process of wireless data transmission. This layer needs to take measures to increase authentication and access control for each equipment to effectively ensure the data security of the perception control layer.
- The intelligent equipment at the network layer will bring the greatest risk to the whole cyber-physical system, no matter whether it is in a central network or a distributed network. On the one hand, as the data transmission channel of the perception control layer and the application layer, the transmitted information is easily attacked; on the other hand, because of the access network, the data transmission is susceptible to be interfered. Attackers may obtain data by an external network or electromagnetic leakage during transmission, causing data leakage. This layer needs to adopt a reasonable data transmission model to improve the reliability of data transmission.
- The intelligent equipment at the application layer not only requires the collecting and sensing equipment to realize the real-time collection and communication of data information, but also requires the use of advanced technologies such as big data analysis and machine learning to evaluate and respond to collected data, and issue control instructions when necessary. So as to realize the remote visual monitoring and behavior control of intelligent equipment. Attackers at this layer will inject malicious code into the network and control some network nodes, which will cause the entire system to be paralyzed. This layer should take measures to set different management permissions to system administrators, senior administrators and ordinary administrators, which can effectively protect the security and reliability of the system.

IV. Data Transmission Model to Improve System Seliability

Existing oil field data transmissions are based on GPS, WIFI, etc., and safety and reliability analysis of these transmissions has not been involved, especially for some remote areas may not be suitable. In view of this, several data transmission models are given with the help of wireless communication technology.

- If the distance between the intelligent equipment and the monitoring center is short, the single well transmission model is usually used. According to the data length of the parameters such as temperature, oil pressure, casing pressure, load, power, etc., the point-to-point wireless communication technology is used to process the data. Common point-point wireless communication technologies include modulation and demodulation, coding and decoding [16], etc.
- If the distance between the intelligent equipment and the monitoring center is long, the multi-well transmission model is usually used. The channel from the wellhead controller to the information- controlling center can not work due to a failure. The information- controlling center will obtain data according to the information broadcast by the intelligent equipment to other channels. The whole network will not be paralyzed because any single node cannot work. If the equipment on one of the channels between the intelligent equipment and the relay station is powered off or fails to work for other reasons, make full use of the channel statistical characteristics between the intelligent equipment and the relay station and use the data from another channel for joint processing without rewiring or calling other equipment. Common multi-point wireless communication models include three-node network models and multi-source multi-relay network models [17], etc.

V. Conclusions and Future Work

In this paper, we introduce the intelligent oilfield monitoring system based on cyber-physical fusion technology. And then, data transmission security strategies are given. Meanwhile, data transmission models for improving system are shown, which can ensure data of intelligent oilfield safe and reliable.

Our introduced concept of the intelligent oilfield monitoring system based on cyber-physical fusion technology has various promising future research directions. For example, we can apply the cyber-physical system model to other industrial fields around the world.

Acknowledgment

This work was financially supported by Innovation and Entrepreneurship Training program for college student of

Authorized licensed use limited to: East Carolina University. Downloaded on June 20,2021 at 10:25:23 UTC from IEEE Xplore. Restrictions apply.

Shaanxi Province (S202010705025), the Special Scientific Research project of education department of Shaanxi Province (18JK0626) and the National Natural Science Foundation of Shaanxi Province (2020GY-038).

REFERENCES

[1] Li Renfa, Yang Fan, Xie Guo, Huang Jing and Duan Mengqin, "Survey of modeling methods in cyber-physical system," Journal on Communication, vol. 37, no. 5, pp. 165–175.

[2] E. A. Lee, "Cyber Physical Systems: Design Challenges," 2008 11th IEEE International Symposium on Object and Component-Oriented Real-time Distributed Computing(ISORC), IEEE. 2008: 363-369.

[3] N. Leavitt, "Researchers fight to keep implanted medical devices safe from hackers." Computer, vol. 43, no. 8, pp. 11-14.

[4] C Tricaud, Y. Q. Chen, "Optimal Mobile Actuator/Sensor Network Motion strategy for Parameter Estimation in a class of Cyber Physical System," American Control Conference, IEEE. 2009, pp. 367-372.

[5] E. Mills, "Hackers broke into FAA air traffic control system," THE Wall Street Journal, 2009-05-07(A6).

[6] P. Derler, E. A. Lee, and A. S. Vincentelli, "Modeling cyber-physical systems," Proceeding of the IEEE, 2012, vol. 100, pp. 13-28.

[7] Shi Chenbo, Miao Quan, and Chen Qixin, "Key technology and application of the energy internet based on cyber physical," Journal of Tsinghua University (Science and Technology), vol. 56, no. 9, pp. 930-936, 941.

[8] Liu Chun, Huang Ranran, and Han Daojun, "Goal Oriented Approach for Analazing Event Model of Cyber-physical Systems," Computer Science, vol. 44, no. 4, pp. 100-103.

[9] Cui Yanling, Jin Beihong, and Zhang Fusang, "Highway Traffic Condition Detection with Data Fusion," Cheinese Journal of Computer, vol. 40, no. 8, pp. 1798-1812.

[10] Cao Zhenli, "A model of cyber-physical system for pig house," Jiangsu Agricultural Sciences, vol. 45, no. 5, pp. 193-196.

[11] Zhang Wen, "Research on Model and Technology of coal Mine cyber-physical system," Internet of Things Technologies, vol. 1, pp. 97-98.

[12] Shan Jinpeng, "Research on the Architecture of DISTRIBUTED Generation Cyber-Physical System," Electric Power Information and Communication Technology, vol. 17, no. 3, pp. 73-78.

[13] Zhang Heng, "Research on Security Theory of Cyber-Physical System," Zhejiang University, 2015.

[14] Peng Kunlun, Peng Wei, Wang Dongxia, and Xing Qianqian, "Research Survey on Security Issues in Cyber-Physical systems," Netinfo Security, vol. 7, pp. 20-28.

[15] Wang Jingyi, Sun Xuhua, Pu Hongbo, and Fu Xu, "A model of information physical fusion system for oil field," Petrochemical Industry Technology, vol. 8, pp. 28,74.

[16] Sun Xuhua, Pu Hongbo, Fu Xu, and Jingyi Wang, "Research on Intelligent Oilfield Data Transmission Scheme Based on Channel Coding Technology," Electronic Component and Information Technology, vol. 4, no. 2, pp. 103-104.

[17] Wang Jingyi, Sun Xuhua, Pu Hongbo, and Fu Xu, "A data transmission method of digital oilfield monitoring system based on Internet of Things."4th International Conference on Intelligent Computing and Signal Processing (ICSP 2019),vol. 1237, pp.1-6.

Authorized licensed use limited to: East Carolina University. Downloaded on June 20,2021 at 10:25:23 UTC from IEEE Xplore. Restrictions apply.

附件7

尊敬的国家自然科学基金委员会科研诚信建设办公室：

本人是西安石油大学教师，本人实名举报我校王静怡老师存在多处涉嫌学术不端情况，王静怡老师在学术研究以及职称评审中学术不端、违反公平竞争的基本原则，并且王静怡老师主持国基金在研项目一项，因此，本人向国基金科研诚信建设办公室实名举报。

举报材料的内容包括王静怡老师的学习、工作经历、承担科研项目情况、项目申报及成果发表中涉嫌存在学术不端的情况。

1.王静怡老师的教育经历为本、硕、博均为通信工程。具体学习经历为：

2010/03~2016/06，西安电子科技大学，通信与信息系统，博士

2007/09~2010/03，西安电子科技大学，通信与信息系统，硕士

2002/09~2006/07，西安邮电大学，通信工程，学士

具体工作经历为：

2016/07~至今，西安石油大学计算机学院，教师

2.王静怡老师主持的 3 项科研项目及相应项目的研究内容为：

（1）无线 MARC 系统中联合网络-信道编码的优化设计研究（18JK0626），陕西省教育厅基础研究项目，2018.01-2021.04，2 万，结题

研究内容：本项目针对无线通信应用中多址接入中继信道（MARC）模型，研究联合网络-信道编码的优化设计方法。通过对理想信道下半速率可逆码和速率兼容网络 LDPC 码删余算法的优化设计，基于 RS 码和 LDPC 码的中继混合译码转发策略，研究非理想信道下适用于多源 MARC 系统的最佳阈值优化方法，以改善目的节点的比特错误概率（Bit Error Ratio,BER）性能。通过本项目的研究，将会为联合网络-信道编码优化设计提供理论支撑，研究成果可应用于未来无线通信系统中。研究内容包含以下三点：①提出一种叠加 LDPC 编码方法，设计新型高斯近似密度进化算法。②系统研究联合网络-信道编码理论及设计算法。③充分利用信道统计特性设计软输出迭代译码算法。

（2）基于信息物理融合的智能油田监控系统关键技术研究（2020GY-038），陕西省科技厅重点研发计划项目一般项目-工业领域，2019.01-2020.12/2020.01-2021.12，5 万，在研

研究内容：本研究基于信息物理融合，拟采用信道编码、干扰消除等无线通信相关技术建立智能油田监控系统，以更好满足油田现场对数据采集、远程传输和实时控制等应用需求。具体为：首先，针对油田信息物理监控系统安全威胁，以保障系统安全运行为目的，提出安全防护措施；然后，针对油田信息物理系统的数据传输可靠性问题，基于信道编码、干扰消除和中继技术分别设计传输方案，并进一步对所提方案不同阶段以及不同通信模型的性能展开深入研究，以改善不同传输方案下系统的可靠性能；最后，采用 BP 神经网络的数据训练方法对采集到的数据流进行实时监测，提高预警的时效性。

（3）基于遥感大数据的汾渭平原空气质量时空特征及其驱动力研究与模拟（62002286），国家自然科学基金委员会青年基金项目，2021.01-2023.12，1/1，24 万，在研

研究内容：未知。

3. 王静怡在国基金项目申请、实施中存在的涉嫌学术不端行为分别有：

（1）基于遥感大数据的汾渭平原空气质量时空特征及其驱动力研究与模拟（62002286）项目申请中列入申请书的论文 8 篇中有 6 篇存在涉嫌重复发表及 1

篇提供虚假信息。

王静怡老师在基于遥感大数据的汾渭平原空气质量时空特征及其驱动力研究与模拟（62002286）项目申报中列入申请书的论文有：

[1] Jingyi Wang*, Shuling Che, Ying Li and Junlong Wang, Optimal design of Joint network LDPC Codes over Orthogonal Multiple-Access Relay Channel. International Journal of Grid and Utility Computing, UK., 2016, 7(2): 68-74.

[2] Jingyi Wang*, Ying Li, Daolong Wu and Baoming Bai. A distributed RS code based hybrid forward strategy for MARC. Gummi Fasern Kunstst, 2016, 69(14): 706-713.

[3] 王静怡, 李晓明*. 近 20a 中国耕地数量变化趋势及其驱动因子分析. 中国农业资源与划分,2019,40(08):171-176.

[4] 王静怡*, 李颖, 孙岳. 适用于网络 LDPC 码的速率兼容算法. 西安电子科技大学学报,2013, 40(2): 13-17.

[5] Jingyi Wang, Xiaoming Li*.Research on the changing trend of farmland area in China and its driving factors from 1996 to 2016. IOP Conference Series: Earth and Environmental Science(EES), 6 月 22 日~24 日, 珠海, 中国, 2018.

[6] Jingyi Wang*, Shuling Che, Ying Li and Junlong Wang. Optimal design of the joint network LDPC codes for half-duplex coopreative multi-Access relay channel. 2013 5th International Conference on Intelligent. 2013. USA: IEEE, 622-625.

[7] 王静怡*, 李颖, 孙岳. 速率兼容网络 LDPC 码的设计. 第十七届全国青年通信学术年会, 7 月 29 日~31 日, 秦皇岛, 中国, 2013

[8] Wang Jingyi*, Sun Xuhua, Bu Hongbo, Fu Xu. A data transmission method of digital oilfield monitoring system based on Internet of Things,2019 4th International Conference on Intelligent Computing and Signal Processing, Journal of Physics: Conference Series, 2019,1237(2).

列入基于遥感大数据的汾渭平原空气质量时空特征及其驱动力研究与模拟（62002286）申请书的论文存在 6 篇次重复表及 1 篇提供虚假信息的涉嫌学术不端情况：

①文章[1]和文章[6]属于英文一稿双发，文章[6]2013 年发表，文章[1]2016 年发表。文章[1]首页虽有标注了文章[1]为文章[6]的改写和扩展，但两篇文章整体内容、结构、图表以及结论雷同，且整段整段的文字写法均完全一样，雷同率至少超过 60%以上，属于明显不符合成果发表规范。

另文章[6]“Optimal design of the joint network LDPC codes for half-duplex coopreative multi-Access relay channel”在 EI 数据库中经过检索不存在，后通过文章发表时间、页码范围搜索发现文章[6]可能为：

Jingyi Wang, Shuling Che, Ying Li, Optimal design of the Joint network LDPC Codes over Orthogonal Multiple-Access Relay Channel. 2013 5th International Conference on Intelligent Networking and Collaborative Systems, 2013. XI’AN: IEEE, 622-625。另于王静怡 2016 年 4 月博士论文末尾攻读博士期间论文成果（博士论文 99 页）未发现会议论文“Optimal design of the joint network LDPC codes for half-duplex coopreative multi-Access relay channel”而是会议论文“Optimal design of the Joint network LDPC Codes over Orthogonal Multiple-Access Relay Channel”。

由此可见王静怡老师为避免论文同名易被发现一稿双发，将文章[6]名称由“Optimal design of the Joint network LDPC Codes over Orthogonal Multiple-Access Relay Channel”篡改成了“Optimal design of the joint network LDPC codes for half-duplex coopreative multi-Access relay channel”，但在[1]的首页王静怡老师准确写出 2013 年会议论文名称为“Optimal design of the Joint network LDPC Codes over Orthogonal Multiple-Access Relay Channel”。将会议名称由“2013 5th International Conference on Intelligent Networking and Collaborative Systems”改为了“2013 5th International Conference on Intelligent”，会议举办地由“XI’AN”改为了“USA”，可见此番篡改论文名称、会议名称、会议举办地属于刻意为之。

②文章[5]和[3]属于中英文一稿双发，文章[5]英文先于 2018 年在国内举办的国际会议发表，文章[3]为 2019 年在国内中文期刊发表。文章[3]中对文章之前已经发表情况未做任何说明，也没有引用[5]。王静怡第一次重复发表始于 2013 年，2016 年第二次重复发表时在文章[1]的首页还标注了此论文曾经发表，此次为改写扩展的说明。但在 2019 年第三次重复发表时，却在文章[3]中对文章[5]曾经发表过没有做任何说明，这说明王静怡重复发表是明知故犯。为了避免被易于发现一稿双发，文章[5]的名字“Research on the changing trend of farmland area in China and its driving factors **from 1996 to 2016**”在文章[3]再次重复发表时改成了“**近 20 年**中国耕地数量变化趋势及其驱动因子分析”。文章[3]在文章[5]的 20 篇参考文献基础上仅增加了 3 篇参考文献，文章[5]和[3]雷同率超过 90%，文章[3]和[5]整体内容、结构、图表以及结论高度雷同，仅仅在第一部分介绍部分有少量差异，其余均雷同，雷同率超过 90%。

③文章[4]和[7]属于中文一稿双发。文章[4]于 2013 年 4 月于西安电子科技大学学报上发表，文章[7]于 2013 年 7 月底在会议上发表。文章[4]和[7]完全雷同。

（2）基于遥感大数据的汾渭平原空气质量时空特征及其驱动力研究与模拟（62002286）项目执行中，王静怡老师在成果发表中存在研究成果与项目申请书研究内容不一致、滥标项目号等问题。

截止目前，标注国基金“基于遥感大数据的汾渭平原空气质量时空特征及其驱动力研究与模拟（62002286）”论文总计有 11 篇，其中文章[9]研究土地盐碱化与项目申请书研究内容无关，为一作非通讯作者论文；文章[10]-[11]为标注国基金（62002286）王静怡老师有署名论文，论文内容与项目申请书研究内容“汾渭平原空气质量”无关；文章[12]-[19]为标注国基金（62002286）王静怡老师无署名论文 8 篇，论文内容与项目申请书研究内容“汾渭平原空气质量”无关。在“基于遥感大数据的汾渭平原空气质量时空特征及其驱动力研究与模拟（62002286）”项目执行已经 3 年的时间里，在标注国基金（62002286）的 11 篇论文中，王静怡仅发表 1 篇一作非通讯期刊论文，且 11 篇论文成果的研究内容均与申请书研究内容“汾渭平原空气质量”无关。

标注国基金（62002286）的一作非通讯作者的论文：

[9]Wang Jingyi, Li Xiaoming*.Comparison on quantitative inversion of characteristic ions in salinized soils with hyperspectral based on support vector regression and partial least squares regression[J].European Journal of Remote Sensing, 2020, 53 (1): 340-348.(标注国家自然科学基金青年基金项目 620022860，陕西省科技厅重点研发计划项目 2020GY-038，陕西省教育厅基础研究项目 18JK0626）权威期刊，根据王静怡博士论文致谢（博士论文 98 页）判断通信作者李晓明疑为王静怡丈夫，其研究方向恰为土地整治。

标注国基金（62002286）的参与署名论文：

[10]阿茹罕,原晓斌,慕晓冬*,王静怡.结合扩展多属性剖面与快速局部 RX 算法的高光谱异常目标检测[J].光子学报,2021,50(09):297-307.（标注国家自然科学基金青年基金项目 62002286）权威期刊,CSCD 收录的 EI 源刊

[11]王彩玲,张育春*,王静怡.水体透射光谱的多特征融合 COD 含量估算研究[J].应用光学,2021,42(03):488-493.(标注国家自然科学基金青年基金项目 62002286）核心期刊

标注国基金（62002286）的未参与署名论文：

[12]程国建,冯亭亭.基于 DSA-UFLD 模型的车道线检测算法[J].智能计算机与应用,2023,13(03):182-187.（标注国家自然科学基金青年基金项目 62002286）一般期刊

[13]程国建,卞晨亮*.基于目标识别的钢材缺陷检测方法[J].计算机工程与设计,2022,43(10):2977-2983.（标注国家自然科学基金青年基金项目 62002286）核心期刊

[14]程国建,卞晨亮,陈琛,杨倬.带注意力机制的神经网络用于跑道线检测[J].计算机工程与应用,2023,59(05):169-175.（标注国家自然科学基金青年基金项目 62002286）核心期刊，CSCD 扩展版

[15]程国建,李碧,万晓龙,姚卫华;魏新善.基于 SqueezeNet 卷积神经网络的岩石薄片图像分类研究[J].矿物岩石,2021,41(04):94-101.（标注国家自然科学基金青年基金项目 62002286）核心期刊，CSCD 扩展版

[16]程国建,刘宁,万晓龙,魏新善.结合 SKNet 与 U-Net 的盐体识别方法[J].油气地质与采收率,2022,29(01):62-68.（标注国家自然科学基金青年基金项目 62002286）核心期刊，CSCD

[17]G. Cheng, L. Li, Z. Yang and X. Qiang, "Research on Seismic Signal Noise Reduction Algorithm based on Deep Learning," 2022 7th International Conference on Intelligent Computing and Signal Processing (ICSP), Xi'an, China, 2022, pp. 70-73, doi: 10.1109/ICSP54964.2022.9778355.（标注国家自然科学基金青年基金项目 62002286，未下载到原文）

[18]谯英,李代先,周少丹.油田勘探开发云平台数据存储模型研究与实践[J].西安石油大学学报(自然科学版),2021,36(06):128-133.（标注国家自然科学基金青年基金项目 62002286）核心期刊，没有西安石油大学人员依然标注基金号

[19]Wang C., Song X. & Zhang J. Hyperspectral image classification based on clustering dimensionality reduction and multi-scale feature fusion. Machine Vision and Applications 33, 90 (2022).（标注国家自然科学基金青年基金项目 62002286）

根据国科金监处〔2022〕73 号关于对唐永永等发表的论文存在**重复发表**、篡改数据和未经同意使用他人署名等问题并**在项目申请材料中存在虚假信息**的处理决定、国科金监处〔2022〕75 号关于对张义平等发表的论文存在伪造、篡改图片和**重复发表**等问题的处理决定、关于对张开飞等发表的论文存在抄袭、**重复发表**及擅自使用他人署名等问题并在**项目申请书中存在虚假信息**处理结果的通报等相关处理案例，王静怡在项目申报、执行过程中存在 10 年内三次连续重复发表和申请材料中存在虚假信息等情况，请国家自然科学基金委核查处理。

综上，在“基于遥感大数据的汾渭平原空气质量时空特征及其驱动力研究与模拟（62002286）”项目申请中，王静怡老师在申请书中提交的作为工作基础的 8 篇论文中 6 篇涉嫌重复发表，并且为了避免被发现重复发表，1 篇论文名称、

会议名称、会议举办地信息均不正确。王静怡在研究成果发表中 3 次重复发表，并且在先的重复发表（2016 年第二次重复发表）还在论文首页对重复发表做了所谓的解释说明，在后发生的重复发表（2019 年第三次重复发表）却故意隐瞒已经发表的事实。这属于明知故犯的学术不端。在国基金项目（62002286）执行中，王静怡老师在成果发表过程中存在恶意重复发表（文章[5]和[3]，在[3]故意隐瞒[5]已经发表的事实），提供虚假信息，在与国基金项目（62002286）申请书研究内容不一致的成果中标注项目号（62002286）等一系列学术不端情况。“基于遥感大数据的汾渭平原空气质量时空特征及其驱动力研究与模拟（62002286）”项目执行至今已 3 年，仅在土壤盐碱化方向发表文章 1 篇（文章[9]），与“基于遥感大数据的汾渭平原空气质量”无关；另标注国基金项目（62002286）的其余 10 篇（文章[10]-[19]），王静怡参与末位署名 2 篇，未参与署名 8 篇（其中文章[18]不仅王静怡未署名且西安石油大学未参与署名单位），以上 10 篇文章研究内容均与“基于遥感大数据的汾渭平原空气质量”无关。“基于遥感大数据的汾渭平原空气质量时空特征及其驱动力研究与模拟（62002286）”执行至今已 3 年，标注基金号（62002286）的 11 篇文章中无 1 篇研究“基于遥感大数据的汾渭平原空气质量”。王静怡老师在陕西省科技厅、教育厅项目申请、执行过程中也同样存在国基金项目类似的问题（一作发表的成果与项目申请书研究内容不一致，列入研究基础的论文 6 篇次涉嫌重复发表，提供虚假信息，参与或不参与署名的与项目申请书研究内容不一致的成果标注基金号等问题），因陕西省科技厅、教育厅项目项目与国家自然科学基金委无关，在此不再详述。王静怡老师的涉嫌学术不端行为，在 2023 年西安石油大学职称评审期间（2023/11/3-2023/12/1），本人已经实名向西安石油大学纪委及人事处举报，西安石油大学纪委及人事处转交科技处，科技处转交计算机学院调查，计算机学院包庇纵容，职能部门推诿搪塞。在此，恳请国家自然科学基金委请国家自然科学基金委员会对王静怡项目申请、执行过程中存在的问题本着对财政经费执行效率、科研风气、学术道德负责的态度，发现一起、查处一起，做到事实清楚、程序合法，公平公正的调查处理。

附件：数据库下载的文章 及王静怡博士论文电子版

此致

敬礼

2023 年 12 月 12 日

为节省页面,王静怡博士论文电子版此处不再重复列出,详见本文总第89-204页

Optimal design of joint network LDPC codes over orthogonal multiple-access relay channels

Jingyi Wang*, Shuling Che and Ying Li

State Key Laboratory of Integrated Service Networks (ISN),
Xidian University,
Xi'an 710071, China
Email: wangjy@stu.xidian.edu.cn
Email: shlche@mail.xidian.edu.cn
Email: ying.lili1973@gmail.com
*Corresponding author

Junlong Wang

Huawei Technologies Co. Ltd.,
Xi'an 710071, China
Email: 401834748@qq.com

Abstract: Optimisation of degree distribution for joint network LDPC code over orthogonal Multiple-Access Relay Channels (MARC) is investigated in this paper. We first use a differential evolution algorithm to optimise the degree distribution of the joint network LDPC code over orthogonal MARC based on Gaussian approximation. Then, using a modified differential evolution algorithm, we design a rate-compatible network LDPC code, which is equivalent to designing a single code with different Signal-to-Noise Ratio (SNR). Simulation results show that the gap between Bit Error Rate (BER) performance of the former algorithm and the decoding threshold is about 0.4 dB and that between the capacity limit and decoding threshold is less than 0.7 dB at $BER = 10^{-6}$. Simultaneously, the gap between BER performance of the latter algorithm and the decoding threshold is about 0.52 dB and that between the capacity limit and the decoding threshold is less than 0.46 dB at $BER = 10^{-7}$.

Keywords: network LDPC code; multiple-access relay network; Gaussian approximation; differential evolution; capacity limit.

Reference to this paper should be made as follows: Wang, J., Che, S., Li, Y. and Wang, J. (2016) 'Optimal design of joint network LDPC codes over orthogonal multiple-access relay channels', *Int. J. Grid and Utility Computing*, Vol. 7, No. 1, pp.68–74.

Biographical notes: Jingyi Wang is currently working towards the PhD degree in Communication and Information System at Xidian University. She received her Master's degree in Telecommunications Engineering from Xidian University in 2010. Her research interests include channel coding and network coding.

Shuling Che is currently an Associate Professor at the School of Telecommunications Engineering, Xidian University. She received her PhD in Communication and Information System from Xidian University in 2008. Her research interest includes channel coding.

Ying Li is currently a Professor at the School of Telecommunications Engineering, Xidian University. She received her PhD in Communication and Information System from Xidian University in 2005. Her research interests include channel coding, wireless network coding and MIMO theory.

Junlong Wang is currently working in Huawei Technologies Co. Ltd. He received his Master's degree in Communication and Information System from Xidian University in 2011.

This paper is a revised and expanded version of a paper entitled 'Optimal design of the joint network LDPC codes over orthogonal multi-access relay channel' presented at the '2013 5th International Conference on Intelligent Networking and Collaborative Systems', Xi'an, China, 9 September 2013.

Copyright © 2016 Inderscience Enterprises Ltd.

1 Introduction

In wireless communications (Shen et al., 2012), cooperation relay networks (Cover and Gamal, 1979; Nosratinia et al., 2004; Laneman et al., 2004) have recently attracted substantial research efforts with many promising techniques of improving performance in terms of throughput, coverage or diversity gain. In relay networks, one or multiple Relay Nodes (RNs) assist the sources in transmitting information. Optimal designs of relay networks have attracted extensive attentions owing to their ability to increase communication capacity. One of the earlier works on this subject dealt with the application of the LDPC code to single-source single-relay networks (Razaghi and Yu, 2007). To improve the performance of the single-source single-relay system, a class of bilayer LDPC codes is designed in Azmi et al. (2008) and Cances and Meghdadi (2009).

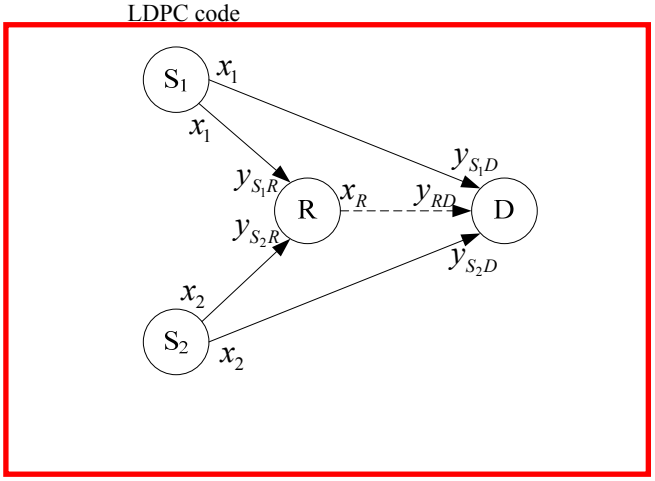
Based on the principle of the bilayer LDPC codes, the authors proposed a class of the joint network LDPC code with network coding (Zhang and Minier, 2013). And then it helps the relay to jointly re-encode the messages from the two sources and send the parity bits to the destination (Li et al., 2009). Moreover, Li et al. (2010) analysed the capacity approaching ability of the joint network LDPC codes. In this paper, we study two different methods of approaching capacity limit of two different transmission modes of a two-source single-relay system with joint network LDPC code, in which the first one requires the same code words transmitted at the two sources and the latter requires different code words transmitted at the two sources.

The rest of the paper is organised as follows. Section 2 presents the system model and then describes the operation of the system throughout different stages of the two cooperation strategies. Section 3 explains the design of two different optimisation methods. Numerical and simulation results are given in Section 4 and finally, the paper is concluded in Section 5.

2 System model

Our system is a two-slot wireless relay network consisting of two sources, one relay and one destination, as shown in Figure 1. Two different transmission modes of the system are described below, which are called Symmetry Cooperation Transmission (SCT) and Asymmetry Cooperation Transmission (ACT). The broadcast stage is followed by the cooperation stage.

Figure 1 Multi-access relay channel model with joint network LDPC code



2.1 The broadcast stage

In this stage, the sources S_i ($i=1,2$) broadcast their LDPC coded signals x_i ($i=1,2$), which are received by both relay R and destination D.

2.1.1 SCT mode

We express the received signals at the relay R and the destination D as follows:

$$y_{S_iR} = h_{S_iR}x_i + n_{S_iR} \tag{1}$$

$$y_{S_iD} = h_{S_iD}x_i + n_{S_iD} \tag{2}$$

where y_{S_iR} and y_{S_iD} are the corresponding received signal by R and D, respectively, h_{S_iR} and h_{S_iD} denote the associated channel gain and n_{S_iR} (n_{S_iD}) denotes a zero-mean Gaussian random variable with a variance $\sigma^2_{S_iR}$ ($\sigma^2_{S_iD}$).

2.1.2 ACT mode

We assume that $P^{(1)}_{S_i}$ ($i=1,2$) is the transmit power of S_i and $w^{(1)}_{S_i}$ ($i=1,2$) is a bit of an LDPC code transmitted by S_i in this stage. Then the received signals at R and D can be written as

$$y_{S_iR} = h_{S_iR}\cdot\sqrt{P^{(1)}_{S_i}}w^{(1)}_{S_i} + n_{S_iR} \tag{3}$$

$$y^{(1)}_{S_iD} = h^{(1)}_{S_iD}\cdot\sqrt{P^{(1)}_{S_i}}w^{(1)}_{S_i} + n^{(1)}_{S_iD} \tag{4}$$

where y_{S_iR}, h_{S_iR} and n_{S_iR} are as defined earlier, while $y^{(1)}_{S_iD}$, $h^{(1)}_{S_iD}$ and $n^{(1)}_{S_iD}$ are the corresponding parametric between S_i and D, where the superscript (1) represents the broadcast stage.

2.2 The cooperation stage

In this stage, after decoding the received signals correctly, R jointly re-encodes the messages of the two sources and sends parity bits x_R of the code words to D.

2.2.1 SCT mode

After x_i is decoded correctly, R jointly re-encodes the messages of the two sources and sends x_R to D. The received signal at D is

$$y_{RD} = h_{RD}x_R + n_{RD} \tag{5}$$

where y_{RD} and n_{RD} are the corresponding parametric between R and D.

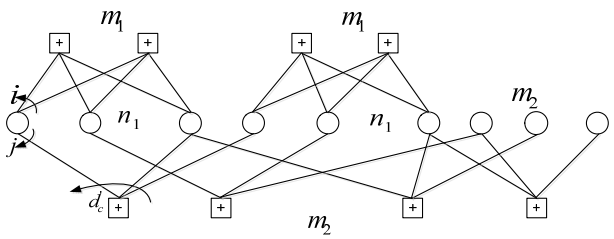
At last, D receives the signals y_{S_iD} and y_{RD}, respectively, from S_i and R. The parity check matrix of the joint network LDPC code can be written as

$$\mathbf{H} = \begin{pmatrix} \mathbf{H}_1 & \mathbf{0} & \mathbf{0} \\ \mathbf{0} & \mathbf{H}_1 & \mathbf{0} \\ \mathbf{A} & \mathbf{B} & \mathbf{C} \end{pmatrix} \tag{6}$$

where $\mathbf{H_1}$ denotes the same parity-check matrix of the constituent codes at the two sources S_i, $\mathbf{H_3} = (\mathbf{ABC})$ denotes the parity-check matrix generated by R and $\mathbf{0}$ represents the all-zero matrix.

Assume that each source uses an $(n_1, n_1 - m_1)$ irregular LDPC code with code length n_1 and parity length m_1. According to Li et al. (2010), the Tanner graph of the joint network LDPC code is shown in Figure 2, where the upper sub-graph denotes the encoding at the sources and the lower sub-graph denotes the encoding at the relay. This code includes $2m_1$ upper check nodes, m_2 lower check nodes and $2n_1 + m_2$ variable nodes. A variable node is of degree (i,j), $1 \le i \le d_v$ and $1 \le j \le d_v'$, where $i(j)$ is its upper (lower) degree and $d_v(d_v')$ is its maximum upper (lower) degree. In addition, $\lambda_{i,j}$ represents the proportion of the number of edges connected to the variable nodes with the degree (i,j).

Figure 2 The Tanner graph of the joint network LDPC code



2.2.2 ACT mode

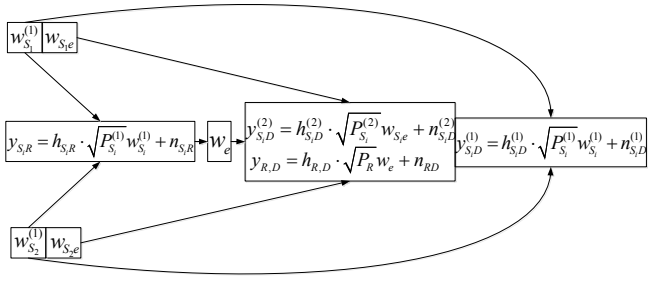
The source $S_i (i = 1,2)$ uses rate-compatible extension method from an entire LDPC code word $w_{S_i 2} = \left[w_{S_i}^{(1)}, w_{S_i e} \right]$ extended from the original code word $w_{S_i}^{(1)}$, and $w_{S_i e}$ carries additional parity-check bits as shown in Figure 3. R only generates two additional parity-check bits $w_{S_1 e}$ and $w_{S_2 e}$ from S_1 and S_2, respectively. Then network-coded code word $w_e = w_{S_1 e} \oplus w_{S_2 e}$. The received signals at D are

$$y_{S_i D}^{(2)} = h_{S_i D}^{(2)} \cdot \sqrt{P_{S_i}^{(2)}} w_{S_i e} + n_{S_i D}^{(2)} \tag{7}$$

$$y_{RD} = h_{RD} \cdot \sqrt{P_R} w_e + n_{RD} \tag{8}$$

where $P_{S_i 2}$ (P_R) is the transmit power of S_i (R) in the second stage. The other parameters were defined earlier, where the superscript (2) represents the cooperation stage.

Figure 3 Diagram of the multi-access relay channel model with joint network LDPC code



Then, D receives the signals $y_{S_i D}^{(1)}$ $\left(y_{S_i D}^{(2)} \right)$ and y_{RD}, respectively, from the two sources and the relay. First, D decodes y_{RD} and then obtains the network-coded code word $w_e = w_{S_1 e} \oplus w_{S_2 e}$. Second, D obtains $w_{S_1 e}$ and $w_{S_2 e}$ by iterative decoding with $y_{S_i D}^{(2)}$ and w_e. Different from the rate-compatible LDPC code designed in Li et al. (2009), the received SNR for $w_{S_i}^{(1)}$ and $w_{S_i e}$ are different. Using (4), (7) and (8), the SNR for the decoding of $w_{S_i}^{(1)}$ and $w_{S_i e}$ can be written, respectively, as

$$SNR_{S_i D} = \frac{\left| h_{S_i D}^{(1)} \right|^2 P_{S_i}^{(1)}}{N_0} \tag{9}$$

$$SNR'_{S_i D} = \frac{\left(h_{S_i D}^{(2)} \sqrt{P_{S_i}^{(2)}} + h_{RD} \sqrt{P_R} \right)^2}{N_0} \tag{10}$$

Finally, we decode $w_{S_1}^{(1)}$ and $w_{S_2}^{(1)}$ correctly by using the Belief Propagation (BP) iterative decoding algorithm with $w_{S_1 2} = \left[w_{S_1}^{(1)}, w_{S_1,e} \right]$ and $w_{S_2 2} = \left[w_{S_2}^{(1)}, w_{S_2,e} \right]$, respectively, at D.

3 Optimisation of degree distribution

3.1 SCT mode

3.1.1 Preliminary

Definition 1: *Decoding threshold of joint network LDPC code is defined as*

$$\sigma^* = \sup \left\{ \sigma : \lim_{L \to +\infty} m_L > M \right\} \tag{11}$$

where L is the maximum iteration number, m_L denotes the mean value of the Log-Likelihood Ratio (*LLR*) message of a code bit at the Lth decoding iteration and M is the *LLR* mean value corresponding to the target error probability.

Then with the knowledge in Li et al. (2010), $2m_L$ is the *LLR* variance value. When $\sigma < \sigma^*$, m_L will be greater than M, which means that the target error probability can be achieved. When $\sigma \ge \sigma^*$, the iterative decoding cannot achieve the target error probability.

3.1.2 Calculation of decoding threshold σ_{SD}^*

Algorithm 1: Given degree distribution of the LDPC code at the sources, let σ_{SD} and σ_{RD} represent the channel parameters of source–destination link and relay–destination link, respectively. We denote the target error probability as $P_e = 10^{-6}$ $(M = 45)$ and the maximum iteration number as L. Let $\Delta\sigma_{SD}$ denote a step length, and then Algorithm 1 can be described as follows.

- *Step 1: Initialisation.* The initialised value of the average mean value of the *LLR* message output by the check node is $m^{'l} = n^{'l} = 0$ (l is the iteration number and $l = 0$ in the first iteration) (Li et al., 2010).

- *Step 2: Updating.* When the iteration number $l < L$, update the mean values of the *LLR* messages at the variable node and the check node, and then calculate the mean value m_l of the *LLR* message during this iteration using the method in Li et al. (2010). If $m_l < M$, add the iteration number by 1 (l = l +1) and continue Step 2. If $m_l \geq M$, $\sigma_{SD} = \sigma_{SD} + \Delta\sigma_{SD}$, and go to Step 1.
- *Step 3: Stopping criterion.* If $l \geq L$ and $m_l < M$ during this iteration, stop the whole process, and the code capacity is defined as $\sigma^*_{SD} = \sigma_{SD} - \Delta\sigma_{SD}$. Otherwise, output the threshold value of channel parameter as $\sigma^*_{SD} = \sigma_{SD}$.

Using Algorithm 1, we can obtain the corresponding σ^*_{SD} from a given degree distribution of the upper layer LDPC code.

3.1.3 *Optimal design of the degree distribution of the lower layer LDPC code*

Our goal is to search the optimal degree distribution of the network LDPC code, which can approach the capacity limit. Here we use differential evolution algorithm to optimal design of the network LDPC code ensembles.

Algorithm 2. Assume that N relay code sets of the network LDPC code structure are randomly generated, denoting their degree distributions of variable node as $\lambda_{i,j}(d)$, $0 \leq i \leq d_v$, $0 \leq j \leq d'$, $d = 1,2,\ldots, N$. The degree of the lower check nodes is fixed as d'_c.

- *Step 1: Initialisation.* Initialise that degree distribution as

$$C(d) = \left\{\lambda_{i,j}(d), 0 \leq i \leq d_v, 0 \leq j \leq d'_v\right\}, d = 1,2,\ldots N \quad (12)$$

- *Step 2: Performance estimation of code sets.* Calculate the code capacity $\sigma^*(d)$ of each code set $C(d)$ through Algorithm 1, and search the optimal code ensemble meeting $C^* = \arg\max_{1\leq d\leq N}\sigma^*(d)$. The degree distribution of the optimal code ensemble corresponding to the maximum code capacity is $C^* = \left\{\lambda^*_{i,j}, 0 \leq i \leq d_v, 0 \leq j \leq d'_v\right\}$.
- *Step 3: Code set updating.* Select $\tilde{N}$ code sets from $\{C(d)\}_{d=1}^{N}$ at random and denote their degree distributions as $\tilde{C}(k) = \left\{\lambda_{i,j}(k), 0 \leq i \leq d_v, 0 \leq j \leq d'_v\right\}, k = 1,2,\ldots,\tilde{N}$. Then, update the degree distribution of the code ensemble: $C^* = C^* + \alpha\sum_{k=1}^{\tilde{N}}(-1)^{k-1}\tilde{C}(k)$, where $\alpha < 1$ is the step length.
- *Step 4: Stopping criterion.* If reaching the preset number of iteration and $m_l < M$, stop the iteration process. The degree distribution of the optimal code ensemble is defined as $C^* = \left\{\lambda^*_{i,j}, 0 \leq i \leq d_v, 0 \leq j \leq d'_v\right\}$; otherwise, go to Step 3.

Remark: *Restrictive conditions must be met for Steps 1 and 3:*

$$\begin{cases} \sum_{i\geq 0, j\geq 0}\lambda_{i,j} = 1 \\ \lambda_i = \frac{1}{\eta}\sum_{j\geq 0}\frac{i}{i+j}\lambda_{i,j} \\ \eta = \sum_i\sum_j\frac{i}{i+j}\lambda_{i,j} \\ d'_c = \frac{1-\eta}{\sum_j\frac{\lambda_{0,j}}{j}} \end{cases} \quad (13)$$

where η is the proportion of the total number of edges in the upper sub-graph. The total number of upper layer edges of a source node is $E = \frac{n_1}{\sum_{i\geq 2}\lambda_i/i} = \frac{k_1}{\sum_{j\geq 2}\rho_j/j}$ and the total number of edges of the bilayer network LDPC relay code is $E' = 2E + k_2 \cdot d'_c$, so $\eta = \frac{2E}{E'}$.

3.2 *ACT mode*

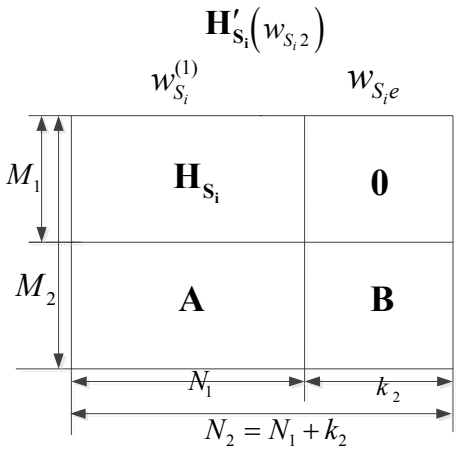
3.2.1 *Ensemble description of the joint network LDPC code*

We assume that R decodes the received signal from S_i correctly. The code rate R_1 of both S_1 and S_2 depends on $R_1 \leq C(SNR_{S_1R})$ and $R_1 \leq C(SNR_{S_2R})$, where $C(SNR_{S_iR})$ is the capacity when *SNR* of the channel between S_i and R is SNR_{S_iR}. Here we assume $R_1 = C(SNR_{S_1R}) = C(SNR_{S_2R})$.

In addition, the distance between S_i and D is farther than the distance between S_i and R, so the channel gain h_{S_iD} is smaller than h_{S_iR} and SNR_{S_iD} is smaller than SNR_{S_iR}. Here we assume $R_1 > C(SNR_{S_1D}) = C(SNR_{S_2D})$. And the capacity between the source and destination link is smaller than the capacity between the source and relay link. According to Shannon theorem, when the rate is greater than the channel capacity, the system cannot decode correctly after more iterations, so extra check bits are generated to help decode.

Figure 4 shows the extended parity-check matrix $\mathbf{H}'_{\mathbf{S}_i}(\mathbf{w}_{\mathbf{S}_i 2})$, where $\mathbf{H}_{\mathbf{S}_i}$ denotes the parity-check matrix of the code word $w^{(1)}_{S_i}$ at the two sources $S_i(i = 1,2)$, w_{S_ie} denotes additional parity-check bits of the entire code word w_{S_i2} and $\mathbf{0}$ represents the all-zero matrix. The rate of the entire code word is $R_2 = \frac{N_1 - (k_1 + k_2)}{N_1 + k_2}$. We find a proper k_2, which must meet $R_2 \leq C(SNR_{S_1D}) = C(SNR_{S_2D})$.

Figure 4 Rate-compatible structure of the parity-check matrix for the relay code



R_1 and R_2 satisfy the following relationship:

$$R_1 = \frac{N_1 - k_1}{N_1} > R_2 = \frac{N_1 - (k_1 + k_2)}{N_1 + k_2} \tag{14}$$

As far as we know, the decoding performance depends on the parity-check matrix, while the degree distribution of the code ensembles determines parity-check matrix. So the design of the parity-check matrix $\mathbf{H}'_{\mathbf{S}_i}$ is equivalent to find the optimal degree distribution based on a given construction algorithm.

3.2.2 *Optimal design of the degree distribution of the joint network LDPC code*

According to the above analysis, when SNR_{S_iD} is given, we can determine the number of extra parity bits. In addition, D decodes the received information of S_i correctly; it is required to satisfy the formula

$$R_1 \le C\left(SNR_{S_iD}\right) + C\left(SNR'_{S_iD}\right) \tag{15}$$

When the transmit power and the channel gains are given, we can obtain the theoretical minimum SNR by (15). Our optimal goal is to find the relay extended code ensemble, whose threshold of SNR is approaching the theoretical extreme value.

Compared with the rate-compatible LDPC code of the single-source single-relay system, the two-source single-relay system uses the linear network-coded method at R, which achieves the same cooperative diversity to the single-source single-relay system and D decodes the received signal of S_1 and S_2 separately. Here the two-source single-relay system can be equal to two separate single-source single-relay systems for rate-compatible LDPC code. Therefore, we can use the algorithm in Cances and Meghdadi (2009) to optimise the design of the rate-compatible extended code ensemble of S_1 and S_2 separately, while linear network-coded is used at the relay.

4 Simulation results

4.1 *SCT mode*

Assume each source node employs an $(n_1, n_1 - m_1)$ LDPC code with $\lambda(x) = 0.23403x + 0.21242x^2 + 0.1469x^5 + 0.102840x^6 + 0.30381x^{19}$ and $\rho(x) = 0.71875x^7 + 0.28125x^8$, where $n_1 = 22164$ and $m_1 = 11082$. $SNR_{RD} = 3$ dB and the two source–destination links are assumed to be symmetric. Using Algorithm 1, four different parameters of the joint network LDPC codes are obtained and listed in Table 1, where σ_{RD}^2 represents the channel parameter between the relay and the destination link.

Table 1 Four optimal joint network LDPC codes

Code ensembles	*Code A*	*Code B*	*Code C*	*Code D*
d'_v	2	2	2	2
d'_c	4	4	4	7
k_2	2814	4814	2814	2814
σ_{RD}	0.5	0.5	0.8	0.5
η	0.942065	0.904808	0.942065	0.902835
σ^*_{SD}	1.0568	1.0987	1.0393	1.1116
Threshold (E_bN_0)	0.155039dB	0.115123dB	0.2018dB	–0.22877dB
Sum capacity (E_bN_0)	–0.24536dB	–0.517620dB	–0.143948dB	–0.24536dB
Gap	0.400399dB	0.632743dB	0.345748dB	0.01666dB

Using Algorithm 2, four optimal degree distributions of the joint network LDPC codes are given in Tables 2–5.

Table 2 Degree distributions of code A

$\lambda_{i,j}$	$\lambda_{i,0}$	$\lambda_{i,1}$	$\lambda_{i,2}$
$i = 2$	0.193815	0.00543635	0.04612661
$i = 3$	0.171369	0.019109592	0.02409292
$i = 6$	0.129299	0.006342408	0.00494214
$i = 7$	0.09485	8.2369E-05	0.00259462
$i = 20$	0.273877	0.000432436	0.00181212
$i = 0$	0	0.0030528	0.02276564

Table 3 Degree distributions of code B

$\lambda_{i,j}$	$\lambda_{i,0}$	$\lambda_{i,1}$	$\lambda_{i,2}$
$i = 2$	0.07441004	0.20599344	0
$i = 3$	0.19208258	0.00015819031	0
$i = 6$	0.1327018904	0.00013842	0.0001681903
$i = 7$	0.09266986	0.000326381	0.0001779641
$i = 20$	0.27426244	0.0005152496	0.0021751167
$i = 0$	0	0.0237936797	0.000009887

Table 4 Degree distributions of code C

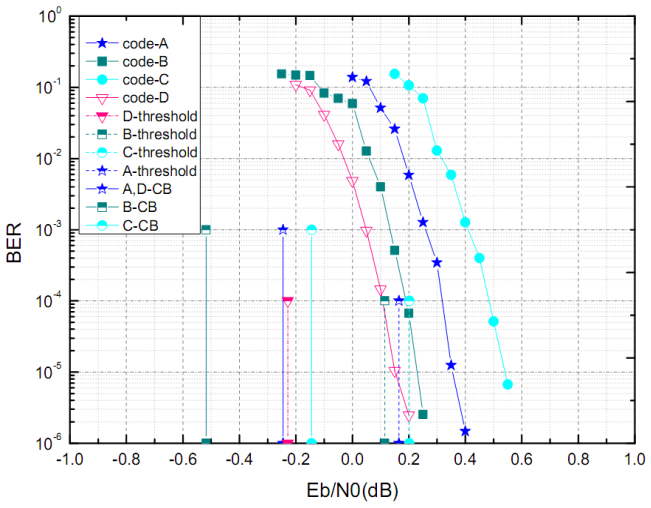
$\lambda_{i,j}$	$\lambda_{i,0}$	$\lambda_{i,1}$	$\lambda_{i,2}$
$i=2$	0.1206132872	0.0	0.0
$i=3$	0.1001453763	0.0000219458	0.0
$i=6$	0.1860514424	0.0002767963	0.000016798
$i=7$	0.1964141036	0.0002114936	0.0000212906
$i=20$	0.3858558271	0.0003262453	0.0000362551
i = 0	0.0	0.0041565109	0.0206487529

Table 5 Degree distributions of code D

$\lambda_{i,j}$	$\lambda_{i,0}$	$\lambda_{i,1}$	$\lambda_{i,2}$
$i=2$	0.1112574229	0.013643762	0.1818773738
$i=3$	0.09172912663	0.0876831253	0.0571696344
$i=6$	0.13223499235	0.00032560828	0.00015708008
$i=7$	0.092674986	4.568455E-05	6.788722E-05
$i=20$	0.274059093	0.00010113293	0.000217037
$i=0$	0	0.00351717946	0.02072694417

The BER curves of four codes are illustrated in Figure 5. We see that the gap between the decoding threshold of four codes obtained by searching the maximum decoding threshold σ_{SD}^{*} and capacity limit is less than 0.7 dB, and that between BER performance and decoding threshold is less than 0.4 dB. Since the lower check degree of Code D is bigger and more information bits are contained in the check equation, it outperforms Code A by 0.2 dB at $BER=10^{-5}$. Another important observation is that Code B has a gain of about 0.15 dB over Code A at $BER=10^{-5}$ and the performance gain of Code D is about 0.1 dB over Code B at $BER=10^{-5}$. This indicates that increasing the degrees of lower layer check nodes is better than increasing the numbers of parity bits to improve system performance. When the noise variances between the *R* and *D* link are increased, the system decoding performance will be reduced and Code A will have a gain of about 0.2 dB over Code C at $BER=10^{-5}$.

Figure 5 Performance of the joint network LDPC codes



4.2 ACT mode

Assume each source node employs LDPC code-1 and code-2 listed in Cances and Meghdadi (2009, Table 1). The two source–destination links are assumed to be symmetric. The distance between S_i and D is normalised to unity and d denotes the normalised distances between S_i and R. The channel gain $|h_{S_1D}|^2=|h_{S_2D}|^2=1$, $|h_{S_1R}|^2=|h_{S_2R}|^2=\frac{1}{d^{\alpha}}$ and $|h_{RD}|^2=\frac{1}{(1-d)^{\alpha}}$, where we assume that $\alpha=2$ is the path loss exponent and $d=0.25$. The power allocation among S_i and R is fixed as $P_{S_1}^{(1)}/2=P_{S_2}^{(1)}/2=P_{S_12}=P_{S_22}=P_R/2=P_T/8$, and $w_{S_i}^{(1)}$ and w_{S_i2} have the rate $R_1=1/2$ and $R_2=1/4$, respectively. Table 6 gives the optimum LDPC code ensemble of w_{S_i2} via the algorithm in Cances and Meghdadi (2009) and the network-coded method at the relay. And the node probability set of w_{S_12} is $h_1(2)=0.1978$, $h_1(i)=1$ for $i\in\{3,6,7,8,10,14,16,20,30,33\}$, the node probability set of w_{S_22} is $h_1(3)=0.1576$, $h_1(i)=1$ for $i\in\{2,4,7,8,10,14,16,20,30,33\}$, where $h_1(i)$ denotes the probability of a variable node that has a degree of *i* and falls in the region of region-1 (i.e. $\mathbf{H_1}$ and **A**, namely region-1; **0** and **B**, namely region-2.)

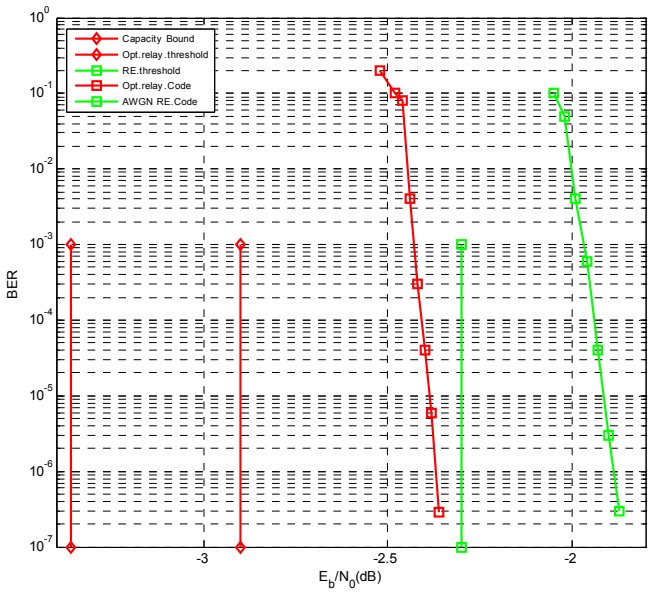
Table 6 Rate-compatible extended LDPC code ensembles

Code ensembles	*Extended code ensemble 1*	*Extended code ensemble 2*
λ_2	0.13370307136	0.06600453943
λ_3	0.02829823403	0.11086569074
λ_4	0.02371830093	0.07247855957
λ_5	0.00295003743	0.00422715433
λ_6	0.05593270965	0.03891266928
λ_7	0.00474956026	0.06403186741
λ_8	0.05605071114	0.03722942404
λ_9	0.11366862967	0.15231465261
λ_{10}	0.06932587957	0
λ_{11}	0.00125745345	0.00502688622
λ_{12}	0.00044250561	0
λ_{13}	0.00081494784	0
λ_{14}	0.00087763614	0.05326214450
λ_{15}	0.00027656601	0
λ_{16}	0.19417146355	0.13551266623
λ_{17}	0.20455190775	0
λ_{20}	0.00118001497	0.00411290691
λ_{22}	0.00186589867	0.16077657776
λ_{26}	0.00009587622	0
λ_{30}	0.10553758901	0.09505384861
ρ_8	0	0.22602708425
ρ_9	0.99563763215	0.77391198379

In simulations, the code lengths of $w_{S_i}^{(1)}$ and w_{S_i2} are $N_1=20000$ and $N_2=2N_1=40000$, respectively. We compare the BER performance between the optimum LDPC

code ensemble and the repetition code under the AWGN channel, when the repetition code has $w_{S_i e} = w_{S_i}^{(1)}$ and D receives $w_{S_i}^{(1)}$ from source S_i and R at the same time. Figure 6 shows the BER performance of the optimised relay code ensemble and the repetition code. It is seen that the relay code ensemble optimised via the algorithm in Cances and Meghdadi (2009) can achieve about 0.5 dB gain over the repetition scheme. The gap between the BER performance of the optimised relay code ensemble of the rate-compatible LDPC and the decoding threshold is about 0.52 dB, and the gap between the decoding threshold and the capacity limit is less than 0.46 dB.

Figure 6 The BER performance comparison between the optimised relay code and the repetition code



5 Conclusions

In this paper, we employed the differential evolution method to design degree distribution of different transmission modes of the joint network LDPC code for a two-source single-relay system. The performance of the new codes we designed showed significant BER performance gain for a two-source single-relay system with symmetric AWGN channels.

Acknowledgements

We are grateful to anonymous referees for their invaluable suggestions. This work is supported by the National Natural Science Foundation of China (Nos. 61072064, 61101148 and 61001131).

References

Azmi, M.H., Yuan, J., Ning, J. and Huynh, H.Q. (2008) 'Improved bilayer LDPC codes using irregular check node degree distribution', *Proceedings of the IEEE International Symposium on Information Theory*, 6–11 July, Toronto, Canada, pp.141–145.

Cances, J.P. and Meghdadi, V. (2009) 'Optimized low density parity check codes designs for half duplex relay channels', *IEEE Transactions on Wireless Communications*, Vol. 8, No. 7, pp.3390–3395.

Cover, T. and Gamal, A.E. (1979) 'Capacity theorems for the relay channel', *IEEE Transactions on Information Theory*, Vol. 25, pp.572–584.

Laneman, J., Tse, D. and Wornell, G. (2004) 'Cooperative diversity in wireless networks: efficient protocols and outage behavior', *IEEE Transactions on Information Theory*, Vol. 50, No. 12, pp.3062–3080.

Li, Y., Song, G.H. and Wang, L.L. (2009) 'Design of joint network-low density parity check codes based on the EXIT charts', *IEEE Communications Letters*, Vol. 13, No. 8, pp.600–602.

Li, Y., Song, G.H. and Wang, L.L. (2010) 'Analysis of the joint network LDPC codes over orthogonal multi-access relay channel', *IEEE Communications Letters*, Vol. 14, No. 2, pp.184–186.

Nosratinia, A., Hunter, T.E. and Hedayat, A. (2004) 'Cooperative communication in wireless networks', *IEEE Communications Magazine.*, Vol. 42, No. 10, pp.74–80.

Razaghi, P. and Yu, W. (2007) 'Bilayer low-density parity-check codes for decode-and-forward in relay channels', *Transactions on Information Theory*, Vol. 3, No. 10, pp.3723–3739.

Shen, Y., Pei, Q., Xu, Q. and Zhang, Z. (2012) 'The multimedia service session handoff method in heterogeneous wireless networks', *International Journal of Grid and Utility Computing*, Vol. 3, No. 1, pp.68–77.

Zhang, Y. and Minier, M. (2013) 'How network coding system constrains packet pollution attacks in wireless sensor networks', *International Journal of Grid and Utility Computing*, Vol. 4, Nos. 2–3, pp.197–203.

A Distributed RS code based hybrid Forward strategy for MARC

Jingyi Wang*, Ying Li, Daolong Wu, Baoming Bai

State Key Lab. of ISN, Xidian University, Xi'an, China

Abstract: To combat the effects of error propagation in error-prone multiple-user multiple-relay (MUMR) wireless networks, a Reed-Solomon (RS) code based hybrid decoded-and-forward (DF) strategy is proposed. In this paper, we introduce a proposed hybrid DF strategy for the MUMR wireless networks. We propose a threshold to analyse and only forwards those bits whose log-likelihood ratios (LLRs) are larger than this threshold. Furthermore, we investigate the optimization of the threshold by minimizing the bit error rate (BER), and this technique is applied to separated cooperation and combined cooperation, respectively. Both separated cooperation and combined cooperation strategy are discussed in the optimization of the threshold. Using the suggested design guidelines in this paper, we show that the performance gap for different scenarios between the MUMR wireless networks with error-free relay and that with the proposed scheme is only 0.01dB at BER=10-6 over both additive white Gaussian noise (AWGN) channel and fading channel. In addition, the effectiveness of our proposed method in mitigating error propagation in error-prone MUMR wireless networks, which demonstrates that the proposed scheme may have potential use in MUMR wireless networks.

Keywords: network coding; relaying strategies; RS code; error propagation; threshold

1. Introduction

Cooperative wireless relay networks [1-3] have recently attracted substantial research efforts. Many promising techniques are proposed to improve the performance in terms of throughput, coverage or diversity gain. In relay networks, one or multiple relay nodes (RNs) can be used to assist the sources in transmitting information. Early works on cooperative communications suggested three types of relay transmission protocol [3]: amplify-and-forward (AF), decode-and-forward (DF) and compress-and-forward (CF).

For practical DF cooperative networks, the potential error propagation limits the attainable end-to-end performance. Hence, various methods have been proposed to mitigate the effects of error propagation imposed by the RNs [4-7]. In [4], authors introduced a distributed turbo-code for the DF scheme. This approach was then extended by [5] and [6] to soft re-encoding at the relay in order to cope with erroneous or unreliable bits at the relay. Authors in [7] proposed to calculate the log-likelihood ratio (LLR) of received bits at the relay. If the LLR of a bit falls below a predetermined threshold, the relay blocks the bit and does not forward it to the destination. This method can avoid errors propagation to the destination in some extent.

Another limitation of cooperative communication systems is their low throughput as compared to that of MIMO systems. To increase the throughput of such networks, network coding was proposed to reduce the traffic in such networks [8,9]. Although the application of network coding to relay networks seems to be natural and beneficial, of which earlier schemes only used in two-user one-relay networks [10]. The design of network coding rarely applied in multiple-user single-relay (MUMR) networks. In [11], physical-layer network coding was studied to multiple-user single-relay networks, which is not optimal for network with multiple relays. Moreover, previous work[10-12] studied binary network coding which represented a special case of general finite field network coding. However, binary network coding is generally not optimal for multiple-user multiple-relay (MUMR) wireless networks in terms of transmission efficiency e.g., frame error rate, energy efficiency [13]. Most of the network coding theory applied to wireless networks based on the assumption that the data is delivered with error-free or all error can be corrected by error correcting coding scheme. However, such an assumption without any error checking schemes (such as ARQ) is impractical as error will propagate to all terminals. So we adopt a reliable threshold at the relays to control error propagation. By calculating LLR values for the bits sent from the sources, the relays apply non-binary network coding based on maximum distance separable codes (MDS) to MUMR wireless networks with arbitrary M ($M \geq 2$) users and N ($N \geq 1$) relays. In this paper, we study different scenarios of source-relay channels, as well as different schemes of applying the LLR threshold at the relays. The results show that separated cooperation has better performance than combined cooperation using optimal threshold.

The rest of this paper is organized as follows. Section 2 presents the system model and then describes the operation of the system throughout different slots of the cooperation strategy. Section 3 analyses the

performance of the system, as well as optimizes the threshold with minimum end-to-end BER as a target. Section 4 presents simulation results, and the paper is concluded in Section 5.

2. System Description

2.1 System Model

The wireless relay network with orthogonal channels consists of *M* sources S_i $(i=1,2,\cdots,M)$, *N* relays R_j $(j=1,2,\cdots,N)$ and one destination D, as shown in Fig.1. The transmission between the *M* sources and the destination will be implemented through two slots.

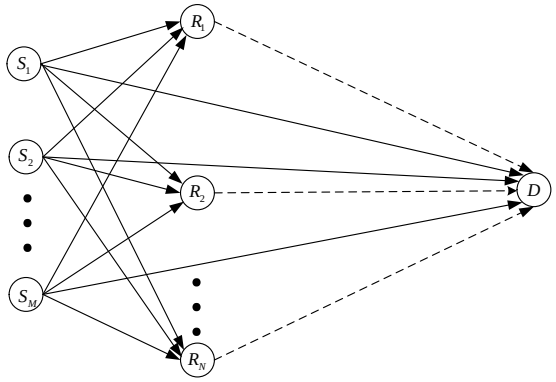


Fig.1 Wireless network with *M* sources and *N* relays

In the first slot, the *M* sources broadcast their coded symbol X_i^t ($i=1,2,\cdots,M$) with rate R_i ($i=1,2,\cdots,M$) to the *N* relays and the destination D, where the superscript *t* represents time throughout this paper. Then we have

$$Y_{S_i,D}^t = h_{S_i,D}^t X_i^t + N_{S_i,D}^t \tag{1}$$

$$Y_{S_i,R_j}^t = h_{S_i,R_j}^t X_i^t + N_{S_i,R_j}^t \tag{2}$$

where $Y_{S_i,D}^t$ and Y_{S_i,R_j}^t are the corresponding signal received by the relay R_j and the destination D respectively, $N_{S_i,D}^t$ and N_{S_i,R_j}^t are the zero-mean additive Gaussian random variables with variance $\sigma_{S_i,D}^2$ and σ_{S_i,R_j}^2 respectively. $h_{S_i,D}^t$ and h_{S_i,R_j}^t are the associated fading, with subscripts indicating the specific channel.

In the second slot, the relay R_j calculates the LLR values of the bits sent from all the sources. If the LLR of a bit falls below a predetermined threshold, the relay R_j blocks the bit and does not forward it to the destination. After this process, the relay R_j re-encodes the selected bits and forwards the encoded sequence to the destination. Let $X_{R_j}^t$ be the coded symbol transmitted by the relay R_j. The received signal at the destination is

$$Y_{R_j,D}^t = h_{R_j,D} X_{R_j}^t + N_{R_j,D}^t \tag{3}$$

where $Y_{R_j,D}^t$ is the received signal at the destination D from the relay R_j, $N_{R_j,D}^t$ is a zero-mean additive Gaussian random variable with variance $\sigma_{R_j,D}^2$.

In this paper, we consider two forwarding schemes. The first scheme is that the relays cooperate with each source individually. In this scheme, each relay determines which users bits can be forwarded independently. The second scheme is that the relays cooperate with all the *M* sources. To be more specific, only when all the LLR values of all the *M* sources are larger than the threshold, can the relay re-encode these bits and forward them to the destination. No matter which scheme is employed, the forwarded symbol $X_{R_j}^t$ is the coded symbol of the

selected bits. A detailed discussion will be given in the next section. The superscript t will be omitted in the following formula for simplicity.

2.1 RS code based Network Coding Scheme

In the relay R_j, the transmitted signal $X_{R_j}^t$ can be written as

$$X_{R_j} = \sum_{i=1}^{M} g_{i,j} \hat{X}_{i,j} \tag{4}$$

where $\hat{X}_j = \left[\hat{X}_{1,j} \hat{X}_{2,j} \cdots \hat{X}_{M,j} \right]$ is the estimation of the source messages at the relay R_j. And $g_{i,j}$ is the network coding coefficient used at the relay R_j. $g_{i,j} = 0$ means that the relay node R_j will not forward to the i-th source.

Let

$$\mathbf{P} = \begin{bmatrix} g_{1,1} & g_{1,2} & \cdots & g_{1,N} \\ g_{2,1} & g_{2,2} & \cdots & g_{2,N} \\ \vdots & & & \vdots \\ g_{M,1} & g_{M,2} & \cdots & g_{M,N} \end{bmatrix} \tag{5}$$

where the matrix $\mathbf{P}$ defines the network coding scheme used by the N relays. Combining $\mathbf{P}$ with an $M \times M$ identity matrix, we can have

$$\begin{aligned} \mathbf{G} &= \begin{bmatrix} g_{1,1} & g_{1,2} & \cdots & g_{1,N} & 1 & 0 & \cdots & 0 \\ g_{2,1} & g_{2,2} & \cdots & g_{2,N} & 0 & 1 & \cdots & 0 \\ \vdots & & & \vdots & & & \ddots & \\ g_{M,1} & g_{M,2} & \cdots & g_{M,N} & 0 & 0 & 0 & 1 \end{bmatrix} \\ &= \left[\mathbf{P} \quad \mathbf{I}_{M \times M} \right] \end{aligned} \tag{6}$$

Apparently, $\mathbf{G}$ is a generator matrix of a RS code with length $M+N$. In other words, the network coding matrix $\mathbf{P}$ can be designed via the help of RS coding theory.

3. Forward Strategy

In this section, we assume that no channel coding is used by the source and the relays. Based on the principle discussed in [7], we study the forward strategy at the relays. If the LLR of the bit is below the preset threshold, the relays stay silent and transmit nothing. Otherwise, the network coded symbols are sent. We calculate optimum decoding threshold for two possible scenarios to obtain minimum BER.

3.1 Threshold based forwarding

Assume BPSK modulation is employed by the sources. Let $\Lambda_{x_i}^j$ denote the LLR of the bit of the i-th user at R_j. We have

$$\begin{aligned} \Lambda_{x_i}^j &= \ln \frac{p\left(x_i = 1 \middle| y_{S_i,R_j}, h_{S_i,R_j} \right)}{p\left(x_i = -1 \middle| y_{S_i,R_j}, h_{S_i,R_j} \right)} = \ln \frac{p\left(y_{S_i,R_j} \middle| x_i = 1, h_{S_i,R_j} \right)}{p\left(y_{S_i,R_j} \middle| x_i = -1, h_{S_i,R_j} \right)} \\ &= 2 y_{S_i,R_j} h_{S_i,R_j} \Big/ \sigma_{S_i,R_j}^2 \end{aligned} \tag{7}$$

where $p(\cdot)$ indicates the conditional probability density function. It is well-known that the sign of $\Lambda_{x_i}^j$ is the hard decision value, and the magnitude is a good measure of the reliability of the bit. R_j estimates the original data as

$$\hat{x}_i^j = sign\left(\Lambda_{x_i}^j \right) \tag{8}$$

where $sign(\cdot)$ is the signature function. The instantaneous BER in terms of $\Lambda_{x_i}^j$ at the R_j can be computed by

$$P_{e-S_i,R_j} = \frac{1}{1+e^{\left|\Lambda_{x_i}^j\right|}} \tag{9}$$

Let P_{eT} be the pre-determined threshold, which means that the relay does not forward the estimated bit $\hat{x}_i^j$ to the destination unless $P_{e-S_i,R_j} \le P_{eT}$. According to (9), we have

$$P_{e-S_i,R_j} = \frac{1}{1+e^{\left|\Lambda_{x_i}^j\right|}} \le P_{eT}$$

or

$$\left|\Lambda_{x_i}^j\right| \ge \ln\left(\frac{1}{P_{eT}} - 1\right) = \Lambda_0 \tag{10}$$

From (7)-(10), $\Lambda_{x_i}^j$ provides the reliable information of the maximum a-posteriori probability decision, which minimizes the error probability.

3.2 Optimization of Threshold

3.2.1 Optimization for separated Cooperation

In the separated cooperation, the relay R_j will evaluate the quality of the received signal from each user. If the LLR exceeds in the preset threshold, the relay decodes and forwards the restored data to D. Otherwise, it keeps silent in the second slot. The transmitted signal can be written as

$$X_{R_j} = \sum_{i=1}^{M} g_{i,j}\hat{X}_{i,j} \tag{11}$$

where $g_{i,j} = 0$ if $\left|\Lambda_{x_i}^j\right| < \Lambda_{S_i 0}$, and $g_{i,j} \neq 0$ if $\left|\Lambda_{x_i}^j\right| \ge \Lambda_{S_i 0}$, $\Lambda_{S_i 0}$ is the threshold of set of S_i.

Let $P_{S_i e}^{sep}$ be the average BER at the destination when separated cooperation is employed. The optimal threshold $\Lambda_{S_i 0}^{opt}$ will be determined by minimizing $P_{S_i e}^{sep}$. More specifically, we have

$$\min_{\Lambda_{S_i 0}} \quad P_{S_i e}^{sep} \tag{12}$$

$$s.t. \quad \Lambda_{S_i 0} > 0 \tag{13}$$

This is a linear programming problem. We use the following probability distribution function to obtain the optimum $\Lambda_{S_i 0}^{opt}$.

There are two events causing the erroneous signal at D. One is that the relay stays silent and an error happens in direct transmission. The other is that the relay forwards the bit to the destination and an error still happens. Since the two events are mutually exclusive, $P_{S_i e}^{sep}$ can be written as

$$P_{S_i e}^{sep} = P_{S_i e}^1 + P_{S_i e}^2 \tag{14}$$

where $P_{S_i e}^1$ and $P_{S_i e}^2$ are the error probabilities corresponding to the first and second event, respectively. They can be computed by

$$P_{S_i e}^1 = P_{S_i}^{(SD)} Pr\left[\left|\Lambda_{x_i}\right| < \Lambda_{S_i 0}\right] \tag{15}$$

$$\begin{aligned} P_{S_i e}^2 &= Pr\left[\hat{X}_{i,j} = 1 \middle| X_i = -1, \left|\Lambda_{x_i}\right| \ge \Lambda_{S_i 0}\right] \\ &= P_{S_i}^{(MAC)}\left(1 - P_{S_i,R_j}^e\right) + P_{S_i}^{(X)} \cdot P_{S_i,R_j}^e \end{aligned} \tag{16}$$

where $P_{S_i}^{(SD)}$ indicates the bit error probability that an error happens in the source-destination link, $P_{S_i}^{(MAC)}$ is the bit error probability that an error happens when the destination decodes by using the signals from both $S_i - D$ link and $R_j - D$ link, $P_{S_i}^{(X)}$ is the bit error probability that an error happens when the destination decodes by using the signals from both $S_i - D$ link and $R_j - D$ link. P_{S_i,R_j}^{e} is the error probability that the R_j decodes messages from the S_i unsuccessfully..

Based on (11)-(16), we can easily compute optimum thresholds to minimize the error probability. It is shown that the optimal thresholds $\Lambda_{S_i 0}^{opt}$ in the case of separated cooperation can be expressed as

$$\Lambda_{S_i 0}^{opt} = \log\left(\frac{P_{S_i}^{(X)} - P_{S_i}^{(MAC)}}{P_{S_i}^{(SD)}} - 1 \right) \tag{17}$$

3.2.2 Combined Cooperation

In this method, R_j evaluates the quality of the received signals from each user. If each LLR satisfies the preset requirement simultaneously, the relay R_j decodes and forwards the restored data to D. Otherwise, the output is null when one of them is null. The transmitted signal can be written as

$$X_{R_j} = \begin{cases} \sum_{i=1}^{M} g_{i,j} \hat{X}_{i,j}, & \left|\Lambda_{x_i}\right| > \Lambda_{S_i 0} \quad \textit{for all } i \\ 0, & \textit{otherwise} \end{cases} \tag{18}$$

where $\Lambda_{S_i 0}$ is the threshold set for forwarding the bits of S_i at the relay R_j.

Let P_e^{com} be the average BER at the destination when combined cooperation is employed. The optimal thresholds $\Lambda_{S_1 0}^{opt}, \Lambda_{S_2 0}^{opt}, \cdots, \Lambda_{S_M 0}^{opt}$ will be determined by minimizing P_e^{com}. More specifically, we have

$$\min_{\Lambda_{S_1 0}, \Lambda_{S_2 0}, \cdots, \Lambda_{S_M 0}} P_e^{com} \tag{19}$$

$$s.t. \quad \Lambda_{S_i 0} > 0, \quad i = 1, 2, \cdots, M. \tag{20}$$

Let $T_{S_1 S_2 \cdots S_M}^{e}$ denotes the event that the bit of S_i is decoded incorrectly at the relays, $T_{S_1 S_2 \cdots S_M}^{c}$ denotes the event that the bit of S_i is decoded correctly at the relays and $T_{S_1 S_2 \cdots S_M}^{x}$ denotes the event that the nulled bit of S_i at the relays. Assume $P = \left\{ \text{sgn}\left(\Lambda_{x_1}\right) \neq x_1, \text{sgn}\left(\Lambda_{x_2}\right) \neq x_2, \cdots \text{sgn}\left(\Lambda_{x_M}\right) \neq x_M \right\}$, $U \in P$ and $U \neq \varnothing$; $T = \left\{ \left|\Lambda_{x_1}\right| > \Lambda_{S_1,0}, \left|\Lambda_{x_2}\right| > \Lambda_{S_2,0}, \cdots \left|\Lambda_{x_M}\right| > \Lambda_{S_M,0} \right\}$; $Q = \left\{ \left|\Lambda_{x_1}\right| < \Lambda_{S_1,0}, \left|\Lambda_{x_2}\right| < \Lambda_{S_2,0}, \cdots \left|\Lambda_{x_1}\right| < \Lambda_{S_M,0} \right\}$, $V \in Q$ and $V \neq \varnothing$ respectively. The probabilities of $T_{S_1 S_2 \cdots S_M}^{e}$, $T_{S_1 S_2 \cdots S_M}^{e}$ and $T_{S_1 S_2 \cdots S_M}^{x}$ can be defined as

$$\begin{aligned} \Pr\left[T_{S_1 S_2 \cdots S_M}^{e} \right] &= \Pr\left[U \middle| T \right] \\ \Pr\left[T_{S_1 S_2 \cdots S_M}^{c} \right] &= 1 - \Pr\left[U \middle| T \right] \\ \Pr\left[T_{S_1 S_2 \cdots S_M}^{x} \right] &= \Pr\left[V \right] \end{aligned} \tag{21}$$

Consequently, the bit error probability at D is expressed as

$$P_e^{com} = P_{S_1 S_2 \cdots S_M}^{(SD)} \Pr\left[T_{S_1 S_2 \cdots S_M}^{x} \right] + P_{S_1 S_2 \cdots S_M}^{(MAC)} \Pr\left[T_{S_1 S_2 \cdots S_M}^{c} \right] + P_{S_1 S_2 \cdots S_M}^{(X)} \Pr\left[T_{S_1 S_2 \cdots S_M}^{e} \right] \tag{22}$$

where $P_{S_1S_2\cdots S_M}^{(SD)}$ indicates the bit error probability that an error happens in the source-destination link, $P_{S_1S_2\cdots S_M}^{(MAC)}$ is the bit error probability that an error happens when the destination decodes by using the signals from both $S_i - D$ link and $R - D$ link, $P_{S_1S_2\cdots S_M}^{(X)}$ is the bit error probability that an error happens in the cooperative transmission from S_i and R_j to D.

By using numerical integration to evaluate the expressions, we obtain all the elements of P_e^{com}; allowing us to obtain their numerical values for a specific ($\Lambda_{S_1 0}, \Lambda_{S_2 0}\cdots, \Lambda_{S_M 0}$) set. Finally, by using a numerical optimization algorithm (such as gradient descent), we can obtain the optimal set of ($\Lambda_{S_1 0}, \Lambda_{S_2 0}\cdots, \Lambda_{S_M 0}$) (denoted as ($\Lambda_{S_1 0}^{opt}, \Lambda_{S_2 0}^{opt}\cdots, \Lambda_{S_M 0}^{opt}$), respectively) optimized for minimize P_e^{com}.

4. Simulation Results

We study an example with four users, four relays and orthogonal channels among sources and relays. Assuming that each source node employs a (3824,1912) irregular LDPC code with degree distribution $\lambda(x) = 0.21606x + 0.1576x^2 + 0.154x^4 + 0.01848x^5 + 0.04312x^6 + 0.41074x^{18}$, $\rho(x) = x^8$. We assume the RS code coefficients are in the finite field $\mathrm{GF}(2^8)$, which is constructed based on the minimal polynomial $p(X) = 1 + X^2 + X^3 + X^4 + X^8$. We simulated all thresholding types in addition to the cases of without any thresholding , with the preset thresholding, with the optimal thresholding at the relays.

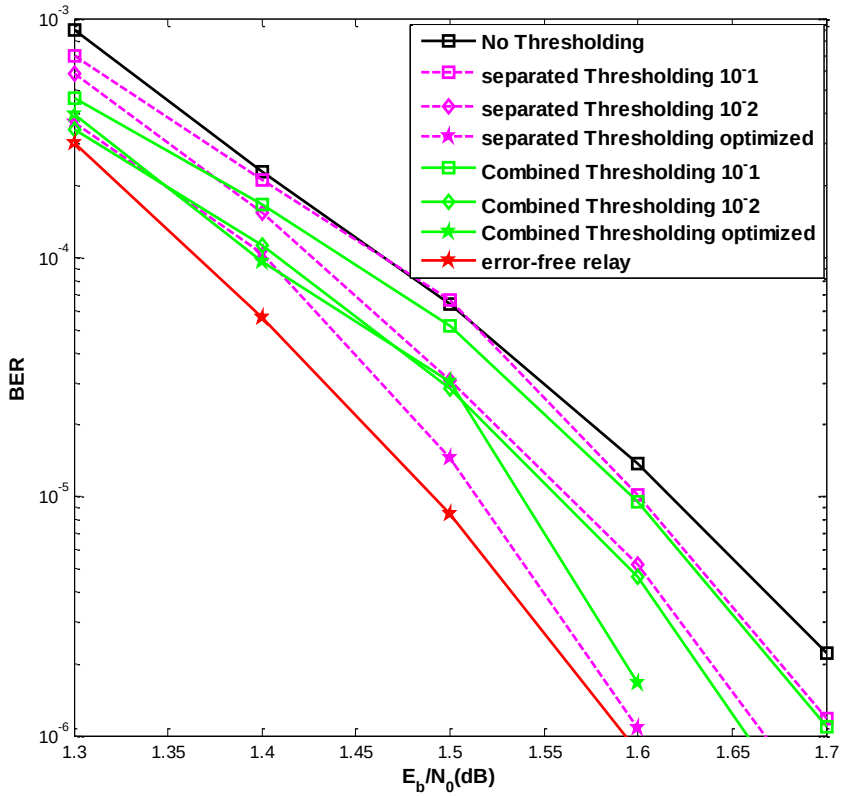


Fig.2 BER performance over AWGN channel

The results are depicted in Fig.2 for $SNR_{S_i,R_j} = SNR_{D,R_j}$, $N_{R_j,D} = 0.3$ over AWGN channel. We can see that the significant gain that separate thresholds provides over no thresholding at the relays, with the performance of separate thresholds displaying a gain of more than 0.18 dB at $\mathrm{BER} = 10^{-6}$ over no thresholding. Although we see a matching performance of combined thresholding and separate thresholding for $P_{eT} = 10^{-1}, 10^{-2}$. For $E_b / N_0 < 1.5\,\mathrm{dB}$, we find no difference between combined thresholding optimized and combined thresholding

$P_{eT}=10^{-2}$, but after that point we see that P_D^e using combined thresholding optimized is better than $P_{eT}=10^{-2}$. Finally we notice that the performance of combined thresholding performs worse than separate thresholds.

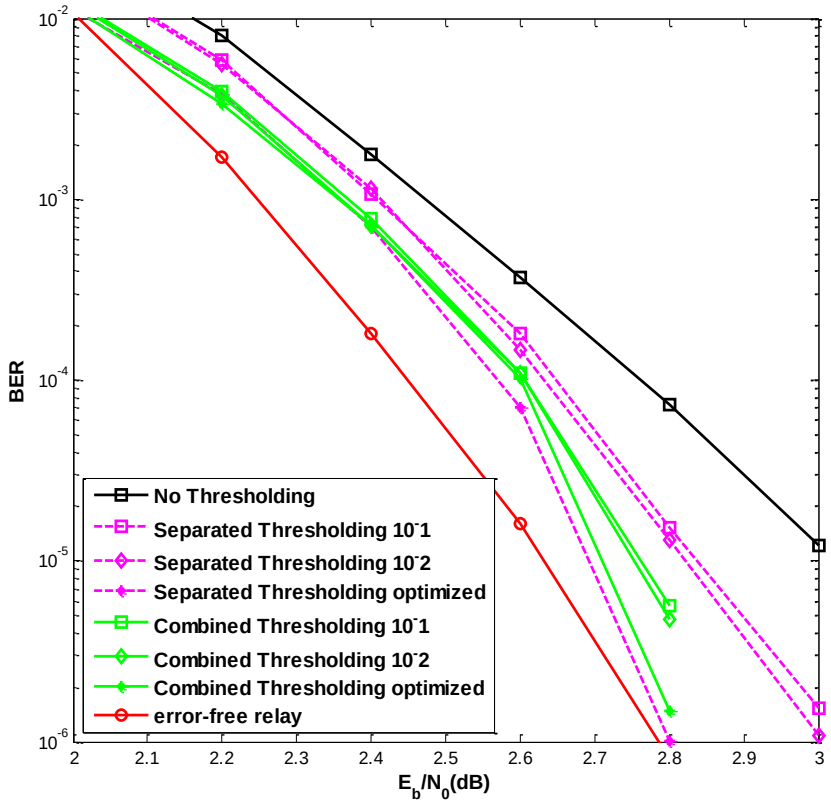


Fig.3 BER performance over Rayleigh fading channel

The results for the case are depicted in Fig.3 for $SNR_{S_i,R_j}=SNR_{D,R_j}+2$, $N_{R_j,D}=0.3$. Throughout the simulations, the channel is assumed that Rayleigh fading channel with $E\left[\left|h_{S_i,R_j}\right|^2\right]=E\left[\left|h_{S_i,D}\right|^2\right]=E\left[\left|h_{R_j,D}\right|^2\right]=1$. We can see that the significant gain that optimized thresholdes provides over no thresholding at the relays, with the performance of separated thresholds displaying a gain of more than 0.3dB and combined thresholds more than 0.2dB at BER $=10^{-5}$ over no thresholding. We see a matching performance of separated thresholding and combined thresholding for $P_{eT}=10^{-1}, P_{eT}=10^{-2}$. For $E_b/N_0<0.6$ dB, we find no difference of combined thresholding for all cases, but after that point we notice that the performance of combined thresholding optimized becomes better than $P_{eT}=10^{-1}, P_{eT}=10^{-2}$. However, we notice that the performance of separated thresholding for thresholding optimized performs better than $P_{eT}=10^{-1}, P_{eT}=10^{-2}$. We see that P_D^e using separated thresholding optimized performs better gain than other thresholds (where the performance without thresholding is significantly worse).

5. Conclusion

In this paper, a RS code based hybrid DF strategy at the relays has been proposed to mitigate error propagation in MUMR wireless networks. Our proposed technique relies on finding the reliability of bits at the relays, which can used to block the forwarding of unreliable bits. In addition, the optimal threshold derivation is derived to minimize bit error ratio (BER), and this technique is applied to separated cooperation and combined cooperation, respectively. Simulation results show that 0.01dB performance improvement with the proposed scheme in MUMR wireless networks at BER equal to 10-6 could be obtained when our proposed method was employed over both an AWGN channel and a fading channel. Applying the achieved guidelines, the noticeable performance improvement compared to of MUMR wireless networks with no the optimal threshold. This large performance gain could be achieved at the cost of slightly increased computational complexity. In terms of complexity it was shown that the performance of the optimal threshold for the separated cooperation was close to the combined cooperation while reducing the computational complexity of the LLR of the bit. In this paper, the effectiveness of our proposed method in mitigating error propagation in error-prone MUMR wireless

networks, which demonstrates that the proposed scheme may have potential use in MUMR wireless networks. However, their use in these specific scenarios needs further detailed analysis.

Acknowledgements

The authors acknowledge the 973 Program (2012CB316100).

References

[1] T. Cover and A. E. Gamal. “Capacity theorems for the relay channel”. IEEE Tran. Inf. Theory, 1979. 25, pp. 572-584.
[2] A. Nosratinia, T. E. Hunter, and A. Hedayat. “Cooperative Communication in Wireless Networks,” IEEE Communications Magazine, 2004, 42(10), pp. 74-80.
[3] J. Laneman, D. Tse, and G. Wornell. “Cooperative Diversity in Wireless Networks: Efficient Protocols and Outage Behavior”. IEEE Transactions on Information Theory, 2004, 50(12), pp. 3062-3080.
[4] B. Zhao and M.C. Valenti. “Distributed turbo codes diversity for the Relay Channel”. IEE Electronics Letters, 2003, 39(10), pp. 786-787.
[5] H. H. Sneessens, J. Louveaux, and L. Vandendorpe. “Turbo-coded decode-and-forward strategy resilient to relay errors”. in Proc. IEEE Int. Conf. Acoustics, Speech and Signal Processing ICASSP 2008, 2008, pp. 3213-3216.
[6] Y. Li, B. Vucetic, T. Wong, and M. Dohler. “Distributed Turbo Coding with Soft Information Relaying in Multihop Relay Networks”. IEEE Journal on Selected Areas in Communications, 2006, 24(11), pp. 2040-2050.
[7] H. V. Khuong and H. Y. Kong. “LLR-based decode-and-forward protocol for relay networks and closed-form ber expressions,” IE-ICE Tran. Fundamentals, 2006, 89, pp. 1832-1841.
[8] S. Li, R. W. Yeung, and N. Cai. “Linear network coding”. IEEE Tran. Inf. Theory, 2003, 49(2), pp. 371-381.
[9] R. Koetter and M. Mdard. “An algebraic approach to network coding”. IEEE/ACM Tran. Netw., 2003, pp. 782-795.
[10] C. Hausl, and J. Hagenauer, “Iterative network and channel decoding for the two-way relay channel”. in Proc. IEEE International Conference on Communication, 2006, 4, pp. 1568-1573.
[11] A. Y. C. Peng, S. Yousefi, and L. M. Kim, “On error analysis and distributed phase steering for wireless network coding over fading channels,” IEEE Tran. Wireless Commun, 2009, 8(11), pp. 5639-5649.
[12] M. Xiao and T. Aulin, “Optimal decoding and performance analysis of a noisy channel network with network coding,” IEEE Trans. Commun., 2009, 57, pp. 1402-1412.
[13] M. Xiao and M. Skoglund, “Multiple-user cooperative communications based on linear network coding,” IEEE Trans. Commun, 2010, 58, pp. 3345-3351.
[14] S. Y. Li, R. Yeung, and N. Cai, “Linear network coding”, IEEE Trans. Inform. Theory, 2003, 49(2), pp.371-381.
[15] S.W. Kim and E.Y. Kim, “Optimum receive antenna selection minimizing error probability,” WCNC2003, 2003, 1, pp.441-447.

第40卷，第8期
2019年8月
中国农业资源与区划
Chinese Journal of Agricultural Resources and Regional Planning
Vol. 40，No. 8，pp171-176
August，2019

doi：10.7621/cjarrp.1005-9121.20190821

中文文章叫近20年，英文文章是1996 to 2016，文章完全一样

·资源利用·

近20年中国耕地数量变化趋势及其驱动因子分析*

王静怡[1]，李晓明[2※]

（1. 西安石油大学计算机学院，陕西西安 710065；2. 陕西省土地工程建设集团有限责任公司，西安 710075）

摘 要 【目的】研究“二调”前后近20年我国耕地面积的变化趋势及其影响因子，为促进耕地保护和土地资源的高效集约节约利用提供决策支撑。【方法】基于1996—2016年耕地数量的原始统计数据，利用数据挖掘技术选用ARIMA模型，基于两次全国土地调查时间段耕地数量数据进行相互预测和反推，即利用1996—2008年耕地数量数据预测2009年耕地数量，利用2009—2016年数据反推2008年耕地数量，从而实现数据的校正和比值归一化的目的，进一步研究近20年内我国耕地数量的变化趋势，并通过相关性分析研究遴选出其驱动因子。【结果】趋势研究结果表明，近20年内我国耕地数量呈现逐年递减的趋势，其中2004年之前递减速度较快，之后递减速度趋缓。相关性分析结果显示，第一产值增加值占比、年末总人口数，以及城镇人口数是影响耕地数量变化的重要驱动因子，其相关系数分别为0.959，-0.918，-0.896。【结论】从研究结果可以推论，我国在社会经济发展中的产业结构布局，以及城镇化建设进程对耕地数量变化产生了重要的影响。

关键词 数据挖掘 ARIMA模型 耕地数量 变化趋势 驱动因子

中图分类号：P96 **文献标识码**：A **文章编号**：1005-9121【2019】08171-06

0 引言

我国是一个农业大国，耕地资源直接关系到国家粮食安全问题，是确保“中国人的饭碗牢牢端在自己手中”的重要基础。同时，在加快推进我国社会主义现代化建设进程中，经济建设对土地的旺盛需求也对耕地保护带来了极大的挑战[1]。对于我国耕地的变化趋势及其影响驱动力的研究，一直都是一个热点问题，甚至有专家学者通过史册文献资料的查证对过去300年我国部分省区耕地资源数量变化及驱动因素进行了研究[2]。

目前，对于我国耕地变化趋势的研究，多基于对统计数据进行分析，从空间尺度上可以分为国家尺度和区域尺度的研究。其中，对于国家尺度上的研究，由于统计标准、技术手段等多种因素的限制，2008—2009年数据发生明显的跳跃式变化，所以绝大部分的研究均处于2008年之前的部分时间段内，如毕于运等[3]通过对我国建国至1996年实有耕地面积的收集整理研究分析了其变化分析；李秀彬[4]对1999年我国前20年耕地面积变化的总体趋势、空间特征和驱动因子进行了研究；曹银贵[5]研究分析了1996—2005年全国耕地变化的情况及其影响的主要因子；黄忠华、吴次芳等利用1978—2007年我国耕地、经济增长、城镇化、地方财政收入数据分析了社会经济因素对耕地变化的影响[6]。以上研究均将时间局限在2008年之前，而回避了2008—2009年耕地统计数据跳跃的现象，这不利于科学研究我国耕地的变化趋势和指导耕地保护工作。对于区域尺度，如省级，甚至市县级尺度，由于统计基数较小，受统计方法、技术标准等因素的影响不大，几乎各个省份区域都有专家对其耕地变化和驱动因子进行了大量研究，如郭丽英等[7]

收稿日期：2018-03-26

作者简介：王静怡（1984—），女，陕西榆林人，博士、讲师。研究方向：资源利用和数据科学

※通讯作者：李晓明（1983—），男，山东烟台人，博士、高级工程师，硕士生导师。研究方向：土地资源利用和遥感信息。Email：xmlisdc@126.com

* 资助项目：陕西省教育厅科研计划项目“无线MARC系统中联合网络—信道编码的优化设计研究”（18JK0626）

(C)1994-2022 China Academic Journal Electronic Publishing House. All rights reserved. http://www.cnki.net

分析了 1996—2008 年我国沿海地区耕地变化的基本态势、时空特征及其主导成因；吴霞等[8]选取 1997—2014 年宁夏耕地面积数据分析耕地面积变化趋势及其驱动因子；武江民等[9]专门针对甘肃兰州市研究其耕地动态变化与驱动力的定量关系。还有学者则基于基于国家、区域、省域、市县不同尺度研究了中国耕地变化的驱动力[10]；

20 世纪 80 年代以来，随着遥感等 3S 技术的发展应用，诸多学者开始不仅仅局限于统计数据的应用，开始借助遥感信息技术对耕地变化进行研究。如张国平、刘纪元等[11]利用中国资源环境数据库及遥感影像对 20 世纪 80 年代末至 2000 年的中国耕地时空变化进行了分析；田光进、庄大方等[12]通过对遥感图像解译研究 80 年代末与 90 年代末 10 年间耕地时空动态变化特征；刘旭华，王劲峰等使用中国 1987—1989 年和 2000 年两期土地利用遥感调查数据，探索定量化研究国家尺度土地利用变化的驱动力[13,14]；许丽丽等[15]基于中分辨率卫星遥感数据，深入分析了 2000—2010 年中国耕地变化及其空间差异，并对中国耕地占补平衡政策的实施效果进行了评估；李景刚等[16]选取 1983—2001 年 NOAA 等遥感数据分析了北方 13 省的耕地变化与驱动力。遥感信息技术的应用开拓了耕地变化研究的新途径，但是由于遥感解译的精度仍有待于进一步提高，所以一定程度上制约了对于耕地变化的研究。

多来以来，我国对于耕地数量的数据统计有多种来源，其中以国土资源部的统计数据被认为最权威[17]。由于遥感影像解译精度，与实地调查统计相比仍有一定差距，所以大部分学者仍采用统计数据进行研究，而且大多避开了数据有明显变化的过渡年份。目前仅有极少数学者对过渡年份前后时间段的统计数据变化一并进行了相关的分析[17,18]。针对两次全国土地调查的统计数据的跳跃式变化，文章研究提出了基于数据挖掘技术研究分析两个时间段的数量关系，以更科学地反映耕地数量的变化趋势，同时基于校正数值研究影响耕地变化的驱动因子，这在目前的研究中尚未见到，对于科学反映我国耕地变化趋势具有积极的意义。

1 数据与方法

1.1 数据获取

1.1.1 全国耕地数量数据

我国耕地数量，尤其是历史时期的耕地数量，长期以来难以确定。国家土地管理部门从 1986 年开始，每年统计并公布我国耕地的增减情况，虽然还有其他职能部门的统计数据，但仍以国土资源部的数据最为权威[17]。为准确掌握全国耕地数量，1984—1996 年国务院安排开展了全国第一次大规模的土地利用现状调查，数据成果统计到了 1996 年 10 月 31 日，结果表明，1996 年全国耕地面积约为 1.300 亿 hm^2（19.51 亿亩）[18]，这一统计数据被认为具有最高可信度[19]。随后，1996—2008 年耕地面积数据均可直接从统计公报中查得。

为进一步准确掌握耕地土地基础数据，国家于 2007 年 7 月 1 日起，启动了第二次全国土地调查，数据统计时间节点为 2009 年 12 月 31 日，统计结果显示 2009 年我国耕地面积为 1.354 亿 hm^2（20.31 亿亩）[18]。随后的每年都有二调变更调查，2007—2016 年每年的全国耕地面积都可以从国家土地调查成果服务平台直接查得。由于第二次全国土地调查采用的技术方法的改进等原因，2008 年与 2009 年的耕地数量存在“跳跃”现象，为科学分析耕地的变化趋势，这一现象问题在后文中进行了着重的研究处理。

1.1.2 驱动因子数据

土地与人类社会的经济发展密不可分，全国耕地变化是在地理背景制约下、社会经济条件、灾害等自然条件共同驱动下发生的[1]，为探索研究耕地变化的驱动因子，该文主要选取了 3 方面共 17 个因子指标做遴选分析：一方面是反映全国经济发展水平的综合类指标，包括国民总收入、国内生产总值、第一产业增加值及比例、第二产业增加值及比例、第三产业增加值及比例、人均国内生产总值、工业增加值、建筑业增加值、农业总产值；另一方面是反映社会城镇化水平的指标，包括年末总人口、城镇人口、乡村人口；还有第三方面是反映自然灾害的指标，包括受灾面积和粮食产量[20]。上述因子指标近 20 年的数据均

(C)1994-2022 China Academic Journal Electronic Publishing House. All rights reserved. http://www.cnki.net

直接从国家统计局网站查得。

1.2　研究方法

该文研究通过对近 20 年全国耕地数量数据的分析处理，研究其变化趋势，进而通过与选取的因子进行相关性分析，研究其变化的驱动因子。其中，在对 1996—2016 年耕地面积的数据分析中，针对 2008—2009 年数据的跳跃现象，通过数据挖掘，一方面利用 1996—2008 年数据预测 2009 年数据，另一方面利用 2009—2016 年数据反推 2008 年数据，基于上述两种相互预测或反推得出的数值，分析 2008 年和 2009 年耕地数量的数据比例关系，进而对 1996—2016 年耕地面积数据进行比值归一化，以探索研究耕地面积的变化趋势。

该文在数据挖掘预测中，通过遴选对比最终采用的为 ARIMA 模型，即自回归积分滑动平均模型(Autoregressive Integrated Moving Average Model)，是由博克思(Box)和詹金斯(Jenkins)提出的著名时间序列预测方法，主要是指将非平稳时间序列转化为平稳时间序列，然后将因变量仅对它的滞后值以及随机误差项的现值和滞后值进行回归所建立的模型，适用于该文的研究。

2　近 20 年耕地数量变化趋势分析

2.1　基于耕地数量原始统计数据的变化趋势及分析

通过对收集整理的 1996—2016 年耕地数量数据分析，如图 1，可以看出，1996—2008 年全国耕地面积逐年减少，其中以 2000—2004 年递减速度最快；2008—2009 年耕地面积数据出现跳跃，由 1.217 亿 hm^2(18.26 亿亩)增至 1.354 亿 hm^2(20.31 亿亩)；2009—2016 年耕地面积递减速度非常缓慢。

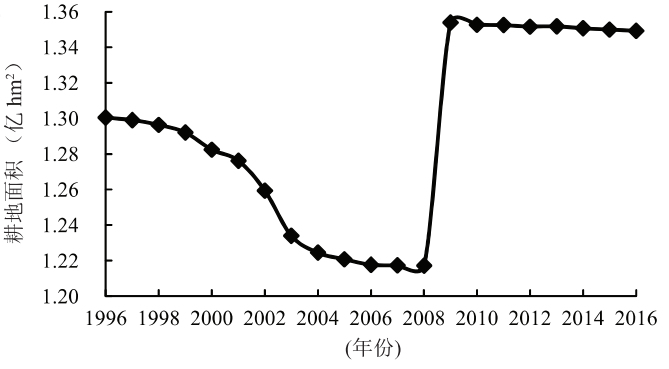


图 1　1996—2016 年基于原始统计数据的耕地数量变化趋势

1996 年国家完成了第一次大规模的土地利用现状调查；2009 年第二次全国土地利用现状调查完成。由此可见，2008—2009 年耕地面积数据的跳跃正是一调与二调数据的分界年份。全国耕地面积是否真的增多了约 0.14 亿 hm^2(2 亿亩)，经文献查阅分析[17,18,21]，主要原因在于二调采用了更为先进的技术手段，将以往少报的耕地面积统计入库，进一步提高了数据的准确度。所以，近 20 年全国耕地数量的统计数据是基于两次不同的技术水平，可直接分别研究各自时段内的变化趋势，但如果要研究连续 20 年时间段内的变化趋势，就须对两个时间段的数据进行校正，使之具有可对比性。

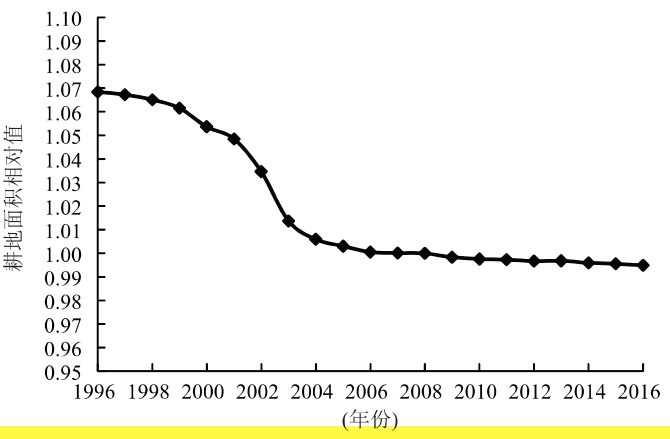


图 2　1996—2016 年基于校正后相对数据的耕地变化趋势

2.2　基于数据挖掘的耕地数量校正

数据挖掘技术在时间序列上具有强有力的预测功能，该文首先利用 1996—2008 年耕地数量数据，预测 2009 年的耕地数量，由此得出 2009 年与 2008 年耕地数量的比值关系 α；然后利用 2009—2016 年耕地数量数据，反推 2008 年的耕地数量，由此得出 2009 年与 2008 年耕地数量的比值关系 β；为更为科学地反映 2009 年与 2008 年耕地数量的比值关系，取利用正向预测与反向反推两种方法得出的 α 与 β 的算数平均值 ρ 作为实际的数量比值关系。

该文研究在预测过程中，利用 SPSS 软件，通过比较分析，在正向预测 2009 年数值和反向反推 2008

(C)1994-2022 China Academic Journal Electronic Publishing House. All rights reserved.　http://www.cnki.net

年数值中均选用 ARIMA 模型，其中正向预测选用的模型为 ARIMA（1，1，2）（$r^2=0.975^{**}$），反向反推选用的模型为 ARIMA（1，1，4）（$r^2=0.966^{**}$），两者均在 0.01 水平呈现显著性。由此，基于 1996—2008 年数据预测得出的 2009 年耕地数量为 1.213 387 亿 hm^2（18.200 8 亿亩），基于 2009—2016 年数据反推得出的 2008 年耕地数量为 1.353 987 亿 hm^2（20.309 8 亿亩），进一步可得出 $\alpha=996\ 899.887\ E-6$，$\beta=999\ 895.617\ E-6$，则 $\rho=998\ 397.752\ E-6$，由此推测 2009 年与 2008 年耕地数量的比值为998 397.752 E－6，即可为两个时间段数据的校正系数。

2.3 基于耕地数量校正相对值的变化趋势分析

为进一步客观的反映近 20 年的耕地数量变化趋势，对全部年份数据进行比值归一化及系数校正，在前文研究基础上，首先对 1996—2008 年全部原始耕地数量数据以 2008 年耕地数量为基数计算得到的比值即为其耕地数量相对值，对 2009—2016 年全部原始耕地数量数据以 2009 年耕地数量为基数计算得到的比值，再乘以校正系数 ρ，即为其相应年份的耕地数量相对值。由此可以得出 1996—2016 年耕地数量的变化趋势，如图 2 所示，可以看出，近 20 年全国耕地数量是呈现递减趋势的，其中 2004 年以前，递减速度较快，2004 年以后耕地数量递减速度较缓，尤其是 2006 年以后耕地数量递减速度趋于稳定。

3 耕地数量变化驱动因子分析

该文研究共收集了 1996—2016 年共 17 个因子指标，首先进行描述性特征统计，如表 1 所示；然后，通过分析耕地数量与各因子指标的相关性（表 2），进行对比分析，以此遴选出耕地数量变化的驱动因子。

表 1 1996—2016 年各因子指标的描述性统计特征

因子	最小值	最大值	平均值	标准差
国民总收入（亿元）	70 780	741 140	304 446.950	225 956.601
国内生产总值（亿元）	71 814	744 127	305 718.670	226 519.843
第一产业增加值（亿元）	13 878	63 671	31 240.710	17 742.619
第一产业增加值占比（%）	8.556	19.325	12.114	3.280
第二产业增加值（亿元）	33 828	296 236	135 629.240	94 949.577
第二产业增加值占比（%）	39.810	47.559	45.327	1.999
第三产业增加值（亿元）	24 107	384 220	138 848.860	114 605.836
第三产业增加值占比（%）	33.569	51.634	42.560	4.472
人均国内生产总值（亿元）	5 898	53 980	22 872	16 332.770
工业增加值（亿元）	29 530	247 860	116 532.760	79 508.293
建筑业增加值（亿元）	4 393	49 522	19 623	15 992.727
年末总人口（万人）	122 389	138 271	131 047.710	4 702.171
城镇人口（万人）	37 304	79 298	58 413.240	12 989.267
乡村人口（万人）	58 973	85 085	72 634.480	8 313.397
农业总产值（亿元）	13 540	59 288	28 842.620	16 570.347
粮食产量（万 t）	43 070	62 144	52 326.480	5 812.061
受灾面积（万 hm^2）	2 177	5 468.8	4 100.948 0	1 070.630

由表 2 可以看出，基于原始统计的耕地面积研究其与各因子指标的相关性，由于数据的跳跃不足以反映耕地变化的实际趋势，与各因子指标的相关性均不高。基于校正后的耕地数量的相对值，研究其与各因子指标的相关性，可以发现，与第一产值增加值占比的相关性最高，相关系数高达 0.959；与年末总人口的相关性次之，为负相关，系数为 －0.918，城镇人口和乡村人口与之的相关性也较高，即第一产业增加值占比，总人口以及城镇人口数量与耕地数量的变化相关性较好，是重要的驱动因子。由此，可以推论出国家产业结构布局调整、我国城镇化建设水平是影响我国耕地数量变化的重要因素条件。耕地作为第一产

(C)1994-2022 China Academic Journal Electronic Publishing House. All rights reserved. http://www.cnki.net

表 2　耕地面积与各因子的相关系数矩阵

	原始统计耕地面积	校正后耕地面积相对值		原始统计耕地面积	校正后耕地面积相对值
原始统计耕地面积	1	-0.142	人均国内生产总值	0.651	-0.749
校正后耕地面积相对值	-0.142	1	工业增加值	0.638	-0.784
国民总收入	0.649	-0.746	建筑业增加值	0.688	-0.716
国内生产总值	0.652	-0.745	年末总人口	0.433	-0.918
第一产业增加值	0.663	-0.736	城镇人口	0.488	-0.896
第一产业增加值占比	-0.274	0.959	乡村人口	-0.518	0.88
第二产业增加值	0.647	-0.774	农业总产值	0.686	-0.709
第二产业增加值占比	-0.519	0.259	粮食产量	0.752	-0.524
第三产业增加值	0.649	-0.717	受灾面积	-0.514	0.708

业的最重要的载体之一，与第一产业增加值密切正相关，我国产业结构中对于第一产业布局要求会直接诱使我国耕地的变化。而城镇化建设过程中，一方面由于城镇建设会直接占用大量的耕地，另一方面，城镇化建设中大量的农民人口直接进入城镇生活，或者进城务工而导致耕地撂荒，所以城镇化建设水平与耕地变化呈现密切的负相关。

4　结论与讨论

土地本身既有自然属性，又有社会属性，对于耕地数量的统计长期以来受社会、经济、政策等诸多因素的影响，导致难以对其进行长时间序列的趋势研究。该文研究的时间序列跨度全国两次土地调查的统计数据，两个时间阶段的数据具有明显的跳跃性，但并不代表 2009 年耕地数量真的比 2008 年大幅度增长。究其原因，主要是由于第二次全国土地调查中应用遥感等新方法、统一了标准，提高了调查的技术水平和准确度，使原来因少报、漏报、瞒报等各种原因未被统计到的耕地重新统计入库，所以要研究跨两个阶段的整体变化趋势，就必须研究建立其数值量化关系。该文通过数据挖掘，并对耕地数量进行校正和比值归一化，研究结果比较准确地反映了我国耕地变化趋势的实际情况。

研究结果表明，近 20 年，我国耕地数量呈现递减趋势，其中 2004 年以前递减速度较快，2004 年以后递减速度趋缓，我国产业结构布局方面，主要是第一产业增加值占比，以及我国人口总数方面，主要是城镇化人口数量是影响变化的主要驱动因子。由于 1999 年后开始生态退耕导致耕地数量迅速减少[17,22]，2004 年国家《土地管理法》修订后强调要加强耕地保护，实行占补平衡，对我国耕地的数量变化产生了积极作用。该文仅对近 20 年我国耕地数量的变化趋势进行了分析；现在国家加强耕地保护，不仅以数量为基础，更关注质量，以产能为核心，实现数量、质量和生态的三位一体保护[23]，下一步将对全国耕地质量的变化趋势进一步分析研究。同时，该文研究通过相关性分析研究提出了主要驱动因子，下一步还将进一步对驱动因子的贡献率进行量化分析研究。

该文研究仅对 1996—2016 年耕地数量的变化趋势进行了分析研究，由于对诸多指标因子数据统计的完整性需求，未对更长时间的耕地变化趋势进行研究。下一步，将在对统计数据分析的基础上，通过对遥感影像的数据挖掘，深入研究更长时间序列的变化趋势。

参考文献

[1] 赵其国，周生路，吴绍华，等. 中国耕地资源变化及其可持续利用与保护对策. 土壤学报，2006，43（4）：662－672.

[2] 葛全胜，戴君虎，何凡能，等. 过去 300 年中国部分省区耕地资源数量变化及驱动因素分析. 自然科学进展，2003，13（8）：825－832.

[3] 毕于运，郑振源. 建国以来中国实有耕地面积增减变化分析. 资源科学，2000，22（2）：8－12.

[4] 李秀彬. 中国近 20 年来耕地面积的变化及其政策启示. 自然资源学报，1999，14（4）：329－333.

(C)1994-2022 China Academic Journal Electronic Publishing House. All rights reserved.　http://www.cnki.net

[5] 曹银贵，袁春，周伟，等. 中国耕地变化的驱动因子及其省域差异分析. 中国土地科学，2008，22（2）：17－22.
[6] 黄忠华，吴次芳，杜雪君. 我国耕地变化与社会经济因素的实证分析. 自然资源学报，2009，24（2）：192－199.
[7] 郭丽英，王道龙，王介勇. 中国沿海地区耕地变化及其成因分析. 中国农业资源与区划，2012，33（1）：6－10.
[8] 吴霞，王世荣，尚红莺，等. 宁夏近 18 年来耕地面积动态变化及驱动力分析. 中国农业资源与区划，2017，38（8）：98－104.
[9] 武江民，赵学茂，党国锋. 甘肃兰州市耕地动态变化与驱动力关系定量研究. 干旱区资源与环境，2010，24（12）：33－38.
[10] 于天，曹银贵，许婧雪. 基于不同尺度的中国耕地变化驱动力研究进展. 中国农学通报，2016，32（24）：194－198.
[11] 张国平，刘纪远，张增祥. 近 10 年来中国耕地资源的时空变化分析. 地理学报，2003，58（3）：323－332.
[12] 田光进，庄大方，刘明亮. 近 10 年中国耕地资源时空变化特征. 地球科学进展，2003，18（1）：30－36.
[13] 刘旭华，王劲峰，刘纪远，等. 国家尺度耕地变化驱动力的定量分析方法. 农业工程学报，2005，21（4）：56－60.
[14] 刘旭华，王劲峰，刘明亮，等. 中国耕地变化驱动力分区研究. 中国科学 D 辑地球科学，2005，35（11）：1087－1095.
[15] 许丽丽，李宝林，袁烨城，等. 2000—2010 年中国耕地变化与耕地占补平衡政策效果分析. 资源科学，2015，37（8）：1543－1551.
[16] 李景刚，何春阳，史培军，等. 近 20 年中国北方 13 省的耕地变化与驱动力. 地理学报，2004，59（2）：274－282.
[17] 封志明，刘宝勤，杨艳昭. 中国耕地资源数量变化的趋势分析与数据重建：1949—2003. 自然资源学报，2005，20（1）：35－43.
[18] 谭永忠，何巨，岳文泽，等. 全国第二次土地调查前后中国耕地面积变化的空间格局. 自然资源学报，2017，32（2）：186－197.
[19] Lin G C S，HO S P S. China's land resources and land-use change：insights from the 1996 land survey. land Use Policy，2003，20（2）：87－107.
[20] 傅泽强，蔡运龙，杨友孝，等. 中国粮食安全与耕地资源变化的相关分析. 自然资源学报，2001，16（4）：313－319.
[21] 张雅琼，杨子生. 我国两次土地资源调查的对比分析. 国土资源科技管理，2013，30（2）：100－104.
[22] 徐宪立，蔡玉梅，张科利，等. 耕地资源动态变化及其影响因素分析. 中国人口·资源与环境，2005，15（3）：75－79.
[23] 谭永忠，吴次芳，王庆日，等. “耕地总量动态平衡”政策驱动下中国的耕地变化及其生态环境效应. 自然资源学报，2005，20（5）：727－734.

RESEARCH ON THE CHANGE TREND OF FARMLAND QUANTITY IN CHINA FOR RECENT 20 YEARS AND ITS DRIVING FACTORS*

Wang Jingyi[1], Li Xiaoming[2]※

(1. Xi'an Shiyou University, Xi'an, Shaanxi 710065, China;
2. Shaanxi Provincial Land Engineering Construction Group, Xi'an, Shaanxi 710075, China)

Abstract The research aims to research the changing trend of farmland quantity for recent 20 years before and after the second national land use survey. It could provide decision support for farmland protection and efficient use of land resources. The original data of farmland area from 1996 to 2016 were collected, data mining technology was introduced, and ARIMA model was chosen to predict the farmland quantity each other based on the farmland area of the twice land use survey, which meant to predict the farmland quantity of 2009 with the farmland quantity of the years from 1996 to 2008, and to predict the farmland quantity of 2008 inversely with the farmland quantity of the years from 2009 to 2016, so the original farmland area data could be corrected and normalized. Then the changing trend of farmland quantity for recent 20 years was studied furtherly and correlation analysis was used to study the driving factors. The trend research result showed, the farmland area decreased year by year for recent 20 years, the decreasing rate was faster before 2004, and then it decreased slowly. The correlation analysis result showed, the added value proportion of primary industry, the total population, and the urban population were the most important driving factors which influenced the farmland quantity change, their coefficients were 0.959, －0.918 and －0.896 respectively. It could be concluded by the result that the industry configuration and the urbanization could affect the farmland quantity with the development of social economy.

Keywords data mining; ARIMA model; farmland quantity; change trend; driving factors

(C)1994-2022 China Academic Journal Electronic Publishing House. All rights reserved. http://www.cnki.net

doi:10.3969/j.issn.1001-2400.2013.02.003

适用于网络 LDPC 码的速率兼容算法

王静怡[1,2]，李 颖[1,2]，孙 岳[1,2]

(1. 西安电子科技大学 综合业务网理论及关键技术国家重点实验室，陕西 西安 710071；
2. 电信科学研究院 无线移动通信国家重点实验室，北京 100083)

摘要：提出了一种可以获得最小比特错误概率的网络低密度奇偶校验(LDPC)码速率兼容删余算法，并推导了该算法的译码错误概率. 该算法基于网络 LDPC 码的结构特点，以达到译码最小比特错误概率为目标，在网络 LDPC 码的 Tanner 图上搜索出需要删余的变量节点，以获得最优的删余图样. 仿真结果表明，该算法比现有算法在 BER 为 10^{-4} 时有 0.4 dB 的性能增益.

关键词：多址接入中继网络；LDPC 码；网络 LDPC 码；速率兼容；删余

中图分类号：TN911.22 **文献标识码**：A **文章编号**：1001-2400(2013)02-0013-05

Rate-compatible network LDPC codes

WANG Jingyi[1,2], *LI Ying*[1,2], *SUN Yue*[1,2]

(1. State Key Lab. of Integrated Service Networks, Xidian Univ., Xi'an 710071, China; 2. State Key Lab. of Wireless Mobile Communications, China Academy of Telecommunication Technology, Beijing 100083, China)

Abstract: A rate-compatible puncturing algorithm for network LDPC codes is proposed to achieve the minimum error probability, and decoding error probability is derived. The algorithm for finding variable nodes to be deleted based on the tanner graph of network LDPC codes is proposed, which is aimed at minimizing the decoding error probability and optimizing the puncturing pattern. Simulation results illustrate that, at BER = 10^{-4}, the proposed rate-compatible network LDPC codes have a coding gain of about 0.4 dB compared with the codes obtained via the existing punctured methods.

Key Words: multi-access relay network; low-density parity-check (LDPC) codes; network LDPC code; rate-compatible; puncturing

由于无线移动信道具有衰落和时变特性，为最大限度地利用信道容量，可采用链路自适应技术，使信道编码速率、调制方式、信号功率等参数能够随信道质量的变化而变化. 链路自适应技术的基础是速率兼容纠错码的设计，其基本概念由文献[1]首次提出，速率兼容低密度奇偶校验(LDPC)码的设计则是近几年的研究热点. 文献[2-3]通过分组和排序操作，将 LDPC 码的变量节点按照迭代恢复次数进行分类，设计了 LDPC 码速率兼容删余算法，可以获得比随机删余更好的性能. 文献[4]首次提出了一种基于有限域上非零元素二进制镜像的缩短码构造方案，用来实现低码率的速率兼容多元 LDPC 码. 文献[5]研究了码率从 1/10 到 5/6 的灵活变化的非规则多元 LDPC 码比特级缩短算法. 文献[6]以多维累加交叉并行级联单奇偶校验码为母码，对奇偶校验比特按组删余，构建了一组速率兼容编码.

上述速率兼容算法都是针对点对点通信链路设计的. 然而，随着无线通信技术的发展和中继协作传输技术的引入，信道编码的设计也从点对点链路推广至无线中继网络. 对于多址接入中继网络，有多个节点同时

收稿日期：2012-06-09 网络出版时间：2012-11-16

基金项目：国家自然基金资助项目(61072064)；国家科技重大专项资助项目(2010ZX03003-003-03)；长江学者和创新团队发展计划资助项目(IRT0852)；中央高校科研业务费专项资金资助项目(K50510010026)

作者简介：王静怡(1984－)，女，西安电子科技大学博士研究生，E-mail：wangjy@stu.xidian.edu.cn.

网络出版地址：http://www.cnki.net/kcms/detail/61.1076.TN.20121116.0924.201302.16_009.html

(C)1994-2023 China Academic Journal Electronic Publishing House. All rights reserved. http://www.cnki.net

需要中继节点帮助转发数据,在中继节点设计有效的联合网络-信道编码算法,可在改善接收端性能的同时,有效提高转发效率. 文献[7]利用 LDPC 码,针对多址接入中继信道设计了一种网络 LDPC 码,并指出可以通过调整中继节点转发数据量来实现中继转发效率和接收端译码性能的有效折中. 与单个 LDPC 码相比,网络 LDPC 码的校验矩阵包括了源节点和中继节点所采用 LDPC 码的校验矩阵,因此其本质上可看做是一种多用户码. 另外,单个 LDPC 码的所有编码比特是在同一个信道中传输,所有编码比特受到相同的噪声干扰,网络 LDPC 码的编码比特则由对应的源节点和中继节点分别传输,不同传输链路将会受到不同的噪声干扰. 笔者将根据网络 LDPC 码的上述特性,设计相应的速率兼容算法.

1 适用于多址接入中继信道的网络 LDPC 码

由两个源节点、一个中继节点和一个目的节点构成的多址接入中继网络模型如图 1 所示. 两个源节点与目的节点之间的信息传输由广播发送和中继转发两个阶段完成. 在广播阶段,两个源节点分别向中继节点和目的节点广播发送编码序列 X_1 和 X_2;在中继转发阶段,中继节点首先对接收信号进行译码,得到两个源节点的估计数据,然后对译码得到的估计数据重新进行联合编码,并将编码序列 X_R 转发至目的节点. 目的节点则根据收到的信号进行联合译码,得到两个源节点的估计信息.

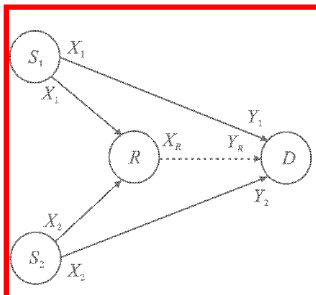


图 1 多址接入中继信道模型

目的节点将两个源节点和中继节点采用的 LDPC 码综合考虑,可得到如下校验矩阵:

$$\boldsymbol{H}=\begin{bmatrix}\boldsymbol{H}_1 & \boldsymbol{0} & \boldsymbol{0}\\ \boldsymbol{0} & \boldsymbol{H}_1 & \boldsymbol{0}\\ \boldsymbol{A} & \boldsymbol{B} & \boldsymbol{C}\end{bmatrix}, \tag{1}$$

其中,$\boldsymbol{H}_1$ 是源节点采用 LDPC 码的校验矩阵,$\boldsymbol{H}_3=[\boldsymbol{A},\boldsymbol{B},\boldsymbol{C}]$,是中继节点采用 LDPC 码的校验矩阵,$\boldsymbol{0}$ 是零矩阵. 由于式(1)中包含了源节点和中继节点所采用 LDPC 码的校验矩阵,并且中继节点是对两个源节点的数据进行联合编码,因此文献[7]称之为网络 LDPC 码,该码的 Tanner 图如图 2 所示.

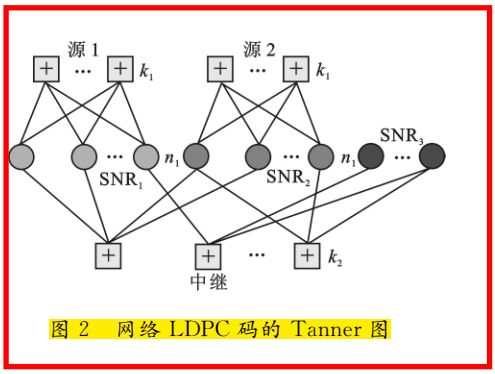


图 2 网络 LDPC 码的 Tanner 图

图 2 中网络 LDPC 码的 Tanner 图包含上下两层子图,其中上层子图包含 $2k_1$ 个校验节点,它们与变量节点的连接关系由 $\boldsymbol{H}_1$ 确定;下层子图包括 k_2 个校验节点,它们与变量节点的连接关系由式(1)中的 $\boldsymbol{H}_3$ 确定. 图中每个变量节点的度用 (i,j) 表示,其中 i 为变量节点与上层校验节点相连的边数,j 为变量节点与下层校验节点相连的边数. 用 d_c 和 d_c' 分别表示上层和下层校验节点的度数.

2 速率兼容网络 LDPC 码的设计

由图 2,网络 LDPC 码的变量节点包含两个源节点所采用的 LDPC 码的变量节点和中继节点所采用的联合 LDPC 码的变量节点,且不同变量节点通过不同的信道达到目的节点. 因此,需要考虑上述特点对删除变量节点恢复概率的影响,并由此设计适用于网络 LDPC 码的速率兼容算法.

2.1 几个定义

定义 1 若被删余的校验比特所对应的变量节点在迭代过程中接收到非零信息,则无论获得的信息正确与否,都称之为“恢复”[2].

定义 2 译码中第 n 次迭代时才恢复的被删除的变量节点称为 n 步恢复变量节点,用 n-SR 表示,而所有 n-SR 构成的集合则用 G_n 表示[2].

图 3 给出了一个包含 1-SR 节点、2-SR 节点的恢复树,其中竖线圆表示幸存的删余变量节点 S(v),横线圆表示未删余变量节点,方块表示校验节点.

第296页,共397页
(C)1994-2023 China Academic Journal Electronic Publishing House. All rights reserved. http://www.cnki.net

定义 3　如果一个一步恢复的删余变量节点至少与一个校验节点相连,且与这个校验节点相连的变量节点没有被完全删余掉,那么称这个校验节点为幸存校验节点[2]. 图 3 中的校验节点 S_1 和 S_2 即为幸存校验节点,而校验节点 D 则为死校验节点.

定义 4　幸存校验节点相连的其余未被删除的变量节点称为幸存变量节点.

由图 2 可见,网络 LDPC 码的编码比特是通过 3 个不同信道到达接收端的,因此,在设计网络 LDPC 码的删余算法时,不仅要考虑被删余变量节点的幸存邻居变量节点数,还要考虑每个幸存邻居变量节点受到的噪声大小. 下面,引入等效幸存变量节点数的概念.

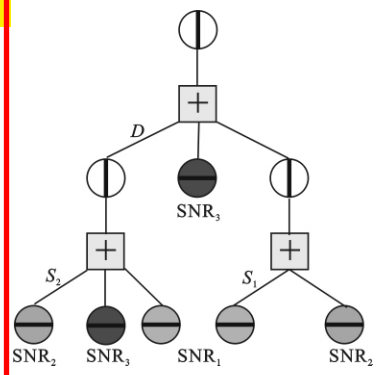


图 3　网络 LDPC 码的恢复树

定义 5　假设网络 LDPC 码所有编码比特在传输过程中受 K 种噪声干扰,其对应的噪声方差分别为 $\sigma_1^2>\sigma_2^2>\cdots>\sigma_K^2$,令每个受到噪声干扰最大(噪声功率为 σ_1^2)的幸存邻居变量节点的等效幸存邻居变量节点数为 1,则受其他噪声干扰的幸存邻居变量节点的等效幸存邻居变量节点数定义为

$$\alpha_i=\left\{\log\left(1-\varphi\left(\frac{2}{\sigma_i^2}\right)\right)\Big/\left[\log\left(1-\varphi\left(\frac{2}{\sigma_1^2}\right)\right)\right]\right\}\leqslant 1\quad,\quad i=1,2,\cdots,K\quad, \tag{2}$$

其中

$$\varphi(x)=\begin{cases}\dfrac{1}{(4\pi x)^{1/2}}\displaystyle\int_R\tanh\frac{u}{2}\exp\left(-\frac{(u-x)^2}{4x}\right)\mathrm{d}u\quad, & x>0\quad,\\ 0\quad, & x=0\quad.\end{cases}$$

2.2　译码恢复错误概率

将网络 LDPC 码的删余变量节点 v 的所有幸存邻居变量节点按照其所通过信道的噪声功率的大小分为 b 类,假设第 t 类的噪声功率为 $\sigma_t^2(t=1,2,\cdots,b)$,且 $\sigma_1^2>\sigma_2^2>\cdots>\sigma_b^2$,并设第 t 类包括 S_t 个变量节点,记为 $\{v_1^t,\cdots,v_s^t,\cdots,v_{S_t}^t\}$. 与 LDPC 码类似,首先估计每次迭代过程中删余网络 LDPC 码的每个变量节点的均值更新,并由此计算该节点的恢复错误概率.

由于网络 LDPC 码的译码同样包括变量节点更新和校验节点更新,但图 2 给出的 Tanner 图表明,网络 LDPC 码的校验节点更新实际上包括上层校验节点和下层校验节点更新. 下面将分析在迭代译码过程中,速率兼容删余的网络 LDPC 码的变量节点和校验节点的均值更新过程.

假设校验节点的度分布分别为 $\rho^{\mathrm{up}}(x)=\sum_{k=1}^{d_c}\rho_k^{\mathrm{up}}x^{k-1}$ 和 $\rho^{\mathrm{low}}(x)=\sum_{k=1}^{d_c'}\rho_k^{\mathrm{low}}x^{k-1}$;$\eta$ 是上层变量节点与校验节点相连的边数占总边数的比例;$\lambda_{i,j}$ 是与度为 (i,j) 的变量节点连接的边数占总边数的比例;$m_{i,j}^{l-1}$ 和 $n_{i,j}^{l-1}$ 分别表示第 $(l-1)$ 次迭代时,变量节点传给上下层的校验节点的对数似然比的均值. 第 l 次迭代时,上下层校验节点的均值更新过程如下:

(1) 当上下层的校验节点向被删余的度为 (i,j) 的变量节点 $v\in G_{l+1}$ 传递消息时,该消息的对数似然比的均值分别为

$$m'^{l}=\sum_k\rho_k^{\mathrm{up}}\varphi^{-1}\left\{\left[\frac{1}{\eta}\sum_{i\geqslant 0,j\geqslant 0}\frac{i}{i+j}\lambda_{i,j}\varphi(m_{i,j}^{l-1})\right]^{\sum_{t=1}^{b}S_t\alpha_t}\right\}\quad, \tag{3}$$

$$n'^{l}=\sum_k\rho_k^{\mathrm{low}}\varphi^{-1}\left\{\left[\frac{1}{1-\eta}\sum_{i\geqslant 0,j\geqslant 0}\frac{j}{i+j}\lambda_{i,j}\varphi(n_{i,j}^{l-1})\right]^{\sum_{t=1}^{b}S_t\alpha_t}\right\}\quad, \tag{4}$$

其中,α_t 表示每个幸存邻居变量节点 v_s^t 的等效幸存邻居变量节点数,S_t 表示与变量节点 v 相连的校验节点没有被删余的变量节点数,变量节点 v 的总等效幸存邻居变量节点数为 $\sum_{t=1}^{b}S_t\alpha_t$.

(2) 当上下层的校验节点向没有删余的度为 (i,j) 的变量节点 v 传递消息时,该消息的对数似然比的均值[7]分别为

$$m'^{l}=\sum_k\rho_k^{\mathrm{up}}\varphi^{-1}\left\{\left[\frac{1}{\eta}\sum_{i\geqslant 0,j\geqslant 0}\frac{i}{i+j}\lambda_{i,j}\varphi(m_{i,j}^{l-1})\right]^{k-1}\right\}\quad, \tag{5}$$

(C)1994-2023 China Academic Journal Electronic Publishing House. All rights reserved.　http://www.cnki.net

$$n'^{l}=\sum_{k}\rho_{k}^{\text{low}}\varphi^{-1}\left\{\left[\frac{1}{1-\eta}\sum_{i\geqslant 0,j\geqslant 0}\frac{j}{i+j}\lambda_{i,j}\varphi(n_{i,j}^{l-1})\right]^{k-1}\right\}\quad(6)$$

上下层变量节点的均值更新过程如下：

第 l 次迭代时，度为 (i,j) 的变量节点传给上下层校验节点的对数似然比消息均值[7]分别为

$$m_{i,j}^{l}=\begin{cases}(i-1)m'^{l}+jn'^{l}+m_{u_0}, & i\neq 0,\ j\geqslant 0\\ jn'^{l}+m'_{u_0}, & i=0,\ j\geqslant 1\end{cases}\quad(7)$$

$$n_{i,j}^{l}=\begin{cases}im'^{l}+(j-1)n'^{l}+m_{u_0}, & i\neq 0,\ j\geqslant 1\\ (j-1)n'^{l}+m'_{u_0}, & i=0,\ j\geqslant 1\\ im'^{l}+m_{u_0}, & i\neq 0,\ j=0\end{cases}\quad(8)$$

若变量节点被删掉，则 $m_{u_0}(m'_{u_0})=0$；若变量节点为由源节点发送至目的节点的信息比特，则 $m_{u_0}=2/\sigma_{SD}^{2}$；若变量节点为中继节点发送至目的节点的信息比特，则 $m'_{u_0}=2/\sigma_{RD}^{2}$. 第 1 次迭代时，校验节点的初始值 $m'^{0}=n'^{0}=0$.

因此，变量节点传给上下层校验节点的平均的消息均值分别为

$$m^{l}=\frac{1}{\eta}\sum_{i\geqslant 0,j\geqslant 0}\frac{i}{i+j}\lambda_{i,j}m_{i,j}^{l},\quad(9)$$

$$n^{l}=\frac{1}{1-\eta}\sum_{i\geqslant 0,j\geqslant 0}\frac{j}{i+j}\lambda_{i,j}n_{i,j}^{l}.\quad(10)$$

经过 L 次迭代后，码比特的平均消息均值为

$$m_{L}=\eta m^{L}+(1-\eta)n^{L}.\quad(11)$$

此时，网络 LDPC 码的被删余变量节点的恢复错误概率为

$$P_{e}(v)=Q\left[(m_{L}/2)^{1/2}\right],\quad(12)$$

其中 $Q(x)=\frac{1}{(2\pi)^{1/2}}\int_{x}^{\infty}\exp\left(-\frac{t^{2}}{2}\right)\mathrm{d}t$.

2.3 网络 LDPC 码的速率兼容算法

由式(3)和(4)可知，等效幸存邻居变量节点数 $\sum_{t=1}^{b}S_{t}\alpha_{t}$ 越小，更新得到的均值 m'^{l} 和 n'^{l} 的值越大，进而迭代后的变量节点 m_{L} 的均值也越大，同时由式(12)得到的恢复错误概率 $P_{e}(v)$ 越小. 因此，在搜索节点时，需要寻找当前具有最小等效邻居的变量节点进行删余操作. 与文献[2]设计的 LDPC 码的删余算法相似，所提出的网络 LDPC 码速率兼容算法主要包括分组和排序两个操作.

2.3.1 分组

将所有删余的变量节点按照迭代恢复次数分成 K 组 $G_{1},G_{2},\cdots,G_{K}$，其中 $G_{l}(1\leqslant l\leqslant K)$ 是经过 l 次迭代才能恢复的所有变量节点的集合.

(1) 给定一个 $M\times N$ 网络 LDPC 码的校验矩阵，初始化 $R_{\infty}=\{1,2,\cdots,M\}$，$G_{\infty}=\{1,2,\cdots,N\}$，$l=1$.

(2) 遍历集合 R_{∞}，找出行重最小的行集合 r.

(3) 遍历集合 G_{∞}，找出列重最小的列集合 c.

(4) 选出所有(2)和(3)相交的元素的集合，$w=\{(r^{*},c^{*}),r^{*}\in r,c^{*}\in c\}$，作为候选对.

(5) 在集合 w 中选出具有最小等效幸存邻居变量节点数的元素，记为 (r_{j}^{*},c_{k}^{*}). 若有多对满足条件，则随机选出其中一对，归入第 l 次迭代可以恢复的集合 G_{l}，更新 $R_{\infty}=R_{\infty}\setminus r_{j}^{*}$ 和 $G_{\infty}=G_{\infty}\setminus c_{k}^{*}$.

(6) 若集合 G_{∞} 为空，则停止迭代；否则，跳至(7).

(7) 若集合 R_{∞} 不为空，则跳至(2)；否则，若步骤(5)中有多于一对满足条件，则 $l=l+1$，跳至(2).

其中，$G_{\infty}(R_{\infty})$ 表示每次迭代后更新的列(行)的集合；$r(c)$ 表示第 l 次迭代时，在集合 $R_{\infty}(G_{\infty})$ 选出的行(列)重最小的行(列)集合；$G_{l}=\{(r_{1}^{*},c_{1}^{*}),(r_{2}^{*},c_{2}^{*}),\cdots\}$；$R_{\infty}=R_{\infty}\setminus r_{j}^{*}$ $(G_{\infty}=G_{\infty}\setminus c_{k}^{*})$ 表示集合 $R_{\infty}(G_{\infty})$ 去掉元素 $r_{j}^{*}(c_{k}^{*})$ 后的集合 $R_{\infty}(G_{\infty})$.

第298页，共397页
(C)1994-2023 China Academic Journal Electronic Publishing House. All rights reserved. http://www.cnki.net

计算最大可达码率[2] 为

$$R_{\max}=R_0\Big/\Big(1-\sum_{j=1}^{K}|G_j|/n\Big)\quad , \tag{13}$$

其中,R_0 是母码的码率,n 是母码的码长.

在给定母码基础上,设计 Q 个码率的子码,对应码率记为 $R_0\leqslant R_1\leqslant\cdots\leqslant R_Q\leqslant R_{\max}$. 假设所设计码的码率为 R_j,需要删余的节点数为[2]

$$np_j=\lfloor n(R_j-R_0)/R_j\rfloor\quad ,\quad 0\leqslant j\leqslant Q\quad . \tag{14}$$

2.3.2　组内排序

依次对 $G_l(1\leqslant l\leqslant K)$ 内的变量节点进行排序.

(1) 给定一个 $M\times N$ 网络 LDPC 码的校验矩阵,初始化 $R_\infty=\{1,2,\cdots,M\}$,$l=1$,$j=1$,$P_0=\varnothing$.

(2) 若 $j>Q$,则停止迭代;否则,$P_j=P_{j-1}$.

(3) $\Delta=np_j-|P_j|$.

(4) 若 $\Delta=0$,$j=j+1$,则跳至(2).

(5) 根据集合 G_l 定义 $C_l\overset{\mathrm{d}}{=\!=}\{c_1^*,c_2^*,\cdots\}$,从 C_l 中选出列重最大的变量节点的集合 $c_{\max}^*$,并从 $c_{\max}^*$ 中找出具有最小数量的死校验节点的变量节点 $c_{\max}^{**}$. 如果有多个满足条件,则随机选出其中一个,归入排序的集合 P_j,更新 $P_j=P_j\bigcup\{c_{\max}^{**}\}$,$G_l=G_l\backslash\{c_{\max}^{**}\}$,$R_\infty=R_\infty\backslash r_{\max}^{**}$,$\Delta=\Delta-1$.

(6) 若 G_l 为空,$l=l+1$,则 $R_\infty=\{1,2,\cdots,M\}$.

(7) 跳至(4).

其中,(1)中的 $l=1$ 表示从 G_1 开始将各 G_l 内的变量节点排序,$j=1$ 表示初始码率为 R_1;(3) 计算需要删余 np_j 个节点,除了上次迭代删余的 $|P_j|$ 个节点外,本次还需要删余 Δ 个节点;(5) 中的集合 $c_{\max}$ 表示最大列重的变量节点的集合,同时意味着该集合包含的变量节点的幸存校验节点数最多;P_j 表示要达到码率 R_j,所需删余的变量节点的列集合;$r_{\max}^{**}$ 表示列为 $c_{\max}^{**}$ 的变量节点所在的行.

经过上述分组和组内排序操作,将 $G_l(1\leqslant l\leqslant K)$ 中的变量节点按照 l 从小到大删余,而在同一个 G_l 中,按照变量节点的列号从小到大删余,直到删掉 np_j 个节点.

3　仿真结果

仿真中两个信源节点采用的 LDPC 码的码率均为 0.5,度分布为

$$\lambda(x)=0.23403x+0.21242x^2+0.1469x^5+0.102840x^6+0.30381x^{19}$$

和

$$\rho(x)=0.71875x^7+0.28125x^8\quad .$$

根据文献[7],假设所采用的网络 LDPC 码的度序列分布为:$\lambda_{0,2}=0.028043$,$\lambda_{2,0}=0.188139$,$\lambda_{2,1}=0.019382$,$\lambda_{2,2}=0.026283$,$\lambda_{3,0}=0.191239$,$\lambda_{3,1}=0.003360$,$\lambda_{3,2}=0.001150$,$\lambda_{6,0}=0.085989$,$\lambda_{6,1}=0.000980$,$\lambda_{6,2}=0.063446$,$\lambda_{7,0}=0.059576$,$\lambda_{7,2}=0.044374$,$\lambda_{20,0}=0.176218$,$\lambda_{20,1}=0.003570$,$\lambda_{20,2}=0.108251$,$\rho_6^{\mathrm{low}}=0.943049$,$\rho_7^{\mathrm{low}}=0.056951$.

假设两个源节点所采用 LDPC 码的码长均为 2 048,中继节点联合编码的 LDPC 码的校验比特数为 628,此时网络 LDPC 码(母码)的码率为 0.444. 根据式(14),可以得到对该网络 LDPC 码进行删余获得的最大码率为 0.733. 利用文中所提算法对该网络 LDPC 码删余可以得到码率分别为 0.5、0.6 和 0.7 的子码. 利用文献[2]中的算法和随机删余也可得到同样码率的网络 LDPC 子码.

假设源节点和中继节点均采用 BPSK 调制方式,源节点与中继节点,源节点与目的节点,以及中继节点与目的节点之间的信道均为高斯白噪声信道,中继节点与目的节点之间的信噪比固定为 5 dB,且中继节点可以正确

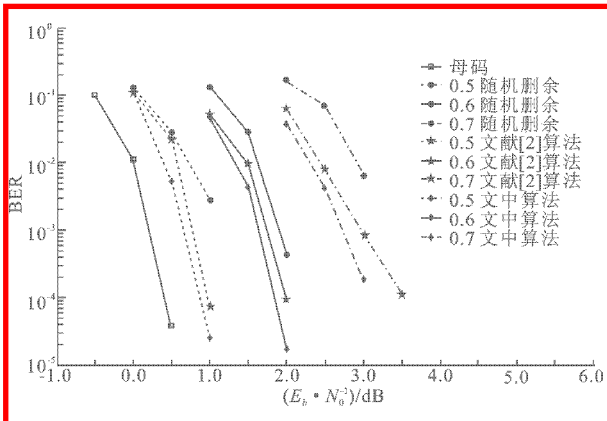


图 4　网络 LDPC 码的删余性能对比

(下转第 47 页)

(C)1994-2023 China Academic Journal Electronic Publishing House. All rights reserved.　http://www.cnki.net

scientific.net/AMR.311-313.2009.

[4] Bozorg M, Termeh F. Domains of PID Controller Coefficients which Guarantee Stability and Performance for LTI Ttime-delay [J]. Automaic, 2011, 47(9): 2122-2125.

[5] 杨莹，李俊民，陈国培. 一类广义混杂系统的随机稳定性及稳定化[J]. 西安电子科技大学学报，2010，37(5)：866-871.
Yang Ying, Li Junmin, Chen Guopei. Stochastic Stability and Stabilization for a Class of Singular Hybrid Systems[J]. Journal of Xidian University, 2010, 37(5): 866-871.

[6] 徐亚兰，陈建军. 压电柔性机械臂的轨迹跟踪控制[J]. 西安电子科技大学学报，2008，35(3)：504-507.
Xu Yalan, Chen Jianjun. Trajectory Tracking Control for the Flexible Link Robot Manipulator Using Piezoelectric Materious [J]. Journal of Xidian University, 2008, 35(3): 504-507.

（编辑：郭　华）

（上接第 17 页）

译出两个源节点的发送数据. 图 4 比较了 3 种不同算法得到的网络 LDPC 码在上述信道假设下的误比特性能，图中横坐标 E_b/N_0 表示源节点与目的节点之间链路的信噪比变化，且假设两个源节点与目的节点之间的链路是对称的.

由图 4 可以看出，随着删余比特的增加，采用所提算法得到的网络 LDPC 码的性能增益也随之增加. 当码率为 0.5，比特误码率(BER)为 10^{-3} 时，采用所提算法性能优于随机删余算法 0.45 dB；当码率为 0.5，BER 为 10^{-4} 时，采用所提算法比文献[2]中算法的性能改善 0.15 dB. 在码率为 0.6，BER 为 10^{-3} 时，所提算法相对于随机删余算法性能改善了 0.3 dB，相对于文献[2]中算法性能改善了 0.2 dB. 当码率为 0.7，SNR 为 3 dB 时，所提算法的 BER 为 10^{-5}，相比于随机删余算法的 10^{-3} 有了明显提升，而 BER 为 10^{-4} 时，所提算法比文献[2]中算法性能增益改善了 0.4 dB.

4　结 束 语

根据网络 LDPC 码的结构特点，以最小化恢复错误概率为目标，设计了一种网络 LDPC 码的速率兼容删余算法. 不同于已有的算法[2]，该算法利用被删余的变量节点的恢复原则和受到的噪声干扰大小设计了不同码率下的删余方案，在不增加系统复杂度的前提下，只需要一对编码译码器即可实现网络 LDPC 码的码率自适应. AWGN 信道下的仿真结果表明，在同等条件下，采用文中所提算法获得的速率兼容网络 LDPC 码比采用文献[2]中算法得到的速率兼容网络 LDPC 码有更好的性能.

参考文献：

[1] Hagenauer J. Rate-Compatible Punctured Convolutional Codes (RCPC codes) and Their Applications [J]. IEEE Trans on Communication, 1988, 36(4): 389-400.

[2] Ha J, Kim J, Klinc D, et al. Rate-Compatible Punctured Low-Density Parity-Check Codes with Short Block Lengths [J]. IEEE Trans on Inform Theory, 2006, 52(2): 728-738.

[3] Ha J, Kim J, Klinc D, et al. Rate-Compatible Puncturing of Low-Density Parity-Check Codes [J]. IEEE Trans on Inform Theory, 2004, 50(11): 2824-2836.

[4] Zhou Lin, Bai Baoming, Xu Ming. Design of Nonlinary Rate-compatible LDPC Codes Utilizing Bit-wise Shortening Method [J]. IEEE Communication Letters, 2010, 14(10): 963-965.

[5] 周林，白宝明，邵军虎，等. 多元 LDPC 码的速率兼容技术研究[J]. 西安电子科技大学学报，2011，38(1)：147-152.
Zhou Lin, Bai Baoming, Shao Junhu, et al. On Nonbinary Rate-compatible LDPC Codes [J]. Journal of Xidian University, 2011, 38(1): 147-152.

[6] 郭凯，陈彦辉，李建东. 一种对奇偶校验比特按组删余的速率兼容编码[J]. 西安电子科技大学学报，2009，36(5)：782-787.
Guo Kai, Chen Yanhui, Li Jiandong. Rate-compatible Codes Based on Puncturing Parity Check Bits in Group [J]. Journal of Xidian University, 2009, 36(5): 782-787.

[7] Li Y, Song G H, Wang L L. Analysis of the Joint Network LDPC Codes over Orthogonal Multi-Access Relay Channel [J]. IEEE Commun Lett, 2010, 14(2): 184-186.

（编辑：齐淑娟）

(C)1994-2023 China Academic Journal Electronic Publishing House. All rights reserved.　http://www.cnki.net

PAPER • OPEN ACCESS

Research on the changing trend of farmland area in China and its driving factors from 1996 to 2016

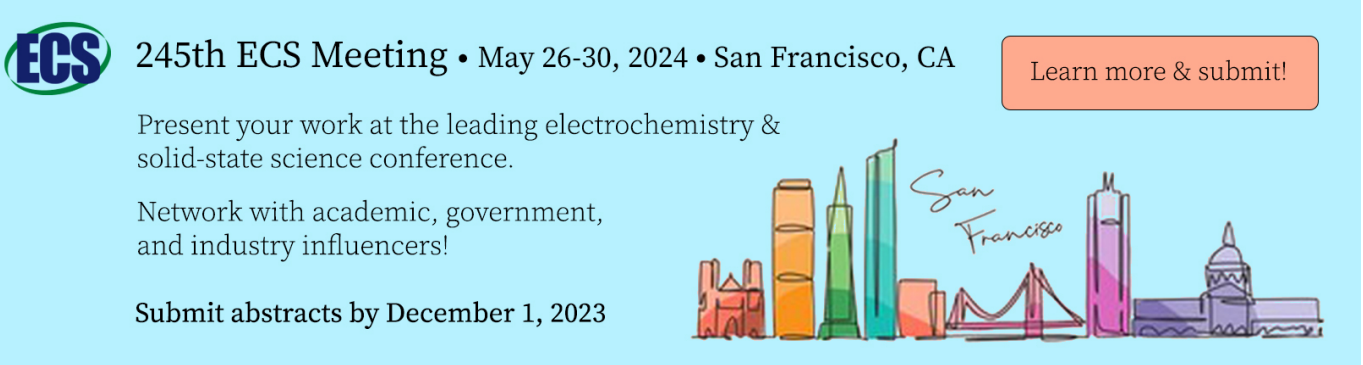
To cite this article: J Y Wang and X M Li 2018 *IOP Conf. Ser.: Mater. Sci. Eng.* **392** 062097

View the article online for updates and enhancements.

中文文章叫近20年，英文文章是1996 to 2016,文章完全一样

You may also like

- The 300 years cropland changes reflecting climate impacts and social resilience at the Yellow River–Huangshui River Valley, China
Qiong Chen, Liang Emlyn Yang, Jing Luo et al.
- Analysis and Research on the Value of Farmland Transfer Based on Environmental Protection Evaluation System
Zhenyu Zhang, Minghua Tian, Jianjun Li et al.
- High Standard Farmland Construction and Soil Conservation Evaluation
Jing Zhang and Lu Sun



This content was downloaded from IP address 219.144.164.16 on 16/11/2023 at 00:29

Research on the changing trend of farmland area in China and its driving factors from 1996 to 2016

J Y Wang [1] and X M Li[2*]

[1]Xi'an Shiyou University, Xi'an China, 710065

[2]Shaanxi Provincial Land Engineering Construction Group，Xi'an China, 710075

*Corresponding author: xmlisdc@126.com

Abstract. The paper was to research the changing trend of farmland area from 1996 to 2016. The original data of farmland area of China in these years were collected, data mining technology was used, and ARIMA model was chosen to predict each other between the two periods of 1996-2008 and 2008-2016, so the original farmland area data could be corrected and normalized. Then correlation analysis was used to study the driving factors. The trend research result showed, the farmland area decreased from 1996 to 2016, the decreasing rate was faster before 2004, and then it decreased slowly. The correlation analysis result showed, the added value proportion of primary industry, the total population, and the urban population were the most important driving factors, their coefficients were 0.959, -0.918 and -0.896 respectively. It could be concluded by the result that the industry configuration and the urbanization could affect the farmland area changing with the development of social economy.

1. Introduction

China is a great agricultural country, and the farmland is one very important resource which is related to food security. However, the vigorous demand for lands brings great challenge for farmland protection with the promotion of socialist modernization construction [1]. The research on farmland area change and its driving factors in China has always been one popular problem. The statement was refuted that China's cultivated land has been descending since 1957 based on the analysis of the actual change of the cultivated land area [2]. The farmland area changing trend, spatial characteristics and the driving factors in China for a period of time before 2007 were studied [3-5]. And in different scales such as the scale of province or in some part of China, the dynamic change trend of farmland was studied [6-8]. Since 1980s, with the development and application of 3S technology, many scholars studied the farmland change using the RS images such as Landsat TM images [9, 10]. And the analysis approaches in the study of the driving forces of land use change in large regions were explored by using digital satellite remote sensing data of China [11]. Not only the changes in China's cultivated land but also those in some provinces were analyzed based on remote sensing data such as Landsat TM/ETM+, NOAA, SPOT dataset [12, 13].

The statistic data sources of cultivated land in China are various, for example, the international organizations such as FAQ, WRI (the world resources institute), and different departments of China such as MLR (the ministry of land and resources), MOA (the ministry of agriculture), the bureau of statistics of PRC. However, the statistical data supplied by MLR are considered the most authoritative [14]. But the data from the MLR are not regularly entire in the demanded periods, and there was a jumping phenomenon with the farmland area from 2008 to 2009, that's because the data of 2008 was

Content from this work may be used under the terms of the Creative Commons Attribution 3.0 licence. Any further distribution of this work must maintain attribution to the author(s) and the title of the work, journal citation and DOI.
Published under licence by IOP Publishing Ltd

based on the first national land use survey, and the data of 2009 was based on the second national land use survey, that's seemly illogical. At present, most scholars analyze the farmland area change by the exiting data directly while ignoring the accuracy of the statistic data, or they just focused on some periods before 2008 or after 2009 evading the jumping years. Only a few scholars researched the farmland area in different historical periods [14, 15]. In this paper, the researched years included the years of before and after the second national land use survey. The method of data mining was introduced to analyze the relation between the two periods of the years before 2008 and the years after 2009, so the changing trend of China's farmland area could be reflected more scientifically. At the same time, the driving factors were studied based on data normalization. And this is not found in the present research, which could be useful for studying China's farmland changing trend.

2. Data and methods

2.1. Data acquisition

2.1.1. Data of farmland area in China

The farmland area of China, especially in the historical periods, has been hard for statistic for a long time. The national department of land management have been announcing the changing situation each year since 1986. In order to obtain the veracious statistical data of farmland in China, the first national land use survey was operated from 1984 to 1996. The survey result showed there was 1.95 billon mu (1 mu = 666.66 m^2) of farmland in China by the day of Oct.31 1996 [15], which was considered the most credible result at that time [16]. Then, the farmland area of each year from 1996 to 2008 can all be obtained from the statistical bulletin of the year.

In order to obtain more veracious statistical data of farmland, the second national land use survey was operated from 2007 to 2009. The survey result showed there was 2.03 billon mu of farmland in China by the year of 2009 [15]. And since then the land use change survey has been operated each year. And the farmland area from 2007 to 2016 can be obtained from the national service platform of land use survey result. Because new methods and technologies were applied with the second national land use survey, some farmlands which were not found in the first survey were found in the second survey, and there was a jumping phenomenon with the farmland area from 2008 to 2009, which would be specially researched after a while for analyzing the changing trend of farmland area.

2.1.2. Data of driving factors

Land is closely related to the human social and economic development. The national farmland change is influenced by the geographical and climate conditions, social and economic development, flood and waterlogging disaster and so on [1]. For researching the driving factors influencing the farmland changing, three kinds of factors were introduced for comparison and selection. One kind were the comprehensive factors reflecting the national economic development, and they were the gross national income (GNI), the gross domestic product (GDP), the primary industry added value and its ratio, the second industry added value and its ratio, the third industry added value and its ratio, the gross agricultural output value, per capita GDP, industrial added value, architectural added value. Another kind were special factors reflecting the level of urbanization, and they were the national population, the urban population, and the rural population. The third kind was the special factors reflecting the natural disaster, and they were the damage area and the grain yield. There were in total of 17 factors which were used for analysis [17]. And data of all factors for the recent 20 years could be obtained from the web site of the national bureau of statistics.

2.2. Study methods

In this paper, the national farmland area dada from 1996 to 2016 years were collected and analysed to study the changing trend, and the correlation analysis was operated to research the driving factors. While studying the changing trend of farmland from 1996 to 2016, according to the found jumping

phenomenon with the data from 2008 to 2009, the data mining technology was introduced. First, the farmland area of the year 2009 can be predicted with the data of 1996 to 2008. And the farmland area of the year 2008 can also be predicted reversely with the data of 2009 to 2016. Then, based on the predicted data and the practically collected data of the farmland of the years 2008 and 2009, the mathematical ratio relation between the farmland area of 2008 and 2009 could be analysed and obtained, so the jumping phenomenon could be solved with the ratio. At last, all the farmland data from 1996 to 2016 should be normalized for researching the changing trend more scientifically.

ARIMA (Autoregressive Integrated Moving Average) model was chosen for prediction with data mining, which was promoted by Box and Jenkins, it's a very famous and useful time-sequence forecast method, and that's just the needed one in this paper.

3. Analysis on the farmland area changing trend from 1996 to 2016

3.1. The analysis based on the original statistic data of farmland area

By collecting and analysing the original statistic data of farmland area for years of 1996-2016, the result showed that the national farmland area decreased year by year, as Figure1, and the decreasing speed was the most quick from 2000 to 2004. While the farmland area jumped from 1.826 billion mu in 2008 to 2.031 billion mu in 2009. And after 2009, the farmland area decreased very slowly.

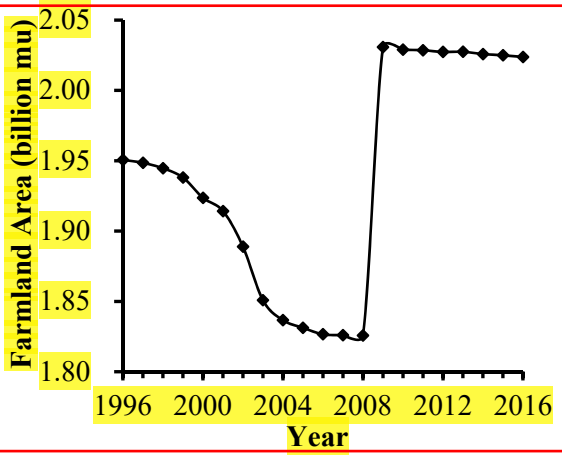


Figure 1. Changing Trend for Farmland Area of 1966-2016 Based on Original Statistic Data

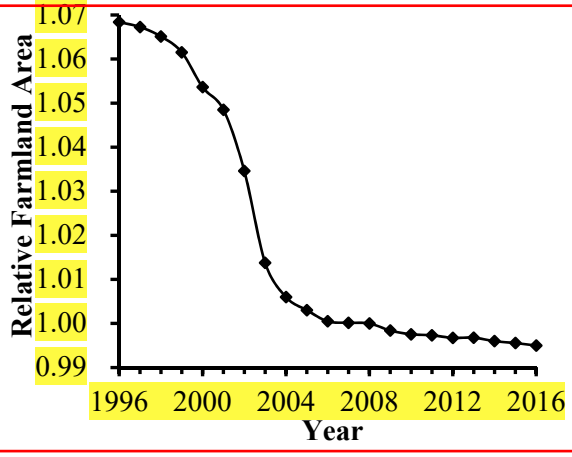


Figure 2. Changing Trend for Farmland Area of 1966-2016 Based on Revised Statistic Data

China finished the first national land use survey in 1996, and the second in 2009, so the jumping phenomenon just happened in the division years of the twice land use survey. Whether the national farmland increased by about 200 million mu in the year of 2009 or not should be studied deeply. And by reviewing literatures [14, 15, 18], it could be concluded that the main reason was that more advanced technologies were introduced while the second land use survey, so some farmlands lost of statistic in the first land use survey were found in the second time, and the accuracy of the statistic result was improved. In this paper, the farmland data for the recent 20 years were based on twice different land use survey and different technology conditions. We can easily studied the changing trend in each period before or after the second land use survey, while all the data of farmland area must be revised and normalized if we want to study the continual time-sequence changing trend from 1996 to 2016, then they might be comparable.

3.2. Revision of farmland area based on data mining technology

Data mining technology is much useful for time-sequence prediction, and by that, in this paper, the farmland area of the year 2009 was predicted with the farmland data of the years from 1996 to 2008, the ratio α between the farmland area of 2009 and that of 2008 could be obtained. And the farmland area of the year 2008 was also predicted reversely with the farmland data of the years from 2009 to

2016, the ratio β between the farmland area of 2009 and that of 2008 could also be obtained. Then, for reflecting the ratio more scientifically, we could get the ratio ρ by the average of α and β.

SPSS software was used for prediction in this paper, by analyzing and comparing, the model of ARIMA was used in both of the prediction and the reverse prediction. The model used while predicting the farmland area of the year 2009 was ARIMA(1,1,2) (r^2=0.975**), and the model used while predicting reversely the farmland area of the 2008 was ARIMA(1,1,4) (r^2=0.966**), both of the two models were significant in the level of 0.01, with that, the predicted farmland area of the year 2009 was 1820.08 million mu, the reversely predicted farmland area of the year 2008 was 2030.98 million mu, so we can get α=0.996899887, β=0.999895617, and then ρ=0.998397752, so we could use the ρ value as the revision ratio of the data of the two different periods.

3.3. Trend analysis based on the revised data of farmland area

All the original farmland area data were revised with the ratio ρ and normalized into relative values for reflecting the changing trend more scientifically. Based on the study of the previous paper, the relative farmland area of the years from 1996 to 2008 were calculated with the denominator of the farmland area of the year 2008, the relative farmland area of the years from 2009 to 2016 were calculated with the denominator of the farmland area of the year 2009 while revised by multiply the ratio ρ. Then the continual changing trend of farmland area from 1996 to 2016 could be obtained, shown as Figure 2, which showed the national farmland area decreased year by year. Before the 2004, the decreasing rate was faster, and after that the decreasing rate trends to be slower, especially after 2009, the farmland area trends to be stable.

4. Analysis on driving factors

A total of 17 factors were collected in this paper, and their descriptive statistical characters were shown in table 1. In order to study the driving factors, correlations between the farmland area and the factors were analysed, and then, by comparing the correlation coefficients shown as table 2. the driving factors could be chosen out.

Table 1. Descriptive Statistical Characters of All Factors from 1996 to 2016

Factors	*Min.*	*Max.*	*Ave.*	*Std.*	Factors	*Min.*	*Max.*	*Ave.*	*Std.*
x_1	7078	74114	30444.70	225956.60	x_{10}	589.8	5398	2287.2	16332.77
x_2	7181.4	74412.7	30571.87	226519.84	x_{11}	2953	24786	11653.28	79508.29
x_3	1387.8	6367.1	3124.07	17742.62	x_{12}	439.3	4952.2	1962.3	15992.73
x_4	8.556	19.325	12.11	3.28	x_{13}	122389	138271	131047.71	4702.17
x_5	3382.8	29623.6	13562.92	94949.58	x_{14}	37304	79298	58413.24	12989.27
x_6	39.810	47.559	45.33	2.00	x_{15}	58973	85085	72634.48	8313.40
x_7	2410.7	38422	13884.89	114605.84	x_{16}	43070	62144	52326.48	5812.06
x_8	33.569	51.634	42.56	4.47	x_{17}	21770	54688	41009.48	10706.30
x_9	1354	5928.8	2884.26	16570.35					

**In the table, x_1 means the gross national income (GNI), billion yuan; x_2 means the gross domestic product (GDP), billion yuan; x_3 means the primary industry added value, billion yuan; x_4 means the proportion of primary industry added value, %; x_5 means the second industry added value, billion yuan; x_6 means the proportion of second industry added value, %; x_7 means the third industry added value, billion yuan; x_8 means the proportion of third industry added value, %; x_9 means gross agricultural output value, billion yuan; x_{10} means per capita GDP, billion yuan; x_{11} means industrial added value, billion yuan; x_{12} means architectural added value, billion yuan; x_{13} means the national population, $*10^4$; x_{14} means the urban population, $*10^4$; x_{15} means the rural population, $*10^4$; x_{16} means the grain yield, $*10^4$ t; x_{17} means damage area, $*10^3$ ha; and the same as follows.*

Table 2. Correlation Coefficients between Original/Relative Farmland Area and Factors

	Original data	Relative data		Original data	Relative data
Relative data	-0.142	1.000	x_9	0.686	-0.709
x_1	0.649	-0.746	x_{10}	0.651	-0.749
x_2	0.652	-0.745	x_{11}	0.638	-0.784
x_3	0.663	-0.736	x_{12}	0.688	-0.716
x_4	-0.274	0.959	x_{13}	0.433	-0.918
x_5	0.647	-0.774	x_{14}	0.488	-0.896
x_6	-0.519	0.259	x_{15}	-0.518	0.880
x_7	0.649	-0.717	x_{16}	0.752	-0.524
x_8	0.433	-0.819	x_{17}	-0.514	0.708

As shown in table 2, the correlation coefficients between the original farmland area and the factors were poor because of the jumping phenomenon. However, by analyzing the correlations between the revised farmland area and the factors, we could find, the proportion of the first industry added value had the best correlation with the farmland area, its coefficient was up to 0.959. The national total population was secondary to it, and its correlation coefficient was -0.918, then the urban population and the rural population were secondary to that sequentially, which means the first industry added value, the national total population, the urban population and the rural population were the most important driving factors. According to the research result, we could conclude that it was mainly the national industry structure and the urbanization construction that influence the farmland changing.

5. Conclusion and discussion

Land has both of its own natural and social characters, and it's just all of the factors including society, economy, and policy factors that influence the statistics of farmland area for a long time. So it's difficult for a long-time changing trend research. The period studied in this paper was across twice national land use survey, and there happened to be a jumping phenomenon, but this couldn't reflect the boost of farmland area from 2008 to 2009. The reasons of the phenomenon were studied, that was mainly because RS, GIS and some other new technologies were applied in the second national land use survey, the survey and statistics were more standardized, so the accuracy was apparently promoted, which made the farmlands lost of statistics before found in the second land use survey. Therefore, in order to study the changing trend for a period across twice land use survey, the quantitative relation of the farmland area between the twice survey must be studied and obtained. In this paper, with data mining technology, revision and normalization of farmland area, the research result could reflect the changing trend more actually.

Research results showed China's farmland area decreased year by year from 1996 to 2016, especially before 2004, the decreasing rate was fast, and after that year the decreasing rate tended to be slow. As to the driving factors, it's the proportion of the primary industry added value in the aspect of the national industry structure and the national population, the urban population in the aspect of urbanization construction which were the main driving factors influencing the farmland changing. Because of the ecological restoration after the year of 1999, the farmland decreased rapidly [14, 19]. In 2004, the land management law was revised, which strengthened the protection and the requisition-compensation balance of farmland, and that's much useful for retaining farmland. In this paper, only the farmland area data from 1996 to 2016 were used to study the changing trend, and in present time, China pay much attention to farmland protection, not only including the quantity, but including the land quality with core of productivity in order to realize the protection of the trinity of quantity, quality and ecology [20]. In the future research, the changing trend of farmland area would be studied deeply.

The years of 1966 to 2016 were introduced in this paper to study the changing trend because the demand of statistical data for longer-time sequence was difficult to be satisfied. In future research, based on the collected statistical data, the data mining, remote sensing interpretation and some other methods would be applied to compensate the lack of some factors, so we wish we could obtain a longer time-sequence changing trend.

References

[1] Zhao Q G, Zhou S L, Wu S H and Ren K. 2006. Cultivated Land Resources and Strategies for Its Sustainable Utilization and Protection in China, *Acta Pedologica Sinica*,43(4): 662-72.
[2] Bi Y Y and Zheng Z Y. 2000. The Actual Changes of Cultivated Area Since The Founding of New China**,** *Resources Science*, 22(2): 8-12.
[3] Li X B. 1999. Change of arable land area in China during the past 20 years and its policy implications, *Journal of Natural Resources*, 14(4): 329-33.
[4] Cao Y G, Yuan C, Zhou W, Tao J and Hua R. 2008. Analysis on D iving Forces and Provincial Differences of Cultivated Land Change in China. *China Land Science*, 22(2): 17-22.
[5] Huang Z H and Wu C F. 2009. Empirical Study of Cultivated Land Change and Socio-economic Factors in China. *Journal of Natural Resources*. 24(2): 192-9.
[6] Yu T, Cao Y G and Xu J X. 2016. Driving Force of Cultivated Land Change in China Based on Different Scales. *Chinese Agricultural Science Bulletin*, 2016, 32(24): 194-8.
[7] Wu X, Wang S R, Shang H Y and Wang Z J. 2017. Analysis of Dynamic Change and Driving Forces of Cultivated Land in NingXia During The Past 18 Years. *Chinese Journal of Agricultural Resources and Regional Planning*. 38(8):98-104.
[8] Guo L Y, Wang D L and Wang J Y. 2012. Analysis of the Arable Land Change and Its Causes in the Eastern Coastal China Over the Last Decades. *Chinese Journal of Agricultural Resources and Regional Planning*. 33(1):6-10.
[9] Zhang G P, Liu J Y and Zhang Z X. 2003. Spatial-temporal Changes of Cropland in China for the Past 10 Years Based on Remote Sensing. *Acta Geographica Sinica*. 58(3): 323-32.
[10] Tian G J, Zhuang D F and Liu M L. 2003. The Spatial-temporal Dynamic Change of Cultivated Land in China in 1990s. *Advance in Earth Sciences*. 18(1): 30-6.
[11] Liu X H,Wang J F,Liu J Y, Liu M L and Meng B. 2005. Quantitative Analysis Approaches to the Driving Forces of Cultivated Land Changes on A National Scale.*Transactions of the Chinese Society of Agricultural Engineering*. 21(4):56-60.
[12] Xu L L, Li B L, Yuan Y C, Gao X Z, Liu H J and Dong G H. 2015. Changes in China's Cultivated Land and the Evaluation of Land Requisition-Compensation Balance Policy from 2000 to 2010. *Resources Science*. 37(8): 1543-51.
[13] Li J G, He C Y, Shi P J, Chen J, Gu Z H and Xu W. 2004. Change Process of Cultivated Land and Its Driving Forces in Northern China during 1983-2001. *Acta Geographica Sinica*. 59(2): 274-82.
[14] Feng Z M, Liu B Q and Yang Z. A Study of the Chaning Trend of Chines Cultivated Land Amount and Data Reconstructing:1949-2003. *Journal of Natural Resources*, 20(1): 35-43.
[15] Tan Y Z, He J, Yue W Z, Zhang L and Wang Q R. 2017. Spatial Pattern Change of the Cultivated Land before and after the Second National Land Survey in China. *Journal of Natural Resources*, 32(2): 186-97.
[16] Lin G C S, Ho S P S. 2003. China's land resources and land-use change: insights from the 1996 land survey. *Land Use Policy*, 20(2): 87-107.
[17] Fu Z Q, Cai Y L, Yang Y X and Dai E F. 2001. Research on the Relationship of Cultivated Land Change and Food Security in China. *Journal of Natural Resources*, 16(4): 313-9.
[18] Zhang Y Q and Yang Z S. 2013. Comparative Analysis of Two Investigations of Land Resource in China. *Scientific and Technological Management of Land and Resources*. 30(2): 100-4.
[19] Xu X L, Cai Y M, Zhang K L and Zheng W Y. 2005. Study on Dynamic Change of Cultivated Land Resources and Causes of the Changes. *China Population Resources and Environment.* 15(3): 75-9.
[20] Tan Y Z, Wu C F, Wang Q R, Zhou L Q and Yan D. 2005. The Change of Cultivated Land and Ecological Environment Effects Driven by the Policy of Dynamic Equilibrium of the Total Cultivated Land. *Journal of Natural Resources*. 20(5): 727-34.

Optimal Design of the Joint Network LDPC Codes over Orthogonal Multi-Access Relay Channel

Jingyi Wang
State Key Lab of ISN
Xidian University
Xi'an, China
Email: wangjy@stu.xidian.edu.cn

Shuling Che
State Key Lab of ISN
Xidian University
Xi'an, China
Email: shlche@mail.xidian.edu.cn

Ying Li
and Junlong Wang
State Key Lab of ISN
Xidian University
Xi'an, China
Email:ying.lili1973@gmail.com

***Abstract*—Optimization of degree distribution of the joint network LDPC code for orthogonal multiple-access relay channel (MARC) is investigated in this paper. We first calculated the code capacity of the source-destination link of orthogonal MARC based on a Gaussian approximation,where two sources communicate with one destination in the presence of one relay. Then, a new generalized differential evolution algorithm is developed to iteratively improve the degree distribution of the joint network LDPC code. Simulation results show that, the gap between bit error rate (BER) performance of our designed codes and the decoding threshold is about 0.4dB, and that between the capacity limit and decoding threshold is less than 0.7dB at BER $= 10^{-6}$.**

***Index Terms*—Network LDPC Code; multi-access relay network; Gaussian approximation; differential evolution; capacity limit.**

I. Introduction

In wireless communications, cooperation relay networks[1][2][3] have recently attracted substantial research efforts with many promising techniques of improving performance in term of throughput, coverage or diversity gain. In relay networks, one or multiple relay nodes (RNs) to assist the sources in transmitting information.Optimal designs of Relay networks have attracted extensive attentions due to that they can increase the communication capacity. One of the earlier works on this subject is the application of LDPC code to the single-source single-relay networks [4]. To improve the performance of the single-source single-relay system, a class of bilayer LDPC codes is designed in[5][6].

Based on the principle of the bilayer LDPC codes, the authors proposed a class of the joint network LDPC code which helps the relay jointly re-encodes the messages from the two sources and sends the parity bits to the destination [7]. Moreover, the authors analyzed the capacity approaching ability of the joint network LDPC codes in [8]. In this paper, we study the problem of approaching capacity limit of a two-source single-relay multiple-access relay network with the joint network LDPC code, in which the two source-to-relay channels and the two source-to-destination channels are under the same channel parameters.Then, a new generalized differential evolution algorithm is developed to optimal the degree distribution of the joint network LDPC code.

The rest of this paper is organized as follows. Section II presents the system model and then describes the operation of the system throughout different stages of the cooperation strategy. Section III explains the optimum design method of degree distribution of the joint network LDPC code. Section IV presents simulation results, and Section VI concludes the paper.

II. System Model

Our system is a two-slot wireless relay network consisting of two sources, one relay and one destination, as shown in Fig.1.

In the first slot, sources $S_i(i = 1, 2)$ broadcast their LDPC coded signals $X_i(i = 1, 2)$, which are received by both relay R and destination D. We express the received bits as

$$Y_{S_i,R} = X_i + N_{S_i,R} \quad (1)$$

$$Y_{S_i,D} = X_i + N_{S_i,D} \quad (2)$$

where $i = 1, 2.X_i$ is the LDPC coded signal sent from source node S_i, while $Y_{S_i,R}$ and $Y_{S_i,D}$ are the corresponding received signal by the relay R and the destination D respectively. Finally, $N_{S_i,R}$ is a zero-mean additive Gaussian random variable with variance $\sigma^2_{S_i,R}$, and $N_{S_i,D}$ is a zero-mean additive Gaussian random variable with variance $\sigma^2_{S_i,D}$.

In the second slot, after decoding the received signals correctly, R jointly re-encodes the messages of the two sources and sends k_2 parity bits X_R to D. The received bits at the destination D is

$$Y_{R,D} = X_R + N_{R,D} \quad (3)$$

where X_R denotes the signal corresponding to the parity bits, and $N_{R,D}$ is a zero-mean additive Gaussian random variable with variance $\sigma^2_{R,D}$.

At last, the destination D can decode the information data of two sources by using the received signals Y_1, Y_2 and Y_R respectively from the two sources and relay. Therefore, X_1, X_2, and X_R can be treated as an equivalent super code which is called as the joint network LDPC code in [7]. The parity check matrix of the joint network LDPC code can be written as

$$\mathbf{H} = \begin{pmatrix} \mathbf{H_1} & \mathbf{0} & \mathbf{0} \\ \mathbf{0} & \mathbf{H_1} & \mathbf{0} \\ \mathbf{A} & \mathbf{B} & \mathbf{C} \end{pmatrix} \quad (4)$$

978-0-7695-4988-0/13 $26.00 © 2013 IEEE
DOI 10.1109/INCoS.2013.116

IEEE computer society

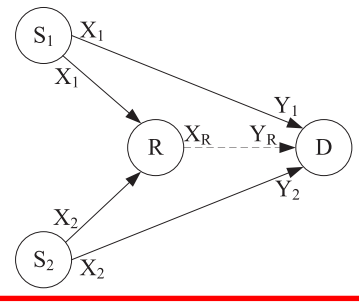


Fig. 1. The model of the joint network LDPC code based relaying scheme

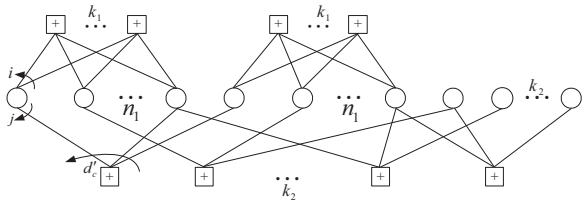


Fig. 2. Tanner graph of the joint network LDPC code

where $\mathbf{H_1}$ denotes the same parity-check matrix of the constituent codes at the two sources $S_i(i=1,2)$, $\mathbf{H_3}=(\mathbf{ABC})$ denotes the parity-check matrix generated by R, and $\mathbf{0}$ represents the all-zero matrix.

Assume that each source uses an (n_1, n_1-k_1) irregular LDPC code with code length n_1 and parity length k_1. According to [8], the Tanner graph of the joint network LDPC code is shown in Fig.2, where the upper sub-graph denotes the encoding at the sources and the lower sub-graph denots the encoding at the relay. This code includes $2k_1$ upper check nodes, k_2 lower check nodes and $2n_1+k_2$ variable nodes. A variable node is of degree (i,j), $1\le i\le d_v$ and $1\le i\le d_v^{'}$, where i (j) is its upper (lower) degree, and d_v $(d_v^{'})$ is its maximum upper (lower) degree. In addition, $\lambda_{i,j}$ represents the proportion of the number of edges connected to the variable nodes with the degree (i,j).

III. Optimization Of Degree Distribution

A. Preliminary

Definition 1: Decoding threshold of joint network LDPC code is defined as

$$\sigma^* = sup\{\sigma : \lim_{L\to+\infty} m_L > M\} \tag{5}$$

where L is the maximum iteration number, m_L denotes the mean value of the log-likelihood ratio (LLR) message of a code bit at L-th decoding iteration and M is the LLR mean value corresponding to the target error probability. Then with the knowledge in [8], $2m_L$ is the LLR variance value. When $\sigma<\sigma^*$, m_L will be greater than M, which means that the target error probability can be achieved. When $\sigma\ge\sigma^*$, the iterative decoding can not achieve the target error probability.

B. Calculation of decoding threshold σ^*_{SD}

Algorithm 1: Given degree distributions of the LDPC code at the sources, let σ_{SD} and σ_{RD} represent the channel parameters of source-destination link and relay-destination link respectively. We denote the target error probability as $P_e=10^{-6}(M=45)$ [8], and the maximum iteration number as L. Let $\Delta\sigma_{SD}$ denote a step length, and then algorithm 1 can be described as follows:

Step 1: Initialization

The initialized value of the average mean value of the LLR message output by the check node is $m^{'l}=n^{'l}=0$ (l is the iteration number, and $l=0$ in the first iteration)[8].

Step 2: Updating

When the iteration number $l<L$, update the mean values of the LLR messages at the variable node and the check node respectively, and then calculate the mean value (m_l) of the LLR message during this iteration using the method in [8]. If $m_l<M$, add the iteration number by 1 $(l=l+1)$, and continue Step 2. If $m_l\ge M$, $\sigma_{SD}=\sigma_{SD}+\Delta\sigma_{SD}$, and go to Step 1.

Step 3: Stopping criterion

If $l\ge L$ and $m_l<M$ during this iteration, stop the whole process, and the code capacity is defined as $\sigma^*_{SD}=\sigma_{SD}-\Delta\sigma_{SD}$. Otherwise, output the threshold value of channel parameter as $\sigma^*_{SD}=\sigma_{SD}$.

Using Algorithm 1, we can obtain the corresponding σ^*_{SD} from a given degree distribution of the upper layer LDPC code.

C. Optimal Design Of Degree Distribution Of The Lower Layer LDPC Code

Our goal is to search the optimal degree distribution of the network LDPC code, which can approach the capacity limit. Here we use differential evolution algorithm to optimal design of the network LDPC code sets.

Algorithm 2: Assume that N relay code sets of the network LDPC code structure are randomly generated, denoting their degree distributions of variable node as $\lambda_{i,j}(d), 0\le i\le d_v, 0\le j\le d_v^{'}, d=1,2,...N$. The degree of the lower check nodes is fixed as $d_c^{'}$.

Step 1: Initialization

Initialize that degree distribution as

$$C(d)=\{\lambda_{i,j}(d), 0\le i\le d_v, 0\le j\le d_v^{'}\}, d=1,2,\cdots,N. \tag{6}$$

Step 2: Performance estimation of code set

Calculate the code capacity $\sigma^*(d)$ of each code set $C(d)$ through the Algorithm 1, and search the optimal code set meeting $C^*=\arg\max_{1\le d\le N}\sigma^*(d)$. The degree distribution of the optimal code set corresponding to the maximum code capacity is $C^*=\{\lambda^*_{i,j}, 0\le i\le d_v, 0\le j\le d_v^{'}\}$.

Step 3: Code set updating

Select $\widetilde{N}$ code sets from $\{C(d)\}_{d=1}^{N}$ at random, and denote their degree distribution as $\widetilde{C}(k)=\{\lambda_{i,j}(k), 0\le i\le d_v, 0\le j\le d_v^{'}\}, k=1,2,\cdots,\widetilde{N}$. Then update the degree distribution of the code set: $C^*=C^*+\alpha\Sigma_{k=1}^{\widetilde{N}}(-1)^{k-1}\widetilde{C}(k)$, where $\alpha<1$ is the step length.

TABLE I
FOUR DIFFERENT PARAMETERS OF THE JOINT NETWORK LDPC CODES

Code Set	Code A	Code B	Code C	Code D
$d_v^{'}$	2	2	2	2
$d_c^{'}$	4	4	4	7
k_2	2814	4814	2814	2814
σ_{RD}	0.5	0.5	0.8	0.5
η	0.942065	0.904808	0.942065	0.902835
σ_{SD}^*	1.0568	1.0987	1.0393	1.1116
Threshold	0.15504dB	0.11512dB	0.20180dB	-0.22877dB
Capacity Limit	-0.24536dB	-0.51762dB	-0.14395dB	-0.24536dB
Gap	0.40040dB	0.63274dB	0.34575dB	0.01666dB

Step 4: Stopping criterion

If reaching the preset number of iteration and $m_l < M$, stop the iteration process. The degree distribution of the optimal code set is defined as $C^* = \{\lambda_{i,j}^*, 0 \le i \le d_v, 0 \le j \le d_v^{'}\}$; Otherwise, go to Step 3.

Remark: Restrictive conditions must be met for Step 1 and Step 3.

$$\begin{cases} \sum\limits_{i\ge 0, j\ge 0} \lambda_{i,j} = 1 \\ \lambda_i = \frac{1}{\eta} \sum\limits_{j\ge 0} \frac{i}{i+j} \lambda_{i,j} \\ \eta = \sum\limits_i \sum\limits_j \frac{i}{i+j} \lambda_{i,j} \\ d_c^{'} = \frac{1-\eta}{\sum\limits_j \frac{\lambda_{0,j}}{j}} \end{cases} \tag{7}$$

where η is the proportion of the total number of edges in the upper sub-graph. The total number of upper-layer edges of a source node is $E = \frac{n_1}{\sum\limits_{i\ge 2} \frac{\lambda_i}{i}} = \frac{k_1}{\sum\limits_{j\ge 2} \frac{\rho_j}{j}}$, and the total number of edges of the bilayer network LDPC code is $E^{'} = 2E + k_2 \cdot d_c^{'}$, so $\eta = \frac{2E}{E^{'}}$.

IV. SIMULATION RESULTS

Assume each source node employs an $(n_1, n_1 - k_1)$ LDPC code with $\lambda(x) = 0.23403x + 0.21242x^2 + 0.1469x^5 + 0.102840x^6 + 0.30381x^{19}$, and $\rho(x) = 0.71875x^7 + 0.28125x^8$, where $n_1 = 22164, k_1 = 11082$. $\text{SNR}_{RD} = 3\text{dB}$ and the two source-destination links are assumed to be symmetric. Using the Algorithm 1, four different parameters of the joint network LDPC codes, are obtained and listed in Table I, where σ_{RD}^2 represents the channel parameter between the relay-destination link.

Using the Algorithm 2, four optimal degree distributions of the joint network LDPC codes are given in Table II III IV.

The BER curves of four codes are illustrated in Fig.3. We see that the gap between the decoding threshold of four codes obtained by searching the maximum decoding threshold σ_{SD}^* and capacity limit is less than 0.7dB, and that between BER performance and decoding threshold is less than 0.4dB. Since the lower check degree of Code D is bigger and more information bits are contained in the check equation, it outperforms Code A by 0.2dB gains at BER $= 10^{-5}$. Another important observation is that Code B has a gain of about 0.15dB over Code A at BER $= 10^{-5}$ and the performance gain of Code D is about 0.1dB over Code B at BER $= 10^{-5}$. This indicates that increasing degrees of lower-layer check nodes is better than increasing the numbers of parity bits to improve system performance. When the noise variance between R-D link is increased, the system decoding performance will be reduced and Code A will have a gain of about 0.2dB over Code C at BER $= 10^{-5}$.

TABLE II
THE OPTIMAL DEGREE DISTRIBUTIONS OF CODE A

$\lambda_{i,j}$	$\lambda_{i,0}$	$\lambda_{i,1}$	$\lambda_{i,2}$
$i=2$	0.193815	0.00543635	0.04612661
$i=3$	0.171369	0.019109592	0.02409292
$i=6$	0.129299	0.006342408	0.00494214
$i=7$	0.09485	0.00008237	0.00259462
$i=20$	0.273877	0.000432436	0.00181212
$i=0$	0	0.0030528	0.02276564

TABLE III
THE OPTIMAL DEGREE DISTRIBUTIONS OF CODE B

$\lambda_{i,j}$	$\lambda_{i,0}$	$\lambda_{i,1}$	$\lambda_{i,2}$
$i=2$	0.07441004	0.20599344	0
$i=3$	0.19208258	0.0001582	0
$i=6$	0.13270189	0.00013842	0.00016819
$i=7$	0.09266986	0.00032638	0.00017797
$i=20$	0.27426244	0.00051525	0.0021752
$i=0$	0	0.0237937	0.0000099

TABLE IV
THE OPTIMAL DEGREE DISTRIBUTIONS OF CODE C

$\lambda_{i,j}$	$\lambda_{i,0}$	$\lambda_{i,1}$	$\lambda_{i,2}$
$i=2$	0.1206132	0	0
$i=3$	0.1001453	0.0000219	0
$i=6$	0.1860514	0.0002767	0.0000167
$i=7$	0.1964141	0.0002114	0.0000212
$i=20$	0.3858558	0.0003262	0.0000362
$i=0$	0	0.0041565	0.0206487

TABLE V
THE OPTIMAL DEGREE DISTRIBUTIONS OF CODE D

$\lambda_{i,j}$	$\lambda_{i,0}$	$\lambda_{i,1}$	$\lambda_{i,2}$
$i=2$	0.1112574	0.0136437	0.1818773
$i=3$	0.0917291	0.0876831	0.0571696
$i=6$	0.1322349	0.0003256	0.0001570
$i=7$	0.0926749	0.0000457	0.0000678
$i=20$	0.2740590	0.0001011	0.000217
$i=0$	0	0.0035171	0.0207269

V. CONCLUSION

In this paper, we employed differential evolution method to design degree distribution of the joint network LDPC code

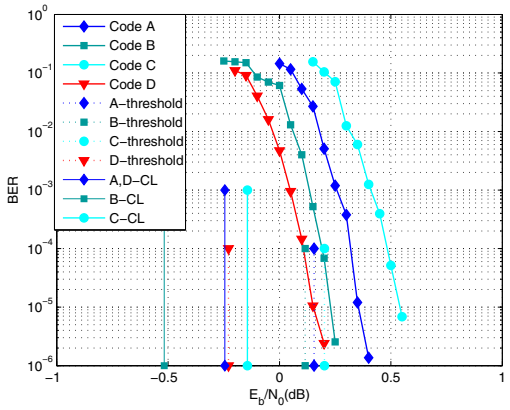


Fig. 3. Performance of the joint network LDPC codes

for a two-source single-relay system, under the assumption of symmetric AWGN channel. The performance of the new codes we designed have significant BER performance gain for a two-source single-relay system with symmetric channels.

ACKNOWLEDGMENT

This work was supported by NSFC(61072064) and NSFC(61101148).

REFERENCES

[1] T. Cover and A. E. Gamal, "Capacity theorems for the relay channel," *IEEE Trans. Inf. Theory.*, vol. 25, pp. 572-584, Sep. 1979.

[2] A. Nosratinia, T. E. Hunter, and A. Hedayat, "Cooperative Communication in Wireless Networks," *IEEE Communications Magazine.*, vol. 42, no. 10, pp.74-80, October 2004.

[3] J. Laneman, D. Tse, and G. Wornell, "Cooperative Diversity in Wireless Networks: Efficient Protocols and Outage Behavior," *IEEE Transactions on Information Theory.*, vol. 50, no. 12, pp. 3062-3080, December 2004.

[4] P. Razaghi and W. Yu, "Bilayer low-density parity-check codes for decode-and-forward in relay channels," *IEEE Trans. Inf. Theory.*, vol. 3, no. 10, pp. 3723-3739, Oct. 2007.

[5] M. H.Azmi, J. Yuan, J. Ning and H. Q.Huynh, "Improved Bilayer LDPC Code Using Irregular Check Node Degree Distribution ," *in Proc. IEEE Int'l Symposium on Information Theory.*, Toronto, Canada, July. 2008.

[6] J. P.Cances and V. Meghdadi, "Optimized Low Density Parity Check Codes Designs for Half Duplex Relay Channels," *IEEE Trans. Wireless Commun.*,vol. 8, no. 7, pp. 3390-3395, July. 2009.

[7] Y. Li, G. H. Song, and L. L. Wang, "Design of joint network-low density parity check codes based on the EXIT charts," *IEEE Commun. Lett.*, vol. 13, no. 8, pp. 600-602, Aug. 2009.

[8] Y. Li, G. H. Song, and L. L. Wang, "Analysis of the joint network LDPC codes over orthogonal multi-access relay channel," *IEEE Commun. Lett.*, vol. 14, no. 2, pp. 184-186, Feb. 2010.

The Design of Rate Compatible Network LDPC Codes

Jingyi Wang，Ying Li，Yue Sun，
State Key Lab. of Integrated Service Networks, Xidian Univ., Xi'an , China

Abstract: This paper studies the design of rate compatible network LDPC codes and proposes a rate-compatible puncturing algorithm, which can obtain the minimum error probability. First, based on the structure of network LDPC codes, the recovery error probability is derived. Then an algorithm of finding variable nodes to be deleted based on the tanner graph of network LDPC codes is proposed, which is aimed at minimizing the decoding error probability and optimizing the puncturing pattern. Simulation results show that the proposed methods of rate-compatible network-LDPC codes have 0.4dB of gain at $BER=10^{-4}$ in error performance compare to the existing punctured methods.

Keywords: multi-access relay channel; Network-LDPC code; rate-compatible; puncturing

速率兼容网络 LDPC 码的设计

王静怡，，李颖，孙岳
西安电子科技大学　综合业务网理论及关键技术国家重点实验室，西安，中国，710071

摘　要：本文研究了网络 LDPC 码的速率兼容算法设计，提出了一种可以获得最低译码错误概率的速率兼容删余算法。首先针对网络 LDPC 码的结构特点，推导了译码恢复错误概率，并基于网络 LDPC 码的 Tanner 图搜索需要删余的变量节点，并以达到最小译码错误概率为目标，获得最优的删余图样。仿真结果表明，与采用现有算法获得的网络 LDPC 码相比，采用所提的改进速率兼容算法获得的网络 LDPC 码的性能在 $BER=10^{-4}$ 时有 0.4 个 dB 的性能增益。

关键词：多址接入信道；网络 LDPC 码；速率兼容；删余

1　引言

无线通信系统中采用中继协作传输技术，可以获取额外的分集增益，从而改善系统性能。但是，对于多址接入中继网络，有多个节点同时需要中继节点帮助转发数据，传统的译码转发或者放大转发模式，会使得中继转发效率降低。因此，通过在中继节点设计有效的联合网络-信道编码算法，在改善接收端性能的同时提高转发效率，是目前的研究热点之一。文献[4]利用低密度奇偶校验(LDPC)码，针对多址接入中继信道设计了一种网络 LDPC 码，并指出可以通过调整中继节点转发数据量来实现中继转发效率和接收端译码性能的有效折中。但是，文中并没有给出具体实现算法，本文将在此基础上，研究适用于网络 LDPC 码的速率兼容算法。

速率兼容码的概念由文献[1]首次提出，文中研究了速率兼容卷积码的设计。删余是实现速率兼容的一种常用方法，即通过将低码率母码中的某些编码比特删余来获取高码率码。速率兼容 LDPC 码的设计是近几年研究热点，文献[2，3]通过分组和排序操作，将 LDPC 码的变量节点按照迭代恢复次数进行分类，设计了 LDPC 码速率兼容删余算法。

资助信息：国家自然基金项目(61072064)；国家科技重大专项(2010ZX03003-003-03)；长江学者和创新团队发展计划资助(IRT0852)；中央高校科研业务费专项资金项目(K50510010026).

(C)1994-2023 China Academic Journal Electronic Publishing House. All rights reserved.　http://www.cnki.net

2 适用于多址接入中继信道的网络 LDPC 码

由两个源节点和一个中继节点构成的多址接入中继网络模型如图 1 所示，两个源节点与目的节点之间的信息传输由广播发送和中继转发两个阶段完成。在广播阶段，两个源节点分别向中继节点和目的节点广播发送编码序列 X_1 和 X_2；在中继转发阶段，中继节点首先对接收信号进行译码，得到两个源节点的估计数据，然后对译码得到的估计数据重新进行联合编码，并将编码序列 X_R 转发至目的节点。目的节点则根据收到的信号进行联合译码，得到两个源节点的估计信息。

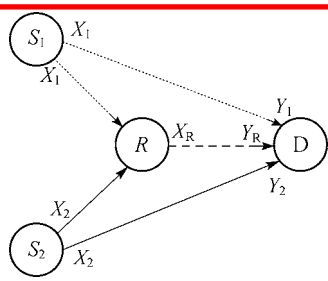


图 1　多址接入中继信道模型

在目的节点端将两个源节点和中继节点采用的 LDPC 码综合考虑，得到如下校验矩阵

$$\boldsymbol{H}=\begin{pmatrix}\boldsymbol{H}_1 & \boldsymbol{0} & \boldsymbol{0}\\ \boldsymbol{0} & \boldsymbol{H}_1 & \boldsymbol{0}\\ \boldsymbol{A} & \boldsymbol{B} & \boldsymbol{C}\end{pmatrix} \qquad (1)$$

式中，$\boldsymbol{H}_1$ 是源节点采用 LDPC 码的校验矩阵，$\boldsymbol{H}_3=(\boldsymbol{A}\quad \boldsymbol{B}\quad \boldsymbol{C})$ 是中继节点采用 LDPC 码的校验矩阵和 $\boldsymbol{0}$ 是零矩阵。由于式(1)中包括了源节点和中继节点所采用 LDPC 码的校验矩阵，并且中继节点是对两个源节点的数据进行联合编码，因此文献[4]称之为网络 LDPC 码，该码的 Tanner 图如图 2 所示。

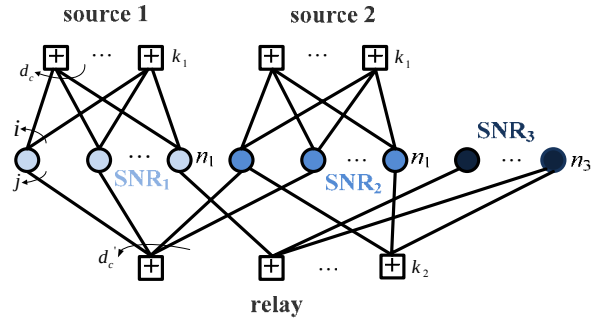


图 2　网络 LDPC 码的 Tanner 图

由图 2，网络 LDPC 码的 Tanner 图中包含上下两层子图，其中上层子图包含 $2k_1$ 个校验节点，它们与变量节点连接关系由式(1)中的 $\boldsymbol{H}_1$ 确定；下层子图包括 k_2 个校验节点，它们与变量节点的连接关系由式(1)中的 $\boldsymbol{H}_3$ 确定。图中每个变量节点的度用 (i,j) 表示，其中 i 为变量节点与上层校验节点相连的边数，j 为变量节点与下层校验节点相连的边数，d_c 和 d_c' 分别表示上层和下层校验节点的度数。

3 速率兼容网络 LDPC 码的设计

3.1 几个定义

定义 1(n 步恢复变量节点)：第 n 次迭代译码时才可以恢复的被删除的变量节点称为 n 步恢复变量节点，用 n-SR 表示。n-SR 的集合用群 G_n 表示。

定义 2(幸存校验节点)：如果一个一步恢复的删余变量节点至少与一个校验节点相连，且与这个校验节点相连的其它变量节点没有都被删余掉，那么这个校验节点就是幸存校验节点。图 3 中的校验节点 S_1 和 S_2 即为幸存校验节点。相反，校验节点 D 即为死校验节点。

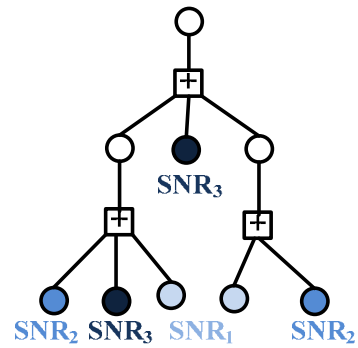


图 3　网络 LDPC 码的恢复树(横线圆表示幸存的变量节点 $S(v)$，竖线圆表示删掉的变量节点)

定义 3(幸存变量节点)：与幸存校验节点相连的其它没有被删除的变量节点称为幸存变量节点。

定义 4(等效幸存邻居变量节点数)：假设网络 LDPC 码所有编码比特在传输过程中受 K 种噪声干扰，对应噪声方差分别为 $\sigma_1^2>\sigma_2^2>\cdots>\sigma_K^2$，令每个受到噪声干扰最大(噪声功率为 σ_1^2)的幸存邻居变量节点的等效幸存邻居变量节点数为 1，则受其他噪声干扰的幸存邻居变量节点的等效幸存邻居变量节点数定义为

$$\alpha_i=\left(\log\left[1-\phi\left[\frac{2}{\sigma_i^2}\right]\right]\Big/\log\left[1-\phi\left[\frac{2}{\sigma_1^2}\right]\right]\right)\leqslant 1 \qquad ()$$

(C)1994-2023 China Academic Journal Electronic Publishing House. All rights reserved.　http://www.cnki.net

式中，$i=1,2,\cdots,K$。

$$\phi(x)=\begin{cases}\dfrac{1}{\sqrt{4\pi x}}\displaystyle\int_R \tanh\frac{u}{2}e^{-\frac{(u-x)^2}{4x}}su & x>0\\ 0 & x=0\end{cases}。$$

3.2 译码恢复错误概率

将网络 LDPC 码的删余变量节点 v 的所有幸存邻居变量节点按照其所通过信道的噪声功率的大小分为 b 类，假设第 t 类的噪声功率为 $\sigma_t^2(t=1,2,\cdots,b)$，且 $\sigma_1^2>\sigma_2^2>\cdots>\sigma_b^2$,并设第 t 类包括 S_t 个变量节点，记为 $\{v_1^t,\cdots,v_s^t,\cdots v_{S_t}^t\}$。与 LDPC 码类似，首先估计每次迭代过程中网络 LDPC 码的每个变量节点的均值更新，并由此计算该节点的恢复错误概率。

$\rho^{up}(x)=\sum_{k=1}^{d_c}\rho_k^{up}x^{k-1}$ $\rho^{low}(x)=\sum_{k=1}^{d_c'}\rho_k^{low}x^{k-1}$ 假设校验节点的度分布分别为 $\rho^{up}(x)=\sum_{k=1}^{d_c}\rho_k^{up}x^{k-1}$ 和 $\rho^{low}(x)=\sum_{k=1}^{d_c'}\rho_k^{low}x^{k-1}$，其中 η 是上层变量节点与校验节点相连的边数占总边数的比例，$\lambda_{i,j}$ 是与度为 (i,j) 的变量节点连接的边数占总边数的比例。$m_{i,j}^{l-1}$ 和 $n_{i,j}^{l-1}$ 分别表示第 $(l-1)$ 次迭代时，变量节点传给上下层的校验节点的对数似然比的均值。第 l 次迭代时，上下层校验节点的均值更新过程如下：

$$m^{'l}=\sum_k\rho_k^{up}\phi^{-1}\left(\left(\frac{1}{\eta}\sum_{i\geqslant0,j\geqslant0}\frac{i}{i+j}\lambda_{i+j}\phi(m_{i,j}^{l-1})\right)^{\sum_{t=1}^{b}S_t\alpha_t}\right)$$

$$n^{'l}=\sum_k\rho_k^{low}\phi^{-1}\left(\left(\frac{1}{1-\eta}\sum_{i\geqslant0,j\geqslant0}\frac{j}{i+j}\lambda_{i+j}\phi(n_{i,j}^{l-1})\right)^{\sum_{t=1}^{b}S_t\alpha_t}\right)\quad()(1)$$

当上下层的校验节点向被删余的度为 (i,j) 变量节点 $v\in G_{l+1}$ 传递消息时，该消息的对数似然比的均值分别为:

$$m^{'l}=\sum_k\rho_k^{up}\phi^{-1}\left(\left(\frac{1}{\eta}\sum_{i\geqslant0,j\geqslant0}\frac{i}{i+j}\lambda_{i+j}\phi(m_{i,j}^{l-1})\right)^{\sum_{t=1}^{b}S_t\alpha_t}\right)$$

$$n^{'l}=\sum_k\rho_k^{low}\phi^{-1}\left(\left(\frac{1}{1-\eta}\sum_{i\geqslant0,j\geqslant0}\frac{j}{i+j}\lambda_{i+j}\phi(n_{i,j}^{l-1})\right)^{\sum_{t=1}^{b}S_t\alpha_t}\right)$$

其中，α_t 表示每个幸存邻居变量节点的等效幸存邻居变量节点数，S_t 表示与变量节点 v 相连的校验节点没有被删余的变量节点数，变量节点 m_L v 的总等效幸存邻居变量节点数为 $\sum_{t=1}^{b}S_t\alpha_t$。

(2) 当上下层的校验节点向没有删余的度为 (i,j) 的变量节点传递消息时，该消息的对数似然比的均值分别为：

$$m^{'l}=\sum_k\rho_k^{up}\phi^{-1}\left(\left(\frac{1}{\eta}\sum_{i\geqslant0,j\geqslant0}\frac{i}{i+j}\lambda_{i+j}\phi(m_{i,j}^{l-1})\right)^{k-1}\right)$$

$$n^{'l}=\sum_k\rho_k^{low}\phi^{-1}\left(\left(\frac{1}{1-\eta}\sum_{i\geqslant0,j\geqslant0}\frac{j}{i+j}\lambda_{i+j}\phi(n_{i,j}^{l-1})\right)^{k-1}\right)$$

上下层变量节点的均值更新过程如下：

假设 $m^{'l}$ 和 $n^{'l}$ 分别表示第 l 次迭代时，上层和下层的校验节点传给变量节点的对数似然比消息均值。第 l 次迭代时，度为 (i,j) ()变量节点传给上下层校验节点的对数似然比消息均值分别为[4]

$$m_{i,j}^{l}=\begin{cases}(i-1)m^{'l}+jn^{'l}+m_{u_0} & i\neq0,j\geqslant0\\ jn^{'l}+m_{u_0}^{'} & i=0,j\geqslant1\end{cases}\qquad(7)$$

$$n_{i,j}^{l}=\begin{cases}im^{'l}+(j-1)n^{'l}+m_{u_0} & i\neq0,j\geqslant1\\ (j-1)n^{'l}+m_{u_0}^{'} & i=0,j\geqslant1\\ im^{'l}+m_{u_0} & i\neq0,j=0\end{cases}$$

若变量节点被删掉，则 $m_{u_0}(m_{u_0}^{'})=0$；若变量节点为由源节点发送至目的节点的信息比特，则 $m_{u_0}=2/\sigma_{SD}^2$；若变量节点为中继节点发送至目的节点的信息比特，则 $m_{u_0}^{'}=2/\sigma_{RD}^2$。第一次迭代时，校验节点的初始值 $m^{'(0)}=n^{'(0)}=0$。

因此，变量节点传给上下层校验节点的平均的消息均值分别为：

$$m^{l}=\frac{1}{\eta}\sum_{i\geqslant0,j\geqslant0}\frac{i}{i+j}\lambda_{i+j}m_{i,j}^{l}$$

$$n^{l}=\frac{1}{1-\eta}\sum_{i\geqslant0,j\geqslant0}\frac{j}{i+j}\lambda_{i+j}n_{i,j}^{l}$$

经过 L 次迭代后，码比特的平均消息均值为：

$$m_L=\eta m^L+(1-\eta)n^L$$

此时，网络 LDPC 码的被删余变量节点的恢复错误概率为：

$$P_e(v)=Q(\sqrt{m_L/2})$$

其中

$$Q(x)=\frac{1}{\sqrt{2\pi}}\int_x^{\infty}e^{-t^2/2}\mathrm{d}t。$$

(C)1994-2023 China Academic Journal Electronic Publishing House. All rights reserved. http://www.cnki.net

3.3 网络 LDPC 码的速率兼容算法

由公式(3)和(4)可知，等效幸存邻居变量节点数 $\sum_{t=1}^{b} S_t \alpha_t$ 越小，更新得到的均值 m'^{l} 和 n'^{l} 的值越大，进而迭代后的变量节点 m_L 的均值也越大，同时由公式(12)得到的恢复错误概率越小。因此，在搜索节点时，需要寻找当前具有最小等效邻居的变量节点进行删余操作。与文献[2]设计的 LDPC 码的删余算法相似，所提出的网络 LDPC 码速率兼容算法主要包括分组和排序两个操作。

分组：

(1) 给定一个 $M \times N$ [D1]网络 LDPC 码的校验矩阵，初始化 $R_\infty = \{1,2,\cdots,M\}$，$G_\infty = \{1,2,\cdots,N\}$，$l=1$；[D2]

(2) 遍历集合 R_∞，找出行重最小的行集合 r；[D3]

(3) 遍历集合 G_∞，找出列重最小的列集合 c；[D4]

(4) 选出所有(2)(3)相交的[D5]元素的集合 $w = \{(r^*, c^*), r^* \in r, c^* \in c\}$，作为候选对；

(5) 在集合 w 中选出具有最小等效幸存邻居变量节点数的元素，记为 (r_j^*, c_k^*)。若有多对满足条件，随机选出其中一对，归[D6]入第 l 次迭代可以恢复的集合 G_l，[D7]更新 $R_\infty = R_\infty \setminus r_j^*$ 和 $G_\infty = G_\infty \setminus c_k^*$；

(6) 若集合 G_∞ 为空，停止迭代，否则跳至(7)；

(7) 若集合 R_∞ 不为空，跳至(2)；否则若步骤(5)中有多于一对满足条件，则 $l = l+1$，跳至(2)。

接下来计算最大可达码率[2]为：

$$R_{\max} = \frac{R_0}{1 - \sum_{j=1}^{K} \left| G_j \right| / n} \tag{13}$$

式中，R_0 是母码的码率，n_i 是母码的码长。

[D8]如果要设计码率为 R_j 的码子，需要删余的节点数为[2]：

$$np_j = \left\lfloor \frac{n(R_j - R_0)}{R_j} \right\rfloor$$

式中 i，$0 \leqslant j \leqslant M$。

组内排序：

(1) 给定一个 $M \times N$ 网络 LDPC 码的校验矩阵[D9]，初始化 $R_\infty = \{1,2,\cdots,M\}$，$l=1$，$j=1$，$P_0 = \phi$；$R_0 \leqslant R_1 \leqslant \cdots \leqslant R_M \leqslant R_{\max}$

(2) 若 $j > M$，停止迭代[D10]；否则，$0 \leqslant j \leqslant M$ $P_j = P_{j-1}$；

(3) $\Delta = np_j - \left| P_j \right|$；[D11]

(4) 若 $\Delta = 0$，$j = j+1$ [D12]，跳至(2[D3])；

(5) 根据集合 G_l 定义 $C_l = \{c_1^*, c_2^*, \cdots\}$，从 C_l 中选出列重最大的变量节点的集合 $c_{\max}^*$，并从 $c_{\max}^*$ 中找出具有最小数量的死校验节点[D14]的变量节点 $c_{\max}^{**}$。如果有多个满足条件，随机选出其中一个，归入排序的集合 P_j，更新 $P_j = P_j \bigcup \{c_{\max}^{**}\}$，$G_l = G_l \setminus \{c_{\max}^{**}\}$，$\Delta = \Delta - 1$，$R_\infty = R_\infty \setminus r_{\max}^{**}$；

(6) 若 G_l 为空，$l = l+1$，$R_\infty = \{1,2,\cdots,M\}$；

(7) 跳至(4)。

经过上述分组和组内排序操作，将 $G_l (1 < l < K)$ () 变量节点按照 l 从小到大删余，而在同一个 G_l 中，按照变量节点的列号从小到大删余，直到删掉 np_j 个节点。

4 仿真结果

仿真中两个源节点采用的 LDPC 码的码长均为 2048，码率均为 0.5，度分布为：$\lambda(x) = 0.23403x + 0.21242x^2 + 0.1469x^5 + 0.102840x^6 + 0.30381x^{19}$ 和 $\rho(x) = 0.71875x^7 + 0.28125x^8$。中继节点采用的 LDPC 码的校验比特数为 628。假设信道模型为理想加性高斯白噪声(AWGN)信道，源节点和中继节点均采用 BPSK 调制方式。中继节点与目的节点之间的信噪比固定为 5dB。中继节点可以正确译码得到两个源节点的发送数据。图 4 和图给出了母码经过本文所改进算法(intentional)、现有算法(original)[2]和随机删余(random)所得到的码率为 0.5、0.6 和 0.7 的网络 LDPC 子码的 BER 性能对比。

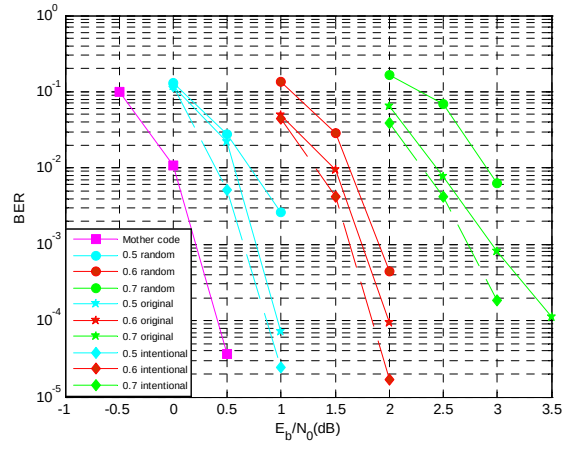


图 4 网络 LDPC 码的删余性能对比

由图 4 和图 5 可以看出，随着删余比特的增加，

(C)1994-2023 China Academic Journal Electronic Publishing House. All rights reserved. http://www.cnki.net

采用所提算法得到的网络 LDPC 码的性能增益也随之增加。当码率为 0.5， BER=10^{-3} 时，采用所提算法性能优于随机算法 0.45dB；当码率为 0.5，BER=10^{-4} 时，采用所提算法比文献[2]中算法的性能改善 0.15dB。在码率为 0.6， BER=10^{-3} 时，所提算法相对于随机算法性能增益为 0.3dB,相对于文献[2]中算法性能增益为 0.2dB。当码率为 0.7，SNR=3dB 时，所提算法的 BER 为 10^{-5} ，相比于随机算法的 10^{-3} 有了明显提升，而 BER=10^{-4} 时，所提算法比文献[2]中算法性能能增益改善 0.4 dB。

5 结论

文章首先介绍了网络 LDPC 码的结构及基本原理,然后针对其结构特性推导了译码恢复错误概率,并详述了适用于网络 LDPC 码的上下层变量节点和校验节点均值更新理论,接着介绍了网络 LDPC 码的速率兼容删余算法,最后对所设计的算法进行仿真,与现有算法相比，本文所提出的改进速率兼容算法在 BER=10^{-4} 时有 0.4dB 的性能增益。

参 考 文 献

[1] Hagenauer J. Rate-Compatible Punctured Convolutional Codes (RCPC codes) and Their Applications[J] . IEEE Trans on Communication, 1988, 36(4) : 389-400.

[2] J. Ha, J. Kim, D. Klinc, and S. W. McLaughlin, “Rate-Compatible Punctured Low-Density Parity-Check Codes With Short Block Lengths”, IEEE trans. Inform. Theory, vol. 52, no. 2, pp. 728-738, Feb. 2006.

[3] J. Ha, J. Kim, D. Klinc, and S. W. McLaughlin, “Rate-Compatible Puncturing of Low-Density Parity-Check Codes ”, IEEE trans. Inform. Theory, vol. 50, no. 11, pp. 2824-2836, NOV. 2004.

[4] Y. Li, G. H. Song, and L. L. Wang, “Design of joint network-low density parity check codes based on the EXIT charts”, IEEE Commun. Lett., vol. 13, no. 8, pp. 600-602, Aug. 2009.

(C)1994-2023 China Academic Journal Electronic Publishing House. All rights reserved. http://www.cnki.net

PAPER • OPEN ACCESS

A data transmission method of digital oilfield monitoring system based on Internet of Things

To cite this article: Jingyi Wang *et al* 2019 *J. Phys.: Conf. Ser.* **1237** 022065

View the article online for updates and enhancements.

You may also like

- Smart Parking System based on Improved OCR Model
Rami Bassam and Fars Samann
- New AlGaN/GaN HEMTs employing both a floating gate and a field plate
Jiyong Lim, Young-Hwan Choi, Young-Shil Kim et al.
- Motorcycle Start-stop System based on Intelligent Biometric Voice Recognition
A Winda, W R E Byan, Sofyan et al.



This content was downloaded from IP address 219.144.164.16 on 04/12/2023 at 06:53

IOP Conf. Series: Journal of Physics: Conf. Series **1237** (2019) 022065 doi:10.1088/1742-6596/1237/2/022065

A data transmission method of digital oilfield monitoring system based on Internet of Things

Jingyi Wang, Xuhua Sun, Hongbo Bu and Xu Fu

School of Computer Science, Xi'an Shiyou University, Xi'an 710065, China

jywang@xsyu.edu.cn

Abstract. To combat the effects that artificial patrols oilfield, artificial inputs production data and the accident is not handed in time, a novel data transmission method is proposed for digital oilfield to make data safe and reliable. Firstly, an oilfield monitoring system based on the Internet of Thing is introduced. Then the proposed method introduces a threshold and only forwards those data which meet the requirements. Furthermore, the proposed data transmission strategy is discussed in detail. It is shown in simulation that the gap between the gain performance of the proposed strategy with the optimal threshold and error-free relay station is only 0.01 dB at $BER = 10^{-6}$.

1. Introduction

It is well-known that Internet of Things (IoT) has gained enough attention from different researchers in industry. IoT communication mainly deals with the exchange of information between objects, people and objects and people. The IoT technology integrates Radio-Frequency, sensor, and nanotechnology, which will be an important technology to change people's life and lifestyle[1].

With the continuous development of computer technology and information technology, the concept of digital oilfield construction will be a kind of highly efficient and refined oilfield construction management mode gradually. The established oilfield based on the IoT realizes the interconnection between objects and the Internet, and the real-time communication and information transmission between proprietary equipment. The monitoring centre can complete the management, statistics and monitoring of relevant data by the collected production data quickly and efficiently. Yang Yubin[2] has proposed a remote monitoring system of pumping unit based on the IoT, which can monitor the operation of pumping unit in real time and not optimize problems such as packet loss and accuracy during the transmission process of specific data. Yang Lei[3] has constructed an overall hardware framework of the well site security IoT system and studied the security information acquisition and transmission subsystem and the three-layer architecture of security monitoring centre, but did not study the accuracy transmission process of data. Khan et al.[4] has proposed a new architecture-based IoT for the oil and gas industry, which makes the data simple, safe, reliable, fast and collected by smart devices, but did not give a specific framework. Gharibi et al.[5] has proposed a reliable, safe and scalable sensor system that can monitor oil and gas equipment, and specific performance is not given.

In order to ensure unmanned operation of equipment with low signal-to-noise ratio and reliable coordination and communication of remote data, this paper establishes a remote transmission monitoring system for oilfield based on the new Internet of Things technology. The established system is characterized by flexible network formation, low cost, high efficiency, safety and reliability, and

Content from this work may be used under the terms of the Creative Commons Attribution 3.0 licence. Any further distribution of this work must maintain attribution to the author(s) and the title of the work, journal citation and DOI.
Published under licence by IOP Publishing Ltd

convenient maintenance. The main thing is that a wireless data transmission scheme is proposed in digital oilfield based on the Internet of Things.

2. System Description

In this section, a novel smart monitoring system of digital oilfield based on IoT is given and then a multi-well cascade data transmission method is presented.

2.1. A novel smart monitoring system of digital oilfield based on IoT

This system consists of smart senor object, smart gateway and data processing centre (see Fig.1). Each part is responsible for its own specific function in order to improve the ability of the entire monitoring system between interconnected oil wells.

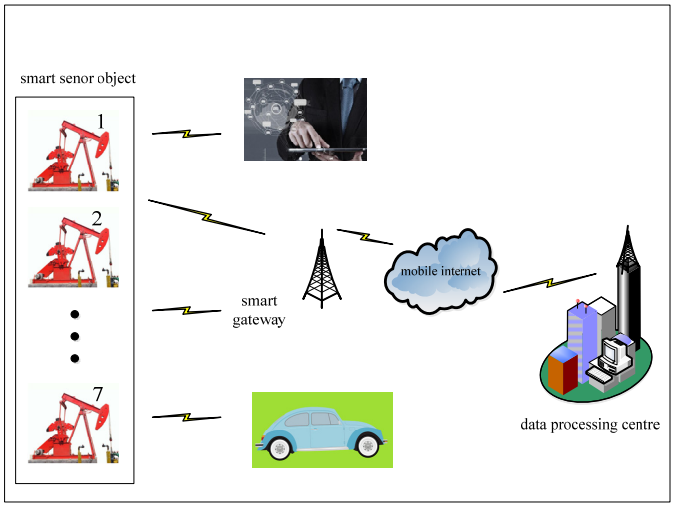


Fig.1 A smart monitoring system of digital oilfield based on IoT

Each smart senor object is a transmitting equipment, which is used to measure and gather data (electricity, load etc.) and send data to the data processing centre. It can independently make data decisions without human intervention. Once the smart senor object has collected the data, it will send useful information to the data processing centre in time. It can prevent abnormal situations from occurring on emergency. If the equipment on the wellheads needs to be repaired or maintained, the smart senor object can inform the data processing centre.

The smart gateway is a translator that acts as a relay between the smart senor object and the data processing centre. If the channel between the smart senor object and the data processing centre is unusable, the smart gateway will be able to send information that transmitted by the smart senor object.

The data processing centre is a terminal equipment, which collects and analyses the data from the source equipment. It also extracts useful information from the received data based on different data analysis methods, and then analyses problems and takes effective measures against emergencies.

These three components interrelate with each other in a transmission process to ensure the whole system safe and reliable.

2.2. System model of data transmission

According to the system structure, a multi-well collective relay communication mode is proposed. Its topological structure was shown in Fig.2.

The WHC receives the collected data from each wireless instrument, processes the data and then sends it to the data processing centre. At the same time, the WHC receives the command from the centre and controls the normal operation of various devices in the whole system.

Wireless ZigBee instrument equipment can be used to collect current, temperature, pressure, load, displacement and other data. After that, the data information is sent to the WHC.

Relay stations are mainly to process and forward data information to the data processing centre, so as to expand the transmission distance of network.

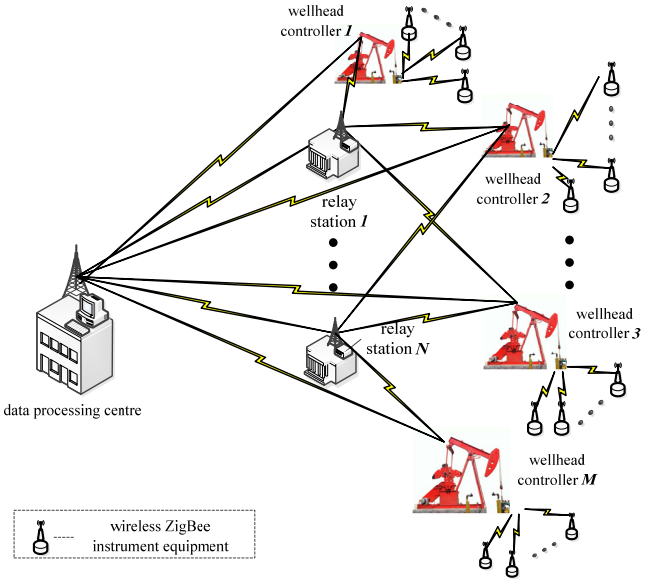


Fig. 2 The topological structure of the process of transmitting data

Fig.2 can be modelled as the network model shown in Fig.3. The transmission process of the whole network is composed of two stages as follows:

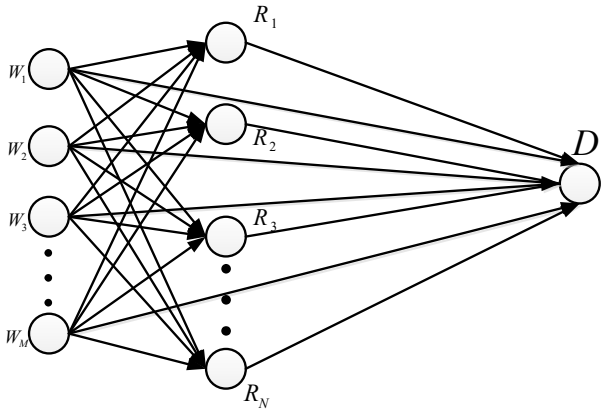


Fig.3 The wireless network model with M WHCs and N relay stations

In the first stage, M WHCs broadcast their collected data X_i^t ($i=1,2,\cdots,M$) to the N relay stations and the data processing centre D, where the superscript t represents time throughout this paper. Then we have

$$Y_{i,D}^t = h_{i,D}^t X_i^t + N_{i,D}^t \tag{1}$$

$$Y_{i,j}^t = h_{i,j}^t X_i^t + N_{i,j}^t \tag{2}$$

where $Y_{i,D}^t$ and $Y_{i,j}^t$ are the corresponding data information received by the relay station R_j and the data processing centre D respectively, $N_{i,D}^t$ and $N_{i,j}^t$ are the noise random variables.

In the second stage, the relay station R_j processes the data sent from all the WHCs. If the data information does not meet the requirements of the system, the relay station R_j blocks the data information and does not forward it to the data processing centre. After this process, the relay station

R_j re-processes the data and forwards the selected data sequence to the data processing centre. Let X_j^t be the data transmitted by the relay station R_j. The received data at the data processing centre is

$$Y_{j,D}^t = h_{j,D} X_j^t + N_{j,D}^t \tag{3}$$

where $Y_{j,D}^t$ is the received data information at the data processing centre D from the relay station R_j, $N_{j,D}^t$ is a noise random variable.

3. Transmission Strategy

In this section, a transmission strategy is deduced based on the research results in the paper [6]. If the bit log-likelihood ratio (LLR) of the received data is below the predetermined threshold, the relay station keeps still and does not send any information. Otherwise, the selected data are sent. We obtain optimum threshold by minimizing error bit probability.

3.1. Description of Threshold

Let Λ_i^j represents the bit LLR of the data of the i-th WHC at the R_j. We obtain

$$\begin{aligned}\Lambda_{x_i}^j &= \ln \frac{p(x_i = 1 \mid y_{i,j}, h_{i,j})}{p(x_i = -1 \mid y_{i,j}, h_{i,j})} = \ln \frac{p(y_{i,j} \mid x_i = 1, h_{i,j})}{p(y_{i,j} \mid x_i = -1, h_{i,j})} \\ &= 2 y_{i,j} h_{i,j} / \sigma_{i,j}^2\end{aligned} \tag{4}$$

where $p(\cdot)$ denote the conditional probability density function. Assuming that $N_{i,j}^t$ is the zero-mean additive Gaussian random variable with variance $\sigma_{i,j}^2$. And apparently, the magnitude of Λ_i^j is a reliable standard of the accurate data. The data of the WHC is estimated by R_j as

$$\hat{x}_i^j = sign(\Lambda_i^j) \tag{5}$$

where $sign(\cdot)$ is the signum function. The instantaneous error bit probability of Λ_i^j at the relay station R_j can be expressed by

$$P_{i,j} = \frac{1}{1 + e^{|\Lambda_i^j|}} \tag{6}$$

Let P_{eT} be the predetermined threshold, which means that the relay station transmits the estimated data $\hat{x}_i^j$ to the data processing centre in case of $P_{i,j} \le P_{eT}$. According to (6), we obtain

$$P_{i,j} = \frac{1}{1 + e^{|\Lambda_i^j|}} \le P_{eT}$$

or

$$|\Lambda_i^j| \ge \ln\left(\frac{1}{P_{eT}} - 1\right) = \Lambda_0 \tag{7}$$

From equations (4)-(7), Λ_i^j can provide the effective information of the maximum a-posteriori probability decision, which can minimize the error bit probability.

3.2. Optimization of Threshold

The relay station R_j estimates the value of the received data from each WHC. If the data bit LLR exceeds the predetermined threshold, the relay station operates and transmits the restored data to the data processing centre D. Otherwise, it keeps steady in the second stage. The transmitted data can be expressed as

$$X_j = \sum_{i=1}^{M} g_{i,j} \hat{X}_{i,j} \tag{8}$$

where $g_{i,j} = 0$ if $\left|\Lambda_i^j\right| < \Lambda_{i0}$, and $g_{i,j}$=1 if $\left|\Lambda_i^j\right| \geq \Lambda_{i0}$, Λ_{i0} is the threshold of set S_i.

Let P_i be the average error bit probability at the data processing centre. The optimal threshold Λ_{i0}^{opt} will be determined by minimizing P_i. So we have

$$\begin{aligned} &\min_{\Lambda_{i0}} \quad P_i \\ &s.t. \quad \Lambda_{i0} > 0 \end{aligned} \tag{9}$$

Therefore, equation(9) is a linear programming problem. Then, we can use the following probability distribution expression to solve the optimal threshold $\Lambda_{S_i 0}^{opt}$.

At the data processing centre D, two factors contribute to error information. One is that the relay station keeps steady and error data occurred in the direct link between WHC and data processing centre. The other one is that the relay station transmits the data information to the data processing centre and error data still occurred. Since these two factors are independent of each other, P_i can be expressed as

$$P_i = P_i^1 + P_i^2 \tag{10}$$

where P_i^1 and P_i^2 are the error data probabilities corresponding to the first and second factor, respectively. These two parts can be expressed

$$P_i^1 = P_i^{(WD)} \cdot Pr[\left|\Lambda_i\right| < \Lambda_{i0}] \tag{11}$$

$$\begin{aligned} P_i^2 &= Pr[\hat{X}_{i,j} = 1 \mid X_i = -1, \left|\Lambda_i\right| \geq \Lambda_{i0}] \\ &= P_i^{(MAC)} \cdot (1 - P_{i,j}^e) + P_i^{(X)} \cdot P_{i,j}^e \end{aligned} \tag{12}$$

where $P_i^{(WD)}$ is the error data probability that error data occurred in the WHC-data processing centre link. When the information is correct at the relay station R_j, $P_i^{(MAC)}$ is the error data probability that error occurred at the data processing centre by using the data information from both $W_i - D$ link and $R_j - D$ link. When the information is error at the relay station R_j, $P_i^{(X)}$ is the error data probability that error occurred at the data processing centre by using the data information from both $W_i - D$ link and $R_j - D$ link. $P_{i,j}^e$ is the error data probability that the relay station R_j operates the data information from the WHC by mistake. The expression of $Pr[\left|\Lambda_i\right| < \Lambda_{i0}]$ and $P_{i,j}^e$ are shown in [7].

Based on equations (10)-(12), we can easily solve the optimum threshold by minimizing the error data probability. And apparently, the optimal threshold Λ_{i0}^{opt} can be expressed

$$\Lambda_{i0}^{opt} = \log\left(\frac{P_i^{(X)} - P_i^{(MAC)}}{P_i^{(WD)}} - 1\right) \tag{13}$$

4. Simulation Results

We use a specific example with four WHCs, four relay stations, one data processing centre, and AWGN orthogonal channel with $SNR_{i,j} = SNR_{D,j}$ and $N_{j,D} = 0.3$. Assuming that each WHC transmits the coded data by using a (3824, 1912) irregular LDPC code with degree distribution $\lambda(x) = 0.21606x + 0.1576x^2 + 0.154x^4 + 0.01848x^5 + 0.04312x^6 + 0.41074x^{18}$, $\rho(x) = x^8$. At the relay stations, we operate data by using the RS code coefficients in the finite field GF(2^8), which is constructed based on the minimal polynomial $p(X) = 1 + X^2 + X^3 + X^4 + X^8$. The simulated results with all the threshold types including without any threshold, the preset threshold, the optimal threshold.

In Fig.4, we can see that the proposed strategy with $P_{eT}=10^{-1}$ provides more than 0.18dB gain performance at $BER=10^{-6}$ (bit error rate, *BER*) over no threshold. The gap between the proposed strategy with the optimal threshold and error-free relay station is only 0.01dB at $BER=10^{-6}$ .The proposed strategy with the optimal threshold has clear advantages over the others.

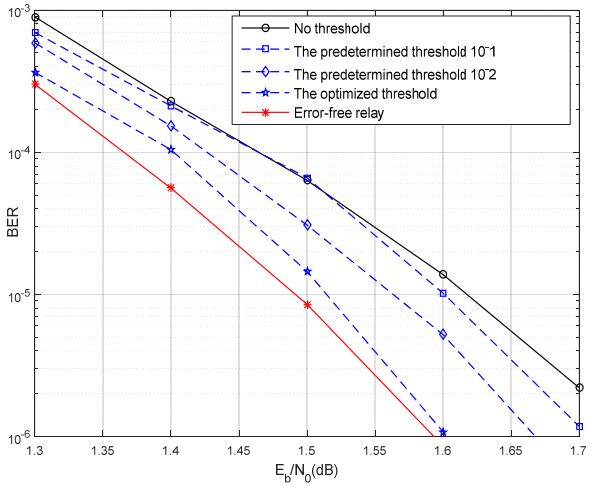


Fig.4 *BER* performance over AWGN channel

5. Conclusion

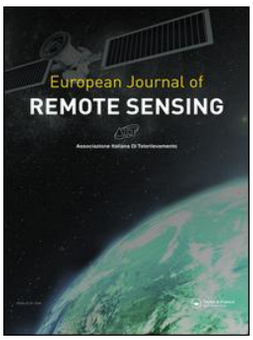
In this paper, an oilfield monitoring system based on the Internet of Thing is established. And then, a data transmission strategy with a threshold in digital oilfield is proposed. The novel strategy has been adopted in the linear programming problem to derive the instantaneous error data probability. The optimal threshold for the proposed strategy is obtained with respect to the minimized instantaneous error data probability. It is shown in simulation that the proposed strategy has significant effect on gain performance. In other word, it can make data of digital oilfield safe and reliable.

Acknowledgments

This work was financially supported by Innovation and Entrepreneurship Training program for college student of Shaanxi Province (201819040) and Special Scientific Research project of education department of Shaanxi Province (18JK0626).

References

[1] Atzori L., Iera A., et al. The internet of things: A survey[J]. Computer networks, 2010, 54(15):2787-2805.
[2] Chen Honglong. An experimental platform for remote monitoring of pumoing unit group based on Internet of Things[J]. 2016,33(2):114-116(in Chinese).
[3] Yang Lei. Research on Safety Monitoring System for Oilfield Well Sites Based on Internet of Things[D]. Xi'an: Xi'an Shiyou University,2016:13-25(in Chinese).
[4] W. Z. Khan, M Y Aalsalem., et al. M S Hossian and M Atiquzzaman. A reliable Internet of Things based architecture for oil and gas industry[C]. 2017 19th International Conference on Advanced Communication Technology(ICACT), Bongpyeong, 2017:705-710.
[5] Gharibi W, Aalsalem M, et al. Monitoring gas and oil fields with reliable wireless sensing and Internet of Things[C]. International Conference on Radar, Antenna, Microwave, Electronics, and Telecommunications. 2017:188-191.
[6] H. V. Khuong and H. Y. Kong, LLR-based decode-and-forward protocol for relay networks and closed-form ber expressions[J]. IEICE Trans. Fundamentals, 2006,E89A:1832-1841.
[7] Wang Jingyi. Study on Channel Codes in Wireless Relay Systems[D]. Xi'an: Xidian University,2016:47-60(in Chinese).



European Journal of Remote Sensing

ISSN: (Print) (Online) Journal homepage: https://www.tandfonline.com/loi/tejr20

Comparison on quantitative inversion of characteristic ions in salinized soils with hyperspectral based on *support vector regression* and *partial least squares regression*

Jingyi Wang & Xiaoming Li

To cite this article: Jingyi Wang & Xiaoming Li (2020) Comparison on quantitative inversion of characteristic ions in salinized soils with hyperspectral based on *support vector regression* and *partial least squares regression* , European Journal of Remote Sensing, 53:1, 340-348, DOI: 10.1080/22797254.2020.1854622

To link to this article: https://doi.org/10.1080/22797254.2020.1854622

© 2020 The Author(s). Published by Informa UK Limited, trading as Taylor & Francis Group.

Published online: 09 Dec 2020.

Submit your article to this journal

Article views: 23

View related articles

View Crossmark data

Full Terms & Conditions of access and use can be found at https://www.tandfonline.com/action/journalInformation?journalCode=tejr20

EUROPEAN JOURNAL OF REMOTE SENSING
2020, VOL. 53, NO. 1, 340–348
https://doi.org/10.1080/22797254.2020.1854622

Taylor & Francis
Taylor & Francis Group

OPEN ACCESS Check for updates

Comparison on quantitative inversion of characteristic ions in salinized soils with hyperspectral based on *support vector regression* and *partial least squares regression*

Jingyi Wang[a] and Xiaoming Li[b]

[a]College of Computer Science, Xi'an Shiyou University, Xi'an, China; [b]Key Laboratory of Degraded and Unused Land Consolidation Engineering, Ministry of Natural Resources, Xi'an, China

ABSTRACT

This study aimed to investigate quantitative inversion of salt ions. Now, most research on hyperspectral characters in salinized soils focus on quantitative inversion of salt content, but few on ions. Original hyperspectral data were collected and calculated average as reflectance (R), the logarithm of the reciprocal of R (Log(1/R)) and continual removed reflectance (R_{cr}) were also used. Correlations between salt content and ions were calculated, three ions were chosen as characteristic. SVR and PLSR methods were used to derive inversion models. Results showed both methods provided accurate measurement. For modeling precision, no matter which hyperspectral characters based on, inversion models derived with SVR were more accurate than PLSR. For test precision, inversion models derived with SVR were also more accurate. Inversion model of Cl^- based on R was the most accurate, followed by that based on R_{cr}, while the inversion model of K^+ based on R_{cr} was the most accurate. All the inversion models of Na^+ based on R, Log(1/R) and R_{cr} had good test precision. In conclusion, the accuracy of the quantitative inversion model with SVR was higher than PLSR, the best hyperspectral characters for inversion models were chosen, making a useful diagnostic tool for soil salinity.

ARTICLE HISTORY
Received 29 December 2019
Revised 19 November 2020
Accepted 19 November 2020

KEYWORDS
Quantitative inversion; soil salinization ions; hyperspectral data; characteristic bands

Introduction

Soil salinization is a global problem for resource and environment, being one of the most important barriers for land productivity. The area of salinized soils in China is about 3 600 × 10^4 ha, distributed in the regions of Shaanxi, Gansu, Ningxia, Qinghai, Xinjiang, and the east coastal areas (Yang, 2008). The national strategy to guarantee food safety intends to maintain the area of farmland in these regions, as well as to ensure no decrease in farmland quality. This requires soil salinization to be addressed early and warned and controlled adequately. Traditional methods of monitoring soil salinization consist of collecting soil samples and analyzing them in laboratory. While the precision of such methods is adequate, it is time-consuming and labor-intensive, making it hard to monitor a large area of land. As the electromagnetic technology was introduced, it enabled quick diagnosis of soil salinization at medium scales (Li et al., 2010). However, using this technology to monitor on a large scale is difficult. The development of remote sensing technology and particularly the application of hyperspectral technology that provide high resolution and abundant spectrum information enabled the quantitative inversion of salinization characters (Yao et al., 2013a). Remote sensing also enabled the realization of whole cover RS monitoring from the point scale to regional scale.

Soil salinization results from some conditions including land hydrologic, climatic, geologic, terrain conditions, and the human activities. And the spectral responses for salinized soil are closely related with its physical and chemical characteristics (Zhu et al., 2017). A number of national and international research have been conducted on quantitative inversion and monitoring for soil salinization with spectral characters. Some studies focused on the mining of hyperspectral data, extracting the hyperspectral characters having the best correlations with soil salt information, such as reflectance (R) (Duan et al., 2017), reciprocal of reflectance (1/R) (Yao et al., 2013a), logarithm of the reciprocal of reflectance (Log(1/R)), continual removed reflectance (R_{cr}) (Ding et al., 2012), and derivative transformations (J. Wang et al., 2009; D. Zhang et al., 2014), allowing them to derive the quantitative inversion models. Other studies focused on methods for deriving inversion models, such as multiple regression (Kelimu et al., 2016), support vector regression (SVR), partial least square regression (PLSR) (Dai et al., 2015; Qu et al., 2009), and artificial neutral networks (J. Wang et al., 2009). Some scholars used fused hyperspectral data and other primary data (such as electromagnetic data) to derive quantitative

CONTACT Xiaoming Li xmlihyc@126.com Key Laboratory of Degraded and Unused Land Consolidation Engineering, Ministry of Natural Resources, Xi'an, China

© 2020 The Author(s). Published by Informa UK Limited, trading as Taylor & Francis Group.
This is an Open Access article distributed under the terms of the Creative Commons Attribution License (http://creativecommons.org/licenses/by/4.0/), which permits unrestricted use, distribution, and reproduction in any medium, provided the original work is properly cited.

inversion models (Yao et al., 2013b, 2013a), while others applied the quantitative models with remote sensing image interpretation on larger scales (Kelimu et al., 2016). Recently, most researchers focus on the quantitative inversion of the total salt content using hyperspectral data, and only few scholars studied the quantitative inversion of salt ions (Dai et al., 2015; Liu et al., 2016; H. J. Wang et al., 2018). Furthermore, this specific research was limited to only one method to derive the inversion model. In this paper, quantitative inversion models of salt ions were derived using two different methods (SVR and PLSR), based on hyperspectral transformation data. The accuracy of each method was compared to indicate which would make the most useful diagnostic tool for soil salinization detection and monitoring at large regional scales.

Data and methods

Data collection

The study area was located in a typical salinized field where the soil type is *arenosols* by WRB classification in Dingbian County, north of Shaanxi province, which is shown in Figure 1. The soil salinization in this area is so severe that it has become one of the most serious limitations for agriculture, the crops are hard to grow. To empirically study the quantitative inversion of soil salinization, a large range of soil salinization is needed. Therefore, 70 sample points over different grades of salinization were selected randomly by viewing soil salt accumulation but not just by equal distance. All sampling points consisted of bare soil with no vegetation cover. 42 and 28 sample points were used to derive the inversion models and for precision testing, respectively. On each sample point, the hyperspectral data was collected first; then, the topsoil (0 ~ 10 cm) was sampled separately.

The hyperspectral data of reflectance were collected outdoors between 11:00, 14:00, using a FieldSpec 4 HR by ASD. The sampling intervals of the spectrum were 1.4 nm with a band wavelength of 350–1000 nm and 2 nm with the band wavelength of 1001–2500 nm; the resampling interval was 1 nm. The spectrum average was defined as 10, denoting that the reflectance was collected 10 times for each sample point.

Calibration was performed in the field before each measurement, using a whiteboard. Hyperspectral data were collected 10 times on each sample point. Additionally, some pretreatments were made in laboratory: the spectral data were loaded in the ViewSpecPro software, abnormal data were eliminated, and the average values were calculated as the hyperspectral characteristic values for a given sample point. In this paper, the hyperspectral characters of reflectance (R), the logarithm of the reciprocal of reflectance ($\mathrm{Log}(1/R)$), and the continual removed reflectance (R_{cr}) were used for the quantitative inversion; the former two characters were extracted directly using the ViewSpecPro software, whereas R_{cr} was obtained with the ENVI software.

After gathering the spectral data, the topsoil (0 ~ 10 cm) was sampled at each point to measure the salinization variables. All the soil samples were taken back to the laboratory, naturally air-dried, grinded, and sieved through a 2-mm mesh screen. Then, soil extract liquid (the soil/water ratio is 1/5) was made. Subsequently, the salinization characteristics, including the total content of soil salt and eight salinization ions (Ca^{2+}, Mg^{2+}, K^{+}, Na^{+}, SO_4^{2-}, Cl^{-}, CO_3^{2-}, HCO_3^{-}), were obtained through sample analysis (Lu, 1999): gravimetric method was used to determine the total content of soil salt, EDTA titration method was used to determine Ca^{2+} and Mg^{2+}, spectrophotometer was used to determine K^{+} and Na^{+}, EDTA indirect complexometric titration method was used to determine SO_4^{2-}, silver nitrate titration method was used to determine Cl^{-}, and double indicators neutralization titration method was used to determine CO_3^{2-} and HCO_3^{-}.

Methods

A correlation analysis between the total salt content and the eight salinization ions was performed, and the salinization characteristic ions were identified by selecting the high correlation coefficients. For the quantitative inversion of salinization characteristic ions, the correlations between the characteristic ionic content and the hyperspectral characters were analyzed, and the characteristic bands were selected using a correlation coefficient extreme method (Zhu et al., 2017) to derive the inversion models.

The PLSR and SVR methods were used to derive quantitative inversion models. Comparing with the traditional multiple regression method, the PLSR method combined all the advantages of a principal component analysis, typical correlation analysis, and multiple line regression and can be used to derive models even when there are strong correlations among variables and the number of the samples is less than the number of variables, so its precision is better than the traditional regression method (Q. Zhang et al., 2018). On the other hand, Support Vector Regression (SVR) is an application of support vector machine (SVM) to the regression problem, namely, to find a regression plane that minimizes the distance of all the data of a set from the plane (Liang et al., 2013). The SVR function can be expressed as:

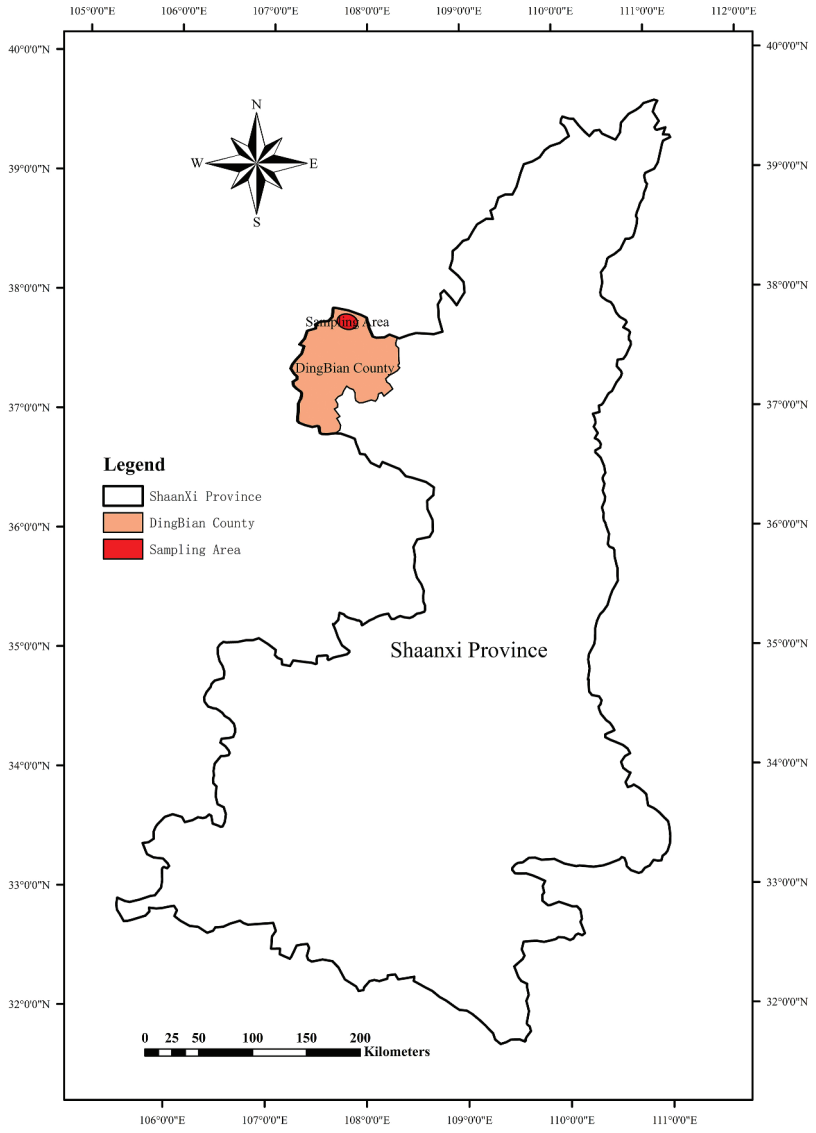


Figure 1. Location of the study area in Shaanxi Province.

$$f(x) = \sum_{i=1}^{N} \left(a_i - a_i^*\right) \cdot k(x, x_i) + b$$

where N is the number of samples, $(a_i \_ a_i^*)$ is the Lagrange multiplier, $k\ (x,\ x_i)$ is the kernel function, and b is the bias term.

For each method, the model precision was compared. All the calculations were realized with Matlab software, and the *PLSR* order in the toolbox and the *libsvm tool* by Chih-Chung Chang and Chih-Jen Lin were used to derive the models. To test the precision of quantitative inversion calculations, both the modeling precision and the test precision were compared. The determination coefficient (r^2) and the root mean square error (RMSE) were compared to determine modeling precision, while the correlations and RMSE between the predicted and the measured value with the test samples were compared to determine test precision.

Results and Discussion

Salinization characteristic ions

The summary statistics of the eight ions and the total salt content are shown in Table 1 The total salt content was from 1.050 g/kg to 29.380 g/kg, and its mean value was 7.690 g/kg, which meant the salinity level in the study area was serious. And that just could explain why the ration of seeding lack in the study area was high, and even nearly bare in some places. As to why the salinity is so serious, the study area is one of the main producing areas for lake salt, and the water in soil contents much soluble salt. When the water moves upwards, especially in the seasons of spring and autumn, the salt could move together, and accumulate on the top soil under the impact of strong evaporation. By the statistical data such as chorography, the salinity of Dingbian County could reach up to 50 g/kg, and even more.

The results of the correlation analysis between the total salt content and eight salinization ions showed

Table 1. Summary statistics for eight salinization ions and the total salt content (TS).

Variables	Sample Quantity (*n*)	Minimum (g/kg)	Maximum (g/kg)	Mean (g/kg)	Standard Deviation (*Std.*)
Ca^{2+}	70	0.050	0.330	0.089	0.057
Mg^{2+}	70	0.010	0.500	0.121	0.099
K^{+}	70	0.017	0.081	0.037	0.018
Na^{+}	70	0.115	0.787	0.362	0.168
SO_4^{2-}	70	0.070	0.226	0.161	0.045
Cl^{-}	70	0.011	0.694	0.174	0.177
CO_3^{2-}	70	0.001	0.002	0.002	0.001
HCO_3^{-}	70	0.003	0.020	0.013	0.004
TS	70	1.050	29.380	7.690	6.942

that the correlation coefficients of K^{+}, Na^{+}, and Cl^{-} are strong (Table 2), the correlation coefficients of Pearson were 0.861**, 0.953** and 0.987**, respectively, and the correlations were all significant at 0.01 level (2-tailed). It could be concluded that the salinization in our study area was caused by chlorides of potassium and sodium, and the characteristic ions should be K^{+}, Na^{+}, and Cl^{-}.

Table 2. Correlations among total content of soil salt (TS) and salt ions.

	Ca^{2+}	Mg^{2+}	K^{+}	Na^{+}	SO_4^{2-}	Cl^{-}	CO_3^{2-}	HCO_3^{-}	TS
Ca^{2+}	1.000								
Mg^{2+}	0.136	1.000							
K^{+}	0.219	0.777	1.000						
Na^{+}	−0.287	0.661	0.808	1.000					
SO_4^{2-}	−0.429	0.339	0.341	0.517	1.000				
Cl^{-}	−0.109	0.702	0.840	0.954	0.306	1.000			
CO_3^{2-}	−0.330	0.246	0.224	0.447	0.217	0.436	1.000		
HCO_3^{-}	−0.067	−0.182	−0.091	−0.079	−0.061	−0.071	−0.242	1.000	
TS	−0.093	0.776	0.861	0.953	0.340	0.987	0.427	−0.126	1.000

Table 3. Descriptive statistical characteristics of hyperspectral characters for Cl^{-} ion (*n*= 42).

Hyperspectral Character	Band	Min	Max	Mean	*Std.*	*Var.*
R	B465	0.070	1.023	0.282	0.306	0.094
	B1365	0.213	1.264	0.509	0.270	0.073
	B1407	0.188	1.251	0.488	0.274	0.075
	B2210	0.203	1.303	0.510	0.275	0.075
	B2353	0.202	1.296	0.501	0.275	0.076
Log(1/R)	B356	−0.110	1.470	0.889	0.450	0.202
	B1365	−0.195	0.676	0.332	0.212	0.045
	B1406	−0.200	0.727	0.353	0.226	0.051
	B2211	−0.227	0.693	0.331	0.223	0.050
	B2353	−0.228	0.698	0.340	0.227	0.051
R_{cr}	B495	0.743	1.000	0.883	0.073	0.005
	B762	0.804	1.000	0.982	0.045	0.002
	B1371	0.681	0.995	0.899	0.077	0.006
	B2140	0.559	1.000	0.896	0.115	0.013
	B2277	0.535	0.998	0.918	0.122	0.015

Table 4. Descriptive statistical characteristics of hyperspectral characters for K^{+} ion (*n*= 42).

Hyperspectral Character	Band	Min	Max	Mean	*Std.*	*Var.*
R	B486	0.076	1.030	0.292	0.304	0.092
	B1366	0.204	1.234	0.509	0.270	0.073
	B1406	0.188	1.254	0.489	0.274	0.075
	B2211	0.204	1.306	0.510	0.275	0.076
	B2336	0.204	1.272	0.503	0.269	0.072
Log(1/R)	B439	−0.137	1.207	0.736	0.388	0.150
	B1363	−0.206	0.682	0.325	0.215	0.046
	B1406	−0.200	0.727	0.353	0.226	0.051
	B2211	−0.227	0.693	0.331	0.223	0.050
	B2336	−0.218	0.692	0.336	0.224	0.050
R_{cr}	B508	0.764	1.000	0.889	0.066	0.004
	B764	0.802	1.000	0.981	0.046	0.002
	B1371	0.681	0.995	0.899	0.077	0.006
	B2140	0.559	1.000	0.896	0.115	0.013
	B2275	0.536	1.000	0.917	0.121	0.015

Table 5. Descriptive statistical characteristics of hyperspectral characters for Na^+ ion (n= 42).

Hyperspectral Character	Band	Min	Max	Mean	*Std.*	*Var.*
R	B491	0.077	1.035	0.295	0.304	0.092
	B1365	0.213	1.264	0.509	0.270	0.073
	B1406	0.188	1.254	0.489	0.274	0.075
	B2211	0.204	1.306	0.510	0.275	0.076
	B2353	0.202	1.296	0.501	0.275	0.076
Log(1/R)	B354	−0.110	1.475	0.892	0.451	0.203
	B1365	−0.195	0.676	0.332	0.212	0.045
	B1406	−0.200	0.727	0.353	0.226	0.051
	B2211	−0.227	0.693	0.331	0.223	0.050
	B2353	−0.228	0.698	0.340	0.227	0.051
R_{cr}	B495	0.743	1.000	0.883	0.073	0.005
	B764	0.802	1.000	0.981	0.046	0.002
	B1371	0.681	0.995	0.899	0.077	0.006
	B2141	0.560	0.999	0.897	0.114	0.013
	B2275	0.536	1.000	0.917	0.121	0.015

Characteristic bands for ions

The correlations between ionic content and *R* are shown in Figure 2. For the Cl^- ion, for example, the correlations are well within the band range of 350~550 nm. With the band wavelength increasing, the correlation coefficients decreased, but there were two peaks between 1350~1450 nm and 2150~2450 nm, shown on the coefficient curve. In the range from 1750 nm to 2000 nm, the correlation coefficients changed significantly, as this band range was mainly the absorption zone of water vapor, which was more sensitive to water (D. Zhang et al., 2014), meaning the curve jumped significantly, suggesting this band range was not adaptive for quantitative inversion. Given the rule of the correlation coefficient extreme, the bands at 465 nm, 1365 nm, 1407 nm, 2210 nm, and 2353 nm were chosen as the characteristic bands, and the reflectance (*R*) of these bands was used to derive the quantitative inversion model of the ion Cl^-. The correlations between Cl^- content and its reciprocal of reflectance (Log(1/*R*)) are shown in Figure 3, and the coefficient curve indicates that their correlation is negative. With the band wavelength increasing, the correlation coefficients decreased on the whole, their correlations being the strongest between 350 and 550 nm, with peaks in the curve in the band ranges of 1350~1450 nm, 2150~2450 nm, and 2150~2450 nm. Given the rule of correlation coefficient extreme, the bands at 356 nm, 1365 nm, 1406 nm, 2211 nm, and 2353 nm were chosen as characteristic bands, and the reciprocal of reflectance

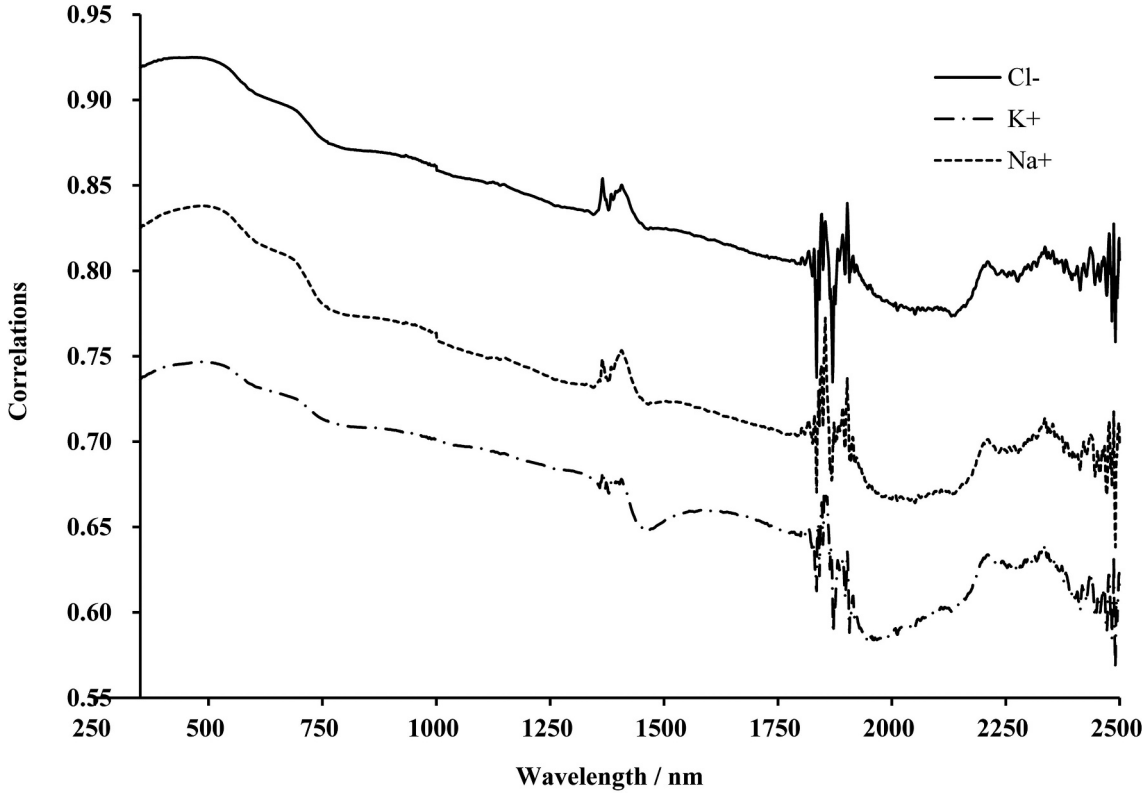


Figure 2. Correlations between reflectance (R) and characteristic ions.

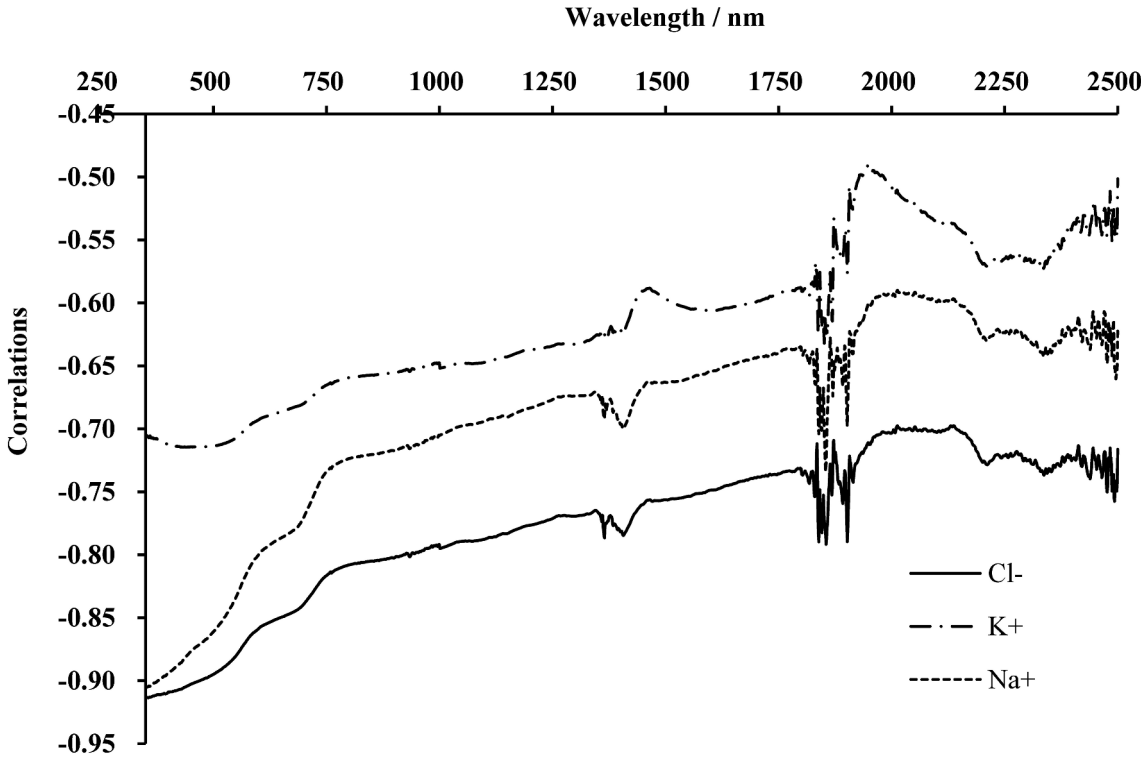


Figure 3. Correlations between Log(1/R) and characteristic ions.

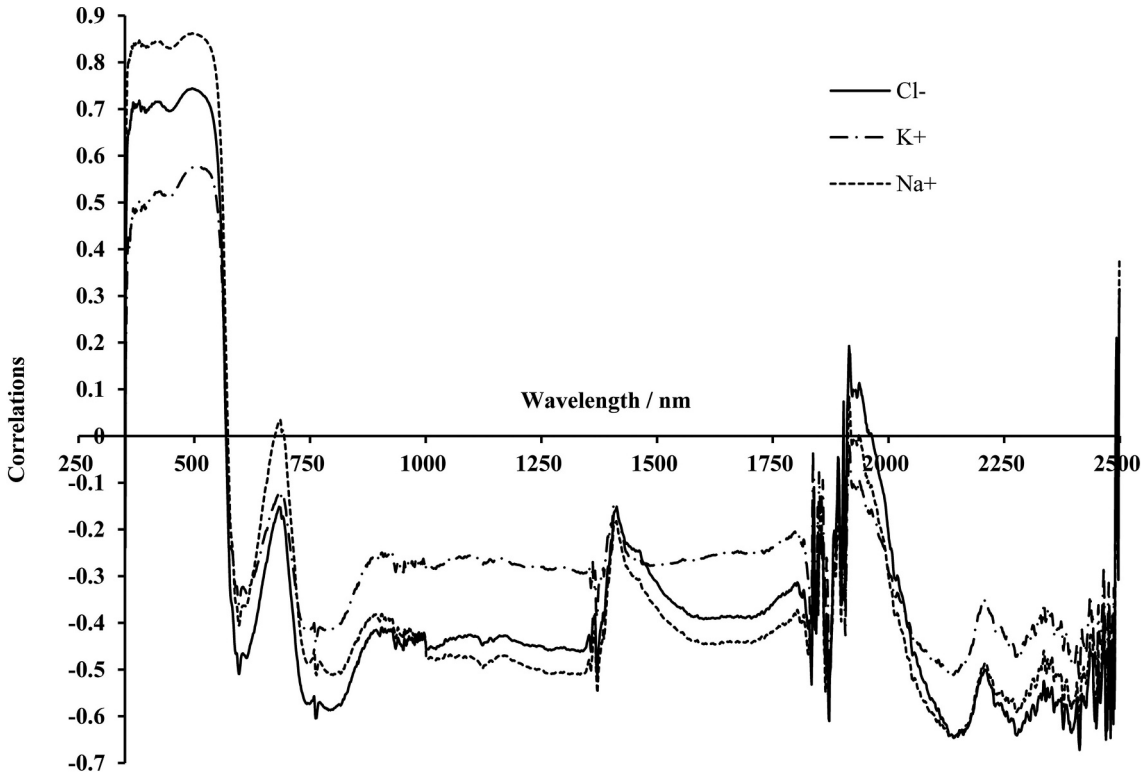


Figure 4. Correlations between R_{cr} and characteristic ions.

(Log(1/R)) of these bands was used to derive the quantitative inversion model of the Cl^- ion. The correlations between Cl^- content and its continual removed reflectance (R_{cr}) are shown in Figure 4. Given the rule of the correlation coefficient extreme, the bands of 495 nm, 762 nm, 1371 nm, 2140 nm, and 2277 nm were chosen as characteristic bands, the continual removed reflectance (R_{cr}) of these bands

was used to derive the quantitative inversion model for the Cl^- ion.

Similarly, for the ion of K^+, the characteristic bands of *R* were 486 nm, 1366 nm, 1406 nm, 2211 nm, and 2336 nm; the characteristic bands of Log(1/*R*) were 439 nm, 1363 nm, 1406 nm, 2211 nm, and 2336 nm; and the characteristic bands of R_{cr} were 508 nm, 764 nm, 1371 nm, 2140 nm, and 2275 nm. Finally, for the ion of Na^+, the characteristic bands of *R* were 491 nm, 1365 nm, 1406 nm, 2211 nm, and 2353 nm; the characteristic bands of Log(1/*R*) were 354 nm, 1365 nm, 1406 nm, 2211 nm, and 2353 nm; and the characteristic bands of R_{cr} were 495 nm, 764 nm, 1371 nm, 2141 nm, and 2275 nm.

Quantitative inversion for characteristic ions and precision test

The descriptive statistical characteristics of all the hyperspectral characters for the ions of Cl^-, K^+, and Na^+ were shown in Tables 3–5 respectively. And the modeling precisions for the quantitative inversion models calculated using each method are shown in Table 6. For the quantitative inversion models of the ions of Cl^-, K^+, and Na^+, with the same hyperspectral character variables, the models derived with SVR had higher r^2 and smaller RMSE than those derived with PLSR, suggesting higher precision by the former method. The models derived using *R*, R_{cr}, and R_{cr} provided the best modeling precision for Cl^-, K^+, and Na^+, respectively. In summary, the models derived with SVR showed higher modeling precision than those derived with PLSR.

Based on the 28 testing samples, the correlations between the predicted values and measured values were compared. The resulting test precisions are shown in Table 7. For the quantitative inversion models of the ion Cl^-, with the same hyperspectral character variables, the RMSE between the predicted values and measured values was smaller, and the slope *k* of the trend line was nearer to 1 with SVR than with PLSR, this suggests that test precision with the former method was higher, and the model derived with *R* had the best test precision. For the quantitative inversion models of the ion K^+, with the same hyperspectral character variables, the RMSE between the predicted values and measured values was smaller, and the slope *k* of the trend line was nearer to 1 with SVR than with PLSR. This suggests that the test precision of the former method was better, and the model derived with R_{cr} had the best test precision. For the quantitative inversion models of the ion Na^+, with the same hyperspectral character variables, the RMSE between the predicted values and measured values with SVR was smaller than that with PLSR, and the slope *k* of the trend lines was nearly the same nearer to 1, but the coefficients of determination r^2 were higher with SVR

Table 6. The modeling precisions of inversion models based on hyperspectral characters (*n*= 42).

			R	Log(*1/R*)	R_{cr}
Cl^-	SVR	RMSE	*0.0483*	*0.0496*	*0.0533*
		r^2	*0.9414*	*0.9397*	*0.9328*
	PLSR	RMSE	*0.0539*	*0.0665*	*0.0851*
		r^2	*0.9249*	*0.8856*	*0.8214*
K^+	SVR	RMSE	*0.0119*	*0.0070*	*0.0065*
		r^2	*0.6458*	*0.8827*	*0.8929*
	PLSR	RMSE	*0.0125*	*0.0124*	*0.0144*
		r^2	*0.5811*	*0.5885*	*0.4501*
Na^+	SVR	RMSE	*0.05430*	*0.0528*	*0.0459*
		r^2	*0.9140*	*0.9194*	*0.9342*
	PLSR	RMSE	*0.0710*	*0.0565*	*0.0603*
		r^2	*0.8420*	*0.9001*	*0.8861*

Table 7. The test precision of the inversion models based on hyperspectral characters (*n*= 28).

			R	Log(*1/R*)	R_{cr}
Cl^-	SVR	RMSE	*0.0791*	*0.0797*	*0.0829*
		y = kx + b	*y = 1.191x + 0.0066*	*y = 1.2146x + 0.0174*	*y = 0.962x+0.0355*
		r^2	*0.8566*	*0.8983*	*0.7413*
	PLSR	RMSE	*0.0824*	*0.1004*	0.0888
		y = kx + b	*y = 1.1924x + 0.002*	*y = 1.395x – 0.0109*	*y = 0.752x + 0.0544*
		r^2	*0.8349*	*0.8789*	*0.6183*
K^+	SVR	RMSE	*0.0116*	*0.0102*	*0.0097*
		y = kx + b	*y = 0.8559x + 0.0123*	*y = 0.8991x + 0.0078*	*y = 0.9239x + 0.0041*
		r^2	*0.6641*	*0.6703*	*0.6610*
	PLSR	RMSE	*0.0186*	*0.0117*	*0.0124*
		y = kx + b	*y = 0.7668x + 0.0104*	*y = 0.8192x + 0.0114*	*y = 0.3161x + 0.024*
		r^2	*0.6792*	*0.5752*	*0.2661*
Na^+	SVR	RMSE	*0.0738*	*0.0769*	*0.0718*
		y = kx + b	*y = 1.0526x + 0.0013*	*y = 1.1706x-0.0289*	*y = 1.1502x – 0.0063*
		r^2	*0.8234*	*0.8384*	*0.8326*
	PLSR	RMSE	*0.0838*	*0.0841*	*0.0903*
		y = kx + b	*y = 0.9786x + 0.0232*	*y = 1.1619x – 0.0225*	*y = 0.9137x + 0.0478*
		r^2	*0.7028*	*0.8700*	*0.7902*

than those with PLSR. It could be concluded that the test precision for the former method was higher, and all the models derived with R, Log(1/R), and R_{cr} had good test precision. In summary, the models derived with SVR showed higher test precision than those derived with PLSR, and that was just accordant to the modeling precision.

Conclusions

This study demonstrated the strong correlations between the total soil salinity and ionic content for K^+, Na^+, and Cl^-, which were chosen as characteristic ions. The hyperspectral characters of R, Log(1/R), and R_{cr} were analyzed to calculate the quantitative inversion of characteristic ions, and the precisions were higher, possibly because salinized soils are more sensitive to absorption and reflectance characters of the spectrum: the more severe the salinization, the higher the reflectance. Hyperspectral data have high resolution, which can reflect the detailed characters of the soil salinization, such as salt ionic content. This, in turn, allows the quantitative inversion of characteristic ions based on hyperspectral characters.

The inversion models derived with SVR had better precision including modeling precision and test precision than those derived with PLSR. The SVR method is based on the statistical learning theory and the minimum structure risk principle, which could provide the best compromise between model complexity and learning ability; hence, its precision is higher than PLSR.

The precisions of the inversion models for characteristic ions based on different hyperspectral characters were different, which indicated that different ions had different sensitive hyperspectral characters. Among the quantitative inversion models derived with SVR, the model for Cl^- derived with the variable of R showed the highest precision, followed by R_{cr}; in addition, both of the models for the two positive ions K^+ and Na^+ derived with the variable of R_{cr} showed the highest precision.

In this paper, the quantitative inversion models were derived with different hyperspectral characters based on different methods, and the precisions were analyzed and compared, which aimed to improve the precision of the quantitative inversion for salinization characteristic ions. The results of this study are particularly relevant for accurate, efficient prevention and recovery of salinized land. Furthermore, on the foundation of the inversion models, they could also be merged with large-scale RS images and big data to improve the efficiency and accuracy of assessment and monitoring of soil salinization on the next study.

Disclosure statement

No potential conflict of interest was reported by the authors.

Funding

This work was supported by the National Natural Science Foundation of China (62002286), the National Natural Science Foundation of Shaanxi Province (2020GY-038) and the Scientific Research Program from Education Department of Shaanxi Provincial Government (18JK0626).

References

Dai, X. J., Zhang, Y. L., Peng, J., Luo, H. P., & Xiang, H. Y. (2015). Prediction and validation of water-soluble salt ions content using hyperspectral data. *Transactions of the Chinese Society of Agricultural Engineering*, *31*(22), 139–145. doi:10.11975/j.issn.1002-6819.2015.22.019

Ding, J. L., Wu, M. C., Liu, H. X., & Li, Z. G. (2012). Study on the soil salinization monitoring based on synthetical hyperspectral index. *Spectroscopy and Spectral Analysis*, *32*(7), 1918–1922. doi:10.3964/j.issn.1000-0593(2012)07-1918-05

Duan, P. C., Xiong, H. G., Li, R. R., & Zhang, L. (2017). A quantitative analysis of the reflectance of the saline soil under different disturbance extent. *Spectroscopy and Spectral Analysis*, *37*(2), 571–576. doi:10.3964/j.issn.1000-0593(2017)02-0571-06

Kelimu, A., Tiyip, T., Zhang, D., & Nurmemet, I. (2016). Calibration and validation of soil salinity estimation model based on measured hyperspectral and Aster image. *Transactions of the Chinese Society of Agricultural Engineering*, *32*(12), 144–150. doi:10.11975/j.issn.1002-6819.2016.12.021

Li, X. M., Yang, J. S., Liu, M. X., Liu, G. M., & Yao, R. J. (2010). Spatial heterogeneity of soil salinity in typical arid area based on electromagnetic induction. *Transactions of the Chinese Society of Agricultural Engineering*, *26*(12), 97–101. doi: 10.3969/j.issn.1002-6819.2010.12.016

Liang, D., Guang, Q. S., Huang, W. J., Huang, L. S., & Yang, G. J. (2013). Remote sensing inversion of leaf area index based on support vector machine regression in winter wheat. *Transactions of the Chinese Society of Agricultural Engineering*, *29*(7), 117–123. doi: 10.3969/j.issn.1002-6819.2013.07.015

Liu, Y. Q., Chen, H. Y., Wang, R. Y., Chang, C. Y., & Chen, Z. (2016). Quantitative analysis of soil salt and its main ions based on visible/near infrared spectroscopy in estuary area of yellow river. *Scientia Agricultura Sinica*, *49*(10), 1925–1935. doi: 10.3864/j.issn.0578-1752.2016.10.009

Lu, R. K. (1999). *Analysis methods of soil agrochemistry*. China Agricultural Science and Technology Press.

Qu, Y. H., Duan, X. L., Gao, H. Y., Chen, A. P., An, Y. Q., Song, J. L., Zhou, H. M., & He, T. (2009). Quantitative retrieval of soil salinity using hyperspectral data in the region of inner mongolia hetao irrigation district. *Spectroscopy and Spectral Analysis*, *29*(5), 1362–1366. doi:10.3964/j.issn.1000-0593(2009)05-1362-05

Wang, H. J., Jiang, T. C., Yunger, J. A., Li, Y. L., Tian, T., & Wang, J. G. (2018). Hyperspectral inverse model for soil salt ions based on support vector machine. *Transactions of the Chinese Society for Agricultural Machinery*, *49*, 263–270. doi:10.6041/j.issn.1000-1298.2018.05.031

Wang, J., Liu, X. N., Huang, F., Tang, J. L., & Zhao, L. B. (2009). Salinity forecasting of saline soil based on ANN and hyperspectral remote sensing. *Transactions of the Chinese Society of Agricultural Engineering*, *25*(12), 161–166. doi:10.3969/j.issn.1002-6819.2009.12.029

Yang, J. S. (2008). Development and prospect of the research on salt-affected soils in China. *Acta Pedologica Sinica*, *45*(5), 837–845. doi:10.3321/j.issn:0564-3929.2008.05.010

Yao, Y., Ding, J. L., Kelimu, A., Zhang, F., & Lei, L. (2013b). Research on remote sensing monitoring of soil salinization based on measured hyperspectral and EM38 data. *Spectroscopy and Spectral Analysis*, *33*(7), 1917–1921. doi:10.3964/j.issn.1000-0593(2013)07-1917-05

Yao, Y., Ding, J. L., Zhang, F., Zhao, Z. L., & Jiang, H. N. (2013a). Research on model of soil salinization monitoring based on hyperspectral index and EM38. *Spectroscopy and Spectral Analysis*, *33*(6), 1658–1664. doi: 10.3964/j.issn.1000-0593(2013)06-1658-07

Zhang, D., Tiyip, T., Zhang, F., & Kelimu, A. (2014). Application of fractional differential in preprocessing hyperspectral data of saline soil. *Transactions of the Chinese Society of Agricultural Engineering*, *30*(24), 151–160. doi: 10.3969/j.issn.1002-6819.2014.24.018

Zhang, Q., Zhou, B. B., Li, M. J., Wei, Q. P., & Han, Z. H. (2018). Multivariate analysis between meteorological factor and fruit quality of Fuji apple at different locations in China. *Journal of Integrative Agriculture*, *17*(6), 1338–1347. https://doi.org/10.1016/S2095-3119(17)61826-4

Zhu, Y., Shen, G. R., Wang, Z. J., Lu, S. M., Zhi, Y. E., & Xiang, Q. Q. (2017). Soil salt content and its spectral characteristics during microbial remediation processes. *Spectroscopy and Spectral Analysis*, *37*(5): 1507-1513. doi: 10.3964/j.issn.1000-0593(2017)05-1507-07

附录8

尊敬的计算机学院岗位聘用工作小组组长：

刘院长您好！本人对学院拟将王静怡老师聘为教师 7 级岗和李小和老师聘为教师 6 级岗存在异议，对拟将我由教师 7 级岗聘为教师 8 级岗存在异议。具体理由如下：

王静怡老师和李小和老师均存在学术不端问题，符合计算机学院 2024-2026 年专业技术岗位设置与聘用实施方案的工作原则第三条：师德师风是第一标准，实施“一票否决”制的规定。

王静怡老师从读博士开始至今 3 次重复发表，将 3 篇成果变为 6 篇成果，且使用重复发表的成果参与副教授职称评审压线通过，成果不仅存在学术不端且单薄。李小和老师将 1 篇文章聚类分割算法加入不同的因子拆分为 3 篇香肠文章，也属于典型的重复发表，使用这样的重复发表的成果参与副教授职称评审压线通过，成果不仅存在学术不端且单薄。

具体说明如下：

（1）李小和老师一稿三发情况说明：

李小和老师符合职称评审论文条件的论文的“sptially constrained Fuzzy c-means clustering algorithm for image segmentation”（权威三类）和“空间加权模糊 C 均值聚类图像分割算法”（核心二类）以及“adaptive spatially weighted fuzzy c-means clustering for image segmentation”（一般期刊）三篇属于结构、内容、结论、实验等高度重复。

“空间加权模糊 C 均值聚类图像分割算法”发表于 2017 年，“sptially constrained Fuzzy c-means clustering algorithm for image segmentation”发表于 2019 年，“adaptive spatially weighted fuzzy c-means clustering for image segmentation”发表于 2022 年，三篇文章都是研究模糊 C 均值算法用于图像分割。2017 年的论文就已经指出将图像的像素空间关系加到模糊 C 均值算法中可以提高图像分割鲁棒性和准确度。2019 年的论文与 2017 的论文相比就额外加入了一个距离加权因

子，2022 年的论文与 2019 年的论文相比就额外加了一个中值滤波算子。实际上，对模糊 C 均值聚类算法在图像分割应用中加入像素空间约束关系（如各种距离因子、中值算子等等）在 2010 年前后大家都有共识也有很多论文发表，这三篇文章之间的工作变化很小，加距离因子加权或是加中值算子都是常规操作，李小和老师如果要继续发表这样的工作理应在一篇文章中在同样的实验条件、参数设置下进行对比分析。但李小和老师将这样常规的已经形成共识的小的微调操作拆分成三篇文章发表，且三篇文章引言、FCM 算法描述、结构、实验、结论存在高度雷同。李小和老师的这三篇文章存在中英文三次重复发表，属于学术不端行为，因此，李小和老师不符合论文要求“核心以上三篇，至少有一篇权威”的基本要求。

（2）王静怡老师持续进行 3 稿 6 发情况说明：

1.王静怡老师的教育经历为本、硕、博均为通信工程。具体学习经历为：

2010/03~2016/06，西安电子科技大学，通信与信息系统，博士

2007/09~2010/03，西安电子科技大学，通信与信息系统，硕士

2002/09~2006/07，西安邮电大学，通信工程，学士

具体工作经历为：

2016/07~至今，西安石油大学计算机学院，教师

2. 王静怡老师涉嫌学术不端主要表现为成果发表中存在连续多次重复发表的情况。王静怡老师第 1 次重复发表出现在 2013 年读博士期间，第 2 次重复发表出现在 2016 年读博士期间，第 3 次重复发表出现在入职西安石油大学后 2019 年。6 篇论文涉嫌重复发表，具体如下：

(1)读博士期间第 1 次重复发表

[1] 王静怡, 李颖, 孙岳. 速率兼容网络 LDPC 码的设计[C]//中国通信学会. 第十七届全国青年通信学术年会论文集. 西安电子科技大学综合业务网理论及关键技术国家重点实验室, 2012:5.

[2] 王静怡*, 李颖, 孙岳. 适用于网络 LDPC 码的速率兼容算法. 西安电子科技大学学报,2013, 40(2): 13-17.

文章[1]和[2]属于中文一稿双发。文章[1]于 2012 年 7 月底在会议上发表，文章[2]于 2013 年 4 月于西安电子科技大学学报上发表。文章[2]既没有引用文章[1],文章

[2]也没有在首页对文章已经发表过做任何说明，文章[1]和[2]完全雷同，属于重复发表。文章[1]和[2]的名字经过刻意调整顺序重构。

(2)读博士期间第 2 次重复发表

[3] Jingyi Wang, Shuling Che, Ying Li, Optimal design of the Joint network LDPC Codes over Orthogonal Multiple-Access Relay Channel. 2013 5th International Conference on Intelligent Networking and Collaborative Systems, 2013. XI'AN: IEEE, 622-625.

[4] Jingyi Wang*, Shuling Che, Ying Li and Junlong Wang, Optimal design of Joint network LDPC Codes over Orthogonal Multiple-Access Relay Channel. International Journal of Grid and Utility Computing, UK., 2016, 7(1): 68-74.

文章[3]和文章[4]属于英文一稿双发，文章[3]2013 年发表，文章[4]2016 年发表。文章[4]首页虽有标注了文章[4]为文章[3]的改写和扩展，但两篇文章整体内容、结构、图表以及结论雷同，且整段整段的文字写法均完全一样，雷同率至少超过60%以上，也就是说文章[3]和[4]的大部分（过半）雷同，文章[4]不具备科研成果三性中的新颖性，属于明显不符合成果发表规范。

另文章[3]在申报陕西省科技厅项目基于信息物理融合的智能油田监控系统关键技术研究（2020GY-038）（已立项）时论文名字被篡改为 Jingyi Wang*, Shuling Che, Ying Li and Junlong Wang. Optimal design of the joint network LDPC codes for half-duplex coopreative multi-Access relay channel. 2013 5th International Conference on Intelligent. 2013. USA: IEEE, 622-625.

“Optimal design of the joint network LDPC codes for half-duplex coopreative multi-Access relay channel”在 EI 数据库中经过检索不存在，后通过文章发表时间、页码范围搜索发现文章[3]应为：

Jingyi Wang, Shuling Che, Ying Li, Optimal design of the Joint network LDPC Codes over Orthogonal Multiple-Access Relay Channel. 2013 5th International Conference on Intelligent Networking and Collaborative Systems, 2013. XI'AN: IEEE, 622-625。

另于王静怡 2016 年 4 月博士论文末尾攻读博士期间论文成果（博士论文 99 页）未发现会议论文“Optimal design of the joint network LDPC codes for half-duplex

coopreative multi-Access relay channel”而是会议论文“Optimal design of the Joint network LDPC Codes over Orthogonal Multiple-Access Relay Channel”。

由此可见王静怡老师为避免论文同名易被发现一稿双发，将文章[3]名称由“Optimal design of the Joint network LDPC Codes over Orthogonal Multiple-Access Relay Channel”篡改成了“Optimal design of the joint network LDPC codes for half-duplex coopreative multi-Access relay channel”，但在文章[4]的首页王静怡老师准确写出 2013 年会议论文名称为“Optimal design of the Joint network LDPC Codes over Orthogonal Multiple-Access Relay Channel”。王静怡将会议名称由“2013 5th International Conference on Intelligent Networking and Collaborative Systems”改为了“2013 5th International Conference on Intelligent”，会议举办地由“XI’AN”改为了“USA”，可见此番篡改论文名称、会议名称、会议举办地属于刻意为之。

(3)入职西安石油大学后第 3 次重复发表，并作为评职称成果提交压线职称评审论文最低条件

[5] WangJingyi , Li Xiaoming*.Research on the changing trend of farmland area in China and its driving factors from 1996 to 2016[C]. IOP Conference Series Materials Science and Engineering, IOP Conference Series: Earth and Environmental Science(EES), 6 月 22 日~24 日, 珠海, 中国, 2018.

[6]王静怡,李晓明*.近 20 年中国耕地数量变化趋势及其驱动因子分析*[J].中国农业资源与区划,2019,40(08):171-176.

文章[5]和[6]属于中英文一稿双发，文章[5]英文先于 2018 年在国内举办的国际会议发表，文章[6]为 2019 年在国内中文期刊发表。文章[6]中对文章之前已经发表情况未做任何说明，也没有引用[5]。王静怡第 1 次重复发表始于 2013 年，2016 年第 2 次重复发表时在文章[4]的首页还标注了此论文曾经发表，此次为改写扩展的说明。但在 2019 年第 3 次重复发表时，却在文章[6]中对文章[5]曾经发表过没有做任何说明，这说明王静怡重复发表是明知故犯。为了避免被易于发现一稿双发，文章[5]的名字“Research on the changing trend of farmland area in China and its driving factors **from 1996 to 2016**”在文章[6]再次重复发表时改成了“**近 20 年**中国耕地数量变化趋势及其驱动因子分析 ”。文章[6]在文章[5]的 20 篇参考文

献基础上仅增加了 3 篇参考文献，文章[6]和[5]雷同率超过 90%，文章[6]和[5]整体内容、结构、图表以及结论高度雷同，仅仅在第一部分介绍部分有少量差异，其余均雷同，雷同率超过 90%。文章[6]不具备科研成果三性中的新颖性，属于重复发表。

综上，王静怡老师和李小和老师均存在严重的学术不端，不符合**计算机学院 2024-2026 年专业技术岗位设置与聘用实施方案的工作原则第三条师德师风为第一标准的工作原则，应“一票否决”。学院不应将存在学术不端的老师一味向前推，提职升级。**（科研论文李小和老师权威三类 1 篇，核心二类 2 篇；发明专利 2 项。王静怡老师权威二类 1 篇，权威三类 1 篇，核心一类 1 篇；发明专利 2 项。本人权威三类 3 篇，核心一类 1 篇，核心二类 2 篇，核心以上为 6 篇。发明专利 4 项。）**目前**，王静怡老师和李小和老师的拟聘结果尚未公示，本着对学院工作负责的态度，本人将两位老师存在的师德师风问题第一时间向学院岗位聘用工作小组组长反映，请学院对反映的情况积极认真核实，妥善解决。

随信附李小和老师 1 稿 3 发的文章和王静怡老师 3 稿 6 发的文章（重复内容使用黄色标注）。

此致

敬礼

2024 年 7 月 9 日

尊敬的计算机学院岗位聘用工作小组组长：

庞书记您好！本人对学院拟将王静怡老师聘为教师 7 级岗和李小和老师聘为教师 6 级岗存在异议，对拟将我由教师 7 级岗聘为教师 8 级岗存在异议。具体理由如下：

王静怡老师和李小和老师均存在学术不端问题，符合计算机学院 2024-2026 年专业技术岗位设置与聘用实施方案的工作原则第三条：师德师风是第一标准，实施“一票否决”制的规定。

王静怡老师从读博士开始至今 3 次重复发表，将 3 篇成果变为 6 篇成果，且使用重复发表的成果参与副教授职称评审压线通过，成果不仅存在学术不端且单薄。李小和老师将 1 篇文章聚类分割算法加入不同的因子拆分为 3 篇香肠文章，也属于典型的重复发表，使用这样的重复发表的成果参与副教授职称评审压线通过，成果不仅存在学术不端且单薄。

具体说明如下：

（1）李小和老师一稿三发情况说明：

李小和老师符合职称评审论文条件的论文的“sptially constrained Fuzzy c-means clustering algorithm for image segmentation”（权威三类）和“空间加权模糊 C 均值聚类图像分割算法”（核心二类）以及“adaptive spatially weighted fuzzy c-means clustering for image segmentation”（一般期刊）三篇属于结构、内容、结论、实验等高度重复。

“空间加权模糊 C 均值聚类图像分割算法”发表于 2017 年，“sptially constrained Fuzzy c-means clustering algorithm for image segmentation”发表于 2019 年，“adaptive spatially weighted fuzzy c-means clustering for image segmentation”发表于 2022 年，三篇文章都是研究模糊 C 均值算法用于图像分割。2017 年的论文就已经指出将图像的像素空间关系加到模糊 C 均值算法中可以提高图像分割鲁棒性和准确度。2019 年的论文与 2017 的论文相比就额外加入了一个距离加权因

子，2022 年的论文与 2019 年的论文相比就额外加了一个中值滤波算子。实际上，对模糊 C 均值聚类算法在图像分割应用中加入像素空间约束关系（如各种距离因子、中值算子等等）在 2010 年前后大家都有共识也有很多论文发表，这三篇文章之间的工作变化很小，加距离因子加权或是加中值算子都是常规操作，李小和老师如果要继续发表这样的工作理应在一篇文章中在同样的实验条件、参数设置下进行对比分析。但李小和老师将这样常规的已经形成共识的小的微调操作拆分成三篇文章发表，且三篇文章引言、FCM 算法描述、结构、实验、结论存在高度雷同。李小和老师的这三篇文章存在中英文三次重复发表，属于学术不端行为，因此，李小和老师不符合论文要求“核心以上三篇，至少有一篇权威”的基本要求。

（2）王静怡老师持续进行 3 稿 6 发情况说明：

1.王静怡老师的教育经历为本、硕、博均为通信工程。具体学习经历为：

2010/03~2016/06，西安电子科技大学，通信与信息系统，博士

2007/09~2010/03，西安电子科技大学，通信与信息系统，硕士

2002/09~2006/07，西安邮电大学，通信工程，学士

具体工作经历为：

2016/07~至今，西安石油大学计算机学院，教师

2. 王静怡老师涉嫌学术不端主要表现为成果发表中存在连续多次重复发表的情况。王静怡老师第 1 次重复发表出现在 2013 年读博士期间，第 2 次重复发表出现在 2016 年读博士期间，第 3 次重复发表出现在入职西安石油大学后 2019 年。6 篇论文涉嫌重复发表，具体如下：

(1)读博士期间第 1 次重复发表

[1] 王静怡, 李颖, 孙岳. 速率兼容网络 LDPC 码的设计[C]//中国通信学会. 第十七届全国青年通信学术年会论文集. 西安电子科技大学综合业务网理论及关键技术国家重点实验室, 2012:5.

[2] 王静怡*, 李颖, 孙岳. 适用于网络 LDPC 码的速率兼容算法. 西安电子科技大学学报,2013, 40(2): 13-17.

文章[1]和[2]属于中文一稿双发。文章[1]于 2012 年 7 月底在会议上发表，文章[2]于 2013 年 4 月于西安电子科技大学学报上发表。文章[2]既没有引用文章[1],文章

[2]也没有在首页对文章已经发表过做任何说明，文章[1]和[2]完全雷同，属于重复发表。文章[1]和[2]的名字经过刻意调整顺序重构。

(2)读博士期间第 2 次重复发表

[3] Jingyi Wang, Shuling Che, Ying Li, Optimal design of the Joint network LDPC Codes over Orthogonal Multiple-Access Relay Channel. 2013 5th International Conference on Intelligent Networking and Collaborative Systems, 2013. XI'AN: IEEE, 622-625.

[4] Jingyi Wang*, Shuling Che, Ying Li and Junlong Wang, Optimal design of Joint network LDPC Codes over Orthogonal Multiple-Access Relay Channel. International Journal of Grid and Utility Computing, UK., 2016, 7(1): 68-74.

文章[3]和文章[4]属于英文一稿双发，文章[3]2013 年发表，文章[4]2016 年发表。文章[4]首页虽有标注了文章[4]为文章[3]的改写和扩展，但两篇文章整体内容、结构、图表以及结论雷同，且整段整段的文字写法均完全一样，雷同率至少超过60%以上，也就是说文章[3]和[4]的大部分（过半）雷同，文章[4]不具备科研成果三性中的新颖性，属于明显不符合成果发表规范。

另文章[3]在申报陕西省科技厅项目基于信息物理融合的智能油田监控系统关键技术研究（2020GY-038）（已立项）时论文名字被篡改为 Jingyi Wang*, Shuling Che, Ying Li and Junlong Wang. Optimal design of the joint network LDPC codes for half-duplex coopreative multi-Access relay channel. 2013 5th International Conference on Intelligent. 2013. USA: IEEE, 622-625.

“Optimal design of the joint network LDPC codes for half-duplex coopreative multi-Access relay channel”在 EI 数据库中经过检索不存在，后通过文章发表时间、页码范围搜索发现文章[3]应为：

Jingyi Wang, Shuling Che, Ying Li, Optimal design of the Joint network LDPC Codes over Orthogonal Multiple-Access Relay Channel. 2013 5th International Conference on Intelligent Networking and Collaborative Systems, 2013. XI'AN: IEEE, 622-625。

另于王静怡 2016 年 4 月博士论文末尾攻读博士期间论文成果（博士论文 99 页）未发现会议论文“Optimal design of the joint network LDPC codes for half-duplex

coopreative multi-Access relay channel”而是会议论文“Optimal design of the Joint network LDPC Codes over Orthogonal Multiple-Access Relay Channel”。

由此可见王静怡老师为避免论文同名易被发现一稿双发，将文章[3]名称由“Optimal design of the Joint network LDPC Codes over Orthogonal Multiple-Access Relay Channel”篡改成了“Optimal design of the joint network LDPC codes for half-duplex coopreative multi-Access relay channel”，但在文章[4]的首页王静怡老师准确写出 2013 年会议论文名称为“Optimal design of the Joint network LDPC Codes over Orthogonal Multiple-Access Relay Channel”。王静怡将会议名称由“2013 5th International Conference on Intelligent Networking and Collaborative Systems”改为了“2013 5th International Conference on Intelligent”，会议举办地由“XI’AN”改为了“USA”，可见此番篡改论文名称、会议名称、会议举办地属于刻意为之。

(3)入职西安石油大学后第 3 次重复发表，并作为评职称成果提交压线职称评审论文最低条件

[5] WangJingyi , Li Xiaoming*.Research on the changing trend of farmland area in China and its driving factors from 1996 to 2016[C]. IOP Conference Series Materials Science and Engineering, IOP Conference Series: Earth and Environmental Science(EES), 6 月 22 日~24 日, 珠海, 中国, 2018.

[6]王静怡,李晓明*.近 20 年中国耕地数量变化趋势及其驱动因子分析*[J].中国农业资源与区划,2019,40(08):171-176.

文章[5]和[6]属于中英文一稿双发，文章[5]英文先于 2018 年在国内举办的国际会议发表，文章[6]为 2019 年在国内中文期刊发表。文章[6]中对文章之前已经发表情况未做任何说明，也没有引用[5]。王静怡第 1 次重复发表始于 2013 年，2016 年第 2 次重复发表时在文章[4]的首页还标注了此论文曾经发表，此次为改写扩展的说明。但在 2019 年第 3 次重复发表时，却在文章[6]中对文章[5]曾经发表过没有做任何说明，这说明王静怡重复发表是明知故犯。为了避免被易于发现一稿双发，文章[5]的名字“Research on the changing trend of farmland area in China and its driving factors **from 1996 to 2016**”在文章[6]再次重复发表时改成了“**近 20 年**中国耕地数量变化趋势及其驱动因子分析 ”。文章[6]在文章[5]的 20 篇参考文

献基础上仅增加了 3 篇参考文献，文章[6]和[5]雷同率超过 90%，文章[6]和[5]整体内容、结构、图表以及结论高度雷同，仅仅在第一部分介绍部分有少量差异，其余均雷同，雷同率超过 90%。文章[6]不具备科研成果三性中的新颖性，属于重复发表。

综上，王静怡老师和李小和老师均存在严重的学术不端，不符合**计算机学院 2024-2026 年专业技术岗位设置与聘用实施方案的工作原则第三条师德师风为第一标准的工作原则，应“一票否决”。学院不应将存在学术不端的老师一味向前推，提职升级。**（科研论文李小和老师权威三类 1 篇，核心二类 2 篇；发明专利 2 项。王静怡老师权威二类 1 篇，权威三类 1 篇，核心一类 1 篇；发明专利 2 项。本人权威三类 3 篇，核心一类 1 篇，核心二类 2 篇，核心以上为 6 篇。发明专利 4 项。）**目前**，王静怡老师和李小和老师的拟聘结果尚未公示，本着对学院工作负责的态度，本人将两位老师存在的师德师风问题第一时间向学院岗位聘用工作小组组长反映，请学院对反映的情况积极认真核实，妥善解决。

随信附李小和老师 1 稿 3 发的文章和王静怡老师 3 稿 6 发的文章（重复内容使用黄色标注）。

此致

敬礼

2024 年 7 月 9 日

教育部关于印发《新时代高校教师职业行为十项准则》《新时代中小学教师职业行为十项准则》《新时代幼儿园教师职业行为十项准则》的通知

2018-11-16 12:35 来源： 教育部网站

教育部关于印发《新时代高校教师职业行为
十项准则》《新时代中小学教师职业行为
十项准则》《新时代幼儿园教师职业
行为十项准则》的通知
教师〔2018〕16号

各省、自治区、直辖市教育厅（教委），新疆生产建设兵团教育局，有关部门（单位）教育司（局），部属各高等学校、部省合建各高等高校：

为深入贯彻习近平新时代中国特色社会主义思想和党的十九大精神，深入贯彻落实全国教育大会精神，扎实推进《中共中央 国务院关于全面深化新时代教师队伍建设改革的意见》的实施，进一步加强师德师风建设，我部研究制定了《新时代高校教师职业行为十项准则》《新时代中小学教师职业行为十项准则》《新时代幼儿园教师职业行为十项准则》（以下统称准则）。现印发给你们，请结合实际，认真贯彻执行。

一、准则是教师职业行为的基本规范。师德师风是评价教师队伍素质的第一标准。长期以来，广大教师牢记使命、不忘初心，爱岗敬业、教书育人，改革创新、服务社会，作出了重大贡献，党和国家高度肯定，学生、家长和社会普遍尊重。但是，也有个别教师放松自我要求，不能认真履职尽责，甚至出现严重违反师德行为，损害教师队伍整体形象。制定教师职业行为准则，明确新时代教师职业规范，针对主要问题、突出问题划定基本底线，是对广大教师的警示提醒和严管厚爱，是深化师德师风建设，造就政治素质过硬、业务能力精湛、育人水平高超的高素质教师队伍的关键之举。

二、立即部署扎实开展准则的学习贯彻。各地各校要立即行动，结合落实师德师风建设长效机制，开展准则的学习贯彻。要结合本地区、本学校实际进行细化，制定具体化的教师职业行为负面清单及失范行为处理办法，提高针对性、操作性。要做好宣传解读，坚持全覆盖、无死角，采取多种形式帮助广大教师全面理解和准确把握，做到人人应知应做、必知必做，真正把教书育人和自我修养结合起来，时刻自重、自省、自警、自励，自觉做以德立身、以德立学、以德施教、以德育德的楷模，维护教师职业形象，提振师道尊严。

三、把准则要求落实到教师管理具体工作中。要把好教师入口关，在教师招聘、引进时组织开展准则的宣讲，确保每位新入职教师知准则、守底线。要将准则要求体现在教师聘用、聘任合同中，明确有关责任。要强化考核，在教师年度考核、职称评聘、推优评先、表彰奖励等工作中必须进行师德考核，实行师德失范“一票否决”。改进师德考核方式方法，避免形式化、随意化。完善师德考核指标体系，提高科学性、实效性。

四、以有力措施坚决查处师德违规行为。各地各校要按照准则及相应的处理指导意见、处理办法要求，严格举报受理和违规查处。对于发生准则中禁止行为的，要态度坚决，一查到底，依法依规严肃惩处，绝不姑息。对于有虐待、猥亵、性骚扰等严重侵害学生行为的，一经查实，要撤销其所获荣誉、称号，追回相关奖金，依法依规撤销教师资格、解除教师职务、清除出教师队伍，同时还要录入全国教师管理信息系统，任何学校不得再聘任其从事教学、科研及管理等工作。涉嫌违法犯罪的要及时移送司法机关依法处理。要严格落实学校主体责任，建立师德建设责任追究机制，对师德违规行为监管不力、拒不处分、拖延处分或推诿隐瞒等失职失责问题，造成不良影响或严重后果的，要按照干部管理权限严肃追究责任。

各地贯彻落实准则的情况，请及时报告教育部。教育部将适时对落实情况进行督查。

教育部

2018年11月8日

新时代高校教师职业行为十项准则

教师是人类灵魂的工程师，是人类文明的传承者。长期以来，广大教师贯彻党的教育方针，教书育人，呕心沥血，默默奉献，为国家发展和民族振兴作出了重大贡献。新时代对广大教师落实立德树人根本任务提出新的更高要求，为进一步增强教师的责任感、使命感、荣誉感，规范职业行为，明确师德底线，引导广大教师努力成为有理想信念、有道德情操、有扎实学识、有仁爱之心的好老师，着力培养德智体美劳全面发展的社会主义建设者和接班人，特制定以下准则。

一、坚定政治方向。坚持以习近平新时代中国特色社会主义思想为指导，拥护中国共产党的领导，贯彻党的教育方针；不得在教育教学活动中及其他场合有损害党中央权威、违背党的路线方针政策的言行。

二、自觉爱国守法。忠于祖国，忠于人民，恪守宪法原则，遵守法律法规，依法履行教师职责；不得损害国家利益、社会公共利益，或违背社会公序良俗。

三、传播优秀文化。带头践行社会主义核心价值观，弘扬真善美，传递正能量；不得通过课堂、论坛、讲座、信息网络及其他渠道发表、转发错误观点，或编造散布虚假信息、不良信息。

四、潜心教书育人。落实立德树人根本任务，遵循教育规律和学生成长规律，因材施教，教学相长；不得违反教学纪律，敷衍教学，或擅自从事影响教育教学本职工作的兼职兼薪行为。

五、关心爱护学生。严慈相济，诲人不倦，真心关爱学生，严格要求学生，做学生良师益友；不得要求学生从事与教学、科研、社会服务无关的事宜。

六、坚持言行雅正。为人师表，以身作则，举止文明，作风正派，自重自爱；不得与学生发生任何不正当关系，严禁任何形式的猥亵、性骚扰行为。

七、遵守学术规范。严谨治学，力戒浮躁，潜心问道，勇于探索，坚守学术良知，反对学术不端；不得抄袭剽窃、篡改侵吞他人学术成果，或滥用学术资源和学术影响。

八、秉持公平诚信。坚持原则，处事公道，光明磊落，为人正直；不得在招生、考试、推优、保研、就业及绩效考核、岗位聘用、职称评聘、评优评奖等工作中徇私舞弊、弄虚作假。

九、坚守廉洁自律。严于律己，清廉从教；不得索要、收受学生及家长财物，不得参加由学生及家长付费的宴请、旅游、娱乐休闲等活动，或利用家长资源谋取私利。

十、积极奉献社会。履行社会责任，贡献聪明才智，树立正确义利观；不得假公济私，擅自利用学校名义或校名、校徽、专利、场所等资源谋取个人利益。

2022 7th International Conference on Intelligent Computing and Signal Processing (ICSP) | 978-1-6654-7857-1/22/$31.00 ©2022 IEEE | DOI: 10.1109/ICSP54964.2022.9778366

Adaptive spatially weighted fuzzy c-means clustering for image segmentation

Xiaohe Li
School of Computer Science
Xi'an Shiyou University
Xi'an, China
lixh@xsyu.edu.cn

Zhan Qu
School of Petroleum Engineering
Xi'an Shiyou University
Xi'an, China
zhqu@xsyu.edu.cn

***Abstract*—Fuzzy c-means (FCM) clustering algorithm is a popular algorithm in the field of image segmentation. In this paper, an adaptive spatially weighted FCM clustering (ASWFCM) is proposed, to improve the performance of image segmentation. Through defining the weight of each pixel neighborhood and incorporating the spatial weights into the traditional Fuzzy c-means objective function, the image information which related to local spatial is integrated into the segmentation approach. Because of those spatial weights of neighboring pixels are fully adapted to the local image content and can effectively detect the anisotropy of neighborhood, the proposed algorithm improves the robust to noise. Both synthetic and real image experimental results verify the accuracy and the robustness of the ASWFCM method.**

Keywords- clustering, image segmentation, ASWFCM

I. INTRODUCTION

Image segmentation is an important task in image understanding and computer vision [1]. In image segmentation processing, an image is divided into several disjoint regions, each of which has the same characteristics with others, such as gray level, color, texture, and other characteristics. One of the most classical fuzzy clustering methods [3-12] is fuzzy c-means (FCM) algorithm [2]. The advantage of this algorithm is mainly due to the ambiguity introduced by the attributes of each image pixel. However, none of the spatial information in the image context is considered in the standard FCM algorithm, resulting in the performance of the algorithm deteriorates.

In order to improve the effectiveness of the standard FCM, smoothing the image before clustering is an effective method. It should be noted that smoothing filtering operation may result in the loss of image information, especially the loss of important image details at the boundary or edge. Moreover, the trade-off between smoothing and clustering cannot be controlled. Therefore, to improve the performance of image segmentation, researchers put forward a lot of local spatial information should be brought into the standard FCM method. By adding the spatial neighborhood term into objective function of FCM, Ahmed et al. [4] proposed FCM_S algorithm. Through using information obtained in different windows containing the image, each pixel in an image is classified through the accumulated local FCM_S approach [5]. In order to decrease the computational complexity of FCM_S, Chen and Zhang [6] proposed two variant FCM_S1 and FCM_S2, which are replaced with average filtering and median filtering images to simplify FCM_S item neighborhood. FCM_S1, FCM_2, as well as FCM_S have the same key parameter. which is adopted to control the trade-off between a pixel and its neighbors. Because of the fact that the key parameter has a crucial impact on the performance of these approaches, and the selection of the key parameter is carried out through experiments, usually using trial and error experiment, this algorithm has its limitations. Wang et al. [7] adjusted the effect of the neighborhood according to the homogeneousness of the neighboring pixels, but weights for the neighbors of each neighborhood term still have the same value. Krindis and Chatzis [8] presented a fuzzy local information c-means (FLICM) clustering method. By introducing a novel fuzzy local neighborhood factor to the objective function, both image quality and noise robustness are ensured. FLICM, however, the objective function is not set any parameters to control the influence of the factors. Li and Qin [9] improved the robustness of FLICM by using *Lp*-norm distance.

To solve the above problems, an adaptive spatially weighted fuzzy c-means (ASWFCM) method is proposed. Firstly, the weight of each pixel neighborhood is defined, and then combining the weights and the FCM objective function. Due to those spatial weights of neighboring pixels are completely adaptive to the local content of the image, the ASWFCM algorithm proposed in this paper could reduce the impact of noise and other imaging artifacts on image segmentation effectively.

This paper is organized as follows. Sec.1 is the introduction. FCM clustering algorithm is reviewed briefly in Sec.2. In Sec. 3, the detailed proposed algorithm is presented. Both synthetic and real image experimental results are shown in Sec.4, and the conclusion is given in Sec. 5.

II. FUZZY C-MEANS CLUSTERING

The FCM clustering algorithm divides the image X into c clusters by minimizing the objective function

$$J_{\mathrm{FCM}} = \sum_{k=1}^{c}\sum_{i=1}^{n} u_{ik}^{m}\|x_i - v_k\|^2 \qquad (1)$$

where $X = \{x_1, x_2, \ldots, x_n\}$ denotes an image with n pixels, u_{ik} is the membership degree of the pixel i belonging to the cluster k , and satisfies $u_{ik} \in [0,1]$ and $\sum_{k=1}^{c} u_{ik} = 1$ for any pixel i,

Authorized licensed use limited to: Shanghai Jiaotong University. Downloaded on November 17,2023 at 11:42:29 UTC from IEEE Xplore. Restrictions apply.

the prototype of the center of cluster k is denoted as v_k. Parameter m is the weighting exponent on each fuzzy membership which is usually set to 2.

$$u_{ik} = \frac{(\|x_i - v_k\|)^{-2/(m-1)}}{\sum_{j=1}^{c}(\|x_j - v_k\|)^{-2/(m-1)}} \quad (2)$$

$$v_k = \frac{\sum_{i=1}^{n} u_{ik}^m x_i}{\sum_{i=1}^{n} u_{ik}^m} \quad (3)$$

Apparently, the information in image context is not taken into consideration in FCM algorithm. Every pixel is considered as isolated. Therefore, the performance of FCM algorithm is greatly affected by noise.

III. PROPOSED ALGORITHM

In this work, the spatial weights for neighbors of each pixel are defined. Through incorporating the spatial weights into the traditional Fuzzy c-means objective function, an adaptive spatially weighted FCM (ASWFCM) algorithm is proposed to improve the effect.

A. Definition of the local weights

Letting $X = \{x_1, x_2, \ldots, x_n\}$ denotes an image with n pixels, which x_i is the gray value of the ith pixel. For each pixel x_i, the median value of its neighboring pixels value is expressed as follows.

$$m_i = med\{x_r, r \in N_i\} \quad (4)$$

where N_i stands for the set of neighbors falling into a window around x_i. The l_1 distance between x_r and m_i is computed by

$$\sigma_{ir} = |x_r - m_i| \quad (5)$$

The weight for pixel $x_r (x_r \in N_i)$ is defined as

$$\xi_{ir} = \exp\left(-\beta \frac{\sigma_{ir}}{\sigma_i}\right) \quad (6)$$

where β is the strength factor, σ_i represents the maximal value of σ_{ir}.

$$\sigma_i = \max_{r \in N_i} \sigma_{ir} \quad (7)$$

Finally, the obtained weights are normalized so that the sum of them equals to one.

$$w_{ir} = \frac{\xi_{ir}}{\sum_{r \in N_i} \xi_{ir}} \quad (8)$$

The weights for neighborhood N_i is denoted by $W_i = \{w_{ir}, r \in N_i\}$. It can be concluded from (4)-(8) that if a pixel's gray value is far away from the median value of its neighbors, the pixel will have a very small weight. This means that w_{ir} measures the similarity between the pixel x_r and the majority of N_i. That is to say, those weights of neighboring pixels are totally adaptive to the local image content. The calculated weights of two neighborhoods selected from a synthetic image is shown in Figure 1. The Figure 1 (a) gives the pixel's gray values in a neighborhood selected from the boundary area and the estimated weights. The Figure. 1 (b) gives the pixel's gray values in a neighborhood selected from the smooth area and the estimated weights. From Figure. 1, it can be easily seen that weights of noise pixels in the neighborhood are relatively small. The calculated weights in two examples illustrate that this approach could effectively detect the anisotropy of neighborhood.

133	208	197
143	211	194
137	215	**241**

0.0133	0.1600	0.2680
0.0213	0.1390	0.2328
0.0161	0.1153	0.0341

(a)

42	69	66
73	**97**	76
80	**95**	68

0.0115	0.1570	0.1174
0.2312	0.0227	0.1729
0.1147	0.0275	0.1425

(b)

Figure 1. Two neighborhoods selected from a synthetic image and the estimated weights, where edge or noise pixels are highlighted in boldface. (a) neighborhood selected from a boundary area and the estimated weights. (b) neighborhood selected from a smooth area and the estimated weights.

B. ASWFCM algorithm

We incorporate the local spatial weights W_i into the standard FCM objective function and then obtain the novel objective function of ASWFCM below:

$$J_{\text{ASWFCM}} = \sum_{k=1}^{c}\sum_{i=1}^{n} u_{ik}^m \sum_{r \in N_i} w_{ir}\|x_i - v_k\|^2 \quad (9)$$

This novel objective function can be minimized iteratively, which is similar to the traditional FCM algorithm. J_{ASWFCM} in its local minimal extreme could satisfy two conditions

$$u_{ik} = \frac{\left(\sum_{r \in N_i} w_{ir}\|x_r - v_k\|^2\right)^{-1/(m-1)}}{\sum_{j=1}^{c}\left(\sum_{r \in N_i} w_{ir}\|x_r - v_j\|^2\right)^{-1/(m-1)}} \quad (10)$$

$$v_k = \frac{\sum_{i=1}^{n} u_{ik}^m \sum_{r \in N_i} w_{ir} x_r}{\sum_{i=1}^{n} u_{ik}^m} \quad (11)$$

Based on this, the step of ASWFCM algorithm is shown as follows.

Step 1: Setting the number of the clusters c, and the fuzzy parameter m.

Authorized licensed use limited to: Shanghai Jiaotong University. Downloaded on November 17,2023 at 11:42:29 UTC from IEEE Xplore. Restrictions apply.

Step 2: Initializing the membership functions randomly.

Step 3: Calculating weights W_i using (4)-(8).

Step 4: Updating the cluster centers v_k using (11).

Step 5: Updating the membership functions u_{ik} using (10).

Step 6: Exiting if the result is convergence and skipping to Step 4 otherwise.

If the weight $w_{ir} = 0$ for $i \neq r$ and $w_{ir} = 1$ for $i = r$, the ASWFCM algorithm is the same as traditional FCM. In this case, the ASWFCM algorithm can be regarded as an extension of the standard FCM. Compared with those improved FCM-type clustering schemes described in introduction, such as FCM_S, FLICM et al., the main novelty of the ASWFCM algorithm is that the effect of neighborhood is completely adaptive to the local content of the image. And thus the ASWFCM algorithm could reduce the impact of noise and other imaging artifacts on image segmentation effectively.

IV. EXPERIMENTAL RESULTS

In order to verify the accuracy and the robustness of this method, both the synthetic image and real image experimental results are analyzed. In order to further illustrate the effectiveness of the algorithm, the performance between ASWFCM and FCM, FCM_S1, FLICM algorithms is compared. Set the parameters $m = 2$, $\beta = 3$, and $N_R = 9$ (a 3×3 window centered around each pixel) in the experiments.

In condition of "Gaussian" (zero mean), "salt & pepper", hybrid "Gaussian" and "salt & pepper" noise, these four algorithms are applied to a synthetic test image which size is 128×128 pixels, and the test image possesses four classes with intensity values 0, 70, 140 and 210. The results are shown in TABLE I and Figure 2. TABLE I describes the segmentation accuracy (SA) of the four algorithms under different noise, where σ_g denotes the standard deviation of Gaussian noise. Segmentation accuracy is Defined as the ratio of the sum of correctly classified pixels to the total number of pixels [4]. In condition of the synthetic image obtained in "Gaussian" ($\sigma_g = 10$), 5% "salt & pepper" noise and the parameter $c = 4$, the result is shown in Figure 2. From Figure 2, we notice that FCM, FCM_S1 and FLICM are affected by the noise obviously, in other words, all these three algorithms lack enough robustness to noise. Meanwhile, the result obtained by the proposed ASWFCM algorithm removes almost all the additional noise. Combined Table 1 and Figure 2, it could be concluded that the algorithm proposed in this paper is less sensitive to noise than other algorithms and achieves relatively satisfactory results.

TABLE I. SA% OF FOUR METHODS ON SYNTHETIC TEST IMAGE

Noise types and level	FCM	FCM_S1	FLICM	ALWFCM
Gaussian (σ_g=15)	96.54	99.12	99.35	99.62
Gaussian (σ_g=20)	89.74	99.05	99.30	99.49
Gaussian (σ_g=25)	82.50	98.97	99.15	99.29
salt & pepper (10%)	92.66	92.51	90.81	99.07
salt & pepper (15%)	88.84	87.82	85.22	98.20
salt & pepper (20%)	85.31	84.83	79.58	98.10

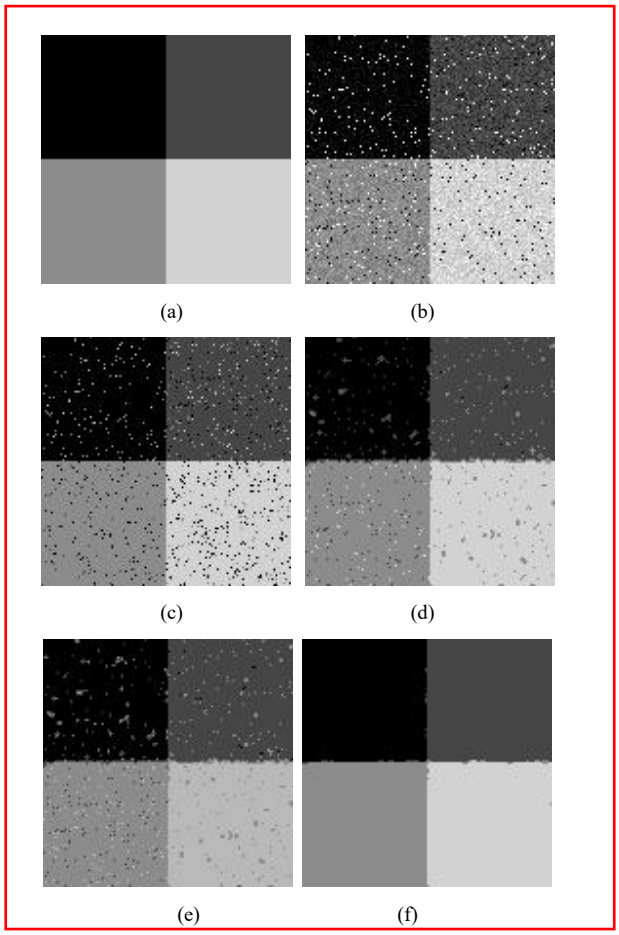


Figure 2. Comparison of segmentation results on synthetic test image. (a) Original image. (b) The same image with hybrid noise. (c) Segemention result obtained by FCM. (d) Ssegemention result obtained by FCM_S1. (e) Segemention result obtained by FLICM result. (f) Segemention result obtained by ASWFCM.

图3的叙述错误，图3(a)是原图，图3(b)是加噪声图

Figure 3 illustrates the clustering results obtained by different algorithms on a real image with 308×242 pixels. Figure 3 (a) shows the real image which in "Gaussian" (σg=10) and 5% "salt & pepper" noise background. Figure 3 (b) is the original image. Figure 3 (c)-(f) present the segmentation results of the four algorithms based on Figure 3 (b), respectively. Due to FCM, FCM_S1 and FLICM are all influenced by hybrid noise, all these three algorithms lack enough robustness to noise, which is shown in Figure 3 (c)-(d). Furthermore, the effect of noise can be basically eliminated through the proposed ASWFCM algorithm, as shown in Figure 3(f). In a word, compared to the above three algorithms, the ASWFCM algorithm proposed in this paper achieves much better segmentation result under hybrid noise condition, and the effectiveness of the algorithm is verified.

Authorized licensed use limited to: Shanghai Jiaotong University. Downloaded on November 17,2023 at 11:42:29 UTC from IEEE Xplore. Restrictions apply.

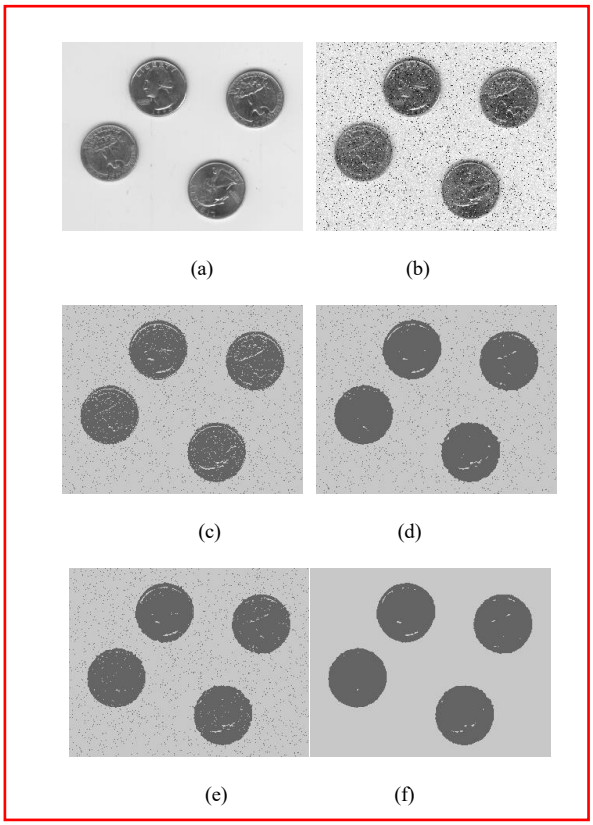


Figure. 3 Comparison of segmentation results on real image. (a) Original image. (b) The same image with hybrid noise. (c) Segemention result obtained by FCM. (d) Segemention result obtained by FCM_S1. (e) Segemention result obtained by FLICM. (f) Segemention result obtained by ASWFCM.

V. CONCLUSIONS

In this paper, the neighboring weights which are completely adaptive to the local content of the image have been defined. This weighting method could not only detect the anisotropy of neighborhoods effectively but also reduce the impact of edges and noise on image. By incorporating those weights into the traditional FCM objective function, a novel adaptive locally weighted fuzzy c-means clustering approach has been presented. Experimental results illustrated that the novel ASWFCM algorithm satisfied both the accuracy and the robustness in image segmentation processsing. Our future work will focus on incorporating the spatial distances of neighboring pixel into the weighting method proposed in this paper.

ACKNOWLEDGMENT

This work is supported by the National Natural Science Foundation of China under grant No. 51974255 as well as The Youth Foundation of Xi'an Shiyou University under grant No. 2013BS021.

REFERENCES

[1] H. Zhang, J.E. Fritts, and S. A Goldman, "Image segmentation evaluation: A survey of unsupervised methods," Computer Vision and Image Understanding, vol. 110(2), pp. 260-180, 2008.

[2] J.C. Bezdek, Pattern recognition with fuzzy objective function algorithms, Plenum, New York, 1981.

[3] X.H. Li, T.Y. Zhang, Z. Qu, "Image segmentation using fuzzy clustering with spatial constraints based on Markov random field via Bayesian theory," IEICE Transactions on Fundamentals of Electronics, Communications and Computer Sciences, vol. E91A(3), pp. 723-729 2008.

[4] M.N. Ahmed et al., "A modified fuzzy c-means algorithm for bias field estimation and segmentation of MRI data," IEEE Trans. Med. Imaging, vol. 21(3), pp. 193–199, 2002.

[5] J. Zhang, et al., "Adaptive image segmentation method based on the fuzzy c-means with spatial information," IET Image Processing, vol. 12(5), pp. 785-792, 2018.

[6] S.C. Chen, D.Q. Zhang, "Robust image segmentation using FCM with spatial constraints based on new kernel-induced distance measure," IEEE Trans. Syst. Man Cybern. B, vol 34(4), pp. 1907–1916, 2004.

[7] Z.M. Wang et al., "An adaptive spatial information-theoretic fuzzy clustering algorithm for image segmentation," Computer Vision and Image Understanding, vol. 117(10), pp. 1412-1420, 2013.

[8] S. Krinidis, V. Chatzis, "A robust fuzzy local information c-means clustering algorithm," IEEE Trans. Image Process, vol. 19(5), pp. 1328-1337, 2010.

[9] F. Li, J. Qin, "Robust fuzzy local information and Lp-norm distance-based image segmentation method," IET Image Processing, vol. 11(4), pp. 217-226, 2017.

[10] J.C. Dunn, "A fuzzy relative of the ISODATA process and its use in detecting compact well separated clusters," J. Cybern., vol. 3(3), pp. 32–57, 1973.

[11] Dhirendra Kumar, R. K. Agrawal, Puneet Kumar, "Bias-Corrected Intuitionistic Fuzzy C-Means With Spatial Neighborhood Information Approach for Human Brain MRI Image Segmentation," IEEE Transactions on Fuzzy Systems, vol. 30(3), pp. 687-700, 2022.

[12] Tao Lei, Peng Liu, Xiaohong Jia et al, "Automatic fuzzy clustering framework for image segmentation," IEEE Transactions on Fuzzy Systems, vol. 28(9), pp. 2078-2091, 2020.

Authorized licensed use limited to: Shanghai Jiaotong University. Downloaded on November 17,2023 at 11:42:29 UTC from IEEE Xplore. Restrictions apply.

Journal of Physics: Conference Series

PAPER • OPEN ACCESS

Spatially Constrained Fuzzy c-Means Clustering Algorithm for Image Segmentation

To cite this article: Xiaohe Li *et al* 2019 *J. Phys.: Conf. Ser.* **1237** 032024

View the article online for updates and enhancements.

You may also like

- Breast density quantification with cone-beam CT: a post-mortem study
Travis Johnson, Huanjun Ding, Huy Q Le et al.
- Simulation studies of mechanical stresses in REBaCuO superconducting ring bulks with infinite and finite height reinforced by metal ring during field-cooled magnetization
H Fujishiro, M D Ainslie, K Takahashi et al.
- An edge-sensitive simplification method for scanned point clouds
Shifan Liu, Jin Liang, Maodong Ren et al.

This content was downloaded from IP address 219.144.164.16 on 16/11/2023 at 00:13

IOP Conf. Series: Journal of Physics: Conf. Series **1237** (2019) 032024 doi:10.1088/1742-6596/1237/3/032024

Spatially Constrained Fuzzy c-Means Clustering Algorithm for Image Segmentation

Xiaohe Li[1, 2], Zhan Qu[2], and Xiaojing Yang[1]

[1]College of Computer Science, Xi'an Shiyou University, Xi'an 710065, China

[2]The Key Laboratory of Well Stability and Fluid & Rock Mechanics in Oil and Gas Reservoir of Shaanxi Province, Xi'an Shiyou University, Xi'an 710065, China

E-mail: lixh@xsyu.edu.cn; zhqu@xsyu.edu.cn; xjyang@xsyu.edu.cn

Abstract. The fuzzy c-means (FCM) clustering is an unsupervised clustering method, which has been widely used in image segmentation. In this paper, a spatially constrained fuzzy c-means clustering algorithm for image segmentation is proposed to overcome the sensitivity of the FCM clustering algorithm to noises and other imaging artifacts. Firstly, the local prior probabilities of pixel classification are defined according to the fuzzy membership function values of neighbouring pixels, and then those local prior probabilities are incorporated into the objective function of the standard FCM. Thus, the local spatial information embedded in the image is incorporated into the FCM algorithm. Experimental results on the synthetic and real images are given to demonstrate the robustness and validity of the proposed algorithm.

1. Introduction

As an important part of image processing, image segmentation is considered to be one of the key and most difficult techniques in computer vision [1]. The goal of image segmentation is to divide an image into several disjoint regions, which are homogeneous with respect to some characteristics such as gray level, color, texture, etc. Fuzzy c-means (FCM) clustering method [2] has been widely used in image segmentation and its success chiefly attributes to the introduction of fuzziness for the belongingness of each image pixel. This allows the clustering procedure to retain more original image information than the crisp or hard segmentation methods. However, the standard FCM clustering method is sensitive to noise and other imaging artifacts, since it does not consider any spatial information in an image.

To solve this problem, a variety of studies incorporating local spatial information into the original FCM clustering method have been proposed [3-10]. In some methods, the spatial context was embedded in the objective function of FCM clustering. Pham [6] applied a spatial penalty on the membership functions. The penalty term leads to an iterative algorithm that allows the estimation of spatially smooth membership functions. A FCM_S algorithm, proposed by Ahmed [7], modified the FCM objective function to compensate the intensity inhomogeneity and allow the labeling of a pixel to be influenced by the labels in its immediate neighborhood. However, this method is very time-consuming to compute the neighborhood terms in each iteration step. To address this problem, Chen and Zhang [8] applied the mean-filter image and the median-filter image to simplify the neighborhood term of FCM_S, and proposed the FCM_S1 and FCM_S2, respectively. The extra mean-filtered image and median-filtered image introduced by these two algorithms can be computed in advance, so the computational complexity can be considerably reduced. Cai [9] proposed a generalized fuzzy c-means algorithm for fast and robust image segmentation. Krindis and Chatzis [10] proposed a fuzzy local

Content from this work may be used under the terms of the Creative Commons Attribution 3.0 licence. Any further distribution of this work must maintain attribution to the author(s) and the title of the work, journal citation and DOI.
Published under licence by IOP Publishing Ltd

information c-means (FLICM) clustering algorithm. In this algorithm, a fuzzy local factor was introduced for solving the problem of noise sensitive and image detail lost. However, the objective function of FLICM is formulated without setting any parameter that controls the effect of this factor. Feng and Chen [11] used the spatial context constraint on the objective function of FCM, which is referred as GFCM. The spatial constraint based on MRF theory is defined as refusable level. The main drawback of the GFCM algorithm is that the hard maximum membership classification is necessary to compute the prior probabilities during the iteration.

Inspired by the ideas of GFCM algorithm, a novel spatially constrained fuzzy c-means (SCFCM) for image segmentation is proposed in this paper. At first, the local prior probabilities of pixel classification are defined according to the fuzzy membership function values of neighboring pixels, then those local prior probabilities are incorporated into the objective function of the standard FCM. Thus, the local spatial information embedded in the image is incorporated into the segmentation process. Therefore, the proposed method can effectively reduce the impact of noises and other imaging artifacts.

The rest of paper is organized as follows. Section 2 reviews the FCM clustering method briefly. The new image segmentation method is presented in Section 3. The experimental comparisons are presented in Section 4. Finally, conclusions are given in Section 5.

2. Fuzzy c-means clustering

The FCM clustering was first proposed by Dunn [12] and further improved by Bezdek [2]. Mathematically, the standard FCM clustering partitions an image X into c clusters by minimizing the objective function

$$J_{\mathrm{FCM}} = \sum_{k=1}^{c}\sum_{i=1}^{n} u_{ik}^{m} \left\| x_i - v_k \right\|^2 \tag{1}$$

where $X = \{x_1, x_2, \ldots, x_n\}$ denotes an image with n pixels, v_k is the prototype of the center of cluster k and u_{ik} is the fuzzy membership function of the pixel i belonging to the cluster k. The fuzzy partition matrix $U = [u_{ik}]$ satisfies

$$U = \left\{ u_{ik} \in [0,1] \middle| \sum_{k=1}^{c} u_{ik} = 1, \forall i, 0 < \sum_{i=1}^{n} u_{ik} < n, \forall k \right\} \tag{2}$$

The parameter m control the fuzziness of the membership function.

Using the Lagrange multiplier method, the objective function J_{FCM} can be minimized iteratively. the update equations of membership functions u_{ik} and the cluster centers v_k are given as follows:

$$u_{ik} = \frac{\left(\left\| x_i - v_k \right\|\right)^{-2/(m-1)}}{\sum_{j=1}^{c}\left(\left\| x_i - v_j \right\|\right)^{-2/(m-1)}} \tag{3}$$

$$v_k = \frac{\sum_{i=1}^{n} u_{ik}^{m} x_i}{\sum_{i=1}^{n} u_{ik}^{m}} \tag{4}$$

Apparently, the FCM algorithm does not use any spatial information in an image. i.e., the segmentation process is solely based on the histogram of image. Therefore, the FCM clustering method is sensitive to noises and imaging artifacts.

3. Proposed Algorithm

In this work, the local prior probabilities of each pixel are defined. Then those probabilities are incorporated into the FCM objective function, and a new spatially constrained fuzzy c-means (SCFCM) algorithm for image segmentation is presented.

3.1 Definition of the local prior probability

Given the membership function u_{ik} of FCM algorithm, the local prior probability is defined as

$$\pi_{ik} = \frac{\left(\sum_{j\in N_i} w_j u_{jk}\right)^b}{\sum_{k=1}^{c}\left(\sum_{j\in N_i} w_j u_{jk}\right)^b} \tag{5}$$

Where b is the constant strength factor, w_j is a weight coefficient depending on their distance from the central pixel. The influence of the neighbouring pixels is controlled by w_j, and it can be obtained by

$$w_j = \exp\left(-\frac{L_{ij}^2}{2d^2}\right) \tag{6}$$

Where L_{ij} is the spatial Euclidian distance between pixels i and j, and $d = (s-1)/4$, s is the size of the neighborhood window. The strength of w_j decreases as the distance between pixel i and j increases.

Comparing to GFCM algorithm, those prior probabilities can be computed directly from the membership functions of neighborhood pixels, and the hard maximum membership segmentation is unnecessary during the iteration. Furthermore, the spatial Euclidian distance between pixels has be incorporated into those prior probabilities. Therefore, the local prior probability defined in this paper has better characteristics, compared with GFCM algorithm.

3.2 SCFCM algorithm

By incorporating the local prior probability π_{ik} into the standard FCM objective function, the objective function of the proposed algorithm is formulated as

$$J_{\text{SCFCM}} = \sum_{k=1}^{c}\sum_{i=1}^{n}(1-\pi_{ik})u_{ik}^m \|x_i - v_k\|^2 \tag{7}$$

Similar to the standard FCM clustering method, the J_{SCFCM} can be minimized iteratively. The membership functions u_{ik} and the cluster centers v_k are updated as follows:

$$v_k = \frac{\sum_{i=1}^{n} u_{ik}^m (1-\pi_{ik}) x_i}{\sum_{i=1}^{n} u_{ik}^m (1-\pi_{ik})} \tag{8}$$

$$u_{ik} = \frac{\left[(1-\pi_{ik})\|x_i - v_k\|^2\right]^{-1/m}}{\sum_{k=1}^{c}\left[(1-\pi_{ik})\|x_i - v_k\|^2\right]^{-1/m}} \tag{9}$$

Thus, the SCFCM algorithm is given as follows:

Step 1: Set the parameter m, and the number of the clusters c.

Step 2: Initialize the membership functions randomly.

Step 3: Calculate the local prior probabilities using (5)-(6).

Step 4: Update the cluster center v_k using (8).

Step 5: Update the membership functions u_{ik} using (9).

Step 6: In case of convergence, exit; Otherwise, go to Step 3.

4. Experimental Results

To demonstrate the robustness and validity of the SCFCM method, we compare the performance of our proposed SCFCM algorithm with the FCM, FCM_S1, FLICM and GFCM algorithms. The experiment will be done on the synthetic and real images corrupted by noises respectively. We set the fuzzy parameter $m=2$, and $b=1.8$ for the proposed algorithm. The size of neighbourhood window is 3×3.

In the first experiment, a synthetic test image with 128×128 pixels, as shown in Fig. 1(a), is used to compare the performance of the proposed algorithm with others. The image contains four classes with intensity values 0, 70, 140 and 210. We compare the performance of above five algorithms on the synthetic test image, which is divided into 4 classes. The test image is corrupted by "Gaussian", "salt & pepper" and hybrid "Gaussian" and "salt & pepper" noises, respectively, and the segmentation results are shown in Table 1 and Fig. 1. Table 1 gives the average segmentation accuracy (SA) of the five algorithms on three different noisy images, where SA is defined as the sum of the correctly classified pixels divided by the sum of the total number of pixels [8]. Fig. 1 shows the results on synthetic test image corrupted by "Gaussian" noises. we can see that FCM, FCM_S1, FLICM and GFCM are, respectively, influenced by the noises more or less., which indicates that these algorithms lack enough robustness to noises, while the proposed SCFCM algorithm removes almost all the added noises. Compared to the FCM, FCM_S1, FLICM and GFCM algorithm, we can see that the proposed SCFCM algorithm achieves much better segmentation.

Table 1 SA% of five algorithms on synthetic test image.

Noise type	FCM	FCM_S1	FLICM	GFCM	SCFCM
Gaussian	98.21	99.08	98.53	98.79	99.98
Salt & Pepper	95.81	95.38	95.92	96.47	98.33
Hybrid noise	94.53	95.68	95.58	95.71	98.55

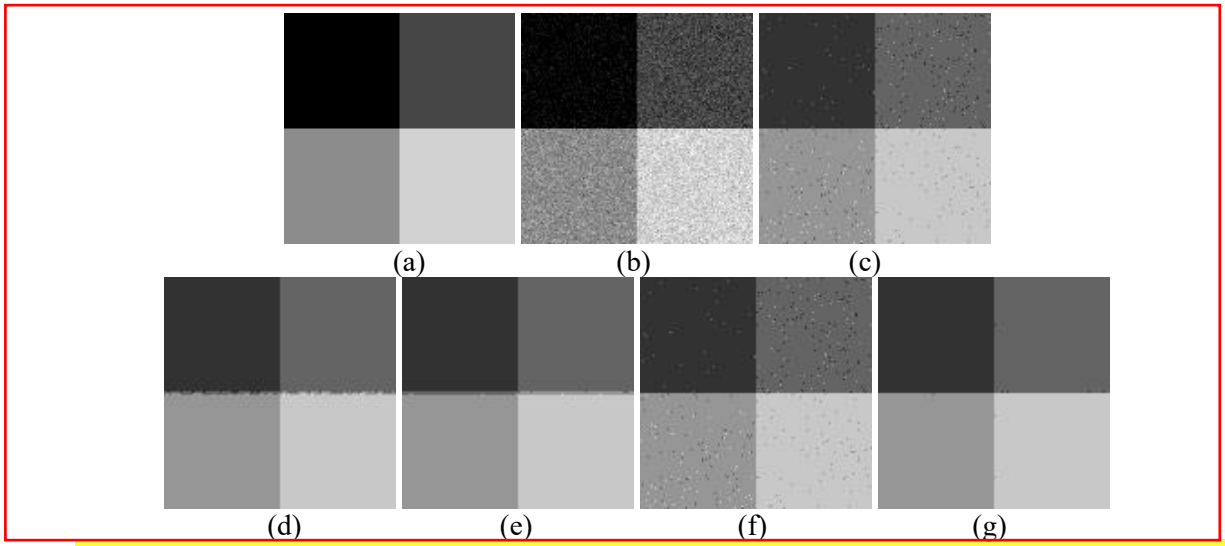


Fig. 1 Segmentation results of five algorithms on synthetic test image. (a) Original image. (b) Noise image. (c) FCM. (d) FCM_S1. (e) FLICM. (f) GFCM. (h) SCFCM.

Fig. 2 presents a comparison of segmentation results on a real image with 308×242 pixels as shown in Fig. 2(a). Fig. 2(b) is the original image corrupted by hybrid "Gaussian" and "salt & pepper" noises. Fig. 2(c)-(g) present the results applying the five algorithms on Fig. 2(b), respectively. We use $c = 2$ in the experiment. Visually, FCM, FCM_S1, FLICM and GFCM are respectively affected by the noises to different extents, while the proposed SCFCM algorithm achieves an outstanding segmentation. From Fig. 2(c)-(g), It can be concluded that the SCFCM algorithm is less sensitive to noises than other algorithms.

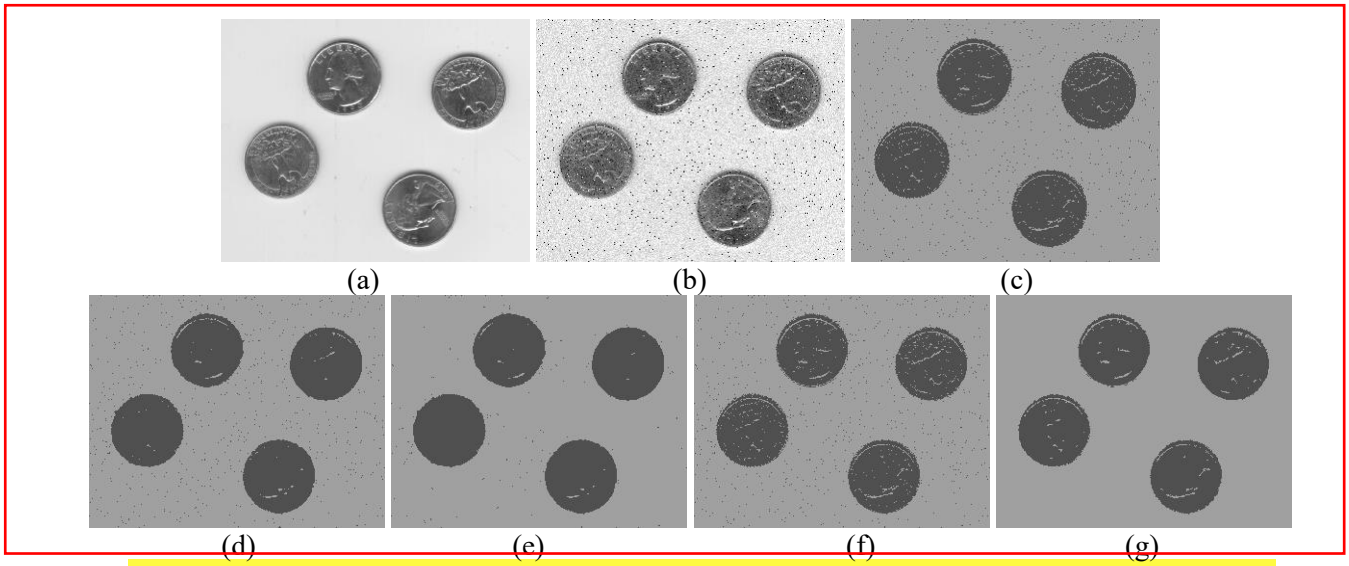


Fig. 2 Segmentation results of five algorithms on a real image corrupted by hybrid "Gaussian" and "salt & pepper" noises. (a) Original image. (b) Noise image. (c) FCM. (d) FCM_S1. (e) FLICM. (f) GFCM. (h) SCFCM.

5. Conclusions

In this paper, we have presented a novel spatially constrained fuzzy c-means clustering algorithm for image segmentation. Firstly, the local prior probabilities of pixels are defined according to the fuzzy membership function values of neighbouring pixels, then those local prior probabilities are incorporated into the objective function of the standard FCM. By this way, the local spatial information embedded in the image is incorporated into the FCM clustering algorithm. Experimental results on the synthetic and real images have demonstrated the robustness and validity of the proposed algorithm.

Acknowledgments

This work was supported by the National Natural Science Foundation of China under grant no. 51674200 and The Youth Foundation of Xi'an Shiyou University under grant no. 2013BS021.

References

[1] H. Zhang, J.E. Fritts, and S. A Goldman. Image segmentation evaluation: A survey of unsupervised methods[J]. Computer Vision and Image Understanding, 2008, 110(2): 260-180.

[2] J.C. Bezdek, Pattern recognition with fuzzy objective function algorithms[M], Plenum, New York, 1981.

[3] X.H. Li, T.Y. Zhang, Z. Qu. Image segmentation using fuzzy clustering with spatial constraints based on Markov random field via Bayesian theory[J]. IEICE Transactions on Fundamentals of Electronics, Communications and Computer Sciences, 2008, E91A(3): 723-729.

[4] F. Li, J. Qin. Robust fuzzy local information and Lp-norm distance-based image segmentation

method[J]. IET Image Processing, 2017, 11(4), 217-226.
[5] J. Zhang, et al. Adaptive image segmentation method based on the fuzzy c-means with spatial information[J]. IET Image Processing, 2018, 12(5): 785-792.
[6] D.L. Pham. Spatial models for fuzzy clustering[J]. Computer vision and image understanding, 2001, 84: 285-297.
[7] M.N. Ahmed, S.M. Yamany, N. Mohamed, A.A. Farag, and T. Moriarty. A modified fuzzy *c*-means algorithm for bias field estimation and segmentation of MRI data[J]. IEEE Trans. Med. Imaging, 2002, 21: 193-199.
[8] S.C. Chen, D.Q. Zhang. Robust image segmentation using FCM with spatial constraints based on new kernel-induced distance measure [J]. IEEE Trans. Syst. Man Cybern. B, 2004, 34(4): 1907–1916.
[9] W.L. Cai, S.C. Chen and D.Q. Zhang. Fast and robust fuzzy c-means clustering algorithms incorporating local information for image segmentation [J]. Pattern Recognition, 2007, 40: 825-838.
[10] S. Krinidis, V. Chatzis. A robust fuzzy local information c-means clustering algorithm[J]. IEEE Trans. Image Process, 2010, 19(5): 1328-1337.
[11] Feng Y. and Chen W. Brain MR image segmentation using fuzzy clustering with spatial constraints based on Markov random field theory[C]. In:Proc of MIAR 2004 (LNCS 3150,Beijing). Berlin: Springer-Verlag, 2014, 188-195.
[12] J.C. Dunn. A fuzzy relative of the ISODATA process and its use in detecting compact well separated clusters[J]. J. Cybern., 1973, 3(3): 32–57.

DOI: 10.3969/j.issn.1673-064X.2017.05.017 中图分类号: TP391.4
文章编号: 1673-064X(2017)05-0102-05 文献标识码: A

空间加权模糊 C 均值聚类图像分割算法

李小和,屈 展,王魁生,卢胜男

(西安石油大学 计算机学院,陕西 西安 710065)

摘要: 为了提高模糊 C 均值聚类(FCM)算法用于图像分割时对噪声的鲁棒性,在 FCM 算法中引入了图像像素的邻域约束,提出一种空间加权模糊 C 均值聚类图像分割算法。首先根据邻域像素的模糊隶属度函数值,定义像素分类标记的局部先验概率,然后将该局部先验概率融入标准的 FCM 算法的目标函数中,从而提出一种空间加权模糊 C 均值聚类图像分割算法。仿真实验通过合成图像和真实图像验证了该算法的有效性和鲁棒性。

关键词: 图像分割算法; 模糊 C 均值聚类; 空间加权

Spatial Weighted Fuzzy C-means Clustering Algorithm for Image Segmentation

LI Xiaohe,QU Zhan,WANG Kuisheng,LU Shengnan

(College of Computer Science,Xi'an Shiyou University,Xi'an 710065,Shaanxi,China)

Abstract: Fuzzy C-means clustering (FCM) is an unsupervised clustering method,which is widely used in image segmentation. A spatial weighted fuzzy C-means clustering algorithm for image segmentation is proposed in order to overcome the sensitivity of the standard FCM algorithm to noises and other imaging artifacts. Firstly,the local prior probabilities of pixel classification marks are defined are defined according to the fuzzy membership function value of neighborhood pixels,and then those local prior probabilities are incorporated into the objective function of the standard FCM. Simulation experiments show the effectiveness and robustness of the proposed algorithm through both synthetic and real images.

Key words: image segmentation algorithm; fuzzy C-means clustering; spatial weighting

李小和,屈展,王魁生,等. 空间加权模糊 C 均值聚类图像分割算法[J]. 西安石油大学学报(自然科学版),2017,32(5):102-106.

LI Xiaohe,QU Zhan,WANG Kuisheng,et al. Spatial weighted fuzzy C-means clustering algorithm for image segmentation[J]. Journal of Xi'an Shiyou University(Natural Science Edition),2017,32(5):102-106.

收稿日期: 2016-09-01

基金项目: 国家自然科学基金项目(51674200);西安石油大学青年科技创新基金项目(2013BS021)

作者简介: 李小和(1974-),男,博士,讲师,研究方向: 图像处理与模式识别。E-mail: lixh@xsyu.edu.cn

(C)1994-2022 China Academic Journal Electronic Publishing House. All rights reserved. http://www.cnki.net

引 言

图像分割是指根据图像的灰度、颜色或者纹理等特征将图像划分成若干个互不相交的区域,使得这些特征在每个区域内表现出一致性或相似性。图像分割是从图像处理到图像分析的关键步骤,也是图像理解的前提和基础[1]。模糊 C 均值聚类[2](Fuzzy C-means,FCM)算法是一种无监督的聚类方法,近年来被广泛地应用于图像分割领域[3-10]。然而标准的 FCM 算法用于图像分割时没有考虑像素的空间位置关系,因此 FCM 算法对噪声特别敏感。

为了进一步提高 FCM 算法用于图像分割时对噪声的鲁棒性,Ahmed 等[5]通过在 FCM 的目标函数中对像素颜色特征引入邻域约束提出了 FCM_S 算法,但 FCM_S 算法在每一步迭代时都需对邻域像素的颜色特征进行一系列计算,因此时间复杂度较大。Chen 等[6]用邻域像素颜色特征的均值或中值取代邻域像素的颜色特征从而提出了 FSM_S1 和 FSM_S2 算法,由于邻域信息的均值或中值可在迭代之前计算,因此,FSM_S1 和 FSM_S2 算法在保持 FSM_S 算法优越性的同时,降低了 FSM_S 算法的复杂度。Pham[7]通过在 FCM 的目标函数中对模糊隶属度函数值引入邻域约束项提出了 RFCM 图像分割算法。Krindis 和 Chatzis 通过在 FCM 目标函数中引入局部邻域因子,提出了 FLICM 算法[8]。Feng 等[9-10]借助马尔可夫随机场(MRF)在 FCM 算法中引入邻域约束,提出了 GFCM 算法。GFCM 算法在每一步迭代过程中,需要通过对像素的模糊隶属度函数值去模糊化得到一个临时分割场,然后运用 MRF 理论计算出像素属于每一类的局部条件概率,最后将该局部条件概率引入到 FCM 算法的目标函数。

为了进一步提高 FCM 图像分割算法对噪声的鲁棒性,本文首先根据邻域像素的模糊隶属度函数值定义像素分类标记的局部先验概率,然后将该局部先验概率融入到标准 FCM 算法的目标函数,提出一种空间加权模糊 C 均值聚类(SWFCM)图像分割算法。

1 模糊 C 均值聚类

给定样本集 $X=\{\boldsymbol{x}_i \mid 1\leqslant i\leqslant N,\text{且}\ \boldsymbol{x}_i\in \mathbf{R}^d\}$,$d$ 为样本空间维数。为了将这 N 个样本划分为 C 类,FCM 算法通过对目标函数迭代优化实现集合划分。FCM 算法[2]的目标函数定义为

$$J_{\mathrm{FCM}}(\boldsymbol{U},\boldsymbol{V})=\sum_{k=1}^{C}\sum_{i=1}^{N}\mu_{ik}^{m}\|\boldsymbol{x}_i-\boldsymbol{v}_k\|^2。\tag{1}$$

式中:$\boldsymbol{U}=[\mu_{ik}]$为模糊隶属度函数值矩阵,$\mu_{ik}$ 为第 i 个样本属于第 k 类的模糊隶属度函数值;$\boldsymbol{V}=[\boldsymbol{v}_1,\boldsymbol{v}_2,\cdots,\boldsymbol{v}_C]$ 为聚类中心矩阵,$\boldsymbol{v}_k$ 为第 k 个类的中心;m 为模糊加权指数,控制聚类结果模糊程度,$m\in[1,+\infty)$。其中 $\boldsymbol{U}$ 满足约束条件

$$\boldsymbol{U}\in\{\mu_{ik}\in[0,1]\mid\sum_{k=1}^{C}\mu_{ik}=1,\forall i,0<\sum_{i=1}^{N}\mu_{ik}<N\forall k\}。\tag{2}$$

FCM 算法的目标函数 J_{FCM} 是样本到聚类中心的距离平方的加权累积和,它反映了在某种差异性定义下的类内紧致一致度,J_{FCM} 越小,聚类的结果越紧致。采用 Lagrange 乘子法可求得在约束条件下使目标函数 J_{FCM} 取局部最小值的必要条件为:

$$\boldsymbol{v}_k=\frac{\sum_{i=1}^{N}\mu_{ik}^{m}\boldsymbol{x}_i}{\sum_{i=1}^{N}\mu_{ik}^{m}},k=1,2,\cdots,C;\tag{3}$$

$$\mu_{ik}=\frac{\|\boldsymbol{x}_i-\boldsymbol{v}_k\|^{-2/(m-1)}}{\sum_{j=1}^{C}\|\boldsymbol{x}_i-\boldsymbol{v}_j\|^{-2/(m-1)}};$$

$$k=1,2,\cdots,C;\ i=1,2,\cdots,N。\tag{4}$$

FCM 算法的具体步骤为:

① 确定聚类数目 C、参数 m,以及迭代停止阈值 ε;

② 采用随机的方法初始化模糊隶属度函数值;

③ 根据式(3),用当前模糊隶属度函数值更新聚类中心;

④ 根据式(4),用当前聚类中心更新模糊隶属度函数值;

⑤ 重复第③到④步,直到满足终止迭代条件:

$$\|\boldsymbol{v}_{\mathrm{new}}-\boldsymbol{v}_{\mathrm{old}}\|<\varepsilon,\tag{5}$$

式中,$\boldsymbol{v}_{\mathrm{new}}$ 为当前迭代的聚类中心,$\boldsymbol{v}_{\mathrm{old}}$ 为前一步迭代的聚类中心。

通过上述步骤,可得到各类的聚类中心,以及各个样本属于各类的模糊隶属度函数值,从而完成模糊聚类划分。若采用 FCM 算法进行图像分割,则这里的样本指的是图像像素的灰度、颜色或者纹理等特征。

2 空间加权模糊 C 均值聚类

在进行图像分割时,为了得到连通区域,通常希望相邻的像素尽可能分割到相同的区域,因此需要在 FCM 算法中引入邻域约束。根据邻域像素的模糊

(C)1994-2022 China Academic Journal Electronic Publishing House. All rights reserved. http://www.cnki.net

隶属度函数值,定义第 i 个像素属于第 k 类的局部先验概率

$$\pi_{ik}=\frac{\sum_{r\in N_i}u_{rk}^{b}}{\sum_{k=1}^{C}\sum_{r\in N_i}u_{rk}^{b}},\tag{6}$$

式中,N_i 为第 i 个像素的邻域,参数 b 为惩罚因子。由式(6)可知,对于任意的 $r\in N_i$,μ_{ik} 越大,π_{ik} 越大。也就是说,图像的第 i 个像素的邻域像素属于第 k 类的模糊隶属度函数值越大时,π_{ik} 越大。

本文将定义的分类标记的局部先验概率 π_{ik} 融入到标准 FCM 的目标函数中,提出了 SWFCM 图像分割算法。SWFCM 算法的目标函数定义为

$$J_{\mathrm{SWFCM}}=\sum_{k=1}^{C}\sum_{i=1}^{N}(1-\pi_{ik})u_{ik}^{m}\|\boldsymbol{x}_i-\boldsymbol{v}_k\|^2。\tag{7}$$

由式(7)和(6)可知,第 i 个像素到第 k 类中心的距离越小,且第 i 个像素及其邻域像素属于第 k 类的模糊隶属度函数值越大时,J_{SWFCM} 越小。因此,最小化目标函数 J_{SWFCM},可使相邻像素尽可能划分到相同的类。

类似标准 FCM 算法,采用 Lagrange 乘子法可求得在约束条件式(2)下使目标函数 J_{SWFCM} 取局部最小的必要条件为:

$$\boldsymbol{v}_k=\frac{\sum_{i=1}^{N}u_{ik}^{m}(1-\pi_{ik})\boldsymbol{x}_i}{\sum_{i=1}^{N}u_{ik}^{m}(1-\pi_{ik})};\tag{8}$$

$$u_{ik}=\frac{[(1-\pi_{ik})\|\boldsymbol{x}_i-\boldsymbol{v}_k\|^2]^{-1/(m-1)}}{\sum_{k=1}^{C}[(1-\pi_{ik})\|\boldsymbol{x}_i-\boldsymbol{v}_k\|^2]^{-1/(m-1)}}。\tag{9}$$

SWFCM 算法的具体步骤为:

① 确定聚类数目 C、参数 m 以及迭代停止阈值 ε;

② 采用随机的方法初始化模糊隶属度函数值;

③ 根据式(6),计算局部概率 π_{ik};

④ 根据式(8),用当前模糊隶属度函数值更新聚类中心;

⑤ 根据式(9),用当前聚类中心更新模糊隶属度函数值;

⑥ 重复第③—⑤步,直到满足终止迭代条件 $\|\boldsymbol{v}_{\mathrm{new}}-\boldsymbol{v}_{\mathrm{old}}\|<\varepsilon$。

根据上述步骤对图像像素进行聚类后,可按照一定的规则对像素的模糊聚类结果进行去模糊化,从而将其转化为确定性分类,完成图像分割。一种比较直接的去模糊化方法是将各个像素划分至其最大模糊隶属度函数值所对应的类。若

$$l_i=\arg\max_{1\leqslant k\leqslant C}\mu_{ik},\tag{10}$$

则将第 i 像素划分到第 l_i 类。

3　实验结果

为了验证本文提出的 SWFCM 图像分割算法的有效性和鲁棒性,选择人工合成图像和真实图像作为测试图像,并将 SWFCM 算法的分割结果与 FCM、FCM_S1、RFCM、FLICM 和 GFCM 算法的分割结果进行对比。选择参数 $\varepsilon=0.0001$,$b=1.6$。由于 FCM 算法在 $m=2$ 时,能够得到比较理想的聚类结果,因此选择参数 $m=2$。邻域系统为二阶邻域系统。

本文首先通过人工合成图像验证 SWFCM 算法的有效性和鲁棒性。合成图像的大小为 96×96 像素,由灰度值分别为 50、100、150 和 200 的 4 类像素组成,然后给该合成图像分别加上高斯噪声、椒盐噪声,以及高斯噪声和椒盐噪声的混合噪声。图 1(a)

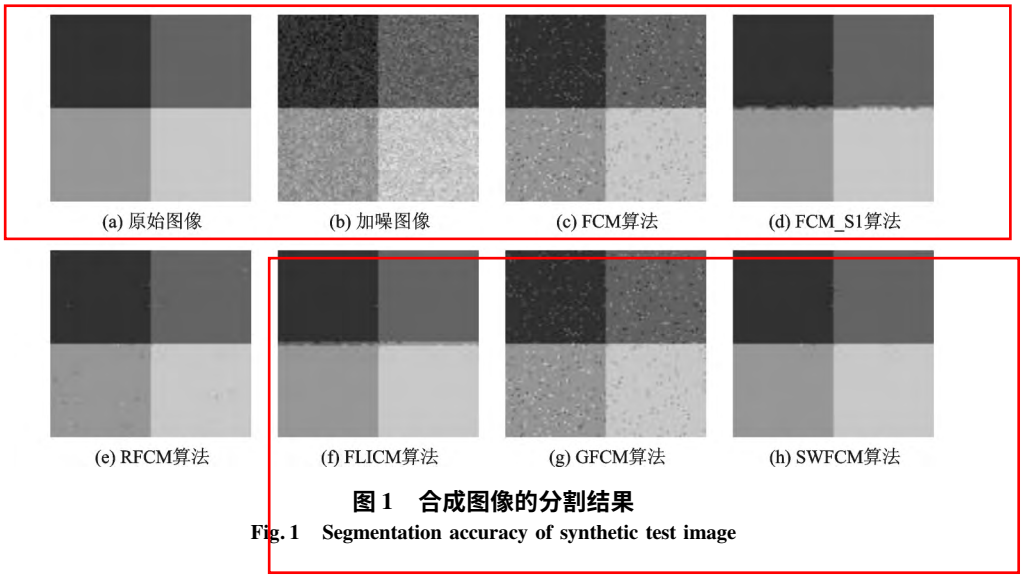


图 1　合成图像的分割结果

Fig. 1　Segmentation accuracy of synthetic test image

(C)1994-2022 China Academic Journal Electronic Publishing House. All rights reserved.　http://www.cnki.net

为原始合成图像，图 1(b) 为加上高斯噪声后的图像。图 1(c) 到(h) 分别为 FCM、FCM_S1、RFCM、FLICM、GFCM 和 SWFCM 算法对图 1(b) 的分割结果。表 1 为 6 种算法在不同噪声下的分割准确率(*SA*) 。这里 *SA* 指的是正确分割的像素数除以图像的总像素数[6] 。参数 $C=4$。由图 1 和表 1 可以发现，FCM、FCM_S1、RFCM、FLICM 和 GFCM 算法在不同程度上受到噪声的影响，分割准确率相对较低，而本文提出的 SWFCM 算法分割准确率最高，能够得到比较理想的分割结果。

表 1 合成图像的分割准确率

Tab. 1 segmentation accuracy on synthetic test image

噪声类型	分割准确率/%					
	FCM	FCM_S1	RFCM	FLICM	GFCM	SWFCM
高斯噪声	94.61	98.69	99.74	98.13	95.29	99.92
椒盐噪声	95.95	93.16	96.39	91.96	96.39	99.80
混合噪声	90.08	92.62	95.29	89.49	90.72	99.35

图 2 为标准测试图像 eight 加上高斯噪声与椒盐噪声的混合噪声后的分割结果。图 2(a) 为 eight 标准测试图像，大小为 308 × 242 像素。图 2(b) 为加上高斯噪声和椒盐噪声后的 eight 图像。图 2(c) 到(h) 分别为 FCM、FCM_S1、RFCM、FLICM、GFCM 和 SWFCM 算法的分割结果。选择参数 $C=2$。通过图 2 可以发现，FCM、FCM_S1、RFCM、FLICM 和 GFCM 算法在一定程度上受到噪声的影响，分割结果相对较差，分割结果包含较多的孤立像素点，本文提出的 SWFCM 算法能够得到比较满意的分割结果。

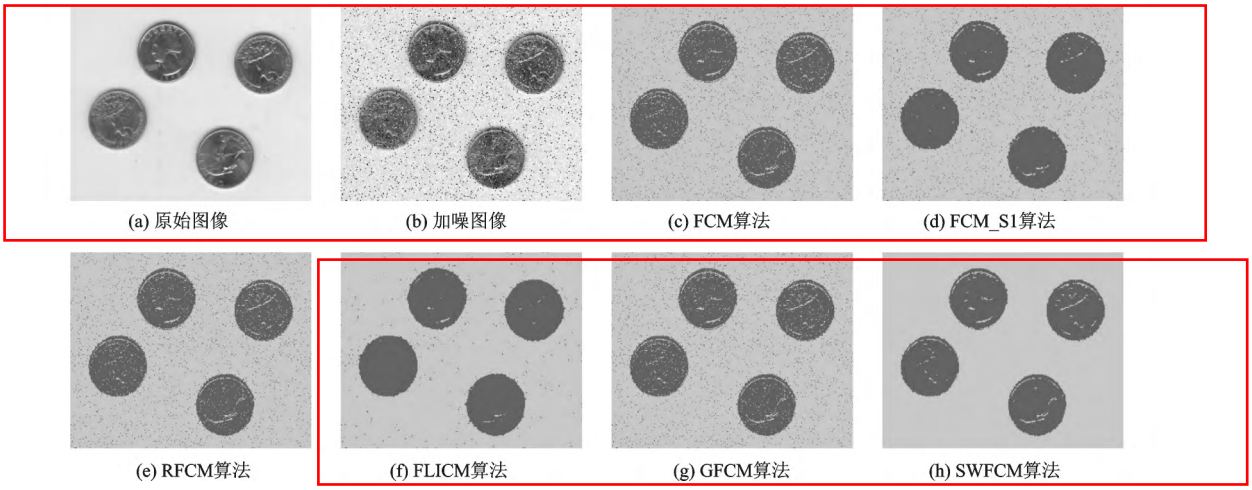


图 2 eight 标准图像加噪声后的分割结果

Fig. 2 Segmentation results of a real image corrupted by noise

4 结 论

标准的 FCM 算法用于图像分割时，由于没考虑相邻像素的关系，对噪声特别敏感，易产生孤立的像素点。为了提高 FCM 图像分割算法对噪声的鲁棒性，本文首先定义了像素分类标记的局部先验概率，然后将该概率融入到 FCM 算法的目标函数中，提出了空间加权模糊聚类图像分割算法。

本文在定义局部先验概率时，没有考虑邻域像素的距离的影响。在式(6) 中引入像素的距离信息，是下一步的研究方向。

参 考 文 献:

[1] ZHANG H，FRITTS J E，GOLDMAN S A. Image segmentation evaluation: a survey of unsupervised methods [J] . Computer Vision and Image Understanding，2008，110(2) : 180-260.

[2] BEZDEK J C. Pattern recognition with fuzzy objective function algorithms [M] . New York: Plenum Press，1981.

[3] LI XH，ZHANG TY，QU Z. Image segmentation using fuzzy clustering with spatial constraints based on Markov random field via Bayesian theory [J] . IEICE Transactions on Fundamentals of Electronics，Communications and Computer Sciences，2008，E91A(3) : 723-729.

[4] LIU G Y，ZHANG Y，WANG A M. Incorporating adaptive

(C)1994-2022 China Academic Journal Electronic Publishing House. All rights reserved. http://www.cnki.net

local information into fuzzy clustering for image segmentation [J]. IEEE Trans. Image Process, 2015, 24(11): 3990-4000.

[5] AHMED M N, YAMANY S M, MOHAMED N, et al. A modified fuzzy C-means algorithm for bias field estimation and segmentation of MRI data [J]. IEEE Transactions on Medical Imaging, 2002, 21(3): 193-199.

[6] CHEN S C, ZHANG D Q. Robust image segmentation using FCM with spatial constraints based on new kernel-induced distance measure [J]. IEEE Transactions on Systems, Man, and Cybernetics: Part B, 2004, 34(4): 1907-1916.

[7] PHAM D L. Spatial models for fuzzy clustering [J]. Computer Vision and Image Understanding, 2001, 84(2): 285-297.

[8] KRINIDIS S, CHATZIS V. A robust fuzzy local information c-means clustering algorithm [J]. IEEE Trans Image Process, 2010, 19(5): 1328-1337.

[9] FENG Y Q, CHEN W F. Brain MR image segmentation using fuzzy clustering with spatial constraints based on Markov random field theory [C]. 2nd International Conference on Information and Computing Science, 2004: 188-195.

[10] 冯衍秋,陈武凡,梁斌,等. 基于 Gibbs 随机场与模糊 C 均值聚类的图像分割新算法 [J]. 电子学报, 2004, 32(4): 645-647.
FENG Yanqiu, CHEN Wufan, LIANG Bin, et al. A new algorithm for image segmentation based on Gibbs random field and fuzzy C-means cluatering [J]. Acta Electronica Sinica, 2004, 32(4): 645-647.

责任编辑: 张新宝

(上接第 101 页)

[8] 高炜欣,胡玉衡,穆向阳,等. 埋弧焊 X 射线焊缝图像缺陷分割检测技术 [J]. 仪器仪表学报, 2011, 32(6): 1215-1224.
GAO Weixin, HU Yuheng, MU Xiangyang, et al. Real-time detection and segmentation of submerged-arc welding defects in X-ray radiography images [J]. Chinese Journal of Scientific Instrument, 2011, 32(6): 1215-1224.

[9] 马婧华,汤宝平,宋涛. 基于自适应本征维数估计流形学习的相空间重构降噪方法 [J]. 振动与冲击, 2015, 34(11): 29-34.
MA Jinghua, TANG Baoping, SONG Tao. Phase space reconstruction method for vibration signal's noise reduction based on adaptive intrinsic dimension estimation manifold learning [J]. Journal of Vibration and Shock, 2015, 34(11): 29-34.

[10] 蒋全胜,贾民平,胡建中,等. 基于拉普拉斯特征映射的故障模式识别方法 [J]. 系统仿真学报, 2008, 20(20): 5710-5713.
JIANG Quansheng, JIA Minping, HU Jianzhong, et al. Method of fault pattern recognition based on laplacian eigenmaps [J]. Journal of System Simulation, 2008, 20(20): 5710-5713.

[11] 王旭辉,舒平,曹立. 基于 ROC 曲线寻优的支持向量机性能研究 [J]. 计算机科学, 2010, 37(8): 240-242.
WANG Xuhui, SHU Ping, CAO Li. Performance evaluation with optimization strategy for support vector machine based on ROC curve [J]. Computer Science, 2010, 37(8): 240-242.

[12] 王欣,高炜欣,武晓朦,等. 基于模糊模式识别的焊缝缺陷图像检测 [J]. 西安石油大学学报(自然科学版), 2016, 31(4): 115-121.
WANG Xin, GAO Weixin, WU Xiaomeng, et al. Image detecting of weld defect based on fuzzy pattern recognition [J]. Journal of Xi'an Shiyou University(Natural Science Edition), 2016, 31(4): 115-121.

[13] 王宏涛,孙剑伟. 基于 BP 神经网络和 SVM 的分类方法研究 [J]. 软件, 2015, 36(11): 96-99.
WANG Hongtao, SUN Jianwei. Research on the classification method based on BP neural network and SVM [J]. Computer Engineering & Software, 2015, 36(11): 96-99.

责任编辑: 董　瑾

(C)1994-2022 China Academic Journal Electronic Publishing House. All rights reserved.　http://www.cnki.net

The Design of Rate Compatible Network LDPC Codes

Jingyi Wang，Ying Li，Yue Sun，
State Key Lab. of Integrated Service Networks, Xidian Univ., Xi'an , China

Abstract: This paper studies the design of rate compatible network LDPC codes and proposes a rate-compatible puncturing algorithm, which can obtain the minimum error probability. First, based on the structure of network LDPC codes, the recovery error probability is derived. Then an algorithm of finding variable nodes to be deleted based on the tanner graph of network LDPC codes is proposed, which is aimed at minimizing the decoding error probability and optimizing the puncturing pattern. Simulation results show that the proposed methods of rate-compatible network-LDPC codes have 0.4dB of gain at $BER=10^{-4}$ in error performance compare to the existing punctured methods.

Keywords: multi-access relay channel; Network-LDPC code; rate-compatible; puncturing

速率兼容网络 LDPC 码的设计

王静怡，，李颖，孙岳
西安电子科技大学　综合业务网理论及关键技术国家重点实验室，西安，中国，710071

摘　要：本文研究了网络 LDPC 码的速率兼容算法设计，提出了一种可以获得最低译码错误概率的速率兼容删余算法。首先针对网络 LDPC 码的结构特点，推导了译码恢复错误概率，并基于网络 LDPC 码的 Tanner 图搜索需要删余的变量节点，并以达到最小译码错误概率为目标，获得最优的删余图样。仿真结果表明，与采用现有算法获得的网络 LDPC 码相比，采用所提的改进速率兼容算法获得的网络 LDPC 码的性能在 $BER=10^{-4}$ 时有 0.4 个 dB 的性能增益。

关键词：多址接入信道；网络 LDPC 码；速率兼容；删余

1　引言

无线通信系统中采用中继协作传输技术，可以获取额外的分集增益，从而改善系统性能。但是，对于多址接入中继网络，有多个节点同时需要中继节点帮助转发数据，传统的译码转发或者放大转发模式，会使得中继转发效率降低。因此，通过在中继节点设计有效的联合网络-信道编码算法，在改善接收端性能的同时提高转发效率，是目前的研究热点之一。文献[4]利用低密度奇偶校验(LDPC)码，针对多址接入中继信道设计了一种网络 LDPC 码，并指出可以通过调整中继节点转发数据量来实现中继转发效率和接收端译码性能的有效折中。但是，文中并没有给出具体实现算法，本文将在此基础上，研究适用于网络 LDPC 码的速率兼容算法。

速率兼容码的概念由文献[1]首次提出，文中研究了速率兼容卷积码的设计。删余是实现速率兼容的一种常用方法，即通过将低码率母码中的某些编码比特删余来获取高码率码。速率兼容 LDPC 码的设计是近几年研究热点，文献[2，3]通过分组和排序操作，将 LDPC 码的变量节点按照迭代恢复次数进行分类，设计了 LDPC 码速率兼容删余算法。

资助信息：国家自然基金项目(61072064)；国家科技重大专项(2010ZX03003-003-03)；长江学者和创新团队发展计划资助(IRT0852)；中央高校科研业务费专项资金项目(K50510010026).

(C)1994-2023 China Academic Journal Electronic Publishing House. All rights reserved.　http://www.cnki.net

2 适用于多址接入中继信道的网络 LDPC 码

由两个源节点和一个中继节点构成的多址接入中继网络模型如图 1 所示，两个源节点与目的节点之间的信息传输由广播发送和中继转发两个阶段完成。在广播阶段，两个源节点分别向中继节点和目的节点广播发送编码序列 X_1 和 X_2；在中继转发阶段，中继节点首先对接收信号进行译码，得到两个源节点的估计数据，然后对译码得到的估计数据重新进行联合编码，并将编码序列 X_R 转发至目的节点。目的节点则根据收到的信号进行联合译码，得到两个源节点的估计信息。

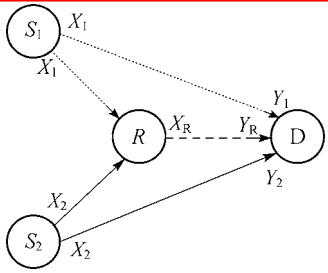


图 1　多址接入中继信道模型

在目的节点端将两个源节点和中继节点采用的 LDPC 码综合考虑，得到如下校验矩阵

$$\boldsymbol{H}=\begin{pmatrix}\boldsymbol{H}_1 & \boldsymbol{0} & \boldsymbol{0}\\ \boldsymbol{0} & \boldsymbol{H}_1 & \boldsymbol{0}\\ \boldsymbol{A} & \boldsymbol{B} & \boldsymbol{C}\end{pmatrix} \qquad (1)$$

式中，$\boldsymbol{H}_1$ 是源节点采用 LDPC 码的校验矩阵，$\boldsymbol{H}_3=(\boldsymbol{A}\quad \boldsymbol{B}\quad \boldsymbol{C})$ 是中继节点采用 LDPC 码的校验矩阵和 $\boldsymbol{0}$ 是零矩阵。由于式(1)中包括了源节点和中继节点所采用 LDPC 码的校验矩阵，并且中继节点是对两个源节点的数据进行联合编码，因此文献[4]称之为网络 LDPC 码，该码的 Tanner 图如图 2 所示。

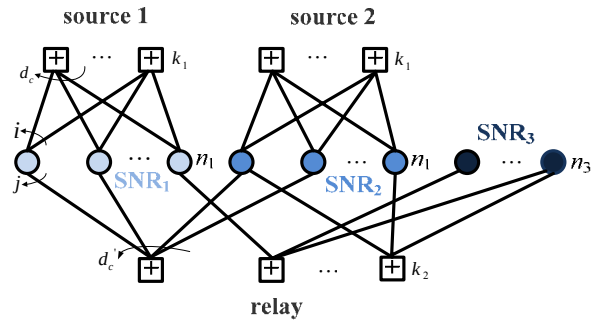


图 2　网络 LDPC 码的 Tanner 图

由图 2，网络 LDPC 码的 Tanner 图中包含上下两层子图，其中上层子图包含 $2k_1$ 个校验节点，它们与变量节点连接关系由式(1)中的 $\boldsymbol{H}_1$ 确定；下层子图包括 k_2 个校验节点，它们与变量节点的连接关系由式(1)中的 $\boldsymbol{H}_3$ 确定。图中每个变量节点的度用 (i,j) 表示，其中 i 为变量节点与上层校验节点相连的边数，j 为变量节点与下层校验节点相连的边数，d_c 和 d_c' 分别表示上层和下层校验节点的度数。

3 速率兼容网络 LDPC 码的设计

3.1 几个定义

定义 1(n 步恢复变量节点)：第 n 次迭代译码时才可以恢复的被删除的变量节点称为 n 步恢复变量节点，用 n-SR 表示。n-SR 的集合用群 G_n 表示。

定义 2(幸存校验节点)：如果一个一步恢复的删余变量节点至少与一个校验节点相连，且与这个校验节点相连的其它变量节点没有都被删余掉，那么这个校验节点就是幸存校验节点。图 3 中的校验节点 S_1 和 S_2 即为幸存校验节点。相反，校验节点 D 即为死校验节点。

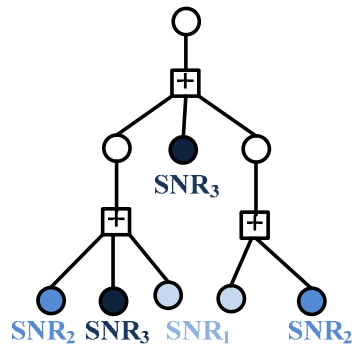


图 3　网络 LDPC 码的恢复树(横线圆表示幸存的变量节点 $S(v)$，竖线圆表示删掉的变量节点)

定义 3(幸存变量节点)：与幸存校验节点相连的其它没有被删除的变量节点称为幸存变量节点。

定义 4(等效幸存邻居变量节点数)：假设网络 LDPC 码所有编码比特在传输过程中受 K 种噪声干扰，对应噪声方差分别为 $\sigma_1^2>\sigma_2^2>\cdots>\sigma_K^2$，令每个受到噪声干扰最大(噪声功率为 σ_1^2)的幸存邻居变量节点的等效幸存邻居变量节点数为 1，则受其他噪声干扰的幸存邻居变量节点的等效幸存邻居变量节点数定义为

$$\alpha_i=\left(\log\left[1-\phi\left[\frac{2}{\sigma_i^2}\right]\right]\Big/\log\left[1-\phi\left[\frac{2}{\sigma_1^2}\right]\right]\right)\leqslant 1 \qquad ()$$

(C)1994-2023 China Academic Journal Electronic Publishing House. All rights reserved.　http://www.cnki.net

式中，$i=1,2,\cdots,K$。

$$\phi(x)=\begin{cases}\dfrac{1}{\sqrt{4\pi x}}\displaystyle\int_R \tanh\frac{u}{2}e^{-\frac{(u-x)^2}{4x}}su & x>0\\ 0 & x=0\end{cases}。$$

3.2 译码恢复错误概率

将网络 LDPC 码的删余变量节点 v 的所有幸存邻居变量节点按照其所通过信道的噪声功率的大小分为 b 类，假设第 t 类的噪声功率为 $\sigma_t^2(t=1,2,\cdots,b)$，且 $\sigma_1^2>\sigma_2^2>\cdots>\sigma_b^2$,并设第 t 类包括 S_t 个变量节点，记为 $\{v_1^t,\cdots,v_s^t,\cdots v_{S_t}^t\}$。与 LDPC 码类似，首先估计每次迭代过程中网络 LDPC 码的每个变量节点的均值更新，并由此计算该节点的恢复错误概率。

$\rho^{up}(x)=\sum_{k=1}^{d_c}\rho_k^{up}x^{k-1}$ $\rho^{low}(x)=\sum_{k=1}^{d_c'}\rho_k^{low}x^{k-1}$ 假设校验节点的度分布分别为 $\rho^{up}(x)=\sum_{k=1}^{d_c}\rho_k^{up}x^{k-1}$ 和 $\rho^{low}(x)=\sum_{k=1}^{d_c'}\rho_k^{low}x^{k-1}$，其中 η 是上层变量节点与校验节点相连的边数占总边数的比例，$\lambda_{i,j}$ 是与度为 (i,j) 的变量节点连接的边数占总边数的比例。$m_{i,j}^{l-1}$ 和 $n_{i,j}^{l-1}$ 分别表示第 $(l-1)$ 次迭代时，变量节点传给上下层的校验节点的对数似然比的均值。第 l 次迭代时，上下层校验节点的均值更新过程如下：

$$m^{'l}=\sum_k\rho_k^{up}\phi^{-1}\left(\left(\frac{1}{\eta}\sum_{i\geqslant0,j\geqslant0}\frac{i}{i+j}\lambda_{i+j}\phi(m_{i,j}^{l-1})\right)^{\sum_{t=1}^{b}S_t\alpha_t}\right)$$

$$n^{'l}=\sum_k\rho_k^{low}\phi^{-1}\left(\left(\frac{1}{1-\eta}\sum_{i\geqslant0,j\geqslant0}\frac{j}{i+j}\lambda_{i+j}\phi(n_{i,j}^{l-1})\right)^{\sum_{t=1}^{b}S_t\alpha_t}\right)\quad()(1)$$

当上下层的校验节点向被删余的度为 (i,j) 变量节点 $v\in G_{l+1}$ 传递消息时，该消息的对数似然比的均值分别为:

$$m^{'l}=\sum_k\rho_k^{up}\phi^{-1}\left(\left(\frac{1}{\eta}\sum_{i\geqslant0,j\geqslant0}\frac{i}{i+j}\lambda_{i+j}\phi(m_{i,j}^{l-1})\right)^{\sum_{t=1}^{b}S_t\alpha_t}\right)$$

$$n^{'l}=\sum_k\rho_k^{low}\phi^{-1}\left(\left(\frac{1}{1-\eta}\sum_{i\geqslant0,j\geqslant0}\frac{j}{i+j}\lambda_{i+j}\phi(n_{i,j}^{l-1})\right)^{\sum_{t=1}^{b}S_t\alpha_t}\right)$$

其中，α_t 表示每个幸存邻居变量节点的等效幸存邻居变量节点数，S_t 表示与变量节点 v 相连的校验节点没有被删余的变量节点数，变量节点 m_L v 的总等效幸存邻居变量节点数为 $\sum_{t=1}^{b}S_t\alpha_t$。

(2) 当上下层的校验节点向没有删余的度为 (i,j) 的变量节点传递消息时，该消息的对数似然比的均值分别为：

$$m^{'l}=\sum_k\rho_k^{up}\phi^{-1}\left(\left(\frac{1}{\eta}\sum_{i\geqslant0,j\geqslant0}\frac{i}{i+j}\lambda_{i+j}\phi(m_{i,j}^{l-1})\right)^{k-1}\right)$$

$$n^{'l}=\sum_k\rho_k^{low}\phi^{-1}\left(\left(\frac{1}{1-\eta}\sum_{i\geqslant0,j\geqslant0}\frac{j}{i+j}\lambda_{i+j}\phi(n_{i,j}^{l-1})\right)^{k-1}\right)$$

上下层变量节点的均值更新过程如下：

假设 $m^{'l}$ 和 $n^{'l}$ 分别表示第 l 次迭代时，上层和下层的校验节点传给变量节点的对数似然比消息均值。第 l 次迭代时，度为 (i,j) ()变量节点传给上下层校验节点的对数似然比消息均值分别为[4]

$$m_{i,j}^{l}=\begin{cases}(i-1)m^{'l}+jn^{'l}+m_{u_0} & i\neq0,j\geqslant0\\ jn^{'l}+m_{u_0}^{'} & i=0,j\geqslant1\end{cases}\qquad(7)$$

$$n_{i,j}^{l}=\begin{cases}im^{'l}+(j-1)n^{'l}+m_{u_0} & i\neq0,j\geqslant1\\ (j-1)n^{'l}+m_{u_0}^{'} & i=0,j\geqslant1\\ im^{'l}+m_{u_0} & i\neq0,j=0\end{cases}$$

若变量节点被删掉，则 $m_{u_0}(m_{u_0}^{'})=0$；若变量节点为由源节点发送至目的节点的信息比特，则 $m_{u_0}=2/\sigma_{SD}^2$；若变量节点为中继节点发送至目的节点的信息比特，则 $m_{u_0}^{'}=2/\sigma_{RD}^2$。第一次迭代时，校验节点的初始值 $m^{'(0)}=n^{'(0)}=0$。

因此，变量节点传给上下层校验节点的平均的消息均值分别为：

$$m^{l}=\frac{1}{\eta}\sum_{i\geqslant0,j\geqslant0}\frac{i}{i+j}\lambda_{i+j}m_{i,j}^{l}$$

$$n^{l}=\frac{1}{1-\eta}\sum_{i\geqslant0,j\geqslant0}\frac{j}{i+j}\lambda_{i+j}n_{i,j}^{l}$$

经过 L 次迭代后，码比特的平均消息均值为：

$$m_L=\eta m^L+(1-\eta)n^L$$

此时，网络 LDPC 码的被删余变量节点的恢复错误概率为：

$$P_e(v)=Q(\sqrt{m_L/2})$$

其中

$$Q(x)=\frac{1}{\sqrt{2\pi}}\int_x^{\infty}e^{-t^2/2}\mathrm{d}t。$$

(C)1994-2023 China Academic Journal Electronic Publishing House. All rights reserved. http://www.cnki.net

3.3 网络 LDPC 码的速率兼容算法

由公式(3)和(4)可知，等效幸存邻居变量节点数 $\sum_{t=1}^{b} S_t \alpha_t$ 越小，更新得到的均值 m'^{l} 和 n'^{l} 的值越大，进而迭代后的变量节点 m_L 的均值也越大，同时由公式(12)得到的恢复错误概率越小。因此，在搜索节点时，需要寻找当前具有最小等效邻居的变量节点进行删余操作。与文献[2]设计的 LDPC 码的删余算法相似，所提出的网络 LDPC 码速率兼容算法主要包括分组和排序两个操作。

分组：

(1) 给定一个 $M \times N$ [D1]网络 LDPC 码的校验矩阵，初始化 $R_\infty = \{1,2,\cdots,M\}$，$G_\infty = \{1,2,\cdots,N\}$，$l=1$；[D2]

(2) 遍历集合 R_∞，找出行重最小的行集合 r；[D3]

(3) 遍历集合 G_∞，找出列重最小的列集合 c；[D4]

(4) 选出所有(2)(3)相交的[D5]元素的集合 $w = \{(r^*, c^*), r^* \in r, c^* \in c\}$，作为候选对；

(5) 在集合 w 中选出具有最小等效幸存邻居变量节点数的元素，记为 (r_j^*, c_k^*)。若有多对满足条件，随机选出其中一对，归[D6]入第 l 次迭代可以恢复的集合 G_l，[D7]更新 $R_\infty = R_\infty \setminus r_j^*$ 和 $G_\infty = G_\infty \setminus c_k^*$；

(6) 若集合 G_∞ 为空，停止迭代，否则跳至(7)；

(7) 若集合 R_∞ 不为空，跳至(2)；否则若步骤(5)中有多于一对满足条件，则 $l = l+1$，跳至(2)。

接下来计算最大可达码率[2]为：

$$R_{\max} = \frac{R_0}{1 - \sum_{j=1}^{K} \left| G_j \right| / n} \tag{13}$$

式中，R_0 是母码的码率，n_i 是母码的码长。

[D8]如果要设计码率为 R_j 的码子，需要删余的节点数为[2]：

$$np_j = \left\lfloor \frac{n(R_j - R_0)}{R_j} \right\rfloor$$

式中 i，$0 \leqslant j \leqslant M$。

组内排序：

(1) 给定一个 $M \times N$ 网络 LDPC 码的校验矩阵[D9]，初始化 $R_\infty = \{1,2,\cdots,M\}$，$l=1$，$j=1$，$P_0 = \phi$；$R_0 \leqslant R_1 \leqslant \cdots \leqslant R_M \leqslant R_{\max}$

(2) 若 $j > M$，停止迭代[D10]；否则，$0 \leqslant j \leqslant M$ $P_j = P_{j-1}$；

(3) $\Delta = np_j - \left| P_j \right|$；[D11]

(4) 若 $\Delta = 0$，$j = j+1$ [D12]，跳至(2[D3])；

(5) 根据集合 G_l 定义 $C_l = \{c_1^*, c_2^*, \cdots\}$，从 C_l 中选出列重最大的变量节点的集合 $c_{\max}^*$，并从 $c_{\max}^*$ 中找出具有最小数量的死校验节点[D14]的变量节点 $c_{\max}^{**}$。如果有多个满足条件，随机选出其中一个，归入排序的集合 P_j，更新 $P_j = P_j \bigcup \{c_{\max}^{**}\}$，$G_l = G_l \setminus \{c_{\max}^{**}\}$，$\Delta = \Delta - 1$，$R_\infty = R_\infty \setminus r_{\max}^{**}$；

(6) 若 G_l 为空，$l = l+1$，$R_\infty = \{1,2,\cdots,M\}$；

(7) 跳至(4)。

经过上述分组和组内排序操作，将 $G_l (1 < l < K)$ () 变量节点按照 l 从小到大删余，而在同一个 G_l 中，按照变量节点的列号从小到大删余，直到删掉 np_j 个节点。

4 仿真结果

仿真中两个源节点采用的 LDPC 码的码长均为 2048，码率均为 0.5，度分布为：$\lambda(x) = 0.23403x + 0.21242x^2 + 0.1469x^5 + 0.102840x^6 + 0.30381x^{19}$ 和 $\rho(x) = 0.71875x^7 + 0.28125x^8$。中继节点采用的 LDPC 码的校验比特数为 628。假设信道模型为理想加性高斯白噪声(AWGN)信道，源节点和中继节点均采用 BPSK 调制方式。中继节点与目的节点之间的信噪比固定为 5dB。中继节点可以正确译码得到两个源节点的发送数据。图 4 和图给出了母码经过本文所改进算法(intentional)、现有算法(original)[2]和随机删余(random)所得到的码率为 0.5、0.6 和 0.7 的网络 LDPC 子码的 BER 性能对比。

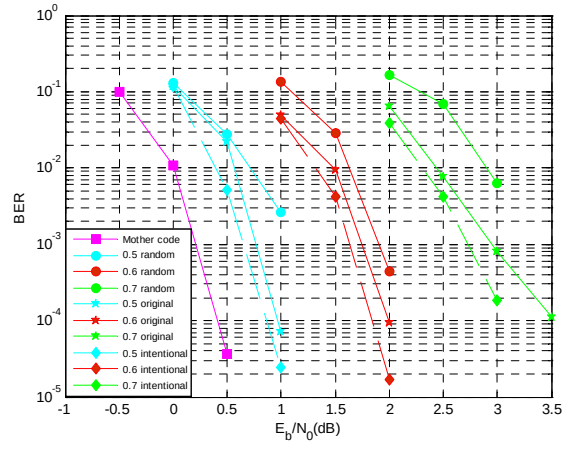


图 4 网络 LDPC 码的删余性能对比

由图 4 和图 5 可以看出，随着删余比特的增加，

(C)1994-2023 China Academic Journal Electronic Publishing House. All rights reserved. http://www.cnki.net

采用所提算法得到的网络 LDPC 码的性能增益也随之增加。当码率为 0.5， BER=10^{-3} 时，采用所提算法性能优于随机算法 0.45dB；当码率为 0.5，BER=10^{-4} 时，采用所提算法比文献[2]中算法的性能改善 0.15dB。在码率为 0.6， BER=10^{-3} 时，所提算法相对于随机算法性能增益为 0.3dB,相对于文献[2]中算法性能增益为 0.2dB。当码率为 0.7，SNR=3dB 时，所提算法的 BER 为 10^{-5} ，相比于随机算法的 10^{-3} 有了明显提升，而 BER=10^{-4} 时，所提算法比文献[2]中算法性能能增益改善 0.4 dB。

5 结论

文章首先介绍了网络 LDPC 码的结构及基本原理,然后针对其结构特性推导了译码恢复错误概率,并详述了适用于网络 LDPC 码的上下层变量节点和校验节点均值更新理论,接着介绍了网络 LDPC 码的速率兼容删余算法,最后对所设计的算法进行仿真,与现有算法相比，本文所提出的改进速率兼容算法在 BER=10^{-4} 时有 0.4dB 的性能增益。

参 考 文 献

[1] Hagenauer J. Rate-Compatible Punctured Convolutional Codes (RCPC codes) and Their Applications[J] . IEEE Trans on Communication, 1988, 36(4) : 389-400.

[2] J. Ha, J. Kim, D. Klinc, and S. W. McLaughlin, “Rate-Compatible Punctured Low-Density Parity-Check Codes With Short Block Lengths”, IEEE trans. Inform. Theory, vol. 52, no. 2, pp. 728-738, Feb. 2006.

[3] J. Ha, J. Kim, D. Klinc, and S. W. McLaughlin, “Rate-Compatible Puncturing of Low-Density Parity-Check Codes ”, IEEE trans. Inform. Theory, vol. 50, no. 11, pp. 2824-2836, NOV. 2004.

[4] Y. Li, G. H. Song, and L. L. Wang, “Design of joint network-low density parity check codes based on the EXIT charts”, IEEE Commun. Lett., vol. 13, no. 8, pp. 600-602, Aug. 2009.

(C)1994-2023 China Academic Journal Electronic Publishing House. All rights reserved. http://www.cnki.net

doi:10.3969/j.issn.1001-2400.2013.02.003

适用于网络 LDPC 码的速率兼容算法

王静怡[1,2]，李 颖[1,2]，孙 岳[1,2]

(1. 西安电子科技大学 综合业务网理论及关键技术国家重点实验室，陕西 西安 710071；
2. 电信科学研究院 无线移动通信国家重点实验室，北京 100083)

摘要：提出了一种可以获得最小比特错误概率的网络低密度奇偶校验(LDPC)码速率兼容删余算法，并推导了该算法的译码错误概率. 该算法基于网络 LDPC 码的结构特点，以达到译码最小比特错误概率为目标，在网络 LDPC 码的 Tanner 图上搜索出需要删余的变量节点，以获得最优的删余图样. 仿真结果表明，该算法比现有算法在 BER 为 10^{-4} 时有 0.4 dB 的性能增益.

关键词：多址接入中继网络；LDPC 码；网络 LDPC 码；速率兼容；删余

中图分类号：TN911.22 **文献标识码**：A **文章编号**：1001-2400(2013)02-0013-05

Rate-compatible network LDPC codes

WANG Jingyi[1,2], *LI Ying*[1,2], *SUN Yue*[1,2]

(1. State Key Lab. of Integrated Service Networks, Xidian Univ., Xi'an 710071, China; 2. State Key Lab. of Wireless Mobile Communications, China Academy of Telecommunication Technology, Beijing 100083, China)

Abstract: A rate-compatible puncturing algorithm for network LDPC codes is proposed to achieve the minimum error probability, and decoding error probability is derived. The algorithm for finding variable nodes to be deleted based on the tanner graph of network LDPC codes is proposed, which is aimed at minimizing the decoding error probability and optimizing the puncturing pattern. Simulation results illustrate that, at BER = 10^{-4}, the proposed rate-compatible network LDPC codes have a coding gain of about 0.4 dB compared with the codes obtained via the existing punctured methods.

Key Words: multi-access relay network; low-density parity-check (LDPC) codes; network LDPC code; rate-compatible; puncturing

由于无线移动信道具有衰落和时变特性，为最大限度地利用信道容量，可采用链路自适应技术，使信道编码速率、调制方式、信号功率等参数能够随信道质量的变化而变化. 链路自适应技术的基础是速率兼容纠错码的设计，其基本概念由文献[1]首次提出，速率兼容低密度奇偶校验(LDPC)码的设计则是近几年的研究热点. 文献[2-3]通过分组和排序操作，将 LDPC 码的变量节点按照迭代恢复次数进行分类，设计了 LDPC 码速率兼容删余算法，可以获得比随机删余更好的性能. 文献[4]首次提出了一种基于有限域上非零元素二进制镜像的缩短码构造方案，用来实现低码率的速率兼容多元 LDPC 码. 文献[5]研究了码率从 1/10 到 5/6 的灵活变化的非规则多元 LDPC 码比特级缩短算法. 文献[6]以多维累加交叉并行级联单奇偶校验码为母码，对奇偶校验比特按组删余，构建了一组速率兼容编码.

上述速率兼容算法都是针对点对点通信链路设计的. 然而，随着无线通信技术的发展和中继协作传输技术的引入，信道编码的设计也从点对点链路推广至无线中继网络. 对于多址接入中继网络，有多个节点同时

收稿日期：2012-06-09 网络出版时间：2012-11-16

基金项目：国家自然基金资助项目(61072064)；国家科技重大专项资助项目(2010ZX03003-003-03)；长江学者和创新团队发展计划资助项目(IRT0852)；中央高校科研业务费专项资金资助项目(K50510010026)

作者简介：王静怡(1984－)，女，西安电子科技大学博士研究生，E-mail：wangjy@stu.xidian.edu.cn.

网络出版地址：http://www.cnki.net/kcms/detail/61.1076.TN.20121116.0924.201302.16_009.html

(C)1994-2023 China Academic Journal Electronic Publishing House. All rights reserved. http://www.cnki.net

需要中继节点帮助转发数据,在中继节点设计有效的联合网络-信道编码算法,可在改善接收端性能的同时,有效提高转发效率. 文献[7]利用 LDPC 码,针对多址接入中继信道设计了一种网络 LDPC 码,并指出可以通过调整中继节点转发数据量来实现中继转发效率和接收端译码性能的有效折中. 与单个 LDPC 码相比,网络 LDPC 码的校验矩阵包括了源节点和中继节点所采用 LDPC 码的校验矩阵,因此其本质上可看做是一种多用户码. 另外,单个 LDPC 码的所有编码比特是在同一个信道中传输,所有编码比特受到相同的噪声干扰,网络 LDPC 码的编码比特则由对应的源节点和中继节点分别传输,不同传输链路将会受到不同的噪声干扰. 笔者将根据网络 LDPC 码的上述特性,设计相应的速率兼容算法.

1 适用于多址接入中继信道的网络 LDPC 码

由两个源节点、一个中继节点和一个目的节点构成的多址接入中继网络模型如图 1 所示. 两个源节点与目的节点之间的信息传输由广播发送和中继转发两个阶段完成. 在广播阶段,两个源节点分别向中继节点和目的节点广播发送编码序列 X_1 和 X_2;在中继转发阶段,中继节点首先对接收信号进行译码,得到两个源节点的估计数据,然后对译码得到的估计数据重新进行联合编码,并将编码序列 X_R 转发至目的节点. 目的节点则根据收到的信号进行联合译码,得到两个源节点的估计信息.

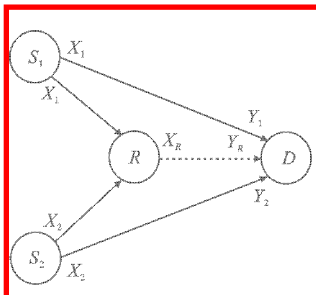


图 1 多址接入中继信道模型

目的节点将两个源节点和中继节点采用的 LDPC 码综合考虑,可得到如下校验矩阵:

$$\boldsymbol{H}=\begin{bmatrix}\boldsymbol{H}_1 & \boldsymbol{0} & \boldsymbol{0}\\ \boldsymbol{0} & \boldsymbol{H}_1 & \boldsymbol{0}\\ \boldsymbol{A} & \boldsymbol{B} & \boldsymbol{C}\end{bmatrix}, \tag{1}$$

其中,$\boldsymbol{H}_1$ 是源节点采用 LDPC 码的校验矩阵,$\boldsymbol{H}_3=[\boldsymbol{A},\boldsymbol{B},\boldsymbol{C}]$,是中继节点采用 LDPC 码的校验矩阵,$\boldsymbol{0}$ 是零矩阵. 由于式(1)中包含了源节点和中继节点所采用 LDPC 码的校验矩阵,并且中继节点是对两个源节点的数据进行联合编码,因此文献[7]称之为网络 LDPC 码,该码的 Tanner 图如图 2 所示.

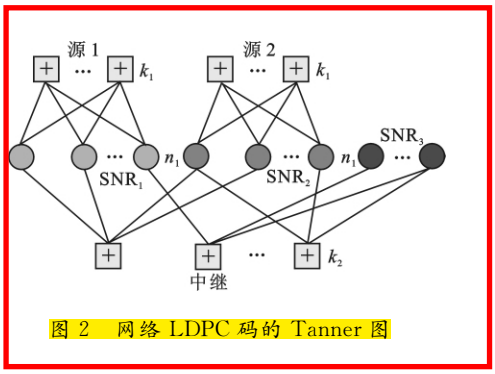


图 2 网络 LDPC 码的 Tanner 图

图 2 中网络 LDPC 码的 Tanner 图包含上下两层子图,其中上层子图包含 $2k_1$ 个校验节点,它们与变量节点的连接关系由 $\boldsymbol{H}_1$ 确定;下层子图包括 k_2 个校验节点,它们与变量节点的连接关系由式(1)中的 $\boldsymbol{H}_3$ 确定. 图中每个变量节点的度用(i,j)表示,其中 i 为变量节点与上层校验节点相连的边数,j 为变量节点与下层校验节点相连的边数. 用 d_c 和 d_c' 分别表示上层和下层校验节点的度数.

2 速率兼容网络 LDPC 码的设计

由图 2,网络 LDPC 码的变量节点包含两个源节点所采用的 LDPC 码的变量节点和中继节点所采用的联合 LDPC 码的变量节点,且不同变量节点通过不同的信道达到目的节点. 因此,需要考虑上述特点对删除变量节点恢复概率的影响,并由此设计适用于网络 LDPC 码的速率兼容算法.

2.1 几个定义

定义 1 若被删余的校验比特所对应的变量节点在迭代过程中接收到非零信息,则无论获得的信息正确与否,都称之为“恢复”[2].

定义 2 译码中第 n 次迭代时才恢复的被删除的变量节点称为 n 步恢复变量节点,用 n-SR 表示,而所有 n-SR 构成的集合则用 G_n 表示[2].

图 3 给出了一个包含 1-SR 节点、2-SR 节点的恢复树,其中竖线圆表示幸存的删余变量节点 S(v),横线圆表示未删余变量节点,方块表示校验节点.

(C)1994-2023 China Academic Journal Electronic Publishing House. All rights reserved. http://www.cnki.net

定义 3　如果一个一步恢复的删余变量节点至少与一个校验节点相连,且与这个校验节点相连的变量节点没有被完全删余掉,那么称这个校验节点为幸存校验节点[2]. 图 3 中的校验节点 S_1 和 S_2 即为幸存校验节点,而校验节点 D 则为死校验节点.

定义 4　幸存校验节点相连的其余未被删除的变量节点称为幸存变量节点.

由图 2 可见,网络 LDPC 码的编码比特是通过 3 个不同信道到达接收端的,因此,在设计网络 LDPC 码的删余算法时,不仅要考虑被删余变量节点的幸存邻居变量节点数,还要考虑每个幸存邻居变量节点受到的噪声大小. 下面,引入等效幸存变量节点数的概念.

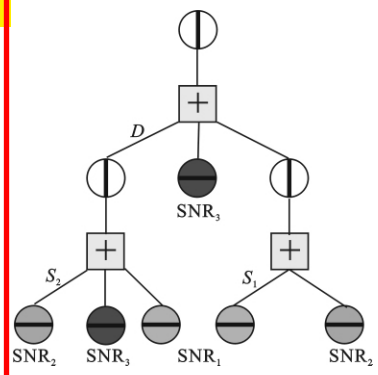


图 3　网络 LDPC 码的恢复树

定义 5　假设网络 LDPC 码所有编码比特在传输过程中受 K 种噪声干扰,其对应的噪声方差分别为 $\sigma_1^2>\sigma_2^2>\cdots>\sigma_K^2$,令每个受到噪声干扰最大(噪声功率为 σ_1^2)的幸存邻居变量节点的等效幸存邻居变量节点数为 1,则受其他噪声干扰的幸存邻居变量节点的等效幸存邻居变量节点数定义为

$$\alpha_i=\left\{\log\left(1-\varphi\left(\frac{2}{\sigma_i^2}\right)\right)\Big/\left[\log\left(1-\varphi\left(\frac{2}{\sigma_1^2}\right)\right)\right]\right\}\leqslant 1\quad,\quad i=1,2,\cdots,K\quad, \tag{2}$$

其中

$$\varphi(x)=\begin{cases}\dfrac{1}{(4\pi x)^{1/2}}\displaystyle\int_R\tanh\frac{u}{2}\exp\left(-\frac{(u-x)^2}{4x}\right)\mathrm{d}u\quad, & x>0\quad,\\ 0\quad, & x=0\quad.\end{cases}$$

2.2　译码恢复错误概率

将网络 LDPC 码的删余变量节点 v 的所有幸存邻居变量节点按照其所通过信道的噪声功率的大小分为 b 类,假设第 t 类的噪声功率为 $\sigma_t^2(t=1,2,\cdots,b)$,且 $\sigma_1^2>\sigma_2^2>\cdots>\sigma_b^2$,并设第 t 类包括 S_t 个变量节点,记为 $\{v_1^t,\cdots,v_s^t,\cdots,v_{S_t}^t\}$. 与 LDPC 码类似,首先估计每次迭代过程中删余网络 LDPC 码的每个变量节点的均值更新,并由此计算该节点的恢复错误概率.

由于网络 LDPC 码的译码同样包括变量节点更新和校验节点更新,但图 2 给出的 Tanner 图表明,网络 LDPC 码的校验节点更新实际上包括上层校验节点和下层校验节点更新. 下面将分析在迭代译码过程中,速率兼容删余的网络 LDPC 码的变量节点和校验节点的均值更新过程.

假设校验节点的度分布分别为 $\rho^{\mathrm{up}}(x)=\sum_{k=1}^{d_c}\rho_k^{\mathrm{up}}x^{k-1}$ 和 $\rho^{\mathrm{low}}(x)=\sum_{k=1}^{d_c'}\rho_k^{\mathrm{low}}x^{k-1}$;$\eta$ 是上层变量节点与校验节点相连的边数占总边数的比例;$\lambda_{i,j}$ 是与度为 (i,j) 的变量节点连接的边数占总边数的比例;$m_{i,j}^{l-1}$ 和 $n_{i,j}^{l-1}$ 分别表示第 $(l-1)$ 次迭代时,变量节点传给上下层的校验节点的对数似然比的均值. 第 l 次迭代时,上下层校验节点的均值更新过程如下:

(1) 当上下层的校验节点向被删余的度为 (i,j) 的变量节点 $v\in G_{l+1}$ 传递消息时,该消息的对数似然比的均值分别为

$$m^{\prime l}=\sum_k\rho_k^{\mathrm{up}}\varphi^{-1}\left\{\left[\frac{1}{\eta}\sum_{i\geqslant 0,j\geqslant 0}\frac{i}{i+j}\lambda_{i,j}\varphi(m_{i,j}^{l-1})\right]^{\sum_{t=1}^{b}S_t\alpha_t}\right\}\quad, \tag{3}$$

$$n^{\prime l}=\sum_k\rho_k^{\mathrm{low}}\varphi^{-1}\left\{\left[\frac{1}{1-\eta}\sum_{i\geqslant 0,j\geqslant 0}\frac{j}{i+j}\lambda_{i,j}\varphi(n_{i,j}^{l-1})\right]^{\sum_{t=1}^{b}S_t\alpha_t}\right\}\quad, \tag{4}$$

其中,α_t 表示每个幸存邻居变量节点 v_s^t 的等效幸存邻居变量节点数,S_t 表示与变量节点 v 相连的校验节点没有被删余的变量节点数,变量节点 v 的总等效幸存邻居变量节点数为 $\sum_{t=1}^{b}S_t\alpha_t$.

(2) 当上下层的校验节点向没有删余的度为 (i,j) 的变量节点 v 传递消息时,该消息的对数似然比的均值[7]分别为

$$m^{\prime l}=\sum_k\rho_k^{\mathrm{up}}\varphi^{-1}\left\{\left[\frac{1}{\eta}\sum_{i\geqslant 0,j\geqslant 0}\frac{i}{i+j}\lambda_{i,j}\varphi(m_{i,j}^{l-1})\right]^{k-1}\right\}\quad, \tag{5}$$

(C)1994-2023 China Academic Journal Electronic Publishing House. All rights reserved.　http://www.cnki.net

$$n'^{l}=\sum_{k}\rho_{k}^{\text{low}}\varphi^{-1}\left\{\left[\frac{1}{1-\eta}\sum_{i\geqslant 0,j\geqslant 0}\frac{j}{i+j}\lambda_{i,j}\varphi(n_{i,j}^{l-1})\right]^{k-1}\right\}. \tag{6}$$

上下层变量节点的均值更新过程如下：

第 l 次迭代时，度为 (i,j) 的变量节点传给上下层校验节点的对数似然比消息均值[7]分别为

$$m_{i,j}^{l}=\begin{cases}(i-1)m'^{l}+jn'^{l}+m_{u_0}, & i\neq 0,\ j\geqslant 0,\\ jn'^{l}+m'_{u_0}, & i=0,\ j\geqslant 1,\end{cases} \tag{7}$$

$$n_{i,j}^{l}=\begin{cases}im'^{l}+(j-1)n'^{l}+m_{u_0}, & i\neq 0,\ j\geqslant 1,\\ (j-1)n'^{l}+m'_{u_0}, & i=0,\ j\geqslant 1,\\ im'^{l}+m_{u_0}, & i\neq 0,\ j=0.\end{cases} \tag{8}$$

若变量节点被删掉，则 $m_{u_0}(m'_{u_0})=0$；若变量节点为由源节点发送至目的节点的信息比特，则 $m_{u_0}=2/\sigma_{SD}^2$；若变量节点为中继节点发送至目的节点的信息比特，则 $m'_{u_0}=2/\sigma_{RD}^2$. 第 1 次迭代时，校验节点的初始值 $m'^{0}=n'^{0}=0$.

因此，变量节点传给上下层校验节点的平均的消息均值分别为

$$m^{l}=\frac{1}{\eta}\sum_{i\geqslant 0,j\geqslant 0}\frac{i}{i+j}\lambda_{i,j}m_{i,j}^{l}, \tag{9}$$

$$n^{l}=\frac{1}{1-\eta}\sum_{i\geqslant 0,j\geqslant 0}\frac{j}{i+j}\lambda_{i,j}n_{i,j}^{l}. \tag{10}$$

经过 L 次迭代后，码比特的平均消息均值为

$$m_L=\eta m^{L}+(1-\eta)n^{L}. \tag{11}$$

此时，网络 LDPC 码的被删余变量节点的恢复错误概率为

$$P_e(v)=Q\left[(m_L/2)^{1/2}\right], \tag{12}$$

其中 $$Q(x)=\frac{1}{(2\pi)^{1/2}}\int_{x}^{\infty}\exp\left(-\frac{t^2}{2}\right)\mathrm{d}t.$$

2.3 网络 LDPC 码的速率兼容算法

由式(3)和(4)可知，等效幸存邻居变量节点数 $\sum_{t=1}^{b}S_t\alpha_t$ 越小，更新得到的均值 m'^{l} 和 n'^{l} 的值越大，进而迭代后的变量节点 m_L 的均值也越大，同时由式(12)得到的恢复错误概率 $P_e(v)$ 越小. 因此，在搜索节点时，需要寻找当前具有最小等效邻居的变量节点进行删余操作. 与文献[2]设计的 LDPC 码的删余算法相似，所提出的网络 LDPC 码速率兼容算法主要包括分组和排序两个操作.

2.3.1 分组

将所有删余的变量节点按照迭代恢复次数分成 K 组 $G_1,G_2,\cdots,G_K$，其中 $G_l(1\leqslant l\leqslant K)$ 是经过 l 次迭代才能恢复的所有变量节点的集合.

(1) 给定一个 $M\times N$ 网络 LDPC 码的校验矩阵，初始化 $R_\infty=\{1,2,\cdots,M\}$，$G_\infty=\{1,2,\cdots,N\}$，$l=1$.

(2) 遍历集合 R_∞，找出行重最小的行集合 r.

(3) 遍历集合 G_∞，找出列重最小的列集合 c.

(4) 选出所有(2)和(3)相交的元素的集合，$w=\{(r^*,c^*),r^*\in r,c^*\in c\}$，作为候选对.

(5) 在集合 w 中选出具有最小等效幸存邻居变量节点数的元素，记为 (r_j^*,c_k^*). 若有多对满足条件，则随机选出其中一对，归入第 l 次迭代可以恢复的集合 G_l，更新 $R_\infty=R_\infty\backslash r_j^*$ 和 $G_\infty=G_\infty\backslash c_k^*$.

(6) 若集合 G_∞ 为空，则停止迭代；否则，跳至(7).

(7) 若集合 R_∞ 不为空，则跳至(2)；否则，若步骤(5)中有多于一对满足条件，则 $l=l+1$，跳至(2).

其中，$G_\infty(R_\infty)$ 表示每次迭代后更新的列(行)的集合；$r(c)$ 表示第 l 次迭代时，在集合 $R_\infty(G_\infty)$ 选出的行(列)重最小的行(列)集合；$G_l=\{(r_1^*,c_1^*),(r_2^*,c_2^*),\cdots\}$；$R_\infty=R_\infty\backslash r_j^*$ $(G_\infty=G_\infty\backslash c_k^*)$ 表示集合 $R_\infty(G_\infty)$ 去掉元素 $r_j^*(c_k^*)$ 后的集合 $R_\infty(G_\infty)$.

第371页，共397页
(C)1994-2023 China Academic Journal Electronic Publishing House. All rights reserved. http://www.cnki.net

计算最大可达码率[2] 为

$$R_{\max}=R_0\Big/\Big(1-\sum_{j=1}^{K}|G_j|/n\Big)\quad , \tag{13}$$

其中,R_0 是母码的码率,n 是母码的码长.

在给定母码基础上,设计 Q 个码率的子码,对应码率记为 $R_0\leqslant R_1\leqslant\cdots\leqslant R_Q\leqslant R_{\max}$. 假设所设计码的码率为 R_j,需要删余的节点数为[2]

$$np_j=\lfloor n(R_j-R_0)/R_j\rfloor\quad ,\quad 0\leqslant j\leqslant Q\quad . \tag{14}$$

2.3.2　组内排序

依次对 $G_l(1\leqslant l\leqslant K)$ 内的变量节点进行排序.

(1) 给定一个 $M\times N$ 网络 LDPC 码的校验矩阵,初始化 $R_\infty=\{1,2,\cdots,M\}$,$l=1$,$j=1$,$P_0=\varnothing$.

(2) 若 $j>Q$,则停止迭代;否则,$P_j=P_{j-1}$.

(3) $\Delta=np_j-|P_j|$.

(4) 若 $\Delta=0$,$j=j+1$,则跳至(2).

(5) 根据集合 G_l 定义 $C_l\xlongequal{\mathrm{d}}\{c_1^*,c_2^*,\cdots\}$,从 C_l 中选出列重最大的变量节点的集合 $c_{\max}^*$,并从 $c_{\max}^*$ 中找出具有最小数量的死校验节点的变量节点 $c_{\max}^{**}$. 如果有多个满足条件,则随机选出其中一个,归入排序的集合 P_j,更新 $P_j=P_j\bigcup\{c_{\max}^{**}\}$,$G_l=G_l\backslash\{c_{\max}^{**}\}$,$R_\infty=R_\infty\backslash r_{\max}^{**}$,$\Delta=\Delta-1$.

(6) 若 G_l 为空,$l=l+1$,则 $R_\infty=\{1,2,\cdots,M\}$.

(7) 跳至(4).

其中,(1)中的 $l=1$ 表示从 G_1 开始将各 G_l 内的变量节点排序,$j=1$ 表示初始码率为 R_1;(3) 计算需要删余 np_j 个节点,除了上次迭代删余的 $|P_j|$ 个节点外,本次还需要删余 Δ 个节点;(5) 中的集合 $c_{\max}$ 表示最大列重的变量节点的集合,同时意味着该集合包含的变量节点的幸存校验节点数最多;P_j 表示要达到码率 R_j,所需删余的变量节点的列集合;$r_{\max}^{**}$ 表示列为 $c_{\max}^{**}$ 的变量节点所在的行.

经过上述分组和组内排序操作,将 $G_l(1\leqslant l\leqslant K)$ 中的变量节点按照 l 从小到大删余,而在同一个 G_l 中,按照变量节点的列号从小到大删余,直到删掉 np_j 个节点.

3　仿真结果

仿真中两个信源节点采用的 LDPC 码的码率均为 0.5,度分布为

$$\lambda(x)=0.23403x+0.21242x^2+0.1469x^5+0.102840x^6+0.30381x^{19}$$

和

$$\rho(x)=0.71875x^7+0.28125x^8\quad .$$

根据文献[7],假设所采用的网络 LDPC 码的度序列分布为:$\lambda_{0,2}=0.028043$,$\lambda_{2,0}=0.188139$,$\lambda_{2,1}=0.019382$,$\lambda_{2,2}=0.026283$,$\lambda_{3,0}=0.191239$,$\lambda_{3,1}=0.003360$,$\lambda_{3,2}=0.001150$,$\lambda_{6,0}=0.085989$,$\lambda_{6,1}=0.000980$,$\lambda_{6,2}=0.063446$,$\lambda_{7,0}=0.059576$,$\lambda_{7,2}=0.044374$,$\lambda_{20,0}=0.176218$,$\lambda_{20,1}=0.003570$,$\lambda_{20,2}=0.108251$,$\rho_6^{\mathrm{low}}=0.943049$,$\rho_7^{\mathrm{low}}=0.056951$.

假设两个源节点所采用 LDPC 码的码长均为 2 048,中继节点联合编码的 LDPC 码的校验比特数为 628,此时网络 LDPC 码(母码)的码率为 0.444. 根据式(14),可以得到对该网络 LDPC 码进行删余获得的最大码率为 0.733. 利用文中所提算法对该网络 LDPC 码删余可以得到码率分别为 0.5、0.6 和 0.7 的子码. 利用文献[2]中的算法和随机删余也可得到同样码率的网络 LDPC 子码.

假设源节点和中继节点均采用 BPSK 调制方式,源节点与中继节点,源节点与目的节点,以及中继节点与目的节点之间的信道均为高斯白噪声信道,中继节点与目的节点之间的信噪比固定为 5 dB,且中继节点可以正确

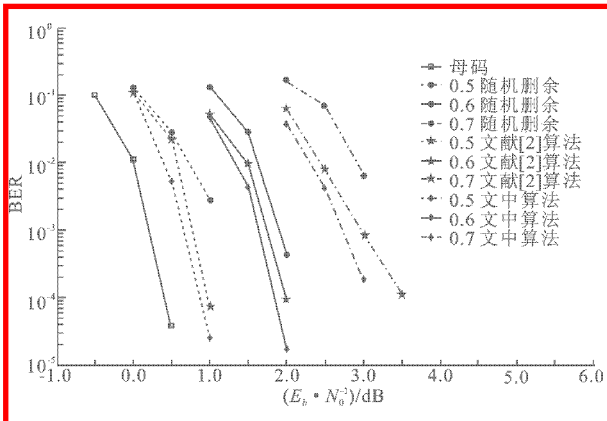


图 4　网络 LDPC 码的删余性能对比

(下转第 47 页)

(C)1994-2023 China Academic Journal Electronic Publishing House. All rights reserved.　http://www.cnki.net

scientific.net/AMR.311-313.2009.

[4] Bozorg M, Termeh F. Domains of PID Controller Coefficients which Guarantee Stability and Performance for LTI Ttime-delay [J]. Automaic, 2011, 47(9): 2122-2125.

[5] 杨莹，李俊民，陈国培. 一类广义混杂系统的随机稳定性及稳定化[J]. 西安电子科技大学学报，2010，37(5)：866-871.
Yang Ying, Li Junmin, Chen Guopei. Stochastic Stability and Stabilization for a Class of Singular Hybrid Systems[J]. Journal of Xidian University, 2010, 37(5): 866-871.

[6] 徐亚兰，陈建军. 压电柔性机械臂的轨迹跟踪控制[J]. 西安电子科技大学学报，2008，35(3)：504-507.
Xu Yalan, Chen Jianjun. Trajectory Tracking Control for the Flexible Link Robot Manipulator Using Piezoelectric Materious [J]. Journal of Xidian University, 2008, 35(3): 504-507.

（编辑：郭　华）

（上接第 17 页）

译出两个源节点的发送数据. 图 4 比较了 3 种不同算法得到的网络 LDPC 码在上述信道假设下的误比特性能，图中横坐标 E_b/N_0 表示源节点与目的节点之间链路的信噪比变化，且假设两个源节点与目的节点之间的链路是对称的.

由图 4 可以看出，随着删余比特的增加，采用所提算法得到的网络 LDPC 码的性能增益也随之增加. 当码率为 0.5，比特误码率(BER)为 10^{-3} 时，采用所提算法性能优于随机删余算法 0.45 dB；当码率为 0.5，BER 为 10^{-4} 时，采用所提算法比文献[2]中算法的性能改善 0.15 dB. 在码率为 0.6，BER 为 10^{-3} 时，所提算法相对于随机删余算法性能改善了 0.3 dB，相对于文献[2]中算法性能改善了 0.2 dB. 当码率为 0.7，SNR 为 3 dB 时，所提算法的 BER 为 10^{-5}，相比于随机删余算法的 10^{-3} 有了明显提升，而 BER 为 10^{-4} 时，所提算法比文献[2]中算法性能增益改善了 0.4 dB.

4　结 束 语

根据网络 LDPC 码的结构特点，以最小化恢复错误概率为目标，设计了一种网络 LDPC 码的速率兼容删余算法. 不同于已有的算法[2]，该算法利用被删余的变量节点的恢复原则和受到的噪声干扰大小设计了不同码率下的删余方案，在不增加系统复杂度的前提下，只需要一对编码译码器即可实现网络 LDPC 码的码率自适应. AWGN 信道下的仿真结果表明，在同等条件下，采用文中所提算法获得的速率兼容网络 LDPC 码比采用文献[2]中算法得到的速率兼容网络 LDPC 码有更好的性能.

参考文献：

[1] Hagenauer J. Rate-Compatible Punctured Convolutional Codes (RCPC codes) and Their Applications [J]. IEEE Trans on Communication, 1988, 36(4): 389-400.

[2] Ha J, Kim J, Klinc D, et al. Rate-Compatible Punctured Low-Density Parity-Check Codes with Short Block Lengths [J]. IEEE Trans on Inform Theory, 2006, 52(2): 728-738.

[3] Ha J, Kim J, Klinc D, et al. Rate-Compatible Puncturing of Low-Density Parity-Check Codes [J]. IEEE Trans on Inform Theory, 2004, 50(11): 2824-2836.

[4] Zhou Lin, Bai Baoming, Xu Ming. Design of Nonlinary Rate-compatible LDPC Codes Utilizing Bit-wise Shortening Method [J]. IEEE Communication Letters, 2010, 14(10): 963-965.

[5] 周林，白宝明，邵军虎，等. 多元 LDPC 码的速率兼容技术研究[J]. 西安电子科技大学学报，2011，38(1)：147-152.
Zhou Lin, Bai Baoming, Shao Junhu, et al. On Nonbinary Rate-compatible LDPC Codes [J]. Journal of Xidian University, 2011, 38(1): 147-152.

[6] 郭凯，陈彦辉，李建东. 一种对奇偶校验比特按组删余的速率兼容编码[J]. 西安电子科技大学学报，2009，36(5)：782-787.
Guo Kai, Chen Yanhui, Li Jiandong. Rate-compatible Codes Based on Puncturing Parity Check Bits in Group [J]. Journal of Xidian University, 2009, 36(5): 782-787.

[7] Li Y, Song G H, Wang L L. Analysis of the Joint Network LDPC Codes over Orthogonal Multi-Access Relay Channel [J]. IEEE Commun Lett, 2010, 14(2): 184-186.

（编辑：齐淑娟）

(C)1994-2023 China Academic Journal Electronic Publishing House. All rights reserved.　http://www.cnki.net

Optimal Design of the Joint Network LDPC Codes over Orthogonal Multi-Access Relay Channel

Jingyi Wang
State Key Lab of ISN
Xidian University
Xi'an, China
Email: wangjy@stu.xidian.edu.cn

Shuling Che
State Key Lab of ISN
Xidian University
Xi'an, China
Email: shlche@mail.xidian.edu.cn

Ying Li
and Junlong Wang
State Key Lab of ISN
Xidian University
Xi'an, China
Email:ying.lili1973@gmail.com

***Abstract*—Optimization of degree distribution of the joint network LDPC code for orthogonal multiple-access relay channel (MARC) is investigated in this paper. We first calculated the code capacity of the source-destination link of orthogonal MARC based on a Gaussian approximation,where two sources communicate with one destination in the presence of one relay. Then, a new generalized differential evolution algorithm is developed to iteratively improve the degree distribution of the joint network LDPC code. Simulation results show that, the gap between bit error rate (BER) performance of our designed codes and the decoding threshold is about 0.4dB, and that between the capacity limit and decoding threshold is less than 0.7dB at BER $= 10^{-6}$.**

***Index Terms*—Network LDPC Code; multi-access relay network; Gaussian approximation; differential evolution; capacity limit.**

I. Introduction

In wireless communications, cooperation relay networks[1][2][3] have recently attracted substantial research efforts with many promising techniques of improving performance in term of throughput, coverage or diversity gain. In relay networks, one or multiple relay nodes (RNs) to assist the sources in transmitting information.Optimal designs of Relay networks have attracted extensive attentions due to that they can increase the communication capacity. One of the earlier works on this subject is the application of LDPC code to the single-source single-relay networks [4]. To improve the performance of the single-source single-relay system, a class of bilayer LDPC codes is designed in[5][6].

Based on the principle of the bilayer LDPC codes, the authors proposed a class of the joint network LDPC code which helps the relay jointly re-encodes the messages from the two sources and sends the parity bits to the destination [7]. Moreover, the authors analyzed the capacity approaching ability of the joint network LDPC codes in [8]. In this paper, we study the problem of approaching capacity limit of a two-source single-relay multiple-access relay network with the joint network LDPC code, in which the two source-to-relay channels and the two source-to-destination channels are under the same channel parameters.Then, a new generalized differential evolution algorithm is developed to optimal the degree distribution of the joint network LDPC code.

The rest of this paper is organized as follows. Section II presents the system model and then describes the operation of the system throughout different stages of the cooperation strategy. Section III explains the optimum design method of degree distribution of the joint network LDPC code. Section IV presents simulation results, and Section VI concludes the paper.

II. System Model

Our system is a two-slot wireless relay network consisting of two sources, one relay and one destination, as shown in Fig.1.

In the first slot, sources $S_i(i = 1, 2)$ broadcast their LDPC coded signals $X_i(i = 1, 2)$, which are received by both relay R and destination D. We express the received bits as

$$Y_{S_i,R} = X_i + N_{S_i,R} \quad (1)$$

$$Y_{S_i,D} = X_i + N_{S_i,D} \quad (2)$$

where $i = 1, 2.X_i$ is the LDPC coded signal sent from source node S_i, while $Y_{S_i,R}$ and $Y_{S_i,D}$ are the corresponding received signal by the relay R and the destination D respectively. Finally, $N_{S_i,R}$ is a zero-mean additive Gaussian random variable with variance $\sigma^2_{S_i,R}$, and $N_{S_i,D}$ is a zero-mean additive Gaussian random variable with variance $\sigma^2_{S_i,D}$.

In the second slot, after decoding the received signals correctly, R jointly re-encodes the messages of the two sources and sends k_2 parity bits X_R to D. The received bits at the destination D is

$$Y_{R,D} = X_R + N_{R,D} \quad (3)$$

where X_R denotes the signal corresponding to the parity bits, and $N_{R,D}$ is a zero-mean additive Gaussian random variable with variance $\sigma^2_{R,D}$.

At last, the destination D can decode the information data of two sources by using the received signals Y_1, Y_2 and Y_R respectively from the two sources and relay. Therefore, X_1, X_2, and X_R can be treated as an equivalent super code which is called as the joint network LDPC code in [7]. The parity check matrix of the joint network LDPC code can be written as

$$\mathbf{H} = \begin{pmatrix} \mathbf{H_1} & \mathbf{0} & \mathbf{0} \\ \mathbf{0} & \mathbf{H_1} & \mathbf{0} \\ \mathbf{A} & \mathbf{B} & \mathbf{C} \end{pmatrix} \quad (4)$$

978-0-7695-4988-0/13 $26.00 © 2013 IEEE
DOI 10.1109/INCoS.2013.116

IEEE computer society

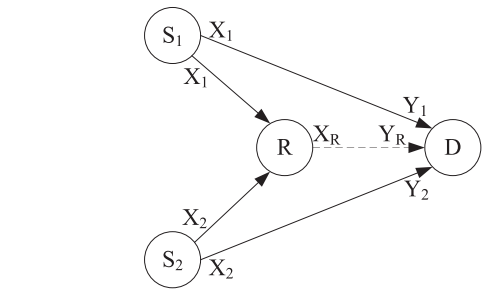


Fig. 1. The model of the joint network LDPC code based relaying scheme

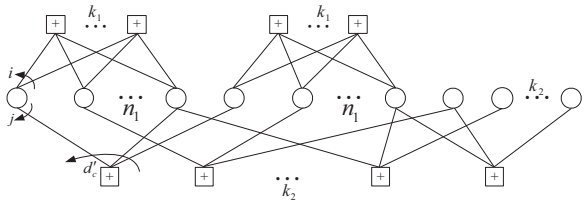


Fig. 2. Tanner graph of the joint network LDPC code

where $\mathbf{H_1}$ denotes the same parity-check matrix of the constituent codes at the two sources $S_i(i=1,2)$, $\mathbf{H_3}=(\mathbf{ABC})$ denotes the parity-check matrix generated by R, and $\mathbf{0}$ represents the all-zero matrix.

Assume that each source uses an (n_1, n_1-k_1) irregular LDPC code with code length n_1 and parity length k_1. According to [8], the Tanner graph of the joint network LDPC code is shown in Fig.2, where the upper sub-graph denotes the encoding at the sources and the lower sub-graph denots the encoding at the relay. This code includes $2k_1$ upper check nodes, k_2 lower check nodes and $2n_1+k_2$ variable nodes. A variable node is of degree (i,j), $1\le i\le d_v$ and $1\le i\le d_v^{'}$, where i (j) is its upper (lower) degree, and d_v $(d_v^{'})$ is its maximum upper (lower) degree. In addition, $\lambda_{i,j}$ represents the proportion of the number of edges connected to the variable nodes with the degree (i,j).

III. Optimization Of Degree Distribution

A. Preliminary

Definition 1: Decoding threshold of joint network LDPC code is defined as

$$\sigma^* = sup\{\sigma : \lim_{L\to+\infty} m_L > M\} \tag{5}$$

where L is the maximum iteration number, m_L denotes the mean value of the log-likelihood ratio (LLR) message of a code bit at L-th decoding iteration and M is the LLR mean value corresponding to the target error probability. Then with the knowledge in [8], $2m_L$ is the LLR variance value. When $\sigma<\sigma^*$, m_L will be greater than M, which means that the target error probability can be achieved. When $\sigma\ge\sigma^*$, the iterative decoding can not achieve the target error probability.

B. Calculation of decoding threshold σ^*_{SD}

Algorithm 1: Given degree distributions of the LDPC code at the sources, let σ_{SD} and σ_{RD} represent the channel parameters of source-destination link and relay-destination link respectively. We denote the target error probability as $P_e=10^{-6}(M=45)$ [8], and the maximum iteration number as L. Let $\Delta\sigma_{SD}$ denote a step length, and then algorithm 1 can be described as follows:

Step 1: Initialization

The initialized value of the average mean value of the LLR message output by the check node is $m^{'l}=n^{'l}=0$ (l is the iteration number, and $l=0$ in the first iteration)[8].

Step 2: Updating

When the iteration number $l<L$, update the mean values of the LLR messages at the variable node and the check node respectively, and then calculate the mean value (m_l) of the LLR message during this iteration using the method in [8]. If $m_l<M$, add the iteration number by 1 $(l=l+1)$, and continue Step 2. If $m_l\ge M$, $\sigma_{SD}=\sigma_{SD}+\Delta\sigma_{SD}$, and go to Step 1.

Step 3: Stopping criterion

If $l\ge L$ and $m_l<M$ during this iteration, stop the whole process, and the code capacity is defined as $\sigma^*_{SD}=\sigma_{SD}-\Delta\sigma_{SD}$. Otherwise, output the threshold value of channel parameter as $\sigma^*_{SD}=\sigma_{SD}$.

Using Algorithm 1, we can obtain the corresponding σ^*_{SD} from a given degree distribution of the upper layer LDPC code.

C. Optimal Design Of Degree Distribution Of The Lower Layer LDPC Code

Our goal is to search the optimal degree distribution of the network LDPC code, which can approach the capacity limit. Here we use differential evolution algorithm to optimal design of the network LDPC code sets.

Algorithm 2: Assume that N relay code sets of the network LDPC code structure are randomly generated, denoting their degree distributions of variable node as $\lambda_{i,j}(d), 0\le i\le d_v, 0\le j\le d_v^{'}, d=1,2,...N$. The degree of the lower check nodes is fixed as $d_c^{'}$.

Step 1: Initialization

Initialize that degree distribution as

$$C(d)=\{\lambda_{i,j}(d), 0\le i\le d_v, 0\le j\le d_v^{'}\}, d=1,2,\cdots,N. \tag{6}$$

Step 2: Performance estimation of code set

Calculate the code capacity $\sigma^*(d)$ of each code set $C(d)$ through the Algorithm 1, and search the optimal code set meeting $C^*=\arg\max_{1\le d\le N}\sigma^*(d)$. The degree distribution of the optimal code set corresponding to the maximum code capacity is $C^*=\{\lambda^*_{i,j}, 0\le i\le d_v, 0\le j\le d_v^{'}\}$.

Step 3: Code set updating

Select $\widetilde{N}$ code sets from $\{C(d)\}_{d=1}^{N}$ at random, and denote their degree distribution as $\widetilde{C}(k)=\{\lambda_{i,j}(k), 0\le i\le d_v, 0\le j\le d_v^{'}\}, k=1,2,\cdots,\widetilde{N}$. Then update the degree distribution of the code set: $C^*=C^*+\alpha\Sigma_{k=1}^{\widetilde{N}}(-1)^{k-1}\widetilde{C}(k)$, where $\alpha<1$ is the step length.

TABLE I
FOUR DIFFERENT PARAMETERS OF THE JOINT NETWORK LDPC CODES

Code Set	Code A	Code B	Code C	Code D
$d_v^{'}$	2	2	2	2
$d_c^{'}$	4	4	4	7
k_2	2814	4814	2814	2814
σ_{RD}	0.5	0.5	0.8	0.5
η	0.942065	0.904808	0.942065	0.902835
σ_{SD}^*	1.0568	1.0987	1.0393	1.1116
Threshold	0.15504dB	0.11512dB	0.20180dB	-0.22877dB
Capacity Limit	-0.24536dB	-0.51762dB	-0.14395dB	-0.24536dB
Gap	0.40040dB	0.63274dB	0.34575dB	0.01666dB

Step 4: Stopping criterion

If reaching the preset number of iteration and $m_l < M$, stop the iteration process. The degree distribution of the optimal code set is defined as $C^* = \{\lambda_{i,j}^*, 0 \le i \le d_v, 0 \le j \le d_v^{'}\}$; Otherwise, go to Step 3.

Remark: Restrictive conditions must be met for Step 1 and Step 3.

$$\begin{cases} \sum\limits_{i\ge 0, j\ge 0} \lambda_{i,j} = 1 \\ \lambda_i = \frac{1}{\eta} \sum\limits_{j\ge 0} \frac{i}{i+j} \lambda_{i,j} \\ \eta = \sum\limits_i \sum\limits_j \frac{i}{i+j} \lambda_{i,j} \\ d_c^{'} = \frac{1-\eta}{\sum\limits_j \frac{\lambda_{0,j}}{j}} \end{cases} \tag{7}$$

where η is the proportion of the total number of edges in the upper sub-graph. The total number of upper-layer edges of a source node is $E = \frac{n_1}{\sum\limits_{i\ge 2} \frac{\lambda_i}{i}} = \frac{k_1}{\sum\limits_{j\ge 2} \frac{\rho_j}{j}}$, and the total number of edges of the bilayer network LDPC code is $E^{'} = 2E + k_2 \cdot d_c^{'}$, so $\eta = \frac{2E}{E^{'}}$.

IV. SIMULATION RESULTS

Assume each source node employs an $(n_1, n_1 - k_1)$ LDPC code with $\lambda(x) = 0.23403x + 0.21242x^2 + 0.1469x^5 + 0.102840x^6 + 0.30381x^{19}$, and $\rho(x) = 0.71875x^7 + 0.28125x^8$, where $n_1 = 22164, k_1 = 11082$. $\text{SNR}_{RD} = 3\text{dB}$ and the two source-destination links are assumed to be symmetric. Using the Algorithm 1, four different parameters of the joint network LDPC codes, are obtained and listed in Table I, where σ_{RD}^2 represents the channel parameter between the relay-destination link.

Using the Algorithm 2, four optimal degree distributions of the joint network LDPC codes are given in Table II III IV.

The BER curves of four codes are illustrated in Fig.3. We see that the gap between the decoding threshold of four codes obtained by searching the maximum decoding threshold σ_{SD}^* and capacity limit is less than 0.7dB, and that between BER performance and decoding threshold is less than 0.4dB. Since the lower check degree of Code D is bigger and more information bits are contained in the check equation, it outperforms Code A by 0.2dB gains at BER $= 10^{-5}$. Another important observation is that Code B has a gain of about 0.15dB over Code A at BER $= 10^{-5}$ and the performance gain of Code D is about 0.1dB over Code B at BER $= 10^{-5}$. This indicates that increasing degrees of lower-layer check nodes is better than increasing the numbers of parity bits to improve system performance. When the noise variance between R-D link is increased, the system decoding performance will be reduced and Code A will have a gain of about 0.2dB over Code C at BER $= 10^{-5}$.

TABLE II
THE OPTIMAL DEGREE DISTRIBUTIONS OF CODE A

$\lambda_{i,j}$	$\lambda_{i,0}$	$\lambda_{i,1}$	$\lambda_{i,2}$
$i=2$	0.193815	0.00543635	0.04612661
$i=3$	0.171369	0.019109592	0.02409292
$i=6$	0.129299	0.006342408	0.00494214
$i=7$	0.09485	0.00008237	0.00259462
$i=20$	0.273877	0.000432436	0.00181212
$i=0$	0	0.0030528	0.02276564

TABLE III
THE OPTIMAL DEGREE DISTRIBUTIONS OF CODE B

$\lambda_{i,j}$	$\lambda_{i,0}$	$\lambda_{i,1}$	$\lambda_{i,2}$
$i=2$	0.07441004	0.20599344	0
$i=3$	0.19208258	0.0001582	0
$i=6$	0.13270189	0.00013842	0.00016819
$i=7$	0.09266986	0.00032638	0.00017797
$i=20$	0.27426244	0.00051525	0.0021752
$i=0$	0	0.0237937	0.0000099

TABLE IV
THE OPTIMAL DEGREE DISTRIBUTIONS OF CODE C

$\lambda_{i,j}$	$\lambda_{i,0}$	$\lambda_{i,1}$	$\lambda_{i,2}$
$i=2$	0.1206132	0	0
$i=3$	0.1001453	0.0000219	0
$i=6$	0.1860514	0.0002767	0.0000167
$i=7$	0.1964141	0.0002114	0.0000212
$i=20$	0.3858558	0.0003262	0.0000362
$i=0$	0	0.0041565	0.0206487

TABLE V
THE OPTIMAL DEGREE DISTRIBUTIONS OF CODE D

$\lambda_{i,j}$	$\lambda_{i,0}$	$\lambda_{i,1}$	$\lambda_{i,2}$
$i=2$	0.1112574	0.0136437	0.1818773
$i=3$	0.0917291	0.0876831	0.0571696
$i=6$	0.1322349	0.0003256	0.0001570
$i=7$	0.0926749	0.0000457	0.0000678
$i=20$	0.2740590	0.0001011	0.000217
$i=0$	0	0.0035171	0.0207269

V. CONCLUSION

In this paper, we employed differential evolution method to design degree distribution of the joint network LDPC code

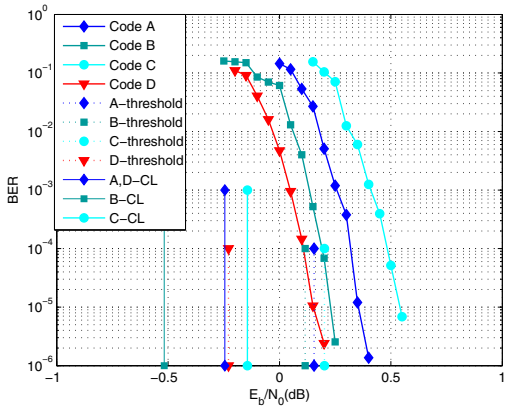


Fig. 3. Performance of the joint network LDPC codes

for a two-source single-relay system, under the assumption of symmetric AWGN channel. The performance of the new codes we designed have significant BER performance gain for a two-source single-relay system with symmetric channels.

ACKNOWLEDGMENT

This work was supported by NSFC(61072064) and NSFC(61101148).

REFERENCES

[1] T. Cover and A. E. Gamal, "Capacity theorems for the relay channel," *IEEE Trans. Inf. Theory.*, vol. 25, pp. 572-584, Sep. 1979.

[2] A. Nosratinia, T. E. Hunter, and A. Hedayat, "Cooperative Communication in Wireless Networks," *IEEE Communications Magazine.*, vol. 42, no. 10, pp.74-80, October 2004.

[3] J. Laneman, D. Tse, and G. Wornell, "Cooperative Diversity in Wireless Networks: Efficient Protocols and Outage Behavior," *IEEE Transactions on Information Theory.*, vol. 50, no. 12, pp. 3062-3080, December 2004.

[4] P. Razaghi and W. Yu, "Bilayer low-density parity-check codes for decode-and-forward in relay channels," *IEEE Trans. Inf. Theory.*, vol. 3, no. 10, pp. 3723-3739, Oct. 2007.

[5] M. H.Azmi, J. Yuan, J. Ning and H. Q.Huynh, "Improved Bilayer LDPC Code Using Irregular Check Node Degree Distribution ," *in Proc. IEEE Int'l Symposium on Information Theory.*, Toronto, Canada, July. 2008.

[6] J. P.Cances and V. Meghdadi, "Optimized Low Density Parity Check Codes Designs for Half Duplex Relay Channels," *IEEE Trans. Wireless Commun.*,vol. 8, no. 7, pp. 3390-3395, July. 2009.

[7] Y. Li, G. H. Song, and L. L. Wang, "Design of joint network-low density parity check codes based on the EXIT charts," *IEEE Commun. Lett.*, vol. 13, no. 8, pp. 600-602, Aug. 2009.

[8] Y. Li, G. H. Song, and L. L. Wang, "Analysis of the joint network LDPC codes over orthogonal multi-access relay channel," *IEEE Commun. Lett.*, vol. 14, no. 2, pp. 184-186, Feb. 2010.

Optimal design of joint network LDPC codes over orthogonal multiple-access relay channels

Jingyi Wang*, Shuling Che and Ying Li

State Key Laboratory of Integrated Service Networks (ISN),
Xidian University,
Xi'an 710071, China
Email: wangjy@stu.xidian.edu.cn
Email: shlche@mail.xidian.edu.cn
Email: ying.lili1973@gmail.com
*Corresponding author

Junlong Wang

Huawei Technologies Co. Ltd.,
Xi'an 710071, China
Email: 401834748@qq.com

Abstract: Optimisation of degree distribution for joint network LDPC code over orthogonal Multiple-Access Relay Channels (MARC) is investigated in this paper. We first use a differential evolution algorithm to optimise the degree distribution of the joint network LDPC code over orthogonal MARC based on Gaussian approximation. Then, using a modified differential evolution algorithm, we design a rate-compatible network LDPC code, which is equivalent to designing a single code with different Signal-to-Noise Ratio (SNR). Simulation results show that the gap between Bit Error Rate (BER) performance of the former algorithm and the decoding threshold is about 0.4 dB and that between the capacity limit and decoding threshold is less than 0.7 dB at $BER = 10^{-6}$. Simultaneously, the gap between BER performance of the latter algorithm and the decoding threshold is about 0.52 dB and that between the capacity limit and the decoding threshold is less than 0.46 dB at $BER = 10^{-7}$.

Keywords: network LDPC code; multiple-access relay network; Gaussian approximation; differential evolution; capacity limit.

Reference to this paper should be made as follows: Wang, J., Che, S., Li, Y. and Wang, J. (2016) 'Optimal design of joint network LDPC codes over orthogonal multiple-access relay channels', *Int. J. Grid and Utility Computing*, Vol. 7, No. 1, pp.68–74.

Biographical notes: Jingyi Wang is currently working towards the PhD degree in Communication and Information System at Xidian University. She received her Master's degree in Telecommunications Engineering from Xidian University in 2010. Her research interests include channel coding and network coding.

Shuling Che is currently an Associate Professor at the School of Telecommunications Engineering, Xidian University. She received her PhD in Communication and Information System from Xidian University in 2008. Her research interest includes channel coding.

Ying Li is currently a Professor at the School of Telecommunications Engineering, Xidian University. She received her PhD in Communication and Information System from Xidian University in 2005. Her research interests include channel coding, wireless network coding and MIMO theory.

Junlong Wang is currently working in Huawei Technologies Co. Ltd. He received his Master's degree in Communication and Information System from Xidian University in 2011.

This paper is a revised and expanded version of a paper entitled 'Optimal design of the joint network LDPC codes over orthogonal multi-access relay channel' presented at the '2013 5th International Conference on Intelligent Networking and Collaborative Systems', Xi'an, China, 9 September 2013.

Copyright © 2016 Inderscience Enterprises Ltd.

1 Introduction

In wireless communications (Shen et al., 2012), cooperation relay networks (Cover and Gamal, 1979; Nosratinia et al., 2004; Laneman et al., 2004) have recently attracted substantial research efforts with many promising techniques of improving performance in terms of throughput, coverage or diversity gain. In relay networks, one or multiple Relay Nodes (RNs) assist the sources in transmitting information. Optimal designs of relay networks have attracted extensive attentions owing to their ability to increase communication capacity. One of the earlier works on this subject dealt with the application of the LDPC code to single-source single-relay networks (Razaghi and Yu, 2007). To improve the performance of the single-source single-relay system, a class of bilayer LDPC codes is designed in Azmi et al. (2008) and Cances and Meghdadi (2009).

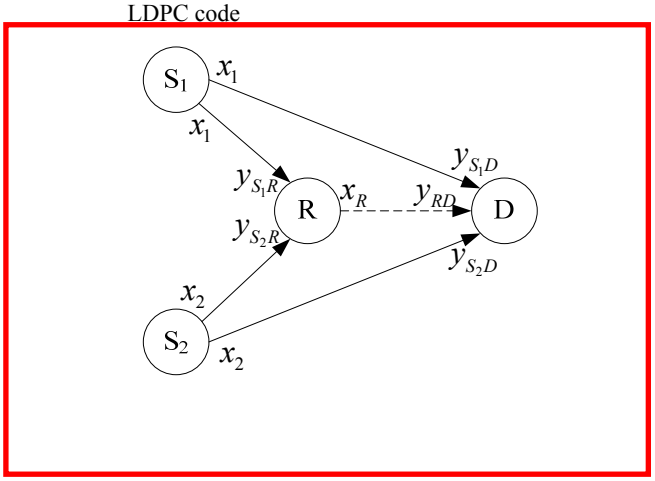
Based on the principle of the bilayer LDPC codes, the authors proposed a class of the joint network LDPC code with network coding (Zhang and Minier, 2013). And then it helps the relay to jointly re-encode the messages from the two sources and send the parity bits to the destination (Li et al., 2009). Moreover, Li et al. (2010) analysed the capacity approaching ability of the joint network LDPC codes. In this paper, we study two different methods of approaching capacity limit of two different transmission modes of a two-source single-relay system with joint network LDPC code, in which the first one requires the same code words transmitted at the two sources and the latter requires different code words transmitted at the two sources.

The rest of the paper is organised as follows. Section 2 presents the system model and then describes the operation of the system throughout different stages of the two cooperation strategies. Section 3 explains the design of two different optimisation methods. Numerical and simulation results are given in Section 4 and finally, the paper is concluded in Section 5.

2 System model

Our system is a two-slot wireless relay network consisting of two sources, one relay and one destination, as shown in Figure 1. Two different transmission modes of the system are described below, which are called Symmetry Cooperation Transmission (SCT) and Asymmetry Cooperation Transmission (ACT). The broadcast stage is followed by the cooperation stage.

Figure 1 Multi-access relay channel model with joint network LDPC code



2.1 The broadcast stage

In this stage, the sources S_i ($i=1,2$) broadcast their LDPC coded signals x_i ($i=1,2$), which are received by both relay R and destination D.

2.1.1 SCT mode

We express the received signals at the relay R and the destination D as follows:

$$y_{S_iR} = h_{S_iR}x_i + n_{S_iR} \tag{1}$$

$$y_{S_iD} = h_{S_iD}x_i + n_{S_iD} \tag{2}$$

where y_{S_iR} and y_{S_iD} are the corresponding received signal by R and D, respectively, h_{S_iR} and h_{S_iD} denote the associated channel gain and n_{S_iR} (n_{S_iD}) denotes a zero-mean Gaussian random variable with a variance $\sigma^2_{S_iR}$ ($\sigma^2_{S_iD}$).

2.1.2 ACT mode

We assume that $P^{(1)}_{S_i}$ ($i=1,2$) is the transmit power of S_i and $w^{(1)}_{S_i}$ ($i=1,2$) is a bit of an LDPC code transmitted by S_i in this stage. Then the received signals at R and D can be written as

$$y_{S_iR} = h_{S_iR}\cdot\sqrt{P^{(1)}_{S_i}}w^{(1)}_{S_i} + n_{S_iR} \tag{3}$$

$$y^{(1)}_{S_iD} = h^{(1)}_{S_iD}\cdot\sqrt{P^{(1)}_{S_i}}w^{(1)}_{S_i} + n^{(1)}_{S_iD} \tag{4}$$

where y_{S_iR}, h_{S_iR} and n_{S_iR} are as defined earlier, while $y^{(1)}_{S_iD}$, $h^{(1)}_{S_iD}$ and $n^{(1)}_{S_iD}$ are the corresponding parametric between S_i and D, where the superscript (1) represents the broadcast stage.

2.2 The cooperation stage

In this stage, after decoding the received signals correctly, R jointly re-encodes the messages of the two sources and sends parity bits x_R of the code words to D.

2.2.1 SCT mode

After x_i is decoded correctly, R jointly re-encodes the messages of the two sources and sends x_R to D. The received signal at D is

$$y_{RD} = h_{RD}x_R + n_{RD} \tag{5}$$

where y_{RD} and n_{RD} are the corresponding parametric between R and D.

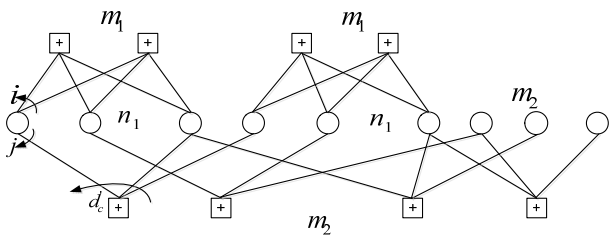
At last, D receives the signals y_{S_iD} and y_{RD}, respectively, from S_i and R. The parity check matrix of the joint network LDPC code can be written as

$$\mathbf{H} = \begin{pmatrix} \mathbf{H}_1 & \mathbf{0} & \mathbf{0} \\ \mathbf{0} & \mathbf{H}_1 & \mathbf{0} \\ \mathbf{A} & \mathbf{B} & \mathbf{C} \end{pmatrix} \tag{6}$$

where $\mathbf{H_1}$ denotes the same parity-check matrix of the constituent codes at the two sources S_i, $\mathbf{H_3} = (\mathbf{ABC})$ denotes the parity-check matrix generated by R and $\mathbf{0}$ represents the all-zero matrix.

Assume that each source uses an $(n_1, n_1 - m_1)$ irregular LDPC code with code length n_1 and parity length m_1. According to Li et al. (2010), the Tanner graph of the joint network LDPC code is shown in Figure 2, where the upper sub-graph denotes the encoding at the sources and the lower sub-graph denotes the encoding at the relay. This code includes $2m_1$ upper check nodes, m_2 lower check nodes and $2n_1 + m_2$ variable nodes. A variable node is of degree (i,j), $1 \le i \le d_v$ and $1 \le j \le d_v'$, where $i(j)$ is its upper (lower) degree and $d_v(d_v')$ is its maximum upper (lower) degree. In addition, $\lambda_{i,j}$ represents the proportion of the number of edges connected to the variable nodes with the degree (i,j).

Figure 2 The Tanner graph of the joint network LDPC code



2.2.2 ACT mode

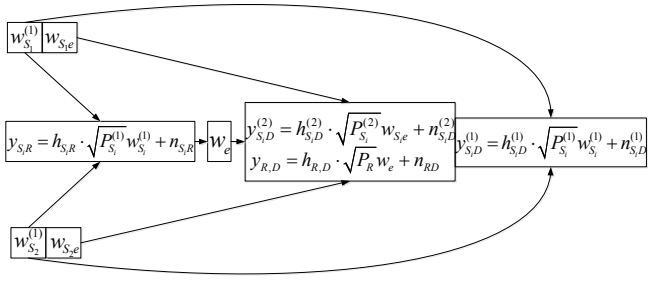
The source $S_i (i = 1,2)$ uses rate-compatible extension method from an entire LDPC code word $w_{S_i 2} = \left[w_{S_i}^{(1)}, w_{S_i e} \right]$ extended from the original code word $w_{S_i}^{(1)}$, and $w_{S_i e}$ carries additional parity-check bits as shown in Figure 3. R only generates two additional parity-check bits $w_{S_1 e}$ and $w_{S_2 e}$ from S_1 and S_2, respectively. Then network-coded code word $w_e = w_{S_1 e} \oplus w_{S_2 e}$. The received signals at D are

$$y_{S_i D}^{(2)} = h_{S_i D}^{(2)} \cdot \sqrt{P_{S_i}^{(2)}} w_{S_i e} + n_{S_i D}^{(2)} \tag{7}$$

$$y_{RD} = h_{RD} \cdot \sqrt{P_R} w_e + n_{RD} \tag{8}$$

where $P_{S_i 2}$ (P_R) is the transmit power of S_i (R) in the second stage. The other parameters were defined earlier, where the superscript (2) represents the cooperation stage.

Figure 3 Diagram of the multi-access relay channel model with joint network LDPC code



Then, D receives the signals $y_{S_i D}^{(1)}$ $\left(y_{S_i D}^{(2)} \right)$ and y_{RD}, respectively, from the two sources and the relay. First, D decodes y_{RD} and then obtains the network-coded code word $w_e = w_{S_1 e} \oplus w_{S_2 e}$. Second, D obtains $w_{S_1 e}$ and $w_{S_2 e}$ by iterative decoding with $y_{S_i D}^{(2)}$ and w_e. Different from the rate-compatible LDPC code designed in Li et al. (2009), the received SNR for $w_{S_i}^{(1)}$ and $w_{S_i e}$ are different. Using (4), (7) and (8), the SNR for the decoding of $w_{S_i}^{(1)}$ and $w_{S_i e}$ can be written, respectively, as

$$SNR_{S_i D} = \frac{\left| h_{S_i D}^{(1)} \right|^2 P_{S_i}^{(1)}}{N_0} \tag{9}$$

$$SNR'_{S_i D} = \frac{\left(h_{S_i D}^{(2)} \sqrt{P_{S_i}^{(2)}} + h_{RD} \sqrt{P_R} \right)^2}{N_0} \tag{10}$$

Finally, we decode $w_{S_1}^{(1)}$ and $w_{S_2}^{(1)}$ correctly by using the Belief Propagation (BP) iterative decoding algorithm with $w_{S_1 2} = \left[w_{S_1}^{(1)}, w_{S_1,e} \right]$ and $w_{S_2 2} = \left[w_{S_2}^{(1)}, w_{S_2,e} \right]$, respectively, at D.

3 Optimisation of degree distribution

3.1 SCT mode

3.1.1 Preliminary

Definition 1: *Decoding threshold of joint network LDPC code is defined as*

$$\sigma^* = \sup \left\{ \sigma : \lim_{L \to +\infty} m_L > M \right\} \tag{11}$$

where L is the maximum iteration number, m_L denotes the mean value of the Log-Likelihood Ratio (*LLR*) message of a code bit at the Lth decoding iteration and M is the *LLR* mean value corresponding to the target error probability.

Then with the knowledge in Li et al. (2010), $2m_L$ is the *LLR* variance value. When $\sigma < \sigma^*$, m_L will be greater than M, which means that the target error probability can be achieved. When $\sigma \ge \sigma^*$, the iterative decoding cannot achieve the target error probability.

3.1.2 Calculation of decoding threshold σ_{SD}^*

Algorithm 1: Given degree distribution of the LDPC code at the sources, let σ_{SD} and σ_{RD} represent the channel parameters of source–destination link and relay–destination link, respectively. We denote the target error probability as $P_e = 10^{-6}$ $(M = 45)$ and the maximum iteration number as L. Let $\Delta\sigma_{SD}$ denote a step length, and then Algorithm 1 can be described as follows.

- *Step 1: Initialisation.* The initialised value of the average mean value of the *LLR* message output by the check node is $m'^{l} = n'^{l} = 0$ (l is the iteration number and $l = 0$ in the first iteration) (Li et al., 2010).

- *Step 2: Updating.* When the iteration number $l < L$, update the mean values of the *LLR* messages at the variable node and the check node, and then calculate the mean value m_l of the *LLR* message during this iteration using the method in Li et al. (2010). If $m_l < M$, add the iteration number by 1 (l = l +1) and continue Step 2. If $m_l \geq M$, $\sigma_{SD} = \sigma_{SD} + \Delta\sigma_{SD}$, and go to Step 1.

- *Step 3: Stopping criterion.* If $l \geq L$ and $m_l < M$ during this iteration, stop the whole process, and the code capacity is defined as $\sigma^*_{SD} = \sigma_{SD} - \Delta\sigma_{SD}$. Otherwise, output the threshold value of channel parameter as $\sigma^*_{SD} = \sigma_{SD}$.

Using Algorithm 1, we can obtain the corresponding σ^*_{SD} from a given degree distribution of the upper layer LDPC code.

3.1.3 *Optimal design of the degree distribution of the lower layer LDPC code*

Our goal is to search the optimal degree distribution of the network LDPC code, which can approach the capacity limit. Here we use differential evolution algorithm to optimal design of the network LDPC code ensembles.

Algorithm 2. Assume that N relay code sets of the network LDPC code structure are randomly generated, denoting their degree distributions of variable node as $\lambda_{i,j}(d)$, $0 \leq i \leq d_v$, $0 \leq j \leq d'$, $d = 1,2,\ldots, N$. The degree of the lower check nodes is fixed as d'_c.

- *Step 1: Initialisation.* Initialise that degree distribution as

$$C(d) = \left\{\lambda_{i,j}(d), 0 \leq i \leq d_v, 0 \leq j \leq d'_v\right\}, d = 1,2,\ldots N \quad (12)$$

- *Step 2: Performance estimation of code sets.* Calculate the code capacity $\sigma^*(d)$ of each code set $C(d)$ through Algorithm 1, and search the optimal code ensemble meeting $C^* = \arg\max_{1\leq d\leq N}\sigma^*(d)$. The degree distribution of the optimal code ensemble corresponding to the maximum code capacity is $C^* = \left\{\lambda^*_{i,j}, 0 \leq i \leq d_v, 0 \leq j \leq d'_v\right\}$.

- *Step 3: Code set updating.* Select $\tilde{N}$ code sets from $\{C(d)\}_{d=1}^{N}$ at random and denote their degree distributions as $\tilde{C}(k) = \left\{\lambda_{i,j}(k), 0 \leq i \leq d_v, 0 \leq j \leq d'_v\right\}, k = 1,2,\ldots,\tilde{N}$. Then, update the degree distribution of the code ensemble: $C^* = C^* + \alpha\sum_{k=1}^{\tilde{N}}(-1)^{k-1}\tilde{C}(k)$, where $\alpha < 1$ is the step length.

- *Step 4: Stopping criterion.* If reaching the preset number of iteration and $m_l < M$, stop the iteration process. The degree distribution of the optimal code ensemble is defined as $C^* = \left\{\lambda^*_{i,j}, 0 \leq i \leq d_v, 0 \leq j \leq d'_v\right\}$; otherwise, go to Step 3.

Remark: *Restrictive conditions must be met for Steps 1 and 3:*

$$\begin{cases} \sum_{i\geq 0, j\geq 0}\lambda_{i,j} = 1 \\ \lambda_i = \frac{1}{\eta}\sum_{j\geq 0}\frac{i}{i+j}\lambda_{i,j} \\ \eta = \sum_i\sum_j\frac{i}{i+j}\lambda_{i,j} \\ d'_c = \frac{1-\eta}{\sum_j\frac{\lambda_{0,j}}{j}} \end{cases} \quad (13)$$

where η is the proportion of the total number of edges in the upper sub-graph. The total number of upper layer edges of a source node is $E = \frac{n_1}{\sum_{i\geq 2}\lambda_i/i} = \frac{k_1}{\sum_{j\geq 2}\rho_j/j}$ and the total number of edges of the bilayer network LDPC relay code is $E' = 2E + k_2 \cdot d'_c$, so $\eta = \frac{2E}{E'}$.

3.2 *ACT mode*

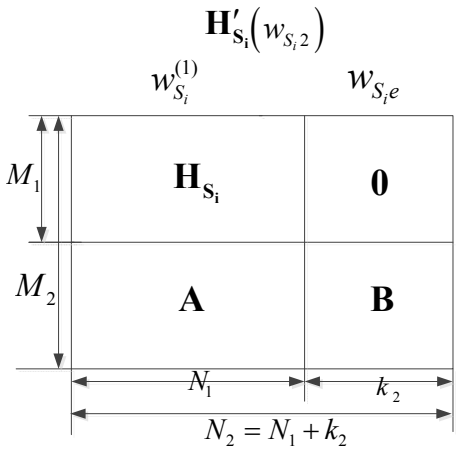
3.2.1 *Ensemble description of the joint network LDPC code*

We assume that R decodes the received signal from S_i correctly. The code rate R_1 of both S_1 and S_2 depends on $R_1 \leq C(SNR_{S_1R})$ and $R_1 \leq C(SNR_{S_2R})$, where $C(SNR_{S_iR})$ is the capacity when *SNR* of the channel between S_i and R is SNR_{S_iR}. Here we assume $R_1 = C(SNR_{S_1R}) = C(SNR_{S_2R})$.

In addition, the distance between S_i and D is farther than the distance between S_i and R, so the channel gain h_{S_iD} is smaller than h_{S_iR} and SNR_{S_iD} is smaller than SNR_{S_iR}. Here we assume $R_1 > C(SNR_{S_1D}) = C(SNR_{S_2D})$. And the capacity between the source and destination link is smaller than the capacity between the source and relay link. According to Shannon theorem, when the rate is greater than the channel capacity, the system cannot decode correctly after more iterations, so extra check bits are generated to help decode.

Figure 4 shows the extended parity-check matrix $\mathbf{H}'_{\mathbf{S}_i}(\mathbf{w}_{\mathbf{S}_i2})$, where $\mathbf{H}_{\mathbf{S}_i}$ denotes the parity-check matrix of the code word $w^{(1)}_{S_i}$ at the two sources $S_i(i = 1,2)$, w_{S_ie} denotes additional parity-check bits of the entire code word w_{S_i2} and $\mathbf{0}$ represents the all-zero matrix. The rate of the entire code word is $R_2 = \frac{N_1 - (k_1 + k_2)}{N_1 + k_2}$. We find a proper k_2, which must meet $R_2 \leq C(SNR_{S_1D}) = C(SNR_{S_2D})$.

Figure 4 Rate-compatible structure of the parity-check matrix for the relay code



R_1 and R_2 satisfy the following relationship:

$$R_1 = \frac{N_1 - k_1}{N_1} > R_2 = \frac{N_1 - (k_1 + k_2)}{N_1 + k_2} \tag{14}$$

As far as we know, the decoding performance depends on the parity-check matrix, while the degree distribution of the code ensembles determines parity-check matrix. So the design of the parity-check matrix $\mathbf{H}'_{\mathbf{S}_i}$ is equivalent to find the optimal degree distribution based on a given construction algorithm.

3.2.2 *Optimal design of the degree distribution of the joint network LDPC code*

According to the above analysis, when SNR_{S_iD} is given, we can determine the number of extra parity bits. In addition, D decodes the received information of S_i correctly; it is required to satisfy the formula

$$R_1 \le C\left(SNR_{S_iD}\right) + C\left(SNR'_{S_iD}\right) \tag{15}$$

When the transmit power and the channel gains are given, we can obtain the theoretical minimum SNR by (15). Our optimal goal is to find the relay extended code ensemble, whose threshold of SNR is approaching the theoretical extreme value.

Compared with the rate-compatible LDPC code of the single-source single-relay system, the two-source single-relay system uses the linear network-coded method at R, which achieves the same cooperative diversity to the single-source single-relay system and D decodes the received signal of S_1 and S_2 separately. Here the two-source single-relay system can be equal to two separate single-source single-relay systems for rate-compatible LDPC code. Therefore, we can use the algorithm in Cances and Meghdadi (2009) to optimise the design of the rate-compatible extended code ensemble of S_1 and S_2 separately, while linear network-coded is used at the relay.

4 Simulation results

4.1 *SCT mode*

Assume each source node employs an $(n_1, n_1 - m_1)$ LDPC code with $\lambda(x) = 0.23403x + 0.21242x^2 + 0.1469x^5 + 0.102840x^6 + 0.30381x^{19}$ and $\rho(x) = 0.71875x^7 + 0.28125x^8$, where $n_1 = 22164$ and $m_1 = 11082$. $SNR_{RD} = 3$ dB and the two source–destination links are assumed to be symmetric. Using Algorithm 1, four different parameters of the joint network LDPC codes are obtained and listed in Table 1, where σ_{RD}^2 represents the channel parameter between the relay and the destination link.

Table 1 Four optimal joint network LDPC codes

Code ensembles	*Code A*	*Code B*	*Code C*	*Code D*
d'_v	2	2	2	2
d'_c	4	4	4	7
k_2	2814	4814	2814	2814
σ_{RD}	0.5	0.5	0.8	0.5
η	0.942065	0.904808	0.942065	0.902835
σ^*_{SD}	1.0568	1.0987	1.0393	1.1116
Threshold (E_bN_0)	0.155039dB	0.115123dB	0.2018dB	–0.22877dB
Sum capacity (E_bN_0)	–0.24536dB	–0.517620dB	–0.143948dB	–0.24536dB
Gap	0.400399dB	0.632743dB	0.345748dB	0.01666dB

Using Algorithm 2, four optimal degree distributions of the joint network LDPC codes are given in Tables 2–5.

Table 2 Degree distributions of code A

$\lambda_{i,j}$	$\lambda_{i,0}$	$\lambda_{i,1}$	$\lambda_{i,2}$
$i = 2$	0.193815	0.00543635	0.04612661
$i = 3$	0.171369	0.019109592	0.02409292
$i = 6$	0.129299	0.006342408	0.00494214
$i = 7$	0.09485	8.2369E-05	0.00259462
$i = 20$	0.273877	0.000432436	0.00181212
$i = 0$	0	0.0030528	0.02276564

Table 3 Degree distributions of code B

$\lambda_{i,j}$	$\lambda_{i,0}$	$\lambda_{i,1}$	$\lambda_{i,2}$
$i = 2$	0.07441004	0.20599344	0
$i = 3$	0.19208258	0.00015819031	0
$i = 6$	0.1327018904	0.00013842	0.0001681903
$i = 7$	0.09266986	0.000326381	0.0001779641
$i = 20$	0.27426244	0.0005152496	0.0021751167
$i = 0$	0	0.0237936797	0.000009887

Table 4 Degree distributions of code C

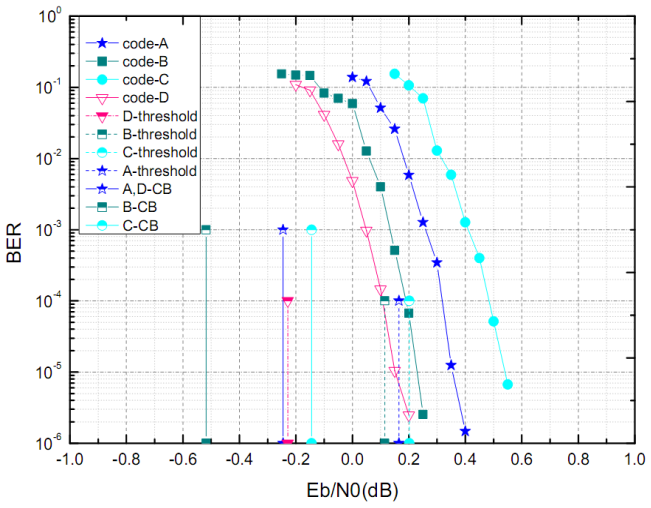
$\lambda_{i,j}$	$\lambda_{i,0}$	$\lambda_{i,1}$	$\lambda_{i,2}$
$i=2$	0.1206132872	0.0	0.0
$i=3$	0.1001453763	0.0000219458	0.0
$i=6$	0.1860514424	0.0002767963	0.000016798
$i=7$	0.1964141036	0.0002114936	0.0000212906
$i=20$	0.3858558271	0.0003262453	0.0000362551
i = 0	0.0	0.0041565109	0.0206487529

Table 5 Degree distributions of code D

$\lambda_{i,j}$	$\lambda_{i,0}$	$\lambda_{i,1}$	$\lambda_{i,2}$
$i=2$	0.1112574229	0.013643762	0.1818773738
$i=3$	0.09172912663	0.0876831253	0.0571696344
$i=6$	0.13223499235	0.00032560828	0.00015708008
$i=7$	0.092674986	4.568455E-05	6.788722E-05
$i=20$	0.274059093	0.00010113293	0.000217037
$i=0$	0	0.00351717946	0.02072694417

The BER curves of four codes are illustrated in Figure 5. We see that the gap between the decoding threshold of four codes obtained by searching the maximum decoding threshold σ_{SD}^{*} and capacity limit is less than 0.7 dB, and that between BER performance and decoding threshold is less than 0.4 dB. Since the lower check degree of Code D is bigger and more information bits are contained in the check equation, it outperforms Code A by 0.2 dB at $BER=10^{-5}$. Another important observation is that Code B has a gain of about 0.15 dB over Code A at $BER=10^{-5}$ and the performance gain of Code D is about 0.1 dB over Code B at $BER=10^{-5}$. This indicates that increasing the degrees of lower layer check nodes is better than increasing the numbers of parity bits to improve system performance. When the noise variances between the *R* and *D* link are increased, the system decoding performance will be reduced and Code A will have a gain of about 0.2 dB over Code C at $BER=10^{-5}$.

Figure 5 Performance of the joint network LDPC codes



4.2 ACT mode

Assume each source node employs LDPC code-1 and code-2 listed in Cances and Meghdadi (2009, Table 1). The two source–destination links are assumed to be symmetric. The distance between S_i and D is normalised to unity and d denotes the normalised distances between S_i and R. The channel gain $|h_{S_1D}|^2=|h_{S_2D}|^2=1$, $|h_{S_1R}|^2=|h_{S_2R}|^2=\frac{1}{d^{\alpha}}$ and $|h_{RD}|^2=\frac{1}{(1-d)^{\alpha}}$, where we assume that $\alpha=2$ is the path loss exponent and $d=0.25$. The power allocation among S_i and R is fixed as $P_{S_1}^{(1)}/2=P_{S_2}^{(1)}/2=P_{S_12}=P_{S_22}=P_R/2=P_T/8$, and $w_{S_i}^{(1)}$ and w_{S_i2} have the rate $R_1=1/2$ and $R_2=1/4$, respectively. Table 6 gives the optimum LDPC code ensemble of w_{S_i2} via the algorithm in Cances and Meghdadi (2009) and the network-coded method at the relay. And the node probability set of w_{S_12} is $h_1(2)=0.1978$, $h_1(i)=1$ for $i\in\{3,6,7,8,10,14,16,20,30,33\}$, the node probability set of w_{S_22} is $h_1(3)=0.1576$, $h_1(i)=1$ for $i\in\{2,4,7,8,10,14,16,20,30,33\}$, where $h_1(i)$ denotes the probability of a variable node that has a degree of *i* and falls in the region of region-1 (i.e. $\mathbf{H_1}$ and **A**, namely region-1; **0** and **B**, namely region-2.)

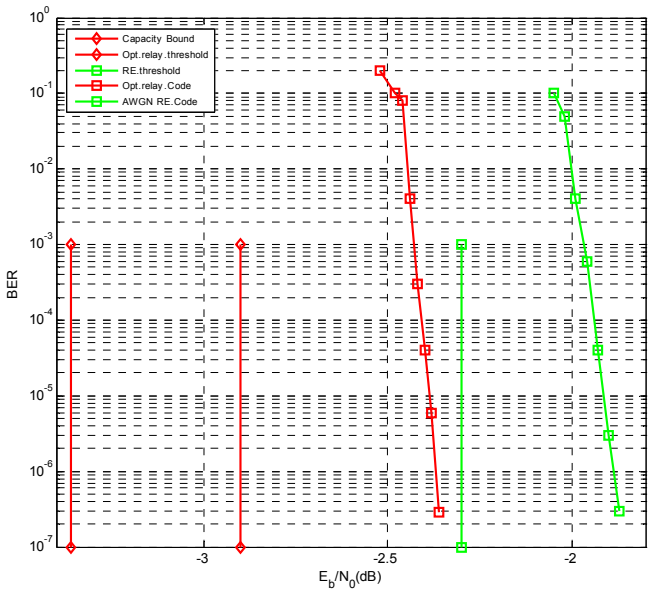
Table 6 Rate-compatible extended LDPC code ensembles

Code ensembles	*Extended code ensemble 1*	*Extended code ensemble 2*
λ_2	0.13370307136	0.06600453943
λ_3	0.02829823403	0.11086569074
λ_4	0.02371830093	0.07247855957
λ_5	0.00295003743	0.00422715433
λ_6	0.05593270965	0.03891266928
λ_7	0.00474956026	0.06403186741
λ_8	0.05605071114	0.03722942404
λ_9	0.11366862967	0.15231465261
λ_{10}	0.06932587957	0
λ_{11}	0.00125745345	0.00502688622
λ_{12}	0.00044250561	0
λ_{13}	0.00081494784	0
λ_{14}	0.00087763614	0.05326214450
λ_{15}	0.00027656601	0
λ_{16}	0.19417146355	0.13551266623
λ_{17}	0.20455190775	0
λ_{20}	0.00118001497	0.00411290691
λ_{22}	0.00186589867	0.16077657776
λ_{26}	0.00009587622	0
λ_{30}	0.10553758901	0.09505384861
ρ_8	0	0.22602708425
ρ_9	0.99563763215	0.77391198379

In simulations, the code lengths of $w_{S_i}^{(1)}$ and w_{S_i2} are $N_1=20000$ and $N_2=2N_1=40000$, respectively. We compare the BER performance between the optimum LDPC

code ensemble and the repetition code under the AWGN channel, when the repetition code has $w_{S_i e} = w_{S_i}^{(1)}$ and D receives $w_{S_i}^{(1)}$ from source S_i and R at the same time. Figure 6 shows the BER performance of the optimised relay code ensemble and the repetition code. It is seen that the relay code ensemble optimised via the algorithm in Cances and Meghdadi (2009) can achieve about 0.5 dB gain over the repetition scheme. The gap between the BER performance of the optimised relay code ensemble of the rate-compatible LDPC and the decoding threshold is about 0.52 dB, and the gap between the decoding threshold and the capacity limit is less than 0.46 dB.

Figure 6 The BER performance comparison between the optimised relay code and the repetition code



5 Conclusions

In this paper, we employed the differential evolution method to design degree distribution of different transmission modes of the joint network LDPC code for a two-source single-relay system. The performance of the new codes we designed showed significant BER performance gain for a two-source single-relay system with symmetric AWGN channels.

Acknowledgements

We are grateful to anonymous referees for their invaluable suggestions. This work is supported by the National Natural Science Foundation of China (Nos. 61072064, 61101148 and 61001131).

References

Azmi, M.H., Yuan, J., Ning, J. and Huynh, H.Q. (2008) 'Improved bilayer LDPC codes using irregular check node degree distribution', *Proceedings of the IEEE International Symposium on Information Theory*, 6–11 July, Toronto, Canada, pp.141–145.

Cances, J.P. and Meghdadi, V. (2009) 'Optimized low density parity check codes designs for half duplex relay channels', *IEEE Transactions on Wireless Communications*, Vol. 8, No. 7, pp.3390–3395.

Cover, T. and Gamal, A.E. (1979) 'Capacity theorems for the relay channel', *IEEE Transactions on Information Theory*, Vol. 25, pp.572–584.

Laneman, J., Tse, D. and Wornell, G. (2004) 'Cooperative diversity in wireless networks: efficient protocols and outage behavior', *IEEE Transactions on Information Theory*, Vol. 50, No. 12, pp.3062–3080.

Li, Y., Song, G.H. and Wang, L.L. (2009) 'Design of joint network-low density parity check codes based on the EXIT charts', *IEEE Communications Letters*, Vol. 13, No. 8, pp.600–602.

Li, Y., Song, G.H. and Wang, L.L. (2010) 'Analysis of the joint network LDPC codes over orthogonal multi-access relay channel', *IEEE Communications Letters*, Vol. 14, No. 2, pp.184–186.

Nosratinia, A., Hunter, T.E. and Hedayat, A. (2004) 'Cooperative communication in wireless networks', *IEEE Communications Magazine.*, Vol. 42, No. 10, pp.74–80.

Razaghi, P. and Yu, W. (2007) 'Bilayer low-density parity-check codes for decode-and-forward in relay channels', *Transactions on Information Theory*, Vol. 3, No. 10, pp.3723–3739.

Shen, Y., Pei, Q., Xu, Q. and Zhang, Z. (2012) 'The multimedia service session handoff method in heterogeneous wireless networks', *International Journal of Grid and Utility Computing*, Vol. 3, No. 1, pp.68–77.

Zhang, Y. and Minier, M. (2013) 'How network coding system constrains packet pollution attacks in wireless sensor networks', *International Journal of Grid and Utility Computing*, Vol. 4, Nos. 2–3, pp.197–203.

PAPER • OPEN ACCESS

Research on the changing trend of farmland area in China and its driving factors from 1996 to 2016

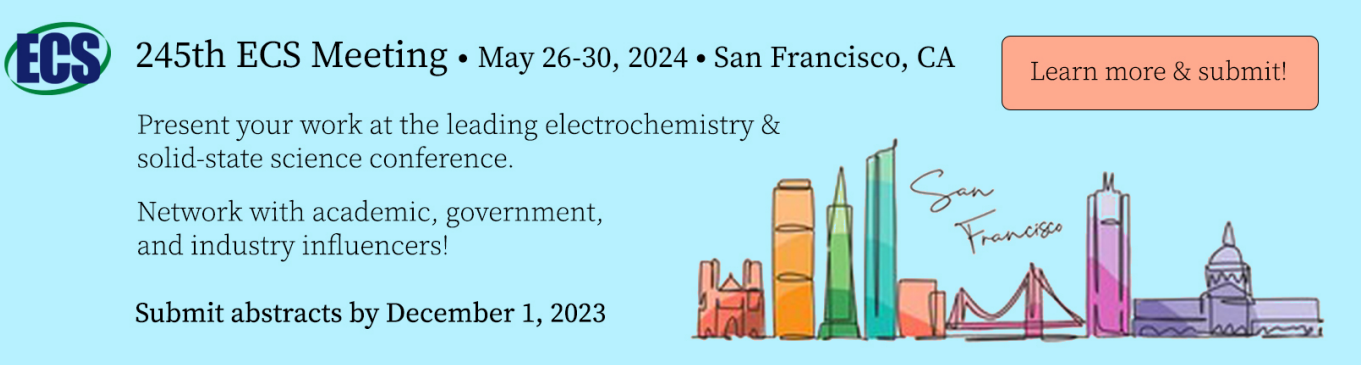
To cite this article: J Y Wang and X M Li 2018 *IOP Conf. Ser.: Mater. Sci. Eng.* **392** 062097

View the article online for updates and enhancements.

中文文章叫近20年，英文文章是1996 to 2016,文章完全一样

You may also like

- The 300 years cropland changes reflecting climate impacts and social resilience at the Yellow River–Huangshui River Valley, China
Qiong Chen, Liang Emlyn Yang, Jing Luo et al.
- Analysis and Research on the Value of Farmland Transfer Based on Environmental Protection Evaluation System
Zhenyu Zhang, Minghua Tian, Jianjun Li et al.
- High Standard Farmland Construction and Soil Conservation Evaluation
Jing Zhang and Lu Sun



This content was downloaded from IP address 219.144.164.16 on 16/11/2023 at 00:29

Research on the changing trend of farmland area in China and its driving factors from 1996 to 2016

J Y Wang [1] and X M Li[2*]

[1]Xi'an Shiyou University, Xi'an China, 710065

[2]Shaanxi Provincial Land Engineering Construction Group，Xi'an China, 710075

*Corresponding author: xmlisdc@126.com

Abstract. The paper was to research the changing trend of farmland area from 1996 to 2016. The original data of farmland area of China in these years were collected, data mining technology was used, and ARIMA model was chosen to predict each other between the two periods of 1996-2008 and 2008-2016, so the original farmland area data could be corrected and normalized. Then correlation analysis was used to study the driving factors. The trend research result showed, the farmland area decreased from 1996 to 2016, the decreasing rate was faster before 2004, and then it decreased slowly. The correlation analysis result showed, the added value proportion of primary industry, the total population, and the urban population were the most important driving factors, their coefficients were 0.959, -0.918 and -0.896 respectively. It could be concluded by the result that the industry configuration and the urbanization could affect the farmland area changing with the development of social economy.

1. Introduction

China is a great agricultural country, and the farmland is one very important resource which is related to food security. However, the vigorous demand for lands brings great challenge for farmland protection with the promotion of socialist modernization construction [1]. The research on farmland area change and its driving factors in China has always been one popular problem. The statement was refuted that China's cultivated land has been descending since 1957 based on the analysis of the actual change of the cultivated land area [2]. The farmland area changing trend, spatial characteristics and the driving factors in China for a period of time before 2007 were studied [3-5]. And in different scales such as the scale of province or in some part of China, the dynamic change trend of farmland was studied [6-8]. Since 1980s, with the development and application of 3S technology, many scholars studied the farmland change using the RS images such as Landsat TM images [9, 10]. And the analysis approaches in the study of the driving forces of land use change in large regions were explored by using digital satellite remote sensing data of China [11]. Not only the changes in China's cultivated land but also those in some provinces were analyzed based on remote sensing data such as Landsat TM/ETM+, NOAA, SPOT dataset [12, 13].

The statistic data sources of cultivated land in China are various, for example, the international organizations such as FAQ, WRI (the world resources institute), and different departments of China such as MLR (the ministry of land and resources), MOA (the ministry of agriculture), the bureau of statistics of PRC. However, the statistical data supplied by MLR are considered the most authoritative [14]. But the data from the MLR are not regularly entire in the demanded periods, and there was a jumping phenomenon with the farmland area from 2008 to 2009, that's because the data of 2008 was

Content from this work may be used under the terms of the Creative Commons Attribution 3.0 licence. Any further distribution of this work must maintain attribution to the author(s) and the title of the work, journal citation and DOI.
Published under licence by IOP Publishing Ltd

based on the first national land use survey, and the data of 2009 was based on the second national land use survey, that's seemly illogical. At present, most scholars analyze the farmland area change by the exiting data directly while ignoring the accuracy of the statistic data, or they just focused on some periods before 2008 or after 2009 evading the jumping years. Only a few scholars researched the farmland area in different historical periods [14, 15]. In this paper, the researched years included the years of before and after the second national land use survey. The method of data mining was introduced to analyze the relation between the two periods of the years before 2008 and the years after 2009, so the changing trend of China's farmland area could be reflected more scientifically. At the same time, the driving factors were studied based on data normalization. And this is not found in the present research, which could be useful for studying China's farmland changing trend.

2. Data and methods

2.1. Data acquisition

2.1.1. Data of farmland area in China

The farmland area of China, especially in the historical periods, has been hard for statistic for a long time. The national department of land management have been announcing the changing situation each year since 1986. In order to obtain the veracious statistical data of farmland in China, the first national land use survey was operated from 1984 to 1996. The survey result showed there was 1.95 billon mu (1 mu = 666.66 m^2) of farmland in China by the day of Oct.31 1996 [15], which was considered the most credible result at that time [16]. Then, the farmland area of each year from 1996 to 2008 can all be obtained from the statistical bulletin of the year.

In order to obtain more veracious statistical data of farmland, the second national land use survey was operated from 2007 to 2009. The survey result showed there was 2.03 billon mu of farmland in China by the year of 2009 [15]. And since then the land use change survey has been operated each year. And the farmland area from 2007 to 2016 can be obtained from the national service platform of land use survey result. Because new methods and technologies were applied with the second national land use survey, some farmlands which were not found in the first survey were found in the second survey, and there was a jumping phenomenon with the farmland area from 2008 to 2009, which would be specially researched after a while for analyzing the changing trend of farmland area.

2.1.2. Data of driving factors

Land is closely related to the human social and economic development. The national farmland change is influenced by the geographical and climate conditions, social and economic development, flood and waterlogging disaster and so on [1]. For researching the driving factors influencing the farmland changing, three kinds of factors were introduced for comparison and selection. One kind were the comprehensive factors reflecting the national economic development, and they were the gross national income (GNI), the gross domestic product (GDP), the primary industry added value and its ratio, the second industry added value and its ratio, the third industry added value and its ratio, the gross agricultural output value, per capita GDP, industrial added value, architectural added value. Another kind were special factors reflecting the level of urbanization, and they were the national population, the urban population, and the rural population. The third kind was the special factors reflecting the natural disaster, and they were the damage area and the grain yield. There were in total of 17 factors which were used for analysis [17]. And data of all factors for the recent 20 years could be obtained from the web site of the national bureau of statistics.

2.2. Study methods

In this paper, the national farmland area dada from 1996 to 2016 years were collected and analysed to study the changing trend, and the correlation analysis was operated to research the driving factors. While studying the changing trend of farmland from 1996 to 2016, according to the found jumping

phenomenon with the data from 2008 to 2009, the data mining technology was introduced. First, the farmland area of the year 2009 can be predicted with the data of 1996 to 2008. And the farmland area of the year 2008 can also be predicted reversely with the data of 2009 to 2016. Then, based on the predicted data and the practically collected data of the farmland of the years 2008 and 2009, the mathematical ratio relation between the farmland area of 2008 and 2009 could be analysed and obtained, so the jumping phenomenon could be solved with the ratio. At last, all the farmland data from 1996 to 2016 should be normalized for researching the changing trend more scientifically.

ARIMA (Autoregressive Integrated Moving Average) model was chosen for prediction with data mining, which was promoted by Box and Jenkins, it's a very famous and useful time-sequence forecast method, and that's just the needed one in this paper.

3. Analysis on the farmland area changing trend from 1996 to 2016

3.1. The analysis based on the original statistic data of farmland area

By collecting and analysing the original statistic data of farmland area for years of 1996-2016, the result showed that the national farmland area decreased year by year, as Figure1, and the decreasing speed was the most quick from 2000 to 2004. While the farmland area jumped from 1.826 billion mu in 2008 to 2.031 billion mu in 2009. And after 2009, the farmland area decreased very slowly.

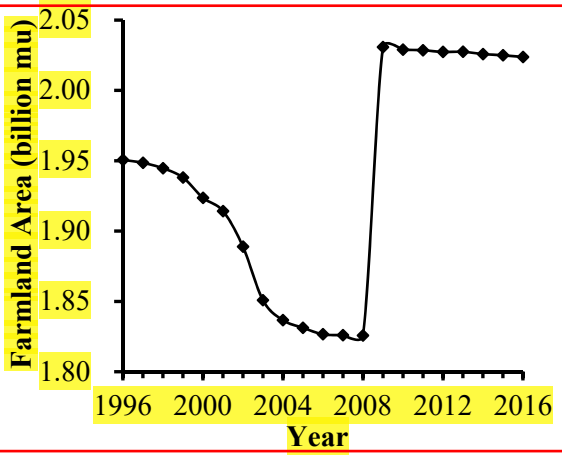


Figure 1. Changing Trend for Farmland Area of 1966-2016 Based on Original Statistic Data

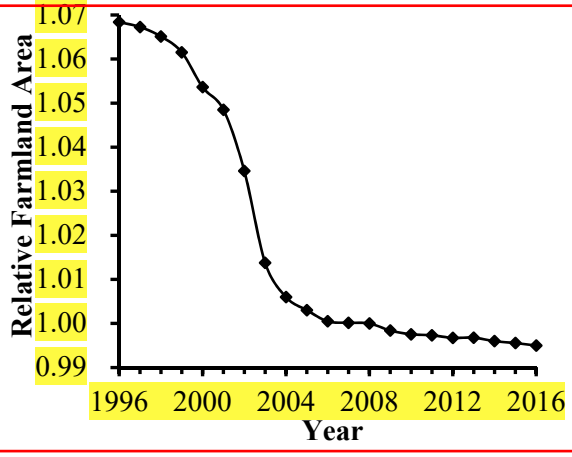


Figure 2. Changing Trend for Farmland Area of 1966-2016 Based on Revised Statistic Data

China finished the first national land use survey in 1996, and the second in 2009, so the jumping phenomenon just happened in the division years of the twice land use survey. Whether the national farmland increased by about 200 million mu in the year of 2009 or not should be studied deeply. And by reviewing literatures [14, 15, 18], it could be concluded that the main reason was that more advanced technologies were introduced while the second land use survey, so some farmlands lost of statistic in the first land use survey were found in the second time, and the accuracy of the statistic result was improved. In this paper, the farmland data for the recent 20 years were based on twice different land use survey and different technology conditions. We can easily studied the changing trend in each period before or after the second land use survey, while all the data of farmland area must be revised and normalized if we want to study the continual time-sequence changing trend from 1996 to 2016, then they might be comparable.

3.2. Revision of farmland area based on data mining technology

Data mining technology is much useful for time-sequence prediction, and by that, in this paper, the farmland area of the year 2009 was predicted with the farmland data of the years from 1996 to 2008, the ratio α between the farmland area of 2009 and that of 2008 could be obtained. And the farmland area of the year 2008 was also predicted reversely with the farmland data of the years from 2009 to

2016, the ratio β between the farmland area of 2009 and that of 2008 could also be obtained. Then, for reflecting the ratio more scientifically, we could get the ratio ρ by the average of α and β.

SPSS software was used for prediction in this paper, by analyzing and comparing, the model of ARIMA was used in both of the prediction and the reverse prediction. The model used while predicting the farmland area of the year 2009 was ARIMA(1,1,2) (r^2=0.975**), and the model used while predicting reversely the farmland area of the 2008 was ARIMA(1,1,4) (r^2=0.966**), both of the two models were significant in the level of 0.01, with that, the predicted farmland area of the year 2009 was 1820.08 million mu, the reversely predicted farmland area of the year 2008 was 2030.98 million mu, so we can get α=0.996899887, β=0.999895617, and then ρ=0.998397752, so we could use the ρ value as the revision ratio of the data of the two different periods.

3.3. Trend analysis based on the revised data of farmland area

All the original farmland area data were revised with the ratio ρ and normalized into relative values for reflecting the changing trend more scientifically. Based on the study of the previous paper, the relative farmland area of the years from 1996 to 2008 were calculated with the denominator of the farmland area of the year 2008, the relative farmland area of the years from 2009 to 2016 were calculated with the denominator of the farmland area of the year 2009 while revised by multiply the ratio ρ. Then the continual changing trend of farmland area from 1996 to 2016 could be obtained, shown as Figure 2, which showed the national farmland area decreased year by year. Before the 2004, the decreasing rate was faster, and after that the decreasing rate trends to be slower, especially after 2009, the farmland area trends to be stable.

4. Analysis on driving factors

A total of 17 factors were collected in this paper, and their descriptive statistical characters were shown in table 1. In order to study the driving factors, correlations between the farmland area and the factors were analysed, and then, by comparing the correlation coefficients shown as table 2. the driving factors could be chosen out.

Table 1. Descriptive Statistical Characters of All Factors from 1996 to 2016

Factors	*Min.*	*Max.*	*Ave.*	*Std.*	Factors	*Min.*	*Max.*	*Ave.*	*Std.*
x_1	7078	74114	30444.70	225956.60	x_{10}	589.8	5398	2287.2	16332.77
x_2	7181.4	74412.7	30571.87	226519.84	x_{11}	2953	24786	11653.28	79508.29
x_3	1387.8	6367.1	3124.07	17742.62	x_{12}	439.3	4952.2	1962.3	15992.73
x_4	8.556	19.325	12.11	3.28	x_{13}	122389	138271	131047.71	4702.17
x_5	3382.8	29623.6	13562.92	94949.58	x_{14}	37304	79298	58413.24	12989.27
x_6	39.810	47.559	45.33	2.00	x_{15}	58973	85085	72634.48	8313.40
x_7	2410.7	38422	13884.89	114605.84	x_{16}	43070	62144	52326.48	5812.06
x_8	33.569	51.634	42.56	4.47	x_{17}	21770	54688	41009.48	10706.30
x_9	1354	5928.8	2884.26	16570.35					

**In the table, x_1 means the gross national income (GNI), billion yuan; x_2 means the gross domestic product (GDP), billion yuan; x_3 means the primary industry added value, billion yuan; x_4 means the proportion of primary industry added value, %; x_5 means the second industry added value, billion yuan; x_6 means the proportion of second industry added value, %; x_7 means the third industry added value, billion yuan; x_8 means the proportion of third industry added value, %; x_9 means gross agricultural output value, billion yuan; x_{10} means per capita GDP, billion yuan; x_{11} means industrial added value, billion yuan; x_{12} means architectural added value, billion yuan; x_{13} means the national population, $*10^4$; x_{14} means the urban population, $*10^4$; x_{15} means the rural population, $*10^4$; x_{16} means the grain yield, $*10^4$ t; x_{17} means damage area, $*10^3$ ha; and the same as follows.*

Table 2. Correlation Coefficients between Original/Relative Farmland Area and Factors

	Original data	Relative data		Original data	Relative data
Relative data	-0.142	1.000	x_9	0.686	-0.709
x_1	0.649	-0.746	x_{10}	0.651	-0.749
x_2	0.652	-0.745	x_{11}	0.638	-0.784
x_3	0.663	-0.736	x_{12}	0.688	-0.716
x_4	-0.274	0.959	x_{13}	0.433	-0.918
x_5	0.647	-0.774	x_{14}	0.488	-0.896
x_6	-0.519	0.259	x_{15}	-0.518	0.880
x_7	0.649	-0.717	x_{16}	0.752	-0.524
x_8	0.433	-0.819	x_{17}	-0.514	0.708

As shown in table 2, the correlation coefficients between the original farmland area and the factors were poor because of the jumping phenomenon. However, by analyzing the correlations between the revised farmland area and the factors, we could find, the proportion of the first industry added value had the best correlation with the farmland area, its coefficient was up to 0.959. The national total population was secondary to it, and its correlation coefficient was -0.918, then the urban population and the rural population were secondary to that sequentially, which means the first industry added value, the national total population, the urban population and the rural population were the most important driving factors. According to the research result, we could conclude that it was mainly the national industry structure and the urbanization construction that influence the farmland changing.

5. Conclusion and discussion

Land has both of its own natural and social characters, and it's just all of the factors including society, economy, and policy factors that influence the statistics of farmland area for a long time. So it's difficult for a long-time changing trend research. The period studied in this paper was across twice national land use survey, and there happened to be a jumping phenomenon, but this couldn't reflect the boost of farmland area from 2008 to 2009. The reasons of the phenomenon were studied, that was mainly because RS, GIS and some other new technologies were applied in the second national land use survey, the survey and statistics were more standardized, so the accuracy was apparently promoted, which made the farmlands lost of statistics before found in the second land use survey. Therefore, in order to study the changing trend for a period across twice land use survey, the quantitative relation of the farmland area between the twice survey must be studied and obtained. In this paper, with data mining technology, revision and normalization of farmland area, the research result could reflect the changing trend more actually.

Research results showed China's farmland area decreased year by year from 1996 to 2016, especially before 2004, the decreasing rate was fast, and after that year the decreasing rate tended to be slow. As to the driving factors, it's the proportion of the primary industry added value in the aspect of the national industry structure and the national population, the urban population in the aspect of urbanization construction which were the main driving factors influencing the farmland changing. Because of the ecological restoration after the year of 1999, the farmland decreased rapidly [14, 19]. In 2004, the land management law was revised, which strengthened the protection and the requisition-compensation balance of farmland, and that's much useful for retaining farmland. In this paper, only the farmland area data from 1996 to 2016 were used to study the changing trend, and in present time, China pay much attention to farmland protection, not only including the quantity, but including the land quality with core of productivity in order to realize the protection of the trinity of quantity, quality and ecology [20]. In the future research, the changing trend of farmland area would be studied deeply.

The years of 1966 to 2016 were introduced in this paper to study the changing trend because the demand of statistical data for longer-time sequence was difficult to be satisfied. In future research, based on the collected statistical data, the data mining, remote sensing interpretation and some other methods would be applied to compensate the lack of some factors, so we wish we could obtain a longer time-sequence changing trend.

References

[1] Zhao Q G, Zhou S L, Wu S H and Ren K. 2006. Cultivated Land Resources and Strategies for Its Sustainable Utilization and Protection in China, *Acta Pedologica Sinica*,43(4): 662-72.
[2] Bi Y Y and Zheng Z Y. 2000. The Actual Changes of Cultivated Area Since The Founding of New China**,** *Resources Science*, 22(2): 8-12.
[3] Li X B. 1999. Change of arable land area in China during the past 20 years and its policy implications, *Journal of Natural Resources*, 14(4): 329-33.
[4] Cao Y G, Yuan C, Zhou W, Tao J and Hua R. 2008. Analysis on D iving Forces and Provincial Differences of Cultivated Land Change in China. *China Land Science*, 22(2): 17-22.
[5] Huang Z H and Wu C F. 2009. Empirical Study of Cultivated Land Change and Socio-economic Factors in China. *Journal of Natural Resources*. 24(2): 192-9.
[6] Yu T, Cao Y G and Xu J X. 2016. Driving Force of Cultivated Land Change in China Based on Different Scales. *Chinese Agricultural Science Bulletin*, 2016, 32(24): 194-8.
[7] Wu X, Wang S R, Shang H Y and Wang Z J. 2017. Analysis of Dynamic Change and Driving Forces of Cultivated Land in NingXia During The Past 18 Years. *Chinese Journal of Agricultural Resources and Regional Planning*. 38(8):98-104.
[8] Guo L Y, Wang D L and Wang J Y. 2012. Analysis of the Arable Land Change and Its Causes in the Eastern Coastal China Over the Last Decades. *Chinese Journal of Agricultural Resources and Regional Planning*. 33(1):6-10.
[9] Zhang G P, Liu J Y and Zhang Z X. 2003. Spatial-temporal Changes of Cropland in China for the Past 10 Years Based on Remote Sensing. *Acta Geographica Sinica*. 58(3): 323-32.
[10] Tian G J, Zhuang D F and Liu M L. 2003. The Spatial-temporal Dynamic Change of Cultivated Land in China in 1990s. *Advance in Earth Sciences*. 18(1): 30-6.
[11] Liu X H,Wang J F,Liu J Y, Liu M L and Meng B. 2005. Quantitative Analysis Approaches to the Driving Forces of Cultivated Land Changes on A National Scale.*Transactions of the Chinese Society of Agricultural Engineering*. 21(4):56-60.
[12] Xu L L, Li B L, Yuan Y C, Gao X Z, Liu H J and Dong G H. 2015. Changes in China's Cultivated Land and the Evaluation of Land Requisition-Compensation Balance Policy from 2000 to 2010. *Resources Science*. 37(8): 1543-51.
[13] Li J G, He C Y, Shi P J, Chen J, Gu Z H and Xu W. 2004. Change Process of Cultivated Land and Its Driving Forces in Northern China during 1983-2001. *Acta Geographica Sinica*. 59(2): 274-82.
[14] Feng Z M, Liu B Q and Yang Z. A Study of the Chaning Trend of Chines Cultivated Land Amount and Data Reconstructing:1949-2003. *Journal of Natural Resources*, 20(1): 35-43.
[15] Tan Y Z, He J, Yue W Z, Zhang L and Wang Q R. 2017. Spatial Pattern Change of the Cultivated Land before and after the Second National Land Survey in China. *Journal of Natural Resources*, 32(2): 186-97.
[16] Lin G C S, Ho S P S. 2003. China's land resources and land-use change: insights from the 1996 land survey. *Land Use Policy*, 20(2): 87-107.
[17] Fu Z Q, Cai Y L, Yang Y X and Dai E F. 2001. Research on the Relationship of Cultivated Land Change and Food Security in China. *Journal of Natural Resources*, 16(4): 313-9.
[18] Zhang Y Q and Yang Z S. 2013. Comparative Analysis of Two Investigations of Land Resource in China. *Scientific and Technological Management of Land and Resources*. 30(2): 100-4.
[19] Xu X L, Cai Y M, Zhang K L and Zheng W Y. 2005. Study on Dynamic Change of Cultivated Land Resources and Causes of the Changes. *China Population Resources and Environment.* 15(3): 75-9.
[20] Tan Y Z, Wu C F, Wang Q R, Zhou L Q and Yan D. 2005. The Change of Cultivated Land and Ecological Environment Effects Driven by the Policy of Dynamic Equilibrium of the Total Cultivated Land. *Journal of Natural Resources*. 20(5): 727-34.

doi：10.7621/cjarrp.1005-9121.20190821

中文文章叫近20年，英文文章是1996 to 2016，文章完全一样

·资源利用·

近20年中国耕地数量变化趋势及其驱动因子分析*

王静怡[1]，李晓明[2※]

（1. 西安石油大学计算机学院，陕西西安 710065；2. 陕西省土地工程建设集团有限责任公司，西安 710075）

摘 要 ［目的］研究“二调”前后近20年我国耕地面积的变化趋势及其影响因子，为促进耕地保护和土地资源的高效集约节约利用提供决策支撑。［方法］基于1996—2016年耕地数量的原始统计数据，利用数据挖掘技术选用ARIMA模型，基于两次全国土地调查时间段耕地数量数据进行相互预测和反推，即利用1996—2008年耕地数量数据预测2009年耕地数量，利用2009—2016年数据反推2008年耕地数量，从而实现数据的校正和比值归一化的目的，进一步研究近20年内我国耕地数量的变化趋势，并通过相关性分析研究遴选出其驱动因子。［结果］趋势研究结果表明，近20年内我国耕地数量呈现逐年递减的趋势，其中2004年之前递减速度较快，之后递减速度趋缓。相关性分析结果显示，第一产值增加值占比、年末总人口数，以及城镇人口数是影响耕地数量变化的重要驱动因子，其相关系数分别为0.959，－0.918，－0.896。［结论］从研究结果可以推论，我国在社会经济发展中的产业结构布局，以及城镇化建设进程对耕地数量变化产生了重要的影响。

关键词 数据挖掘 ARIMA模型 耕地数量 变化趋势 驱动因子

中图分类号：P96 文献标识码：A 文章编号：1005－9121［2019］08171－06

0 引言

我国是一个农业大国，耕地资源直接关系到国家粮食安全问题，是确保“中国人的饭碗牢牢端在自己手中”的重要基础。同时，在加快推进我国社会主义现代化建设进程中，经济建设对土地的旺盛需求也对耕地保护带来了极大的挑战[1]。对于我国耕地的变化趋势及其影响驱动力的研究，一直都是一个热点问题，甚至有专家学者通过史册文献资料的查证对过去300年我国部分省区耕地资源数量变化及驱动因素进行了研究[2]。

目前，对于我国耕地变化趋势的研究，多基于对统计数据进行分析，从空间尺度上可以分为国家尺度和区域尺度的研究。其中，对于国家尺度上的研究，由于统计标准、技术手段等多种因素的限制，2008—2009年数据发生明显的跳跃式变化，所以绝大部分的研究均处于2008年之前的部分时间段内，如毕于运等[3]通过对我国建国至1996年实有耕地面积的收集整理研究分析了其变化分析；李秀彬[4]对1999年我国前20年耕地面积变化的总体趋势、空间特征和驱动因子进行了研究；曹银贵[5]研究分析了1996—2005年全国耕地变化的情况及其影响的主要因子；黄忠华、吴次芳等利用1978—2007年我国耕地、经济增长、城镇化、地方财政收入数据分析了社会经济因素对耕地变化的影响[6]。以上研究均将时间局限在2008年之前，而回避了2008—2009年耕地统计数据跳跃的现象，这不利于科学研究我国耕地的变化趋势和指导耕地保护工作。对于区域尺度，如省级，甚至市县级尺度，由于统计基数较小，受统计方法、技术标准等因素的影响不大，几乎各个省份区域都有专家对其耕地变化和驱动因子进行了大量研究，如郭丽英等[7]

收稿日期：2018-03-26

作者简介：王静怡（1984—），女，陕西榆林人，博士、讲师。研究方向：资源利用和数据科学

※通讯作者：李晓明（1983—），男，山东烟台人，博士、高级工程师，硕士生导师。研究方向：土地资源利用和遥感信息。Email：xmlisdc@126.com

* 资助项目：陕西省教育厅科研计划项目“无线MARC系统中联合网络—信道编码的优化设计研究”（18JK0626）

(C)1994-2022 China Academic Journal Electronic Publishing House. All rights reserved. http://www.cnki.net

分析了 1996—2008 年我国沿海地区耕地变化的基本态势、时空特征及其主导成因；吴霞等[8]选取 1997—2014 年宁夏耕地面积数据分析耕地面积变化趋势及其驱动因子；武江民等[9]专门针对甘肃兰州市研究其耕地动态变化与驱动力的定量关系。还有学者则基于基于国家、区域、省域、市县不同尺度研究了中国耕地变化的驱动力[10]；

20 世纪 80 年代以来，随着遥感等 3S 技术的发展应用，诸多学者开始不仅仅局限于统计数据的应用，开始借助遥感信息技术对耕地变化进行研究。如张国平、刘纪元等[11]利用中国资源环境数据库及遥感影像对 20 世纪 80 年代末至 2000 年的中国耕地时空变化进行了分析；田光进、庄大方等[12]通过对遥感图像解译研究 80 年代末与 90 年代末 10 年间耕地时空动态变化特征；刘旭华，王劲峰等使用中国 1987—1989 年和 2000 年两期土地利用遥感调查数据，探索定量化研究国家尺度土地利用变化的驱动力[13,14]；许丽丽等[15]基于中分辨率卫星遥感数据，深入分析了 2000—2010 年中国耕地变化及其空间差异，并对中国耕地占补平衡政策的实施效果进行了评估；李景刚等[16]选取 1983—2001 年 NOAA 等遥感数据分析了北方 13 省的耕地变化与驱动力。遥感信息技术的应用开拓了耕地变化研究的新途径，但是由于遥感解译的精度仍有待于进一步提高，所以一定程度上制约了对于耕地变化的研究。

多来以来，我国对于耕地数量的数据统计有多种来源，其中以国土资源部的统计数据被认为最权威[17]。由于遥感影像解译精度，与实地调查统计相比仍有一定差距，所以大部分学者仍采用统计数据进行研究，而且大多避开了数据有明显变化的过渡年份。目前仅有极少数学者对过渡年份前后时间段的统计数据变化一并进行了相关的分析[17,18]。针对两次全国土地调查的统计数据的跳跃式变化，文章研究提出了基于数据挖掘技术研究分析两个时间段的数量关系，以更科学地反映耕地数量的变化趋势，同时基于校正数值研究影响耕地变化的驱动因子，这在目前的研究中尚未见到，对于科学反映我国耕地变化趋势具有积极的意义。

1 数据与方法

1.1 数据获取

1.1.1 全国耕地数量数据

我国耕地数量，尤其是历史时期的耕地数量，长期以来难以确定。国家土地管理部门从 1986 年开始，每年统计并公布我国耕地的增减情况，虽然还有其他职能部门的统计数据，但仍以国土资源部的数据最为权威[17]。为准确掌握全国耕地数量，1984—1996 年国务院安排开展了全国第一次大规模的土地利用现状调查，数据成果统计到了 1996 年 10 月 31 日，结果表明，1996 年全国耕地面积约为 1.300 亿 hm^2（19.51 亿亩）[18]，这一统计数据被认为具有最高可信度[19]。随后，1996—2008 年耕地面积数据均可直接从统计公报中查得。

为进一步准确掌握耕地土地基础数据，国家于 2007 年 7 月 1 日起，启动了第二次全国土地调查，数据统计时间节点为 2009 年 12 月 31 日，统计结果显示 2009 年我国耕地面积为 1.354 亿 hm^2（20.31 亿亩）[18]。随后的每年都有二调变更调查，2007—2016 年每年的全国耕地面积都可以从国家土地调查成果服务平台直接查得。由于第二次全国土地调查采用的技术方法的改进等原因，2008 年与 2009 年的耕地数量存在“跳跃”现象，为科学分析耕地的变化趋势，这一现象问题在后文中进行了着重的研究处理。

1.1.2 驱动因子数据

土地与人类社会的经济发展密不可分，全国耕地变化是在地理背景制约下、社会经济条件、灾害等自然条件共同驱动下发生的[1]，为探索研究耕地变化的驱动因子，该文主要选取了 3 方面共 17 个因子指标做遴选分析：一方面是反映全国经济发展水平的综合类指标，包括国民总收入、国内生产总值、第一产业增加值及比例、第二产业增加值及比例、第三产业增加值及比例、人均国内生产总值、工业增加值、建筑业增加值、农业总产值；另一方面是反映社会城镇化水平的指标，包括年末总人口、城镇人口、乡村人口；还有第三方面是反映自然灾害的指标，包括受灾面积和粮食产量[20]。上述因子指标近 20 年的数据均

(C)1994-2022 China Academic Journal Electronic Publishing House. All rights reserved. http://www.cnki.net

直接从国家统计局网站查得。

1.2　研究方法

该文研究通过对近 20 年全国耕地数量数据的分析处理，研究其变化趋势，进而通过与选取的因子进行相关性分析，研究其变化的驱动因子。其中，在对 1996—2016 年耕地面积的数据分析中，针对 2008—2009 年数据的跳跃现象，通过数据挖掘，一方面利用 1996—2008 年数据预测 2009 年数据，另一方面利用 2009—2016 年数据反推 2008 年数据，基于上述两种相互预测或反推得出的数值，分析 2008 年和 2009 年耕地数量的数据比例关系，进而对 1996—2016 年耕地面积数据进行比值归一化，以探索研究耕地面积的变化趋势。

该文在数据挖掘预测中，通过遴选对比最终采用的为 ARIMA 模型，即自回归积分滑动平均模型(Autoregressive Integrated Moving Average Model)，是由博克思(Box)和詹金斯(Jenkins)提出的著名时间序列预测方法，主要是指将非平稳时间序列转化为平稳时间序列，然后将因变量仅对它的滞后值以及随机误差项的现值和滞后值进行回归所建立的模型，适用于该文的研究。

2　近 20 年耕地数量变化趋势分析

2.1　基于耕地数量原始统计数据的变化趋势及分析

通过对收集整理的 1996—2016 年耕地数量数据分析，如图 1，可以看出，1996—2008 年全国耕地面积逐年减少，其中以 2000—2004 年递减速度最快；2008—2009 年耕地面积数据出现跳跃，由 1.217 亿 hm^2(18.26 亿亩)增至 1.354 亿 hm^2(20.31 亿亩)；2009—2016 年耕地面积递减速度非常缓慢。

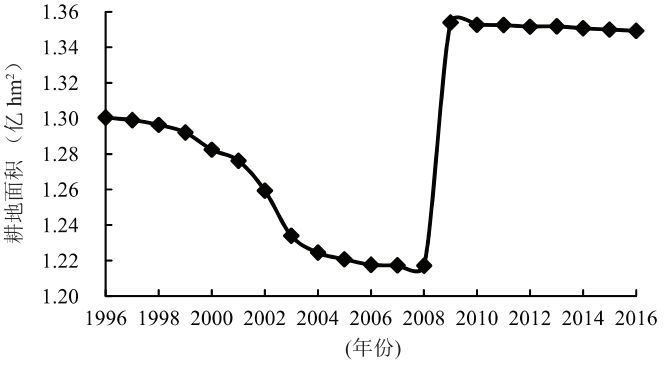


图 1　1996—2016 年基于原始统计数据的耕地数量变化趋势

1996 年国家完成了第一次大规模的土地利用现状调查；2009 年第二次全国土地利用现状调查完成。由此可见，2008—2009 年耕地面积数据的跳跃正是一调与二调数据的分界年份。全国耕地面积是否真的增多了约 0.14 亿 hm^2(2 亿亩)，经文献查阅分析[17,18,21]，主要原因在于二调采用了更为先进的技术手段，将以往少报的耕地面积统计入库，进一步提高了数据的准确度。所以，近 20 年全国耕地数量的统计数据是基于两次不同的技术水平，可直接分别研究各自时段内的变化趋势，但如果要研究连续 20 年时间段内的变化趋势，就须对两个时间段的数据进行校正，使之具有可对比性。

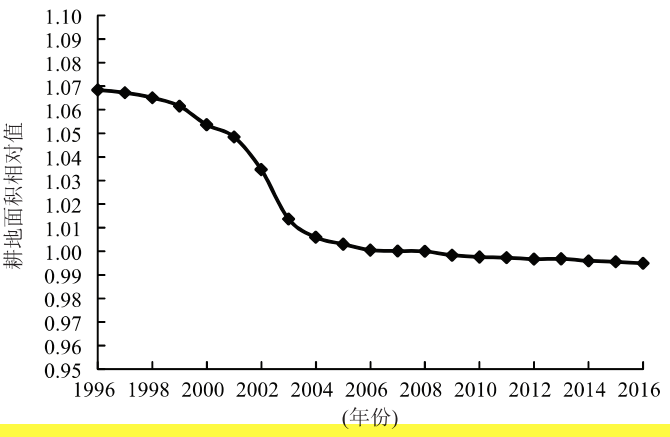


图 2　1996—2016 年基于校正后相对数据的耕地变化趋势

2.2　基于数据挖掘的耕地数量校正

数据挖掘技术在时间序列上具有强有力的预测功能，该文首先利用 1996—2008 年耕地数量数据，预测 2009 年的耕地数量，由此得出 2009 年与 2008 年耕地数量的比值关系 α；然后利用 2009—2016 年耕地数量数据，反推 2008 年的耕地数量，由此得出 2009 年与 2008 年耕地数量的比值关系 β；为更为科学地反映 2009 年与 2008 年耕地数量的比值关系，取利用正向预测与反向反推两种方法得出的 α 与 β 的算数平均值 ρ 作为实际的数量比值关系。

该文研究在预测过程中，利用 SPSS 软件，通过比较分析，在正向预测 2009 年数值和反向反推 2008

(C)1994-2022 China Academic Journal Electronic Publishing House. All rights reserved.　http://www.cnki.net

年数值中均选用 ARIMA 模型，其中正向预测选用的模型为 ARIMA（1，1，2）（$r^2=0.975^{**}$），反向反推选用的模型为 ARIMA（1，1，4）（$r^2=0.966^{**}$），两者均在 0.01 水平呈现显著性。由此，基于 1996—2008 年数据预测得出的 2009 年耕地数量为 1.213 387 亿 hm^2（18.200 8 亿亩），基于 2009—2016 年数据反推得出的 2008 年耕地数量为 1.353 987 亿 hm^2（20.309 8 亿亩），进一步可得出 $\alpha=996\ 899.887\ E-6$，$\beta=999\ 895.617\ E-6$，则 $\rho=998\ 397.752\ E-6$，由此推测 2009 年与 2008 年耕地数量的比值为998 397.752 E－6，即可为两个时间段数据的校正系数。

2.3 基于耕地数量校正相对值的变化趋势分析

为进一步客观的反映近 20 年的耕地数量变化趋势，对全部年份数据进行比值归一化及系数校正，在前文研究基础上，首先对 1996—2008 年全部原始耕地数量数据以 2008 年耕地数量为基数计算得到的比值即为其耕地数量相对值，对 2009—2016 年全部原始耕地数量数据以 2009 年耕地数量为基数计算得到的比值，再乘以校正系数 ρ，即为其相应年份的耕地数量相对值。由此可以得出 1996—2016 年耕地数量的变化趋势，如图 2 所示，可以看出，近 20 年全国耕地数量是呈现递减趋势的，其中 2004 年以前，递减速度较快，2004 年以后耕地数量递减速度较缓，尤其是 2006 年以后耕地数量递减速度趋于稳定。

3 耕地数量变化驱动因子分析

该文研究共收集了 1996—2016 年共 17 个因子指标，首先进行描述性特征统计，如表 1 所示；然后，通过分析耕地数量与各因子指标的相关性（表 2），进行对比分析，以此遴选出耕地数量变化的驱动因子。

表 1 1996—2016 年各因子指标的描述性统计特征

因子	最小值	最大值	平均值	标准差
国民总收入（亿元）	70 780	741 140	304 446.950	225 956.601
国内生产总值（亿元）	71 814	744 127	305 718.670	226 519.843
第一产业增加值（亿元）	13 878	63 671	31 240.710	17 742.619
第一产业增加值占比（%）	8.556	19.325	12.114	3.280
第二产业增加值（亿元）	33 828	296 236	135 629.240	94 949.577
第二产业增加值占比（%）	39.810	47.559	45.327	1.999
第三产业增加值（亿元）	24 107	384 220	138 848.860	114 605.836
第三产业增加值占比（%）	33.569	51.634	42.560	4.472
人均国内生产总值（亿元）	5 898	53 980	22 872	16 332.770
工业增加值（亿元）	29 530	247 860	116 532.760	79 508.293
建筑业增加值（亿元）	4 393	49 522	19 623	15 992.727
年末总人口（万人）	122 389	138 271	131 047.710	4 702.171
城镇人口（万人）	37 304	79 298	58 413.240	12 989.267
乡村人口（万人）	58 973	85 085	72 634.480	8 313.397
农业总产值（亿元）	13 540	59 288	28 842.620	16 570.347
粮食产量（万 t）	43 070	62 144	52 326.480	5 812.061
受灾面积（万 hm^2）	2 177	5 468.8	4 100.948 0	1 070.630

由表 2 可以看出，基于原始统计的耕地面积研究其与各因子指标的相关性，由于数据的跳跃不足以反映耕地变化的实际趋势，与各因子指标的相关性均不高。基于校正后的耕地数量的相对值，研究其与各因子指标的相关性，可以发现，与第一产值增加值占比的相关性最高，相关系数高达 0.959；与年末总人口的相关性次之，为负相关，系数为 －0.918，城镇人口和乡村人口与之的相关性也较高，即第一产业增加值占比，总人口以及城镇人口数量与耕地数量的变化相关性较好，是重要的驱动因子。由此，可以推论出国家产业结构布局调整、我国城镇化建设水平是影响我国耕地数量变化的重要因素条件。耕地作为第一产

(C)1994-2022 China Academic Journal Electronic Publishing House. All rights reserved. http://www.cnki.net

表 2　耕地面积与各因子的相关系数矩阵

	原始统计耕地面积	校正后耕地面积相对值		原始统计耕地面积	校正后耕地面积相对值
原始统计耕地面积	1	-0.142	人均国内生产总值	0.651	-0.749
校正后耕地面积相对值	-0.142	1	工业增加值	0.638	-0.784
国民总收入	0.649	-0.746	建筑业增加值	0.688	-0.716
国内生产总值	0.652	-0.745	年末总人口	0.433	-0.918
第一产业增加值	0.663	-0.736	城镇人口	0.488	-0.896
第一产业增加值占比	-0.274	0.959	乡村人口	-0.518	0.88
第二产业增加值	0.647	-0.774	农业总产值	0.686	-0.709
第二产业增加值占比	-0.519	0.259	粮食产量	0.752	-0.524
第三产业增加值	0.649	-0.717	受灾面积	-0.514	0.708

业的最重要的载体之一，与第一产业增加值密切正相关，我国产业结构中对于第一产业布局要求会直接诱使我国耕地的变化。而城镇化建设过程中，一方面由于城镇建设会直接占用大量的耕地，另一方面，城镇化建设中大量的农民人口直接进入城镇生活，或者进城务工而导致耕地撂荒，所以城镇化建设水平与耕地变化呈现密切的负相关。

4　结论与讨论

土地本身既有自然属性，又有社会属性，对于耕地数量的统计长期以来受社会、经济、政策等诸多因素的影响，导致难以对其进行长时间序列的趋势研究。该文研究的时间序列跨度全国两次土地调查的统计数据，两个时间阶段的数据具有明显的跳跃性，但并不代表 2009 年耕地数量真的比 2008 年大幅度增长。究其原因，主要是由于第二次全国土地调查中应用遥感等新方法、统一了标准，提高了调查的技术水平和准确度，使原来因少报、漏报、瞒报等各种原因未被统计到的耕地重新统计入库，所以要研究跨两个阶段的整体变化趋势，就必须研究建立其数值量化关系。该文通过数据挖掘，并对耕地数量进行校正和比值归一化，研究结果比较准确地反映了我国耕地变化趋势的实际情况。

研究结果表明，近 20 年，我国耕地数量呈现递减趋势，其中 2004 年以前递减速度较快，2004 年以后递减速度趋缓，我国产业结构布局方面，主要是第一产业增加值占比，以及我国人口总数方面，主要是城镇化人口数量是影响变化的主要驱动因子。由于 1999 年后开始生态退耕导致耕地数量迅速减少[17,22]，2004 年国家《土地管理法》修订后强调要加强耕地保护，实行占补平衡，对我国耕地的数量变化产生了积极作用。该文仅对近 20 年我国耕地数量的变化趋势进行了分析；现在国家加强耕地保护，不仅以数量为基础，更关注质量，以产能为核心，实现数量、质量和生态的三位一体保护[23]，下一步将对全国耕地质量的变化趋势进一步分析研究。同时，该文研究通过相关性分析研究提出了主要驱动因子，下一步还将进一步对驱动因子的贡献率进行量化分析研究。

该文研究仅对 1996—2016 年耕地数量的变化趋势进行了分析研究，由于对诸多指标因子数据统计的完整性需求，未对更长时间的耕地变化趋势进行研究。下一步，将在对统计数据分析的基础上，通过对遥感影像的数据挖掘，深入研究更长时间序列的变化趋势。

参考文献

[1] 赵其国，周生路，吴绍华，等. 中国耕地资源变化及其可持续利用与保护对策. 土壤学报，2006，43（4）：662－672.

[2] 葛全胜，戴君虎，何凡能，等. 过去 300 年中国部分省区耕地资源数量变化及驱动因素分析. 自然科学进展，2003，13（8）：825－832.

[3] 毕于运，郑振源. 建国以来中国实有耕地面积增减变化分析. 资源科学，2000，22（2）：8－12.

[4] 李秀彬. 中国近 20 年来耕地面积的变化及其政策启示. 自然资源学报，1999，14（4）：329－333.

(C)1994-2022 China Academic Journal Electronic Publishing House. All rights reserved.　http://www.cnki.net

[5] 曹银贵，袁春，周伟，等. 中国耕地变化的驱动因子及其省域差异分析. 中国土地科学，2008，22（2）：17－22.
[6] 黄忠华，吴次芳，杜雪君. 我国耕地变化与社会经济因素的实证分析. 自然资源学报，2009，24（2）：192－199.
[7] 郭丽英，王道龙，王介勇. 中国沿海地区耕地变化及其成因分析. 中国农业资源与区划，2012，33（1）：6－10.
[8] 吴霞，王世荣，尚红莺，等. 宁夏近 18 年来耕地面积动态变化及驱动力分析. 中国农业资源与区划，2017，38（8）：98－104.
[9] 武江民，赵学茂，党国锋. 甘肃兰州市耕地动态变化与驱动力关系定量研究. 干旱区资源与环境，2010，24（12）：33－38.
[10] 于天，曹银贵，许婧雪. 基于不同尺度的中国耕地变化驱动力研究进展. 中国农学通报，2016，32（24）：194－198.
[11] 张国平，刘纪远，张增祥. 近 10 年来中国耕地资源的时空变化分析. 地理学报，2003，58（3）：323－332.
[12] 田光进，庄大方，刘明亮. 近 10 年中国耕地资源时空变化特征. 地球科学进展，2003，18（1）：30－36.
[13] 刘旭华，王劲峰，刘纪远，等. 国家尺度耕地变化驱动力的定量分析方法. 农业工程学报，2005，21（4）：56－60.
[14] 刘旭华，王劲峰，刘明亮，等. 中国耕地变化驱动力分区研究. 中国科学 D 辑地球科学，2005，35（11）：1087－1095.
[15] 许丽丽，李宝林，袁烨城，等. 2000—2010 年中国耕地变化与耕地占补平衡政策效果分析. 资源科学，2015，37（8）：1543－1551.
[16] 李景刚，何春阳，史培军，等. 近 20 年中国北方 13 省的耕地变化与驱动力. 地理学报，2004，59（2）：274－282.
[17] 封志明，刘宝勤，杨艳昭. 中国耕地资源数量变化的趋势分析与数据重建：1949—2003. 自然资源学报，2005，20（1）：35－43.
[18] 谭永忠，何巨，岳文泽，等. 全国第二次土地调查前后中国耕地面积变化的空间格局. 自然资源学报，2017，32（2）：186－197.
[19] Lin G C S，HO S P S. China's land resources and land-use change：insights from the 1996 land survey. land Use Policy，2003，20（2）：87－107.
[20] 傅泽强，蔡运龙，杨友孝，等. 中国粮食安全与耕地资源变化的相关分析. 自然资源学报，2001，16（4）：313－319.
[21] 张雅琼，杨子生. 我国两次土地资源调查的对比分析. 国土资源科技管理，2013，30（2）：100－104.
[22] 徐宪立，蔡玉梅，张科利，等. 耕地资源动态变化及其影响因素分析. 中国人口·资源与环境，2005，15（3）：75－79.
[23] 谭永忠，吴次芳，王庆日，等. “耕地总量动态平衡”政策驱动下中国的耕地变化及其生态环境效应. 自然资源学报，2005，20（5）：727－734.

RESEARCH ON THE CHANGE TREND OF FARMLAND QUANTITY IN CHINA FOR RECENT 20 YEARS AND ITS DRIVING FACTORS*

Wang Jingyi[1], Li Xiaoming[2]※

(1. Xi'an Shiyou University, Xi'an, Shaanxi 710065, China;
2. Shaanxi Provincial Land Engineering Construction Group, Xi'an, Shaanxi 710075, China)

Abstract The research aims to research the changing trend of farmland quantity for recent 20 years before and after the second national land use survey. It could provide decision support for farmland protection and efficient use of land resources. The original data of farmland area from 1996 to 2016 were collected, data mining technology was introduced, and ARIMA model was chosen to predict the farmland quantity each other based on the farmland area of the twice land use survey, which meant to predict the farmland quantity of 2009 with the farmland quantity of the years from 1996 to 2008, and to predict the farmland quantity of 2008 inversely with the farmland quantity of the years from 2009 to 2016, so the original farmland area data could be corrected and normalized. Then the changing trend of farmland quantity for recent 20 years was studied furtherly and correlation analysis was used to study the driving factors. The trend research result showed, the farmland area decreased year by year for recent 20 years, the decreasing rate was faster before 2004, and then it decreased slowly. The correlation analysis result showed, the added value proportion of primary industry, the total population, and the urban population were the most important driving factors which influenced the farmland quantity change, their coefficients were 0.959, －0.918 and －0.896 respectively. It could be concluded by the result that the industry configuration and the urbanization could affect the farmland quantity with the development of social economy.

Keywords data mining; ARIMA model; farmland quantity; change trend; driving factors

(C)1994-2022 China Academic Journal Electronic Publishing House. All rights reserved. http://www.cnki.net